



TECHNISCHE  
UNIVERSITÄT  
WIEN  
Vienna | Austria

## Dissertation

# The stress tensor in the augmented plane wave based methods and its implementation in the WIEN2k code

by

**Kamal Belbase**  
ORCID: 0000-0002-7817-9456

A thesis submitted for the purpose of obtaining the degree of  
Doctor of Natural Sciences

under the supervision of  
Ao. Univ. Prof. Dipl.-Ing. Dr. techn. Peter Blaha  
Priv. Doz. Dr. Andreas Tröster

in the  
Institute of Material Chemistry  
**Vienna University of Technology**

November, 2021



## **Declaration of Authorship**

I, Kamal Belbase, declare that this thesis titled, “The stress tensor in the augmented plane wave based methods and its implementation in the WIEN2k code” and the work presented in it are my own. I confirm that:

- This work was done wholly or mainly while in candidature for a research degree at this University.
- Where any part of this thesis has previously been submitted for a degree or any other qualification at this University or any other institution, this has been clearly stated.
- Where I have consulted the published work of others, this is always clearly attributed.
- Where I have quoted from the work of others, the source is always given. With the exception of such quotations, this thesis is entirely my own work.
- I have acknowledged all main sources of help.
- Where the thesis is based on work done by myself jointly with others, I have made clear exactly what was done by others and what I have contributed myself.

Signed: Kamal Belbase

---

Date: November 30, 2021

---



# Abstract

In this work I present a detailed derivation of the formalism of the stress tensor for non-relativistic full potential augmented plane wave (APW) based methods. This formalism has been implemented into the WIEN2k code and has been thoroughly tested for various solids. After an introduction into the APW methods and the calculation of the total energy, the derivative of the latter with respect to strain is derived in full detail and simplified as much as possible. The individual contributions due to kinetic, electrostatic and exchange-correlation energy parts are given and the complications due to the decomposition into core and valence states, the decomposition of space into atomic spheres and an interstitial region, the finite (position dependent) basis set and eventually the discontinuity in slope of the basis functions across the sphere boundary in the APW+lo method are discussed in full detail. The implementation for the LDA approximation has been generalized for the GGA approximations of DFT, where an additional contribution to the stress tensor arises. Finally I tested the implementation by comparing the result of the stress tensor formalism with the corresponding results derived from total energy calculations. Both, hydrostatic and non-hydrostatic conditions have been applied and the accuracy of individual stress components has also been tested at finite strain. Typically the calculated stress (pressure) deviates from the one obtained from fits to total energy calculations by less than 1-3 kbar, which does not lead to any significant influence on eg. equilibrium lattice parameters. I also tested the convergence of the stress tensor with respect to basis set, confirmed the superior convergence of the stress tensor in the APW+lo method as compared to LAPW, but still found it necessary to increase the basis set size a bit as compared to total energy calculations. Other convergence parameters remain the same as for total energies. For metals like aluminum the effect of the tetrahedron and Fermi-Dirac (FD) methods on the calculated stress is studied and it was found that the FD method converges much faster with respect to k-points and yields in general more accurate results. Finally, a comparison of our formalism with previous attempts in literature on this topic is given and similarities and differences are pointed out.

## Acknowledgments

First and foremost, I would like to express my sincere gratitude to my Supervisors, Ao. Univ. Prof. Dipl.-Ing. Dr. techn. Peter Blaha and Priv. Doz. Dr. Andreas Tröster for the continuous support and guidance throughout my PhD study and research. Their encouragement and assistance at all times have been immensely valuable. Their guidance helped me in all the time during my research and the preparation of this thesis. I could not have imagined having a better supervisors and mentors for my doctorate.

Besides my advisors, I would like to thank Dr. Fabien Tran for his friendship and presence in times of need. I thank my fellow colleagues: Sohaib, Jan, Leila, Thomas, Mahdiyar, who created a pleasant working atmosphere.

I would like to thank my friends Sudip Paudyal, Shiva Devkota, respected brother Dr Surya Poudel and sister-in-law Prashna Niroula for the wonderful times together.

I am very grateful to all of my family members for their everlasting love and support who have enjoyed every moment of my success.

I acknowledge support by the Austrian Science Fund (FWF) Project P27738-N28 and WIEN2k.

## Kurzfassung

In dieser Arbeit präsentiere ich eine detaillierte Ableitung des Formalismus für den Stresstensor in nicht-relativistischen “full potential augmented plane wave (APW)“ basierenden Methoden. Dieser Formalismus wurde dann in das WIEN2k-Programm programmiert und für verschiedene Festkörper getestet. Nach einer Einleitung in die APW-methode und der Berechnung der Gesamtenergie wird die Ableitung derselben nach dem Strain genauestens hergeleitet und die entsprechenden Gleichungen so weit wie möglich vereinfacht. Die Beiträge von kinetischer, potentieller und austauschkorrelation Energie werden einzeln abgeleitet und die Besonderheiten diskutiert, die durch die Teilung in Core- und Valenzelektronen, die Aufteilung des Raumes in Atomkugeln und einen Zwischenbereich, den endlichen (positionsabhängigen) Basissatz und die Unstetigkeit der Ableitung der Basisfunktionen am Kugelrand auftreten. Die Implementation für die LDA Näherung wurde für die GGA Näherung verallgemeinert, wobei einige zusätzliche Terme auftreten. Schließlich habe ich die Implementation durch einen Vergleich der Resultate des Stresstensors mit jenen aus Gesamtenergieberechnungen getestet. Es wurden hydrostatische und nicht-hydrostatische Bedingungen angewendet und die Genauigkeit auch bei endlichem Druck überprüft. Im Vergleich zu Ergebnissen aus der Gesamtenergie haben die berechneten Drücke einen typischen Fehler von 1-3 kbar, was aber auf entsprechend abgeleitete Größen wie z.B. die Gleichgewichtsgitterkonstanten kaum einen nennenswerten Einfluss hat. Ich habe auch die Konvergenz des Stresstensors mit der Größe des Basissatzes getestet und wie erwartet ein besseres Verhalten der APW+lo Methode gegenüber der LAPW Methode gefunden. Dennoch muss man den Basissatz im Vergleich zu Gesamtenergieberechnungen leicht verbessern, während andere Konvergenzparameter gleich gewählt werden können. Für Metalle wie Al liefert die Fermi-Dirac Methode genauere Ergebnisse als die Tetraedermethode und konvergiert mit weniger k-Punkten. Schlussendlich wird unser Formalismus mit den vorhergehenden Versuchen in der Literatur verglichen und Gemeinsamkeiten bzw. Unterschiede hervorgehoben.

# Contents

<b>List of Figures</b>	<b>ix</b>
<b>List of Tables</b>	<b>xiv</b>
<b>1 Introduction</b>	<b>1</b>
<b>2 Strain and Stress Tensor</b>	<b>4</b>
2.1 Elastic Constants . . . . .	6
<b>3 The APW based methods</b>	<b>8</b>
3.1 Basis Function . . . . .	8
3.1.1 APW . . . . .	8
3.1.2 LAPW . . . . .	10
3.1.3 APW+lo . . . . .	11
3.1.4 LO Orbitals . . . . .	12
3.2 Wave Function . . . . .	13
3.3 Charge density . . . . .	14
<b>4 Total Energy and Potentials</b>	<b>16</b>
4.1 Additional contribution to the kinetic energy . . . . .	18
4.2 Coulomb Potential . . . . .	19
4.3 Madelung potential . . . . .	22
<b>5 Strain variation</b>	<b>25</b>
5.1 Variation of the kinetic energy . . . . .	26
5.2 Variation of the electrostatic energy . . . . .	29
5.3 Variation of the exchange-correlation energy . . . . .	30
5.3.1 Variation of the LDA exchange-correlation energy . . . . .	30
5.3.2 Variation of the GGA exchange-correlation energy . . . . .	31
5.4 Variation of the total energy . . . . .	34
5.5 Variation of the interstitial charge density . . . . .	35
5.6 Variation of the interstitial Coulomb potential . . . . .	37
<b>6 Stress tensor</b>	<b>39</b>
6.1 Electrostatic Stress Tensor . . . . .	40
6.1.1 Coulomb Stress Tensor . . . . .	40
6.1.2 Madelung Stress Tensor . . . . .	44
6.2 Core Correction Stress Tensor . . . . .	48
6.3 Valence Kinetic Stress Tensor . . . . .	52
6.3.1 Additional Surface Integral . . . . .	56

6.4	Valence Correction Stress Tensor . . . . .	59
6.5	Exchange Correlation Stress Tensor . . . . .	69
6.6	Total stress tensor . . . . .	71
<b>7</b>	<b>Pressure</b>	<b>74</b>
7.1	Pressure due to the valence correction stress tensor . . . . .	75
7.2	Pressure due to the valence kinetic stress tensor . . . . .	76
7.2.1	Pressure due to the additional surface integral . . . . .	77
7.3	Pressure due to the core correction stress tensor . . . . .	78
7.4	Pressure due to the exchange correlation stress tensor . . . . .	79
7.5	Pressure due to the electrostatic stress tensor . . . . .	81
7.6	The simple pressure formula . . . . .	82
7.7	Core leakage . . . . .	83
<b>8</b>	<b>Results</b>	<b>90</b>
8.1	Calculations for fcc Aluminum . . . . .	91
8.2	Silicon . . . . .	99
8.3	Tungsten W . . . . .	104
8.4	Low symmetry crystal structures . . . . .	110
8.4.1	ZnO . . . . .	110
8.4.2	Rutile TiO <sub>2</sub> . . . . .	112
8.5	Lattice parameters . . . . .	113
8.6	Accuracy of individual component . . . . .	114
8.7	Elastic constants . . . . .	115
<b>9</b>	<b>Discussion</b>	<b>118</b>
<b>Appendices</b>		<b>123</b>
<b>A</b>	<b>Mathematical tools</b>	<b>124</b>
A.1	Variation of spherical harmonics . . . . .	125
A.2	c coefficients . . . . .	126
A.3	Component derivative of the radial function . . . . .	127
A.4	Integration over the whole unit cell . . . . .	128
<b>B</b>	<b>Real and complex spherical harmonics and density</b>	<b>130</b>
B.1	Sum over atoms . . . . .	131
B.2	k points symmetrization . . . . .	132
B.3	Occupation number . . . . .	132
<b>C</b>	<b>Contribution from the double counting term</b>	<b>134</b>
<b>D</b>	<b>Janak's Identity</b>	<b>136</b>
<b>E</b>	<b>Variation of the electrostatic energy</b>	<b>139</b>
<b>F</b>	<b>Calculation of the strain variation of Kohn-Sham eigenvalue</b>	<b>141</b>
<b>Bibliography</b>		<b>144</b>
<b>10</b>	<b>List of Publication</b>	<b>148</b>



# List of Figures

1.1	The total energy versus volume and its numerical derivative (pressure) for Aluminum. The parabolic curve (red) represents the least square fit using the Birch-Murnaghan ( $E_{BM}$ ) equation and the blue curve presents the numerical derivative i.e $P^{(E)} = -\frac{\partial E_{BM}(\Omega)}{\partial \Omega}$ . $\Omega$ is the volume of the unit cell. At the equilibrium, energy is at a minimum and the pressure is zero. . . . .	2
2.1	A homogeneously stressed body. $X_1$ , $X_2$ , and $X_3$ correspond to the familiar x, y and z axes. Based on its normal (perpendicular to the surface) or tangential (parallel to the surface) components, the stress tensor is decomposed in each face. . . . .	4
2.2	The relationship between strain and stress for a material[21]. . . . .	6
3.1	The division of a unit cell into non-overlapping atom centered spheres with radius $R_a$ located at $\tau_a$ and the interstitial region (IS)—space between the atoms. . . . .	8
7.1	The different contributions to the exchange-correlation pressure (Eqn. (7.31c)) for Al (left panel) and Si (right panel) as function of volume. The bottom plots display the trace of the equation (6.150). $P^{GGA}$ is the trace of the GGA stress tensor ( $\sigma_{\alpha\beta}^{GGA}$ ), $P^{LDA}$ is the LDA like expression, and $P^{GGA,CORR}$ is the GGA correction. . . . .	81
7.2	The behavior of core potential inside and outside of an atomic-sphere for fcc Al before and after the extrapolation with a polynomial. $r$ is the distance from the nucleus and the vertical line at $r = 2.1$ denotes the sphere boundary. Because of the existence of a singularity in the potential at $r = 0$ , $r$ times $V_{00}(r)$ is plotted. The red line represents the potential before extrapolation, the blue line the extrapolated potential using a quadratic equation, and $V_{00}$ represents the spherically symmetric part of the potential. . . . .	86
7.3	Pressure estimated by the simple pressure formula given in equation (7.37) ( <b>a</b> ), and directly from total energy using the least square fit of the Birch-Murnaghan (BM) equation of state ( <b>b</b> ) for fcc Al. The potential outside atomic sphere is the original potential (red curve in Fig. 7.2) and 2p states are considered as core states. . . . .	86
7.4	Same as Fig. 7.3 but the potential at any point outside of an atomic-sphere region is calculated via extrapolation using a quadratic equation (blue curve in Fig. 7.2). . . . .	87

7.5	Pressure estimated via the analytical simple pressure formula using two different expressions of the potential in the region outside of the atomic-sphere. The 2p states are treated as semi-core states. On the left panel, the core potential outside of an atomic sphere is the original potential. On the right panel, the core potential outside the sphere is the extrapolated potential. . . . .	87
7.6	The trace of stress tensor as a function of volume for fcc Al for three different sphere sizes. The 2p states are treated as core states. The core potential outside of an atomic sphere in the panel ( <b>a</b> ) is the original potential (red curve in Fig.7.2) and in the panel ( <b>b</b> ) is the extrapolated potential (blue curve in Fig. 7.2). . . . .	88
8.1	( <b>a</b> ) Energy-volume curves as well as $P^{(E)}$ , ( <b>b</b> ) the negative trace of the full stress tensor $P^{(\sigma)}$ and, ( <b>c</b> ) the difference between $P^{(\sigma)}$ and $P^{(E)}$ as function of $\Omega$ for various $R_a K_{max}$ for fcc Al. The standard tetrahedron method with the Blöchl correction is used for the BZ integration. . . . .	93
8.2	Same as Figure 8.1, but with the tetrahedron method without Blöchl's correction. . . . .	94
8.3	Energy-volume curves as well as $P^{(E)}$ for different k-meshes at $R_a K_{max} = 10$ for fcc Al. The negative trace of the full stress tensor, $P^{(\sigma)}$ , and the difference between $P^{(\sigma)}$ and $P^{(E)}$ as function of $\Omega$ . On the left panel, ( <b>a</b> ), ( <b>b</b> ), and ( <b>c</b> ) are the results using the standard tetrahedron method with Blöchl's correction. On the right panel, ( <b>a1</b> ), ( <b>b1</b> ), and ( <b>c1</b> ) are without Blöchl's correction. . . . .	95
8.4	( <b>a</b> ) Energy-volume curves as well as $P^{(E)}$ , ( <b>b</b> ) the negative trace of the full stress tensor $P^{(\sigma)}$ and, ( <b>c</b> ) the difference between $P^{(\sigma)}$ and $P^{(E)}$ as function of $\Omega$ for various $R_a K_{max}$ for fcc Al. All other input parameters are the same as in Figure 8.1, but the FD method with a broadening parameter of 0.003 Ry is used for the BZ integration. . . . .	97
8.5	Same as Figure 8.3 but the FD method with a broadening parameter 0.005 Ry. . . . .	97
8.6	( <b>a</b> ) Energy-volume curves as well as $P^{(E)}$ for different k-meshes and $R_a K_{max} = 10$ for fcc Al. <b>b</b> ) The negative trace of the full stress tensor, $P^{(\sigma)}$ , and ( <b>c</b> ) the difference between $P^{(\sigma)}$ and $P^{(E)}$ as function of $\Omega$ . The integration in IBZ is carried out using the FD method with a broadening parameter of 0.005 Ry and all remaining input parameters are the same as in Figure 8.3. . . . .	98
8.7	( <b>a</b> ) Energy-volume curves as well as $P^{(E)}$ , ( <b>b</b> ) the negative trace of the full stress tensor $P^{(\sigma)}$ and, ( <b>c</b> ) the difference between $P^{(\sigma)}$ and $P^{(E)}$ as function of $\Omega$ for various $R_a K_{max}$ for Si in the diamond structure. . . . .	100
8.8	( <b>a</b> ) Energy-volume curves as well as $P^{(E)}$ for five different $G_{max}$ in the expansion of the charge density and the potential for Si in the diamond structure. ( <b>b</b> ) The negative trace of the full stress tensor $P^{(\sigma)}$ and ( <b>c</b> ) the difference between $P^{(E)}$ and $P^{(\sigma)}$ as function $\Omega$ . $R_a K_{max} = 10$ and all other input parameters are the same as in Figure 8.7. . . . .	101

8.9 (a) Energy-volume curves as well as $P^{(E)}$ for three different k point meshes for Si in the diamond structure. (b) The negative trace of the full stress tensor $P^{(\sigma)}$ and (c) the difference between $P^{(E)}$ and $P^{(\sigma)}$ as function of $\Omega$ . $R_aK_{max} = 10$ and all other input parameters are the same as in Figure 8.7. . . . .	101
8.10 (a) Energy-volume curves as well as $P^{(E)}$ for four different cutoff values of the angular momentum ( $L''_{max}$ ) of the non-spherical potential for Si in the diamond structure. (b) The negative trace of the full stress tensor $P^{(\sigma)}$ and (c) the difference between $P^{(E)}$ and $P^{(\sigma)}$ as function of $\Omega$ . $R_aK_{max} = 10$ and all other input parameters are the same as in Figure 8.7. . . . .	102
8.11 Pressure $P^{(\sigma)}$ estimated from the trace of the full stress tensor for GaAs at different values of $R_aK_{max}$ as function of $\Omega$ . The vertical lines represent the equilibrium volume predicted directly from the total energy using the least square fit of BM equation. . . . .	104
8.12 (a) Energy-volume curves as well as $P^{(E)} = -\frac{dE(\Omega)}{d\Omega}$ , (b) the negative trace of the full stress tensor $P^{(\sigma)}$ , and (c) the difference between $P^{(\sigma)}$ and $P^{(E)}$ for various $R_aK_{max}$ as function of the unit cell volumes ( $\Omega$ ) for bcc W. Temperature broadening method with a broadening parameter of 0.005 Ry is used for the BZ integration . . . . .	106
8.13 (a) The negative trace of the full stress tensor $P^{(\sigma)}$ and (b) the difference of $P^{(\sigma)}$ from $P^{(E)}$ for different $R_aK_{max}$ as function of $\Omega$ for bcc W. The standard tetrahedron method with Blöchl's correction is used for the BZ integration and all other input parameters are the same as in Figure . . . . .	106
8.14 (a) The negative trace of the full stress tensor $P^{(\sigma)}$ and (b) the deviation of $P^{(\sigma)}$ from $P^{(E)}$ for two different k-meshes as function of $\Omega$ for bcc W. The standard tetrahedron method with Blöchl's correction and Fermi-Dirac (FD) smearing method are used. $R_aK_{max} = 10$ and all other input parameters are the same as in Figure 8.12. . . . .	107
8.15 The trace of the full stress tensor with (red curve) and without (blue curve) the inclusion of APW surface term, Eqn. (6.82), as function of $\Omega$ . The vertical orange line corresponds to the equilibrium lattice predicted directly from the total energy calculation. $R_aK_{max} = 10$ and all the remaining input parameters are the same as in Figure 8.12. . . . .	108
8.16 Convergence of $\sigma_{11}$ according to different $R_aK_{max}$ for the APW+lo and LAPW methods at the equilibrium volume for bcc W. For LAPW two different cases—4f electrons as valence or core— are considered. All other input parameters are the same as in Figure 8.12. . . . .	109
8.17 Comparison of the predicted lattice parameters from the stress tensor calculation and directly from the total energy for six different values of $R_aK_{max}$ in the APW+lo and LAPW methods for bcc W. All other conditions are the same as Figure 8.16. . . . .	109
8.18 (a) Energy-volume curves as well as $P^{(E)}$ , (b) the negative trace of the full stress tensor $P^{(\sigma)}$ , and (c) the difference between $P^{(\sigma)}$ and $P^{(E)}$ for the LDA and GGA as function $\Omega$ for bcc W. $R_aK_{max} = 10$ and all other input parameter are the same as in Fig. 8.12 (a)-(c). . . . .	110

8.19 Elastic constants $C_{12}$ and $C_{11}$ versus the applied strain for fcc AlAs using Eqs. (8.12) and (8.13) (represented by marker points) and Eqs.(8.9) to (8.11) (represented by dashed lines). All input parameters are the same as in Table 8.14. . . . .	117
8.20 Elastic constants $C_{12}$ and $C_{11}$ versus the applied strain for silicon in the diamond structure using Eqs. (8.12) and (8.13) (represented by marker points) and Eqs.(8.9) to (8.11) (represented by dashed lines). All input parameters are the same as in Table 8.13. . . . .	117

# List of Tables

5.1	All quantities that are necessary to calculate the total energy in the undistorted and distorted system. The first and second column contain the quantities for the undistorted and distorted system, respectively. The $\underline{\epsilon}$ symbolizes a symmetrical, infinitesimal strain deformation and $[\underline{\epsilon}]$ is used to indicate quantities after deformation. . . . .	26
7.1	The exchange correlation pressure (in kbar) is decomposed according to equation (7.31c) for seven different volumes of fcc Aluminum. . . . .	80
7.2	The exchange correlation pressure (in kbar) is decomposed according to equation (7.31c) for seven different volumes of Silicon in a diamond structure. . . . .	80
7.3	The predicted lattice parameter ( $a_0$ ) using the analytical simple pressure (SIMP) formula and directly from total energy (ENE) for three different atomic sphere sizes ( $R_a$ ). The 2p states are treated as core states and the core potential outside an atomic sphere is the original potential. . .	88
7.4	Same as Table 7.3, but the 2p states are treated as semi-core states. . .	89
8.1	Predicted equilibrium volume $\Omega_0$ (in Bohr <sup>3</sup> ) and lattice constant $a_0$ (in Bohr) from the analytical stress tensor (superscript $(\sigma)$ ) and directly from the total energy (superscript $(E)$ ) as a function of $R_a K_{max}$ for fcc Al. The standard tetrahedron method with Blöchl's correction is used for k-space integration and all the remaining input parameters are the same as in Figure 8.1. . . . .	93
8.2	Same as Table 8.1, but the tetrahedron method without Blöchl's correction. . . . .	93
8.3	Predicted equilibrium volume $\Omega_0$ (in Bohr <sup>3</sup> ) and lattice constant $a_0$ (in Bohr) from the analytical stress tensor (superscript $(\sigma)$ ) and directly from the total energy (superscript $(E)$ ) as a function of $R_a K_{max}$ for fcc Al. For the BZ integration, the FD method with broadening parameter 0.003 Ry is used. All other input parameters are the same as in Figure 8.4. . . . .	96
8.4	Same as Table 8.3 but temperature broadening with broadening parameter 0.005 Ry. All other input parameters are the same as in Figure 8.5. . . . .	96
8.5	The $\sigma_{11}$ component of various stress tensor contributions of Eqn. (6.164) for fcc Al at the unit cell volume $\Omega = 111.17$ Bohr <sup>3</sup> , which is the equilibrium volume according to the total energy calculation. The stress component in the energy unit is given in the Ry column, in the pressure unit in the kbar column, and $1\text{Ry} = \frac{147105.1641}{\Omega}$ kbar with $\Omega = 111.17$ Bohr <sup>3</sup> . . . . .	99

8.6	Predicted equilibrium volume $\Omega_0$ (in Bohr <sup>3</sup> ) and lattice constant $a_0$ (in Bohr) from the analytical stress tensor (superscript ( $\sigma$ )) and directly from the total energy (superscript ( $E$ )) as a function of $R_a K_{max}$ for Si in the diamond structure. . . . .	100
8.7	Predicted equilibrium volume $\Omega_0$ (in Bohr <sup>3</sup> ) and lattice constant $a_0$ (in Bohr) from the analytical stress tensor (superscript ( $\sigma$ )) and directly from the total energy (superscript ( $E$ )) as a function of $R_a K_{max}$ for GaAs. All input parameters are set to the same value as in Figure 8.11. . . . .	104
8.8	Lattice parameters $a_0^{(E)}$ and $a_0^{(\sigma)}$ (in units of Bohr) of bcc W as predicted from total energy and the analytical stress formalism, respectively, for four different values of $R_a K_{max}$ and using the Fermi-Dirac (FD) and tetrahedron (Tetra) method. . . . .	105
8.9	$\sigma_{\alpha\beta}^{APW}$ (in kbar) as given in Eqn. (6.82) for $\alpha=\beta=1$ for bcc W at the equilibrium according to the APW+lo and LAPW methods. LOs are added in the both method. $R_a K_{max} = 10$ and all input parameters are the same as in Figure 8.12. . . . .	108
8.10	Comparison of the equilibrium lattice parameters (in Bohr), $a_0$ and $c_0$ , of ZnO obtained from the fifth order polynomial fit to the total energy (labeled 'energy') and directly from the stress tensor formalism with and without inclusion of the non-spherical components ( $l=2$ ) in the potential when the core correction, Eqn. (6.48), is calculated. $V_{tot}^c$ represents the sum of the both spherical potential $V_{00}^c$ and non-spherical potential $V_{2m}^c$ . . . . .	112
8.11	Comparison of the equilibrium lattice parameters (Bohr), $a_0$ and $c_0$ , obtained from the fifth order polynomial fit to the total energy (labeled 'energy') and directly from the stress tensor formalism. . . . .	113
8.12	Comparison of the equilibrium lattice parameter $a_0$ (in Bohr) and the bulk modulus (in kbar) obtained from the total energy ( $E$ ) and directly from the stress tensor ( $\sigma$ ) formalism for different elements. . . . .	114
8.13	Comparison of $\sigma_{33}$ (in kbar) calculated using Eqs. (8.8) and (6.163) for silicon in the diamond structure with seven different non-volume conserving tetragonal deformations. The superscripts ( $E$ ) and ( $\sigma$ ) correspond to the energy and stress. . . . .	115
8.14	Comparison of $\sigma_{33}$ (in kbar) calculated using Eqs. (8.8) and (6.163) for fcc AlAs with different non-volume conserving tetragonal deformations. The superscripts ( $E$ ) and ( $\sigma$ ) correspond to the energy and stress. . . . .	115
A.1	The value of $c_{at}$ for different $\alpha$ and t. $\alpha = 1, 2, 3$ represent to x, y, z of the Cartesian coordinate system. . . . .	124
B.1	Pre-factors for different $l$ and m. . . . .	130

# Chapter 1

## Introduction

Many physical and chemical properties such as equilibrium lattice constants, elastic constants, bulk moduli, phonons, phase transitions or chemical bonding depend on the total energy of a system. Furthermore, properties such as the forces on atoms or the stress depend on the derivatives of the total energy. The force is the derivative of the total energy with respect to the atomic position, and stress is a derivative with respect to strain. The derivative can be computed numerically by a finite difference approach, but to do so, the total energy needs to be calculated several times, as shown in Figure 1.1. In Figure 1.1, the marked points represent the selected unit cell volumes at which first-principle density functional theory (DFT)[1, 2] calculations are performed to compute the total energy. The curve to join these points is obtained by a least square fit using the Birch-Murnaghan (BM) equation (Figure 1.1). Consequently, the prediction of the equilibrium volume ( $\Omega_0$ ) based on the information of the total energy becomes more and more expensive with increasing the system size and decreasing the symmetry of the crystal structure. For example, if the structure is hexagonal, the structural optimization becomes a two dimensional problem—at each volume the ratio  $\frac{c}{a}$  needs to be optimized too. The calculations become severely more complicated and tedious if the structure has even lower symmetry such as orthorhombic, monoclinic or triclinic. In such cases, information obtained from the stress tensor is particularly valuable because few calculations can be sufficient to determine the equilibrium configuration. In equilibrium, all components of the stress tensor become zero within the numerical accuracy of the calculation.

The concept of stress is a little different than that of forces. In force calculations, an atom is displaced, and the corresponding energy is calculated. In contrast to forces, in stress calculations, the unit cell is deformed and the effect of this deformation on the total energy needs to be computed. Also, force calculations lead to a change of the atomic positions, whereas stress leads to a change in the size and shape of the unit cell. The immediate effect of deformation on a system is: the cell parameters change, and the atomic positions are modified since they are defined with respect to the deformed lattice parameters.

The stress tensor within Density Functional Theory (DFT) formalism was first introduced by Nielsen and Martin in Refs. [3, 4], and verified using a plane-wave based implementation. This work was limited to the Local Density Approximation (LDA)[5, 6]. Later, the derivation was extended to semilocal exchange-correlations functional by Corso & Resta et. al. [7] and tested again in a pseudopotential based implementa-

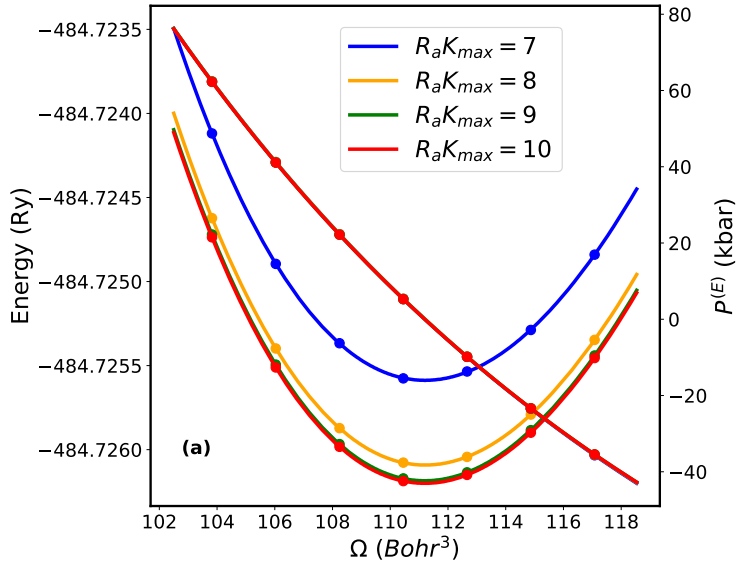


Figure 1.1: The total energy versus volume and its numerical derivative (pressure) for Aluminum. The parabolic curve (red) represents the least square fit using the Birch-Murnaghan ( $E_{BM}$ ) equation and the blue curve presents the numerical derivative i.e  $P^{(E)} = -\frac{\partial E_{BM}(\Omega)}{\partial \Omega}$ .  $\Omega$  is the volume of the unit cell. At the equilibrium, energy is at a minimum and the pressure is zero.

tion. The work was further expanded to the projector augmented wave (PAW) method by Torrent et. al. [8]. In plane-wave pseudopotential calculations, a full structural optimization—optimizing both atomic positions and shape and size of the unit cell—is possible and implemented in many code. On the other hand, in all electron Full Potential Augmented Plane Wave (APW) methods[9, 10, 11], the unit cell can only be optimized by tedious total energy calculations. For the linearized APW (LAPW) method, the stress tensor was first derived by Thonhauser et. al. [12] and implemented in WIEN97 [13, 14]. However, the authors present only the result of the pressure for Al and Si using a simplified approximation of the full stress tensor. The formalism for the full tensor did not work.

Later, in a modified version of the LAPW method proposed by Soler and Williams [15, 16], a stress tensor calculation was published by Nagasako and Oguchi. They provide a rigorous mathematical formalism for both local and semilocal functionals in Refs. [17] and [18], respectively. They tested their implementation for many different elements with different cutoff parameters and also for some compounds. The results are in agreement with numerical results—calculated directly from the total energies. Unfortunately, their approach cannot be used directly in our method since the basis functions used to solve the Kohn-Sham equation are considerably different from ours. In Soler and Williams LAPW, basis functions are mostly defined by plane-waves and only for the chemically important  $l$  ( $l \leq l_{max} : l_{max} = 2$  or  $3$ ), the plane waves are augmented inside the spherical region.

For the standard LAPW method, Klüppelberg in Ref. [19] gives a very elegant mathematical derivation of the stress tensor and also discusses an implementation into the FLEUR code [20]. Unfortunately, the calculated stress and pressure do not agree with

each other as well as with the results obtained directly from the total energy. The author suggests that the possible error may be due to the electrostatic stress tensor and the sum of valence and discontinuity correction. The error in the reported results is so big that it is difficult to identify whether it is due to a numerical or a mathematical problem. Also, in Ref. [19], the result of the so called simple pressure formula is not correct, even though its expression is simple and is calculated using the charge density and potential obtained from regular total energy calculations.

In our calculations, we will closely follow the work of Klüppelberg *et al.* but introduce modifications when necessary. We also make a comparison with the work of Thonhauser et. al, wherever it is possible. In order to make this thesis readable and not to get lost in the mathematical derivations, we divide the thesis into nine different chapters. Chapter 3 gives an overview of the construction of the basis functions and the charge density in APW based methods for describing the valence electrons. Chapter 4 contains the derivation of the total energy on the basis of the Kohn-Sham density functional theory, which will later serve as the starting point for the calculation of the stress tensor. Chapter 5 contains the detailed derivation of the strain variation of the total energy, which was derived in Chapter 4. In Chapter 6 we use all the derivations obtained so far to formulate the stress tensor formalism. In this chapter we also discuss in detail the similarities and differences of our formalism with previously published results. Chapter 7 contains the discussion of pressure as a special case of the stress tensor. In this chapter we also discuss the core leakage problem and the techniques we adopt to mitigate it. In Chapter 8, we present the results of the implementation in the WIEN2k code. Chapter 9 provides a detailed discussion. In the main chapters we provide relevant mathematical steps and we provide detailed derivations in the Appendix. All necessary mathematical concepts that are often used in the main chapters are also discussed in the Appendix.

# Chapter 2

## Strain and Stress Tensor

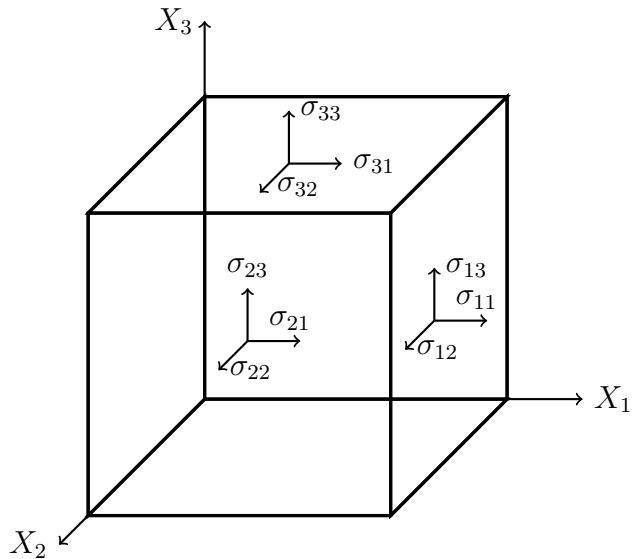


Figure 2.1: A homogeneously stressed body.  $X_1$ ,  $X_2$ , and  $X_3$  correspond to the familiar x, y and z axes. Based on its normal (perpendicular to the surface) or tangential (parallel to the surface) components, the stress tensor is decomposed in each face.

In the previous chapter we have discussed why the calculation of the stress tensor is important and what attempts have been made so far. In this chapter we discuss the strain and stress tensors and their relationship with the elastic constants. Generally speaking, strain represents the deformation of a material from given reference state to its current state. In our calculations strain is applied by reducing or expanding the volume because it is easy to control. The strain is represented by the dimensionless  $3 \times 3$  tensor  $\epsilon_{\alpha\beta}$ , and can be measured by measuring the change in volume compared to the reference volume. We begin our derivation by assuming a system in some initial state with the total energy  $E_0$ . We further assume that the system is strained by an infinitesimal amount of  $\underline{\epsilon}$  and is no longer in its initial state that corresponds to the total energy  $E_0$ . The total energy of the strained system is  $E[\underline{\epsilon}]$  and  $E[\underline{\epsilon}]$  can be expanded around the initial state  $E_0$  using the Taylor series expansion.

$$E[\underline{\epsilon}] = E_0 + \Omega_0 \sum_{\alpha,\beta=1}^3 \sigma_{\alpha\beta} \epsilon_{\alpha\beta} + \mathcal{O}(\epsilon^2), \quad (2.1)$$

where  $\Omega_0$  is the volume of the system correspond to the energy  $E_0$  and  $\mathcal{O}(\epsilon^2)$  implies expansion terms higher order in  $\epsilon$ . The expression of the stress tensor from equation (2.1) after neglecting the higher order terms becomes:

$$\sigma_{\alpha\beta} = \frac{1}{\Omega_0} \left. \frac{dE[\underline{\epsilon}]}{d\underline{\epsilon}_{\alpha\beta}} \right|_{\underline{\epsilon}=0}, \quad (2.2)$$

where  $\alpha$  or  $\beta = 1, 2$ , or  $3$  correspond to the x, y, and z axes of the coordinate system. Expression  $|_{\underline{\epsilon}=0}$  signifies that  $\underline{\epsilon} = 0$  is substituted after performing the derivative so that only the first order variation in the total energy with respect to  $\underline{\epsilon}$  is significant and higher order variations can be neglected. Since strain is unitless, the unit of stress is  $\frac{\text{energy}}{\text{volume}}$ , with the energy and volume being measured in Rydberg (Ry) and Bohr<sup>3</sup>, respectively. Equation (2.2) shows that the stress is the first order variation of the total energy with respect to the applied deformation i.e strain. To specify the stress tensor completely at any point in the system requires nine components which can be seen in equation (2.3) and in Figure 2.1. Equation (2.2) provides the basis for our stress tensor formulation and is used in chapter 6.

$$\sigma_{\alpha\beta} = \begin{pmatrix} \sigma_{11} & \sigma_{12} & \sigma_{13} \\ \sigma_{21} & \sigma_{22} & \sigma_{23} \\ \sigma_{31} & \sigma_{32} & \sigma_{33} \end{pmatrix} \equiv \begin{pmatrix} \sigma_{xx} & \sigma_{xy} & \sigma_{xz} \\ \sigma_{yx} & \sigma_{yy} & \sigma_{yz} \\ \sigma_{zx} & \sigma_{zy} & \sigma_{zz} \end{pmatrix} \quad (2.3)$$

Since the strain tensor is a second rank symmetrical tensor ( $\epsilon_{\alpha\beta} = \epsilon_{\beta\alpha}$ ) the stress tensor is also a second rank symmetrical tensor ( $\sigma_{\alpha\beta} = \sigma_{\beta\alpha}$ ). Because of the symmetrical nature, six independent components are enough to describe the full stress tensor.

Under hydrostatic conditions, the trace of the stress tensor gives the pressure.

$$P = -\frac{1}{3} \sum_{\alpha} \sigma_{\alpha\alpha} \quad (2.4)$$

Equation (2.4) provides the basis for our pressure calculation and is used in Chapter 7 to evaluate the pressure from the total stress tensor. In our manuscript, this is sometimes referred to as ‘simple pressure’.

## 2.1 Elastic Constants

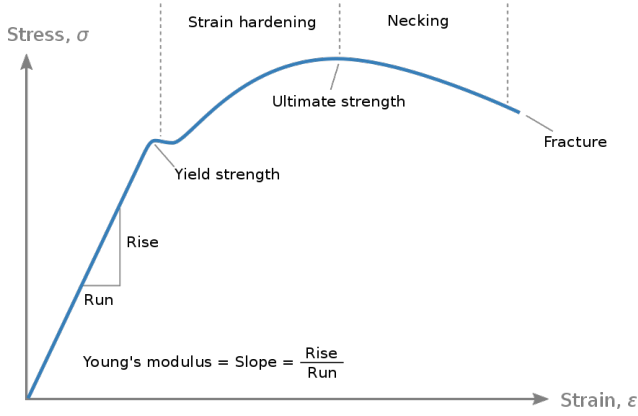


Figure 2.2: The relationship between strain and stress for a material[21].

Elastic constants are the parameters that connect stress to strain within the elastic regime. The elastic regime is defined as the region in which deformation do not exceed a certain limit and the material should return to prior deformation stage after releasing the deformation forces, which is shown by the linear region up to **yield strength** in Fig.2.2. In the figure the area beyond **yield strength** represents the permanent deformation of a material and the material does not regain its original state even after the deformation force is removed. Within the elastic limit, stress is directly proportional to strain according to Hooke's law and the proportionality constants represent the elastic constants. In tensor form, this relationship is defined as

$$\sigma_{\alpha\beta} = \sum_{\gamma\delta} C_{\alpha\beta\gamma\delta} \epsilon_{\gamma\delta}, \quad (2.5)$$

Furthermore,

$$C_{\alpha\beta\gamma\delta} = \left. \frac{d\sigma_{\alpha\beta}}{d\epsilon_{\gamma\delta}} \right|_{\underline{\epsilon}=0} \quad (2.6)$$

$$\stackrel{(2.2)}{=} \frac{1}{\Omega_0} \left. \frac{\partial^2 E[\underline{\epsilon}]}{\partial \epsilon_{\alpha\beta} \partial \epsilon_{\gamma\delta}} \right|_{\underline{\epsilon}=0}, \quad (2.7)$$

where all indices- $\alpha$ ,  $\beta$ ,  $\gamma$ , and  $\delta$ -run from 1 to 3. Equation (2.6) provides a relationship between the stress tensor and the elastic constants. Similar to equation (2.1), elastic constants can be calculated using the Taylor series expansion of the total energy of the system around the equilibrium volume  $\Omega_0$  as a function of strain.

$$E[\underline{\epsilon}] = E(0) + \Omega_0 \sum_{\alpha,\beta=1}^3 \sigma_{\alpha\beta} \epsilon_{\alpha\beta} + \frac{\Omega_0}{2} \sum_{\alpha,\beta,\gamma,\delta=1}^3 C_{\alpha\beta\gamma\delta} \epsilon_{\alpha\beta} \epsilon_{\gamma\delta} + \mathcal{O}(\epsilon^3), \quad (2.8)$$

where  $\sigma_{\alpha\beta}$  and  $\epsilon_{\alpha\beta}$  are the second rank tensors, and the elastic constants  $C_{\alpha\beta\gamma\delta}$  are fourth rank tensors.  $\mathcal{O}(\epsilon^3)$  represent all higher order terms in  $\epsilon$ . By applying the

second order strain variation in equation (2.8) we get equation (2.7). Unlike the stress tensor, elastic constants need 81 elements to completely specify all elastic constants of the crystal. However, due to the symmetry of the crystal, not all elements are independent. Therefore, the number of independent elements is much less than 81. For example, the cubic structure with 48 symmetry operations has only three independent elastic constant, while the hexagonal structure with 24 symmetry operations has five independent elastic constants.

# Chapter 3

## The APW based methods

### 3.1 Basis Function

Introduction of a set of basis functions is necessary to numerically solve Kohn-Sham single-particle equations in density functional theory (DFT) [22, 23] and to define the electron density of a system. In our calculations, we will be using augmented plane wave (APW) methods and their linearized version—LAPW and APW+lo—as basis functions. In the APW based methods, the basis functions are defined according to the behavior of the potential and its effect on wave functions. Near the nuclei, the potential is very strong but still approximately spherical, and the wave functions are similar to those in a free atom, and thus may contain several nodes and a cusp at the nucleus. In the region far away from the nucleus, the potential is weaker, and the wavefunctions are much smoother. Based on these observations, a unit cell is divided into non-overlapping atom-centered spheres and an interstitial region as shown in Figure 3.1. Inside an atom-centered sphere, also known as a muffin-tin region (MT-region), numerical solutions of the Schrödinger equation are used to define the basis functions, whereas in the interstitial plane waves are used. Various flavors of APW-based methods have slightly different basis functions within the spheres. A detailed discussion of the construction of the basis functions is provided in the sections below.

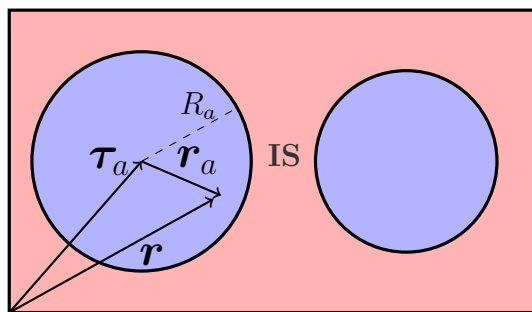


Figure 3.1: The division of a unit cell into non-overlapping atom centered spheres with radius  $R_a$  located at  $\tau_a$  and the interstitial region (IS)—space between the atoms.

#### 3.1.1 APW

APW stands for the augmented plane wave method, first suggested by Slater in Ref. [24, 9], and is defined as:

$$\phi_{\mathbf{kK}}(\mathbf{r}) = \begin{cases} \frac{1}{\sqrt{\Omega}} e^{i(\mathbf{k}+\mathbf{K}) \cdot \mathbf{r}} & \mathbf{r} \in IS \\ \sum_{lm} a_{lm}^{a\mathbf{k}\mathbf{K}} u_l(r_a, E) Y_{lm}(\hat{\mathbf{r}}_a) & \mathbf{r} \in R_a \end{cases} \quad (3.1)$$

Here  $u_l(r_a, E)$  is the solution of the radial Schrödinger equation (equation (3.2)) with a spherically symmetric potential ( $V_{00}$ ) within the non-overlapping atom-centered spheres,  $E$  is the eigenenergy or band energy,  $\Omega$  is the unit cell volume, and  $r_a$  and  $\hat{\mathbf{r}}_a$  are the length and angular part of the local position vector  $\mathbf{r}_a$ . The local position vector,  $\mathbf{r}_a$ , is defined with respect to the atomic center ( $\tau_a$ ) of an atom  $a$  such that  $\mathbf{r}_a = \mathbf{r} - \tau_a$ , see Fig. 3.1. In addition,  $Y_{lm}$  represents a spherical harmonic for a pair of angular momentum quantum numbers  $l$  and  $m$ . The wave vector in the first Brillouin zone is denoted by  $\mathbf{k}$ , and  $\mathbf{K}$  denotes a reciprocal lattice vector. Equation (3.1) shows that each plane wave is augmented within the region of the atomic spheres by a linear combination of radial functions times the spherical harmonics, and the unknown coefficient  $a_{lm}^{a\mathbf{k}\mathbf{K}}$  ensures the continuity of basis functions at the sphere boundary. The point to remember is that when defining the basis function within an atomic domain, only the spherical part of the potential is used in equation (3.2)) and the non-spherical part only enters when solving the total Hamiltonian of the system:

$$\left\{ -\frac{d^2}{dr_a^2} + \frac{l(l+1)}{r_a^2} + V_{00}^a(r_a) - E \right\} r_a u_l(r_a, E) = 0 \quad (3.2)$$

The APW method demands that the basis functions are continuous and this is achieved by matching the functions from inside ( $\mathbf{r} \in R_a$ ) and outside ( $\mathbf{r} \in IS$ ) at the sphere boundary ( $|\mathbf{r}_a| = R_a$ )

$$\sum_{lm} a_{lm}^{a\mathbf{k}\mathbf{K}} u_l(r_a, E) Y_{lm}(\hat{\mathbf{r}}_a) \Big|_{r_a=R_a} = \frac{1}{\sqrt{\Omega}} e^{i(\mathbf{k}+\mathbf{K}) \cdot \mathbf{r}} \Big|_{r_a=R_a} \quad (3.3)$$

At first, using Rayleigh's expansion, the exponential function is expanded into spherical harmonics and spherical Bessel functions ( $j_l$ ).

$$e^{i(\mathbf{k}+\mathbf{K}) \cdot \mathbf{r}} = e^{i(\mathbf{k}+\mathbf{K}) \cdot \tau_a} \sum_{lm} 4\pi i^l Y_{lm}^*((\widehat{\mathbf{k}+\mathbf{K}})) Y_{lm}(\hat{\mathbf{r}}_a) j_l(|\mathbf{k}+\mathbf{K}|r_a) \quad (3.4)$$

Substitution of equation (3.4) in (3.3) and comparing each  $lm$  yields:

$$a_{lm}^{a\mathbf{k}\mathbf{K}} = \frac{4\pi i^l}{\sqrt{\Omega}} e^{i(\mathbf{k}+\mathbf{K}) \cdot \tau_a} Y_{lm}^*((\widehat{\mathbf{k}+\mathbf{K}})) \frac{j_l(|\mathbf{k}+\mathbf{K}|R_a)}{u_l(R_a, E)} \quad (3.5)$$

Equations (3.5) and (3.1) show that the basis functions in the region of the atomic spheres are connected to a particular  $\mathbf{k}$ -point and a reciprocal lattice vector  $\mathbf{K}$  via  $a_{lm}^{a\mathbf{k}\mathbf{K}}$ . In APW, the basis functions within the spheres depend on the exact eigenenergy ( $E$ ), which is unknown prior to the calculations. This leads to the problem that the basis functions need to be re-evaluated for a large number of energies, which can lead to an energy that makes  $u_l(R_a, E)$  very small or even zero at the sphere boundary. In this situation,  $a_{lm}^{a\mathbf{k}\mathbf{K}}$  will blow up due to the presence of  $u_l(R_a, E)$  in the denominator of

equation (3.5). This is known as the **asymptotic problem**; as a result, basis-functions decouple at the boundary. In addition, the basis functions lack the variational freedom in the sense that  $E$  is not permissible to be other than the band energy. As a result, the eigenvalue problem becomes non-linear in energy and has to be solved iteratively for many different energies. This is, however, a computationally expensive process and even more expensive as the number of  $k$ -points increases, the symmetry of the system decreases, the number of atoms increases, and so on. Therefore, to mitigate the previously mentioned problems, we work with subsequent versions: the linearized augmented plane wave (LAPW) and the APW plus local orbital (APW+lo) method.

### 3.1.2 LAPW

In the linearized augmented plane wave method (LAPW), basis functions are defined similarly as in APW but with a different augmentation inside an atomic sphere. As can be seen in equation (3.6), we use a linear combination of the radial functions  $u_l(r_a, E_l^a)$  and their energy derivatives  $\dot{u}_l(r_a, E_l^a)$  in the region of the atomic spheres at a certain energy  $E_l^a$  instead of the radial functions  $u_l(r_a, E)$ , which, in the case of APW are evaluated with the exact eigenenergy. The inclusion of the energy derivative,  $\dot{u}_l(r_a, E_l^a)$ , linearizes the energy dependency of  $u_l$  and makes the basis functions somehow independent of the choice of the energy parameter ( $E_l^a$ ). This ultimately resolves the energy dependency problem associated with APW. This technique was first suggested in Ref. [25, 26].

$$\phi_{k\mathbf{K}}(\mathbf{r}) = \begin{cases} \frac{1}{\sqrt{\Omega}} e^{i(\mathbf{k}+\mathbf{K}) \cdot \mathbf{r}} & \mathbf{r} \in IS \\ \sum_{lm} \left[ a_{lm}^{a\mathbf{k}\mathbf{K}} u_l(r_a, E_l^a) + b_{lm}^{a\mathbf{k}\mathbf{K}} \dot{u}_l(r_a, E_l^a) \right] Y_{lm}(\hat{\mathbf{r}}_a) & \mathbf{r} \in R_a \end{cases} \quad (3.6)$$

Here  $u_l(r_a, E_l^a)$  and  $\dot{u}_l(r_a, E_l^a)$  are the solution of equations (3.2) and (3.7), respectively.

$$\left\{ -\frac{d^2}{dr_a^2} + \frac{l(l+1)}{r_a^2} + V_{00}^a - E_l^a \right\} r_a \dot{u}_l(r_a, E_l^a) = r_a u_l(r_a, E_l^a) \quad (3.7)$$

In the LAPW method, the two constants  $a_{lm}^{a\mathbf{k}\mathbf{K}}$  and  $b_{lm}^{a\mathbf{k}\mathbf{K}}$  are determined by forcing the value and slope of the functions given in equation (3.6) to be continuous across the sphere boundary ( $|\mathbf{r}_a| = R_a$ ) for each  $lm$ .

$$\begin{pmatrix} a_{lm}^{a\mathbf{k}\mathbf{K}} \\ b_{lm}^{a\mathbf{k}\mathbf{K}} \end{pmatrix} = \frac{4\pi i^l}{\sqrt{\Omega}} e^{i(\mathbf{k}+\mathbf{K}) \cdot \mathbf{r}_a} Y_{lm}^*((\widehat{\mathbf{k}+\mathbf{K}})) \underline{\underline{U}}^{-1} \begin{pmatrix} j_l(|\mathbf{k}+\mathbf{K}|R_a) \\ |\mathbf{k}+\mathbf{K}|j'_l(|\mathbf{k}+\mathbf{K}|R_a) \end{pmatrix}, \quad (3.8)$$

where the matrix  $\underline{\underline{U}}^{-1}$  is

$$\underline{\underline{U}}^{-1} = \frac{1}{W_l^a(R_a, E_l^a)} \begin{pmatrix} \dot{u}'_l(R_a, E_l^a) & -\dot{u}_l(R_a, E_l^a) \\ -u'_l(R_a, E_l^a) & u_l(R_a, E_l^a) \end{pmatrix}, \quad (3.9)$$

$u'_l$  represents the first order radial derivative of  $u_l$  and  $W_l^a(R_a, E_l^a)$  is the Wronskian determinant.

$$W_l^a(R_a, E_l^a) = u_l(R_a, E_l^a) \dot{u}_l(R_a, E_l^a) - \dot{u}_l(R_a, E_l^a) u'_l(R_a, E_l^a) \quad (3.10)$$

In principle, the basis function should include all possible  $lm$  inside a sphere but from practical point of view, inclusion of all  $l$  is not possible. Therefore, a truncation after some acceptable value is inevitable, and the truncation value of  $l$  (i.e  $l_{max}$ ) is set up after weighing the accuracy versus efficiency. Accordingly, the LAPW basis functions are continuous in value and slope up to  $l = l_{max}$  with typically  $l_{max} = 8$  to 10 depending on the desired numerical precision.

The solutions of the Schrödinger's equation, eq. (3.2), are normalized

$$\int_0^{R_a} dr_a r_a u_l(r_a, E_l^a) r_a u_l(r_a, E_l^a) = 1 \quad (3.11)$$

The following lines are obtained by multiplying equations (3.7) and (3.2) and subtracting them from each other.

$$\begin{aligned} 1 &= \int_0^{R_a} dr_a \left[ r_a \dot{u}_l(r_a, E_l^a) \frac{d^2 r_a u_l(r_a, E_l^a)}{dr_a^2} - r_a u_l(r_a, E_l^a) \frac{d^2 r_a \dot{u}_l(r_a, E_l^a)}{dr_a^2} \right] \\ &= \int_0^{R_a} dr_a \frac{d}{dr_a} \left[ r_a \dot{u}_l(r_a, E_l^a) (r_a u_l(r_a, E_l^a))' - (r_a \dot{u}_l(r_a, E_l^a))' r_a u_l(r_a, E_l^a) \right] \\ &= -R_a^2 \left( u'_l(R_a, E_l^a) \dot{u}'_l(R_a, E_l^a) - \dot{u}'_l(R_a, E_l^a) u'_l(R_a, E_l^a) \right) \end{aligned} \quad (3.12)$$

From equations (3.10) and 3.12) we get the Wronskian as follows.

$$W_l^a(R_a, E_l^a) = -\frac{1}{R_a^2}$$

The different augmentation of the LAPW method inside the spherical region makes the basis functions energy independent. Unlike in APW, in the LAPW method there is no  $u_l$  in the denominator of the matching coefficients. As a result, there is no asymptotic problem. The basis functions in LAPW describe the energy dependency by a linearized Taylor series and are less accurate compared to APW. In addition, the matching of the slope of the solutions limits the flexibility of the LAPW basis and the number of basis functions needs to be increased to achieve the same accuracy as in APW. Consequently, the secular matrix becomes larger, and convergence in the LAPW becomes slower with respect to the number of basis functions. Despite all this, in LAPW the secular matrix is energy-independent which is a huge advantage compared to the energy-dependent secular matrix in the APW method.

### 3.1.3 APW+lo

A different linearization of the energy dependency was suggested by Sjöstedt *et al.* in Ref. [27]. They used an APW basis, but expanded  $u_l$  at a fixed energy  $E_l^a$ . In order to gain the necessary flexibility, they added a set of local orbitals. These additional functions are local in the sense that they are confined to the region of the atomic spheres.

The local orbitals are defined as linear combination of  $u_{l,lo}(r_a, E_l^a)$  and  $\dot{u}_{l,lo}(r_a, E_l^a)$  to mimic the traditional LAPW basis function. The linear combination is, however, introduced only for physically important angular momenta  $l$ , i.e  $l = 0, 1, 2$  or  $3$  depending on the atom. Consequently, for a given  $l$ , only  $(2l + 1)$  extra basis functions per atom are added. Therefore, the APW+lo basis set consists of APW basis functions from equation (3.1) and the local orbitals (lo) from equation (3.13):

$$\phi_{lo}^a(\mathbf{r}) = \begin{cases} 0 & \mathbf{r} \in IS \\ \left[ a_{l,lo}^a u_{l,lo}(r_a, E_l^a) + b_{l,lo}^a \dot{u}_{l,lo}(r_a, E_l^a) \right] Y_{lm}(\hat{r}_a) & \mathbf{r} \in R_a \end{cases} \quad (3.13)$$

$u_l(r_a, E_l^a)$  and  $\dot{u}_{l,lo}(r_a, E_l^a)$  are, respectively, the solution of equations (3.2) and (3.7), with the same linearization energy ( $E_l^a$ ) used in the original LAPW method. The  $a_{l,lo}^a$  and  $b_{l,lo}^a$  are evaluated by setting the value of the local orbital to zero at the sphere boundary.

$$\frac{a_{l,lo}^a}{b_{l,lo}^a} = -\frac{\dot{u}_{l,lo}(r_a, E_l^a)}{u_{l,lo}(r_a, E_l^a)} \quad (3.14)$$

The local orbitals are normalized inside the sphere.

$$a_{l,lo}^{a2} + b_{l,lo}^{a2} \int_0^{R_a} dr_a r_a^2 \dot{u}_{l,lo}^2(r_a, E_l^a) = 1 \quad (3.15)$$

$$b_{l,lo}^a = \frac{1}{\sqrt{\left(\frac{a_{l,lo}^a}{b_{l,lo}^a}\right)^2 + PE(l)}} \quad (3.16)$$

Here  $PE(l) = \int_0^{R_a} dr_a r_a^2 \dot{u}_{l,lo}^2(R_a, E_l^a)$ . A fictitious plane wave is attached to each  $lo$  to make the local orbitals behave exactly like the original APW under the symmetry operations of the system. Also, in APW+lo, only the value of the basis functions is restricted to match to a plane wave at the boundary of the sphere. As a result, the APW+lo basis is less restricted compared to LAPW and expected to have faster convergence in terms of the number of basis functions[28].

### 3.1.4 LO Orbitals

Local Orbitals (LO) were first introduced by Singh [29, 30] in the LAPW method to describe semi-core states, which are higher (lower) in energy compared to core states (valence states) see figure 3.1, and the linearization energy ( $E_l^a$ ) used in the original LAPW or APW+lo methods to describe the valence states does not lead to a basis which can describe semi-core states. As a result, the LO needs to be defined with a different linearization energy ( $E_{l,LO}^a$ ).

$$\phi_{LO}^a(\mathbf{r}) = \begin{cases} 0 & \mathbf{r} \in IS \\ \left[ a_{l,LO}^a u_l(r_a, E_l^a) + b_{l,LO}^a \dot{u}_l(r_a, E_l^a) + c_{l,LO}^a u_{l,LO}(r_a, E_{l,LO}^a) \right] Y_{lm}(\hat{r}_a) & \mathbf{r} \in R_a \end{cases} \quad (3.17)$$

$u_l(r_a, E_l^a)$  and  $u_{l,LO}(r_a, E_{l,LO}^a)$  are the solutions of equation (3.2) with different energies  $E_l^a$  and  $E_{l,LO}^a$ . The index  $l$  only includes the chemically important  $l$  such that  $l \leq 3$ , and therefore for any  $l$  only  $2l+1$  LOs per atom are added. Also, the unknown coefficients  $a_{l,LO}^a$ ,  $b_{l,LO}^a$ , and  $c_{l,LO}^a$  are determined using the conditions that the value and radial derivative of the LO functions vanish at the sphere boundary and the LO functions are normalized inside the sphere. As the name suggests, the LOs are confined to the region of the atomic spheres but, to preserve the same symmetry property as of the original APW+lo and LAPW, the LOs are connected to a fictitious plane wave at the sphere boundary.

Equations (3.5) and (3.8) show that the matching coefficients contain the phase factor  $e^{i(\mathbf{k}+\mathbf{K}) \cdot \boldsymbol{\tau}_a}$ , which depends on the atomic position  $\boldsymbol{\tau}_a$ . As a result, the basis set of the APW based method changes with a change of an atomic position. This dependency leads to a correction term in the force calculation, which is often referred to as a Pulay correction[32]. We also expect a similar correction for the stress calculation.

## 3.2 Wave Function

The total wave function  $\psi_{v\mathbf{k}}(\mathbf{r})$  for the band  $v$  and given  $\mathbf{k}$  vector is expanded as linear combination of the basis functions as given below.

$$\psi_{v\mathbf{k}}(\mathbf{r}) = \sum_{\mathbf{K}} c_{v\mathbf{k}\mathbf{K}} \phi_{\mathbf{k}\mathbf{K}}(\mathbf{r}), \quad (3.18)$$

where  $c_{v\mathbf{k}\mathbf{K}}$  are expansion coefficients and the summation runs over all reciprocal lattice vectors  $\mathbf{K}$  such that  $|\mathbf{K}| \leq K_{max}$ .  $\phi_{\mathbf{k}\mathbf{K}}(\mathbf{r})$  are the basis functions and their definition was provided in previous sections. Let us recall it once again:

$$\phi_{\mathbf{k}\mathbf{K}}(\mathbf{r}) = \begin{cases} \frac{1}{\sqrt{\Omega}} e^{i(\mathbf{k}+\mathbf{K}) \cdot \mathbf{r}} & \mathbf{r} \in IS \\ \sum_{lm} \sum_{\lambda} a_{lm\lambda}^{a\mathbf{k}\mathbf{K}} u_{l\lambda}(r_a, E_{l\lambda}^a) Y_{lm}(\hat{\mathbf{r}}_a) & \mathbf{r} \in R_a \end{cases} \quad (3.19)$$

Here, the label  $\lambda$  is introduced to distinguish the radial function ( $\lambda=0$ ) and its energy derivative ( $\lambda=1$ ). Equation (3.19) is valid for both APW+lo and LAPW methods, and it shows that the  $\mathbf{K}$  dependency of the basis set in the region of the atomic spheres appears via the matching coefficients. As a result, the total wave functions inside the spheres can be written in the fashion given below.

$$\psi_{v\mathbf{k}}^a(\mathbf{r}) = \sum_{\mathbf{K}} c_{v\mathbf{k}\mathbf{K}} \sum_{lm} a_{lm\lambda}^{a\mathbf{k}\mathbf{K}} u_{l\lambda}(r_a, E_{l\lambda}^a) Y_{lm}(\hat{\mathbf{r}}_a) \quad (3.20)$$

$$= \sum_{lm} \mathbf{A}_{lm\lambda}^{av\mathbf{k}} u_{l\lambda}(r_a, E_{l\lambda}^a) Y_{lm}(\hat{\mathbf{r}}_a), \quad (3.21)$$

where the coefficients

$$\mathbf{A}_{lm\lambda}^{av\mathbf{k}} = \sum_{\mathbf{K}} c_{v\mathbf{k}\mathbf{K}} a_{lm\lambda}^{a\mathbf{k}\mathbf{K}} \quad (3.22)$$

are written as

$$\mathbf{A}_{lm\lambda}^{av\mathbf{k}} = \begin{cases} A_{lm}^{av\mathbf{k}} & \lambda = 0 \\ B_{lm}^{av\mathbf{k}} & \lambda = 1 \end{cases} \quad (3.23)$$

In the presence of a semi core local orbital (LO), we introduce the index  $\lambda = 2$  and the coefficient  $\mathbf{A}_{lm2}^{av\mathbf{k}} = C_{lm,LO}^{av\mathbf{k}}$ . Then,  $E_{l\lambda}^a$  in  $u_{l\lambda}(r_a, E_{l\lambda}^a)$  agrees with the semi core energy  $E_{l,LO}^a$ . In the case of APW+lo,  $B_{lm}^{av\mathbf{k}}$ , which is only present due to the local orbital (lo) and  $A_{lm}^{av\mathbf{k}}$ , contains the contribution of APW and lo, see section 3.1.3.

After collecting all the intermediate steps, the final expression of equation (3.18) is:

$$\psi_{v\mathbf{k}}(\mathbf{r}) = \begin{cases} \frac{1}{\sqrt{\Omega}} \sum_{\mathbf{K}} c_{v\mathbf{k}\mathbf{K}} e^{i(\mathbf{k}+\mathbf{K}).\mathbf{r}} & \mathbf{r} \in IS \\ \sum_{lm} \left( A_{lm}^{av\mathbf{k}} u_l(r_a, E_l^a) + B_{lm}^{av\mathbf{k}} \dot{u}_l(r_a, E_l^a) + C_{lm,LO}^{av\mathbf{k}} u_l(r_a, E_{l,LO}^a) \right) Y_{lm}(\hat{r}_a) & \mathbf{r} \in R_a \end{cases} \quad (3.24)$$

This expression is used explicitly for the construction of the valence charge density in section 3.3 and for the calculation of the valence kinetic stress tensor in section 6.3 and the valence correction stress tensor in section 6.4.

### 3.3 Charge density

In the previous sections, we have defined the basis functions and wave functions to describe the valence electrons. Now, we are going to use them to construct the valence charge density. The valence charge density is defined as:

$$\rho(\mathbf{r}) = \sum_{v\mathbf{k}} n_{v\mathbf{k}} \psi_{v\mathbf{k}}^*(\mathbf{r}) \psi_{v\mathbf{k}}(\mathbf{r}), \quad (3.25)$$

where  $n_{v\mathbf{k}}$  is the occupation number of band  $v$  for a given k-vector  $\mathbf{k}$ . The index  $v$  runs over all occupied valence states and  $\mathbf{k}$  over all k-points of the Brillouin zone. In the APW based methods, because of the dual representation of the wave-functions (equation (3.24)), the charge density is also differently defined in the interstitial region and in the atomic spheres. In the interstitial region it is represented as follows.

$$\begin{aligned} \rho_I(\mathbf{r}) &= \sum_{v\mathbf{k}} n_{v\mathbf{k}} \sum_{\mathbf{KK}'} \frac{c_{v\mathbf{k}\mathbf{K}'}^* c_{v\mathbf{k}\mathbf{K}}}{\Omega} e^{-i(\mathbf{k}+\mathbf{K}')\cdot\mathbf{r}} e^{i(\mathbf{k}+\mathbf{K})\cdot\mathbf{r}} \\ &= \sum_{\mathbf{G}} \rho(\mathbf{G}) e^{i\mathbf{G}\cdot\mathbf{r}} \end{aligned}$$

with

$$\rho(\mathbf{G}) = \sum_{\mathbf{K}} \sum_{\mathbf{K}'} \sum_{v\mathbf{k}} n_{v\mathbf{k}} \frac{c_{v\mathbf{k}\mathbf{K}'}^* c_{v\mathbf{k}\mathbf{K}}}{\Omega} \delta_{\mathbf{G}, \mathbf{K}-\mathbf{K}'} \quad (3.26)$$

where  $\rho(\mathbf{G})$  is the Fourier component of  $\rho_I(\mathbf{r})$  and the index I in  $\rho_I(\mathbf{r})$  indicates the interstitial region. Similarly, the charge density in the atomic spheres is:

$$\begin{aligned}
\rho_a(\mathbf{r}) &= \sum_{v\mathbf{k}} n_{v\mathbf{k}} \sum_{lm} \sum_{l'm'} \left[ A_{lm}^{av\mathbf{k}} u_l(r_a) + B_{lm}^{av\mathbf{k}} \dot{u}_l(r_a) + C_{lm,LO}^{av\mathbf{k}} u_{l,LO}(r_a) \right]^* \\
&\quad \left[ A_{l'm'}^{av\mathbf{k}} u_{l'}(r_a) + B_{l'm'}^{av\mathbf{k}} \dot{u}_{l'}(r_a) + C_{l'm',LO}^{av\mathbf{k}} u_{l,LO}(r_a) \right] Y_{lm}^*(\hat{r}_a) Y_{l'm'}(\hat{r}_a) \\
&= \sum_{LM} \left[ \sum_{v\mathbf{k}} n_{v\mathbf{k}} \sum_{lm} \sum_{l'm'} \left\{ A_{lm}^{av\mathbf{k}*} A_{l'm'}^{av\mathbf{k}} u_l(r_a) u_{l'}(r_a) + A_{lm}^{av\mathbf{k}*} B_{l'm'}^{av\mathbf{k}} u_l(r_a) \dot{u}_{l'}(r_a) \right. \right. \\
&\quad + A_{lm}^{av\mathbf{k}*} C_{l'm',LO}^{av\mathbf{k}} u_l(r_a) u_{l',LO}^a(r_a) + B_{lm}^{av\mathbf{k}*} A_{l'm'}^{av\mathbf{k}} \dot{u}_l(r_a) u_{l'}(r_a) \\
&\quad + B_{lm}^{av\mathbf{k}*} B_{l'm'}^{av\mathbf{k}} \dot{u}_l(r_a) \dot{u}_{l'}(r_a) + B_{lm}^{av\mathbf{k}*} C_{l'm',LO}^{av\mathbf{k}} \dot{u}_l(r_a) u_{l',LO}^a(r_a) + C_{lm,LO}^{av\mathbf{k}*} A_{l'm'}^{av\mathbf{k}} u_{l,LO}(r_a) u_{l'}(r_a) \\
&\quad \left. \left. + C_{lm,LO}^{av\mathbf{k}*} B_{l'm'}^{av\mathbf{k}} u_{l,LO}(r_a) \dot{u}_{l'}(r_a) + C_{lm,LO}^{av\mathbf{k}*} C_{l'm',LO}^{av\mathbf{k}} u_{l,LO}(r_a) u_{l',LO}^a(r_a) \right\} G_{l,l',L}^{m,m',M} \right] Y_{LM}(\hat{r}_a) \\
&= \sum_{LM} \rho_{LM}(r) Y_{LM}(\hat{r}_a)
\end{aligned} \tag{3.27}$$

In the above equations  $u_l(r_a, E_l^a)$  is replaced by  $u_l(r_a)$  and  $u_l^a(r_a, E_{l,LO}^a)$  is replaced by  $u_{l,LO}(r_a)$  for the sake of brevity.  $G_{l,l',L}^{m,m',M}$  denotes a Gaunt number— an integral of three spherical harmonics as given in equation (A.5). Now the total valence density  $\rho(\mathbf{r})$  is written by combining equations (3.26) and (3.27).

$$\rho(\mathbf{r}) = \begin{cases} \sum_{\mathbf{G}}^{G_{max}} \rho(\mathbf{G}) e^{i\mathbf{G}\cdot\mathbf{r}} & \mathbf{r} \in IS \\ \sum_{LM} \rho_{LM}(r) Y_{LM}(\hat{r}_a) & \mathbf{r} \in R_a, \end{cases} \tag{3.28}$$

where  $G_{max}$  is the cutoff value in the expansion of the charge density and it should be at least  $2K_{max}$ . In practice, in order to save computational time, all symmetry operations are used during the construction of the charge density, such as the site symmetry within a sphere and the space group symmetry in the interstitial. Also, the density is a real quantity and is identical among equivalent atoms. The densities among equivalent atoms can be obtained from the representative atom by applying a space group operation. Accordingly, *stars* of  $\mathbf{G}$  are introduced in the interstitial region and the lattice harmonics in the atomic spheres. The *star* are the symmetrized plane waves, and the lattice harmonics are the symmetrized spherical harmonics[33], see Ref. [30] for a detailed explanation. As a result, only a few independent  $\rho(\mathbf{G})$  for the *stars* functions and a few  $LM$  combinations of the lattice harmonics contribute to equation (3.28).

# Chapter 4

## Total Energy and Potentials

According to Refs. [22, 23], the total energy of a system in Kohn-Sham (KS) density functional theory as a function of  $\rho$  is given as:

$$E_{tot}[\rho] = E_{kin}[\rho] + E_{es}[\rho] + E_{xc}[\rho], \quad (4.1)$$

where  $E_{kin}[\rho]$ ,  $E_{es}[\rho]$ , and  $E_{xc}[\rho]$  are the non-interacting kinetic energy, classical Coulomb interaction energy, and exchange-correlation energy, respectively. The non-interacting kinetic energy of the system is given below,

$$E_{kin}[\rho] = \sum_{v\mathbf{k}} n_{v\mathbf{k}} \int_{\Omega} d^3\mathbf{r} \psi_{v\mathbf{k}}^*(\mathbf{r}) \left( -\frac{1}{2} \nabla^2 \right) \psi_{v\mathbf{k}}(\mathbf{r}), \quad (4.2)$$

where  $v$ ,  $\mathbf{k}$ , and  $n_{v\mathbf{k}}$  are the band index,  $\mathbf{k}$ -vector and occupation numbers. The occupation numbers ( $n_{v\mathbf{k}}$ ) are either one or zero according to the occupied and unoccupied bands of insulator and semiconductor. However, they can have fractional values for metallic systems, especially near the Fermi-level.  $\Omega$  is the volume of the system and commonly known as the unit cell volume. There are two different expressions of the kinetic energy operators in practice that will be discussed at the end of this chapter. The electronic wave functions,  $\psi_{v\mathbf{k}}(\mathbf{r})$  in equation (4.2), are obtained as solution of the one-electron KS equation (4.3).

$$\left[ -\frac{1}{2} \nabla^2 + V_{eff}(\mathbf{r}) \right] \psi_{v\mathbf{k}}(\mathbf{r}) = \epsilon_{v\mathbf{k}} \psi_{v\mathbf{k}}(\mathbf{r}) \quad (4.3)$$

where  $V_{eff}(\mathbf{r})$  is the effective potential and it is defined in equation (4.7). The single-particle wave functions— $\psi_{v\mathbf{k}}(\mathbf{r})$ —do not have a strict physical significance. They are formulated using basis functions and the  $\psi_{v\mathbf{k}}(\mathbf{r})$  are used to define the charge density  $\rho(\mathbf{r})$  of a system as explained in section 3.3.

$$\rho(\mathbf{r}) = \sum_{v\mathbf{k}} n_{v\mathbf{k}} \psi_{v\mathbf{k}}^*(\mathbf{r}) \psi_{v\mathbf{k}}(\mathbf{r}) \quad (4.4)$$

Now, multiply the equation (4.3) by  $\psi_{v\mathbf{k}}^*(\mathbf{r})$  from the right, integrate over the unit cell volume  $\Omega$ , and sum over all the occupied states ( $n_{v\mathbf{k}}$ ) in order to get the following expression.

$$\sum_{v\mathbf{k}} n_{v\mathbf{k}} \int_{\Omega} d^3\mathbf{r} \psi_{v\mathbf{k}}^*(\mathbf{r}) \left[ -\frac{1}{2} \nabla^2 + V_{eff}(\mathbf{r}) \right] \psi_{v\mathbf{k}}(\mathbf{r}) = \sum_{v\mathbf{k}} n_{v\mathbf{k}} \int_{\Omega} d^3\mathbf{r} \epsilon_{v\mathbf{k}} \psi_{v\mathbf{k}}^*(\mathbf{r}) \psi_{v\mathbf{k}}(\mathbf{r}) \quad (4.5)$$

Equation (4.5) is solved by using expression (4.4) and the orthogonality condition. Substituting equation (4.5) in equation (4.2), we get:

$$E_{kin}[\rho] = \sum_{v\mathbf{k}} n_{v\mathbf{k}} \epsilon_{v\mathbf{k}} - \int_{\Omega} d^3\mathbf{r} V_{eff}(\mathbf{r}) \rho(\mathbf{r}) \quad (4.6)$$

The effective potential  $V_{eff}(\mathbf{r})$  is defined as a sum of the Coulomb potential  $V_C(\mathbf{r})$  and the exchange correlation potential  $\mu_{xc}(\mathbf{r})$ :

$$V_{eff}(\mathbf{r}) = V_C(\mathbf{r}) + \mu_{xc}(\mathbf{r}) \quad (4.7)$$

The Coulomb potential  $V_C(\mathbf{r})$  is

$$V_C(\mathbf{r}) = \int d^3\mathbf{r}' \frac{\rho(\mathbf{r}')}{|\mathbf{r} - \mathbf{r}'|} - \sum_a \frac{Z_a}{|\mathbf{r} - \boldsymbol{\tau}_a|} \quad (4.8)$$

$Z_a$  is the nuclear charge of an atom  $a$ , located at  $\boldsymbol{\tau}_a$ . Also, the exchange-correlation potential  $\mu_{xc}(\rho)$  is defined as:

$$\mu_{xc}(\rho) = \frac{\delta E_{xc}[\rho]}{\delta \rho(\mathbf{r})} = \frac{\delta}{\delta \rho(\mathbf{r})} [\rho(\mathbf{r}) \epsilon_{xc}(\rho)] \quad (4.9)$$

$\epsilon_{xc}(\rho) = \epsilon_x(\rho) + \epsilon_c(\rho)$  denotes the exchange-correlation energy per particle and it is the sum of the exchange ( $\epsilon_x(\rho)$ ) and correlation ( $\epsilon_c(\rho)$ ) energy per particle. The total exchange-correlation energy is given as:

$$E_{xc}[\rho] = \int_{\Omega} d^3\mathbf{r} \rho(\mathbf{r}) \epsilon_{xc}(\rho), \quad (4.10)$$

where  $\epsilon_{xc}(\rho)$  corresponds to  $\epsilon_{xc}(\rho(\mathbf{r}))$  for LDA and  $\epsilon_{xc}(\rho(\mathbf{r}), \nabla \rho(\mathbf{r}))$  for GGA. During the following derivations,  $\epsilon_{xc}(\rho)$  is used for brevity, except when the exchange correlation energy is discussed explicitly.

$E_{es}[\rho]$  in equation (4.1) contains all possible interactions among all charges in the system i.e. electron-electron, electron-nuclear, and nuclear-nuclear interactions. The expression of  $E_{es}[\rho]$  is given below.

$$\begin{aligned} E_{es}[\rho] &= \frac{1}{2} \left[ \int_{\Omega} d^3\mathbf{r} \int d^3\mathbf{r}' \frac{\rho(\mathbf{r})\rho(\mathbf{r}')}{|\mathbf{r} - \mathbf{r}'|} - \sum_a 2Z_a \int d^3\mathbf{r} \frac{\rho(\mathbf{r})}{|\mathbf{r} - \boldsymbol{\tau}_a|} + \sum_{a \neq b} \frac{Z_a Z_b}{|\boldsymbol{\tau}_a - \boldsymbol{\tau}_b|} \right] \\ &= \frac{1}{2} \left[ \int_{\Omega} d^3\mathbf{r} \rho(\mathbf{r}) \left( \int d^3\mathbf{r}' \frac{\rho(\mathbf{r}')}{|\mathbf{r} - \mathbf{r}'|} - \sum_a \int d^3\mathbf{r} \frac{Z_a}{|\mathbf{r} - \boldsymbol{\tau}_a|} \right) \right. \\ &\quad \left. - \sum_b Z_b \left( \int d^3\mathbf{r} \frac{\rho(\mathbf{r})}{|\mathbf{r} - \boldsymbol{\tau}_a|} - \sum_{a \neq b} \frac{Z_a}{|\boldsymbol{\tau}_a - \boldsymbol{\tau}_b|} \right) \right] \end{aligned} \quad (4.11)$$

The expression inside the first bracket is similar to equation (4.8), and the expression inside the second bracket is a limiting case ( $\mathbf{r} \rightarrow \boldsymbol{\tau}_b$ ) of the equation (4.8), which is also known as the Madelung potential ( $V_M$ ).

$$V_M(\boldsymbol{\tau}_b) = V_C(\mathbf{r} \rightarrow \boldsymbol{\tau}_b) \quad (4.12)$$

$$= \int d^3\mathbf{r} \frac{\rho(\mathbf{r})}{|\mathbf{r} - \boldsymbol{\tau}_b|} - \sum_{a \neq b} \frac{Z_a}{|\boldsymbol{\tau}_a - \boldsymbol{\tau}_b|} \quad (4.13)$$

The equation (4.14) is obtained by substituting the equations (4.8) and (4.13) into (4.11).

$$E_{es}[\rho] = \frac{1}{2} \left[ \int_{\Omega} d^3\mathbf{r} \rho(\mathbf{r}) V_C(\mathbf{r}) - \sum_b Z_b V_M(\boldsymbol{\tau}_b) \right] \quad (4.14)$$

Now, from a final substitution of the equations (4.6), (4.10), and (4.14) into (4.1), we get the total energy of the system.

$$\begin{aligned} E_{tot}[\rho] &= \sum_{v\mathbf{k}} n_{v\mathbf{k}} \epsilon_{v\mathbf{k}} - \int_{\Omega} d^3\mathbf{r} \rho(\mathbf{r}) V_{eff}(\mathbf{r}) + \frac{1}{2} \int_{\Omega} d^3\mathbf{r} \rho(\mathbf{r}) V_C(\mathbf{r}) \\ &\quad - \frac{1}{2} \sum_a Z_a V_M(\boldsymbol{\tau}_a) + \int_{\Omega} d^3\mathbf{r} \rho(\mathbf{r}) \epsilon_{xc}(\mathbf{r}) \\ &= \sum_{v\mathbf{k}} n_{v\mathbf{k}} \epsilon_{v\mathbf{k}} - \frac{1}{2} \int_{\Omega} d^3\mathbf{r} \rho(\mathbf{r}) V_C(\mathbf{r}) - \frac{1}{2} \sum_a Z_a V_M(\boldsymbol{\tau}_a) \\ &\quad + \int_{\Omega} d^3\mathbf{r} \rho(\mathbf{r}) (\epsilon_{xc}(\rho) - \mu_{xc}(\rho)) \end{aligned} \quad (4.15)$$

A detailed discussion of the total energy and its important features are provided in Ref. [34] for the LAPW method. This expression also forms the basis to calculate the stress tensor in Chapter 5, where it will be modified according to the deformation of the system.

## 4.1 Additional contribution to the kinetic energy

In practice there are two different expressions of the kinetic energy:  $\frac{1}{2} \int_{\Omega} d\Omega \psi_{v\mathbf{k}}^*(\mathbf{r}) (-\nabla^2) \psi_{v\mathbf{k}}(\mathbf{r})$  and  $\frac{1}{2} \int_{\Omega} d\Omega \nabla \psi_{v\mathbf{k}}^*(\mathbf{r}) \nabla \psi_{v\mathbf{k}}(\mathbf{r})$ . The latter expression is referred to as the Slater form of kinetic energy since it was first suggested by Slater [24]. These two expressions are equivalent if the basis functions are continuous at the boundary of the atomic spheres, and the interstitial region, both in the value and slope. This can be validated from the following mathematical expression.

According to Green's theorem,

$$\frac{1}{2} \int_{\Omega} d\Omega \nabla \psi_{v\mathbf{k}}^*(\mathbf{r}) \cdot \nabla \psi_{v\mathbf{k}}(\mathbf{r}) = \frac{1}{2} \int_{\Omega} d\Omega \psi_{v\mathbf{k}}^*(\mathbf{r}) (-\nabla^2) \psi_{v\mathbf{k}}(\mathbf{r}) + \frac{1}{2} \oint dS \left( \psi_{v\mathbf{k}}^{*a}(\mathbf{r}) \frac{\partial \psi_{v\mathbf{k}}^a(\mathbf{r})}{\partial r} - \psi_{v\mathbf{k}}^{*IS}(\mathbf{r}) \frac{\partial \psi_{v\mathbf{k}}^{IS}(\mathbf{r})}{\partial r} \right) \quad (4.16)$$

In the LAPW method, both expressions for the kinetic energy are equivalent since value and slope of the basis functions are continuous across the sphere boundary. As a result, the surface integral (second integral of 4.1) will vanish. The story in APW is different, where the basis functions are continuous, but nothing is restricted regarding the continuity of the slope. As a result, the surface integral does not vanish, and the  $\nabla^2$  form of kinetic energy is not equivalent to the Slater form of kinetic energy. The detailed discussion is provided in Ref. [30]. Also, because of the presence of this surface integral, the expression of the full stress tensor in the APW method will be different from the LAPW method.

## 4.2 Coulomb Potential

The Coulomb potential is evaluated using Weinert's method [35]. According to this method, we calculate the interstitial potential using the real interstitial charge density and the multipole moments produced by the total charge (electrons plus nucleus) distribution inside the spheres. The potential at any point outside of the spheres is independent of the actual charge distribution in the region of the spheres but depends only on its multipole moments. Therefore, the rapidly oscillating charge density in the region of the atomic spheres can be replaced by a much more smooth charge density that is zero outside the spheres but generates the correct potential in the interstitial region. In the literature, this smooth charge density is often referred to as the pseudo-charge density. As a result, the interstitial potential is calculated using the actual interstitial charge density plus the pseudo charge density. The calculated potential in the interstitial is also correct at the boundary of the spheres. By solving the electrostatic boundary value problem, the potential at any point within the spheres can be evaluated.

The Poisson equation determining the interstitial potential is:

$$\nabla^2 V_C^I(\mathbf{r}) = -4\pi \tilde{\rho}(\mathbf{r}) \quad (4.17)$$

$$= -4\pi (\rho_I(\mathbf{r}) + \tilde{\rho}_a(\mathbf{r})) \quad (4.18)$$

where  $V_C^I(\mathbf{r})$  is the interstitial Coulomb potential and  $\tilde{\rho}(\mathbf{r})$  is the total charge density in the interstitial—sum of real interstitial charge density ( $\rho_I(\mathbf{r})$ ) and pseudo charge density ( $\tilde{\rho}_a(\mathbf{r})$ ) of the spherical regions.

The Fourier series expansion of  $V_C^I(\mathbf{r})$  and  $\tilde{\rho}(\mathbf{r})$  are:

$$V_C^I(\mathbf{r}) = \sum_{\mathbf{G}} V_C(\mathbf{G}) e^{i\mathbf{G}\cdot\mathbf{r}} \quad (4.19)$$

$$\tilde{\rho}(\mathbf{r}) = \sum_{\mathbf{G}} \tilde{\rho}(\mathbf{G}) e^{i\mathbf{G}\cdot\mathbf{r}} \quad (4.20)$$

Operating on both side of (4.19) by  $\nabla^2$ , we obtain,

$$\nabla^2 V_C^I(\mathbf{r}) = \nabla^2 \sum_{\mathbf{G}} V_C(\mathbf{G}) e^{i\mathbf{G} \cdot \mathbf{r}} \quad (4.21)$$

$$\nabla^2 V_C^I(\mathbf{r}) = - \sum_{\mathbf{G}} \mathbf{G}^2 V_C(\mathbf{G}) e^{i\mathbf{G} \cdot \mathbf{r}} \quad (4.22)$$

Substituting equation (4.20) in equation (4.17) and comparing with (4.22), we get:

$$V_C(\mathbf{G}) = \frac{4\pi}{\mathbf{G}^2} \tilde{\rho}(\mathbf{G}) \quad (4.23)$$

The potential in the interstitial region is obtained by substituting equation (4.23) in equation (4.19) and using  $\tilde{\rho}(\mathbf{G}) = \tilde{\rho}_a(\mathbf{G}) + \rho_I(\mathbf{G})$ :

$$V_C^I(\mathbf{r}) = \sum_{\mathbf{G} \neq 0} \frac{4\pi \tilde{\rho}(\mathbf{G})}{\mathbf{G}^2} e^{i\mathbf{G} \cdot \mathbf{r}} = \sum_{\mathbf{G} \neq 0} \frac{4\pi}{\mathbf{G}^2} (\tilde{\rho}_a(\mathbf{G}) + \rho_I(\mathbf{G})) e^{i\mathbf{G} \cdot \mathbf{r}}, \quad (4.24)$$

where  $\mathbf{G}$  is a reciprocal lattice vector.  $\rho_I(\mathbf{G})$  and  $\tilde{\rho}_a(\mathbf{G})$  are the Fourier components of the interstitial charge density and smooth (pseudo-charge) density, respectively. The potential that is given in equation (4.24) is also correct at the boundary of the spheres i.e  $V_C^I(R_a)$ . Once the potential at the boundary of the spheres is known, the potential at any point inside the spheres can easily be evaluated using equation (4.25). The detailed discussion is provided in Ref. [35], and Eq. (7) of Ref. [35] in our notation is:

$$V_C^a(\mathbf{r}) = V_C^a(\mathbf{r}_a + \boldsymbol{\tau}_a) = \int_{R_a} d^3 \mathbf{r}'_a G(\mathbf{r}_a, \mathbf{r}'_a) \rho^a(\mathbf{r}'_a) - \frac{R_a^2}{4\pi} \oint_S V_C^I(R_a) \frac{\partial G(\mathbf{r}_a, \mathbf{r}'_a)}{\partial n} dS, \quad (4.25)$$

where  $\mathbf{r}_a$  and  $\mathbf{r}'_a$  are positions at any point inside the sphere with respect to the center of sphere  $\boldsymbol{\tau}_a$ .  $V_C^a(\mathbf{r})$  and  $V_C^I(R_a)$  are the Coulomb potential at position  $\mathbf{r}$  and the interstitial Coulomb potential on the sphere boundary  $|\mathbf{r}_a| = R_a$ , respectively.  $\rho^a(\mathbf{r}'_a)$  indicates the electronic charge density of an atom  $a$  at  $\mathbf{r}'_a$ .  $\int_{R_a} d^3 \mathbf{r}'_a$  represents the integration in the region of an atomic sphere  $a$ ,  $\frac{\partial}{\partial n}$  is to denote the normal derivative, and  $\oint_S dS$  represents the surface integral. The Green's function  $G(\mathbf{r}_a, \mathbf{r}'_a)$  determines the potential generated at the point  $\mathbf{r}_a$  due to a charge located at  $\mathbf{r}'_a$ . The expression of the Green's function,  $G(\mathbf{r}_a, \mathbf{r}'_a)$ , as given in the equation (8) in Ref. [35] is:

$$G(\mathbf{r}_a, \mathbf{r}'_a) = 4\pi \sum_{lm} \frac{Y_{lm}^*(\hat{\mathbf{r}}'_a) Y_{lm}(\hat{\mathbf{r}}_a)}{2l+1} \frac{r'_<}{r'_>}^l \left[ 1 - \left( \frac{r'_>}{R_a} \right)^{2l+1} \right] \quad (4.26)$$

Here  $r'_< = \min(r_a, r'_a)$  and  $r'_> = \max(r_a, r'_a)$ . When  $r'_a \rightarrow R_a$  (on the boundary) then  $r'_> = R_a$  i.e.

$$G(\mathbf{r}_a, \mathbf{r}'_a)|_{r'_a=R_a} = 0 \quad (4.27)$$

When  $r'_a \rightarrow 0$  (near the nuclei) then  $r'_> = r_a$ , and only the  $l=0$  term survives in the above summation:

$$\lim_{r'_a \rightarrow 0} G(\mathbf{r}_a, \mathbf{r}'_a) = \lim_{r'_a \rightarrow 0} 4\pi \sum_{lm} \frac{Y_{lm}^*(\hat{\mathbf{r}}'_a) Y_{lm}(\hat{\mathbf{r}}_a)}{2l+1} \frac{r'_a{}^l}{r_a^{l+1}} \left[ 1 - \left( \frac{r_a}{R_a} \right)^{2l+1} \right] \quad (4.28)$$

$$= 4\pi Y_{00}^*(\hat{\mathbf{r}}'_a) Y_{00}(\hat{\mathbf{r}}_a) \frac{1}{r_a} \left( 1 - \frac{r_a}{R_a} \right) \quad (4.29)$$

$$= \frac{1}{r_a} \left( 1 - \frac{r_a}{R_a} \right) \quad (4.30)$$

Similarly, if we take the limit  $r_a \rightarrow 0$  then  $r_> = r'_a$  and only  $l = 0$  term will survive in the summation.

$$\lim_{r_a \rightarrow 0} G(\mathbf{r}_a, \mathbf{r}'_a) = \lim_{r_a \rightarrow 0} \frac{1}{r'_a} \left( 1 - \frac{r'_a}{R_a} \right) \quad (4.31)$$

The normal derivative of the Green's function evaluated at the sphere boundary  $r'_a = R_a$  is

$$\frac{\partial G(\mathbf{r}_a, \mathbf{r}'_a)}{\partial n} = -\frac{4\pi}{R_a^2} \sum_{lm} \left( \frac{r_a}{R_a} \right)^l Y_{lm}^*(\hat{R}_a) Y_{lm}(\hat{r}_a) \quad (4.32)$$

In the limit  $r_a \rightarrow 0$

$$\lim_{r_a \rightarrow 0} \frac{\partial G(\mathbf{r}_a, \mathbf{r}'_a)}{\partial n} = -\frac{4\pi}{R_a^2} \sum_{lm} \delta_{l0} Y_{lm}^*(\hat{r}'_a) Y_{lm}(\hat{r}_a) \quad (4.33)$$

$$= -\frac{1}{R_a^2} \quad (4.34)$$

Inserting all these relations, the final expression of the electrostatic Coulomb potential at any point inside the atomic sphere becomes

$$\begin{aligned} V_C^a(\mathbf{r}) &= \sum_{lm} Y_{lm}(\hat{r}_a) \left\{ \frac{4\pi}{2l+1} \int_0^{R_a} dr'_a r'^{-2} \rho_{lm}^a(r'_a) \frac{r'^l}{r'^{l+1}} \left[ 1 - \left( \frac{r_>}{R_a} \right)^{2l+1} \right] \right. \\ &\quad \left. - \frac{Z_a}{r_a} \left( 1 - \frac{r_a}{R_a} \right) \sqrt{4\pi} \delta_{l0} \delta_{m0} + \left( \frac{r_a}{R_a} \right)^l \sum_{\mathbf{G} \neq 0} e^{i\mathbf{G} \cdot \boldsymbol{\tau}_a} V_C(\mathbf{G}) \oint_S dS e^{i\mathbf{G} \cdot \mathbf{R}_a} Y_{lm}^*(\hat{R}_a) \right\} \end{aligned} \quad (4.35)$$

The potential inside a sphere is expanded in terms of spherical harmonics.

$$V_C^a(\mathbf{r}) = \sum_{lm} V_{lm}^{aC}(r_a) Y_{lm}(\hat{r}_a) \quad (4.36)$$

Comparing equation 4.35 and 4.36.

$$\begin{aligned} V_{lm}^{aC}(r_a) &= \frac{4\pi}{2l+1} \int_0^{R_a} dr'_a r'^{-2} \rho_{lm}^a(r'_a) \frac{r'^l}{r'^{l+1}} \left[ 1 - \left( \frac{r_>}{R_a} \right)^{2l+1} \right] - \frac{Z_a}{r_a} \left( 1 - \frac{r_a}{R_a} \right) \sqrt{4\pi} \delta_{l0} \delta_{m0} \\ &\quad + \left( \frac{r_a}{R_a} \right)^l \sum_{\mathbf{G} \neq 0} e^{i\mathbf{G} \cdot \boldsymbol{\tau}_a} V_C(\mathbf{G}) \oint_S dS e^{i\mathbf{G} \cdot \mathbf{R}_a} Y_{lm}^*(\hat{R}_a) \end{aligned} \quad (4.37)$$

The last line of the above equation is further simplified using the Rayleigh expansion.

$$\begin{aligned} V_{lm}^{aC}(r_a) &= \frac{4\pi}{2l+1} \int_0^{R_a} dr'_a r'^{-2} \rho_{lm}^a(r'_a) \frac{r'_<}{r'^{l+1}} \left[ 1 - \left( \frac{r'_>}{R_a} \right)^{2l+1} \right] - \frac{Z_a}{r_a} \left( 1 - \frac{r_a}{R_a} \right) \sqrt{4\pi} \delta_{l0} \delta_{m0} \\ &\quad + 4\pi i^l \left( \frac{r_a}{R_a} \right)^l \sum_{\mathbf{G} \neq 0} e^{i\mathbf{G} \cdot \boldsymbol{\tau}_a} V_C(\mathbf{G}) j_l(GR_a) Y_{lm}^*(\hat{G}) \end{aligned} \quad (4.38)$$

At the sphere boundary  $r_a = R_a$ , the Coulomb potential is reduced to

$$V_{lm}^{aC}(R_a) = 4\pi i^l \sum_{\mathbf{G} \neq 0} e^{i\mathbf{G} \cdot \boldsymbol{\tau}_a} V_C(\mathbf{G}) j_l(GR_a) Y_{lm}^*(\hat{G}), \quad (4.39)$$

where  $V_C(\mathbf{G})$  is computed using Poisson's equation and given in the equation (4.23). Also, the Coulomb potential at any point inside an atomic sphere is given in equation (4.35). This potential is also a cornerstone for calculating the total energy (4.15) as well as strain variations of the total energy.

### 4.3 Madelung potential

The full Coulomb potential is due to all charges in the system, whereas the Madelung potential at the site  $\boldsymbol{\tau}_a$  is defined as the Coulomb potential due to all charges in the system except the nuclear charge at this site[34]. In other words, the Madelung potential can be regarded as a special case of the total Coulomb potential. The Coulomb potential as given in equation (4.25) is:

$$V_C^a(\mathbf{r}_a + \boldsymbol{\tau}_a) = \int_{R_a} G(\mathbf{r}_a, \mathbf{r}'_a) \rho^a(\mathbf{r}'_a) d^3 \mathbf{r}'_a - \frac{R_a^2}{4\pi} \oint_S V_C^I(\mathbf{R}_a) \frac{\partial G(\mathbf{r}_a, \mathbf{r}'_a)}{\partial n} dS \quad (4.40)$$

The Madelung potential is:

$$V_M(\boldsymbol{\tau}_a) = \lim_{r_a \rightarrow 0} V_C^a(\mathbf{r}_a + \boldsymbol{\tau}_a) \quad (4.41)$$

$$= V_C^a(\boldsymbol{\tau}_a) \quad (4.42)$$

$$= \int_{R_a} G(0, \mathbf{r}'_a) \rho^a(\mathbf{r}'_a) d^3 \mathbf{r}'_a - \frac{R_a^2}{4\pi} \oint_S V_C^I(\mathbf{R}_a) \frac{\partial G(0, \mathbf{r}'_a)}{\partial n} dS \quad (4.43)$$

As we know from the previous section 4.2:

$$G(0, \mathbf{r}'_a) \stackrel{(4.31)}{=} \frac{1}{r'_a} \left( 1 - \frac{r'_a}{R_a} \right) \quad (4.44)$$

$$\frac{\partial G(0, \mathbf{r}'_a)}{\partial n} \stackrel{(4.34)}{=} -\frac{1}{R_a^2} \quad (4.45)$$

With these expressions, equation (4.43) becomes:

$$V_M(\boldsymbol{\tau}_a) = \int_{R_a} \frac{\rho^a(\mathbf{r}'_a)}{r'_a} d^3 \mathbf{r}'_a - \frac{1}{R_a} \int_{R_a} \rho^a(\mathbf{r}'_a) d^3 \mathbf{r}'_a + \frac{1}{4\pi} \oint_S dS \left( V_C^I(\mathbf{R}_a) + \frac{Z_a}{R_a} \right)$$

Applying the limiting condition  $r_a \rightarrow 0$  to the equation (4.35):

$$\lim_{r_a \rightarrow 0} V_C^a(\mathbf{r}) = \lim_{r_a \rightarrow 0} \sum_{lm} Y_{lm}(\hat{r}_a) \left\{ \frac{4\pi}{2l+1} \int_0^{R_a} dr'_a r'^{-2} \rho_{lm}^a(r'_a) \frac{r'^l}{r'^{l+1}} \left[ 1 - \left( \frac{r_>}{R_a} \right)^{2l+1} \right] \right. \\ \left. - \frac{Z_a}{r_a} \left( 1 - \frac{r_a}{R_a} \right) \sqrt{4\pi} \delta_{l0} \delta_{m0} + \left( \frac{r_a}{R_a} \right)^l \sum_{\mathbf{G} \neq 0} e^{i\mathbf{G} \cdot \boldsymbol{\tau}_a} V_C(\mathbf{G}) \oint_S dS e^{i\mathbf{G} \cdot \mathbf{R}_a} Y_{lm}^*(\hat{R}_a) \right\} \quad (4.46)$$

We apply the limiting condition in the first line. When  $r_a \rightarrow 0$  then  $r_> = r'_a$ ,  $r_< = r_a$ , and because of  $(r_a)^l$ , only the  $l=0$  term survives there.

$$\begin{aligned} & \lim_{r_a \rightarrow 0} \sum_{lm} Y_{lm}(\hat{r}_a) \frac{4\pi}{2l+1} \int_0^{R_a} dr'_a r'^{-2} \rho_{lm}^a(r'_a) \frac{r'^l}{r'^{l+1}} \left[ 1 - \left( \frac{r_>}{R_a} \right)^{2l+1} \right] \\ &= \lim_{r_a \rightarrow 0} \sum_{lm} Y_{lm}(\hat{r}_a) \frac{4\pi}{2l+1} \int_0^{R_a} dr'_a r'^{-2} \rho_{lm}^a(r'_a) \frac{r'^l}{r'^{(l+1)}} \left[ 1 - \left( \frac{r'_a}{R_a} \right)^{2l+1} \right] \\ &= Y_{00}(0) \frac{4\pi}{2*0+1} \int_0^{R_a} dr'_a r'^{-2} \rho_{00}^a(r'_a) \frac{1}{r'^{(0+1)}} \left[ 1 - \left( \frac{r'_a}{R_a} \right)^{2*0+1} \right] \\ &= \sqrt{4\pi} \int_0^{R_a} dr'_a r'^{-2} \rho_{00}^a(r'_a) \frac{1}{r'_a} \left[ 1 - \left( \frac{r'_a}{R_a} \right) \right] \\ &= \left\langle \frac{\rho^a(r'_a)}{r'_a} \right\rangle_{R_a} - \frac{Q_a}{R_a} \end{aligned} \quad (4.47)$$

where  $Q_a = \int_{R_a} d^3 \mathbf{r}'_a \rho^a(\mathbf{r}'_a)$  denotes the total electronic charge inside an atomic sphere  $a$  and  $\left\langle \frac{\rho^a(r'_a)}{r'_a} \right\rangle_{R_a} = \sqrt{4\pi} \int_0^{R_a} dr'_a r'_a \rho_{00}(r'_a)$ . Considering the second expression of equation (4.46) and using the fact that the nuclear charge at the site  $\boldsymbol{\tau}_a$  does not contribute to the Madelung potential, we get the following expression:

$$\lim_{r_a \rightarrow 0} \left( \frac{Z_a}{r_a} - \frac{Z_a}{R_a} \right) = -\frac{Z_a}{R_a} \quad (4.48)$$

Now, we will be considering the third term of equation (4.46). Using the Rayleigh expansion to expand the exponential function ( $e^{i\mathbf{G} \cdot \mathbf{R}_a}$ ) in terms of spherical harmonics and applying  $r_a \rightarrow 0$ , we get:

$$\begin{aligned} & \lim_{r_a \rightarrow 0} \sum_{lm} Y_{lm}(\hat{r}_a) \left( \frac{r_a}{R_a} \right)^l \sum_{\mathbf{G} \neq 0} e^{i\mathbf{G} \cdot \boldsymbol{\tau}_a} V_C(\mathbf{G}) \oint_S dS e^{i\mathbf{G} \cdot \mathbf{R}_a} Y_{lm}^*(\hat{R}_a) \\ &= \lim_{r_a \rightarrow 0} \sum_{lm} Y_{lm}(\hat{r}_a) 4\pi i^l \left( \frac{r_a}{R_a} \right)^l \sum_{\mathbf{G} \neq 0} e^{i\mathbf{G} \cdot \boldsymbol{\tau}_a} V_C(\mathbf{G}) j_l(|\mathbf{G}| R_a) Y_{lm}^*(\hat{G}) \end{aligned} \quad (4.49)$$

$$\begin{aligned} &= Y_{00}(0) 4\pi \sum_{\mathbf{G} \neq 0} e^{i\mathbf{G} \cdot \boldsymbol{\tau}_a} V_C(\mathbf{G}) j_0(|\mathbf{G}| R_a) Y_{00}^*(\hat{G}) \\ &= \sum_{\mathbf{G} \neq 0} e^{i\mathbf{G} \cdot \boldsymbol{\tau}_a} V_C(\mathbf{G}) j_0(|\mathbf{G}| R_a) \end{aligned} \quad (4.50)$$

The potential at the sphere boundary is:

$$V_C(\mathbf{R}_a) = \sum_{lm} V_{lm}^{aC}(R_a) Y_{lm}(\hat{r}_a) = \sum_{lm} Y_{lm}(\hat{r}_a) 4\pi i^l \sum_{\mathbf{G} \neq 0} e^{i\mathbf{G} \cdot \boldsymbol{\tau}_a} V_C(\mathbf{G}) j_l(G R_a) Y_{lm}^*(\hat{G})$$

Denoting the spherical average of the potential by  $V_C^0(\mathbf{R}_a)$ .

$$V_C^0(\mathbf{R}_a) = \sum_{\mathbf{G} \neq 0} e^{i\mathbf{G} \cdot \boldsymbol{\tau}_a} V_C(\mathbf{G}) j_0(GR_a) \quad (4.51)$$

Substituting equation (4.51) in (4.50).

$$\lim_{r_a \rightarrow 0} \sum_{lm} Y_{lm}(\hat{r}_a) \left( \frac{r_a}{R_a} \right)^l \sum_{\mathbf{G} \neq 0} e^{i\mathbf{G} \cdot \boldsymbol{\tau}_a} V_C(\mathbf{G}) \oint_S dS e^{i\mathbf{G} \cdot \mathbf{R}_a} Y_{lm}^*(\hat{R}_a) = V_C^0(\mathbf{R}_a) \quad (4.52)$$

The final expression of the Madelung potential is obtained by substituting (4.47),(4.48), and (4.52) in (4.46).

$$V_M(\boldsymbol{\tau}_a) = \frac{1}{R_a} \left[ R_a V_C^0(\mathbf{R}_a) + Z_a - Q_a \right] + \left\langle \frac{\rho^a(\mathbf{r}'_a)}{r'_a} \right\rangle_{R_a} \quad (4.53)$$

In WIEN2k[13, 14], this expression is already implemented in the program file **energy.F**. In the stress calculation, this potential will be used to compute the contribution of the Madelung stress to the total stress tensor, which is discussed in detail in section 6.1.2.

# Chapter 5

## Strain variation

In the previous chapters we have explored various topics that are essential for a complete understanding of the stress tensor. In this chapter we use all of this information to understand how the total energy, the potential, and the charge density of the system change under symmetric infinitesimal strain deformation ( $\underline{\epsilon} \rightarrow 0$ ). As we can see in equation (2.2), the stress tensor is calculated by differentiating the total energy with respect to the strain. The derivation in this thesis is dedicated to the DFT formalism, so the following total energy[34] is the starting point of this derivation.

$$\begin{aligned} E_{tot} = & \sum_{v\mathbf{k}} n_{v\mathbf{k}} \epsilon_{v\mathbf{k}} - \int_{\Omega} d^3\mathbf{r} \rho(\mathbf{r}) V_{eff}(\mathbf{r}) + \frac{1}{2} \int_{\Omega} d^3\mathbf{r} \rho(\mathbf{r}) V_C(\mathbf{r}) \\ & - \frac{1}{2} \sum_{a \in \Omega} Z_a V_M(\boldsymbol{\tau}_a) + \int_{\Omega} d^3\mathbf{r} \rho(\mathbf{r}) \epsilon_{xc}(\mathbf{r}), \end{aligned} \quad (5.1)$$

We have already mentioned that in the stress tensor calculations, a system is distorted by a small strain  $\underline{\epsilon}$  such that  $\underline{\epsilon} \rightarrow 0$  and the first-order change in the total energy is evaluated. Distorting the system means changing the shape and size of the unit cell. As a result, all atoms in the system will be displaced to new positions, and all the quantities that define the total energy ( $E_{tot}$ ) and depend on the shape and size of the unit cell will be changed. The list of changing quantities is given in Table 5.1 below.

Equation (5.1) in the distorted system becomes

$$\begin{aligned} E_{tot}[\underline{\epsilon}] = & \sum_{v\mathbf{k}[\underline{\epsilon}]} n_{v\mathbf{k}[\underline{\epsilon}]} \epsilon_{v\mathbf{k}[\underline{\epsilon}]} - \int_{\Omega[\underline{\epsilon}]} d^3\mathbf{r}_{\epsilon} \rho_{[\underline{\epsilon}]}(\mathbf{r}_{\epsilon}) V_{eff}[\underline{\epsilon}](\mathbf{r}_{\epsilon}) + \frac{1}{2} \int_{\Omega[\underline{\epsilon}]} d^3\mathbf{r}_{\epsilon} \rho_{[\underline{\epsilon}]}(\mathbf{r}_{\epsilon}) V_C[\underline{\epsilon}](\mathbf{r}_{\epsilon}) \\ & - \frac{1}{2} \sum_{a \in \Omega[\underline{\epsilon}]} Z_a V_M[\underline{\epsilon}](\boldsymbol{\tau}_a[\underline{\epsilon}]) + \int_{\Omega[\underline{\epsilon}]} d^3\mathbf{r}_{\epsilon} \rho_{[\underline{\epsilon}]}(\mathbf{r}_{\epsilon}) \epsilon_{xc}[\underline{\epsilon}](\mathbf{r}_{\epsilon}) \end{aligned} \quad (5.2a)$$

$$E_{tot}[\underline{\epsilon}] = E_{kin}[\underline{\epsilon}] + E_{es}[\underline{\epsilon}] + E_{xc}[\underline{\epsilon}] \quad (5.2b)$$

In the following, the Coulomb potential and Madelung potential given in Eqs.(4.8) and (4.13) are defined in the deformed system.

Table 5.1: All quantities that are necessary to calculate the total energy in the undistorted and distorted system. The first and second column contain the quantities for the undistorted and distorted system, respectively. The  $\underline{\epsilon}$  symbolizes a symmetrical, infinitesimal strain deformation and  $[\underline{\epsilon}]$  is used to indicate quantities after deformation.

un-strained system	strained system
$\Omega$	$\Omega[\underline{\epsilon}]$
$n_{v\mathbf{k}}$	$n_{v\mathbf{k}[\underline{\epsilon}]}[\underline{\epsilon}]$
$\epsilon_{v\mathbf{k}}$	$\epsilon_{v\mathbf{k}[\underline{\epsilon}]}[\underline{\epsilon}]$
$\rho(\mathbf{r})$	$\rho[\underline{\epsilon}](\mathbf{r}[\underline{\epsilon}])$
$V_{eff}(\mathbf{r})$	$V_{eff}[\underline{\epsilon}](\mathbf{r}[\underline{\epsilon}])$
$\epsilon_{xc}(\mathbf{r})$	$\epsilon_{xc}[\underline{\epsilon}](\mathbf{r}[\underline{\epsilon}])$
$V_C(\mathbf{r})$	$V_C[\underline{\epsilon}](\mathbf{r}[\underline{\epsilon}])$
$V_M(\mathbf{r})$	$V_M[\underline{\epsilon}](\mathbf{r}[\underline{\epsilon}])$
$\int_{\Omega} d^3\mathbf{r}$	$\int_{\Omega[\underline{\epsilon}]} d^3\mathbf{r}_{\epsilon}$
$\mathbf{G}$	$\mathbf{G}[\underline{\epsilon}]$

$$V_C[\underline{\epsilon}](\mathbf{r}_{\epsilon}) = \int d^3\mathbf{r}'_{\epsilon} \frac{\rho[\underline{\epsilon}](\mathbf{r}'_{\epsilon})}{|\mathbf{r}_{\epsilon} - \mathbf{r}'_{\epsilon}|} - \sum_b \frac{Z_b}{|\mathbf{r}_{\epsilon} - \boldsymbol{\tau}_b[\underline{\epsilon}]|} \quad (5.3)$$

$$V_M[\underline{\epsilon}](\boldsymbol{\tau}_a[\underline{\epsilon}]) = \int d^3\mathbf{r}_{\epsilon} \frac{\rho[\underline{\epsilon}](\mathbf{r}_{\epsilon})}{|\mathbf{r}_{\epsilon} - \boldsymbol{\tau}_a[\underline{\epsilon}]|} - \sum_{b \neq a} \frac{Z_b}{|\boldsymbol{\tau}_a[\underline{\epsilon}] - \boldsymbol{\tau}_b[\underline{\epsilon}]|} \quad (5.4)$$

$\boldsymbol{\tau}_a[\underline{\epsilon}]$  and  $\mathbf{r}_{\epsilon}$  are the atomic position and spatial vector in the distorted system, and their transformation to the un-distorted system is given as:  $\boldsymbol{\tau}_a[\underline{\epsilon}] = (\underline{1} + \underline{\epsilon})\boldsymbol{\tau}_a$  and  $\mathbf{r}_{\epsilon} = (\underline{1} + \underline{\epsilon})\mathbf{r}$ . In the following sections we calculate the variation of kinetic energy, exchange-correlation energy, and electrostatic energy.

## 5.1 Variation of the kinetic energy

The expression of the kinetic energy in an undistorted system according to equation (4.6) is

$$E_{kin} = \sum_{v\mathbf{k}} n_{v\mathbf{k}} \epsilon_{v\mathbf{k}} - \int_{\Omega} d^3\mathbf{r} V_{eff}(\mathbf{r}) \rho(\mathbf{r}) \quad (5.5)$$

In a distorted system, the above equation becomes

$$E_{kin}[\underline{\epsilon}] = \sum_{v\mathbf{k}} n_{v\mathbf{k}[\underline{\epsilon}]}[\underline{\epsilon}] \epsilon_{v\mathbf{k}[\underline{\epsilon}]}[\underline{\epsilon}] - \int_{\Omega[\underline{\epsilon}]} d^3\mathbf{r}_{\epsilon} V_{eff}[\underline{\epsilon}](\mathbf{r}_{\epsilon}) \rho[\underline{\epsilon}](\mathbf{r}_{\epsilon}) \quad (5.6)$$

Back transformation of the integral from a distorted to an undistorted system leads to

$$\int_{\Omega[\underline{\epsilon}]} d^3 \mathbf{r}_\epsilon \rightarrow \det(\underline{1} + \underline{\epsilon}) \int_{\Omega} d^3 \mathbf{r} \quad (5.7)$$

Substitution of equation (5.7) in (5.6) gives

$$E_{kin}[\underline{\epsilon}] = \sum_{v\mathbf{k}} n_{v\mathbf{k}}[\underline{\epsilon}] \epsilon_{v\mathbf{k}}[\underline{\epsilon}] - \det(\underline{1} + \underline{\epsilon}) \int_{\Omega} d^3 \mathbf{r} \rho[\underline{\epsilon}](\mathbf{r}[\underline{\epsilon}]) V_{eff}[\underline{\epsilon}](\mathbf{r}[\underline{\epsilon}]) \quad (5.8)$$

Now we apply the strain variation in equation (5.8).

$$\begin{aligned} \frac{dE_{kin}[\underline{\epsilon}]}{d\epsilon_{\alpha\beta}} \Big|_{\underline{\epsilon}=0} &= \sum_{v\mathbf{k}} \frac{d n_{v\mathbf{k}}[\underline{\epsilon}] \epsilon_{v\mathbf{k}}[\underline{\epsilon}]}{d\epsilon_{\alpha\beta}} \Big|_{\underline{\epsilon}=0} - \delta_{\alpha\beta} \int_{\Omega} d^3 \mathbf{r} \rho(\mathbf{r}) V_{eff}(\mathbf{r}) \\ &\quad - \int_{\Omega} d^3 \mathbf{r} \frac{d}{d\epsilon_{\alpha\beta}} V_{eff}[\underline{\epsilon}](\mathbf{r}[\underline{\epsilon}]) \rho[\underline{\epsilon}](\mathbf{r}[\underline{\epsilon}]) \Big|_{\underline{\epsilon}=0} \end{aligned} \quad (5.9)$$

As explained in Ref.[12], the change in the occupation numbers due to the conservation of the electron number is a second-order effect and is neglected in the stress calculation.

$$\frac{dn_{v\mathbf{k}}[\underline{\epsilon}]}{d\epsilon_{\alpha\beta}} \Big|_{\underline{\epsilon}=0} \rightarrow 0 \quad (5.10)$$

The simplification of the third term of equation (5.9) is discussed in Appendix C, which simplifies equation (5.9) as follows.

$$\begin{aligned} \frac{dE_{kin}[\underline{\epsilon}]}{d\epsilon_{\alpha\beta}} \Big|_{\underline{\epsilon}=0} &= \sum_{v\mathbf{k}} n_{v\mathbf{k}} \frac{d\epsilon_{v\mathbf{k}}[\underline{\epsilon}]}{d\epsilon_{\alpha\beta}} \Big|_{\underline{\epsilon}=0} - \delta_{\alpha\beta} \int_{\Omega} d^3 \mathbf{r} \rho(\mathbf{r}) V_{eff}(\mathbf{r}) - \int_{\Omega} d^3 \mathbf{r} \rho(\mathbf{r}) \frac{dV_{eff}[\underline{\epsilon}](\mathbf{r})}{d\epsilon_{\alpha\beta}} \Big|_{\underline{\epsilon}=0} \\ &\quad - \frac{1}{2} \int_{\Omega} d^3 \mathbf{r} \rho(\mathbf{r}) (r_\beta \partial_\alpha + r_\alpha \partial_\beta) V_{eff}(\mathbf{r}) + \int_{\Omega} d^3 \mathbf{r} V_{eff}(\mathbf{r}) \frac{\rho[\underline{\epsilon}](\mathbf{r}[\underline{\epsilon}])}{d\epsilon_{\alpha\beta}} \end{aligned} \quad (5.11)$$

In the APW based methods, core and valence states are treated differently. The core states are the direct solution of the Dirac equation and they are not expressed using basis functions. The valence states are, however, described in terms of the basis functions. As a result, the strain variation of total eigenvalues is split into the valence and core electron contribution.

$$\sum_{v\mathbf{k}} n_{v\mathbf{k}} \frac{d\epsilon_{v\mathbf{k}}[\underline{\epsilon}]}{d\epsilon_{\alpha\beta}} \Big|_{\underline{\epsilon}=0} = \sum_{v\mathbf{k}} n_{v\mathbf{k}} \frac{d\epsilon_{v\mathbf{k}}^c[\underline{\epsilon}]}{d\epsilon_{\alpha\beta}} \Big|_{\underline{\epsilon}=0} + \sum_{v\mathbf{k}} n_{v\mathbf{k}} \frac{d\epsilon_{v\mathbf{k}}^v[\underline{\epsilon}]}{d\epsilon_{\alpha\beta}} \Big|_{\underline{\epsilon}=0} \quad (5.12)$$

Here the superscripts letters  $c$  and  $v$  are abbreviations for core and valence states. The expressions  $\frac{d\epsilon_{v\mathbf{k}}^c[\underline{\epsilon}]}{d\epsilon_{\alpha\beta}} \Big|_{\underline{\epsilon}=0}$  and  $\frac{d\epsilon_{v\mathbf{k}}^v[\underline{\epsilon}]}{d\epsilon_{\alpha\beta}} \Big|_{\underline{\epsilon}=0}$  are the change of core eigenvalues and valence eigenvalues when a system is strained. The change of core eigenvalues is given below.

$$\begin{aligned} \sum_{v\mathbf{k}} n_{v\mathbf{k}} \frac{d}{d\epsilon_{\alpha\beta}} \epsilon_v^c[\underline{\epsilon}] \Big|_{\underline{\epsilon}=0} &= \sum_{v\mathbf{k}} n_{v\mathbf{k}} \frac{d}{d\epsilon_{\alpha\beta}} \left\langle \psi_v^a[\underline{\epsilon}](\mathbf{r}_\epsilon) \left| -\frac{1}{2} \nabla^2 + V_{eff}[\underline{\epsilon}](\mathbf{r}) \right| \psi_v^a[\underline{\epsilon}](\mathbf{r}_\epsilon) \right\rangle \\ &= \sum_{v\mathbf{k}} n_{v\mathbf{k}} \left\langle \psi_v^a(\mathbf{r}) \left| \frac{dV_{eff}[\underline{\epsilon}](\mathbf{r})}{d\epsilon_{\alpha\beta}} \right| \psi_v^a(\mathbf{r}) \right\rangle \\ &= \int_{R_a} d^3 \mathbf{r}_a \rho_c^a(\mathbf{r}_a) \frac{dV_{eff}[\underline{\epsilon}](\mathbf{r}_a)}{d\epsilon_{\alpha\beta}} \Big|_{\underline{\epsilon}=0} \end{aligned} \quad (5.13)$$

Here  $\rho_c^a(\mathbf{r}_a)$  is the core charge density of an atom  $a$  located at  $\boldsymbol{\tau}_a$ ,  $\int_{R_a}$  represents the integration in the region of the atomic spheres, and  $R_a$  denotes the size of the sphere. In the APW based methods; the core charge density vanishes outside a sphere since it has to be confined to the region of the atomic spheres to fulfill the orthogonality condition: valence states are orthogonal to core states if core states are fully confined to the region of the atomic sphere.

The detail calculation of the change of the valence eigenvalues ( $\frac{d\epsilon_{v\mathbf{k}}^v[\underline{\epsilon}][\underline{\epsilon}]}{d\epsilon_{\alpha\beta}} \Big|_{\underline{\epsilon}=0}$ ) is provided in Appendix F. This derivation is motivated by section (5.2.2) of Ref. [19] and the resulting change in the valence eigenvalues calculated for the LAPW force in Ref. [31]. Here we just recall the final expression, which is:

$$\begin{aligned} \frac{d\epsilon_{v\mathbf{k}}^v[\underline{\epsilon}][\underline{\epsilon}]}{d\epsilon_{\alpha\beta}} \Big|_{\underline{\epsilon}=0} &= 2\Re \left\langle \frac{d\psi_{v\mathbf{k}}[\underline{\epsilon}](\mathbf{r}[\underline{\epsilon}])}{d\epsilon_{\alpha\beta}} \Big|_{\underline{\epsilon}=0} \left| \hat{H}_{eff}(\mathbf{r}) - \epsilon_{v\mathbf{k}} \right| \psi_{v\mathbf{k}} \right\rangle + \left\langle \psi_{v\mathbf{k}} \left| \frac{1}{2}(\partial_\alpha \partial_\beta + \partial_\beta \partial_\alpha) \right| \psi_{v\mathbf{k}} \right\rangle \\ &+ \left\langle \psi_{v\mathbf{k}} \left| \frac{dV_{eff}[\underline{\epsilon}](\mathbf{r}[\underline{\epsilon}])}{d\epsilon_{\alpha\beta}} \Big|_{\underline{\epsilon}=0} \right| \psi_{v\mathbf{k}} \right\rangle \end{aligned} \quad (5.14)$$

Here  $\frac{d\psi_{v\mathbf{k}}[\underline{\epsilon}](\mathbf{r}[\underline{\epsilon}])}{d\epsilon_{\alpha\beta}} \Big|_{\underline{\epsilon}=0}$  has an explicit dependency in  $\underline{\epsilon}$  and implicit dependency through  $\mathbf{r}_\epsilon$ . Use of the frozen augmentation approximation[37], an explicit dependency on  $\underline{\epsilon}$  as a result of linear response is discarded in the matching condition while keeping the implicit  $\underline{\epsilon}$  dependency. The following relation is obtained by substituting equation (5.13) and (5.14) in equation (5.12).

$$\begin{aligned} \sum_{v\mathbf{k}} n_{v\mathbf{k}} \frac{d\epsilon_{v\mathbf{k}}[\underline{\epsilon}][\underline{\epsilon}]}{d\epsilon_{\alpha\beta}} \Big|_{\underline{\epsilon}=0} &= \int_{R_a} d^3 r_a \rho_c^a(\mathbf{r}_a) \frac{dV_{eff}[\underline{\epsilon}](\mathbf{r}_a)}{d\epsilon_{\alpha\beta}} \Big|_{\underline{\epsilon}=0} \\ &+ \sum_{v\mathbf{k}} n_{v\mathbf{k}} \left\{ 2\Re \left\langle \frac{d\psi_{v\mathbf{k}}[\underline{\epsilon}](\mathbf{r}[\underline{\epsilon}])}{d\epsilon_{\alpha\beta}} \Big|_{\underline{\epsilon}=0} \left| \hat{H}_{eff}(\mathbf{r}) - \epsilon_{v\mathbf{k}} \right| \psi_{v\mathbf{k}} \right\rangle \right. \\ &\quad \left. + \left\langle \psi_{v\mathbf{k}} \left| \frac{1}{2}(\partial_\alpha \partial_\beta + \partial_\beta \partial_\alpha) \right| \psi_{v\mathbf{k}} \right\rangle + \left\langle \psi_{v\mathbf{k}} \left| \frac{dV_{eff}[\underline{\epsilon}](\mathbf{r}[\underline{\epsilon}])}{d\epsilon_{\alpha\beta}} \Big|_{\underline{\epsilon}=0} \right| \psi_{v\mathbf{k}} \right\rangle \right\} \end{aligned} \quad (5.15)$$

To further simplify the above equation, we use the following relationship.

$$\begin{aligned} \sum_{v\mathbf{k}} n_{v\mathbf{k}} \left\langle \psi_{v\mathbf{k}} \left| \frac{dV_{eff}[\underline{\epsilon}](\mathbf{r}[\underline{\epsilon}])}{d\epsilon_{\alpha\beta}} \Big|_{\underline{\epsilon}=0} \right| \psi_{v\mathbf{k}} \right\rangle &= \int_{\Omega} d^3 r \rho_v(\mathbf{r}) \left[ \frac{\delta V_{eff}[\underline{\epsilon}](\mathbf{r})}{\delta \epsilon_{\alpha\beta}} \Big|_{\underline{\epsilon}=0} \right. \\ &\quad \left. + \frac{1}{2} (r_\beta \partial_\alpha + r_\alpha \partial_\beta) V_{eff}(\mathbf{r}) \right] \end{aligned} \quad (5.16a)$$

and

$$\rho(\mathbf{r}) = \rho_c^a(\mathbf{r}_a) + \rho_v(\mathbf{r}) \quad (5.16b)$$

Substituting equations (5.16a) and (5.16b) in (5.15), and substituting equation (5.15) in (5.9) gives the final expression for the strain variation of kinetic energy.

$$\begin{aligned}
\frac{E_{kin}[\underline{\epsilon}]}{d\epsilon_{\alpha\beta}} \Big|_{\underline{\epsilon}=0} &= 2 \sum_{v\mathbf{k}} n_{v\mathbf{k}} \Re \left\langle \frac{d\psi_{v\mathbf{k}}[\underline{\epsilon}](\mathbf{r}[\underline{\epsilon}])}{d\epsilon_{\alpha\beta}} \Big|_{\underline{\epsilon}=0} \right| \widehat{H}_{eff}(\mathbf{r}) - \epsilon_{v\mathbf{k}} \left| \psi_{v\mathbf{k}} \right\rangle \\
&+ \frac{1}{2} \sum_{v\mathbf{k}} n_{v\mathbf{k}} \int_{\Omega} d^3\mathbf{r} \psi_{v\mathbf{k}}^*(\mathbf{r}) (\partial_{\alpha}\partial_{\beta} + \partial_{\beta}\partial_{\alpha}) \psi_{v\mathbf{k}}(\mathbf{r}) \\
&- \delta_{\alpha\beta} \int_{\Omega} d^3\mathbf{r} \rho(\mathbf{r}) V_{eff}(\mathbf{r}) - \frac{1}{2} \int_{\Omega} d^3\mathbf{r} \rho_c^a(\mathbf{r}) (r_{\beta}\partial_{\alpha} + r_{\alpha}\partial_{\beta}) V_{eff}(\mathbf{r}) \\
&- \int_{\Omega} d^3\mathbf{r} V_{eff}(\mathbf{r}) \frac{d\rho[\underline{\epsilon}](\mathbf{r}[\underline{\epsilon}])}{d\epsilon_{\alpha\beta}}
\end{aligned} \tag{5.17}$$

## 5.2 Variation of the electrostatic energy

The electrostatic energy according to equation (4.14) is

$$E_{es} = \frac{1}{2} \int_{\Omega} d^3\mathbf{r} \rho(\mathbf{r}) V_C(\mathbf{r}) - \frac{1}{2} \sum_{a \in \Omega} Z_a V_M(\boldsymbol{\tau}_a) \tag{5.18}$$

The Coulomb potential ( $V_C(\mathbf{r})$ ) and the Madelung potential ( $V_M(\boldsymbol{\tau}_a)$ ) are given in equations (4.8) and (4.13). Equation (5.18) in the distorted system is

$$E_{es}[\underline{\epsilon}] = \frac{1}{2} \int_{\Omega[\underline{\epsilon}]} d^3\mathbf{r}_{\epsilon} \rho[\underline{\epsilon}](\mathbf{r}[\underline{\epsilon}]) V_C[\underline{\epsilon}](\mathbf{r}[\underline{\epsilon}]) - \frac{1}{2} \sum_{a \in \Omega[\underline{\epsilon}]} Z_a V_M[\underline{\epsilon}](\boldsymbol{\tau}_a[\underline{\epsilon}]) \tag{5.19}$$

$$= E_C[\underline{\epsilon}] + E_M[\underline{\epsilon}] \tag{5.20}$$

Substitution of strained Coulomb and Madelung potential, equations (5.3) and (5.4), in equation (5.19) gives the strained Coulomb and Madelung energy.

$$E_C[\underline{\epsilon}] = +\frac{1}{2} \int_{\Omega[\underline{\epsilon}]} d^3\mathbf{r}_{\epsilon} \rho[\underline{\epsilon}](\mathbf{r}_{\epsilon}) \left[ \int d^3\mathbf{r}'_{\epsilon} \frac{\rho[\underline{\epsilon}](\mathbf{r}'_{\epsilon})}{|\mathbf{r}_{\epsilon} - \mathbf{r}'_{\epsilon}|} - \sum_b \frac{Z_b}{|\mathbf{r}_{\epsilon} - \boldsymbol{\tau}_b[\underline{\epsilon}]|} \right] \tag{5.21}$$

$$E_M[\underline{\epsilon}] = -\frac{1}{2} \sum_{a \in \Omega} Z_a \left[ \int d^3\mathbf{r}_{\epsilon} \frac{\rho[\underline{\epsilon}](\mathbf{r}_{\epsilon})}{|\mathbf{r}_{\epsilon} - \boldsymbol{\tau}_a[\underline{\epsilon}]|} - \sum_{b \neq a} \frac{Z_b}{|\boldsymbol{\tau}_a[\underline{\epsilon}] - \boldsymbol{\tau}_b[\underline{\epsilon}]|} \right] \tag{5.22}$$

The strain variation of equation (5.20) is

$$\frac{dE_{es}[\underline{\epsilon}]}{d\epsilon_{\alpha\beta}} \Big|_{\underline{\epsilon}=0} = \frac{dE_C[\underline{\epsilon}]}{d\epsilon_{\alpha\beta}} \Big|_{\underline{\epsilon}=0} + \frac{dE_M[\underline{\epsilon}]}{d\epsilon_{\alpha\beta}} \Big|_{\underline{\epsilon}=0} \tag{5.23}$$

The rigorous mathematical steps used to simplify equation (5.23) and to obtain equation (5.24) are provided in Appendix E. There we used a partial back-substitution technique similar to that of Ref. [19], since the integrals involved in the electrostatic stress are impossible to evaluate analytically. The technique provided in Ref. [19] offers a considerable simplification. The main advantage of this technique is to isolate the strain derivative of the density, which is later canceled with similar expressions

of the double-counting part of the kinetic stress and the variation of the Kohn-Sham eigenvalues. Hence, the ultimate expression of a strained variation of the electrostatic energy according to equation (E.7) is

$$\begin{aligned} \frac{dE_{es}[\underline{\epsilon}]}{d\epsilon_{\alpha\beta}} &= \int_{\Omega} d^3\mathbf{r} \frac{d\rho[\underline{\epsilon}](\mathbf{r}[\underline{\epsilon}])}{d\epsilon_{\alpha\beta}} \Big|_{\underline{\epsilon}=0} V_C(\mathbf{r}) + \frac{1}{2} \frac{d}{d\epsilon_{\alpha\beta}} \left\{ \int_{\Omega[\underline{\epsilon}]} d^3\mathbf{r}_\epsilon \rho((\underline{1}-\underline{\epsilon})\mathbf{r}_\epsilon) V_C[\underline{\epsilon}](\mathbf{r}_\epsilon) \right\}_{\underline{\epsilon}=0} \\ &\quad - \frac{1}{2} \sum_{a \in \Omega} Z_a \frac{d}{d\epsilon_{\alpha\beta}} V_M[\underline{\epsilon}](\boldsymbol{\tau}_a[\underline{\epsilon}]) \Big|_{\underline{\epsilon}=0} \end{aligned} \quad (5.24)$$

In the above equation, modified or deformed Coulomb and Madelung potentials are used. The definition of  $(V_C[\underline{\epsilon}](\mathbf{r}[\underline{\epsilon}]))$  and  $(V_M[\underline{\epsilon}](\boldsymbol{\tau}_a[\underline{\epsilon}]))$  in equation (5.19) is a little different than in equation (5.24). In equation (5.19), the Coulomb and Madelung potential are defined using the strained density  $(\rho[\underline{\epsilon}](\mathbf{r}_\epsilon))$ . However, in equations (5.24) they are defined using the charge density of unstrained system but smeared over the strained system i.e  $\rho((\underline{1}-\underline{\epsilon})\mathbf{r}_\epsilon)$ , see equations (5.25a) and (5.25b). The rationale behind these definitions are that the valence density of the un-strained system is smeared over the strained lattice and, the core density of the unstrained system is moved along with the nuclei to the position of the nuclei in the strained lattice and smeared over the strained lattice.

$$V_C[\underline{\epsilon}](\mathbf{r}_\epsilon) = \int d^3\mathbf{r}'_\epsilon \frac{\rho((\underline{1}-\underline{\epsilon})\mathbf{r}'_\epsilon)}{|\mathbf{r}_\epsilon - \mathbf{r}'_\epsilon|} - \sum_b \frac{Z_b}{|\mathbf{r}_\epsilon - \boldsymbol{\tau}_b[\underline{\epsilon}]|} \quad (5.25a)$$

$$V_M^a[\underline{\epsilon}](\boldsymbol{\tau}_a[\underline{\epsilon}]) = \int d^3\mathbf{r}_\epsilon \frac{\rho((\underline{1}-\underline{\epsilon})\mathbf{r}_\epsilon)}{|\mathbf{r}_\epsilon - \boldsymbol{\tau}_a[\underline{\epsilon}]|} - \sum_{b \neq a} \frac{Z_b}{|\boldsymbol{\tau}_a[\underline{\epsilon}] - \boldsymbol{\tau}_b[\underline{\epsilon}]|} \quad (5.25b)$$

## 5.3 Variation of the exchange-correlation energy

### 5.3.1 Variation of the LDA exchange-correlation energy

In this section, a variation of the exchange-correlation energy within the framework of the Local Density Approximation (LDA) is discussed. We first consider the exchange-correlation energy of an undistorted system as given in equation (4.10).

$$E_{xc}^{LDA} = \int_{\Omega} d^3\mathbf{r} \rho(\mathbf{r}) \epsilon_{xc}(\rho(\mathbf{r})) \quad (5.26)$$

In the distorted system, it becomes:

$$E_{xc}^{LDA}[\epsilon] = \int_{\Omega[\epsilon]} d^3\mathbf{r}_\epsilon \rho[\epsilon](\mathbf{r}_\epsilon) \epsilon_{xc}(\rho[\epsilon](\mathbf{r}_\epsilon)) \quad (5.27)$$

The following expression results from a back transformation of the integral from a distorted to an undistorted system.

$$E_{xc}^{LDA}[\epsilon] = \det(\underline{1} + \underline{\epsilon}) \int_{\Omega} d^3\mathbf{r} \rho[\epsilon](\mathbf{r}[\epsilon]) \epsilon_{xc}(\rho[\epsilon](\mathbf{r}[\epsilon])) \quad (5.28)$$

The change in exchange-correlation energy according to the applied strained is

$$\frac{dE_{xc}^{LDA}[\epsilon]}{d\epsilon_{\alpha\beta}} \Big|_{\epsilon=0} = \delta_{\alpha\beta} \int_{\Omega} d^3\mathbf{r} \rho(\mathbf{r}) \epsilon_{xc}(\rho(\mathbf{r})) + \int_{\Omega} d^3\mathbf{r} \frac{\partial \rho[\epsilon](\mathbf{r}[\epsilon]) \epsilon_{xc}(\rho[\epsilon](\mathbf{r}[\epsilon]))}{\partial \epsilon_{\alpha\beta}} \Big|_{\epsilon=0} \quad (5.29)$$

The first integral is in its simplest possible form, and further simplification is only needed for the second integral.

$$\begin{aligned} \int_{\Omega} d^3\mathbf{r} \frac{\partial}{\partial \epsilon_{\alpha\beta}} \rho[\epsilon](\mathbf{r}[\epsilon]) \epsilon_{xc}(\rho[\epsilon](\mathbf{r}[\epsilon])) &= \int_{\Omega} d^3\mathbf{r} \frac{\partial [\rho(\mathbf{r}) \epsilon_{xc}(\rho(\mathbf{r}))]}{\partial \rho(\mathbf{r})} \frac{\partial \rho[\epsilon](\mathbf{r}[\epsilon])}{\partial \epsilon_{\alpha\beta}} \Big|_{\epsilon=0} \\ &= \int_{\Omega} d^3\mathbf{r} \frac{\partial \rho[\epsilon](\mathbf{r}[\epsilon])}{\partial \epsilon_{\alpha\beta}} \Big|_{\epsilon=0} \mu_{xc}(\rho(\mathbf{r})) \end{aligned} \quad (5.30)$$

Hence the final expression of equation (5.29) is

$$\frac{dE_{xc}^{LDA}[\epsilon]}{d\epsilon_{\alpha\beta}} \Big|_{\epsilon=0} = \delta_{\alpha\beta} \int_{\Omega} d^3\mathbf{r} \rho(\mathbf{r}) \epsilon_{xc}(\rho(\mathbf{r})) + \int_{\Omega} d^3\mathbf{r} \frac{\partial \rho[\epsilon](\mathbf{r}[\epsilon])}{\partial \epsilon_{\alpha\beta}} \Big|_{\epsilon=0} \mu_{xc}(\rho(\mathbf{r})) \quad (5.31)$$

### 5.3.2 Variation of the GGA exchange-correlation energy

In contrast to the LDA, the GGA exchange-correlation energy not only depends on the charge density but also on its gradient [38, 39]. The GGA exchange-correlation energy in the undistorted system is defined as:

$$E_{xc}^{GGA} = \int_{\Omega} d^3\mathbf{r} \rho(\mathbf{r}) \epsilon_{xc}(\rho(\mathbf{r}), \nabla \rho(\mathbf{r})) \quad (5.32)$$

In the distorted system, it becomes:

$$E_{xc}^{GGA}[\epsilon] = \int_{\Omega[\epsilon]} d^3\mathbf{r}_{\epsilon} \rho[\epsilon](\mathbf{r}_{\epsilon}) \epsilon_{xc}(\rho[\epsilon](\mathbf{r}_{\epsilon}), \nabla_{\epsilon} \rho[\epsilon](\mathbf{r}_{\epsilon})) \quad (5.33)$$

Back transformation of the integral from a distorted to an undistorted system gives the following expression:

$$E_{xc}^{GGA}[\epsilon] = \det((\underline{1} + \underline{\epsilon})) \int_{\Omega} d^3\mathbf{r} \rho[\epsilon](\mathbf{r}[\epsilon]) \epsilon_{xc}(\rho[\epsilon](\mathbf{r}[\epsilon]), \nabla[\epsilon] \rho[\epsilon](\mathbf{r}[\epsilon]))$$

The change in GGA exchange correlation energy according to the applied strained is:

$$\begin{aligned} \frac{dE_{xc}^{GGA}[\epsilon]}{d\epsilon_{\alpha\beta}} \Big|_{\underline{\epsilon}=0} &= \frac{d}{d\epsilon_{\alpha\beta}} \left[ \det((\underline{1} + \underline{\epsilon})) \int_{\Omega} d^3\mathbf{r} \rho[\epsilon](\mathbf{r}[\epsilon]) \epsilon_{xc}(\rho[\epsilon](\mathbf{r}[\epsilon]), \nabla[\epsilon] \rho[\epsilon](\mathbf{r}[\epsilon])) \right]_{\underline{\epsilon}=0} \\ &= \delta_{\alpha\beta} \int_{\Omega} d^3\mathbf{r} \rho(\mathbf{r}) \epsilon_{xc}(\rho(\mathbf{r}), \nabla \rho(\mathbf{r})) + \int_{\Omega} d^3\mathbf{r} \frac{d\rho[\epsilon](\mathbf{r}[\epsilon])}{d\epsilon_{\alpha\beta}} \Big|_{\underline{\epsilon}=0} \epsilon_{xc}(\rho(\mathbf{r}), \nabla \rho(\mathbf{r})) \\ &\quad + \int_{\Omega} d^3\mathbf{r} \rho(\mathbf{r}) \frac{d}{d\epsilon_{\alpha\beta}} \epsilon_{xc}(\rho[\epsilon](\mathbf{r}[\epsilon]), \nabla[\epsilon] \rho[\epsilon](\mathbf{r}[\epsilon])) \Big|_{\underline{\epsilon}=0} \end{aligned} \quad (5.34)$$

The first and second terms are similar to the LDA expression, equation (5.31), and they are already in their simplest form. Therefore we try to further simplify the third term of the above equation in the following lines.

$$\frac{d}{d\epsilon_{\alpha\beta}}\epsilon_{xc}(\rho[\epsilon](\mathbf{r}[\epsilon]), \nabla[\epsilon]\rho[\epsilon](\mathbf{r}[\epsilon]))\Big|_{\underline{\epsilon}=0} = \frac{\partial\epsilon_{xc}}{\partial\rho(\mathbf{r})}\frac{\partial\rho[\epsilon](\mathbf{r}[\epsilon])}{\partial\epsilon_{\alpha\beta}}\Big|_{\underline{\epsilon}=0} + \frac{\partial\epsilon_{xc}}{\partial(\partial_\mu\rho(\mathbf{r}))}\frac{\partial(\partial_\mu[\epsilon]\rho[\epsilon](\mathbf{r}[\epsilon]))}{d\epsilon_{\alpha\beta}}\Big|_{\underline{\epsilon}=0} \quad (5.35)$$

where,

$$(\nabla\rho(\mathbf{r}))_\mu = \partial_\mu\rho(\mathbf{r}), \quad (5.36)$$

and  $\epsilon_{xc}$  in the right hand side is equivalent to  $\epsilon_{xc}(\rho(\mathbf{r}), \nabla\rho(\mathbf{r}))$ . The relationship of the nabla operator ( $\nabla$ ) between the strained and the unstrained system is:

$$\nabla_\mu[\epsilon]\rho(\mathbf{r}) = \partial_\mu[\epsilon]\rho(\mathbf{r}) = (\delta_{\mu\nu} - \epsilon_{\mu\nu})\partial_\mu\rho(\mathbf{r}) \quad (5.37)$$

$$\frac{\partial}{\partial\epsilon_{\alpha\beta}}\frac{\partial_\mu[\epsilon]\rho[\epsilon](\mathbf{r}[\epsilon])}{\partial\epsilon_{\alpha\beta}}\Big|_{\underline{\epsilon}=0} = \frac{\partial(\partial_\mu[\epsilon])\rho(\mathbf{r})}{\partial\epsilon_{\alpha\beta}}\Big|_{\underline{\epsilon}=0} + \partial_\mu\frac{\partial\rho[\epsilon](\mathbf{r}[\epsilon])}{\partial\epsilon_{\alpha\beta}}\Big|_{\underline{\epsilon}=0} \quad (5.38)$$

and

$$\begin{aligned} \frac{\partial\partial_\mu[\epsilon]\rho(\mathbf{r})}{\partial\epsilon_{\alpha\beta}}\Big|_{\underline{\epsilon}=0} &= -\frac{\partial\epsilon_{\mu\nu}}{\partial\epsilon_{\alpha\beta}}\Big|_{\underline{\epsilon}=0}\partial_\mu\rho(\mathbf{r}) = -\frac{1}{2}(\delta_{\mu\alpha}\delta_{\nu\alpha}\partial_\nu\rho(\mathbf{r}) + \delta_{\nu\alpha}\delta_{\mu\alpha}\partial_\nu\rho(\mathbf{r})) \\ &= -\frac{1}{2}(\delta_{\mu\alpha}\partial_\beta\rho(\mathbf{r}) + \delta_{\mu\beta}\partial_\alpha\rho(\mathbf{r})) \end{aligned} \quad (5.39)$$

Using equations (5.39) and (5.38) in (5.35):

$$\begin{aligned} \frac{\partial\epsilon_{xc}}{\partial(\partial_\mu\rho(\mathbf{r}))}\frac{\partial_\mu[\epsilon]\rho(\mathbf{r})}{\partial\epsilon_{\alpha\beta}}\Big|_{\underline{\epsilon}=0} &= -\frac{1}{2}(\delta_{\mu\alpha}\partial_\beta\rho(\mathbf{r}) + \delta_{\mu\beta}\partial_\alpha\rho(\mathbf{r}))\frac{\partial\epsilon_{xc}}{\partial(\partial_\mu\rho(\mathbf{r}))} \\ &= -\frac{1}{2}\left(\frac{\partial\epsilon_{xc}}{\partial(\partial_\alpha\rho(\mathbf{r}))}\partial_\beta\rho(\mathbf{r}) + \frac{\partial\epsilon_{xc}}{\partial(\partial_\beta\rho(\mathbf{r}))}\partial_\alpha\rho(\mathbf{r})\right) \end{aligned} \quad (5.40)$$

A further simplification of the first term inside the bracket is:

$$\frac{\partial\epsilon_{xc}}{\partial(\partial_\alpha\rho(\mathbf{r}))}\partial_\beta\rho(\mathbf{r}) = \frac{\partial\epsilon_{xc}}{\partial(\partial_\alpha\rho(\mathbf{r}) \cdot \partial_\alpha\rho(\mathbf{r}))}\frac{\partial(\partial_\alpha\rho(\mathbf{r}) \cdot \partial_\alpha\rho(\mathbf{r}))}{\partial\partial_\alpha\rho(\mathbf{r})}\partial_\beta\rho(\mathbf{r}) \quad (5.41)$$

$$= \frac{\partial\epsilon_{xc}}{\partial\sigma}2\partial_\alpha\rho(\mathbf{r})\partial_\beta\rho(\mathbf{r}) \quad (5.42)$$

Here, we have introduced  $\sigma = \nabla\rho(\mathbf{r}) \cdot \nabla\rho(\mathbf{r})$  in the same manner as defined in the Libxc online manual [40]. In a spin-polarized system, this notation will be slightly different as it needs to be defined separately for each spin state. The simple expression of  $\sigma$  for the spin-up ( $\uparrow$ ), spin down ( $\downarrow$ ), and mixed spin states is given below, but their use in the case of spin-polarization is provided while the stress contribution of the GGA exchange correlation energy is calculated in section 6.5.

$$\sigma[0] = \nabla\rho(\mathbf{r})_\uparrow \cdot \nabla\rho(\mathbf{r})_\uparrow, \quad \sigma[1] = \nabla\rho(\mathbf{r})_\downarrow \cdot \nabla\rho(\mathbf{r})_\uparrow, \quad \sigma[2] = \nabla\rho(\mathbf{r})_\downarrow \cdot \nabla\rho(\mathbf{r})_\downarrow \quad (5.43)$$

Substituting equation (5.41) into (5.40):

$$\frac{\partial\epsilon_{xc}}{\partial(\partial_\mu\rho(\mathbf{r}))} \frac{\partial_\mu[\epsilon]\rho(\mathbf{r})}{\partial\epsilon_{\alpha\beta}} = -\partial_\alpha\rho(\mathbf{r})\partial_\beta\rho(\mathbf{r}) \left( \frac{\partial\epsilon_{xc}}{\partial\sigma} + \frac{\partial\epsilon_{xc}}{\partial\sigma} \right) \quad (5.44)$$

$$= -2 \partial_\alpha\rho(\mathbf{r})\partial_\beta\rho(\mathbf{r}) \frac{\partial\epsilon_{xc}}{\partial\sigma} \quad (5.45)$$

If we collect all the intermediate expressions and substitute them into the third integral of equation (5.34) we get:

$$\begin{aligned} \int_\Omega d^3\mathbf{r}\rho(\mathbf{r}) \frac{\partial}{\partial\epsilon_{\alpha\beta}}\epsilon_{xc}(\rho[\epsilon](\mathbf{r}[\epsilon]), \nabla[\epsilon]\rho[\epsilon](\mathbf{r}[\epsilon])) &= -2 \int_\Omega d^3\mathbf{r}\rho(\mathbf{r})\partial_\alpha\rho(\mathbf{r})\partial_\beta\rho(\mathbf{r}) \frac{\partial\epsilon_{xc}}{\partial\sigma} \\ &\quad + \int_\Omega d^3\mathbf{r}\rho(\mathbf{r}) \left\{ \frac{\partial\epsilon_{xc}}{\partial\rho(\mathbf{r})} \frac{d\rho[\epsilon](\mathbf{r}[\epsilon])}{d\epsilon_{\alpha\beta}} \right. \\ &\quad \left. + \frac{\partial\epsilon_{xc}}{\partial(\partial_\mu\rho(\mathbf{r}))} \partial_\mu \frac{d\rho[\epsilon](\mathbf{r}[\epsilon])}{d\epsilon_{\alpha\beta}} \right\} \end{aligned} \quad (5.46)$$

The first expression of equation (5.46) is already in its simplest form. In the following lines we further simplify the second integral. To solve the second integral we use the following relationship.

$$\int_\Omega d^3\mathbf{r}\rho(\mathbf{r}) \frac{\partial\epsilon_{xc}}{\partial(\partial_\mu\rho(\mathbf{r}))} \partial_\mu \frac{d\rho[\epsilon](\mathbf{r}[\epsilon])}{d\epsilon_{\alpha\beta}} = - \int_\Omega d^3\mathbf{r} \frac{d\rho[\epsilon](\mathbf{r}[\epsilon])}{d\epsilon_{\alpha\beta}} \partial_\mu \left[ \rho(\mathbf{r}) \frac{\partial\epsilon_{xc}}{\partial(\partial_\mu\rho(\mathbf{r}))} \right] \quad (5.47)$$

This relation hold true only if the integrand is smooth inside the integration domain. Now let's look at the second integral of equation (5.46) and manipulate it using (5.47).

$$\begin{aligned} \int_\Omega d^3\mathbf{r}\rho(\mathbf{r}) \left\{ \frac{\partial\epsilon_{xc}}{\partial\rho(\mathbf{r})} \frac{d\rho[\epsilon](\mathbf{r}[\epsilon])}{d\epsilon_{\alpha\beta}} + \frac{\partial\epsilon_{xc}}{\partial(\partial_\mu\rho(\mathbf{r}))} \partial_\mu \frac{d\rho[\epsilon](\mathbf{r}[\epsilon])}{d\epsilon_{\alpha\beta}} \right\} &= - \int_\Omega d^3\mathbf{r} \frac{d\rho[\epsilon](\mathbf{r}[\epsilon])}{d\epsilon_{\alpha\beta}} \epsilon_{xc} + \int_\Omega d^3\mathbf{r} \frac{d\rho[\epsilon](\mathbf{r}[\epsilon])}{d\epsilon_{\alpha\beta}} \epsilon_{xc} \\ &\quad + \int_\Omega d^3\mathbf{r}\rho(\mathbf{r}) \left\{ \frac{\partial\epsilon_{xc}}{\partial\rho(\mathbf{r})} \frac{d\rho[\epsilon](\mathbf{r}[\epsilon])}{d\epsilon_{\alpha\beta}} + \frac{\partial\epsilon_{xc}}{\partial(\partial_\mu\rho(\mathbf{r}))} \partial_\mu \frac{d\rho[\epsilon](\mathbf{r}[\epsilon])}{d\epsilon_{\alpha\beta}} \right\} \\ &= \int_\Omega d^3\mathbf{r} \frac{d\rho[\epsilon](\mathbf{r}[\epsilon])}{d\epsilon_{\alpha\beta}} \left\{ \epsilon_{xc}(\rho(\mathbf{r}), \nabla\rho(\mathbf{r})) + \frac{\partial\epsilon_{xc}}{\partial\rho(\mathbf{r})} - \partial_\mu \left[ \rho(\mathbf{r}) \frac{\partial\epsilon_{xc}}{\partial(\partial_\mu\rho(\mathbf{r}))} \right] \right\} \\ &\quad - \int_\Omega d^3\mathbf{r} \frac{d\rho[\epsilon](\mathbf{r}[\epsilon])}{d\epsilon_{\alpha\beta}} \epsilon_{xc} \\ &= - \int_\Omega d^3\mathbf{r} \frac{d\rho[\epsilon](\mathbf{r}[\epsilon])}{d\epsilon_{\alpha\beta}} \epsilon_{xc} + \int_\Omega d^3\mathbf{r} \frac{d\rho[\epsilon](\mathbf{r}[\epsilon])}{d\epsilon_{\alpha\beta}} \mu_{xc} \end{aligned} \quad (5.48)$$

where  $\mu_{xc}$  (equivalent to  $\mu_{xc}(\rho(\mathbf{r}), \nabla\rho(\mathbf{r}))$ ) is the exchange correlation potential, which is defined as follows.

$$\begin{aligned} \mu_{xc} &= \epsilon_{xc} + \frac{\partial\epsilon_{xc}}{\partial\rho(\mathbf{r})} - \partial_\mu \left[ \rho(\mathbf{r}) \frac{\partial\epsilon_{xc}}{\partial(\partial_\mu\rho(\mathbf{r}))} \right] \\ &= \frac{\partial[\rho(\mathbf{r})\epsilon_{xc}]}{\partial\rho(\mathbf{r})} - \nabla \cdot \frac{\partial[\rho(\mathbf{r})\epsilon_{xc}]}{\partial\nabla\rho(\mathbf{r})} \end{aligned}$$

We get the final expression for the strain variation in GGA exchange-correlation energy by substituting equation (5.48) into (5.46) and the final expression of (5.46) into equation (5.34).

$$\begin{aligned} \left. \frac{dE_{xc}^{GGA}[\epsilon]}{d\epsilon_{\alpha\beta}} \right|_{\epsilon=0} &= \delta_{\alpha\beta} \int_{\Omega} d^3\mathbf{r} \rho(\mathbf{r}) \epsilon_{xc} + \int_{\Omega} d^3\mathbf{r} \frac{d\rho[\epsilon](\mathbf{r}[\epsilon])}{d\epsilon_{\alpha\beta}} \mu_{xc} \\ &\quad - 2 \int_{\Omega} d^3\mathbf{r} \rho(\mathbf{r}) \partial_{\alpha}\rho(\mathbf{r}) \partial_{\beta}\rho(\mathbf{r}) \frac{\partial\epsilon_{xc}}{\partial\sigma} \end{aligned} \quad (5.49)$$

The first and second term in equation (5.49) are similar to equation (5.31). The remaining term represents the additional correction due to a change in the  $\nabla\rho(\mathbf{r})$  with the applied strain. By combining equation (5.31) and (5.49), we write the variation in exchange correlation energy as follows, which applies to both LDA and GGA.

$$\begin{aligned} \left. \frac{dE_{xc}[\epsilon]}{d\epsilon_{\alpha\beta}} \right|_{\epsilon=0} &= \delta_{\alpha\beta} \int_{\Omega} d^3\mathbf{r} \rho(\mathbf{r}) \epsilon_{xc} + \int_{\Omega} d^3\mathbf{r} \frac{d\rho[\epsilon](\mathbf{r}[\epsilon])}{d\epsilon_{\alpha\beta}} \mu_{xc} \\ &\quad - \delta_{GGA} 2 \int_{\Omega} d^3\mathbf{r} \rho(\mathbf{r}) \partial_{\alpha}\rho(\mathbf{r}) \partial_{\beta}\rho(\mathbf{r}) \frac{\partial\epsilon_{xc}}{\partial\sigma}, \end{aligned} \quad (5.50)$$

where  $\delta_{GGA}$  is zero unless GGA exchange correlation energy is used. In the above equation  $\epsilon_{xc}$  [ $\mu_{xc}$ ] is equivalent to  $\epsilon_{xc}(\rho(\mathbf{r}))$  [ $\mu_{xc}(\rho(\mathbf{r}))$ ] for LDA and  $\epsilon_{xc}(\rho(\mathbf{r}), \nabla\rho(\mathbf{r}))$  [ $\mu_{xc}(\rho(\mathbf{r}), \nabla\rho(\mathbf{r}))$ ] for GGA.

## 5.4 Variation of the total energy

So far we have calculated the strain variation of each contribution to the total energy. In this section we calculate the strain variation of the total energy using all the expressions we derived in previous sections. Here first we take the total energy in undistorted system, equation (5.2b), and apply the strain variation on it.

$$\left. \frac{dE_{tot}[\underline{\epsilon}]}{d\epsilon_{\alpha\beta}} \right|_{\underline{\epsilon}=0} = \left. \frac{dE_{kin}[\underline{\epsilon}]}{d\epsilon_{\alpha\beta}} \right|_{\underline{\epsilon}=0} + \left. \frac{dE_{xc}[\underline{\epsilon}]}{d\epsilon_{\alpha\beta}} \right|_{\underline{\epsilon}=0} + \left. \frac{dE_{es}[\underline{\epsilon}]}{d\epsilon_{\alpha\beta}} \right|_{\underline{\epsilon}=0} \quad (5.51)$$

The expressions on the right-hand side of equation (5.51) are already available in sections 5.1, 5.2, and 5.3, respectively. Here we insert them into equation (5.51) and get

$$\begin{aligned}
\left. \frac{dE_{tot}[\underline{\epsilon}]}{d\epsilon_{\alpha\beta}} \right|_{\underline{\epsilon}=0} = & 2 \sum_{v\mathbf{k}} n_{v\mathbf{k}} \Re \left\langle \left. \frac{d\psi_{v\mathbf{k}}[\underline{\epsilon}](\mathbf{r}[\underline{\epsilon}])}{d\epsilon_{\alpha\beta}} \right|_{\underline{\epsilon}=0} \left| \hat{H}_{eff}(\mathbf{r}) - \epsilon_{v\mathbf{k}} \right| \psi_{v\mathbf{k}} \right\rangle \\
& + \frac{1}{2} \sum_{v\mathbf{k}} n_{v\mathbf{k}} \int_{\Omega} d^3\mathbf{r} \psi_{v\mathbf{k}}^*(\mathbf{r}) (\partial_{\alpha}\partial_{\beta} + \partial_{\beta}\partial_{\alpha}) \psi_{v\mathbf{k}}(\mathbf{r}) - \delta_{\alpha\beta} \int_{\Omega} d^3\mathbf{r} \rho(\mathbf{r}) V_{eff}(\mathbf{r}) \\
& - \frac{1}{2} \int_{\Omega} d^3\mathbf{r} \rho_c^a(\mathbf{r}) (r_{\beta}\partial_{\alpha} + r_{\alpha}\partial_{\beta}) V_{eff}(\mathbf{r}) - \cancel{\int_{\Omega} d^3\mathbf{r} V_{eff}(\mathbf{r}) \frac{d\rho[\underline{\epsilon}](\mathbf{r}[\underline{\epsilon}])}{d\epsilon_{\alpha\beta}}} \\
& + \delta_{\alpha\beta} \int_{\Omega} d^3\mathbf{r} \rho(\mathbf{r}) \epsilon_{xc} + \cancel{\int_{\Omega} d^3\mathbf{r} \frac{d\rho[\epsilon](\mathbf{r}[\epsilon])}{d\epsilon_{\alpha\beta}} \mu_{xc}} \\
& - \delta_{GGA} 2 \int_{\Omega} d^3\mathbf{r} \rho(\mathbf{r}) \partial_{\alpha}\rho(\mathbf{r}) \partial_{\beta}\rho(\mathbf{r}) \frac{\partial\epsilon_{xc}}{\partial\sigma} \\
& + \cancel{\int_{\Omega} d^3\mathbf{r} \frac{d\rho[\underline{\epsilon}](\mathbf{r}[\underline{\epsilon}])}{d\epsilon_{\alpha\beta}} V_C(\mathbf{r})} + \frac{1}{2} \frac{\delta}{\delta\epsilon_{\alpha\beta}} \left\{ \int_{\Omega[\underline{\epsilon}]} d^3\mathbf{r}_{\epsilon} \rho((\underline{\epsilon}-\underline{\epsilon})\mathbf{r}_{\epsilon}) V_C[\underline{\epsilon}](\mathbf{r}_{\epsilon}) \right\}_{\underline{\epsilon}=0} \\
& - \frac{1}{2} \sum_a Z_a \frac{\delta}{\delta\epsilon_{\alpha\beta}} V_M[\underline{\epsilon}](\boldsymbol{\tau}_a[\underline{\epsilon}]) \Big|_{\underline{\epsilon}=0}
\end{aligned}$$

The final expression is:

$$\begin{aligned}
\left. \frac{dE_{tot}[\underline{\epsilon}]}{d\epsilon_{\alpha\beta}} \right|_{\underline{\epsilon}=0} = & 2 \sum_{v\mathbf{k}} n_{v\mathbf{k}} \Re \left\langle \left. \frac{d\psi_{v\mathbf{k}}[\underline{\epsilon}](\mathbf{r}[\underline{\epsilon}])}{d\epsilon_{\alpha\beta}} \right|_{\underline{\epsilon}=0} \left| \hat{H}_{eff}(\mathbf{r}) - \epsilon_{v\mathbf{k}} \right| \psi_{v\mathbf{k}} \right\rangle \\
& + \frac{1}{2} \sum_{v\mathbf{k}} n_{v\mathbf{k}} \int_{\Omega} d^3\mathbf{r} \psi_{v\mathbf{k}}^*(\mathbf{r}) (\partial_{\alpha}\partial_{\beta} + \partial_{\beta}\partial_{\alpha}) \psi_{v\mathbf{k}}(\mathbf{r}) \\
& - \frac{1}{2} \int_{\Omega} d^3\mathbf{r} \rho_c^a(\mathbf{r}) (r_{\beta}\partial_{\alpha} + r_{\alpha}\partial_{\beta}) V_{eff}(\mathbf{r}) \\
& + \delta_{\alpha\beta} \int_{\Omega} d^3\mathbf{r} \rho(\mathbf{r}) (\epsilon_{xc} - \mu_{xc}) - \delta_{GGA} 2 \int_{\Omega} d^3\mathbf{r} \rho(\mathbf{r}) \partial_{\alpha}\rho(\mathbf{r}) \partial_{\beta}\rho(\mathbf{r}) \frac{\partial\epsilon_{xc}}{\partial\sigma} \\
& - \delta_{\alpha\beta} \int_{\Omega} d^3\mathbf{r} \rho(\mathbf{r}) V_C(\mathbf{r}) + \frac{1}{2} \frac{\delta}{\delta\epsilon_{\alpha\beta}} \left\{ \int_{\Omega[\underline{\epsilon}]} d^3\mathbf{r}_{\epsilon} \rho((\underline{\epsilon}-\underline{\epsilon})\mathbf{r}_{\epsilon}) V_C[\underline{\epsilon}](\mathbf{r}_{\epsilon}) \right\}_{\underline{\epsilon}=0} \\
& - \frac{1}{2} \sum_a Z_a \frac{\delta}{\delta\epsilon_{\alpha\beta}} V_M[\underline{\epsilon}](\boldsymbol{\tau}_a[\underline{\epsilon}]) \Big|_{\underline{\epsilon}=0} \tag{5.52}
\end{aligned}$$

Equation (5.52) is the final expression of the strain variation in total energy. This expression is used in Chapter 6 to evaluate 'ready-to-implement' form of the total stress tensor formalism. Furthermore, the strain variation of the interstitial charge density and the interstitial Coulomb potential is required when the Coulomb stress tensor is further simplified in section 6.1.1. These two variations are discussed in the following sections.

## 5.5 Variation of the interstitial charge density

The Fourier series expansion of the charge density in the interstitial is

$$\rho_I(\mathbf{r}) = \sum_{\mathbf{G}} \rho_I(\mathbf{G}) e^{i\mathbf{G}\cdot\mathbf{r}} \tag{5.53}$$

with

$$\rho_I(\mathbf{G}) = \frac{1}{\Omega} \int_{\Omega} d^3 \mathbf{r} \rho_I(\mathbf{r}) e^{-i\mathbf{G} \cdot \mathbf{r}} \quad (5.54)$$

When a system is strained by a small amount ( $\underline{\epsilon} \rightarrow 0$ )

$$\rho_I[\underline{\epsilon}](\mathbf{G}[\underline{\epsilon}]) = \frac{1}{\Omega[\underline{\epsilon}]} \int_{\Omega[\underline{\epsilon}]} d^3 \mathbf{r}_\epsilon \rho_I[\underline{\epsilon}](\mathbf{r}_\epsilon) e^{-i\mathbf{G}[\underline{\epsilon}] \cdot \mathbf{r}_\epsilon} \quad (5.55)$$

As we have discussed in section 5.2, we replace the physically strained electronic charge density  $\rho_I[\underline{\epsilon}](\mathbf{r}_\epsilon)$  by the ‘smeared’ charge density  $\rho_I((\underline{1} - \underline{\epsilon})\mathbf{r})$ .

$$\begin{aligned} \rho_I[\underline{\epsilon}](\mathbf{G}[\underline{\epsilon}]) &= \frac{1}{\Omega[\underline{\epsilon}]} \int_{\Omega[\underline{\epsilon}]} d^3 \mathbf{r}_\epsilon \rho_I((\underline{1} - \underline{\epsilon})\mathbf{r}_\epsilon) e^{-i\mathbf{G}[\underline{\epsilon}] \cdot \mathbf{r}_\epsilon} \\ &= \frac{1}{\Omega} \int_{\Omega} d^3 \mathbf{r} \rho_I((\underline{1} - \underline{\epsilon})\mathbf{r}[\underline{\epsilon}]) e^{-i\mathbf{G} \cdot \mathbf{r}} \\ &= \frac{1}{\Omega} \int_{\Omega} d^3 \mathbf{r} \rho_I((\underline{1} - \underline{\epsilon})(\underline{1} + \underline{\epsilon})\mathbf{r}) e^{-i\mathbf{G} \cdot \mathbf{r}} \\ &= \frac{1}{\Omega} \int_{\Omega} d^3 \mathbf{r} \rho_I(\mathbf{r}) e^{-i\mathbf{G} \cdot \mathbf{r}} \\ &= \rho_I(\mathbf{G}) \end{aligned} \quad (5.56)$$

A similar concept will be used for the pseudo-charge density  $\tilde{\rho}_a$ .

$$\tilde{\rho}_a[\underline{\epsilon}](\mathbf{G}[\underline{\epsilon}]) = \tilde{\rho}_a(\mathbf{G}) \quad (5.57a)$$

This concept is different from Klüppelberg et. al (equation (3.25) in Ref. [19]) and it greatly simplifies the electrostatic stress tensor in the interstitial, which we see in section 6.1.1. We see from the above equations that the Fourier components of the plane wave charge density as well as pseudo-charge density are independent of whether the system is strained or not.

$$\rho_I[\underline{\epsilon}](\mathbf{G}[\underline{\epsilon}]) = \rho_I(\mathbf{G}) \quad (5.58)$$

$$\tilde{\rho}_a[\underline{\epsilon}](\mathbf{G}[\underline{\epsilon}]) = \tilde{\rho}_a(\mathbf{G}) \quad (5.59)$$

Which gives

$$\left. \frac{\partial}{\partial \epsilon_{\alpha\beta}} \right|_{\underline{\epsilon}=0} \rho_I[\underline{\epsilon}](\mathbf{G}[\underline{\epsilon}]) = 0 \quad (5.60)$$

$$\left. \frac{\partial}{\partial \epsilon_{\alpha\beta}} \right|_{\underline{\epsilon}=0} \tilde{\rho}_a[\underline{\epsilon}](\mathbf{G}[\underline{\epsilon}]) = 0 \quad (5.61)$$

## 5.6 Variation of the interstitial Coulomb potential

In the interstitial region, the Coulomb potential is defined as:

$$V_C(\mathbf{r}) = \sum_{\mathbf{G} \neq 0} V_C(\mathbf{G}) e^{i\mathbf{G} \cdot \mathbf{r}}, \quad (5.62)$$

where  $\mathbf{G} = 0$  is excluded because  $\mathbf{G}$  is in the denominator in the expression of  $V_C(\mathbf{G})$ , see equation (4.23). In the strained system:

$$V_C[\underline{\epsilon}](\mathbf{r}[\underline{\epsilon}]) = \sum_{\mathbf{G} \neq 0} V_C[\underline{\epsilon}](\mathbf{G}[\underline{\epsilon}]) e^{i\mathbf{G}[\underline{\epsilon}] \cdot \mathbf{r}[\underline{\epsilon}]} \quad (5.63)$$

$$V_C[\underline{\epsilon}](\mathbf{r}[\underline{\epsilon}]) = \sum_{\mathbf{G} \neq 0} V_C[\underline{\epsilon}](\mathbf{G}[\underline{\epsilon}]) e^{i(\mathbf{G} \cdot \mathbf{r} + O(\underline{\epsilon}^2))} \quad (5.64)$$

The strain variation of the equation (5.64)

$$\frac{\partial}{\partial \epsilon_{\alpha\beta}} V_C[\underline{\epsilon}](\mathbf{r}[\underline{\epsilon}]) \Big|_{\underline{\epsilon}=0} = \sum_{\mathbf{G} \neq 0} \frac{\partial V_C[\underline{\epsilon}](\mathbf{G}[\underline{\epsilon}])}{\partial \epsilon_{\alpha\beta}} \Big|_{\underline{\epsilon}=0} e^{i\mathbf{G} \cdot \mathbf{r}} \quad (5.65)$$

Writing the equation (4.23) in the deformed system gives

$$V_C[\underline{\epsilon}](\mathbf{G}[\underline{\epsilon}]) = \frac{4\pi}{\mathbf{G}[\underline{\epsilon}]^2} \tilde{\rho}[\underline{\epsilon}](\mathbf{G}[\underline{\epsilon}]) = \frac{4\pi}{\mathbf{G}[\underline{\epsilon}]^2} \left( \tilde{\rho}_a[\underline{\epsilon}](\mathbf{G}[\underline{\epsilon}]) + \rho_I[\underline{\epsilon}](\mathbf{G}[\underline{\epsilon}]) \right) \quad (5.66)$$

Apply  $\frac{\partial}{\partial \epsilon_{\alpha\beta}} \Big|_{\underline{\epsilon}=0}$  on both sides of the above equation:

$$\begin{aligned} \frac{\partial}{\partial \epsilon_{\alpha\beta}} V_C[\underline{\epsilon}](\mathbf{G}[\underline{\epsilon}]) \Big|_{\underline{\epsilon}=0} &= \frac{\partial}{\partial \epsilon_{\alpha\beta}} \frac{4\pi}{\mathbf{G}[\underline{\epsilon}]^2} \left( \tilde{\rho}_a[\underline{\epsilon}](\mathbf{G}[\underline{\epsilon}]) + \rho_I[\underline{\epsilon}](\mathbf{G}[\underline{\epsilon}]) \right) \Big|_{\underline{\epsilon}=0} \\ &= \frac{\partial}{\partial \epsilon_{\alpha\beta}} \frac{4\pi}{\mathbf{G}[\underline{\epsilon}]^2} \Big|_{\underline{\epsilon}=0} \left( \tilde{\rho}_a(\mathbf{G}) + \rho_I(\mathbf{G}) \right) + \frac{4\pi}{\mathbf{G}^2} \frac{\partial}{\partial \epsilon_{\alpha\beta}} \left( \tilde{\rho}_a[\underline{\epsilon}](\mathbf{G}[\underline{\epsilon}]) + \rho_I[\underline{\epsilon}](\mathbf{G}[\underline{\epsilon}]) \right) \Big|_{\underline{\epsilon}=0} \end{aligned} \quad (5.67)$$

Equations (5.58) and (5.59) show that the Fourier components of the plane wave charge density and pseudo-charge density remain the same even if the system is deformed. Therefore, the contribution of the second term of the equation (5.67) vanishes. However, in equation (5.31a) of Ref. [19], the author assumed the Fourier components of the plane wave charge density is independent of the strain but not the Fourier components of the pseudo charge density. This leads to a different expression of the strain variation of the Coulomb potential than our equation (5.68). In equation (5.32) in Ref. [19], the variation of the Coulomb potential is considered, and this expression contains the contribution from the change of the pseudo-charge density, which is not present in our formulation.

$$\frac{\partial}{\partial \epsilon_{\alpha\beta}} V_C[\underline{\epsilon}](\mathbf{G}[\underline{\epsilon}]) \Big|_{\underline{\epsilon}=0} = \frac{\partial}{\partial \epsilon_{\alpha\beta}} \frac{4\pi}{\mathbf{G}[\underline{\epsilon}]^2} \Big|_{\underline{\epsilon}=0} \left( \tilde{\rho}_a(\mathbf{G}) + \rho_I(\mathbf{G}) \right)$$

Using equation (A.15), we get

$$\frac{\partial}{\partial \epsilon_{\alpha\beta}} V_C[\underline{\epsilon}](\mathbf{G}[\underline{\epsilon}]) \Big|_{\underline{\epsilon}=0} = \frac{4\pi}{\mathbf{G}^2} 2\hat{\mathbf{G}}_\alpha \hat{\mathbf{G}}_\beta (\tilde{\rho}_a(\mathbf{G}) + \rho_I(\mathbf{G})) \quad (5.68)$$

The change in the Coulomb potential is only due to the change of the reciprocal lattice vector. Now, the final expression of the strain variation of the Coulomb potential in the interstitial region is:

$$\frac{\partial}{\partial \epsilon_{\alpha\beta}} V_C[\underline{\epsilon}](\mathbf{G}[\underline{\epsilon}]) \Big|_{\underline{\epsilon}=0} = \frac{8\pi \hat{\mathbf{G}}_\alpha \hat{\mathbf{G}}_\beta}{\mathbf{G}^2} (\tilde{\rho}_a(\mathbf{G}) + \rho_I(\mathbf{G})) \stackrel{(4.23)}{=} 2\hat{\mathbf{G}}_\alpha \hat{\mathbf{G}}_\beta V_C(\mathbf{G}) \quad (5.69)$$

# Chapter 6

## Stress tensor

In the previous chapter we defined and calculated the variation of energies according to the strain applied in the system. In this chapter we use this information to define the total stress tensor. The total stress tensor is defined as

$$\sigma_{\alpha\beta} = \frac{1}{\Omega} \left. \frac{dE_{tot}[\underline{\epsilon}]}{d\epsilon_{\alpha\beta}} \right|_{\underline{\epsilon}=0} \quad (6.1)$$

The variation of the total energy according to applied strained is provided in equation (5.52). Using equation (5.52)

$$\begin{aligned} \sigma_{\alpha\beta} &= -\frac{\delta_{\alpha\beta}}{\Omega} \int_{\Omega} d^3\mathbf{r} \rho(\mathbf{r}) V_C(\mathbf{r}) + \frac{1}{2\Omega} \frac{d}{d\epsilon_{\alpha\beta}} \left\{ \int_{\Omega[\underline{\epsilon}]} d^3\mathbf{r}_\epsilon \rho((\underline{1} - \underline{\epsilon})\mathbf{r}_\epsilon) V_C[\underline{\epsilon}](\mathbf{r}_\epsilon) \right\}_{\underline{\epsilon}=0} \\ &\quad - \frac{1}{2\Omega} \sum_a Z_a \frac{d}{d\epsilon_{\alpha\beta}} V_M[\underline{\epsilon}](\boldsymbol{\tau}_a[\underline{\epsilon}]) \Big|_{\underline{\epsilon}=0} - \frac{1}{2\Omega} \sum_a \int_{\Omega} d^3\mathbf{r} \rho_c^a(\mathbf{r}) (r_\beta \partial_\alpha + r_\alpha \partial_\beta) V_{eff}(\mathbf{r}) \\ &\quad + \frac{1}{2\Omega} \sum_{v\mathbf{k}} n_{v\mathbf{k}} \int_{\Omega} d^3\mathbf{r} \psi_{v\mathbf{k}}^*(\mathbf{r}) (\partial_\alpha \partial_\beta + \partial_\beta \partial_\alpha) \psi_{v\mathbf{k}}(\mathbf{r}) \\ &\quad + \frac{2}{\Omega} \sum_{v\mathbf{k}} n_{v\mathbf{k}} \Re \left\langle \frac{d\psi_{v\mathbf{k}}[\underline{\epsilon}][\underline{\epsilon}](\mathbf{r}[\underline{\epsilon}])}{d\epsilon_{\alpha\beta}} \right\rangle_{\underline{\epsilon}=0} \left| \widehat{H}_{eff}(\mathbf{r}) - \epsilon_{v\mathbf{k}} \right| \psi_{v\mathbf{k}} \rangle \\ &\quad + \frac{\delta_{\alpha\beta}}{\Omega} \int_{\Omega} d^3\mathbf{r} \rho(\mathbf{r}) (\epsilon_{xc} - \mu_{xc}) - \frac{2\delta_{GGA}}{\Omega} \int_{\Omega} d^3\mathbf{r} \rho(\mathbf{r}) \partial_\alpha \rho(\mathbf{r}) \partial_\beta \rho(\mathbf{r}) \frac{\partial \epsilon_{xc}}{\partial \sigma} \end{aligned}$$

For the sake of brevity, we introduce short stress notations for the expressions at the right hand side of the above equation and decompose the electronic states into core and valence.

$$\sigma_{\alpha\beta} = \sigma_{\alpha\beta}^{es} + \sigma_{\alpha\beta}^{core} + \sigma_{\alpha\beta}^{val,kin} + \sigma_{\alpha\beta}^{val,corr} + \sigma_{\alpha\beta}^{xc}, \quad (6.2)$$

where  $\sigma_{\alpha\beta}^{es}$ ,  $\sigma_{\alpha\beta}^{core}$ ,  $\sigma_{\alpha\beta}^{val,kin}$ ,  $\sigma_{\alpha\beta}^{val,corr}$ , and  $\sigma_{\alpha\beta}^{xc}$  are the contributions in the total stress tensor from electrostatic energy, core correction, valence kinetic energy, valance correction,

and exchange correlation energy, respectively.

$$\begin{aligned}\sigma_{\alpha\beta}^{es} &= -\frac{\delta_{\alpha\beta}}{\Omega} \int_{\Omega} d^3\mathbf{r} \rho(\mathbf{r}) V_C(\mathbf{r}) + \frac{1}{2\Omega} \frac{d}{d\epsilon_{\alpha\beta}} \left\{ \int_{\Omega[\underline{\epsilon}]} d^3\mathbf{r}_\epsilon \rho((\underline{1} - \underline{\epsilon})\mathbf{r}_\epsilon) V_C[\underline{\epsilon}](\mathbf{r}_\epsilon) \right\}_{\underline{\epsilon}=0} \\ &\quad - \frac{1}{2\Omega} \sum_a Z_a \frac{d}{d\epsilon_{\alpha\beta}} V_M[\underline{\epsilon}](\boldsymbol{\tau}_a[\underline{\epsilon}]) \Big|_{\underline{\epsilon}=0}\end{aligned}\quad (6.3a)$$

$$\sigma_{\alpha\beta}^{core} = -\frac{1}{2\Omega} \sum_a \int_{\Omega} d^3\mathbf{r} \rho_c^a(\mathbf{r}) (r_\beta \partial_\alpha + r_\alpha \partial_\beta) V_{eff}(\mathbf{r}) \quad (6.3b)$$

$$\sigma_{\alpha\beta}^{val,kin} = \frac{1}{2\Omega} \sum_{v\mathbf{k}} n_{v\mathbf{k}} \int_{\Omega} d^3\mathbf{r} \psi_{v\mathbf{k}}^*(\mathbf{r}) (\partial_\alpha \partial_\beta + \partial_\beta \partial_\alpha) \psi_{v\mathbf{k}}(\mathbf{r}) \quad (6.3c)$$

$$\sigma_{\alpha\beta}^{val,corr} = \frac{2}{\Omega} \sum_{v\mathbf{k}} n_{v\mathbf{k}} \Re \left\langle \frac{d\psi_{v\mathbf{k}}[\underline{\epsilon}](\mathbf{r}[\underline{\epsilon}])}{d\epsilon_{\alpha\beta}} \Big|_{\underline{\epsilon}=0} \left| \widehat{H}_{eff}(\mathbf{r}) - \epsilon_{v\mathbf{k}} \right| \psi_{v\mathbf{k}} \right\rangle \quad (6.3d)$$

$$\begin{aligned}\sigma_{\alpha\beta}^{xc} &= \frac{\delta_{\alpha\beta}}{\Omega} \int_{\Omega} d^3\mathbf{r} \rho(\mathbf{r}) (\epsilon_{xc} - \mu_{xc}) \\ &\quad - \frac{2\delta_{GGA}}{\Omega} \int_{\Omega} d^3\mathbf{r} \rho(\mathbf{r}) \partial_\alpha \rho(\mathbf{r}) \partial_\beta \rho(\mathbf{r}) \frac{\partial \epsilon_{xc}}{\partial \sigma}\end{aligned}\quad (6.3e)$$

Most of the above expressions are in their general form. Therefore, further simplification is needed and is provided in the following sections.

## 6.1 Electrostatic Stress Tensor

The electrostatic stress tensor ( $\sigma_{\alpha\beta}^{es}$ ) is determined from the variation in electrostatic energy according to the applied strain. The expression of  $\sigma_{\alpha\beta}^{es}$  as given in equation (6.3a) is:

$$\begin{aligned}\sigma_{\alpha\beta}^{es} &= -\frac{\delta_{\alpha\beta}}{\Omega} \int_{\Omega} d^3\mathbf{r} \rho(\mathbf{r}) V_C(\mathbf{r}) + \frac{1}{2\Omega} \frac{d}{d\epsilon_{\alpha\beta}} \left|_{\underline{\epsilon}=0} \int_{\Omega[\underline{\epsilon}]} d^3\mathbf{r}_\epsilon \rho((\underline{1} - \underline{\epsilon})\mathbf{r}_\epsilon) V_C[\underline{\epsilon}](\mathbf{r}_\epsilon)\right. \\ &\quad \left. - \frac{1}{2\Omega} \sum_{a\in\Omega} Z_a \frac{d}{d\epsilon_{\alpha\beta}} \Big|_{\underline{\epsilon}=0} V_M^a[\underline{\epsilon}](\boldsymbol{\tau}_a[\underline{\epsilon}])\right.\end{aligned}\quad (6.4)$$

The first term of the above equation is in its simplest possible form. The remaining second and third terms need to be further simplified. For this purpose, we consider the Coulomb stress tensor ( $\sigma_{\alpha\beta}^C$ ) and the Madelung stress tensor ( $\sigma_{\alpha\beta}^M$ ) separately as follows.

### 6.1.1 Coulomb Stress Tensor

The expression of the Coulomb stress tensor ( $\sigma_{\alpha\beta}^C$ ) is:

$$\sigma_{\alpha\beta}^C = \frac{1}{2\Omega} \frac{d}{d\epsilon_{\alpha\beta}} \left|_{\underline{\epsilon}=0} \int_{\Omega[\underline{\epsilon}]} d^3\mathbf{r}_\epsilon \rho((\underline{1} - \underline{\epsilon})\mathbf{r}_\epsilon) V_C[\underline{\epsilon}](\mathbf{r}_\epsilon)\right. \quad (6.5a)$$

The strained Coulomb potential ( $V_C[\underline{\epsilon}](\mathbf{r}_\epsilon)$ ) is given in equation (5.25a).  $\rho((\underline{1} - \underline{\epsilon})\mathbf{r}_\epsilon)$  is the electronic charge density of an undistorted lattice but smeared over a distorted lattice.

$$V_C[\underline{\epsilon}](\mathbf{r}_\epsilon) = \int d^3\mathbf{r}'_\epsilon \frac{\rho((\underline{1} - \underline{\epsilon})\mathbf{r}'_\epsilon)}{|\mathbf{r}_\epsilon - \mathbf{r}'_\epsilon|} - \sum_b \frac{Z_b}{|\mathbf{r}_\epsilon - \boldsymbol{\tau}_b[\underline{\epsilon}]|} \quad (6.6)$$

The right hand side of equation (6.5a) is

$$\begin{aligned} \frac{d}{d\epsilon_{\alpha\beta}} \left|_{\underline{\epsilon}=0} \right. \int_{\Omega[\underline{\epsilon}]} d^3\mathbf{r}_\epsilon \rho((\underline{1} - \underline{\epsilon})\mathbf{r}_\epsilon) V_C[\underline{\epsilon}](\mathbf{r}_\epsilon) &= \frac{d}{d\epsilon_{\alpha\beta}} \left|_{\underline{\epsilon}=0} \right. \det(\underline{1} + \underline{\epsilon}) \int_{\Omega} d^3\mathbf{r} \rho(\mathbf{r}) V_C[\underline{\epsilon}](\mathbf{r}[\underline{\epsilon}]) \\ &= \delta_{\alpha\beta} \int_{\Omega} d^3\mathbf{r} \rho(\mathbf{r}) V_C(\mathbf{r}) + \int_{\Omega} d^3\mathbf{r} \rho(\mathbf{r}) \frac{dV_C[\underline{\epsilon}](\mathbf{r}[\underline{\epsilon}])}{d\epsilon_{\alpha\beta}} \Big|_{\underline{\epsilon}=0} \end{aligned}$$

Equation (6.5a) becomes

$$2\Omega\sigma_{\alpha\beta}^C = \delta_{\alpha\beta} \int_{\Omega} d^3\mathbf{r} \rho(\mathbf{r}) V_C(\mathbf{r}) + \int_{\Omega} d^3\mathbf{r} \rho(\mathbf{r}) \frac{dV_C[\underline{\epsilon}](\mathbf{r}[\underline{\epsilon}])}{d\epsilon_{\alpha\beta}} \Big|_{\underline{\epsilon}=0} \quad (6.7)$$

A decomposition of the integrals into interstitial and spheres according to equation (A.36) gives the following expression.

$$\begin{aligned} 2\Omega\sigma_{\alpha\beta}^C &= \delta_{\alpha\beta} \int_{\Omega} d^3\mathbf{r} \Theta_{IS}(\mathbf{r}) \rho(\mathbf{r}) V_C(\mathbf{r}) + \int_{\Omega} d^3\mathbf{r} \Theta_{IS}(\mathbf{r}) \rho(\mathbf{r}) \frac{dV_C[\underline{\epsilon}](\mathbf{r}[\underline{\epsilon}])}{d\epsilon_{\alpha\beta}} \Big|_{\underline{\epsilon}=0} + \\ &\quad \delta_{\alpha\beta} \sum_a \int_{\Omega} d^3\mathbf{r} \Theta_a(\mathbf{r}) \rho(\mathbf{r}) V_C(\mathbf{r}) + \sum_a \int_{\Omega} d^3\mathbf{r} \Theta_a(\mathbf{r}) \rho(\mathbf{r}) \frac{dV_C[\underline{\epsilon}](\mathbf{r}[\underline{\epsilon}])}{d\epsilon_{\alpha\beta}} \Big|_{\underline{\epsilon}=0} \quad (6.8) \\ &= 2\Omega\sigma_{\alpha\beta}^{C,IS} + 2\Omega\sigma_{\alpha\beta}^{C,R_a} \quad (6.9) \end{aligned}$$

where  $\Theta_{IS}(\mathbf{r})(\Theta_a(\mathbf{r}))$  is a Heavyside type of step function, and it is used to separate the integration domains.  $\Theta_{IS}(\mathbf{r})(\Theta_a(\mathbf{r}))$  is 1 in the interstitial (atomic spheres) region and 0 in the region of the atomic spheres (interstitial). In equation (6.9), the Coulomb stress tensor is divided into  $\sigma_{\alpha\beta}^{C,IS}$  and  $\sigma_{\alpha\beta}^{C,R_a}$ , which denote the Coulomb stress tensor in interstitial and in the region of the atomic sphere.

The simplification of the Coulomb stress tensor will be carried out separately in the interstitial region and the atomic spheres. The simplification in the interstitial is much easier since the density and potential are in their simplest form i.e. plane wave expansion. First, we consider the interstitial electrostatic stress and move on to the region of the atomic spheres.

$$2\Omega\sigma_{\alpha\beta}^{C,IS} = \delta_{\alpha\beta} \int_{\Omega} d^3\mathbf{r} \Theta_{IS}(\mathbf{r}) \rho(\mathbf{r}) V_C(\mathbf{r}) + \int_{\Omega} d^3\mathbf{r} \Theta_{IS}(\mathbf{r}) \rho(\mathbf{r}) \frac{dV_C[\underline{\epsilon}](\mathbf{r}[\underline{\epsilon}])}{d\epsilon_{\alpha\beta}} \Big|_{\underline{\epsilon}=0} \quad (6.10)$$

In the APW based methods, both the charge density and potential at the interstitial region are expanded via Fourier series as given in equations (3.26) and (5.62). To simplify the r.h.s of the above equation, we recall equations (3.26) and (5.62) for the charge density and potential, and for the strain variation of the Coulomb potential, we recall equation (5.69).

$$2\Omega\sigma_{\alpha\beta}^{C,IS} = \sum_{\mathbf{G}} \sum_{\mathbf{G}'\neq 0} \delta_{\alpha\beta} \int_{\Omega} d^3\mathbf{r} \Theta_{IS}(\mathbf{r}) \rho^*(\mathbf{G}) V_C(\mathbf{G}') e^{-i(\mathbf{G}-\mathbf{G}')\cdot\mathbf{r}} + \sum_{\mathbf{G}} \sum_{\mathbf{G}'\neq 0} \int_{\Omega} d^3\mathbf{r} \Theta_{IS}(\mathbf{r}) \rho^*(\mathbf{G}) 2\hat{\mathbf{G}}'_{\alpha} \hat{\mathbf{G}}'_{\beta} V_C(\mathbf{G}') e^{-i(\mathbf{G}-\mathbf{G}')\cdot\mathbf{r}} \quad (6.11)$$

The Fourier transform of three-dimensional step function is

$$\Theta(\mathbf{G} - \mathbf{G}') = \frac{1}{\Omega} \int_{\Omega} d^3\mathbf{r} \Theta_{IS}(\mathbf{r}) e^{-i(\mathbf{G}-\mathbf{G}')\cdot\mathbf{r}} \quad (6.12)$$

Using this relation, the interstitial Coulomb stress becomes

$$2\Omega\sigma_{\alpha\beta}^{C,IS} = \Omega \sum_{\mathbf{G}} \sum_{\mathbf{G}'\neq 0} \rho^*(\mathbf{G}) \left( \delta_{\alpha\beta} V_C(\mathbf{G}') + 2\hat{\mathbf{G}}'_{\alpha} \hat{\mathbf{G}}'_{\beta} V_C(\mathbf{G}') \right) \Theta(\mathbf{G} - \mathbf{G}') \quad (6.13)$$

Again, from equation (6.9), the electrostatic stress tensor in the atomic spheres is

$$2\Omega\sigma_{\alpha\beta}^{C,R_a} = \delta_{\alpha\beta} \sum_a \int_{\Omega} d^3\mathbf{r} \Theta_a(\mathbf{r}) \rho(\mathbf{r}) V_C(\mathbf{r}) + \sum_a \int_{\Omega} d^3\mathbf{r} \Theta_a(\mathbf{r}) \rho(\mathbf{r}) \frac{dV_C[\underline{\epsilon}](\mathbf{r}[\underline{\epsilon}])}{d\underline{\epsilon}_{\alpha\beta}} \Big|_{\underline{\epsilon}=0} \quad (6.14)$$

The first expression of the above equation is already in its simplest form, so the focus will be given to solve the second integral. It is clear from Eq. (6.14) that to evaluate the second integral we need to calculate the strain variation of the Coulomb potential. Two different approaches are available in Refs. [12] and [19] to calculate the change in the potential under infinitesimal strain, but due to the lack of sufficient results it is unclear which approach works best for the original LAPW method. In Ref. [12], the authors suggest that the strain potential can be determined directly from the strained charge density using Poisson's equation. In contrast, in Ref. [19] an explicit derivation of the strain variation of the Coulomb potential using Weinert's method was presented. We tried to work with the expression provided in Ref. [19] first, but unfortunately this resulted in huge errors in the calculated stress tensor and we could not figure out where the problem was actually originating from. Therefore, in the following, we use a different approach to simplify the strain variation of the Coulomb potential.

We first consider equation (5.25a) and the integral involved in equation (5.25a) is transformed back from the strain to unstrained system, which ultimately results in the following expression.

$$V_C[\epsilon](\mathbf{r}[\underline{\epsilon}]) = \int d^3\mathbf{r}' \frac{\det(1 + \underline{\epsilon}) \rho(\mathbf{r}')} {|\mathbf{r}[\underline{\epsilon}] - \mathbf{r}'[\underline{\epsilon}]|} - \sum_b \frac{Z_b}{|\mathbf{r}[\underline{\epsilon}] - \boldsymbol{\tau}_b[\underline{\epsilon}]|} \quad (6.15)$$

As we can see in Eq.(6.14) we need the strained variation of Eq. (6.15) only inside the atomic spheres. In general, an integral in Eq.(6.15) should be evaluated over the entire crystal, but based on the references [17],[43],and [45] this integral is only considered within the unit cell in the following manipulation.

The change of the strained Coulomb potential with respect to strain is:

$$\frac{dV_C[\epsilon](\mathbf{r}[\underline{\epsilon}])}{d\epsilon_{\alpha\beta}} \Big|_{\underline{\epsilon}=0} = \delta_{\alpha\beta} \int d^3\mathbf{r}' \frac{\rho(\mathbf{r}')}{|\mathbf{r} - \mathbf{r}'|} + \int d^3\mathbf{r}' \frac{d}{d\epsilon_{\alpha\beta}} \frac{\rho(\mathbf{r}')}{|\mathbf{r}[\underline{\epsilon}] - \mathbf{r}'[\underline{\epsilon}]|} \Bigg|_{\underline{\epsilon}=0} \quad (6.16)$$

$$- \sum_b \frac{d}{d\epsilon_{\alpha\beta}} \frac{Z_b}{|\mathbf{r}[\underline{\epsilon}] - \boldsymbol{\tau}_b[\underline{\epsilon}]|} \Bigg|_{\underline{\epsilon}=0} \quad (6.17)$$

$$= \delta_{\alpha\beta} \left\{ \int d^3\mathbf{r}' \frac{\rho(\mathbf{r}')}{|\mathbf{r} - \mathbf{r}'|} - \sum_b \frac{Z_b}{|\mathbf{r} - \boldsymbol{\tau}_b|} \right\} + \delta_{\alpha\beta} \sum_b \frac{Z_b}{|\mathbf{r} - \boldsymbol{\tau}_b|} + \left\{ \int d^3\mathbf{r}' \frac{d}{d\epsilon_{\alpha\beta}} \frac{\rho(\mathbf{r}')}{|\mathbf{r}[\underline{\epsilon}] - \mathbf{r}'[\underline{\epsilon}]|} \Bigg|_{\underline{\epsilon}=0} - \sum_b \frac{d}{d\epsilon_{\alpha\beta}} \frac{Z_b}{|\mathbf{r}[\underline{\epsilon}] - \boldsymbol{\tau}_b[\underline{\epsilon}]|} \Bigg|_{\underline{\epsilon}=0} \right\} \quad (6.18)$$

In equation (6.18), the second expression in the curly bracket and the third expression on the first line are the same but have opposite sign, and they are introduced to make subsequent calculations easier. The expression in the first curly bracket is nothing else than the Coulomb potential. The expressions in the second curly bracket need to be further simplified, and this is achieved using the following relationships:

$$\begin{aligned} & \frac{d}{d\epsilon_{\alpha\beta}} \frac{1}{|\mathbf{r}[\epsilon] - \mathbf{r}'[\epsilon]|} \Bigg|_{\underline{\epsilon}=0} \\ & \stackrel{(A.15)}{=} -\frac{1}{|\mathbf{r} - \mathbf{r}'|} ((\widehat{\mathbf{r} - \mathbf{r}'})_\alpha (\widehat{\mathbf{r} - \mathbf{r}'})_\beta) \\ & \stackrel{(A.1)}{=} -\frac{1}{|\mathbf{r} - \mathbf{r}'|} \sum_{t,t'=-1}^1 c_{\alpha t} c_{\beta t'} Y_{1t}(\hat{\mathbf{r}}) Y_{1t'}(\hat{\mathbf{r}}) \end{aligned} \quad (6.19)$$

Similarly,

$$\begin{aligned} & \frac{d}{d\epsilon_{\alpha\beta}} \frac{1}{|\mathbf{r}[\epsilon] - \boldsymbol{\tau}_b[\epsilon]|} \Bigg|_{\underline{\epsilon}=0} \\ & = -\frac{1}{|\mathbf{r} - \boldsymbol{\tau}_b|} ((\widehat{\mathbf{r} - \boldsymbol{\tau}_b})_\alpha (\widehat{\mathbf{r} - \boldsymbol{\tau}_b})_\beta) \\ & = -\frac{1}{|\mathbf{r} - \boldsymbol{\tau}_b|} \sum_{t,t'=-1}^1 c_{\alpha t} c_{\beta t'} Y_{1t}(\hat{\mathbf{r}}) Y_{1t'}(\hat{\mathbf{r}}) \end{aligned} \quad (6.20)$$

Also, the expression in the first curly bracket in equation (6.18) will be replaced by the following relation.

$$V_C(\mathbf{r}) = \int d^3\mathbf{r}' \frac{\rho(\mathbf{r}')}{|\mathbf{r} - \mathbf{r}'|} - \sum_b \frac{Z_b}{|\mathbf{r} - \boldsymbol{\tau}_b|} \quad (6.21)$$

Substituting the equations (6.19), (6.20), and (6.21) in equation (6.18).

$$\begin{aligned} \frac{dV_C[\epsilon](\mathbf{r}[\underline{\epsilon}])}{d\epsilon_{\alpha\beta}} \Big|_{\underline{\epsilon}=0} &= \delta_{\alpha\beta} V_C(\mathbf{r}) + \delta_{\alpha\beta} \sum_b \frac{Z_b}{|\mathbf{r} - \boldsymbol{\tau}_b|} \\ &\quad - V_C(\mathbf{r}) \sum_{t,t'=-1}^1 c_{\alpha t} c_{\beta t'} Y_{1t}(\hat{\mathbf{r}}) Y_{1t'}(\hat{\mathbf{r}}) \end{aligned} \quad (6.22)$$

Substituting equation (6.22) in equation (6.14) yields

$$\begin{aligned} 2\Omega\sigma_{\alpha\beta}^{C,R_a} &= 2\delta_{\alpha\beta} \sum_a \int_{\Omega} d^3\mathbf{r} \Theta_a(\mathbf{r}) \rho(\mathbf{r}) V_C(\mathbf{r}) + \delta_{\alpha\beta} \sum_b \int_{\Omega} d^3\mathbf{r} \Theta_b(\mathbf{r}) \rho(\mathbf{r}) \frac{Z_b}{|\mathbf{r} - \boldsymbol{\tau}_b|} \\ &\quad - \sum_a \sum_{t,t'=-1}^1 c_{\alpha t} c_{\beta t'} \int_{\Omega} d^3\mathbf{r} \Theta_a(\mathbf{r}) \rho(\mathbf{r}) V_C(\mathbf{r}) Y_{1t}(\hat{\mathbf{r}}) Y_{1t'}(\hat{\mathbf{r}}) \end{aligned} \quad (6.23)$$

The final Coulomb stress tensor is obtained by substituting equations (6.23) and (6.13) in equation (6.9):

$$\begin{aligned} 2\Omega\sigma_{\alpha\beta}^C &= \Omega \sum_{\mathbf{G}} \sum_{\mathbf{G}' \neq 0} \rho^*(\mathbf{G}) \left( \delta_{\alpha\beta} V_C(\mathbf{G}') + 2\hat{\mathbf{G}}'_\alpha \hat{\mathbf{G}}'_\beta V_C(\mathbf{G}') \right) \Theta(\mathbf{G} - \mathbf{G}') \\ &\quad - \sum_a \sum_{t,t'=-1}^1 c_{\alpha t} c_{\beta t'} \int_{\Omega} d^3\mathbf{r} \Theta_a(\mathbf{r}) \rho(\mathbf{r}) V_C(\mathbf{r}) Y_{1t}(\hat{\mathbf{r}}) Y_{1t'}(\hat{\mathbf{r}}) \\ &\quad + 2\delta_{\alpha\beta} \sum_a \int_{\Omega} d^3\mathbf{r} \Theta_a(\mathbf{r}) \rho(\mathbf{r}) V_C(\mathbf{r}) \\ &\quad + \delta_{\alpha\beta} \sum_b \int_{\Omega} d^3\mathbf{r} \Theta_b(\mathbf{r}) \rho(\mathbf{r}) \frac{Z_b}{|\mathbf{r} - \boldsymbol{\tau}_b|} \end{aligned} \quad (6.24)$$

### 6.1.2 Madelung Stress Tensor

The Madelung stress tensor  $\sigma_{\alpha\beta}^M$  is:

$$\sigma_{\alpha\beta}^M = -\frac{1}{2\Omega} \sum_{a \in \Omega} Z_a \frac{d}{d\epsilon_{\alpha\beta}} \Big|_{\underline{\epsilon}=0} V_M^a[\underline{\epsilon}](\boldsymbol{\tau}_a[\underline{\epsilon}]) \quad (6.25)$$

The strained Madelung ( $V_M^a[\underline{\epsilon}](\boldsymbol{\tau}_a[\underline{\epsilon}])$ ) potential as given in equation (5.25b):

$$V_M^a[\underline{\epsilon}](\boldsymbol{\tau}_a[\underline{\epsilon}]) = \int d^3\mathbf{r}'_\epsilon \frac{\rho((1-\underline{\epsilon})\mathbf{r}'_\epsilon)}{|\mathbf{r}'_\epsilon - \boldsymbol{\tau}_a[\underline{\epsilon}]|} - \sum_{b \neq a} \frac{Z_b}{|\boldsymbol{\tau}_a[\underline{\epsilon}] - \boldsymbol{\tau}_b[\underline{\epsilon}]|} \quad (6.26)$$

As usual, the integral will be transformed back to the undeformed system, and steps similar to those for the Coulomb stress will be followed here.

$$\begin{aligned}
\frac{dV_M^a[\underline{\epsilon}](\boldsymbol{\tau}_a[\underline{\epsilon}])}{d\epsilon_{\alpha\beta}} \Big|_{\underline{\epsilon}=0} &= \delta_{\alpha\beta} \int d^3\mathbf{r}' \frac{\rho(r')}{|\mathbf{r}' - \boldsymbol{\tau}_a|} + \int d^3\mathbf{r}' \frac{d}{d\epsilon_{\alpha\beta}} \frac{\rho(r')}{|\mathbf{r}'[\underline{\epsilon}] - \boldsymbol{\tau}_a[\underline{\epsilon}]|} \Big|_{\underline{\epsilon}=0} - \sum_{b \neq a} \frac{d}{d\epsilon_{\alpha\beta}} \frac{Z_b}{|\boldsymbol{\tau}_a[\underline{\epsilon}] - \boldsymbol{\tau}_b[\underline{\epsilon}]|} \Big|_{\underline{\epsilon}=0} \\
&\stackrel{(6.19),(6.20)}{=} \delta_{\alpha\beta} \int d^3\mathbf{r}' \frac{\rho(r')}{|\mathbf{r}' - \boldsymbol{\tau}_a|} - \sum_{t,t'=-1}^1 c_{\alpha t} c_{\beta t'} \left\{ \int_{\Omega} d^3\mathbf{r}' \frac{\rho(r')}{|\mathbf{r}' - \boldsymbol{\tau}_a|} - \sum_{b \neq a} \frac{Z_b}{|\boldsymbol{\tau}_a - \boldsymbol{\tau}_b|} \right\} Y_{1t} Y_{1t'} \\
&\stackrel{(4.13)}{=} \delta_{\alpha\beta} \int d^3\mathbf{r}' \frac{\rho(r')}{|\mathbf{r}' - \boldsymbol{\tau}_a|} - \sum_{t,t'=-1}^1 c_{\alpha t} c_{\beta t'} V_M(\boldsymbol{\tau}_a) Y_{1t}(\hat{\boldsymbol{\tau}}_a) Y_{1t'}(\hat{\boldsymbol{\tau}}_a)
\end{aligned} \tag{6.27}$$

Substituting (6.27) in (6.25):

$$2\Omega\sigma_{\alpha\beta}^M = -\delta_{\alpha\beta} \sum_a Z_a \int d^3\mathbf{r} \frac{\rho(r)}{|\mathbf{r} - \boldsymbol{\tau}_a|} + \sum_a Z_a \sum_{t,t'=-1}^1 c_{\alpha t} c_{\beta t'} V_M(\boldsymbol{\tau}_a) Y_{1t}(\hat{\boldsymbol{\tau}}_a) Y_{1t'}(\hat{\boldsymbol{\tau}}_a) \tag{6.28}$$

The first expression in equation (6.28) is similar to the last expression in equation (6.24) but with opposite sign. As a result, in the final stress formula, they cancel out.

The electrostatic stress tensor is obtained via substituting equations (6.24) and (6.28) in (6.4):

$$\begin{aligned}
2\Omega\sigma_{\alpha\beta}^{es} &= -2\delta_{\alpha\beta} \int_{\Omega} d^3\mathbf{r} \rho(\mathbf{r}) V_C(\mathbf{r}) + 2\Omega\sigma_{\alpha\beta}^C + 2\Omega\sigma_{\alpha\beta}^M \\
&= -2\delta_{\alpha\beta} \int_{\Omega} d^3\mathbf{r} \rho(\mathbf{r}) V_C(\mathbf{r}) + \Omega \sum_{\mathbf{G}} \sum_{\mathbf{G}' \neq 0} \rho^*(\mathbf{G}) \left( \delta_{\alpha\beta} V_C(\mathbf{G}') + 2\widehat{\mathbf{G}}'_\alpha \widehat{\mathbf{G}}'_\beta V_C(\mathbf{G}') \right) \Theta(\mathbf{G} - \mathbf{G}') \\
&\quad - \sum_a \sum_{t,t'=-1}^1 c_{\alpha t} c_{\beta t'} \int_{\Omega} d^3\mathbf{r} \Theta_a(\mathbf{r}) \rho(\mathbf{r}) V_C(\mathbf{r}) Y_{1t}(\hat{\mathbf{r}}) Y_{1t'}(\hat{\mathbf{r}}) \\
&\quad + 2\delta_{\alpha\beta} \sum_a \int_{\Omega} d^3\mathbf{r} \Theta_a(\mathbf{r}) \rho(\mathbf{r}) V_C(\mathbf{r}) + \cancel{\delta_{\alpha\beta} \sum_b \int_{\Omega} d^3\mathbf{r} \Theta_a(\mathbf{r}) \rho(\mathbf{r}) \frac{Z_b}{|\mathbf{r} - \boldsymbol{\tau}_b|}} \\
&\quad - \cancel{\delta_{\alpha\beta} \sum_a Z_a \int d^3\mathbf{r} \frac{\rho(r)}{|\mathbf{r} - \boldsymbol{\tau}_a|}} + \sum_a Z_a \sum_{t,t'=-1}^1 c_{\alpha t} c_{\beta t'} V_M(\boldsymbol{\tau}_a) Y_{1t}(\hat{\boldsymbol{\tau}}_a) Y_{1t'}(\hat{\boldsymbol{\tau}}_a) \\
&= \Omega \sum_{\mathbf{G}} \sum_{\mathbf{G}' \neq 0} \rho^*(\mathbf{G}) \left( -\delta_{\alpha\beta} V_C(\mathbf{G}') + 2\widehat{\mathbf{G}}'_\alpha \widehat{\mathbf{G}}'_\beta V_C(\mathbf{G}') \right) \Theta(\mathbf{G} - \mathbf{G}') \\
&\quad - \sum_a \sum_{t,t'=-1}^1 c_{\alpha t} c_{\beta t'} \int_{\Omega} d^3\mathbf{r} \Theta_a(\mathbf{r}) \rho(\mathbf{r}) V_C(\mathbf{r}) Y_{1t}(\hat{\mathbf{r}}) Y_{1t'}(\hat{\mathbf{r}}) \\
&\quad + \sum_a Z_a \sum_{t,t'=-1}^1 c_{\alpha t} c_{\beta t'} V_M(\boldsymbol{\tau}_a) Y_{1t}(\hat{\boldsymbol{\tau}}_a) Y_{1t'}(\hat{\boldsymbol{\tau}}_a)
\end{aligned}$$

Now the final expression of the electrostatic stress tensor becomes

$$\begin{aligned}
2\Omega\sigma_{\alpha\beta}^{es} = & \Omega \sum_{\mathbf{G}} \sum_{\mathbf{G}' \neq 0} \rho^*(\mathbf{G}) \left( -\delta_{\alpha\beta} V_C(\mathbf{G}') + 2\widehat{\mathbf{G}}'_\alpha \widehat{\mathbf{G}}'_\beta V_C(\mathbf{G}') \right) \Theta(\mathbf{G} - \mathbf{G}') \\
& - \sum_{t,t'=-1}^1 c_{\alpha t} c_{\beta t'} \int_{\Omega} d^3 \mathbf{r} \Theta_a(\mathbf{r}) \rho(\mathbf{r}) V_C(\mathbf{r}) Y_{1t}(\hat{\mathbf{r}}) Y_{1t'}(\hat{\mathbf{r}}) \\
& + \sum_a Z_a \sum_{t,t'=-1}^1 c_{\alpha t} c_{\beta t'} V_M(\boldsymbol{\tau}_a) Y_{1t}(\hat{\boldsymbol{\tau}}_a) Y_{1t'}(\hat{\boldsymbol{\tau}}_a)
\end{aligned} \tag{6.29}$$

The first line in the above equation calculates the interstitial electrostatic stress tensor, and it originates from the Coulomb stress tensor. The remaining expressions evaluate the electrostatic stress tensor in the region of atomic spheres. Equation (6.29) shows that all necessary terms, such as the charge density and the potential, to compute the electrostatic stress tensor are already available from a regular total energy calculation. Additional effort may be required to simplify the first expression in the second line because it contains a surface integral of four spherical harmonics (one from the charge density, one from the potential, and two from the unit vector expansion). According to equation (A.4), the surface integral of four spherical harmonics is equivalent to a sum of the products of two Gaunt numbers. Also, the  $l$  and  $m$  that are required to calculate the Gaunt numbers are coming from the charge density and potential, which are already restricted according to the symmetry of the crystal structure. As a result, the calculation of equation (6.29) does not raise the overall computational burden. In our WIEN2k implementation, the first line of the above equation is calculated in the routine `xcpot3.F` using the Fast Fourier Transform (FFT) field, and all remaining terms are calculated in the subroutine `finl_elect_str.f`.

In the following, we will compare our electrostatic stress tensor with previous works in Refs.[12, 19]. The expression of the electrostatic stress tensor (EST) given in equation (6.29) is different compared to the equations in Ref. [19] and equation (10) in Ref. [12]. In Ref. [12], only ideas but no explicit expressions are provided regarding the problem how to simplify EST, and thus no one-to-one comparison can be made. In Ref. [19], the general expressions (5.20a) and (5.20b) are similar to our equation (6.4). However, deviations start to emerge when further steps are executed to simplify these expressions.

The derivation provided in section 5.5 shows that Fourier components of the plane wave charge density ( $\rho_I(\mathbf{G})$ ) and pseudo-charge density ( $\tilde{\rho}_a(\mathbf{G})$ ) do not change when the system is deformed. In section 5.5, during the calculation of strained Fourier components of pseudo-charge density, the physically strained pseudo-charge density is replaced by a smeared pseudo-charge density, shown in equation (5.57a). This concept is similar to that used to compute the strained Fourier components of the plane wave charge density but it is completely different from the approach used in Ref. [19]. Because of this, our interstitial Coulomb stress tensor is much more straightforward and entirely different from the one reported in Refs. [19] and [12]. In Ref. [19], Fourier components of the plane wave charge density are independent of strain (equation (5.29b)) but not the pseudo charge density (equation (5.31a)). In our formulation, the Coulomb stress tensor of the interstitial region appears due to a change of  $\mathbf{G}$ , but in Ref. [19] this contribution appears due to the change of  $\mathbf{G}$ , pseudo-charge density, and step-function. The change of step function contributes a surface integral (first line in equation (5.39)

in Ref. [19]). However, from our calculation, we obtain no such surface term. On the other hand, the difference with Thonhauser et. al. (equation (5.54) in Thonhauser thesis) is due to the use of a different scaling technique for the charge density: equation (7) in Ref. [12].

Similar to the Coulomb stress tensor in the interstitial, inside the spheres also our expression (second line of equation (6.29)) is simple and straightforward to use compared to equations (5.36) and (5.38) in Ref. [19]. In equation (6.29), the required quantities like charge density and potential are already at our disposal from a regular DFT calculation executed to evaluate the total energy. As a result, no additional effort is required other than calculating the products of two Gaunt numbers. In contrast, expressions in Ref. [19] are much more involved. In Ref. [19], the strain variation of the smeared charge density and potential is required according to equations (5.28) and (5.36), respectively. These expressions are difficult to evaluate, especially the strain variation of the potential (equation (5.36) in Ref. [19]) since it is intertwined to the interstitial potential, the second line of equation (5.36) in [19], which in turn is controlled by the pseudo-charge inside the spheres. On the other hand, we can not make any comparison with Thonhauser *et al.*, in Ref. [12], since the authors literally only provide rough ideas how to solve the Coulomb integral without presenting the final outcome explicitly.

We know that the Madelung potential is a special case of the Coulomb potential, as shown in equation (4.41). This also suggests that the strain variation of the Madelung potential is a special case of the strain variation of the Coulomb potential, which can be seen by a comparison of equations (6.16) and (6.27). We already noted that the strain variation of Coulomb potential, as well as Coulomb stress tensor resulting from our derivation, are entirely different from the expressions reported in Refs. [19] and [12]. As a result, the strain variation of the Madelung potential of our calculation is expected to be different from a corresponding expression in Refs. [19] and [12]. Again, the last term of the equation (6.29) is associated to the Madelung stress tensor, which is very simple and easy to compute compared to the combination of equations (5.37) and (5.38) in Ref. [19].

The comparison with Ref.[17], however, is not straightforward. This is because the authors use different augmentation in the region of atomic spheres, similar to what is defined in Refs.[15, 16]. For this reason, the basis functions and thus the charge density inside atomic spheres differ from those used in the original LAPW method. As a result, a one-to-one comparison of equation (6.29) with the corresponding equation, (47) in Ref.[17], is not possible inside the atomic spheres. The first term in equation (6.29), however, is similar to the first term in equation (47) in Ref.[17]. This is due to the fact that in both works the required quantities are expanded in terms of plane waves in the interstitial region. We also compare equation (6.29) with the corresponding terms in Ref.[3], which was derived for the pseudopotential method. We observe that the first term in equation (6.29) corresponds to the second term in Ref.[3] if  $V_C(\mathbf{G})$  is replaced by equation (4.23) in our work. This is because in both works plane wave expansions of the required charge density and potential are used.

## 6.2 Core Correction Stress Tensor

The core correction contribution to the total stress tensor as given in equation (6.3b) is

$$\sigma_{\alpha\beta}^{core} = -\frac{1}{2\Omega} \int_{\Omega} d^3\mathbf{r} \rho_c(\mathbf{r}) (r_{\beta}\partial_{\alpha} + r_{\alpha}\partial_{\beta}) V_{eff}(\mathbf{r}) \quad (6.30)$$

$$= -\frac{1}{\Omega} \sum_{a \in \Omega} \int_{R_a} d^3\mathbf{r}_a \rho_c^a(\mathbf{r}_a) \frac{1}{2} (\mathbf{r}_{a\alpha}\partial_{\beta} + \mathbf{r}_{a\beta}\partial_{\alpha}) V_{eff}^a(\mathbf{r}_a), \quad (6.31)$$

where  $\rho_c^a(\mathbf{r}_a)$  represents the core charge density, and it is confined, in principle, to the interior of the atomic spheres.  $V_{eff}^a(\mathbf{r}_a)$  is the effective or total potential in the system,  $\int_{R_a}$  denotes the integration domain inside an atomic sphere region, and the summation index  $a$  runs over all the equivalent and non-equivalent atoms in the unit cell.

When the unit cell is deformed, the core states change in two different ways: First, the core states will move along with the nuclei to a position in the strained unit cell. Second, the total potential in the unit cell will be changed, and core states will interact with that modified potential. Equation (6.30) suggests that the core correction is coming from this second change. The following lines illustrate the necessary steps to simplify equation (6.31).

Inside an atomic sphere, the potential is expanded in terms of spherical harmonics. For the sake of brevity, in the following lines we will be using  $V_{eff}^a(\mathbf{r}_a) = V(\mathbf{r})$

$$V(\mathbf{r}) = \sum_{l,m} V_{l,m}(\mathbf{r}) Y_{l,m}(\hat{\mathbf{r}}) \quad (6.32)$$

The partial derivative of the length of a radial vector along the Cartesian direction  $\alpha$  is

$$\frac{\partial r}{\partial r_{\alpha}} = \partial_{\alpha} r = \partial_{\alpha} \left[ \sum_{\alpha} \mathbf{r}_{\alpha}^2 \right]^{\frac{1}{2}} = \frac{\mathbf{r}_{\alpha}}{\sqrt{\sum_{\alpha} \mathbf{r}_{\alpha}^2}} = \hat{\mathbf{r}}_{\alpha} \quad (6.33)$$

Also,

$$\partial_{\alpha} = \frac{\partial}{\partial r_{\alpha}} = \frac{\partial}{\partial r} \frac{\partial r}{\partial r_{\alpha}} = \hat{\mathbf{r}}_{\alpha} \frac{\partial}{\partial r} \quad (6.34)$$

$$\begin{aligned} \partial_{\alpha} V(\mathbf{r}) &= \sum_{l,m} \left( Y_{l,m}(\hat{\mathbf{r}}) \partial_{\alpha} V_{l,m}(\mathbf{r}) + V_{l,m}(\mathbf{r}) \partial_{\alpha} Y_{l,m}(\hat{\mathbf{r}}) \right) \\ &= \sum_{l,m} \left( Y_{l,m}(\hat{\mathbf{r}}) \hat{\mathbf{r}}_{\alpha} V'_{l,m}(\mathbf{r}) + \frac{V_{l,m}(\mathbf{r})}{r} r \partial_{\alpha} Y_{l,m}(\hat{\mathbf{r}}) \right) \\ &\stackrel{(A.8)}{=} \sum_{l,m} \left( Y_{l,m}(\hat{\mathbf{r}}) \hat{\mathbf{r}}_{\alpha} V'_{l,m}(\mathbf{r}) + \frac{V_{l,m}(\mathbf{r})}{r} \sum_{s=\pm 1}^1 \sum_{t=-1}^1 c_{\alpha}^{st}(l, m) Y_{l+s, m+t}(\hat{\mathbf{r}}) \right) \end{aligned} \quad (6.35)$$

The prime in  $V'_{l,m}(\mathbf{r})$  denotes the radial derivative, the summation over  $s$  takes  $+1$  and  $-1$  only, and  $t$  runs from  $-1$  to  $+1$ . In the above equation, the loop over  $l$  and  $s$  has

to be such that  $l + s$  is always positive. The expressions of  $c_\alpha^{st}(l, m)$  are provided in section A.2. The angular derivative of the spherical harmonics produces a change of angular quantum number ( $l$ ) of the spherical harmonics to its nearest value only by  $\pm 1$ . The implication of this result is that a **s**-like shape of the effective potential can only change to a **p**-like shape but not directly to **d**-like shape. However, a **p**-like shape can transform to **s**-like shape or **d**-like shape according to  $s = -1$  or  $s = +1$ , respectively.

Also,

$$\partial_\alpha V(\mathbf{r}) = \sum_{l,m} \left( V'_{l,m}(\mathbf{r}) \sum_{t=-1}^1 c_{\alpha t} Y_{1t}(\hat{\mathbf{r}}) Y_{l,m}(\hat{\mathbf{r}}) + \frac{V_{l,m}(\mathbf{r})}{r} \sum_{s=\pm 1} \sum_{t=-1}^1 c_\alpha^{st}(l, m) Y_{l+s, m+t}(\hat{\mathbf{r}}) \right) \quad (6.36)$$

We expand the radial vector components in terms of spherical harmonics:

$$r_\beta = \hat{\mathbf{r}}_\beta r \stackrel{(A.1)}{=} r \sum_{t'=-1}^1 c_{\beta t'} Y_{1t'}(\hat{\mathbf{r}}) \quad (6.37)$$

Multiplying equation (6.36) by (6.37):

$$\begin{aligned} r_\beta \partial_\alpha V(\mathbf{r}) &= \sum_{l,m} \left( r V'_{l,m}(\mathbf{r}) \sum_{t,t'=-1}^1 c_{\alpha t} c_{\beta t'} Y_{1t'}(\hat{\mathbf{r}}) Y_{1t}(\hat{\mathbf{r}}) Y_{l,m}(\hat{\mathbf{r}}) \right. \\ &\quad \left. + V_{l,m}(\mathbf{r}) \sum_{s=\pm 1} \sum_{t,t'=-1}^1 c_\alpha^{st}(l, m) c_{\beta t'} Y_{1t'}(\hat{\mathbf{r}}) Y_{l+s, m+t}(\hat{\mathbf{r}}) \right) \end{aligned} \quad (6.38)$$

The product of two spherical harmonics can be replaced by a Gaunt number according to equation (A.4).

$$\begin{aligned} r_\beta \partial_\alpha V(\mathbf{r}) &= \sum_{l,m} \left( r V'_{l,m}(\mathbf{r}) \sum_{t,t'=-1}^1 c_{\alpha t} c_{\beta t'} \sum_{s=0}^2 \sum_{\nu=-s}^s G_{s,1,1}^{\nu, t, t'} Y_{s\nu}(\hat{\mathbf{r}}) Y_{l,m}(\hat{\mathbf{r}}) \right. \\ &\quad \left. + V_{l,m}(\mathbf{r}) \sum_{s=\pm 1} \sum_{t,t'=-1}^1 c_\alpha^{st}(l, m) c_{\beta t'} Y_{1t'}(\hat{\mathbf{r}}) Y_{l+s, m+t}(\hat{\mathbf{r}}) \right) \end{aligned} \quad (6.39)$$

Interchanging  $\alpha$  and  $\beta$ :

$$\begin{aligned} r_\alpha \partial_\beta V(\mathbf{r}) &= \sum_{l,m} \left( r V'_{l,m}(\mathbf{r}) \sum_{t,t'=-1}^1 c_{\alpha t} c_{\beta t'} \sum_{s=0}^2 \sum_{\nu=-s}^s G_{s,1,1}^{\nu, t, t'} Y_{s\nu}(\hat{\mathbf{r}}) Y_{l,m}(\hat{\mathbf{r}}) \right. \\ &\quad \left. + V_{l,m}(\mathbf{r}) \sum_{s=\pm 1} \sum_{t,t'=-1}^1 c_\beta^{st}(l, m) c_{\alpha t'} Y_{1t'}(\hat{\mathbf{r}}) Y_{l+s, m+t}(\hat{\mathbf{r}}) \right) \end{aligned} \quad (6.40)$$

Adding the expressions (6.39) and (6.40):

$$\begin{aligned} \frac{1}{2} (r_\beta \partial_\alpha + r_\alpha \partial_\beta) V(\mathbf{r}) &= \sum_{l,m} \sum_{t,t'=-1}^1 \left( r V'_{l,m}(\mathbf{r}) c_{\alpha t} c_{\beta t'} \sum_{s=0}^2 \sum_{\nu=-s}^s G_{s,1,1}^{\nu, t, t'} Y_{s\nu}(\hat{\mathbf{r}}) Y_{l,m}(\hat{\mathbf{r}}) \right. \\ &\quad \left. + V_{l,m}(\mathbf{r}) \sum_{s=\pm 1} \frac{c_\beta^{st}(l, m) c_{\alpha t'} + c_\alpha^{st}(l, m) c_{\beta t'}}{2} Y_{1t'}(\hat{\mathbf{r}}) Y_{l+s, m+t}(\hat{\mathbf{r}}) \right) \end{aligned} \quad (6.41)$$

The total charge density is a real quantity:

$$\rho(\mathbf{r}) = \sum_{l',m'} \rho_{l',m'}(r) Y_{l',m'}(\hat{\mathbf{r}}) = \sum_{l',m'} \rho_{l',m'}^*(r) Y_{l',m'}^*(\hat{\mathbf{r}}) \quad (6.42)$$

Substituting equation (6.41) in (6.31):

$$\begin{aligned} \Omega \sigma_{\alpha\beta}^C &= \sum_{l,m} \sum_{l',m'} \sum_{t,t'=-1}^1 \left( I_1 c_{\alpha t} c_{\beta t'} \sum_{s=0}^2 \sum_{\nu=-s}^s G_{s,1,1}^{\nu,t,t'} G_{l',l,s}^{m',m,\nu} \right. \\ &\quad \left. + I_2 \sum_{s=\pm 1} \frac{c_{\beta}^{st}(l,m)c_{\alpha t'} + c_{\alpha}^{st}(l,m)c_{\beta t'}}{2} G_{l',1,l+s}^{m',t',m+t} \right), \end{aligned} \quad (6.43)$$

where  $I_1$  and  $I_2$  are the abbreviation of the following integrals:

$$I_1 = - \int_0^{R_a} r_a^3 dr_a \rho_{l',m'}^*(r_a) \frac{dV_{l,m}(r_a)}{dr_a} \quad (6.44)$$

$$I_2 = - \int_0^{R_a} r_a^2 dr_a \rho_{l',m'}^*(r_a) V_{l,m}(r_a) \quad (6.45)$$

In the APW based methods, the core density is assumed to be spherically symmetric and confined within a spherical region. It is also assumed that its spherical nature remains intact even for the strained system, which means that  $l'$  and  $m'$  of the charge density in equation (6.43) are zero. The underlying assumption is that when a system is deformed, the core states simply move to a new position along with the nucleus, and the stress contribution comes through the change in the shape of the potential. Core states are lying so deep in energy and are so localized that their spherical nature persists even after the system is deformed. On the other hand, the total potential is spreading over the entire crystal, and thus the indexes  $l, m$  of potential can have both spherical and non-spherical indexes. However, due to the product of two Gaunt numbers  $G_{s,1,1}^{\nu,t,t'} G_{l',l,s}^{m',m,\nu}$ ,  $l$  and  $m$  can have only very few non-spherical components. This concept is similar to the core correction for the force calculation. In the calculation of forces, densities are assumed to be spherical too, but the potential they interact with has both spherical ( $l = 0$ ) and non-spherical components ( $l = 1$ ), see equation (A4) in Ref.[31].

The product of two Gaunt numbers with  $l', m' = 0$  is:

$$\begin{aligned} G_{s,1,1}^{\nu,t,t'} G_{l',l,s}^{m',m,\nu} &= G_{s,1,1}^{\nu,t,t'} G_{0,l,s}^{0,m,\nu} \\ &= G_{s,1,1}^{\nu,t,t'} \int_S dS Y_{00}^*(\hat{\mathbf{r}}) Y_{lm}(\hat{\mathbf{r}}) Y_{s\nu}(\hat{\mathbf{r}}) \\ &= G_{s,1,1}^{\nu,t,t'} \frac{(-1)^m}{\sqrt{4\pi}} \delta_{l,s} \delta_{-m,\nu} \\ &= \frac{(-1)^m}{\sqrt{4\pi}} G_{l,1,1}^{-m,t,t'} \end{aligned} \quad (6.46)$$

$$\begin{aligned}
G_{l',1,l+s}^{m',t',m+t} &= G_{0,1,l+s}^{0,t',m+t} \\
&= \frac{(-1)^{t'}}{\sqrt{4\pi}} \delta_{1,l+s} \delta_{-t',m+t}
\end{aligned} \tag{6.47}$$

The final expression of core-correction stress is obtained by substituting equations (6.46) and (6.47) in (6.43).

$$\begin{aligned}
\Omega \sigma_{\alpha\beta}^C &= \sum_{l,m} \sum_{t,t'=-1}^1 \left( I_1 c_{\alpha t} c_{\beta t'} \frac{(-1)^m}{4\pi} G_{l,1,1}^{-m,t,t'} + \right. \\
&\quad \left. I_2 \sum_{s=\pm 1} \frac{c_{\beta}^{st}(l,m) c_{\alpha t'} + c_{\alpha}^{st}(l,m) c_{\beta t'}}{2} \frac{(-1)^{t'}}{4\pi} \delta_{1,l+s} \delta_{-t',m+t} \right)
\end{aligned} \tag{6.48}$$

with integrals,

$$I_1 = - \int_0^{R_a} r_a^3 dr_a \sqrt{4\pi} \rho_{00}^*(r_a) \frac{dV_{lm}(r_a)}{dr_a} \tag{6.49}$$

$$I_2 = - \int_0^{R_a} r_a^2 dr_a \sqrt{4\pi} \rho_{00}^*(r_a) V_{lm}(r_a) \tag{6.50}$$

Equation (6.48) shows that the stress components ( $\alpha, \beta$ ) enter in the equation via  $c_{\alpha t}$ ,  $c_{\beta t'}$ ,  $c_{\alpha}^{st}(l,m)$ , and  $c_{\beta}^{st}(l,m)$  and these coefficients result from a change in potential (radial derivative of  $V_{lm}(\mathbf{r})$ ) and spherical harmonics (angular derivative of spherical harmonics  $Y_{lm}(\hat{\mathbf{r}})$ ).

For a Gaunt number  $G_{l,1,1}^{-m,t,t'}$ , the indices  $[l, 1, 1]$  are required to satisfy the triangle rule and their sum needs to be even [46]. These conditions restrict  $l$  to be 0 and 2,  $l=0$  is the primary component and  $l=2$  acts as an extra correction term, which does not always exist. In a cubic structure,  $l=2$  never appears because of symmetry (for example, with site symmetry  $m3m$ ,  $l$  of the charge density can be 0,4,6), a  $l=2$  term appears only in the lower symmetric crystal structures (for example, a hexagonal system). As can be seen above, we assumed that the core density is always spherical, and  $l = 2$  appears due to the non-spherical nature introduced in the total potential when the system is deformed. This concept is similar to the core correction of the force calculation. In the force calculation, atoms are displaced, and in the core correction,  $l=1$  appears in the potential. In the stress calculation, the system is deformed and  $l=2$  appears in the potential as a core correction.

Equation (6.31) is similar to corresponding expression in Refs.[12, 19]. Equation (21) in Thonhauser *et al.* has a different sign than in our expression. On the other hand, we do not see such a term in Ref.[17]. In section 4.1 in Ref. [12], the authors make an argument that “the core correction vanishes for pure pressure”, but from our calculation we could not validate such a rationale. The core correction given in Thonhauser et. al. is:

$$\Omega\sigma_{\alpha\beta}^C = \sum_a \int_{R_a} \rho_a^{core}(\mathbf{r}) \mathbf{r}_\beta \nabla_\alpha V(\mathbf{r}) d^3r \quad (6.51)$$

Mathematically, the negative trace or pure pressure from equation (6.51) is:

$$3\Omega P = - \sum_a \int_{R_a} d^3r \rho_a^{core}(\mathbf{r}) \mathbf{r}_a \nabla V(\mathbf{r}) \quad (6.52)$$

This expression does not seem to vanish as claimed in Ref. [12]. In appendix D, we show that the trace of core correction stress i.e.  $\sum_{\alpha=\beta} \sigma_{\alpha\beta}^C$  is equivalent to twice the core kinetic energy.

### 6.3 Valence Kinetic Stress Tensor

The kinetic stress tensor for the valence electrons is given in equation (6.3c).

$$\Omega\sigma_{\alpha\beta}^{val,kin} = \frac{1}{2} \sum_{v\mathbf{k}} n_{v\mathbf{k}} \int_{\Omega} d^3\mathbf{r} \psi_{v\mathbf{k}}^*(\mathbf{r}) (\partial_\alpha \partial_\beta + \partial_\beta \partial_\alpha) \psi_{v\mathbf{k}}(\mathbf{r}) \quad (6.53)$$

The integration over the unit cell is evaluated separately in the two regions— in the atomic spheres and in the interstitial.

$$\begin{aligned} \Omega\sigma_{\alpha\beta}^{val,kin} &= \frac{1}{2} \int_{\Omega} d^3\mathbf{r} \psi_{v\mathbf{k}}^*(\mathbf{r}) (\partial_\alpha \partial_\beta + \partial_\beta \partial_\alpha) \psi_{v\mathbf{k}}(\mathbf{r}) \\ &= \frac{1}{2} \int_{\Omega} d^3\mathbf{r} \Theta_{IS}(\mathbf{r}) \psi_{v\mathbf{k}}^*(\mathbf{r}) (\partial_\alpha \partial_\beta + \partial_\beta \partial_\alpha) \psi_{v\mathbf{k}}(\mathbf{r}) \\ &\quad + \frac{1}{2} \int_{\Omega} d^3\mathbf{r} \Theta_a(\mathbf{r}) \psi_{v\mathbf{k}}^*(\mathbf{r}) (\partial_\alpha \partial_\beta + \partial_\beta \partial_\alpha) \psi_{v\mathbf{k}}(\mathbf{r}) \\ &= \frac{1}{2} \int_{\Omega} d^3\mathbf{r} \Theta_{IS}(\mathbf{r}) \psi_{v\mathbf{k}}^*(\mathbf{r}) (\partial_\alpha \partial_\beta + \partial_\beta \partial_\alpha) \psi_{v\mathbf{k}}(\mathbf{r}) \\ &\quad + \frac{1}{2} \sum_{a \in \Omega} \int_{R_a} d^3\mathbf{r} \psi_{v\mathbf{k}}^*(\mathbf{r}) (\partial_\alpha \partial_\beta + \partial_\beta \partial_\alpha) \psi_{v\mathbf{k}}(\mathbf{r}) \\ &= \Omega\sigma_{\alpha\beta}^{kin,IS} + \Omega\sigma_{\alpha\beta}^{kin,R_a} \end{aligned} \quad (6.54)$$

$\Omega\sigma_{\alpha\beta}^{kin,IS}$  and  $\Omega\sigma_{\alpha\beta}^{kin,R_a}$  are the valence kinetic stress in the interstitial region and in the region of the atomic spheres. The interstitial part will be simplified as given below:

$$\begin{aligned} \Omega\sigma_{\alpha\beta}^{kin,IS} &= \frac{1}{2} \sum_{v\mathbf{k}} n_{v\mathbf{k}} \int_{\Omega} d^3\mathbf{r} \Theta_{IS}(\mathbf{r}) \psi_{v\mathbf{k}}^*(\mathbf{r}) (\partial_\alpha \partial_\beta + \partial_\beta \partial_\alpha) \psi_{v\mathbf{k}}(\mathbf{r}) \\ &\stackrel{(3.20)}{=} \frac{1}{2} \sum_{v\mathbf{k}} n_{v\mathbf{k}} \sum_{\mathbf{KK}'} c_{v\mathbf{k}\mathbf{K}}^* c_{v\mathbf{k}\mathbf{K}'} \int_{\Omega} d^3\mathbf{r} \Theta_{IS}(\mathbf{r}) \phi_{\mathbf{k}\mathbf{K}}^*(\mathbf{r}) (\partial_\alpha \partial_\beta + \partial_\beta \partial_\alpha) \phi_{\mathbf{k}\mathbf{K}'}(\mathbf{r}) \\ &\stackrel{(3.6)}{=} \frac{1}{2} \sum_{v\mathbf{k}} n_{v\mathbf{k}} \sum_{\mathbf{KK}'} c_{v\mathbf{k}\mathbf{K}}^* c_{v\mathbf{k}\mathbf{K}'} \frac{1}{\Omega} \int_{\Omega} d^3\mathbf{r} \Theta_{IS}(\mathbf{r}) e^{-i(\mathbf{k}+\mathbf{K}) \cdot \mathbf{r}} (\partial_\alpha \partial_\beta + \partial_\beta \partial_\alpha) e^{i(\mathbf{k}+\mathbf{K}') \cdot \mathbf{r}} \\ &= \sum_{v\mathbf{k}} n_{v\mathbf{k}} \sum_{\mathbf{KK}'} c_{v\mathbf{k}\mathbf{K}}^* c_{v\mathbf{k}\mathbf{K}'} \frac{1}{\Omega} \int_{\Omega} d^3\mathbf{r} \Theta_{IS}(\mathbf{r}) e^{-i(\mathbf{k}+\mathbf{K}) \cdot \mathbf{r}} i(\mathbf{k}+\mathbf{K}')_\alpha i(\mathbf{k}+\mathbf{K}')_\beta e^{i(\mathbf{k}+\mathbf{K}') \cdot \mathbf{r}} \\ &= - \sum_{v\mathbf{k}} n_{v\mathbf{k}} \sum_{\mathbf{KK}'} c_{v\mathbf{k}\mathbf{K}}^* c_{v\mathbf{k}\mathbf{K}'} (\mathbf{k}+\mathbf{K}')_\alpha (\mathbf{k}+\mathbf{K}')_\beta \frac{1}{\Omega} \int_{\Omega} d^3\mathbf{r} \Theta_{IS}(\mathbf{r}) e^{-i(\mathbf{K}-\mathbf{K}') \cdot \mathbf{r}} \end{aligned}$$

The final expression of the interstitial part of the valence kinetic stress is:

$$\Omega \sigma_{\alpha\beta}^{kin,IS} \stackrel{(A.41)}{=} - \sum_{v\mathbf{k}} n_{v\mathbf{k}} \sum_{\mathbf{K}\mathbf{K}'} c_{v\mathbf{k}\mathbf{K}}^* c_{v\mathbf{k}\mathbf{K}'} (\mathbf{k} + \mathbf{K}')_\alpha (\mathbf{k} + \mathbf{K}')_\beta \Theta(\mathbf{K} - \mathbf{K}') \quad (6.55)$$

The valence kinetic stress in the atomic spheres will be simplified in the following lines. For the sake of brevity, the explicit energy dependency will be dropped from the radial function and its energy derivative i.e  $u_{l\lambda}(r, E_l^a) \equiv u_{l\lambda}(r)$  and  $\dot{u}_{l\lambda}(r, E_l^a) \equiv \dot{u}_{l\lambda}(r)$ .

$$\Omega \sigma_{\alpha\beta}^{kin,R_a} = \frac{1}{2} \sum_{v\mathbf{k}} n_{v\mathbf{k}} \sum_{a \in \Omega} \int_{R_a} d^3\mathbf{r} \psi_{v\mathbf{k}}^*(\mathbf{r}) (\partial_\alpha \partial_\beta + \partial_\beta \partial_\alpha) \psi_{v\mathbf{k}}(\mathbf{r}) \quad (6.56)$$

$$\stackrel{(3.24)}{=} \frac{1}{2} \sum_{v\mathbf{k}} n_{v\mathbf{k}} \sum_{a \in \Omega} \sum_{LL'} \sum_{\lambda\lambda'} A_{L'\lambda'}^{av\mathbf{k}*} A_{L\lambda}^{av\mathbf{k}} \int_{R_a} d^3\mathbf{r} u_{l'\lambda'}(r) Y_{L'}^*(\hat{\mathbf{r}}) (\partial_\alpha \partial_\beta + \partial_\beta \partial_\alpha) u_{l\lambda}(r) Y_L(\hat{\mathbf{r}}) \quad (6.57)$$

Here  $L$  represent the combine index of  $l$  and  $m$ . In the following lines, each part of equation (6.57) will be simplified, and during the simplification, an argument of the spherical harmonics will be dropped for brevity i.e  $Y_L(\hat{\mathbf{r}}) = Y_{lm}(\hat{\mathbf{r}}) \equiv Y_{lm}$

$$\begin{aligned} \partial_\alpha (u_{l\lambda}(r) Y_{lm}(\hat{\mathbf{r}})) &= \partial_\alpha u_{l\lambda}(r) Y_{lm} + u_{l\lambda}(r) \partial_\alpha Y_{lm} \\ &\stackrel{(A.8)}{=} \hat{r}_\alpha u'_{l\lambda}(r) Y_{lm} + \frac{u_{l\lambda}(r)}{r} \sum_{s=\pm 1} \sum_{t=-1}^1 c_\alpha^{st}(l, m) Y_{l+s, m+t} \\ &\stackrel{(A.1)}{=} \sum_{t=-1} c_{\alpha t} Y_{1t} u'_{l\lambda}(r) Y_{lm} + \frac{u_{l\lambda}(r)}{r} \sum_{s=\pm 1} \sum_{t=-1}^1 c_\alpha^{st}(l, m) Y_{l+s, m+t} \\ &\stackrel{(A.4)}{=} \sum_{t=-1} c_{\alpha t} u'_{l\lambda}(r) \sum_{s,\nu} G_{s,1,l}^{\nu,t,m} Y_{s\nu} + \frac{u_{l\lambda}(r)}{r} \sum_{s=\pm 1} \sum_{t=-1}^1 c_\alpha^{st}(l, m) Y_{l+s, m+t} \end{aligned} \quad (6.58)$$

And

$$\begin{aligned} \partial_\beta \partial_\alpha (u_{l\lambda}(r) Y_{lm}(\hat{\mathbf{r}})) &= \sum_{t=-1} c_{\alpha t} \sum_{s,\nu} G_{s,1,l}^{\nu,t,m} [\partial_\beta u'_{l\lambda}(r) Y_{s\nu} + u'_{l\lambda}(r) \partial_\beta Y_{s\nu}] \\ &\quad + \left[ \partial_\beta \left( \frac{u_{l\lambda}(r)}{r} \right) \sum_{s=\pm 1} \sum_{t=-1}^1 c_\alpha^{st}(l, m) Y_{l+s, m+t} + \frac{u_{l\lambda}(r)}{r} \sum_{s=\pm 1} \sum_{t=-1}^1 c_\alpha^{st}(l, m) \partial_\beta Y_{l+s, m+t} \right] \\ &= \sum_{t,t'=-1} c_{\alpha t} c_{\beta t'} \sum_{s,\nu} G_{s,1,l}^{\nu,t,m} u''_{l\lambda}(r) Y_{1t'} Y_{s\nu} \\ &\quad + \sum_{t,t'=-1} c_{\alpha t} \sum_{s,\nu} G_{s,1,l}^{\nu,t,m} \frac{u'_{l\lambda}(r)}{r} \sum_{s'=\pm 1} c_\beta^{s't'}(s, \nu) Y_{s+s', \nu+t'} \\ &\quad + \left[ \frac{u'_{l\lambda}(r)}{r} - \frac{u_{l\lambda}(r)}{r^2} \right] \sum_{s=\pm 1} \sum_{t,t'=-1}^1 c_\alpha^{st}(l, m) c_{\beta t'} Y_{1t'} Y_{l+s, m+t} \\ &\quad + \frac{u_{l\lambda}(r)}{r^2} \sum_{s,s'=\pm 1} \sum_{t,t'=-1}^1 c_\alpha^{st}(l, m) c_\beta^{s't'}(l+s, m+t) Y_{l+s+s', m+t+t'} \end{aligned} \quad (6.59)$$

Substituting (6.58) and (6.59) in (6.57), we get:

$$\begin{aligned}
\Omega \sigma_{\alpha\beta}^{kin,R_a} = & \frac{1}{2} \sum_{v\mathbf{k}} n_{v\mathbf{k}} \sum_{a \in \Omega} \sum_{LL'} \sum_{\lambda\lambda'} A_{L'\lambda'}^{av\mathbf{k}*} A_{L\lambda}^{av\mathbf{k}} \\
& \left\{ \sum_{t,t'=-1} \left( c_{\alpha t} c_{\beta t'} + c_{\beta t} c_{\alpha t'} \right) \sum_{s,\nu} G_{s,1,l}^{\nu,t,m} \int_0^{R_a} r_a^2 dr_a u_{l'\lambda'}(r) u_{l\lambda}''(r) \oint_S dS Y_{l'm'}^* Y_{1t'} Y_{s\nu} \right. \\
& + \sum_{t,t'=-1} \sum_{s,\nu} \sum_{s'=\pm 1} G_{s,1,l}^{\nu,t,m} \left( c_{\alpha t} c_{\beta}^{s't'}(s,\nu) + c_{\beta t} c_{\alpha}^{s't'}(s,\nu) \right) \int_0^{R_a} r_a dr_a u_{l'\lambda'}(r) u_{l\lambda}'(r) \\
& \times \oint_S dS Y_{l'm'}^* Y_{s+s',\nu+t'} + \sum_{s=\pm 1} \sum_{t,t'=-1}^1 \left( c_{\alpha}^{st}(l,m) c_{\beta t'} + c_{\beta}^{st}(l,m) c_{\alpha t'} \right) \\
& \times \int_0^{R_a} r_a^2 dr_a u_{l'\lambda'}(r) \left[ \frac{u_{l\lambda}'(r)}{r} - \frac{u_{l\lambda}(r)}{r^2} \right] \oint_S dS Y_{l'm'}^* Y_{1t'} Y_{l+s,m+t} + \\
& \sum_{s,s'=\pm 1} \sum_{t,t'=-1}^1 \left( c_{\alpha}^{st}(l,m) c_{\beta}^{s't'}(l+s,m+t) + c_{\beta}^{st}(l,m) c_{\alpha}^{s't'}(l+s,m+t) \right) \\
& \times \int_0^{R_a} dr_a u_{l'\lambda'}(r) u_{l\lambda}(r) \oint_S dS Y_{l'm'}^* Y_{l+s+s',m+t+t'} \Bigg\} \tag{6.60}
\end{aligned}$$

Using equations (A.5) and (A.4) for the surface integrals:

$$\begin{aligned}
\Omega \sigma_{\alpha\beta}^{kin,R_a} = & \frac{1}{2} \sum_{v\mathbf{k}} n_{v\mathbf{k}} \sum_{a \in \Omega} \sum_{LL'} \sum_{\lambda\lambda'} A_{L'\lambda'}^{av\mathbf{k}*} A_{L\lambda}^{av\mathbf{k}} \\
& \left\{ \sum_{t,t'=-1} \left( c_{\alpha t} c_{\beta t'} + c_{\beta t} c_{\alpha t'} \right) \sum_{s,\nu} G_{s,1,l}^{\nu,t,m} G_{l',1,s}^{m',t',\nu} \int_0^{R_a} r_a^2 dr_a u_{l'\lambda'}(r) u_{l\lambda}''(r) \right. \\
& + \sum_{t,t'=-1} \sum_{s,\nu} \sum_{s'=\pm 1} G_{s,1,l}^{\nu,t,m} \left( c_{\alpha t} c_{\beta}^{s't'}(s,\nu) + c_{\beta t} c_{\alpha}^{s't'}(s,\nu) \right) \delta_{l',s+s'} \delta_{m',\nu+t'} \int_0^{R_a} r_a dr_a u_{l'\lambda'}(r) u_{l\lambda}'(r) \\
& + \sum_{s=\pm 1} \sum_{t,t'=-1}^1 \left( c_{\alpha}^{st}(l,m) c_{\beta t'} + c_{\beta}^{st}(l,m) c_{\alpha t'} \right) G_{l',1,l+s}^{m',t',m+t} \int_0^{R_a} r_a^2 dr_a u_{l'\lambda'}(r) \left[ \frac{u_{l\lambda}'(r)}{r} - \frac{u_{l\lambda}(r)}{r^2} \right] \\
& + \sum_{s,s'=\pm 1} \sum_{t,t'=-1}^1 \left( c_{\alpha}^{st}(l,m) c_{\beta}^{s't'}(l+s,m+t) + c_{\beta}^{st}(l,m) c_{\alpha}^{s't'}(l+s,m+t) \right) \delta_{l',l+s+s'} \delta_{m',m+t+t'} \\
& \times \int_0^{R_a} dr_a u_{l'\lambda'}(r) u_{l\lambda}(r) \Bigg\} \tag{6.61}
\end{aligned}$$

The second line of the equation (6.61) contains a sum of the products of two Gaunt numbers:

$$\sum_{s\nu} G_{s,1,l}^{\nu,t,m} G_{l',1,s}^{m',t',\nu} \tag{6.62}$$

The origin of this expression is the product of four spherical harmonics  $Y_{l'm'} Y_{lm} Y_{1t} Y_{1t'}$ , which can be rearranged differently as given below:

$$\begin{aligned}
\oint_S ds Y_{l'm'} Y_{lm} Y_{1t} Y_{1t'} = & \sum_{s\nu} G_{s,1,1}^{\nu,t,t'} \oint_S ds Y_{l'm'} Y_{lm} Y_{s\nu} \\
= & \sum_{s\nu} G_{s,1,1}^{\nu,t,t'} G_{l',l,s}^{m',m,\nu} \tag{6.63}
\end{aligned}$$

The equation (6.63) is advantageous over (6.62), since  $s$  takes only 0 and 2 in equation (6.63), whereas  $s$  in equation (6.62) runs from  $l - 1$  to  $l + 1$ . The final result is the same, but reduce the computational burden by reducing the number of necessary loop operations from  $l_{max} \times l_{max} \times (l_{max} + 1)$  to  $l_{max} \times l_{max} \times 2$ .

Finally, the final expression of the valence kinetic stress tensor is obtained by substituting the equations (6.55) and (6.61) into equation (6.54).

$$\begin{aligned}
\Omega\sigma_{\alpha\beta}^{val,kin} &= \Omega\sigma_{\alpha\beta}^{kin,IS} + \Omega\sigma_{\alpha\beta}^{kin,R_a} \\
&= - \sum_{v\mathbf{k}} n_{v\mathbf{k}} \sum_{\mathbf{KK}'} z_{v\mathbf{k}\mathbf{K}}^* z_{v\mathbf{k}\mathbf{K}'} (\mathbf{k} + \mathbf{K}')_\alpha (\mathbf{k} + \mathbf{K}')_\beta \Theta(\mathbf{K} - \mathbf{K}') \\
&\quad + \frac{1}{2} \sum_{v\mathbf{k}} n_{v\mathbf{k}} \sum_{a \in \Omega} \sum_{L'L'} \sum_{\lambda\lambda'} A_{L'\lambda'}^{av\mathbf{k}*} A_{L\lambda}^{av\mathbf{k}} \\
&\quad \times \left\{ \sum_{t,t'=-1} \left( c_{\alpha t} c_{\beta t'} + c_{\beta t} c_{\alpha t'} \right) \sum_{s,\nu} G_{s,1,l}^{\nu,t,m} G_{l',1,s}^{m',t',\nu} \int_0^{R_a} r_a^2 dr_a u_{l'\lambda'}(r) u_{l\lambda}''(r) \right. \\
&\quad + \sum_{t,t'=-1} \sum_{s,\nu} \sum_{s'=\pm 1} G_{s,1,l}^{\nu,t,m} \left( c_{\alpha t} c_{\beta}^{s't'}(s, \nu) + c_{\beta t} c_{\alpha}^{s't'}(s, \nu) \right) \delta_{l',s+s'} \delta_{m',\nu+t'} \\
&\quad \times \int_0^{R_a} r_a dr_a u_{l'\lambda'}(r) u_{l\lambda}'(r) + \sum_{s=\pm 1} \sum_{t,t'=-1}^1 \left( c_{\alpha}^{st}(l, m) c_{\beta t'} + c_{\beta}^{st}(l, m) c_{\alpha t'} \right) \\
&\quad \times G_{l',1,l+s}^{m',t',m+t} \int_0^{R_a} r_a^2 dr_a u_{l'\lambda'}(r) \left[ \frac{u_{l\lambda}'(r)}{r} - \frac{u_{l\lambda}(r)}{r^2} \right] \\
&\quad + \sum_{s,s'=\pm 1} \sum_{t,t'=-1}^1 \left( c_{\alpha}^{st}(l, m) c_{\beta}^{s't'}(l+s, m+t) + c_{\beta}^{st}(l, m) c_{\alpha}^{s't'}(l+s, m+t) \right) \\
&\quad \times \delta_{l',l+s+s'} \delta_{m',m+t+t'} \int_0^{R_a} dr_a u_{l'\lambda'}(r) u_{l\lambda}(r) \Big\} \tag{6.64}
\end{aligned}$$

Equation (6.64) is the same as the corresponding expression in Ref.[19]. In Ref.[12], equation (16) represents the kinetic stress tensor and it has a different sign compared to equation (6.64). If the author took the further steps as described above to simplify equation (16), the expression of the valence kinetic stress tensor in Ref.[12] would be the same as in equation (6.64) with opposite sign. Moreover, it is suggested in Ref.[12] to use the so called Slater form of the kinetic energy in order to avoid the discontinuity correction. With the continuous radial derivative in the LAPW method, the Slater form and  $\nabla^2$  form of the kinetic energy is equivalent, see section 4.1. In our stress tensor formalism, however, we have an additional surface contribution only in the case of the APW method as described in section 6.3.1. With Ref.[17] we can only compare in the interstitial region and equation (33) in Ref.[17] is the same as the first term of equation (6.64). The first in equation (6.64) is also similar to the first term in Ref.[3], which is derived using the pseudo-potential method. Equation (6.64) has many summation and the computational effort to evaluate such multiple summations operations is demanding. Also, in the above equation wavefunctions are involved directly, and calculations with wave functions are more expensive than with the density. Consequently, the evaluation of the kinetic stress tensor requires appreciably more computational time and memory than that of the electrostatic stress.

### 6.3.1 Additional Surface Integral

As we discussed in section 4.1, in the case of the APW+lo method, if we use  $\nabla \cdot \nabla$  form of the kinetic energy operator an additional surface integral needs to be addressed. The surface integral represents the discontinuity in the slope (radial derivative) of the basis function. This integral vanishes in the case of the LAPW method because the basis functions are continuous due to the matching of the slope at the surface boundary. Before embarking any further discussion, let us recall equation (4.1),

$$\frac{1}{2} \int_{\Omega} d\Omega \nabla \psi_{v\mathbf{k}}^* \cdot \nabla \psi_{v\mathbf{k}} = \frac{1}{2} \int_{\Omega} d\Omega \psi_{v\mathbf{k}}^* (-\nabla^2) \psi_{v\mathbf{k}} + \frac{1}{2} \oint dS \left( \psi_{v\mathbf{k}}^* \frac{\partial \psi_{v\mathbf{k}}^a}{\partial r} - \psi_{v\mathbf{k}}^{*IS} \frac{\partial \psi_{v\mathbf{k}}^{IS}}{\partial r} \right) \quad (6.65)$$

Here for the sake of brevity  $\psi_{v\mathbf{k}}^a(\mathbf{r})$  and  $\psi_{v\mathbf{k}}^{IS}(\mathbf{r})$  are written as  $\psi_{v\mathbf{k}}^a$  and  $\psi_{v\mathbf{k}}^{IS}$ . The second expression of equation (6.65) is the surface term. This section focuses on solving the surface integral and its variation with respect to strain. First we consider interstitial wave functions and calculate their derivative at the boundary of the sphere.

$$\psi_{v\mathbf{k}}^{IS} = \sum_{v\mathbf{k}\mathbf{K}} \frac{c_{v\mathbf{k}\mathbf{K}}}{\sqrt{\Omega}} e^{i(\mathbf{k}+\mathbf{K}) \cdot \mathbf{r}} \quad (6.66)$$

$$= \sum_{v\mathbf{k}\mathbf{K}} \frac{c_{v\mathbf{k}\mathbf{K}}}{\sqrt{\Omega}} e^{i(\mathbf{k}+\mathbf{K}) \cdot \boldsymbol{\tau}_a} e^{i(\mathbf{k}+\mathbf{K}) \cdot \mathbf{r}_a} \quad (6.67)$$

We transferred the vector of the global coordinate system i.e  $\mathbf{r}$  into the vector of the local coordinate system i.e  $\mathbf{r}_a$  using  $\mathbf{r} = \mathbf{r}_a + \boldsymbol{\tau}_a$ . To solve equation (6.67) we use a Rayleigh expansion:  $e^{i(\mathbf{k}+\mathbf{K}) \cdot \mathbf{r}_a} = 4\pi i^l Y_{lm}^*(\widehat{\mathbf{k}+\mathbf{K}}) Y_{lm}(\hat{\mathbf{r}}_a) j_l(|\mathbf{k}+\mathbf{K}|r_a)$

$$\psi_{v\mathbf{k}}^{IS} = \sum_{v\mathbf{k}\mathbf{K}} \frac{c_{v\mathbf{k}\mathbf{K}}}{\sqrt{\Omega}} 4\pi i^l e^{i(\mathbf{k}+\mathbf{K}) \cdot \boldsymbol{\tau}_a} Y_{lm}^*(\widehat{\mathbf{k}+\mathbf{K}}) j_l(|\mathbf{k}+\mathbf{K}|r_a) Y_{lm}(\hat{\mathbf{r}}_a) \quad (6.68)$$

The radial derivative of equation (6.68) is

$$\frac{\partial \psi_{v\mathbf{k}}^{IS}}{\partial r} = \sum_{v\mathbf{k}\mathbf{K}} \frac{c_{v\mathbf{k}\mathbf{K}}}{\sqrt{\Omega}} 4\pi i^l e^{i(\mathbf{k}+\mathbf{K}) \cdot \boldsymbol{\tau}_a} Y_{lm}^*(\widehat{\mathbf{k}+\mathbf{K}}) |\mathbf{k}+\mathbf{K}| j'_l(|\mathbf{k}+\mathbf{K}|r_a) Y_{lm}(\hat{\mathbf{r}}_a) \quad (6.69)$$

When calculating the surface integral we require the following relationship.

$$\begin{aligned} \frac{\partial \psi_{v\mathbf{k}}^{IS}}{\partial r} \Big|_{r=R_a} &= \sum_{v\mathbf{k}\mathbf{K}} \frac{c_{v\mathbf{k}\mathbf{K}}}{\sqrt{\Omega}} 4\pi i^l e^{i(\mathbf{k}+\mathbf{K}) \cdot \boldsymbol{\tau}_a} Y_{lm}^*(\widehat{\mathbf{k}+\mathbf{K}}) |\mathbf{k}+\mathbf{K}| j'_l(|\mathbf{k}+\mathbf{K}|R_a) Y_{lm}(\hat{\mathbf{r}}_a) \\ &= F_{lm}^{av\mathbf{k}} Y_{lm}(\hat{\mathbf{r}}_a), \end{aligned} \quad (6.70)$$

where

$$F_{lm}^{av\mathbf{k}} = \sum_{v\mathbf{k}\mathbf{K}} \frac{c_{v\mathbf{k}\mathbf{K}}}{\sqrt{\Omega}} 4\pi i^l e^{i(\mathbf{k}+\mathbf{K}) \cdot \boldsymbol{\tau}_a} Y_{lm}^*(\widehat{\mathbf{k}+\mathbf{K}}) |\mathbf{k}+\mathbf{K}| j'_l(|\mathbf{k}+\mathbf{K}|R_a) \quad (6.71)$$

let us recall equation (3.20)

$$\psi_{v\mathbf{k}}^a = \sum_{lm} \mathbf{A}_{lm\lambda}^{av\mathbf{k}} u_{l\lambda}(r_a, E_l^a) Y_{lm}(\hat{\mathbf{r}}_a), \quad (6.72)$$

where the label  $\lambda$  distinguishes the radial function ( $\lambda=0$ ) and its energy derivative ( $\lambda=1$ ). In the case of APW+lo, the energy derivative term comes from local orbitals (lo). For the sake of brevity,  $u_{l\lambda}(r_a, E_l^a)$  will be replaced by  $u_{l\lambda}(r_a)$ . The radial derivative of equation (6.72) at the boundary of the sphere is

$$\frac{\partial \psi_{v\mathbf{k}}^a}{\partial r} \Big|_{r=R_a} = \sum_{lm} \sum_{\lambda} \mathbf{A}_{lm\lambda}^{avk} u'_{l\lambda}(R_a) Y_{lm}(\hat{r}_a) \quad (6.73)$$

Using the above expressions, the surface integral term of equation (6.65) becomes

$$S = \frac{1}{2} \oint dS \left( \psi_{v\mathbf{k}}^* \frac{\partial \psi_{v\mathbf{k}}^a}{\partial r} - \psi_{v\mathbf{k}}^* \text{IS} \frac{\partial \psi_{v\mathbf{k}}^{\text{IS}}}{\partial r} \right) \quad (6.74)$$

$$= \sum_{lm} \sum_{\lambda} \mathbf{A}_{lm\lambda}^{avk*} u_{l\lambda}(R_a) \left\{ \sum_{\lambda'} \mathbf{A}_{lm\lambda'}^{avk} u'_{l\lambda'}(R_a) - F_{lm}^{avk} \right\} \quad (6.75)$$

When the system is deformed, the surface integral will be deformed as follows:

$$S[\underline{\epsilon}] = \frac{1}{2} \sum_{lm} \sum_{\lambda} \mathbf{A}_{lm\lambda}^{avk[\underline{\epsilon}]*} u_{l\lambda}[\underline{\epsilon}](R_a) \left\{ \sum_{\lambda'} \mathbf{A}_{lm\lambda'}^{avk[\underline{\epsilon}]} u'_{l\lambda'}[\underline{\epsilon}](R_a) - F_{lm}^{avk[\underline{\epsilon}]} \right\} \quad (6.76)$$

Using the frozen augmentation approximation [31, 37] i.e  $u_{l\lambda}[\underline{\epsilon}](R_a) \rightarrow u_{l\lambda}(R_a)$  equation (6.76) is

$$S[\underline{\epsilon}] = \frac{1}{2} \sum_{lm} \sum_{\lambda} \mathbf{A}_{lm\lambda}^{avk[\underline{\epsilon}]*} u_{l\lambda}(R_a) \left\{ \sum_{\lambda'} \mathbf{A}_{lm\lambda'}^{avk[\underline{\epsilon}]} u'_{l\lambda'}(R_a) - F_{lm}^{avk[\underline{\epsilon}]} \right\} \quad (6.77)$$

The strain variation of equation (6.77) is

$$\begin{aligned} \frac{dS[\underline{\epsilon}]}{d\epsilon_{\alpha\beta}} &= \frac{1}{2} \sum_{lm} \sum_{\lambda} \frac{d\mathbf{A}_{lm\lambda}^{avk[\underline{\epsilon}]*}}{d\epsilon_{\alpha\beta}} u_{l\lambda}(R_a) \left\{ \sum_{\lambda'} \mathbf{A}_{lm\lambda'}^{avk} u'_{l\lambda'}(R_a) - F_{lm}^{avk} \right\} \\ &+ \sum_{lm} \sum_{\lambda} \mathbf{A}_{lm\lambda}^{avk*} u_{l\lambda}(R_a) \left\{ \sum_{\lambda'} \frac{d\mathbf{A}_{lm\lambda'}^{avk[\underline{\epsilon}]} }{d\epsilon_{\alpha\beta}} u'_{l\lambda'}(R_a) - \frac{dF_{lm}^{avk[\underline{\epsilon}]} }{d\epsilon_{\alpha\beta}} \right\}, \end{aligned} \quad (6.78)$$

where

$$\begin{aligned} \frac{dF_{lm}^{avk[\underline{\epsilon}]} }{d\epsilon_{\alpha\beta}} &= \sum_{v\mathbf{k}[\underline{\epsilon}] \mathbf{K}[\underline{\epsilon}]} \frac{c_{v\mathbf{k}\mathbf{K}}}{\sqrt{\Omega}} 4\pi i^l e^{i(\mathbf{k}+\mathbf{K}) \cdot \tau_a} \left( \frac{dY_{lm}^*(\widehat{\mathbf{k}+\mathbf{K}}[\underline{\epsilon}])}{d\epsilon_{\alpha\beta}} |\mathbf{k}+\mathbf{K}| j'_l(|\mathbf{k}+\mathbf{K}| R_a) \right. \\ &\quad \left. + Y_{lm}^*(\widehat{\mathbf{k}+\mathbf{K}}) \frac{d|\mathbf{k}[\underline{\epsilon}]+\mathbf{K}[\underline{\epsilon}]| j'_l(|\mathbf{k}[\underline{\epsilon}]+\mathbf{K}[\underline{\epsilon}]| R_a)}{d\epsilon_{\alpha\beta}} \right) \end{aligned} \quad (6.79)$$

To further simplify equation (6.79), we use the following relations:

$$\frac{dY_{lm}^*(\widehat{\mathbf{k}+\mathbf{K}}[\underline{\epsilon}])}{d\epsilon_{\alpha\beta}} = -\frac{1}{2} \sum_{s=\pm 1} \sum_{t,t'=-1}^1 \left[ (\widehat{\mathbf{k}+\mathbf{K}})_\alpha c_\beta^{st}(l,m) + (\widehat{\mathbf{k}+\mathbf{K}})_\beta c_\alpha^{st}(l,m) \right] Y_{l+s,m+t}^*(\widehat{\mathbf{k}+\mathbf{K}}) \quad (6.80a)$$

$$\frac{d(|\mathbf{k}[\underline{\epsilon}] + \mathbf{K}[\underline{\epsilon}]|j'_l(|\mathbf{k}[\underline{\epsilon}] + \mathbf{K}[\underline{\epsilon}]|R_a))}{d\epsilon_{\alpha\beta}} = -\frac{(\mathbf{k} + \mathbf{K})_\alpha(\mathbf{k} + \mathbf{K})_\beta}{|\mathbf{k} + \mathbf{K}|} j'_l(|\mathbf{k} + \mathbf{K}|R_a) + |\mathbf{k} + \mathbf{K}|R_a j''_l(|\mathbf{k} + \mathbf{K}|R_a) \quad (6.80b)$$

Substituting equations (6.80a) and (6.80b) into equation (6.79)

$$\begin{aligned} \frac{dF_{lm}^{avk[\underline{\epsilon}]} }{d\epsilon_{\alpha\beta}} &= \sum_{v\mathbf{k}[\underline{\epsilon}]\mathbf{K}[\underline{\epsilon}]} \frac{c_v\mathbf{k}\mathbf{K}}{\sqrt{\Omega}} 4\pi i^l e^{i(\mathbf{k}+\mathbf{K})\cdot\tau_a} \\ &\times \left( -\frac{1}{2} \sum_{s=\pm 1} \sum_{t,t'=-1}^1 \left[ (\widehat{\mathbf{k}+\mathbf{K}})_\alpha c_\beta^{st}(l,m) + (\widehat{\mathbf{k}+\mathbf{K}})_\beta c_\alpha^{st}(l,m) \right] \right. \\ &\times Y_{l+1,m+t}^*(\widehat{\mathbf{k}+\mathbf{K}})|\mathbf{k}+\mathbf{K}|j'_l(|\mathbf{k}+\mathbf{K}|R_a) \\ &\left. + Y_{lm}^*(\widehat{\mathbf{k}+\mathbf{K}}) \left[ -\frac{(\mathbf{k}+\mathbf{K})_\alpha(\mathbf{k}+\mathbf{K})_\beta}{|\mathbf{k}+\mathbf{K}|} j'_l(|\mathbf{k}+\mathbf{K}|R_a) + |\mathbf{k}+\mathbf{K}|R_a j''_l(|\mathbf{k}+\mathbf{K}|R_a) \right] \right) \end{aligned}$$

Let us introduce a new notation  $\mathbf{F}_{lm}^{avk}(\alpha, \beta)$  so that

$$\begin{aligned} \mathbf{F}_{lm}^{avk}(\alpha, \beta) &= \frac{dF_{lm}^{avk[\underline{\epsilon}]} }{d\epsilon_{\alpha\beta}} \\ &= \sum_{\mathbf{K}} \frac{c_v\mathbf{k}\mathbf{K}}{\sqrt{\Omega}} 4\pi i^l e^{i(\mathbf{k}+\mathbf{K})\cdot\tau_a} \\ &\times \left( -\frac{1}{2} \sum_{s=\pm 1} \sum_{t,t'=-1}^1 \left[ (\widehat{\mathbf{k}+\mathbf{K}})_\alpha c_\beta^{st}(l,m) + (\widehat{\mathbf{k}+\mathbf{K}})_\beta c_\alpha^{st}(l,m) \right] \right. \\ &\times Y_{l+1,m+t}^*(\widehat{\mathbf{k}+\mathbf{K}})|\mathbf{k}+\mathbf{K}|j'_l(|\mathbf{k}+\mathbf{K}|R_a) \\ &\left. + Y_{lm}^*(\widehat{\mathbf{k}+\mathbf{K}}) \left[ -\frac{(\mathbf{k}+\mathbf{K})_\alpha(\mathbf{k}+\mathbf{K})_\beta}{|\mathbf{k}+\mathbf{K}|} j'_l(|\mathbf{k}+\mathbf{K}|R_a) + |\mathbf{k}+\mathbf{K}|R_a j''_l(|\mathbf{k}+\mathbf{K}|R_a) \right] \right) \end{aligned}$$

The detailed derivation of  $\frac{dA_{lm\lambda}^{avk[\underline{\epsilon}]*}}{d\epsilon_{\alpha\beta}}$  can be found in section 6.4. Here, we introduce also a new notation  $\mathbf{D}_{lm0}^{avk}(\alpha, \beta)$  so that

$$\begin{aligned} \mathbf{D}_{lm0}^{avk}(\alpha, \beta) &= \frac{dA_{lm0}^{avk[\underline{\epsilon}]*}}{d\epsilon_{\alpha\beta}} \\ &= -\sum_{\mathbf{K}} \frac{c_v\mathbf{k}\mathbf{K}}{\sqrt{\Omega}} 4\pi i^l e^{i(\mathbf{k}+\mathbf{K})\cdot\tau_a} \left( Y_{lm}^*(\widehat{\mathbf{k}+\mathbf{K}}) \frac{j'_l(|\mathbf{k}+\mathbf{K}|R_a)}{u_l(R_a)} R_a \frac{(\mathbf{k}+\mathbf{K})_\alpha(\mathbf{k}+\mathbf{K})_\beta}{|\mathbf{k}+\mathbf{K}|} \right. \\ &\left. + \frac{1}{2} \sum_{s=\pm 1} \sum_{t,t'=-1}^1 \left[ (\mathbf{k}+\mathbf{K})_\alpha c_\beta^{st}(l,m) + (\mathbf{k}+\mathbf{K})_\beta c_\alpha^{st}(l,m) \right] \frac{Y_{l+1,m+t}^*(\widehat{\mathbf{k}+\mathbf{K}})}{|\mathbf{k}+\mathbf{K}|} \frac{j_l(|\mathbf{k}+\mathbf{K}|R_a)}{u_l(R_a)} \right) \end{aligned}$$

Substituting the above equations into Equation (6.78), we get:

$$\begin{aligned} \frac{dS[\underline{\epsilon}]}{d\epsilon_{\alpha\beta}} &= \frac{1}{2} \sum_{lm} \sum_{\lambda} \mathbf{D}_{lm}^{avk}(\alpha, \beta) u_{l\lambda}(R_a) \left\{ \sum_{\lambda'} \mathbf{A}_{lm\lambda'}^{avk} u'_{l\lambda'}(R_a) - F_{lm}^{avk} \right\} \\ &+ \frac{1}{2} \sum_{lm} \sum_{\lambda} \mathbf{A}_{lm\lambda}^{avk*} u_{l\lambda}(R_a) \left\{ \sum_{\lambda'} \mathbf{D}_{lm}^{avk}(\alpha, \beta) u'_{l\lambda'}(R_a) - \mathbf{F}_{lm}^{avk}(\alpha, \beta) \right\} \quad (6.81) \end{aligned}$$

We assign  $\frac{1}{\Omega} \frac{dS[\underline{\epsilon}]}{d\epsilon_{\alpha\beta}}$  as  $\sigma_{\alpha\beta}^{APW}$ . The superscript *APW* is to specify that the contribution becomes significant only if APW+lo is used.

$$\begin{aligned}\sigma_{\alpha\beta}^{APW} = & \frac{1}{2\Omega} \sum_{lm} \sum_{\lambda} \mathbf{D}_{lm}^{avk}(\alpha, \beta) u_{l\lambda}(R_a) \left\{ \sum_{\lambda'} \mathbf{A}_{lm\lambda'}^{avk} u'_{l\lambda'}(R_a) - F_{lm}^{avk} \right\} \\ & + \frac{1}{2\Omega} \sum_{lm} \sum_{\lambda} \mathbf{A}_{lm\lambda}^{avk*} u_{l\lambda}(R_a) \left\{ \sum_{\lambda'} \mathbf{D}_{lm}^{avk}(\alpha, \beta) u'_{l\lambda'}(R_a) - \mathbf{F}_{lm}^{avk}(\alpha, \beta) \right\}\end{aligned}\quad (6.82)$$

This additional surface integral needs to be added to our total stress tensor formalism, equation (6.2), if the APW+lo basis functions are used. In the case of the LAPW method, the slope of the basis functions at the boundary of the sphere is continuous and therefore the contribution of the expression in equation (6.75) disappears. Consequently, the contribution of equation (6.82) also disappears.

## 6.4 Valence Correction Stress Tensor

When a system is deformed, both valence and core eigenvalues will be changed. The change of the core eigenvalue together with the double-counting term gives the core correction, which is discussed in section 6.2. Likewise, the variation of valence eigenvalues gives the valence correction. General expression of the valence correction stress tensor according to equation (6.3c) is

$$\sigma_{\alpha\beta}^{val,corr} = \frac{2}{\Omega} \sum_{v\mathbf{k}} n_{v\mathbf{k}} \Re \left\langle \frac{d\psi_{v\mathbf{k}}[\underline{\epsilon}](\mathbf{r}[\underline{\epsilon}])}{d\epsilon_{\alpha\beta}} \Bigg|_{\underline{\epsilon}=0} \left| \hat{H}_{eff}(\mathbf{r}) - \epsilon_{v\mathbf{k}} \right| \psi_{v\mathbf{k}} \right\rangle \quad (6.83)$$

The valence correction is sometimes referred to as incomplete basis set (IBS) correction because it originates from the fact that there is a finite number of basis functions. In the APW based methods, the valence wave functions are approximated and the basis function used to expand them as in equation (3.18) are incomplete. As a consequence, the strain variation of the eigenfunctions can no longer be expected to be expandable in terms of the same basis functions. Also, our basis functions have an atomic position ( $\boldsymbol{\tau}_a$ ) dependency, which means if the position of an atomic is displaced, our basis functions will be displaced along with it. These two effects contribute to  $\sigma_{\alpha\beta}^{val,corr}$ .

$\psi_{v\mathbf{k}}(\mathbf{r})$  represents the valence states and they are distributed over the entire unit cell. Therefore, the integration limit in the above equation is over the whole unit cell, but adopting the technique given in Ref. [19] demonstrates that the interstitial part of the integral will not contribute because the plane waves are a complete basis set. Let's consider only  $\frac{\delta\psi_{v\mathbf{k}}[\underline{\epsilon}](\mathbf{r}[\underline{\epsilon}])}{\delta\epsilon_{\alpha\beta}} \Bigg|_{\underline{\epsilon}=0}$  and manipulate as given below.

$$\begin{aligned}
\left. \frac{d\psi_{v\mathbf{k}[\underline{\epsilon}]}(\mathbf{r}[\underline{\epsilon}])}{d\epsilon_{\alpha\beta}} \right|_{\underline{\epsilon}=0} &= \sum_{\mathbf{K}} \frac{d}{d\epsilon_{\alpha\beta}} \Bigg|_{\underline{\epsilon}=0} \left[ c_{v\mathbf{k}[\underline{\epsilon}]\mathbf{K}[\underline{\epsilon}][\underline{\epsilon}]} \cdot \phi_{\mathbf{k}[\underline{\epsilon}]\mathbf{K}[\underline{\epsilon}][\underline{\epsilon}]}(\mathbf{r}[\underline{\epsilon}]) \right] \\
&= \sum_{\mathbf{K}} \frac{d}{d\epsilon_{\alpha\beta}} \Bigg|_{\underline{\epsilon}=0} \left[ \frac{c_{v\mathbf{k}[\underline{\epsilon}]\mathbf{K}[\underline{\epsilon}][\underline{\epsilon}]}[\underline{\epsilon}]}{\sqrt{\Omega[\underline{\epsilon}]}} \cdot \sqrt{\Omega[\underline{\epsilon}]} \phi_{\mathbf{k}[\underline{\epsilon}]\mathbf{K}[\underline{\epsilon}][\underline{\epsilon}]}(\mathbf{r}[\underline{\epsilon}]) \right] \\
&= \sum_{\mathbf{K}} \left( \frac{d}{d\epsilon_{\alpha\beta}} \left[ \frac{c_{v\mathbf{k}[\underline{\epsilon}]\mathbf{K}[\underline{\epsilon}][\underline{\epsilon}]}[\underline{\epsilon}]}{\sqrt{\Omega[\underline{\epsilon}]}} \right] \Bigg|_{\underline{\epsilon}=0} \sqrt{\Omega} \phi_{\mathbf{k}\mathbf{K}}(\mathbf{r}) + \frac{c_{v\mathbf{k}\mathbf{K}}}{\sqrt{\Omega}} \frac{d}{d\epsilon_{\alpha\beta}} \left[ \sqrt{\Omega[\underline{\epsilon}]} \phi_{\mathbf{k}[\underline{\epsilon}]\mathbf{K}[\underline{\epsilon}][\underline{\epsilon}]}(\mathbf{r}[\underline{\epsilon}]) \right]_{\underline{\epsilon}=0} \right) \tag{6.84}
\end{aligned}$$

The first term in the above equation is proportional to the basis functions, so it does not contribute to equation (6.83). The second term, for the interstitial region, can be further simplified as given below:

$$\sqrt{\Omega[\underline{\epsilon}]} \phi_{\mathbf{k}[\underline{\epsilon}]\mathbf{K}[\underline{\epsilon}][\underline{\epsilon}]}(\mathbf{r}[\underline{\epsilon}]) = \sqrt{\Omega[\underline{\epsilon}]} \frac{e^{i(\mathbf{k}[\underline{\epsilon}]+\mathbf{K}[\underline{\epsilon}])\mathbf{r}[\underline{\epsilon}]}}{\sqrt{\Omega[\underline{\epsilon}]}} = e^{i(\mathbf{k}+\mathbf{K})\mathbf{r}+O(\underline{\epsilon}^2)} \tag{6.85}$$

Equation (6.85) in first order approximation becomes:

$$\frac{d}{d\epsilon_{\alpha\beta}} \left[ \sqrt{\Omega[\underline{\epsilon}]} \phi_{\mathbf{k}[\underline{\epsilon}]\mathbf{K}[\underline{\epsilon}][\underline{\epsilon}]}(\mathbf{r}[\underline{\epsilon}]) \right]_{\underline{\epsilon}=0} \longrightarrow 0 \tag{6.86}$$

The valence correction as given in equation (6.83) can thus be simplified as an integral over the atomic spheres:

$$\begin{aligned}
\sigma_{\alpha\beta}^{val,corr} &= \frac{2}{\Omega} \sum_{v\mathbf{k}} n_{v\mathbf{k}} \Re \left[ \int_{R_a} d^3 r_a \left( \sum_{\mathbf{K}} \frac{c_{v\mathbf{k}\mathbf{K}}}{\sqrt{\Omega}} \frac{d}{d\epsilon_{\alpha\beta}} \left[ \sqrt{\Omega[\underline{\epsilon}]} \phi_{\mathbf{k}[\underline{\epsilon}]\mathbf{K}[\underline{\epsilon}][\underline{\epsilon}]}(\mathbf{r}_a[\underline{\epsilon}]) \right]_{\underline{\epsilon}=0} \right)^* (\hat{H}_{eff} - \epsilon_v(\mathbf{k})) \psi_{v\mathbf{k}}(\mathbf{r}) \right] \\
&= \frac{2}{\Omega} \sum_{v\mathbf{k}} n_{v\mathbf{k}} \Re(I_{\alpha\beta}^{av}(\mathbf{k})) \tag{6.87}
\end{aligned}$$

In the above expression,  $R_a$  represents the integration domain is inside an atomic sphere  $a$  only, and  $I_{\alpha\beta}^{av}(\mathbf{k})$  is the representation of the term inside the square bracket.  $\Re$  is to denote the real part of a complex number.

$$I_{\alpha\beta}^{av}(\mathbf{k}) = \int_{R_a} d^3 r_a \left( \sum_{\mathbf{K}} \frac{c_{v\mathbf{k}\mathbf{K}}}{\sqrt{\Omega}} \frac{d}{d\epsilon_{\alpha\beta}} \left[ \sqrt{\Omega[\underline{\epsilon}]} \phi_{\mathbf{k}[\underline{\epsilon}]\mathbf{K}[\underline{\epsilon}][\underline{\epsilon}]}(\mathbf{r}_a[\underline{\epsilon}]) \right]_{\underline{\epsilon}=0} \right)^* (\hat{H}_{eff} - \epsilon_v(\mathbf{k})) \psi_{v\mathbf{k}}(\mathbf{r}) \tag{6.88}$$

In a strained system, the basis function,  $\phi_{\mathbf{k}\mathbf{K}}(\mathbf{r})$ , is given as:

$$\phi_{\mathbf{k}[\underline{\epsilon}]\mathbf{K}[\underline{\epsilon}][\underline{\epsilon}]}(\mathbf{r}[\underline{\epsilon}]) = \sum_{lm\lambda} a_{lm\lambda}^{a\mathbf{k}[\underline{\epsilon}]\mathbf{G}[\underline{\epsilon}]} u_{l\lambda}(\underline{\epsilon})(r_a[\underline{\epsilon}]) Y_{lm}(\hat{r}_a[\underline{\epsilon}]) \tag{6.89}$$

and using the frozen augmentation approximation[31].

$$u_{l\lambda}[\underline{\epsilon}](r_a[\underline{\epsilon}]) \longrightarrow u_{l\lambda}(r_a[\underline{\epsilon}]) \quad (6.90)$$

the strained variation in equation (6.89) is:

$$\frac{d}{d\epsilon_{\alpha\beta}} \left[ \sqrt{\Omega[\underline{\epsilon}]} \phi_{\mathbf{k}[\underline{\epsilon}]\mathbf{K}[\underline{\epsilon}]}(\mathbf{r}[\underline{\epsilon}]) \right]_{\underline{\epsilon}=0} = \sum_{lm\lambda} \left[ \frac{d}{d\epsilon_{\alpha\beta}} \sqrt{\Omega[\underline{\epsilon}]} a_{lm\lambda}^{a\mathbf{k}[\underline{\epsilon}]\mathbf{K}[\underline{\epsilon}]} \right]_{\underline{\epsilon}=0} u_{l\lambda}^a(r_a) Y_{lm}(\hat{\mathbf{r}}_a) \quad (6.91a)$$

$$+ \sqrt{\Omega} \sum_{lm\lambda} a_{lm\lambda}^{a\mathbf{k}\mathbf{K}} \left[ \frac{d}{d\epsilon_{\alpha\beta}} u_{l\lambda}^a(r_a[\underline{\epsilon}]) \right]_{\underline{\epsilon}=0} Y_{lm}(\hat{\mathbf{r}}_a) \quad (6.91b)$$

$$+ \sqrt{\Omega} \sum_{lm\lambda} a_{lm\lambda}^{a\mathbf{k}\mathbf{K}} u_{l\lambda}^a(r_a) \left[ \frac{d}{d\epsilon_{\alpha\beta}} Y_{lm}(\hat{\mathbf{r}}_a[\underline{\epsilon}]) \right]_{\underline{\epsilon}=0} \quad (6.91c)$$

Substituting equations (6.91a), (6.91b), and (6.91c) in (6.88). The integral  $I_{\alpha\beta}^{av}(\mathbf{k})$  can be split into three different parts. These three different expressions originate from the variation of matching coefficients, radial functions and spherical harmonics according to the strain.

$$I_{\alpha\beta}^{av}(\mathbf{k}) = I_{\alpha\beta}^{av(1)}(\mathbf{k}) + I_{\alpha\beta}^{av(2)}(\mathbf{k}) + I_{\alpha\beta}^{av(3)}(\mathbf{k}), \quad (6.92)$$

where  $I_{\alpha\beta}^{av(1)}(\mathbf{k})$ ,  $I_{\alpha\beta}^{av(2)}(\mathbf{k})$ , and  $I_{\alpha\beta}^{av(3)}(\mathbf{k})$  are given below:

$$I_{\alpha\beta}^{av(1)}(\mathbf{k}) = \sum_{\mathbf{K}} \sum_{lm\lambda} \frac{c_{v\mathbf{k}\mathbf{K}}^*}{\sqrt{\Omega}} \int_{R_a} d^3 r_a \left( \left[ \frac{d}{d\epsilon_{\alpha\beta}} \sqrt{\Omega[\underline{\epsilon}]} a_{lm\lambda}^{a\mathbf{k}[\underline{\epsilon}]\mathbf{K}[\underline{\epsilon}]} \right]_{\underline{\epsilon}=0} u_{l\lambda}^a(r_a) Y_{lm}(\hat{\mathbf{r}}_a) \right)^* (\hat{H}_{eff} - \epsilon_v(\mathbf{k})) \psi_{v\mathbf{k}}(\mathbf{r}) \quad (6.93)$$

$$I_{\alpha\beta}^{av(2)}(\mathbf{k}) = \sum_{\mathbf{K}} \sum_{lm\lambda} \frac{c_{v\mathbf{k}\mathbf{K}}^*}{\sqrt{\Omega}} \int_{R_a} d^3 r_a \left( \sqrt{\Omega} a_{lm\lambda}^{a\mathbf{k}\mathbf{K}} \left[ \frac{d}{d\epsilon_{\alpha\beta}} u_{l\lambda}^a(r_a[\underline{\epsilon}]) \right]_{\underline{\epsilon}=0} Y_{lm}(\hat{\mathbf{r}}_a) \right)^* (\hat{H}_{eff} - \epsilon_v(\mathbf{k})) \psi_{v\mathbf{k}}(\mathbf{r}) \quad (6.94)$$

$$I_{\alpha\beta}^{av(3)}(\mathbf{k}) = \sum_{\mathbf{K}} \sum_{lm\lambda} \frac{c_{v\mathbf{k}\mathbf{K}}^*}{\sqrt{\Omega}} \int_{R_a} d^3 r_a \left( \sqrt{\Omega} a_{lm\lambda}^{a\mathbf{k}\mathbf{K}} u_{l\lambda}^a(r_a) \left[ \frac{d}{d\epsilon_{\alpha\beta}} Y_{lm}(\hat{\mathbf{r}}_a[\underline{\epsilon}]) \right]_{\underline{\epsilon}=0} \right)^* (\hat{H}_{eff} - \epsilon_v(\mathbf{k})) \psi_{v\mathbf{k}}(\mathbf{r}) \quad (6.95)$$

To solve equation (6.93), the matching coefficients are defined for a deformed system:

$$\begin{pmatrix} a_{lm}^{a\mathbf{k}[\underline{\epsilon}]\mathbf{K}[\underline{\epsilon}]} \\ b_{lm}^{a\mathbf{k}[\underline{\epsilon}]\mathbf{K}[\underline{\epsilon}]} \end{pmatrix} \equiv 4\pi i^l e^{i(\mathbf{k}[\underline{\epsilon}] + \mathbf{K}[\underline{\epsilon}])\tau_a[\underline{\epsilon}]} Y_{lm}^*(\mathbf{k}[\underline{\epsilon}] + \widehat{\mathbf{K}}[\underline{\epsilon}]) \underline{U}^{-1} \cdot \begin{pmatrix} j_l(|\mathbf{k}[\underline{\epsilon}] + \mathbf{K}[\underline{\epsilon}]| R_a) \\ |\mathbf{k}[\underline{\epsilon}] + \mathbf{K}[\underline{\epsilon}]| j'_l(|\mathbf{k}[\underline{\epsilon}] + \mathbf{K}[\underline{\epsilon}]| R_a) \end{pmatrix} e^{i(\mathbf{k} + \mathbf{K})\tau_a + O(\underline{\epsilon}^2)} \quad (6.96)$$

The expression suggests that the change in the matching coefficients is due to the change of  $Y_{lm}$  and  $j_l$  according to the change of  $\mathbf{K}$  and  $\mathbf{k}$  when the lattice is deformed. Also,  $\underline{U}^{-1}$  does not depend on strain according to the frozen augmentation approximation.

$$\begin{aligned} \frac{d}{d\epsilon_{\alpha\beta}} \left[ \sqrt{\Omega[\underline{\epsilon}]} \begin{pmatrix} a_{lm}^{a\mathbf{k}[\underline{\epsilon}]\mathbf{K}[\underline{\epsilon}]} \\ b_{lm}^{a\mathbf{k}[\underline{\epsilon}]\mathbf{K}[\underline{\epsilon}]} \end{pmatrix} \right]_{\underline{\epsilon}=0} &= 4\pi i^l e^{i(\mathbf{k} + \mathbf{K})\tau_a} \left\{ \frac{dY_{lm}^*(\mathbf{k}[\underline{\epsilon}] + \widehat{\mathbf{K}}[\underline{\epsilon}])}{d\epsilon_{\alpha\beta}} \Big|_{\underline{\epsilon}=0} \underline{U}^{-1} \cdot \begin{pmatrix} j_l(|\mathbf{k} + \mathbf{K}| R_a) \\ |\mathbf{k} + \mathbf{K}| j'_l(|\mathbf{k} + \mathbf{K}| R_a) \end{pmatrix} \right. \\ &\quad \left. + Y_{lm}^*(\mathbf{k} + \widehat{\mathbf{K}}) \underline{U}^{-1} \cdot \frac{d}{d\epsilon_{\alpha\beta}} \left[ \begin{pmatrix} j_l(|\mathbf{k}[\underline{\epsilon}] + \mathbf{K}[\underline{\epsilon}]| R_a) \\ |\mathbf{k}[\underline{\epsilon}] + \mathbf{K}[\underline{\epsilon}]| j'_l(|\mathbf{k}[\underline{\epsilon}] + \mathbf{K}[\underline{\epsilon}]| R_a) \end{pmatrix} \right]_{\underline{\epsilon}=0} \right\} \end{aligned} \quad (6.97)$$

From equation (A.10):

$$\frac{d}{d\epsilon_{\alpha\beta}} \left|_{\underline{\varepsilon}=0} \right. Y_{lm}(|\widehat{\mathbf{k}+\mathbf{K}}|[\underline{\varepsilon}]) = -\frac{1}{2} \sum_{s=\pm 1} \sum_{t,t'=-1}^1 [c_{\alpha t'} c_{\beta}^{st}(l,m) + c_{\beta t'} c_{\alpha}^{st}(l,m)] Y_{1t'}((\widehat{\mathbf{k}+\mathbf{K}})) Y_{l+s,m+t}((\widehat{\mathbf{k}+\mathbf{K}}))$$

Also,

$$\begin{aligned} \frac{d}{d\epsilon_{\alpha\beta}} \left[ \left( \frac{j_l(|\mathbf{k}|[\underline{\varepsilon}] + \mathbf{K}|[\underline{\varepsilon}]|R_a)}{|\mathbf{k}|[\underline{\varepsilon}] + \mathbf{K}|[\underline{\varepsilon}]|j'_l(|\mathbf{k}|[\underline{\varepsilon}] + \mathbf{K}|[\underline{\varepsilon}]|R_a)} \right) \right]_{\underline{\varepsilon}=0} &= \frac{d}{d|\mathbf{k}+\mathbf{K}|} \left( \frac{j_l(|\mathbf{k}+\mathbf{K}|R_a)}{|\mathbf{k}+\mathbf{K}| j'_l(|\mathbf{k}+\mathbf{K}|R_a)} \right) \frac{d|\mathbf{k}|[\underline{\varepsilon}] + \mathbf{K}|[\underline{\varepsilon}]}{d\epsilon_{\alpha\beta}} \Big|_{\underline{\varepsilon}=0} \\ &\stackrel{(A.15)}{=} -(\widehat{\mathbf{k}+\mathbf{K}})_{\alpha} (\widehat{\mathbf{k}+\mathbf{K}})_{\beta} |\mathbf{k}+\mathbf{K}| \left( \frac{R_a j'_l(|\mathbf{k}+\mathbf{K}|R_a)}{j'_l(|\mathbf{k}+\mathbf{K}|R_a) + |\mathbf{k}+\mathbf{K}|R_a j''_l(|\mathbf{k}+\mathbf{K}|R_a)} \right) \end{aligned} \quad (6.98)$$

Substituting (6.98) and (6.98) in (6.97):

$$\begin{aligned} \frac{d}{d\epsilon_{\alpha\beta}} \left[ \sqrt{\Omega[\underline{\varepsilon}]} \left( \frac{a_{lm}^{a\mathbf{k}\mathbf{K}}[\underline{\varepsilon}]}{b_{lm}^{a\mathbf{k}\mathbf{K}}[\underline{\varepsilon}]} \right) \right]_{\underline{\varepsilon}=0} &= 4\pi i^l e^{i(\mathbf{k}+\mathbf{K})\tau_a} \left\{ \right. \\ \left[ -\frac{1}{2} \sum_{s=\pm 1} \sum_{t,t'=-1}^1 [c_{\alpha t'} c_{\beta}^{st}(l,m) + c_{\beta t'} c_{\alpha}^{st}(l,m)] Y_{1t'}((\widehat{\mathbf{k}+\mathbf{K}})) Y_{l+s,m+t}((\widehat{\mathbf{k}+\mathbf{K}})) \right] \underline{\underline{U}}^{-1} \cdot \left( \frac{j_l(|\mathbf{k}+\mathbf{K}|R_a)}{|\mathbf{k}+\mathbf{K}| j'_l(|\mathbf{k}+\mathbf{K}|R_a)} \right) \\ \left. - Y_{lm}^*(\widehat{\mathbf{k}+\mathbf{K}}) \underline{\underline{U}}^{-1} \cdot (\widehat{\mathbf{k}+\mathbf{K}})_{\alpha} (\widehat{\mathbf{k}+\mathbf{K}})_{\beta} |\mathbf{k}+\mathbf{K}| \left( \frac{R_a j'_l(|\mathbf{k}+\mathbf{K}|R_a)}{j'_l(|\mathbf{k}+\mathbf{K}|R_a) + |\mathbf{k}+\mathbf{K}|R_a j''_l(|\mathbf{k}+\mathbf{K}|R_a)} \right) \right\} \end{aligned} \quad (6.99)$$

The left hand side of the equation is

$$\sqrt{\Omega} \left( \frac{d_{lm0}^{a\mathbf{k}\mathbf{K}}(\alpha, \beta)}{d_{lm1}^{a\mathbf{k}\mathbf{K}}(\alpha, \beta)} \right) \equiv \frac{d}{d\epsilon_{\alpha\beta}} \left[ \sqrt{\Omega[\underline{\varepsilon}]} \left( \frac{a_{lm}^{a\mathbf{k}\mathbf{K}}[\underline{\varepsilon}]}{b_{lm}^{a\mathbf{k}\mathbf{K}}[\underline{\varepsilon}]} \right) \right]_{\underline{\varepsilon}=0} \quad (6.100)$$

The notation  $d_{lm\lambda}^{a\mathbf{k}\mathbf{K}}(\alpha, \beta)$  suggests that when a system is deformed, the matching will be different in each directions ( $\alpha = 1, 2, 3$ ) because  $(\mathbf{k}+\mathbf{K})_{\alpha}$  is different for  $\alpha = 1, 2, 3$ .  $d_{lm\lambda}^{a\mathbf{k}\mathbf{K}}(\alpha, \beta)$  arises due to the change in k points in the Brillouin zone and the reciprocal lattice vector  $\mathbf{K}$  in the interstitial when the system is deformed.

Now,

$$\begin{aligned} \left( \frac{d_{lm0}^{a\mathbf{k}\mathbf{K}}(\alpha, \beta)}{d_{lm1}^{a\mathbf{k}\mathbf{K}}(\alpha, \beta)} \right) &= \frac{4\pi i^l e^{i(\mathbf{k}+\mathbf{K})\tau_a}}{\sqrt{\Omega}} \left\{ \left[ -\frac{1}{2} \sum_{s=\pm 1} \sum_{t,t'=-1}^1 [c_{\alpha t'} c_{\beta}^{st}(l,m) + c_{\beta t'} c_{\alpha}^{st}(l,m)] Y_{1t'}(\widehat{\mathbf{r}}) Y_{l+s,m+t}(\widehat{\mathbf{r}}) \right] \underline{\underline{U}}^{-1} \cdot \left( \frac{j_l(|\mathbf{k}+\mathbf{K}|R_a)}{|\mathbf{k}+\mathbf{K}| j'_l(|\mathbf{k}+\mathbf{K}|R_a)} \right) \right. \\ &\quad \left. - Y_{lm}^*(\widehat{\mathbf{k}+\mathbf{K}}) \underline{\underline{U}}^{-1} \cdot (\widehat{\mathbf{k}+\mathbf{K}})_{\alpha} (\widehat{\mathbf{k}+\mathbf{K}})_{\beta} |\mathbf{k}+\mathbf{K}| \left( \frac{R_a j'_l(|\mathbf{k}+\mathbf{K}|R_a)}{j'_l(|\mathbf{k}+\mathbf{K}|R_a) + |\mathbf{k}+\mathbf{K}|R_a j''_l(|\mathbf{k}+\mathbf{K}|R_a)} \right) \right\} \end{aligned} \quad (6.101)$$

From equation (6.93):

$$I_{\alpha\beta}^{av(1)}(\mathbf{k}) = \sum_{\mathbf{K}} \sum_{lm\lambda} \frac{c_{v\mathbf{k}\mathbf{K}}^*}{\sqrt{\Omega}} \int_{R_a} d^3 r_a \left( \left[ \frac{d}{d\epsilon_{\alpha\beta}} \sqrt{\Omega[\underline{\varepsilon}]} a_{lm\lambda}^{a\mathbf{k}\mathbf{K}}[\underline{\varepsilon}] \right]_{\underline{\varepsilon}=0} u_{l\lambda}^a(r_a) Y_{lm}(\widehat{\mathbf{r}}_a) \right)^* (\widehat{H}_{eff} - \epsilon_v(\mathbf{k})) \psi_{v\mathbf{k}}(\mathbf{r}) \quad (6.102a)$$

$$= \sum_{\mathbf{K}} \sum_{lm\lambda} c_{v\mathbf{k}\mathbf{K}}^* \int_{R_a} d^3 r_a \left( d_{lm\lambda}^{a\mathbf{k}\mathbf{K}}(\alpha, \beta) u_{l\lambda}^a(r_a) Y_{lm}(\widehat{\mathbf{r}}_a) \right)^* (\widehat{H}_{eff} - \epsilon_v(\mathbf{k})) \psi_{v\mathbf{k}}(\mathbf{r}) \quad (6.102b)$$

$$= \sum_{lm\lambda} \int_{R_a} d^3 r_a \left( D_{lm\lambda}^{av\mathbf{k}}(\alpha, \beta) u_{l\lambda}^a(r_a) Y_{lm}(\widehat{\mathbf{r}}_a) \right)^* (\widehat{H}_{eff} - \epsilon_v(\mathbf{k})) \psi_{v\mathbf{k}}(\mathbf{r}) \quad (6.102c)$$

The capital D coefficients in the above equation are defined as

$$D_{lm\lambda}^{av\mathbf{k}}(\alpha, \beta) = \sum_{\mathbf{K}} c_{v\mathbf{k}\mathbf{K}} d_{lm\lambda}^{a\mathbf{k}\mathbf{K}}(\alpha, \beta) \quad (6.103)$$

Furthermore, the total Hamiltonian  $H_{eff}$  is split into spherical and non-spherical parts, according to the spherical and non-spherical parts of the potential.

$$H_{eff} = H_{sph}^a + H_{non-sph}^a \quad (6.104)$$

$$= H_{sph}^a + \sum_{L''>0} V_{L''}^{a\text{eff}}(r_a) Y_{L''}(\hat{\mathbf{r}}_a) \quad (6.105)$$

The subscript  $L''$  represents the combination of  $l''$  and  $m''$ . Owing to equation (6.104), the integral  $I_{\alpha\beta}^{av\ (1)}(\mathbf{k})$  splits into the spherical and non-spherical parts.

$$I_{\alpha\beta}^{av\ (1)}(\mathbf{k}) = I_{\alpha\beta}^{av1\ sph}(\mathbf{k}) + I_{\alpha\beta}^{av1\ non-sph}(\mathbf{k}) \quad (6.106)$$

The functions  $I_{\alpha\beta}^{av1\ sph}(\mathbf{k})$  and  $I_{\alpha\beta}^{av1\ non-sph}(\mathbf{k})$  are defined as

$$I_{\alpha\beta}^{av1\ sph}(\mathbf{k}) = \sum_{lm\lambda} \int_{R_a} d^3 r_a (D_{lm\lambda}^{av\mathbf{k}}(\alpha, \beta) u_{l\lambda}^a(r_a) Y_{lm}(\hat{\mathbf{r}}_a))^* (\hat{H}_{sph} - \epsilon_v(\mathbf{k})) \psi_{v\mathbf{k}}(\mathbf{r}) \quad (6.107)$$

$$I_{\alpha\beta}^{av1\ non-sph}(\mathbf{k}) = \sum_{lm\lambda} \int_{R_a} d^3 r_a (D_{lm\lambda}^{av\mathbf{k}}(\alpha, \beta) u_{l\lambda}^a(r_a) Y_{lm}(\hat{\mathbf{r}}_a))^* \hat{H}_{non-sph} \psi_{v\mathbf{k}}(\mathbf{r}) \quad (6.108)$$

We know that the radial function  $u_l^a(r_a)$  and its energy derivative  $\dot{u}_l^a(r_a)$  are the solution of the following two equations:

$$H_{sph}^a u_l^a = E_l^a u_l^a \quad (6.109)$$

$$H_{sph}^a \dot{u}_l^a = u_l^a + E_l^a \dot{u}_l^a \quad (6.110)$$

Combining these two equations:

$$H_{sph}^a u_{l\lambda}^a = E_l^a u_{l\lambda}^a + \delta_{\lambda 1} u_l^a \quad (6.111)$$

Also,

$$(H_{sph}^a - \epsilon_{v\mathbf{k}}) u_{l\lambda}^a = (E_l^a - \epsilon_{v\mathbf{k}}) u_{l\lambda}^a + \delta_{\lambda 1} u_l^a \quad (6.112)$$

This suggests:

$$\begin{aligned} (H_{sph}^a - \epsilon_{v\mathbf{k}}) \psi_{v\mathbf{k}}(\mathbf{r}) &\stackrel{(3.6)}{=} \sum_{L'\lambda'} A_{L'\lambda'} (H_{sph}^a - \epsilon_{v\mathbf{k}}) u_{l'\lambda'}^a(r_a) Y_{L'}(\hat{\mathbf{r}}_a) \\ &= \sum_{L'\lambda'} A_{L'\lambda'}^{\text{av}\mathbf{k}} [(E_{l'}^a - \epsilon_{v\mathbf{k}}) u_{l'\lambda'}^a(r_a) + \delta_{\lambda' 1} u_{l'}^a(r_a)] Y_{L'}(\hat{\mathbf{r}}_a) \end{aligned} \quad (6.113)$$

After collecting all the intermediate calculations, equation (6.107) becomes:

$$\begin{aligned}
I_{\alpha\beta}^{av1 sph}(\mathbf{k}) &= \sum_{L\lambda} \sum_{L'\lambda'} D_{L\lambda}^{av\mathbf{k}*}(\alpha, \beta) A_{L'\lambda'}^{av\mathbf{k}} \int_0^{R_a} r_a^2 dr_a u_{l\lambda}^a(r_a) \left[ (E_l^a - \epsilon_{v\mathbf{k}}) u_{l'\lambda'}^a(r_a) + \delta_{\lambda'1} u_{l'}^a(r_a) \right] \underbrace{\oint ds Y_L(\hat{\mathbf{r}}_a) Y_{L'}(\hat{\mathbf{r}}_a)}_{\delta_{L'L}} \\
&= \sum_{L\lambda\lambda'} D_{L\lambda}^{av\mathbf{k}*}(\alpha, \beta) A_{L\lambda'}^{av\mathbf{k}} \int_0^{R_a} r_a^2 dr_a u_{l\lambda}^a(r_a) \left[ (E_l^a - \epsilon_{v\mathbf{k}}) u_{l\lambda'}^a(r_a) + \delta_{\lambda'1} u_{l'}^a(r_a) \right] \\
&= \sum_{L\lambda\lambda'} D_{L\lambda}^{av\mathbf{k}*}(\alpha, \beta) A_{L\lambda'}^{av\mathbf{k}} \left[ (E_l^a - \epsilon_{v\mathbf{k}}) \int_0^{R_a} r_a^2 dr_a u_{l\lambda}^a(r_a) u_{l\lambda'}^a(r_a) + \delta_{\lambda'1} \int_0^{R_a} r_a^2 dr_a u_{l\lambda}^a(r_a) u_l^a(r_a) \right] \\
&= \sum_{L\lambda\lambda'} D_{L\lambda}^{av\mathbf{k}*}(\alpha, \beta) A_{L\lambda'}^{av\mathbf{k}} \left[ (E_l^a - \epsilon_{v\mathbf{k}}) \delta_{\lambda'1} \|u_{l\lambda}^a\|^2 + \delta_{\lambda'1} \delta_{\lambda',0} \right]
\end{aligned} \tag{6.114}$$

Similarly, the non-spherical part as given in equation (6.108) is:

$$I_{\alpha\beta}^{av1 non-sph}(\mathbf{k}) = \sum_{L''>0} \sum_{L\lambda} \sum_{L'\lambda'} D_{L\lambda}^{av\mathbf{k}*}(\alpha, \beta) A_{L'\lambda'}^{av\mathbf{k}} \int_{R_a} d^3 r_a u_{l\lambda}^a(r_a) V_{L''}^{a eff}(r_a) u_{l'\lambda'}^a(r_a) Y_L^*(\hat{\mathbf{r}}_a) Y_{L''}(\hat{\mathbf{r}}_a) Y_{L'}(\hat{\mathbf{r}}_a) \tag{6.115}$$

$$= \sum_{L''>0} \sum_{L\lambda} \sum_{L'\lambda'} D_{L\lambda}^{av\mathbf{k}*}(\alpha, \beta) A_{L'\lambda'}^{av\mathbf{k}} \int_0^{R_a} r_a^2 dr_a u_{l\lambda}^a(r_a) V_{L''}^{a eff}(r_a) u_{l'\lambda'}^a(r_a) \oint ds Y_L^*(\hat{\mathbf{r}}_a) Y_{L''}(\hat{\mathbf{r}}_a) Y_{L'}(\hat{\mathbf{r}}_a) \tag{6.116}$$

$$= \sum_{L''>0} \sum_{L\lambda} \sum_{L'\lambda'} D_{L\lambda}^{av\mathbf{k}*}(\alpha, \beta) A_{L'\lambda'}^{av\mathbf{k}} G_{l,l'',l'}^{m,m'',m'} \int_0^{R_a} r_a^2 dr_a u_{l\lambda}^a(r_a) V_{L''}^{a eff}(r_a) u_{l'\lambda'}^a(r_a) \tag{6.117}$$

For the sake of brevity, we define an integral:

$$V_{l,L'',l'}^{a\lambda\lambda'} = \int_0^{R_a} r_a^2 dr_a u_{l\lambda}^a(r_a) V_{L''}^{eff}(\mathbf{r}_a) u_{l'\lambda'}^a(r_a) \tag{6.118}$$

The final expression of (6.106) is obtained by substituting equations (6.114) and (6.117) in (6.106).

$$\begin{aligned}
I_{\alpha\beta}^{av(1)}(\mathbf{k}) &= \sum_{L\lambda\lambda'} D_{L\lambda}^{av\mathbf{k}*}(\alpha, \beta) A_{L\lambda'}^{av\mathbf{k}} \left[ (E_l^a - \epsilon_{v\mathbf{k}}) \delta_{\lambda\lambda'} \|u_{l\lambda'}^a\|^2 + \delta_{\lambda'1} \delta_{\lambda,0} \right] \\
&\quad + \sum_{L''>0} \sum_{L\lambda} \sum_{L'\lambda'} D_{L\lambda}^{av\mathbf{k}*}(\alpha, \beta) A_{L'\lambda'}^{av\mathbf{k}} G_{l,l'',l'}^{m,m'',m'} V_{l,L'',l'}^{a\lambda\lambda'}
\end{aligned} \tag{6.119}$$

Furthermore, we use the strain variation of the radial function to evaluate equation (6.91b).

$$\begin{aligned}
\frac{\delta u_{l\lambda}^a(r_a[\underline{\epsilon}])}{\delta \epsilon_{\alpha\beta}} &= \frac{\partial u_{l\lambda}^a(r_a)}{\partial r_a} \frac{\partial r_a[\underline{\epsilon}]}{\partial \epsilon_{\alpha\beta}} \stackrel{(A.15)}{=} \hat{\mathbf{r}}_{a\alpha} \hat{\mathbf{r}}_{a\beta} r_a u_{l\lambda}^{a\prime}(r_a) \\
&\stackrel{(A.16)}{=} r_a u_{l\lambda}^{a\prime}(r_a) \sum_{t,t'=-1} c_{\alpha t} c_{\beta t'} Y_{1t}(\hat{\mathbf{r}}_a) Y_{1t'}(\hat{\mathbf{r}}_a)
\end{aligned} \tag{6.120}$$

Equation (6.94) becomes

$$I_{\alpha\beta}^{av(2)}(\mathbf{k}) = \sum_{\mathbf{K}} \sum_{lm\lambda} c_{v\mathbf{k}\mathbf{K}}^* \int_{R_a} d^3 r_a \hat{\mathbf{r}}_{a\alpha} \hat{\mathbf{r}}_{a\beta} r_a (a_{lm\lambda}^{a\mathbf{K}} u_{l\lambda}^{a\prime}(r_a) Y_{lm}(\hat{\mathbf{r}}_a))^* (\hat{H}_{eff} - \epsilon_v(\mathbf{k})) \psi_{v\mathbf{k}}(\mathbf{r}) \tag{6.121}$$

$$= \sum_{lm\lambda} \int_{R_a} d^3 r_a \hat{\mathbf{r}}_{a\alpha} \hat{\mathbf{r}}_{a\beta} r_a (A_{lm\lambda}^{av\mathbf{k}} u_{l\lambda}^{a\prime}(r_a) Y_{lm}(\hat{\mathbf{r}}_a))^* (\hat{H}_{eff} - \epsilon_v(\mathbf{k})) \psi_{v\mathbf{k}}(\mathbf{r}) \tag{6.122}$$

$$= I_{\alpha\beta}^{av(2)sph}(\mathbf{k}) + I_{\alpha\beta}^{av(2)non sph}(\mathbf{k}) \tag{6.123}$$

Integral  $I_{\alpha\beta}^{av(2)}(\mathbf{k})$  is splitted into the  $I_{\alpha\beta}^{av(2)sph}(\mathbf{k})$  and  $I_{\alpha\beta}^{av(2)non sph}(\mathbf{k})$  by the same reasoning that are used to simplify equation (6.106). First considering the spherical part  $I_{\alpha\beta}^{av(2)sph}(\mathbf{k})$  and using (6.113):

$$\begin{aligned} I_{\alpha\beta}^{av(2)sph}(\mathbf{k}) &= \sum_{L\lambda} \sum_{L'\lambda'} A_{L\lambda}^{av\mathbf{k}*} A_{L'\lambda'}^{av\mathbf{k}} \int_0^{R_a} r_a^3 dr_a u_{l\lambda}^{a\prime}(r_a) \left[ (E_{l'}^a - \epsilon_{v\mathbf{k}}) u_{l'\lambda'}^a(r_a) + \delta_{\lambda'1} u_{l'}^a(r_a) \right] \\ &\oint ds \hat{\mathbf{r}}_{a\alpha} \hat{\mathbf{r}}_{a\beta} Y_L^*(\hat{\mathbf{r}}_a) Y_{L'}(\hat{\mathbf{r}}_a) \end{aligned} \quad (6.124)$$

The surface integral is:

$$\begin{aligned} \oint ds \hat{\mathbf{r}}_{a\alpha} \hat{\mathbf{r}}_{a\beta} Y_L^*(\hat{\mathbf{r}}_a) Y_{L'}(\hat{\mathbf{r}}_a) &\stackrel{(A.16)}{=} \sum_{t,t'=-1} c_{\alpha t} c_{\beta t'} \oint ds Y_L^*(\hat{\mathbf{r}}_a) Y_{L'}(\hat{\mathbf{r}}_a) Y_{1t}(\hat{\mathbf{r}}_a) Y_{1t'}(\hat{\mathbf{r}}_a) \\ &\stackrel{(A.4)}{=} \sum_{t,t'=-1} c_{\alpha t} c_{\beta t'} \sum_{s,\nu} G_{s,1,1}^{\nu,t,t'} \oint ds Y_L^*(\hat{\mathbf{r}}_a) Y_{L'}(\hat{\mathbf{r}}_a) Y_{s\nu} \\ &\stackrel{(A.5)}{=} \sum_{t,t'=-1} c_{\alpha t} c_{\beta t'} \sum_{s,\nu} G_{s,1,1}^{\nu,t,t'} G_{l,l',s}^{m,m',\nu} \end{aligned} \quad (6.125)$$

Define an integral:

$$J_{ll'}^{a\lambda\lambda'} = \int_0^{R_a} r_a^3 dr_a u_{l\lambda}^{a\prime}(r_a) u_{l'\lambda'}^a(r_a) \quad (6.126)$$

From the substitution of equations (6.125) and (6.126) in (6.124), we get:

$$I_{\alpha\beta}^{av(2)sph}(\mathbf{k}) = \sum_{L\lambda} \sum_{L'\lambda'} A_{L\lambda}^{av\mathbf{k}*} A_{L'\lambda'}^{av\mathbf{k}} \sum_{t,t'=-1} c_{\alpha t} c_{\beta t'} \sum_{s,\nu} G_{s,1,1}^{\nu,t,t'} G_{l,l',s}^{m,m',\nu} \left[ (E_{l'}^a - \epsilon_{v\mathbf{k}}) J_{ll'}^{a\lambda\lambda'} + \delta_{\lambda'1} J_{ll'}^{a\lambda0} \right] \quad (6.127)$$

The non-spherical part of the integration is:

$$\begin{aligned} I_{\alpha\beta}^{av(2)non sph}(\mathbf{k}) &= \sum_{L''>0} \sum_{L\lambda} \sum_{L'\lambda'} A_{L\lambda}^{av\mathbf{k}*} A_{L'\lambda'}^{av\mathbf{k}} \int_{R_a} d^3 r_a \hat{\mathbf{r}}_{a\alpha} \hat{\mathbf{r}}_{a\beta} r_a u_{l\lambda}^{a\prime}(r_a) Y_L^*(\hat{\mathbf{r}}_a) V_{L''}^{eff}(r_a) Y_{L''}(\hat{\mathbf{r}}_a) u_{l'\lambda'}^a(r_a) Y_{L'}(\hat{\mathbf{r}}_a) \\ &= \sum_{L''>0} \sum_{L\lambda} \sum_{L'\lambda'} A_{L\lambda}^{av\mathbf{k}*} A_{L'\lambda'}^{av\mathbf{k}} \int_0^{R_a} r_a^3 dr_a u_{l\lambda}^{a\prime}(r_a) V_{L''}^{eff}(r_a) u_{l'\lambda'}^a(r_a) \oint ds \hat{\mathbf{r}}_{a\alpha} \hat{\mathbf{r}}_{a\beta} Y_L^*(\hat{\mathbf{r}}_a) Y_{L''}(\hat{\mathbf{r}}_a) Y_{L'}(\hat{\mathbf{r}}_a) \end{aligned}$$

The surface integral in the above equation is:

$$\begin{aligned} \oint ds \hat{\mathbf{r}}_{a\alpha} \hat{\mathbf{r}}_{a\beta} Y_L^*(\hat{\mathbf{r}}_a) Y_{L'}(\hat{\mathbf{r}}_a) Y_{L''}(\hat{\mathbf{r}}_a) &= \sum_{t,t'=-1} c_{\alpha t} c_{\beta t'} \oint ds Y_{1t}(\hat{\mathbf{r}}_a) Y_{1t'}(\hat{\mathbf{r}}_a) Y_{L''}(\hat{\mathbf{r}}_a) Y_{L'}(\hat{\mathbf{r}}_a) Y_L^*(\hat{\mathbf{r}}_a) \\ &\stackrel{(A.4)}{=} \sum_{t,t'=-1} c_{\alpha t} c_{\beta t'} \sum_{s,\nu} G_{s,1,1}^{\nu,t,t'} \oint ds Y_{s\nu}(\hat{\mathbf{r}}_a) Y_{L''}(\hat{\mathbf{r}}_a) Y_{L'}(\hat{\mathbf{r}}_a) Y_L^*(\hat{\mathbf{r}}_a) \\ &\stackrel{(A.4)}{=} \sum_{t,t'=-1} c_{\alpha t} c_{\beta t'} \sum_{s,\nu} G_{s,1,1}^{\nu,t,t'} \sum_{s',\nu'} G_{s',l'',l'}^{s',m'',m'} \oint ds Y_{s\nu}(\hat{\mathbf{r}}_a) Y_{s',\nu'}(\hat{\mathbf{r}}_a) Y_L^*(\hat{\mathbf{r}}_a) \\ &\stackrel{(A.5)}{=} \sum_{t,t'=-1} c_{\alpha t} c_{\beta t'} \sum_{s,\nu} G_{s,1,1}^{\nu,t,t'} \sum_{s',\nu'} G_{s',l'',l'}^{s',m'',m'} G_{l,s,s'}^{m,\nu,\nu'} \\ &= \sum_{t,t'=-1} \sum_{s,\nu} \sum_{s',\nu'} c_{\alpha t} c_{\beta t'} G_{s,1,1}^{\nu,t,t'} G_{s',l'',l'}^{s',m'',m'} G_{l,s,s'}^{m,\nu,\nu'} \end{aligned} \quad (6.128)$$

The integral  $I_{\alpha\beta}^{av \text{ (2)non sph}}(\mathbf{k})$  becomes:

$$I_{\alpha\beta}^{av \text{ (2)non sph}}(\mathbf{k}) = \sum_{L'' > 0} \sum_{L\lambda} \sum_{L'\lambda'} A_{L\lambda}^{av\mathbf{k}*} A_{L'\lambda'}^{av\mathbf{k}} \sum_{t,t'=-1} \sum_{s\nu} \sum_{s'\nu'} c_{\alpha t} c_{\beta t'} G_{s,1,1}^{\nu,t,t'} G_{s',l'',l'}^{\nu',m'',m'} G_{l,s,s'}^{m,\nu,\nu'} \\ \int_0^{R_a} r_a^3 dr_a u_{l\lambda}^{at}(r_a) V_{L''}^{eff}(r_a) u_{l'\lambda'}^{at}(r_a) \quad (6.129)$$

To shorten the expression, define yet another integral:

$$W_{l,L'',l'}^{a\lambda\lambda'} = \int_0^{R_a} r_a^3 dr_a u_{l\lambda}^{at}(r_a) V_{L''}^{eff}(r_a) u_{l'\lambda'}^{at}(r_a) \quad (6.130)$$

The final expression of the second integral is:

$$I_{\alpha\beta}^{av \text{ (2)}}(\mathbf{k}) = \sum_{L\lambda} \sum_{L'\lambda'} A_{L\lambda}^{av\mathbf{k}*} A_{L'\lambda'}^{av\mathbf{k}} \sum_{t,t'=-1} c_{\alpha t} c_{\beta t'} \sum_{s,\nu} G_{s,1,1}^{\nu,t,t'} G_{l,l',s}^{m,m',\nu} \left[ (E_{l'}^a - \epsilon_{v\mathbf{k}}) J_{ll'}^{a\lambda\lambda'} + \delta_{\lambda'1} J_{ll'}^{a\lambda0} \right] \\ + \sum_{L'' > 0} \sum_{L\lambda} \sum_{L'\lambda'} A_{L\lambda}^{av\mathbf{k}*} A_{L'\lambda'}^{av\mathbf{k}} \sum_{t,t'=-1} \sum_{s\nu} \sum_{s'\nu'} c_{\alpha t} c_{\beta t'} G_{s,1,1}^{\nu,t,t'} G_{s',l'',l'}^{\nu',m'',m'} G_{l,s,s'}^{m,\nu,\nu'} W_{l,L'',l'}^{a\lambda\lambda'} \quad (6.131)$$

In the following lines, integral  $I_{\alpha\beta}^{av \text{ (3)}}(\mathbf{k})$  will be evaluated. Using

$$\frac{d}{d\epsilon_{\alpha\beta}} \Bigg|_{\underline{\epsilon}=0} Y_{lm}(\widehat{\mathbf{r}}_a[\underline{\epsilon}]) \stackrel{(A.10)}{=} \frac{1}{2} \sum_{s=\pm 1} \sum_{t,t'=-1}^1 [c_{\alpha t'} c_{\beta}^{st}(l, m) + c_{\beta t'} c_{\alpha}^{st}(l, m)] Y_{1t'}(\widehat{\mathbf{r}}_a) Y_{l+s, m+t}(\widehat{\mathbf{r}}_a)$$

the integral given in (6.95) becomes:

$$I_{\alpha\beta}^{av \text{ (3)}}(\mathbf{k}) = \frac{1}{2} \sum_{lm\lambda} \sum_{s=\pm 1} \sum_{t,t'=-1}^1 [c_{\alpha t'} c_{\beta}^{st}(l, m) + c_{\beta t'} c_{\alpha}^{st}(l, m)] \\ \int_{R_a} d^3 r_a (A_{lm\lambda}^{av\mathbf{k}} u_{l\lambda}^a(r_a) Y_{1t'}(\widehat{\mathbf{r}}_a) Y_{l+s, m+t}(\widehat{\mathbf{r}}_a))^* (\widehat{H}_{eff} - \epsilon_v(\mathbf{k})) \psi_{v\mathbf{k}}(\mathbf{r}) \\ = \frac{1}{2} \sum_{lm\lambda} \sum_{s=\pm 1} \sum_{t,t'=-1}^1 [c_{\alpha t'} c_{\beta}^{st}(l, m) + c_{\beta t'} c_{\alpha}^{st}(l, m)] \left[ I_{\alpha\beta}^{av \text{ (3)sph}}(\mathbf{k}) + I_{\alpha\beta}^{av \text{ (3)non sph}}(\mathbf{k}) \right] \quad (6.132)$$

The spherical part is:

$$I_{\alpha\beta}^{av \text{ (3)sph}}(\mathbf{k}) = \sum_{L'\lambda'} A_{L\lambda}^{av\mathbf{k}*} A_{L'\lambda'}^{av\mathbf{k}} \int_{R_a} d^3 r_a u_{l\lambda}^a(r_a) Y_{1t'}^*(\widehat{\mathbf{r}}_a) Y_{l+s, m+t}^*(\widehat{\mathbf{r}}_a) [(E_{l'}^a - \epsilon_{v\mathbf{k}}) u_{l'\lambda'}^a(r_a) + \delta_{\lambda'1} u_{l'\lambda'}^a(r_a)] Y_{L'\lambda'}(\widehat{\mathbf{r}}_a) \\ = \sum_{L'\lambda'} A_{L\lambda}^{av\mathbf{k}*} A_{L'\lambda'}^{av\mathbf{k}} \int_0^{R_a} r_a^2 dr_a u_{l\lambda}^a(r_a) [(E_{l'}^a - \epsilon_{v\mathbf{k}}) u_{l'\lambda'}^a(r_a) + \delta_{\lambda'1} u_{l'\lambda'}^a(r_a)] \oint ds Y_{L'\lambda'}(\widehat{\mathbf{r}}_a) Y_{1t'}^*(\widehat{\mathbf{r}}_a) Y_{l+s, m+t}^*(\widehat{\mathbf{r}}_a) \\ = \sum_{L'\lambda'} A_{L\lambda}^{av\mathbf{k}*} A_{L'\lambda'}^{av\mathbf{k}} G_{l,1,l+s}^{m,t',m+t} \int_0^{R_a} r_a^2 dr_a u_{l\lambda}^a(r_a) [(E_{l'}^a - \epsilon_{v\mathbf{k}}) u_{l'\lambda'}^a(r_a) + \delta_{\lambda'1} u_{l'\lambda'}^a(r_a)] \\ = \sum_{L'\lambda'} A_{L\lambda}^{av\mathbf{k}*} A_{L'\lambda'}^{av\mathbf{k}} G_{l,1,l+s}^{m,t',m+t} \{(E_{l'}^a - \epsilon_{v\mathbf{k}}) \delta_{\lambda,\lambda'} \|u_{l\lambda}^a\|^2 + \delta_{\lambda'1} \delta_{\lambda,0}\} \quad (6.133)$$

and the non-spherical part is:

$$\begin{aligned}
I_{\alpha\beta}^{av \ (3) non sph}(\mathbf{k}) &= \sum_{L''>0} \sum_{L'\lambda'} A_{L\lambda}^{av\mathbf{k}*} A_{L'\lambda'}^{av\mathbf{k}} \int_{R_a} d^3 r_a u_{l\lambda}^a(r_a) Y_{1t'}^*(\widehat{\mathbf{r}_a}) Y_{l+s,m+t}^*(\widehat{\mathbf{r}_a}) V_{L''}^{eff}(\mathbf{r}_a) Y_{L''}(\widehat{\mathbf{r}_a}) u_{l'\lambda'}^a(r_a) Y_{L'}(\widehat{\mathbf{r}_a}) \\
&= \sum_{L''>0} \sum_{L'\lambda'} A_{L\lambda}^{av\mathbf{k}*} A_{L'\lambda'}^{av\mathbf{k}} \int_0^{R_a} r_a^2 dr_a u_{l\lambda}^a(r_a) V_{L''}^{eff}(\mathbf{r}_a) u_{l'\lambda'}^a(r_a) \oint ds Y_{1t'}^*(\widehat{\mathbf{r}_a}) Y_{l+s,m+t}^*(\widehat{\mathbf{r}_a}) Y_{L''}(\widehat{\mathbf{r}_a}) Y_{L'}(\widehat{\mathbf{r}_a}) \\
&= \sum_{L''>0} \sum_{L'\lambda'} A_{L\lambda}^{av\mathbf{k}*} A_{L'\lambda'}^{av\mathbf{k}} \int_0^{R_a} r_a^2 dr_a u_{l\lambda}^a(r_a) V_{L''}^{eff}(\mathbf{r}_a) u_{l'\lambda'}^a(r_a) \sum_{s',\nu'} G_{s',l'',l'}^{v',m''} \oint ds Y_{s',\nu'} Y_{1t'}^*(\widehat{\mathbf{r}_a}) Y_{l+s,m+t}^*(\widehat{\mathbf{r}_a}) \\
&= \sum_{L''>0} \sum_{L'\lambda'} A_{L\lambda}^{av\mathbf{k}*} A_{L'\lambda'}^{av\mathbf{k}} \sum_{s',\nu'} G_{s',l'',l'}^{v',m''} G_{s',1,l+s}^{v',t',m+t} \int_0^{R_a} r_a^2 dr_a u_{l\lambda}^a(r_a) V_{L''}^{eff}(\mathbf{r}_a) u_{l'\lambda'}^a(r_a)
\end{aligned} \tag{6.134}$$

The final expression of  $I_{\alpha\beta}^{av \ (3)}(\mathbf{k})$  is:

$$\begin{aligned}
I_{\alpha\beta}^{av \ (3)}(\mathbf{k}) &= \frac{1}{2} \sum_{s=\pm 1} \sum_{t,t'=-1}^1 [c_{\alpha t'} c_{\beta}^{st}(l,m) + c_{\beta t'} c_{\alpha}^{st}(l,m)] \sum_{L\lambda} \sum_{L'\lambda'} A_{L\lambda}^{av\mathbf{k}*} A_{L'\lambda'}^{av\mathbf{k}} \\
&\quad \times \left\{ G_{l,1,l+s}^{m,t',m+t} \left\{ (E_{l'}^a - \epsilon_{v\mathbf{k}}) \delta_{\lambda,\lambda'} \|u_{l\lambda'}^a\|^2 + \delta_{\lambda'1} \delta_{\lambda,0} \right\} + \right. \\
&\quad \left. \sum_{L''>0} \sum_{s,\nu} G_{s,l'',l'}^{v',m''} G_{s,1,l+s}^{v',t',m+t} V_{l,L'',l'}^{a\lambda\lambda'} \right\}
\end{aligned} \tag{6.135}$$

The integral  $I_{\alpha\beta}^{av \ (3)}(\mathbf{k})$  arises from the change of spherical harmonics with respect to strain. According to equation (A.12), in the case of pure pressure (also known as hydrostatic condition), this change will vanish. Therefore, for pure pressure, which amounts to the trace of the full stress tensor, integral  $I_{\alpha\beta}^{av \ (3)}(\mathbf{k})$  does not contribute.

Now, substituting  $I_{\alpha\beta}^{av \ (1)}(\mathbf{k})$ ,  $I_{\alpha\beta}^{av \ (2)}(\mathbf{k})$ , and  $I_{\alpha\beta}^{av \ (3)}(\mathbf{k})$  in (6.92)

$$I_{\alpha\beta}^{av}(\mathbf{k}) = \sum_{L\lambda\lambda'} D_{L\lambda}^{av\mathbf{k}*}(\alpha, \beta) A_{L\lambda}^{av\mathbf{k}} \left[ (E_l^a - \epsilon_{v\mathbf{k}}) \delta_{\lambda\lambda'} \|u_{l\lambda'}^a\|^2 + \delta_{\lambda'1} \delta_{\lambda,0} \right] \tag{6.136}$$

$$+ \sum_{L\lambda} \sum_{L'\lambda'} A_{L\lambda}^{av\mathbf{k}*} A_{L'\lambda'}^{av\mathbf{k}} \sum_{t,t'=-1} c_{\alpha t'} c_{\beta t'} \sum_{s,\nu} G_{s,1,1}^{v,t,t'} G_{l,l',s}^{m,m',\nu} \left[ (E_{l'}^a - \epsilon_{v\mathbf{k}}) J_{ll'}^{a\lambda\lambda'} + \delta_{\lambda'1} J_{ll'}^{a\lambda0} \right] \tag{6.137}$$

$$+ \frac{1}{2} \sum_{s=\pm 1} \sum_{t,t'=-1}^1 [c_{\alpha t'} c_{\beta}^{st}(l,m) + c_{\beta t'} c_{\alpha}^{st}(l,m)] \times \sum_{L'\lambda'} A_{L\lambda}^{av\mathbf{k}*} A_{L'\lambda'}^{av\mathbf{k}} G_{l,1,l+s}^{m,t',m+t} \left\{ (E_{l'}^a - \epsilon_{v\mathbf{k}}) \delta_{\lambda,\lambda'} \|u_{l\lambda'}^a\|^2 + \delta_{\lambda'1} \delta_{\lambda,0} \right\} \tag{6.138}$$

$$+ \sum_{L''} \sum_{L\lambda} \sum_{L'\lambda'} D_{L\lambda}^{av\mathbf{k}*}(\alpha, \beta) A_{L'\lambda'}^{av\mathbf{k}} G_{l,l'',l'}^{m,m'',m'} V_{l,L'',l'}^{a\lambda\lambda'} \tag{6.139}$$

$$+ \sum_{L''} \sum_{L\lambda} \sum_{L'\lambda'} A_{L\lambda}^{av\mathbf{k}*} A_{L'\lambda'}^{av\mathbf{k}} \sum_{t,t'=-1} \sum_{s\nu} \sum_{s'\nu'} c_{\alpha t'} c_{\beta t'} G_{s,1,1}^{v,t,t'} G_{s',l'',l'}^{v',m''} G_{l,s,s'}^{m,\nu,\nu'} W_{l,L'',l'}^{a\lambda\lambda'} \tag{6.140}$$

$$+ \frac{1}{2} \sum_{s=\pm 1} \sum_{t,t'=-1}^1 [c_{\alpha t'} c_{\beta}^{st}(l,m) + c_{\beta t'} c_{\alpha}^{st}(l,m)] \sum_{L\lambda} \sum_{L'\lambda'} A_{L\lambda}^{av\mathbf{k}*} A_{L'\lambda'}^{av\mathbf{k}} \times \sum_{L''} \sum_{s',\nu'} G_{s',l'',l'}^{v',m''} G_{s',1,l+s}^{v',t',m+t} V_{l,L'',l'}^{a\lambda\lambda'} \tag{6.141}$$

In the integral  $I_{\alpha\beta}^{av}(\mathbf{k})$ , (6.136) to (6.138) are due to the spherical part and (6.139) to (6.141) due to non-spherical parts of the potential in the Hamiltonian. As a result, the total integral  $I_{\alpha\beta}^{av}(\mathbf{k})$  can be written for spherical and non-spherical part separately as given below.

$$I_{\alpha\beta}^{av}(\mathbf{k}) = I_{\alpha\beta}^{av sph}(\mathbf{k}) + I_{\alpha\beta}^{av non-sph}(\mathbf{k}) \quad (6.142)$$

Finally, the simplest version of the valence correction will be obtained by substituting equation (6.142) in (6.87).

$$\sigma_{\alpha\beta}^{val,corr} = \frac{2}{\Omega} \sum_{v\mathbf{k}} n_{v\mathbf{k}} \Re(I_{\alpha\beta}^{av}(\mathbf{k})), \quad (6.143)$$

with the spherical part of integral ( $I_{\alpha\beta}^{av}(\mathbf{k})$ ) is

$$\begin{aligned} I_{\alpha\beta}^{av sph}(\mathbf{k}) &= \sum_{L\lambda\lambda'} D_{L\lambda}^{av\mathbf{k}*}(\alpha, \beta) A_{L\lambda'}^{av\mathbf{k}} \left[ (E_l^a - \epsilon_{v\mathbf{k}}) \delta_{\lambda\lambda'} \|u_{l\lambda'}^a\|^2 + \delta_{\lambda'1} \delta_{\lambda,0} \right] \\ &\quad + \sum_{L\lambda} \sum_{L'\lambda'} A_{L\lambda}^{av\mathbf{k}*} A_{L'\lambda'}^{av\mathbf{k}} \sum_{t,t'=-1} c_{\alpha t} c_{\beta t'} \sum_{s,\nu} G_{s,1,1}^{\nu,t,t'} G_{l,l',s}^{m,m',\nu} \\ &\quad \times \left[ (E_{l'}^a - \epsilon_{v\mathbf{k}}) J_{ll'}^{a\lambda\lambda'} + \delta_{\lambda'1} J_{ll'}^{a\lambda0} \right] \\ &\quad + \frac{1}{2} \sum_{s=\pm 1} \sum_{t,t'=-1}^1 [c_{\alpha t} c_{\beta t'}^s(l, m) + c_{\beta t'} c_{\alpha t}^s(l, m)] \sum_{L'\lambda'} A_{L\lambda}^{av\mathbf{k}*} A_{L'\lambda'}^{av\mathbf{k}} G_{l,1,l+s}^{m,t',m+t} \\ &\quad \times \left\{ (E_{l'}^a - \epsilon_{v\mathbf{k}}) \delta_{\lambda,\lambda'} \|u_{l\lambda'}^a\|^2 + \delta_{\lambda'1} \delta_{\lambda,0} \right\} \end{aligned} \quad (6.144)$$

and the non-spherical part of integral ( $I_{\alpha\beta}^{av}(\mathbf{k})$ ) is

$$\begin{aligned} I_{\alpha\beta}^{av non-sph}(\mathbf{k}) &= \sum_{L''} \sum_{L\lambda} \sum_{L'\lambda'} D_{L\lambda}^{av\mathbf{k}*}(\alpha, \beta) A_{L'\lambda'}^{av\mathbf{k}} G_{l,l'',l'}^{m,m'',m'} V_{l,L'',l'}^{a\lambda\lambda'} \\ &\quad + \sum_{L''} \sum_{L\lambda} \sum_{L'\lambda'} A_{L\lambda}^{av\mathbf{k}*} A_{L'\lambda'}^{av\mathbf{k}} \sum_{t,t'=-1} \sum_{s\nu} \sum_{s'\nu'} c_{\alpha t} c_{\beta t'} G_{s,1,1}^{\nu,t,t'} G_{s',l'',l'}^{s',m'',m'} \\ &\quad \times G_{l,s,s'}^{m,\nu,\nu'} W_{l,L'',l'}^{a\lambda\lambda'} + \frac{1}{2} \sum_{s=\pm 1} \sum_{t,t'=-1}^1 [c_{\alpha t} c_{\beta t'}^s(l, m) + c_{\beta t'} c_{\alpha t}^s(l, m)] \\ &\quad \times \sum_{L\lambda} \sum_{L'\lambda'} A_{L\lambda}^{av\mathbf{k}*} A_{L'\lambda'}^{av\mathbf{k}} \sum_{L''} \sum_{s',\nu'} G_{s',l'',l'}^{s',m'',m'} G_{s',1,l+s}^{\nu',t',m+t} V_{l,L'',l'}^{a\lambda\lambda'} \end{aligned} \quad (6.145)$$

In our WIEN2k implementation, equation (6.143) is implemented in the subroutine `val_corr_stress.f` inside the `lapw2` program. Similar to the kinetic stress, having Gaunt numbers and products of Gaunt numbers makes the valence correction computationally expensive as compared to the electrostatic and exchange stress tensors. The matrix product to calculate  $D_{L\lambda}^{av\mathbf{k}*}(\alpha, \beta)$ , as suggested by equation (6.103), is carried out using a LAPACK routines `dgemm`[41] and `zgemm`[42]. This routine is very efficient to compute the matrix multiplication in a higher dimension and has already been extensively used to calculate  $A_{L\lambda}^{av\mathbf{k}}$  in total energy calculations.

## 6.5 Exchange Correlation Stress Tensor

The exchange correlation stress tensor according to equation (6.3e) is:

$$\sigma_{\alpha\beta}^{xc} = \frac{\delta_{\alpha\beta}}{\Omega} \int_{\Omega} d^3\mathbf{r} \rho(\mathbf{r}) (\epsilon_{xc} - \mu_{xc}) - \frac{2\delta_{GGA}}{\Omega} \int_{\Omega} d^3\mathbf{r} \rho(\mathbf{r}) \partial_{\alpha}\rho(\mathbf{r}) \partial_{\beta}\rho(\mathbf{r}) \frac{\partial\epsilon_{xc}}{\partial\sigma} \quad (6.146)$$

It was already mentioned that  $\delta_{GGA}$  distinguish whether the exchange correlation energy is LDA or GGA. In case of LDA,  $\delta_{GGA} = 0$  and  $\delta_{GGA} = 1$  for GGA. Therefore,

$$\sigma_{\alpha\beta}^{LDA} = \frac{\delta_{\alpha\beta}}{\Omega} \int_{\Omega} d^3\mathbf{r} \rho(\mathbf{r}) (\epsilon_{xc}(\rho(\mathbf{r})) - \mu_{xc}(\rho(\mathbf{r}))) \quad (6.147a)$$

$$\begin{aligned} \sigma_{\alpha\beta}^{GGA} &= \frac{\delta_{\alpha\beta}}{\Omega} \int_{\Omega} d^3\mathbf{r} \rho(\mathbf{r}) (\epsilon_{xc}(\rho(\mathbf{r}), \nabla\rho(\mathbf{r})) - \mu_{xc}(\rho(\mathbf{r}), \nabla\rho(\mathbf{r}))) \\ &\quad - \frac{2}{\Omega} \int_{\Omega} d^3\mathbf{r} \rho(\mathbf{r}) \partial_{\alpha}\rho(\mathbf{r}) \partial_{\beta}\rho(\mathbf{r}) \frac{\partial\epsilon_{xc}(\rho(\mathbf{r}), \nabla\rho(\mathbf{r}))}{\partial\sigma} \end{aligned} \quad (6.147b)$$

$$(6.147c)$$

If we compare  $\Omega\sigma_{\alpha\beta}^{GGA}$  with  $\Omega\sigma_{\alpha\beta}^{LDA}$ , the second term in  $\Omega\sigma_{\alpha\beta}^{GGA}$ , is an additional contribution whose presence is solely due to the change of  $\nabla\rho(\mathbf{r})$  according to the strain. This is a small correction term, which will vanish if we pass from GGA to LDA. The final expression of the GGA stress tensor that contributes to the total stress tensor formula is

$$\Omega\sigma_{\alpha\beta}^{GGA} = \Omega\sigma_{\alpha\beta}^{LDA} - 2 \int_{\Omega} d^3\mathbf{r} \rho(\mathbf{r}) \partial_{\alpha}\rho(\mathbf{r}) \partial_{\beta}\rho(\mathbf{r}) \frac{\partial\epsilon_{xc}}{\partial\sigma} \quad (6.148)$$

Here, the superscript LDA in  $\Omega\sigma_{\alpha\beta}^{LDA}$  indicates that the expression formally agrees with the LDA exchange correlation stress equation (6.147a), but the density ( $\rho(\mathbf{r})$ ) and  $\epsilon_{xc}$  are calculated under GGA approximation. During the implementation, care has to be given as to whether  $\epsilon_{xc}$  is energy per unit particle or energy per unit volume, the latter case often being referred to as energy density. If  $\epsilon_{xc}$  is defined as energy density, the particle density ( $\rho(\mathbf{r})$ ) is already multiplied on it i.e it is  $\rho(\mathbf{r})\epsilon_{xc}$ .

The correction term, the second expression of equation (6.148), is implemented in WIEN2k in a subroutine **stress\_gga.f**. In this subroutine, we take ‘vsigma’ from the Libxc library and according to the Libxc manual [40], ‘vsigma’ is the “first partial derivative of the energy per unit volume in terms of sigma ( $\sigma$ )”. Which implies, if ‘vsigma’ is taken from the Libxc then the particle density ( $\rho$ ) is already multiplied in  $\frac{\partial\epsilon_{xc}}{\partial\sigma}$  i.e ‘vsigma’  $\equiv \rho \frac{\partial\epsilon_{xc}}{\partial\sigma}$ .

Equation (6.148) is similar to equation (20) in Ref. [18]. Some arguments in Ref. [18], however, differ from what we observed in our calculations. In Ref. [18] the authors claim that the GGA correction does not contain any contribution from the atomic spheres. They come to this conclusion analytically, but our derivations and calculations neither support such a conclusion analytically nor numerically. In contrast to their observations, we found that the interstitial contribution  $(\Omega\sigma_{\alpha\beta}^{GGA,CORR})_{Int}$  is always smaller compared to the contribution of the atomic spheres  $(\Omega\sigma_{\alpha\beta}^{GGA,CORR})_{sph}$ .

We even observed that in some cases the interstitial contribution is close to zero. The only plausible explanation for this discrepancy between our observation and the claim in Ref. [18] could be the different ways they define the basis-function and the charge density. To support our arguments the numerical results are presented in the figure 7.1 and Tables 7.1, 7.2.

Again, considering equation (6.148):

$$\Omega\sigma_{\alpha\beta}^{GGA} = \Omega\sigma_{\alpha\beta}^{LDA} - 2 \int_{\Omega} d^3\mathbf{r} \rho(\mathbf{r}) \partial_{\alpha}\rho(\mathbf{r}) \partial_{\beta}\rho(\mathbf{r}) \frac{\partial\epsilon_{xc}}{\partial\sigma} \quad (6.149a)$$

$$\Omega\sigma_{\alpha\beta}^{GGA} = \Omega\sigma_{\alpha\beta}^{LDA} + \Omega\sigma_{\alpha\beta}^{GGA,CORR} \quad (6.149b)$$

The integration in  $\Omega\sigma_{\alpha\beta}^{GGA,CORR}$  will be further divided into the region of the atomic spheres and the interstitial region.

$$\begin{aligned} \Omega\sigma_{\alpha\beta}^{GGA,CORR} &= -2 \int_{\Omega} d^3\mathbf{r} \rho(\mathbf{r}) \partial_{\alpha}\rho(\mathbf{r}) \partial_{\beta}\rho(\mathbf{r}) \frac{\partial\epsilon_{xc}}{\partial\sigma} \\ &= -2 \int_{\Omega} d^3\mathbf{r} \Theta_a(\mathbf{r}) \rho(\mathbf{r}) \partial_{\alpha}\rho(\mathbf{r}) \partial_{\beta}\rho(\mathbf{r}) \frac{\partial\epsilon_{xc}}{\partial\sigma} - 2 \int_{\Omega} d^3\mathbf{r} \Theta_{IS}(\mathbf{r}) \rho(\mathbf{r}) \partial_{\alpha}\rho(\mathbf{r}) \partial_{\beta}\rho(\mathbf{r}) \frac{\partial\epsilon_{xc}}{\partial\sigma} \\ &= (\Omega\sigma_{\alpha\beta}^{GGA,CORR})_{sph} + (\Omega\sigma_{\alpha\beta}^{GGA,CORR})_{int} \end{aligned} \quad (6.150)$$

### Spin polarized case:

For spin up

$$\begin{aligned} \frac{\partial\epsilon_{xc}^{\uparrow}}{\partial(\partial_{\alpha}\rho^{\uparrow}(\mathbf{r}))} \partial_{\beta}\rho^{\uparrow}(\mathbf{r}) &= \frac{\partial\epsilon_{xc}^{\uparrow}}{\partial(\partial_{\alpha}\rho^{\uparrow}(\mathbf{r}).\partial_{\alpha}\rho^{\uparrow}(\mathbf{r}))} \frac{\partial(\partial_{\alpha}\rho^{\uparrow}(\mathbf{r}).\partial_{\alpha}\rho^{\uparrow}(\mathbf{r}))}{\partial\partial_{\alpha}\rho^{\uparrow}(\mathbf{r})} \partial_{\beta}\rho^{\uparrow}(\mathbf{r}) + \\ &\quad \frac{\partial\epsilon_{xc}^{\uparrow}}{\partial(\partial_{\alpha}\rho^{\uparrow}(\mathbf{r}).\partial_{\alpha}\rho^{\downarrow}(\mathbf{r}))} \frac{\partial(\partial_{\alpha}\rho^{\uparrow}(\mathbf{r}).\partial_{\alpha}\rho^{\downarrow}(\mathbf{r}))}{\partial\partial_{\alpha}\rho^{\uparrow}(\mathbf{r})} \partial_{\beta}\rho^{\uparrow}(\mathbf{r}) \end{aligned} \quad (6.151)$$

$$\frac{\partial\epsilon_{xc}^{\uparrow}}{\partial(\partial_{\alpha}\rho^{\uparrow}(\mathbf{r}))} \partial_{\beta}\rho^{\uparrow}(\mathbf{r}) = 2 \frac{\partial\epsilon_{xc}^{\uparrow}}{\partial\sigma[0]} \partial_{\alpha}\rho^{\uparrow}(\mathbf{r}) \partial_{\beta}\rho^{\uparrow}(\mathbf{r}) + \frac{\partial\epsilon_{xc}^{\uparrow}}{\partial\sigma[1]} \partial_{\alpha}\rho^{\downarrow}(\mathbf{r}) \partial_{\beta}\rho^{\uparrow}(\mathbf{r}) \quad (6.152)$$

Similarly

$$\frac{\partial\epsilon_{xc}^{\uparrow}}{\partial(\partial_{\beta}\rho^{\uparrow}(\mathbf{r}))} \partial_{\alpha}\rho^{\uparrow}(\mathbf{r}) = 2 \frac{\partial\epsilon_{xc}^{\uparrow}}{\partial\sigma[0]} \partial_{\beta}\rho^{\uparrow}(\mathbf{r}) \partial_{\alpha}\rho^{\uparrow}(\mathbf{r}) + \frac{\partial\epsilon_{xc}^{\uparrow}}{\partial\sigma[1]} \partial_{\beta}\rho^{\downarrow}(\mathbf{r}) \partial_{\alpha}\rho^{\uparrow}(\mathbf{r}) \quad (6.153)$$

For spin down

$$\frac{\partial\epsilon_{xc}^{\downarrow}}{\partial(\partial_{\alpha}\rho^{\downarrow}(\mathbf{r}))} \partial_{\beta}\rho^{\downarrow}(\mathbf{r}) = 2 \frac{\partial\epsilon_{xc}^{\downarrow}}{\partial\sigma[2]} \partial_{\alpha}\rho^{\downarrow}(\mathbf{r}) \partial_{\beta}\rho^{\downarrow}(\mathbf{r}) + \frac{\partial\epsilon_{xc}^{\downarrow}}{\partial\sigma[1]} \partial_{\alpha}\rho^{\uparrow}(\mathbf{r}) \partial_{\beta}\rho^{\downarrow}(\mathbf{r}) \quad (6.154)$$

$$\frac{\partial\epsilon_{xc}^{\downarrow}}{\partial(\partial_{\beta}\rho^{\downarrow}(\mathbf{r}))} \partial_{\alpha}\rho^{\downarrow}(\mathbf{r}) = 2 \frac{\partial\epsilon_{xc}^{\downarrow}}{\partial\sigma[2]} \partial_{\beta}\rho^{\downarrow}(\mathbf{r}) \partial_{\alpha}\rho^{\downarrow}(\mathbf{r}) + \frac{\partial\epsilon_{xc}^{\downarrow}}{\partial\sigma[1]} \partial_{\beta}\rho^{\uparrow}(\mathbf{r}) \partial_{\alpha}\rho^{\downarrow}(\mathbf{r}) \quad (6.155)$$

Here,

$$\sigma[0] = \partial_{\alpha}\rho^{\uparrow}(\mathbf{r}).\partial_{\alpha}\rho^{\uparrow}(\mathbf{r}) \quad (6.156)$$

$$\sigma[1] = \partial_{\alpha}\rho^{\uparrow}(\mathbf{r}).\partial_{\alpha}\rho^{\downarrow}(\mathbf{r}) \quad (6.157)$$

$$\sigma[2] = \partial_{\alpha}\rho^{\downarrow}(\mathbf{r}).\partial_{\alpha}\rho^{\downarrow}(\mathbf{r}) \quad (6.158)$$

Consider the equation (6.148).

$$\Omega\sigma_{\alpha\beta}^{GGA} = \Omega\sigma_{\alpha\beta}^{LDA} - 2 \int_{\Omega} d^3\mathbf{r} \rho(\mathbf{r}) \partial_{\alpha}\rho(\mathbf{r}) \partial_{\beta}\rho(\mathbf{r}) \frac{\partial\epsilon_{xc}}{\partial\sigma} \quad (6.159)$$

This equation can be written as:

$$\Omega\sigma_{\alpha\beta}^{GGA} = \Omega\sigma_{\alpha\beta}^{LDA} - \frac{1}{2} \int_{\Omega} d^3\mathbf{r} \rho(\mathbf{r}) \left( \frac{\partial\epsilon_{xc}}{\partial(\partial_{\alpha}\rho(\mathbf{r}))} \partial_{\beta}\rho(\mathbf{r}) + \frac{\partial\epsilon_{xc}}{\partial(\partial_{\beta}\rho(\mathbf{r}))} \partial_{\alpha}\rho(\mathbf{r}) \right) \quad (6.160)$$

In the case of spin up and spin down,

$$\Omega\sigma_{\alpha\beta}^{GGA\uparrow} = \Omega\sigma_{\alpha\beta}^{LDA\uparrow} - \frac{1}{2} \int_{\Omega} d^3\mathbf{r} \rho^{\uparrow}(\mathbf{r}) \left( \frac{\partial\epsilon_{xc}^{\uparrow}}{\partial(\partial_{\alpha}\rho^{\uparrow}(\mathbf{r}))} \partial_{\beta}\rho^{\uparrow}(\mathbf{r}) + \frac{\partial\epsilon_{xc}^{\uparrow}}{\partial(\partial_{\beta}\rho^{\uparrow}(\mathbf{r}))} \partial_{\alpha}\rho^{\uparrow}(\mathbf{r}) \right) \quad (6.161a)$$

$$\Omega\sigma_{\alpha\beta}^{GGA\downarrow} = \Omega\sigma_{\alpha\beta}^{LDA\downarrow} - \frac{1}{2} \int_{\Omega} d^3\mathbf{r} \rho^{\downarrow}(\mathbf{r}) \left( \frac{\partial\epsilon_{xc}^{\downarrow}}{\partial(\partial_{\alpha}\rho^{\downarrow}(\mathbf{r}))} \partial_{\beta}\rho^{\downarrow}(\mathbf{r}) + \frac{\partial\epsilon_{xc}^{\downarrow}}{\partial(\partial_{\beta}\rho^{\downarrow}(\mathbf{r}))} \partial_{\alpha}\rho^{\downarrow}(\mathbf{r}) \right) \quad (6.161b)$$

The required derivatives for equations (6.161a) and (6.161b) are available in equations (6.152), (6.153), (6.154), and (6.155). In addition, equations (6.161a) and (6.161b) can be written as given below.

$$\begin{aligned} \Omega\sigma_{\alpha\beta}^{GGA\uparrow} &= \Omega\sigma_{\alpha\beta}^{LDA\uparrow} - 2 \int_{\Omega} d^3\mathbf{r} \rho^{\uparrow}(\mathbf{r}) \partial_{\alpha}\rho^{\uparrow}(\mathbf{r}) \partial_{\beta}\rho^{\uparrow}(\mathbf{r}) \frac{\partial\epsilon_{XC}^{\uparrow}}{\partial\sigma[0]} \\ &\quad - \frac{1}{2} \int_{\Omega} d^3\mathbf{r} \rho^{\uparrow}(\mathbf{r}) \left( \partial_{\alpha}\rho^{\uparrow}(\mathbf{r}) \partial_{\beta}^{\downarrow}\rho(\mathbf{r}) + \partial_{\alpha}^{\downarrow}\rho(\mathbf{r}) \partial_{\beta}\rho^{\uparrow}(\mathbf{r}) \right) \frac{\partial\epsilon_{XC}^{\uparrow}}{\partial\sigma[1]} \end{aligned} \quad (6.162a)$$

$$\begin{aligned} \Omega\sigma_{\alpha\beta}^{GGA\downarrow} &= \Omega\sigma_{\alpha\beta}^{LDA\downarrow} - 2 \int_{\Omega} d^3\mathbf{r} \rho^{\downarrow}(\mathbf{r}) \partial_{\alpha}\rho^{\downarrow}(\mathbf{r}) \partial_{\beta}\rho^{\downarrow}(\mathbf{r}) \frac{\partial\epsilon_{XC}^{\downarrow}}{\partial\sigma[2]} \\ &\quad - \frac{1}{2} \int_{\Omega} d^3\mathbf{r} \rho^{\downarrow}(\mathbf{r}) \left( \partial_{\alpha}\rho^{\downarrow}(\mathbf{r}) \partial_{\beta}^{\uparrow}\rho(\mathbf{r}) + \partial_{\alpha}^{\uparrow}\rho(\mathbf{r}) \partial_{\beta}\rho^{\downarrow}(\mathbf{r}) \right) \frac{\partial\epsilon_{XC}^{\downarrow}}{\partial\sigma[1]} \end{aligned} \quad (6.162b)$$

## 6.6 Total stress tensor

In the previous sections we calculated various contribution to the final stress tensor formula. Here we collect them all to evaluate the total stress tensor. We first recall equation (6.2)

$$\sigma_{\alpha\beta} = \sigma_{\alpha\beta}^{es} + \sigma_{\alpha\beta}^{core} + \sigma_{\alpha\beta}^{val,kin} + \sigma_{\alpha\beta}^{val,corr} + \sigma_{\alpha\beta}^{xc}, \quad (6.163)$$

where  $\sigma_{\alpha\beta}^{es}$ ,  $\sigma_{\alpha\beta}^{core}$ ,  $\sigma_{\alpha\beta}^{val,kin}$ ,  $\sigma_{\alpha\beta}^{val,corr}$ , and  $\sigma_{\alpha\beta}^{xc}$  are provided in equations (6.29), (6.48), (6.64), (6.143), and (6.146) respectively. If the APW+lo basis functions were used, we would have an additional contribution according to equation (6.82). In this case, the equation (6.163) becomes as follows

$$\sigma_{\alpha\beta} = \sigma_{\alpha\beta}^{es} + \sigma_{\alpha\beta}^{core} + \sigma_{\alpha\beta}^{val,kin} + \delta_{APW}\sigma_{\alpha\beta}^{APW} + \sigma_{\alpha\beta}^{val,corr} + \sigma_{\alpha\beta}^{xc}, \quad (6.164)$$

where  $\delta_{APW}$  is to indicate that this contribution is only relevant for APW+lo.

$$\begin{aligned} \sigma_{\alpha\beta}^{es} &= \frac{1}{2} \sum_{\mathbf{G}} \sum_{\mathbf{G}' \neq 0} \rho^*(\mathbf{G}) \left( -\delta_{\alpha\beta} V_C(\mathbf{G}') + 2\hat{\mathbf{G}}'_\alpha \hat{\mathbf{G}}'_\beta V_C(\mathbf{G}') \right) \Theta(\mathbf{G} - \mathbf{G}') \\ &\quad - \frac{1}{2\Omega} \sum_a \sum_{t,t'=-1}^1 c_{\alpha t} c_{\beta t'} \int_{\Omega} d^3 \mathbf{r} \Theta_a(\mathbf{r}) \rho(\mathbf{r}) V_C(\mathbf{r}) Y_{1t}(\hat{\mathbf{r}}) Y_{1t'}(\hat{\mathbf{r}}) \\ &\quad + \frac{1}{2\Omega} \sum_a Z_a \sum_{t,t'=-1}^1 c_{\alpha t} c_{\beta t'} V_M(\boldsymbol{\tau}_a) Y_{1t}(\hat{\boldsymbol{\tau}}) Y_{1t'}(\hat{\boldsymbol{\tau}}) \end{aligned} \quad (6.165a)$$

$$\begin{aligned} \sigma_{\alpha\beta}^{core} &= -\frac{1}{\Omega} \sum_a \sum_{l,m} \sum_{t,t'=-1}^1 \left( c_{\alpha t} c_{\beta t'} \frac{(-1)^m}{4\pi} G_{l,1,1}^{-m,t,t'} \int_0^{R_a} r_a^3 dr_a \sqrt{4\pi} \rho_{00}^*(r_a) \frac{dV_{lm}(r_a)}{dr_a} \right. \\ &\quad \left. + \sum_{s=\pm 1} \frac{c_\beta^{st}(l,m)c_{\alpha t'} + c_\alpha^{st}(l,m)c_{\beta t'}}{2} \frac{(-1)^{t'}}{4\pi} \delta_{1,l+s} \delta_{-t',m+t} \int_0^{R_a} dr_a \sqrt{4\pi} r_a^2 \rho_{00}^*(r_a) V_{lm}(r_a) \right) \end{aligned} \quad (6.165b)$$

$$\begin{aligned} \sigma_{\alpha\beta}^{val,kin} &= \frac{1}{\Omega} \left\{ - \sum_{v\mathbf{k}} n_{v\mathbf{k}} \sum_{\mathbf{KK}'} z_{v\mathbf{k}\mathbf{K}}^* z_{v\mathbf{k}\mathbf{K}'} (\mathbf{k} + \mathbf{K}')_\alpha (\mathbf{k} + \mathbf{K}')_\beta \Theta(\mathbf{K} - \mathbf{K}') \right. \\ &\quad + \frac{1}{2} \sum_{v\mathbf{k}} n_{v\mathbf{k}} \sum_{a \in \Omega} \sum_{LL'} \sum_{\lambda\lambda'} A_{L'\lambda'}^{av\mathbf{k}*} A_{L\lambda}^{av\mathbf{k}} \\ &\quad \times \left\{ \sum_{t,t'=-1} \left( c_{\alpha t} c_{\beta t'} + c_{\beta t} c_{\alpha t'} \right) \sum_{s,\nu} G_{s,1,l}^{\nu,t,m} G_{l',1,s}^{m',t',\nu} \int_0^{R_a} r_a^2 dr_a u_{l'\lambda'}(r) u_{l\lambda}''(r) \right. \\ &\quad + \sum_{t,t'=-1} \sum_{s,\nu} \sum_{s'=\pm 1} G_{s,1,l}^{\nu,t,m} \left( c_{\alpha t} c_{\beta}^{s't'}(s,\nu) + c_{\beta t} c_{\alpha}^{s't'}(s,\nu) \right) \delta_{l',s+s'} \delta_{m',\nu+t'} \\ &\quad \times \int_0^{R_a} r_a dr_a u_{l'\lambda'}(r) u_{l\lambda}'(r) + \sum_{s=\pm 1} \sum_{t,t'=-1}^1 \left( c_\alpha^{st}(l,m) c_{\beta t'} + c_\beta^{st}(l,m) c_{\alpha t'} \right) \\ &\quad \times G_{l',1,l+s}^{m',t',m+t} \int_0^{R_a} r_a^2 dr_a u_{l'\lambda'}(r) \left[ \frac{u_{l\lambda}'(r)}{r} - \frac{u_{l\lambda}(r)}{r^2} \right] \\ &\quad + \sum_{s,s'=\pm 1} \sum_{t,t'=-1}^1 \left( c_\alpha^{st}(l,m) c_{\beta}^{s't'}(l+s,m+t) + c_\beta^{st}(l,m) c_{\alpha}^{s't'}(l+s,m+t) \right) \\ &\quad \times \delta_{l',l+s+s'} \delta_{m',m+t+t'} \int_0^{R_a} dr_a u_{l'\lambda'}(r) u_{l\lambda}(r) \Big\} \end{aligned} \quad (6.165c)$$

$$\begin{aligned} \sigma_{\alpha\beta}^{APW} &= \frac{1}{2\Omega} \sum_{lm} \sum_{\lambda} \mathbf{D}_{lm}^{av\mathbf{k}}(\alpha, \beta) u_{l\lambda}(R_a) \left\{ \sum_{\lambda'} A_{lm\lambda'}^{av\mathbf{k}} u_{l\lambda'}'(R_a) - F_{lm}^{av\mathbf{k}} \right\} \\ &\quad + \frac{1}{2\Omega} \sum_{lm} \sum_{\lambda} A_{lm\lambda}^{av\mathbf{k}*} u_{l\lambda}(R_a) \left\{ \sum_{\lambda'} \mathbf{D}_{lm}^{av\mathbf{k}}(\alpha, \beta) u_{l\lambda'}'(R_a) - \mathbf{F}_{lm}^{av\mathbf{k}}(\alpha, \beta) \right\} \end{aligned} \quad (6.165d)$$

$$\begin{aligned}
\sigma_{\alpha\beta}^{val,corr} = & \frac{2}{\Omega} \sum_a \sum_{v\mathbf{k}} n_{v\mathbf{k}} \Re \left\{ \sum_{L\lambda\lambda'} D_{L\lambda}^{av\mathbf{k}*}(\alpha, \beta) A_{L\lambda'}^{av\mathbf{k}} \left[ (E_l^a - \epsilon_{v\mathbf{k}}) \delta_{\lambda\lambda'} \|u_{l\lambda'}^a\|^2 + \delta_{\lambda'1} \delta_{\lambda,0} \right] \right. \\
& + \sum_{L\lambda} \sum_{L'\lambda'} A_{L\lambda}^{av\mathbf{k}*} A_{L'\lambda'}^{av\mathbf{k}} \sum_{t,t'=-1} c_{\alpha t} c_{\beta t'} \sum_{s,\nu} G_{s,1}^{\nu,t,t'} G_{l,l',s}^{m,m',\nu} \left[ (E_{l'}^a - \epsilon_{v\mathbf{k}}) J_{ll'}^{a\lambda\lambda'} + \delta_{\lambda'1} J_{ll'}^{a\lambda 0} \right] \\
& + \frac{1}{2} \sum_{s=\pm 1} \sum_{t,t'=-1}^1 [c_{\alpha t'} c_{\beta}^{st}(l, m) + c_{\beta t'} c_{\alpha}^{st}(l, m)] \\
& \times \sum_{L'\lambda'} A_{L\lambda}^{av\mathbf{k}*} A_{L'\lambda'}^{av\mathbf{k}} G_{l,1,l+s}^{m,t',m+t} \left\{ (E_{l'}^a - \epsilon_{v\mathbf{k}}) \delta_{\lambda,\lambda'} \|u_{l\lambda'}^a\|^2 + \delta_{\lambda'1} \delta_{\lambda,0} \right\} \\
& + \sum_{L''} \sum_{L\lambda} \sum_{L'\lambda'} D_{L\lambda}^{av\mathbf{k}*}(\alpha, \beta) A_{L'\lambda'}^{av\mathbf{k}} G_{l,l'',l'}^{m,m'',m'} V_{l,L'',l'}^{a\lambda\lambda'} \\
& + \sum_{L''} \sum_{L\lambda} \sum_{L'\lambda'} A_{L\lambda}^{av\mathbf{k}*} A_{L'\lambda'}^{av\mathbf{k}} \sum_{t,t'=-1} \sum_{s\nu} \sum_{s'\nu'} c_{\alpha t} c_{\beta t'} G_{s,1,1}^{\nu,t,t'} G_{s',l'',l'}^{m'',m'} G_{l,s,s'}^{m,\nu,\nu'} W_{l,L'',l'}^{a\lambda\lambda'} \\
& + \frac{1}{2} \sum_{s=\pm 1} \sum_{t,t'=-1}^1 [c_{\alpha t'} c_{\beta}^{st}(l, m) + c_{\beta t'} c_{\alpha}^{st}(l, m)] \sum_{L\lambda} \sum_{L'\lambda'} A_{L\lambda}^{av\mathbf{k}*} A_{L'\lambda'}^{av\mathbf{k}} \\
& \times \left. \sum_{L''} \sum_{s',\nu'} G_{s',l'',l'}^{m'',m'} G_{s',1,l+s}^{\nu',t',m+t} V_{l,L'',l'}^{a\lambda\lambda'} \right\} \quad (6.165e)
\end{aligned}$$

$$\sigma_{\alpha\beta}^{xc} = \frac{\delta_{\alpha\beta}}{\Omega} \int_{\Omega} d^3 r \rho(\mathbf{r}) (\epsilon_{xc} - \mu_{xc}) - \frac{2\delta_{GGA}}{\Omega} \int_{\Omega} d^3 r \rho(\mathbf{r}) \partial_{\alpha} \rho(\mathbf{r}) \partial_{\beta} \rho(\mathbf{r}) \frac{\partial \epsilon_{XC}}{\partial \sigma} \quad (6.165f)$$

Our stress tensor calculation is more general than the derivation given in [19, 12, 17, 18] in the sense that our calculations are valid for APW+lo, LAPW, higher energy local orbitals, and GGA. In the case of GGA and APW+lo, an additional integral must be incorporated, which we discussed in the sections above.

# Chapter 7

## Pressure

The hydrostatic pressure component of a given stress tensor is defined as one third of its negative trace:

$$P = -\frac{1}{3} \sum_{\alpha}^3 \sigma_{\alpha\alpha}, \quad (7.1)$$

Explicitly, with  $\sigma_{\alpha\beta}$  given in equation (6.164)

$$\begin{aligned} P &= -\frac{1}{3} \sum_{\alpha=\beta=1}^3 \left( \sigma_{\alpha\beta}^{val,corr} + \sigma_{\alpha\beta}^{val,kin} + \delta_{APW} \sigma_{\alpha\beta}^{APW} + \sigma_{\alpha\beta}^{core} + \sigma_{\alpha\beta}^{xc} + \sigma_{\alpha\beta}^{es} \right) \quad (7.2) \\ &= P_{val,corr} + P_{val,kin} + \delta_{APW} P_{APW} + P_{core} + P_{xc} + P_{es} \end{aligned} \quad (7.3)$$

The conversion of the full stress formula into a simple pressure formula will be accomplished using the following relations.

As discussed in equation (A.12), the strain variation of the spherical harmonics will not contribute to pressure

$$\sum_{\alpha\alpha} \frac{\delta}{\delta \epsilon_{\alpha\alpha}} \Bigg|_{\underline{\epsilon}=0} Y_{lm}(\hat{\mathbf{r}}[\underline{\epsilon}]) \stackrel{(A.12)}{=} 0 \quad (7.4)$$

The product of the unit vectors is:

$$\sum_{\alpha=\beta} \hat{\mathbf{r}}_{\alpha} \hat{\mathbf{r}}_{\beta} \stackrel{(A.1)}{=} \sum_{t,t'=-1}^1 c_{\alpha t} c_{\beta t'} Y_{1t}(\hat{\mathbf{r}}) Y_{1t'}(\hat{\mathbf{r}}) = 1 \quad (7.5)$$

In the valence correction and valence kinetic stress, the following expression appears repeatedly:

$$\sum_{t,t'=-1}^1 c_{\alpha t} c_{\beta t'} \sum_{s,v} G_{s,1,1}^{v,t,t'} G_{l,l',s}^{m,m',v} \quad (7.6)$$

If we review these derivations closely, it is clear that the product of Gaunt numbers originating from a surface integral of four spherical harmonics, see equation (6.63). With equation (6.63), equation (7.6) simplifies in

$$\sum_{\alpha=\beta} \sum_{t,t'=-1}^1 c_{\alpha t} c_{\beta t'} \sum_{s,v} G_{s,1,1}^{v,t,t'} G_{l,l',s}^{m,m',v} = \sum_{\alpha=\beta} \sum_{t,t'=-1}^1 c_{\alpha t} c_{\beta t'} \oint_S dS Y_{1t}(\hat{\mathbf{r}}) Y_{1t'}(\hat{\mathbf{r}}) Y_{lm}^*(\hat{\mathbf{r}}) Y_{l'm'}(\hat{\mathbf{r}}) \stackrel{(A.1)}{=} \sum_{\alpha=\beta} \oint_S dS \hat{\mathbf{r}}_\alpha \hat{\mathbf{r}}_\beta Y_{lm}^*(\hat{\mathbf{r}}) Y_{l'm'}(\hat{\mathbf{r}}) \quad (7.7)$$

$$= \delta_{ll'} \delta_{mm'} \quad (7.8)$$

Also,

$$\sum_{\alpha=\beta} (\widehat{\mathbf{k} + \mathbf{K}})_\alpha (\widehat{\mathbf{k} + \mathbf{K}})_\beta = \frac{1}{|\mathbf{k} + \mathbf{K}|} \quad (7.9)$$

In the following sections, individual stress contribution will be considered once again and hydrostatic conditions will be applied.

## 7.1 Pressure due to the valence correction stress tensor

The pressure resulting from the valence correction stress is:

$$P_{val,corr} = -\frac{1}{3} \sum_{\alpha} \frac{2}{\Omega} \sum_{v\mathbf{k}} n_{v\mathbf{k}} \Re \left\langle \frac{d\psi_{v\mathbf{k}[\underline{\epsilon}]}(\mathbf{r}[\underline{\epsilon}])}{d\epsilon_{\alpha\alpha}} \Big|_{\underline{\epsilon}=0} \left| \hat{H}_{eff}(\mathbf{r}) - \epsilon_{v\mathbf{k}} \right| \psi_{v\mathbf{k}} \right\rangle \quad (7.10)$$

$$\stackrel{(6.143)}{=} -\frac{2}{3\Omega} \sum_{av\mathbf{k}} n_{v\mathbf{k}} \Re(I_{\alpha\alpha}^{av}(\mathbf{k})), \quad (7.11)$$

where  $\Re(I_{\alpha\alpha}^{av}(\mathbf{k}))$  is the real part of integral  $I_{\alpha\alpha}^{av}(\mathbf{k})$  as defined in equations (6.144) and (6.145), respectively, for spherical and non-spherical parts of the Hamiltonian. But the expression of  $I_{\alpha\alpha}^{av}(\mathbf{k})$  in the pressure calculation can be simplified because some contributions to pressure disappear. For example, the last line in equations (6.144) and (6.145) contains the contribution of the strain variation of spherical harmonics, and according to equation (7.4), this does not contribute. Also, the second last line of equations (6.144) and (6.145) is simplified using equation (7.8). As a result, the expression of  $I_{\alpha\alpha}^{av}(\mathbf{k})$  becomes:

$$I_{\alpha\alpha}^{av}(\mathbf{k}) = I_{\alpha\alpha}^{av sph}(\mathbf{k}) + I_{\alpha\alpha}^{av non-sph}(\mathbf{k}) \quad (7.12)$$

The spherical part is:

$$I_{\alpha\alpha}^{av sph}(\mathbf{k}) = \sum_{L\lambda\lambda'} D_{L\lambda}^{av\mathbf{k}*} A_{L\lambda'}^{av\mathbf{k}} \left[ (E_l^a - \epsilon_{v\mathbf{k}}) \delta_{\lambda\lambda'} \|u_{l\lambda'}^a\|^2 + \delta_{\lambda'1} \delta_{\lambda,0} \right] \quad (7.13)$$

$$+ \sum_{L\lambda\lambda'} A_{L\lambda}^{av\mathbf{k}*} A_{L\lambda'}^{av\mathbf{k}} \left[ (E_l^a - \epsilon_{v\mathbf{k}}) J_l^{a\lambda\lambda'} + \delta_{\lambda'1} J_l^{a\lambda0} \right] \quad (7.14)$$

The  $D_{L\lambda}^{av\mathbf{k}*}$  is from the strain variation of the matching coefficients, and its expression is:

$$\begin{aligned} D_{L0}^{av\mathbf{k}} &= \sum_{\mathbf{K}} c_{v\mathbf{k}\mathbf{K}} \left[ -\frac{4\pi i^l e^{i(\mathbf{k}+\mathbf{K})\tau_a}}{\sqrt{\Omega}} Y_{lm}^*(\widehat{\mathbf{k}+\mathbf{K}}) \underline{\mathcal{U}}^{-1} R_a j'_l(|\mathbf{k}+\mathbf{K}|R_a) \right] \\ D_{L1}^{av\mathbf{k}} &= \sum_{\mathbf{K}} c_{v\mathbf{k}\mathbf{K}} \left[ -\frac{4\pi i^l e^{i(\mathbf{k}+\mathbf{K})\tau_a}}{\sqrt{\Omega}} Y_{lm}^*(\widehat{\mathbf{k}+\mathbf{K}}) \underline{\mathcal{U}}^{-1} \left( j'_l(|\mathbf{k}+\mathbf{K}|R_a) + |\mathbf{k}+\mathbf{K}|R_a j''_l(|\mathbf{k}+\mathbf{K}|R_a) \right) \right] \\ D_{L2}^{av\mathbf{k}} &= 0 \end{aligned}$$

The coefficient  $J_l^a$  in equation (7.14) is defined as:

$$J_l^{a\lambda\lambda'} = \int_0^{R_a} r_a^3 dr_a u_{l\lambda}^{a\prime}(r_a) u_{l\lambda'}^a(r_a) \quad (7.15)$$

The non-spherical part in equation (7.12) can be simplified to:

$$\begin{aligned} I_{\alpha\alpha}^{av\text{non-sph}}(\mathbf{k}) &= \sum_{L''} \sum_{L\lambda} \sum_{L'\lambda'} D_{L\lambda}^{av\mathbf{k}*} A_{L'\lambda'}^{av\mathbf{k}} G_{l,l'',l'}^{m,m'',m'} V_{l,L'',l'}^{a\lambda\lambda'} \\ &\quad + \sum_{L''} \sum_{L\lambda} \sum_{L'\lambda'} A_{L\lambda}^{av\mathbf{k}*} A_{L'\lambda'}^{av\mathbf{k}} G_{l,l'',l'}^{m,m'',m'} W_{l,L'',l'}^{a\lambda\lambda'}, \end{aligned} \quad (7.16)$$

with  $V_{l,L'',l'}^{a\lambda\lambda'}$  and  $W_{l,L'',l'}^{a\lambda\lambda'}$  as follows

$$V_{l,L'',l'}^{a\lambda\lambda'} = \int_0^{R_a} r_a^2 dr_a u_{l\lambda}^a(r_a) V_{L''}^{eff}(\mathbf{r}_a) u_{l'\lambda'}^a(r_a) \quad (7.17)$$

$$W_{l,L'',l'}^{a\lambda\lambda'} = \int_0^{R_a} r_a^3 dr_a u_{l\lambda}^{a\prime}(r_a) V_{L''}^{eff}(r_a) u_{l'\lambda'}^a(r_a) \quad (7.18)$$

Comparing the pressure equations (7.11), (7.14), and (7.16) with the corresponding stress equations (6.143), (6.144), and (6.145) clearly suggest that the pressure equations are way simpler, easy to understand, and easy to implement. The computational burden required to compute the pressure contribution of the valence correction is negligible compared to that of the valence correction stress.

## 7.2 Pressure due to the valence kinetic stress tensor

In this section, we first consider the full valence kinetic stress, and then we apply the hydrostatic condition. The full valence kinetic stress tensor is already simplified in section 6.3 and given in equation (6.64). Equation (6.64) is:

$$\begin{aligned}
\Omega \sigma_{\alpha\beta}^{val,kin} &= \Omega \sigma_{\alpha\beta}^{kin,IS} + \Omega \sigma_{\alpha\beta}^{kin,R_a} \\
&= - \sum_{v\mathbf{k}} n_{v\mathbf{k}} \sum_{\mathbf{KK}'} c_{v\mathbf{k}\mathbf{K}}^* c_{v\mathbf{k}\mathbf{K}'} (\mathbf{k} + \mathbf{K}')_\alpha (\mathbf{k} + \mathbf{K}')_\beta \Theta(\mathbf{K} - \mathbf{K}') + \frac{1}{2} \sum_{v\mathbf{k}} n_{v\mathbf{k}} \sum_{a \in \Omega} \sum_{LL'} \sum_{\lambda\lambda'} A_{L'\lambda'}^{av\mathbf{k}*} A_{L\lambda}^{av\mathbf{k}} \\
&\quad \times \left\{ \sum_{t,t'=-1} \left( c_{\alpha t} c_{\beta t'} + c_{\beta t} c_{\alpha t'} \right) \sum_{s,\nu} G_{s,1,l}^{\nu,t,m} G_{l',1,s}^{m',t',\nu} \int_0^{R_a} r_a^2 dr_a u_{l'\lambda'}(r) u_{l\lambda}''(r) \right. \\
&\quad + \sum_{t,t'=-1} \sum_{s,\nu} \sum_{s'=\pm 1} G_{s,1,l}^{\nu,t,m} \left( c_{\alpha t} c_{\beta}^{s't'}(s,\nu) + c_{\beta t} c_{\alpha}^{s't'}(s,\nu) \right) \delta_{l',s+s'} \delta_{m',\nu+t'} \int_0^{R_a} r_a dr_a u_{l'\lambda'}(r) u_{l\lambda}'(r) \\
&\quad + \sum_{s=\pm 1} \sum_{t,t'=-1}^1 \left( c_{\alpha}^{st}(l,m) c_{\beta t'} + c_{\beta}^{st}(l,m) c_{\alpha t'} \right) G_{l',1,l+s}^{m',t',m+t} \int_0^{R_a} r_a^2 dr_a u_{l'\lambda'}(r) \left[ \frac{u_{l\lambda}'(r)}{r} - \frac{u_{l\lambda}(r)}{r^2} \right] \\
&\quad + \sum_{s,s'=\pm 1} \sum_{t,t'=-1}^1 \left( c_{\alpha}^{st}(l,m) c_{\beta}^{s't'}(l+s,m+t) + c_{\beta}^{st}(l,m) c_{\alpha}^{s't'}(l+s,m+t) \right) \delta_{l',l+s+s'} \delta_{m',m+t+t'} \\
&\quad \left. \times \int_0^{R_a} dr_a u_{l'\lambda'}(r) u_{l\lambda}(r) \right\}
\end{aligned}$$

In the pressure calculation, any expression containing  $c_{\alpha}^{st}(l,m)$  or  $c_{\beta}^{st}(l,m)$  vanishes because these coefficients only enter due to the derivative of spherical harmonics with respect to strain, which according to equation (7.4) disappears.

$$\begin{aligned}
\sum_{\alpha} \Omega \sigma_{\alpha\alpha}^{val,kin} &= - \sum_{v\mathbf{k}} n_{v\mathbf{k}} \sum_{\mathbf{KK}'} c_{v\mathbf{k}\mathbf{K}}^* c_{v\mathbf{k}\mathbf{K}'} (\mathbf{k} + \mathbf{K}')^2 \Theta(\mathbf{K} - \mathbf{K}') \\
&\quad + \sum_{v\mathbf{k}} n_{v\mathbf{k}} \sum_{a \in \Omega} \sum_L \sum_{\lambda\lambda'} A_{L\lambda'}^{av\mathbf{k}*} A_{L\lambda}^{av\mathbf{k}} \int_0^{R_a} r_a^2 dr_a u_{l\lambda'}(r) u_{l\lambda}''(r) \quad (7.19)
\end{aligned}$$

The valence kinetic pressure is:

$$\begin{aligned}
P_{val,kin} &= -\frac{1}{3} \sum_{\alpha} \sigma_{\alpha\alpha}^{val,kin} \\
&= -\frac{1}{3\Omega} \left( - \sum_{v\mathbf{k}} n_{v\mathbf{k}} \sum_{\mathbf{KK}'} c_{v\mathbf{k}\mathbf{K}}^* c_{v\mathbf{k}\mathbf{K}'} (\mathbf{k} + \mathbf{K}')^2 \Theta(\mathbf{K} - \mathbf{K}') \right. \\
&\quad \left. + \sum_{v\mathbf{k}} n_{v\mathbf{k}} \sum_{a \in \Omega} \sum_L \sum_{\lambda\lambda'} A_{L\lambda'}^{av\mathbf{k}*} A_{L\lambda}^{av\mathbf{k}} \int_0^{R_a} r_a^2 dr_a u_{l\lambda'}(r) u_{l\lambda}''(r) \right) \quad (7.20)
\end{aligned}$$

The expression inside the big bracket is nothing but twice the negative of valence kinetic energy ( $-2E_{kin}^{val}$ ). Therefore,

$$P_{val,kin} = \frac{2}{3\Omega} E_{kin}^{val} \quad (7.21)$$

This expression is similar to the corresponding expressions in Refs. [12, 19].

### 7.2.1 Pressure due to the additional surface integral

The stress contribution due to the additional surface integral in the kinetic energy expression in the APW+lo method is discussed in section 6.3.1, and equation (6.82) of the same section is

$$\begin{aligned}\sigma_{\alpha\beta}^{APW} = & \frac{1}{2\Omega} \sum_{lm} \sum_{\lambda} \mathbf{D}_{lm}^{avk}(\alpha, \beta) u_{l\lambda}(R_a) \left\{ \sum_{\lambda'} \mathbf{A}_{lm\lambda'}^{avk} u'_{l\lambda'}(R_a) - F_{lm}^{avk} \right\} \\ & + \frac{1}{2\Omega} \sum_{lm} \sum_{\lambda} \mathbf{A}_{lm\lambda}^{avk*} u_{l\lambda}(R_a) \left\{ \sum_{\lambda'} \mathbf{D}_{lm}^{avk}(\alpha, \beta) u'_{l\lambda'}(R_a) - \mathbf{F}_{lm}^{avk}(\alpha, \beta) \right\}\end{aligned}\quad (7.22)$$

The pressure contribution of equation (7.22) is

$$\begin{aligned}P_{APW} = & -\frac{1}{3} \sum_{\alpha} \sigma_{\alpha\alpha}^{APW} \\ = & -\frac{1}{6\Omega} \sum_{\alpha} \sum_{lm} \sum_{\lambda\lambda'} \left\{ \mathbf{D}_{lm}^{avk}(\alpha, \alpha) u_{l\lambda}(R_a) \left\{ \mathbf{A}_{lm\lambda'}^{avk} u'_{l\lambda'}(R_a) - F_{lm}^{avk} \right\} \right. \\ & \left. + \mathbf{A}_{lm\lambda}^{avk*} u_{l\lambda}(R_a) \left\{ \sum_{\lambda'} \mathbf{D}_{lm}^{avk}(\alpha, \alpha) u'_{l\lambda'}(R_a) - \mathbf{F}_{lm}^{avk}(\alpha, \alpha) \right\} \right\}\end{aligned}\quad (7.23)$$

This contribution does not exist when the LAPW method is used.

### 7.3 Pressure due to the core correction stress tensor

The core correction stress was already discussed and simplified in section 6.2. From equation (6.31)

$$\sigma_{\alpha\beta}^{core} = -\frac{1}{\Omega} \sum_{a \in \Omega} \int_{R_a} d^3 \mathbf{r}_a \rho_c^a(\mathbf{r}_a) \frac{1}{2} (\mathbf{r}_{a\alpha} \partial_{\beta} + \mathbf{r}_{a\beta} \partial_{\alpha}) V_{eff}^a(\mathbf{r}_a) \quad (7.24)$$

The sum of the diagonal elements is

$$\sum_{\alpha} \sigma_{\alpha\alpha}^{core} = -\frac{1}{\Omega} \sum_{a \in \Omega} \int_{R_a} d^3 \mathbf{r}_a \rho_c^a(\mathbf{r}_a) \mathbf{r}_a \nabla V_{eff}^a(\mathbf{r}_a) \quad (7.25)$$

This relation can be further simplified using the Janak's identity (D.15). A detailed discussion of this identity is provided in appendix D. Using equation (D.15), we get:

$$\sum_{\alpha} \sigma_{\alpha\alpha}^{core} = -\frac{2}{\Omega} E_{kin}^{core} \quad (7.26)$$

The core correction pressure is

$$\begin{aligned}P_{core} = & -\frac{1}{3} \sum_{\alpha} \sigma_{\alpha\alpha}^{core} \\ = & \frac{2}{3\Omega} E_{kin}^{core}\end{aligned}\quad (7.27)$$

In Ref. [19], the authors said that the core correction vanishes for pure pressure. We believe that the authors meant to say that its explicit form like in stress would not exist, otherwise one would not be able to retain the full core kinetic energy upon invoking Janak's identity [44].

## 7.4 Pressure due to the exchange correlation stress tensor

The exchange correlation stress tensor according to equation (6.146) is

$$\sigma_{\alpha\beta}^{xc} = \frac{\delta_{\alpha\beta}}{\Omega} \int_{\Omega} d^3 \mathbf{r} \rho(\mathbf{r}) (\epsilon_{xc} - \mu_{xc}) - \frac{2\delta_{GGA}}{\Omega} \int_{\Omega} d^3 \mathbf{r} \rho(\mathbf{r}) \partial_{\alpha} \rho(\mathbf{r}) \partial_{\beta} \rho(\mathbf{r}) \frac{\partial \epsilon_{xc}}{\partial \sigma} \quad (7.28)$$

The form of the exchange-correlation stress tensor depends on the choice of exchange-correlation function. Its expressions for the local density approximation (LDA) and the general gradient approximation (GGA) as given in equations (6.147a) and (6.147c) are:

$$\begin{aligned} \sigma_{\alpha\beta}^{LDA} &\stackrel{(6.147a)}{=} \frac{\delta_{\alpha\beta}}{\Omega} \int_{\Omega} d^3 \mathbf{r} \rho(\mathbf{r}) (\epsilon_{xc}(\rho(\mathbf{r})) - \mu_{xc}(\rho(\mathbf{r}))) \\ \sigma_{\alpha\beta}^{GGA} &\stackrel{(6.147c)}{=} \frac{\delta_{\alpha\beta}}{\Omega} \int_{\Omega} d^3 \mathbf{r} \rho(\mathbf{r}) (\epsilon_{xc}(\rho(\mathbf{r}), \nabla \rho(\mathbf{r})) - \mu_{xc}(\rho(\mathbf{r}), \nabla \rho(\mathbf{r}))) \\ &\quad - \frac{2}{\Omega} \int_{\Omega} d^3 \mathbf{r} \rho(\mathbf{r}) \partial_{\alpha} \rho(\mathbf{r}) \partial_{\beta} \rho(\mathbf{r}) \frac{\partial \epsilon_{xc}}{\partial \sigma} \end{aligned}$$

The exchange correlation pressure is

$$P^{xc} = -\frac{1}{3} \sum_{\alpha} \sigma_{\alpha\alpha}^{xc}$$

Which follows

$$P^{LDA} = -\frac{1}{\Omega} \int_{\Omega} d^3 \mathbf{r} \rho(\mathbf{r}) (\epsilon_{xc}(\rho(\mathbf{r})) - \mu_{xc}(\rho(\mathbf{r}))) \quad (7.29)$$

$$P^{GGA} = -\frac{1}{\Omega} \int_{\Omega} d^3 \mathbf{r} \rho(\mathbf{r}) (\epsilon_{xc}(\rho(\mathbf{r}), \nabla \rho(\mathbf{r})) - \mu_{xc}(\rho(\mathbf{r}), \nabla \rho(\mathbf{r}))) + \frac{2}{3\Omega} \int_{\Omega} d^3 \mathbf{r} \rho(\mathbf{r}) \sigma \frac{\partial \epsilon_{xc}}{\partial \sigma}, \quad (7.30)$$

where  $\sigma = \nabla \rho(\mathbf{r}) \cdot \nabla \rho(\mathbf{r})$ .

The LDA pressure formula is already in its simplest form, but a further simplification is possible for the GGA pressure formula. From equations (7.29) and (7.30) we get:

$$3\Omega P^{GGA} = 3\Omega P^{LDA} + 2 \sum_{\alpha} \int_{\Omega} d^3 \mathbf{r} \rho(\mathbf{r}) \partial_{\alpha} \rho(\mathbf{r}) \partial_{\alpha} \rho(\mathbf{r}) \frac{\partial \epsilon_{xc}}{\partial \sigma} \quad (7.31a)$$

$$P^{GGA} = P^{LDA} + \frac{2}{3\Omega} \int_{\Omega} d^3 \mathbf{r} \rho(\mathbf{r}) |\nabla \rho(\mathbf{r})|^2 \frac{\partial \epsilon_{xc}}{\partial \sigma} \quad (7.31b)$$

$$= P^{LDA} + P^{GGA\_CORR} \quad (7.31c)$$

Similar to the stress  $\Omega \sigma_{\alpha\beta}^{GGA,CORR}$  in equation (6.150),  $P^{GGA,CORR}$  is also divided into the contribution from the atomic spheres  $(P^{GGA,CORR})_{sph}$  and the interstitial region  $(P^{GGA,CORR})_{int}$ .  $(P^{GGA,CORR})_{sph}$  and  $(P^{GGA,CORR})_{int}$  are the trace of the first and second integral of equation (6.150).

In the following Tables 7.1 and 7.2 we present each contribution of equation (7.31c) for Aluminum (Al) and Silicon (Si) at seven different volumes. The GGA correction term

$P^{GGA,CORR}$ , which is decomposed in the atomic spheres region  $(P^{GGA,CORR})_{sph}$  and the interstitial region  $(P^{GGA,CORR})_{int}$ , is also presented. Contrary to what is claimed in Ref.[18],  $(P^{GGA,CORR})_{int}$  is almost zero and  $P^{GGA,CORR}$  is entirely due to the term inside the atomic spheres. The only plausible explanation for the discrepancy between our observation and the claim in Ref. [18] could be the different ways in which they define their basis function and the charge density. In contrast to Al,  $(P^{GGA,CORR})_{int}$  is not entirely negligible for Si.  $(P^{GGA,CORR})_{int}$  for Si is orders of magnitude larger than that for Al. For both elements, the LDA like term ( $P^{LDA}$ ) contributes most to the trace of GGA stress, and the GGA correction is an order of magnitude less than the LDA like term. For  $P^{GGA,CORR}$ , the integration inside the atomic spheres provides the biggest contribution. This can also be seen in Fig. 7.1.

Table 7.1: The exchange correlation pressure (in kbar) is decomposed according to equation (7.31c) for seven different volumes of fcc Aluminum.

Volume( $\text{Bohr}^3$ )	$P^{GGA}$	$P^{LDA}$	$P^{GGA,CORR}$	$(P^{GGA,CORR})_{sph}$	$(P^{GGA,CORR})_{int}$
94.82	18838.40	16828.64	2009.76	2009.73	0.03
97.94	18227.42	16281.17	1946.25	1946.22	0.03
101.07	17655.30	15768.61	1886.68	1886.65	0.03
104.19	17118.44	15287.73	1830.70	1830.67	0.04
107.32	16611.68	14833.90	1777.78	1777.74	0.04
110.45	16134.02	14406.20	1727.82	1727.78	0.04
113.57	15684.42	14003.67	1680.74	1680.69	0.05

Table 7.2: The exchange correlation pressure (in kbar) is decomposed according to equation (7.31c) for seven different volumes of Silicon in a diamond structure.

Volume( $\text{Bohr}^3$ )	$P^{GGA}$	$P^{LDA}$	$P^{GGA,CORR}$	$(P^{GGA,CORR})_{sph}$	$(P^{GGA,CORR})_{int}$
259.66	15385.34	13764.25	1621.09	1610.64	10.46
265.18	15060.14	13472.32	1587.83	1577.37	10.46
270.71	14748.38	13192.48	1555.90	1545.45	10.45
276.23	14449.25	12924.01	1525.24	1514.80	10.44
281.76	14162.00	12666.24	1495.76	1485.33	10.43
287.28	13885.94	12418.54	1467.41	1456.99	10.41
292.81	13620.43	12180.32	1440.11	1429.71	10.40

In the following Fig. 7.1 we plot Table 7.1 in the left panel and Table 7.2 in the right panel.

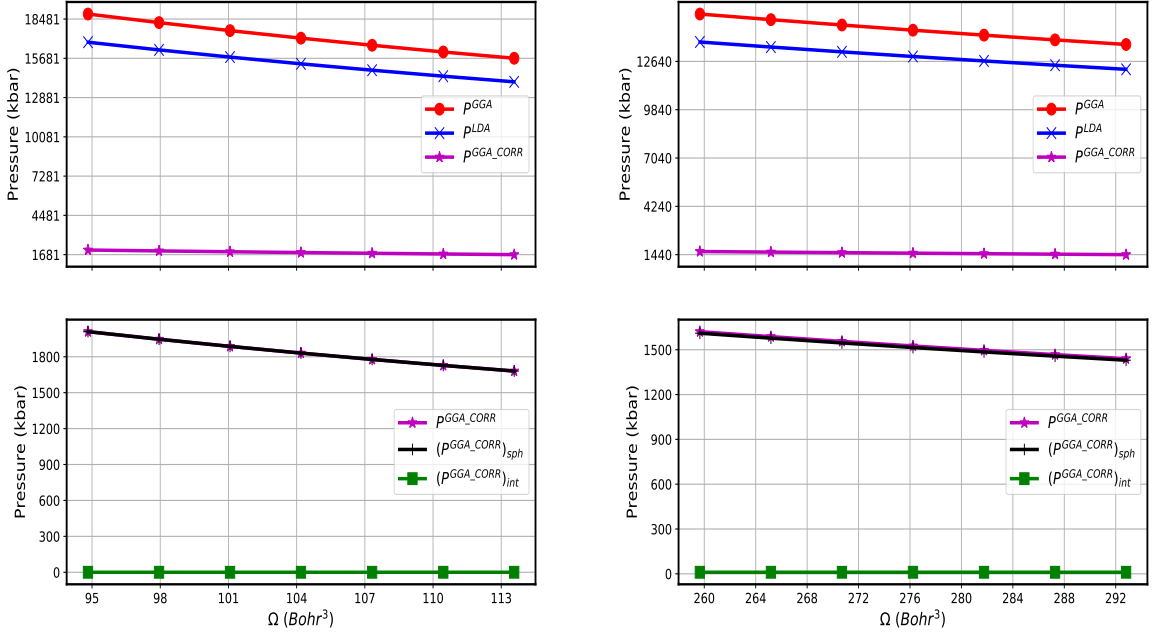


Figure 7.1: The different contributions to the exchange-correlation pressure (Eqn. (7.31c)) for Al (left panel) and Si (right panel) as function of volume. The bottom plots display the trace of the equation (6.150).  $P^{GGA}$  is the trace of the GGA stress tensor ( $\sigma_{\alpha\beta}^{GGA}$ ),  $P^{LDA}$  is the LDA like expression, and  $P^{GGA,CORR}$  is the GGA correction.

The upper panels of Fig. 7.1 show the trace of the total GGA exchange-correlation stress ( $P^{GGA}$ ), which is decomposed into a LDA like term ( $P^{LDA}$ ) and a GGA correction ( $P^{GGA,CORR}$ ).  $P^{GGA,CORR}$  is then further divided into the sphere ( $(P^{GGA,CORR})_{sph}$ ) and the interstitial ( $(P^{GGA,CORR})_{int}$ ) contributions. These contributions are shown in the lower panels of Fig. 7.1. Left panels are for Aluminum and right panels for Silicon.

## 7.5 Pressure due to the electrostatic stress tensor

The electrostatic stress tensor has been discussed in detail in section 6.1, and its contribution to the total stress is provided in equation (6.29). Equation (6.29) is:

$$\begin{aligned}
 2\Omega\sigma_{\alpha\beta}^{es} &= \Omega \sum_{\mathbf{G}} \sum_{\mathbf{G}' \neq 0} \rho^*(\mathbf{G}) \left( -\delta_{\alpha\beta} V_C(\mathbf{G}') + 2\hat{\mathbf{G}}_\alpha \hat{\mathbf{G}}_\beta V_C(\mathbf{G}) \right) \Theta(\mathbf{G} - \mathbf{G}') \\
 &\quad - \sum_{t,t'=-1}^1 c_{\alpha t} c_{\beta t'} \int_{\Omega} d^3 \mathbf{r} \Theta_a(\mathbf{r}) \rho(\mathbf{r}) V_C(\mathbf{r}) Y_{1t}(\hat{\mathbf{r}}) Y_{1t'}(\hat{\mathbf{r}}) \\
 &\quad + \sum_a Z_a \sum_{t,t'=-1}^1 c_{\alpha t} c_{\beta t'} V_M(\boldsymbol{\tau}_a) Y_{1t}(\boldsymbol{\tau}_a) Y_{1t'}(\boldsymbol{\tau}_a)
 \end{aligned} \tag{7.32}$$

The trace of the stress is

$$\begin{aligned}
\sum_{\alpha} 2\Omega \sigma_{\alpha\alpha}^{es} &= \Omega \sum_{\mathbf{G}} \sum_{\mathbf{G}' \neq 0} \rho^*(\mathbf{G}) \left( -3V_C(\mathbf{G}') + 2V_C(\mathbf{G}) \right) \Theta(\mathbf{G} - \mathbf{G}') \\
&\quad - \int_{\Omega} d^3\mathbf{r} \Theta_a(\mathbf{r}) \rho(\mathbf{r}) V_C(\mathbf{r}) \sum_{\alpha} \hat{\mathbf{r}}_{\alpha} \hat{\mathbf{r}}_{\alpha} + \sum_a Z_a V_M(\boldsymbol{\tau}_a) \sum_{\alpha} \hat{\boldsymbol{\tau}}_{\alpha} \hat{\boldsymbol{\tau}}_{\alpha} \\
&\stackrel{(7.5)}{=} -\Omega \sum_{\mathbf{G}} \sum_{\mathbf{G}' \neq 0} \rho^*(\mathbf{G}) V_C(\mathbf{G}') \Theta(\mathbf{G} - \mathbf{G}') - \int_{\Omega} d^3\mathbf{r} \Theta_a(\mathbf{r}) \rho(\mathbf{r}) V_C(\mathbf{r}) \\
&\quad + \sum_a Z_a V_M(\boldsymbol{\tau}_a)
\end{aligned} \tag{7.33}$$

Using the relation:

$$-\Omega \sum_{\mathbf{G}} \sum_{\mathbf{G}' \neq 0} \rho^*(\mathbf{G}) V_C(\mathbf{G}') \Theta(\mathbf{G} - \mathbf{G}') = - \int_{\Omega} d^3\mathbf{r} \Theta_{IS}(\mathbf{r}) \rho(\mathbf{r}) V_C(\mathbf{r}) \tag{7.34}$$

we get:

$$\begin{aligned}
\sum_{\alpha} 2\Omega \sigma_{\alpha\alpha}^{es} &= - \int_{\Omega} d^3\mathbf{r} \Theta_{IS}(\mathbf{r}) \rho(\mathbf{r}) V_C(\mathbf{r}) - \int_{\Omega} d^3\mathbf{r} \Theta_a(\mathbf{r}) \rho(\mathbf{r}) V_C(\mathbf{r}) + \sum_a Z_a V_M(\boldsymbol{\tau}_a) \\
&= - \int_{\Omega} d^3\mathbf{r} \rho(\mathbf{r}) V_C(\mathbf{r}) + \sum_a Z_a V_M(\boldsymbol{\tau}_a)
\end{aligned} \tag{7.35}$$

Finally, electrostatic pressure is:

$$\begin{aligned}
P^{es} &= -\frac{1}{3} \sum_{\alpha} \sigma_{\alpha\alpha}^{es} \\
&= \frac{1}{3} \left( \frac{1}{2\Omega} \int_{\Omega} d^3\mathbf{r} \rho(\mathbf{r}) V_C(\mathbf{r}) - \frac{1}{2\Omega} \sum_a Z_a V_M(\boldsymbol{\tau}_a) \right)
\end{aligned} \tag{7.36}$$

This equation is identical to the electrostatic part of the simple pressure equation (5.64b) in Ref. [19] and equation (32) in Ref. [12].

## 7.6 The simple pressure formula

The so-called simple pressure formula is obtained by summing the pressure contribution of valence correction stress, valence kinetic stress, core correction stress, exchange correctional stress, and electrostatic stress, which are calculated in equations (7.11), (7.21), (7.27), (7.29), and (7.36), respectively. In the case of the APW+lo method, we would have an additional contribution, as described in section 7.2.1.

$$\begin{aligned}
P_{LDA}^{tot} &= P_{val,corr} + P_{val,kin} + \delta_{APW} P_{APW} + P_{core} + P_{xc,LDA}^{tot} + P^{es} \\
&= P_{val,corr} + \frac{2}{3\Omega} E_{kin}^{val} + \delta_{APW} P_{APW} + \frac{2}{3\Omega} E_{kin}^{core} \\
&\quad - \frac{1}{\Omega} \int_{\Omega} d^3\mathbf{r} \rho(\mathbf{r}) \left( \epsilon_{xc}(\rho(\mathbf{r})) - \mu_{xc}(\rho(\mathbf{r})) \right) + \frac{1}{3} \left( \frac{1}{2\Omega} \int_{\Omega} d^3\mathbf{r} \rho(\mathbf{r}) V_C(\mathbf{r}) - \frac{1}{2\Omega} \sum_a Z_a V_M(\boldsymbol{\tau}_a) \right)
\end{aligned}$$

Using LDA, the final expression of the simple pressure formula is

$$\begin{aligned}
P_{LDA}^{tot} = & \frac{2}{3\Omega} E_{kin} + \delta_{APW} P_{APW} - \frac{1}{\Omega} \int_{\Omega} d^3 \mathbf{r} \rho(\mathbf{r}) \left( \epsilon_{xc}(\rho(\mathbf{r})) - \mu_{xc}(\rho(\mathbf{r})) \right) \\
& + \frac{1}{3} \left( \frac{1}{2\Omega} \int_{\Omega} d^3 \mathbf{r} \rho(\mathbf{r}) V_C(\mathbf{r}) - \frac{1}{2\Omega} \sum_a Z_a V_M(\boldsymbol{\tau}_a) \right) + P_{val,corr} \quad (7.37)
\end{aligned}$$

Similarly, using GGA:

$$P_{GGA}^{tot} = P_{LDA}^{tot} + \frac{2}{3\Omega} \int_{\Omega} d^3 \mathbf{r} \rho(\mathbf{r}) \sigma \frac{\partial \epsilon_{XC}}{\partial \sigma} \quad (7.38)$$

The presence of the last term  $P_{val,corr}$  in equation (7.37) is due to the choice of the basis sets, and in the case of position-independent and complete basis sets, this contribution would vanish. Equation (7.37), with the exception to the second term and last correction term, is also similar to the pressure that is derived directly from the total energy in Ref. [44]. The simple pressure formula of Refs. [19, 12] is the same as equation (7.37) for LAPW, and the GGA correction term, the second term of equation (7.38), is similar to the corresponding expression in Ref. [18]. Using the simple pressure formula is much more convenient for calculating hydrostatic pressure because many of the complicated expressions that exist in the full stress tensor vanish. Also, most of the required quantities are already at our disposal from a regular total energy calculation and an additional effort is only required for calculating  $P_{val,corr}$ .

Furthermore, equations (7.37) and (7.38) are simplified as given below:

$$\begin{aligned}
3\Omega P_{LDA}^{tot} & \stackrel{(4.15)}{=} E_{tot} + E_{kin} - \int_{\Omega} d^3 \mathbf{r} \rho(\mathbf{r}) \left( 4\epsilon_{XC}(\rho(\mathbf{r})) - 3\mu_{XC}(\rho(\mathbf{r})) \right) \\
& + \delta_{APW} 3\Omega P_{APW} + 3\Omega P_{val,corr} \quad (7.39)
\end{aligned}$$

$$3\Omega P_{GGA}^{tot} \stackrel{(4.15)}{=} 3\Omega P_{LDA}^{tot} + 2 \int_{\Omega} d^3 \mathbf{r} \rho(\mathbf{r}) \sigma \frac{\partial \epsilon_{XC}}{\partial \sigma} \quad (7.40)$$

## 7.7 Core leakage

In principle, each individual contribution to the pressure formula resembles the trace of a corresponding contribution to the full stress tensor, but for the core correction we used Janak's identity (D.15) to convert the trace of the core correction stress into the core kinetic energy. The detailed derivation of this identity is given in Appendix D. In this derivation, however, it is assumed that the surface integral containing core wave-functions vanishes. This assumption is valid if core states strictly vanish at the sphere boundary and beyond. This is also the basis for the construction of the basis functions in the APW based methods. In the APW based methods, the valence states are orthogonal to the core states as long as the core states are confined in the atomic spheres. This is only possible if the core states are deep in energy and the sphere sizes are large. However, if a system has core states close to the WIEN2k default core separation energy of -6 Ry (for example, 2p states of Al or 5s states in Pt), a portion of the core wave function will eventually spill out from the atomic spheres.

This phenomenon is known as core leakage. In such cases, Janak's identity (D.15), and consequently the simple pressure formulas of equations (7.37) and (7.38) are invalid. The core leakage varies with respect to the size of atomic-spheres and thus the results change with different choices of  $R_a$ . The core leakage can be mitigated in different ways:

1. We can describe them as semi-core states using local orbitals (LO) as described in section 3.1.4.
2. Instead of using Janak's identity, we can work with the expression that directly comes from the trace of the core correction stress and perform an integration well beyond the atomic spheres until the core density really becomes zero. For this we need the wave function and potential outside the spheres.
3. We approximate the core potential outside the atomic spheres, such that it more realistically resembles that of the real solid. The potential is approximated by taking three subsequent points in the vicinity of an atomic sphere boundary using a quadratic equation ie.  $V_{00}(r)|_{r>R_a} = a_0 + a_1 * r + a_2 * r^2$  (in the following it is referred to as the extrapolated potential). The potential is extrapolated outside the atomic sphere as long as it increases. When the potential begins to decrease, it is replaced by the value at which it begins to decrease.

In a total energy calculation, a small core leakage problem is not as severe as compared to a pressure calculation. In the pressure calculation, it is problematic because of Janak's identity. In total energy calculation, the leak portions of core densities from many different atoms are superposed and produce a “crystalline” core density, which has i) non-spherical terms due to the superposition effects, and ii) an interstitial density described by a Fourier series. Actual calculations showed that while a certain amount of core leakage may be numerically irrelevant in a total energy calculation, it may very well turn out to be highly problematic for pressure calculations. In WIEN2k, there is a warning message that pops up to warn the user during the initialization process if the amount of core leakage is appreciable.

To demonstrate these effects explicitly, we present results for fcc Aluminum. This element is chosen because Al has 2p states that can be described as core states or as semi-core states. In general, the amount of core leakage when 2p states are treated as core states is tolerable for total energy calculation except for very small spheres. In the present calculations,  $R_a K_{max}$  is 10,  $G_{max}$  is  $20 \text{ Ry}^{\frac{1}{2}}$ ,  $l_{max}$  is 10, and the cutoff parameter for the non-spherical potential i.e the max of  $L''$  in equation (6.104) is 6. A discrete k-mesh of  $21 \times 21 \times 21$  k-points is reduced to 286 k-points in the irreducible Brillouin zone (IBZ) after exploiting all symmetry operations for a cubic system. Because of symmetry, only '0 0', '4 0', '4 4', '6 0', and '6 4' components are presented in the expansion of the charge density and potential in terms of the lattice harmonics. For the integration in the IBZ, we used the temperature broadening method with a broadening parameter of 0.005 Ry. The local density approximation (LDA) is used to evaluated the exchange correlation energy and potential and a Fast Fourier Transform (FFT) grid of  $90 \times 90 \times 90$  is used to evaluate the exchange energy or potential in the interstitial. The convergence criteria for the energy difference between two self-consistent cycles and charge distance is set at  $10^{-5}$ .

In the original WIEN2k code, the core potential outside an atomic-sphere (beyond  $R_a$ ) is decreasing as the distance from a nucleus increases because  $r * V_{00}(r)$  was kept constant at  $R_a * V_{00}(R_a)$  i.e  $V_{00}(r)|_{r>R_a} = \frac{R_a * V_{00}(R_a)}{r}$  (in the following it is referred to as the original potential). When the simple pressure formula, as given in equation (7.37), is evaluated using this potential, we observed that the pressure is changing according to different choices of atomic spheres radii  $R_a$ , see Fig. 7.3 (a). In Fig. 7.3 (b), the pressure is estimated directly from the total energy using a least square fit with the Birch-Murnaghan (BM) equation of state, and the calculated pressure is insensitive to the choice of  $R_a$ . In these calculations, 1s, 2s, and 2p states of Aluminum are treated as core states. For the sphere size of  $R_a = 2.1$ , 0.8% of the 2p charge is outside of the sphere, and for  $R_a = 2.5$ , only 0.1% is outside. This amount of core leakage is not a problem in total energy calculation and thus for estimating the pressure from it, see Fig. 7.3 (b). However, in analytical pressure calculation, this is a noticeable problem, see Fig. 7.3 (a). This can also be seen in Tables 7.3 and 7.4 below. In our analytical simple pressure formula, the total non-interacting kinetic energy ( $E_{kin}$ ) in equation (7.37) is replaced by equation (4.6), and the spherical part ( $l=0, m=0$  component) of the potential for core electrons in the region outside of the atomic-sphere is calculated by  $V_{00}(r)|_{r>R_a} = \frac{R_a * V_{00}(R_a)}{r}$ .

One approach to solve this problem is to extrapolate the core potential outside the atomic spheres as mentioned above. The modification is achieved via a fitting of a quadratic equation, see Fig. 7.2. The result of such calculations is provided in Fig. 7.4, and do not show any  $R_a$  dependency. Furthermore, we have also treated only 1s and 2s as core states but 2p as semi-core states and described using local orbitals. In this case, for the sphere size of  $R_a = 2.1$ , only 0.08% of 2p charge is outside the sphere, and for  $R_a = 2.5$ , only 0.01% core charge leaks out. From the results presented in Fig. 7.5, it is clear that this amount of core leakage is not a problem in analytical pressure calculations. In Fig. 7.5 (a) and (b), the core potential outside the atomic sphere is the original potential and the extrapolated potential, respectively. Fig. 7.6 shows the same calculation as in Fig. 7.5, but the pressure is estimated by the trace of the full stress tensor. The extrapolation of the core potential is accomplished in a subroutine `extrapolate_potential.f` in `lcore` program.

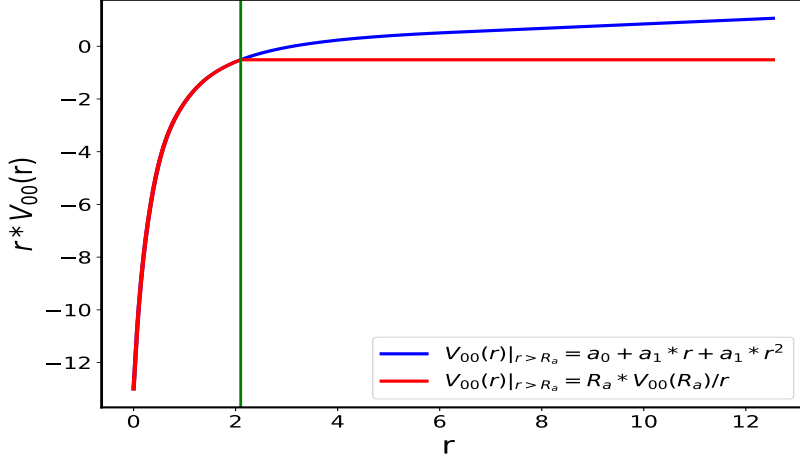


Figure 7.2: The behavior of core potential inside and outside of an atomic-sphere for fcc Al before and after the extrapolation with a polynomial.  $r$  is the distance from the nucleus and the vertical line at  $r = 2.1$  denotes the sphere boundary. Because of the existence of a singularity in the potential at  $r = 0$ ,  $r$  times  $V_{00}(r)$  is plotted. The red line represents the potential before extrapolation, the blue line the extrapolated potential using a quadratic equation, and  $V_{00}$  represents the spherically symmetric part of the potential.

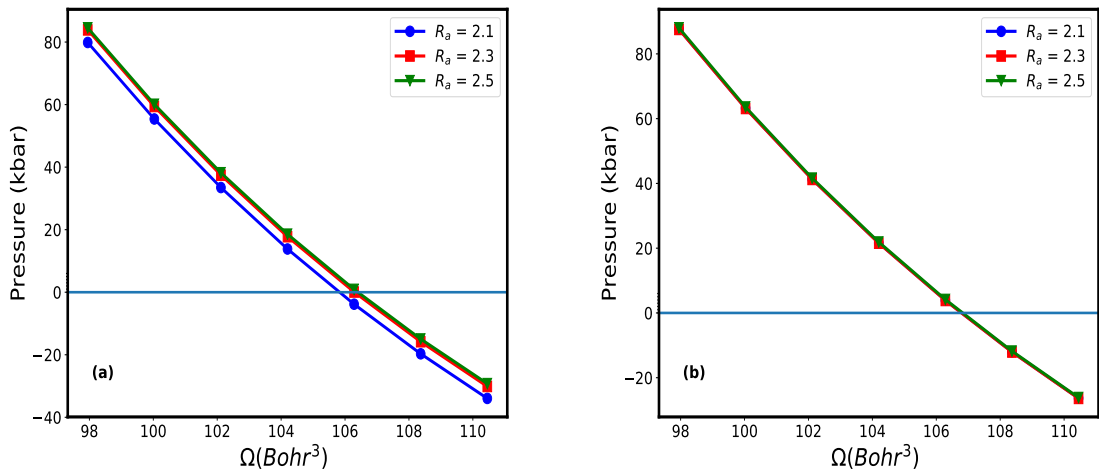


Figure 7.3: Pressure estimated by the simple pressure formula given in equation (7.37) (a), and directly from total energy using the least square fit of the Birch-Murnaghan (BM) equation of state (b) for fcc Al. The potential outside atomic sphere is the original potential (red curve in Fig. 7.2) and 2p states are considered as core states.

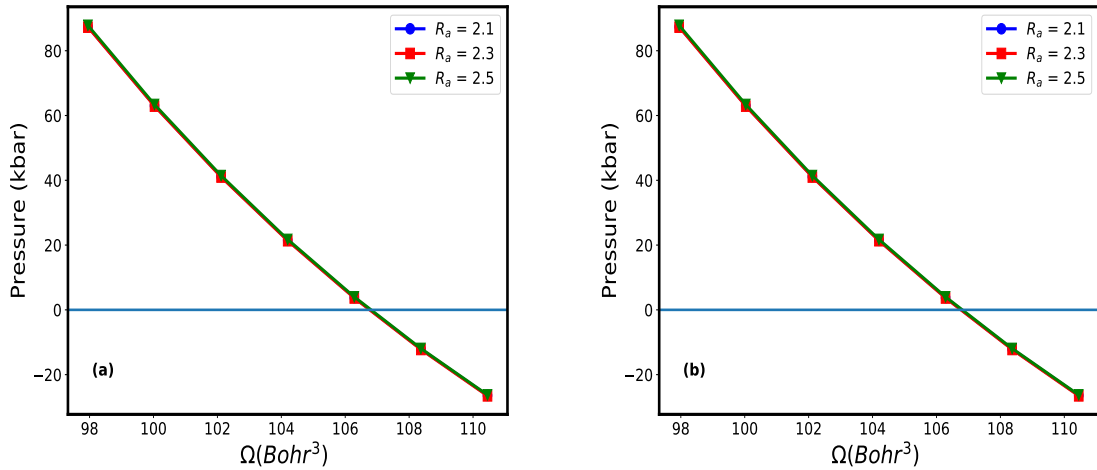


Figure 7.4: Same as Fig. 7.3 but the potential at any point outside of an atomic-sphere region is calculated via extrapolation using a quadratic equation (blue curve in Fig. 7.2).

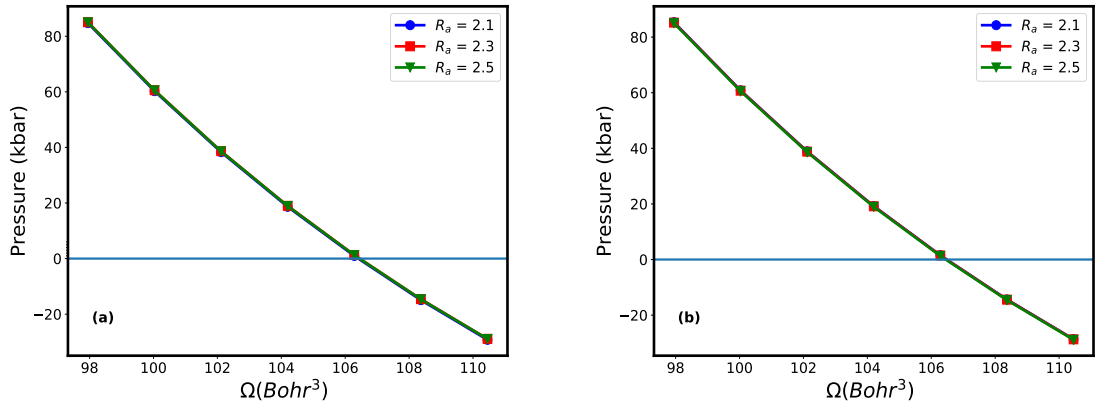


Figure 7.5: Pressure estimated via the analytical simple pressure formula using two different expressions of the potential in the region outside of the atomic-sphere. The 2p states are treated as semi-core states. On the left panel, the core potential outside of an atomic sphere is the original potential. On the right panel, the core potential outside the sphere is the extrapolated potential.

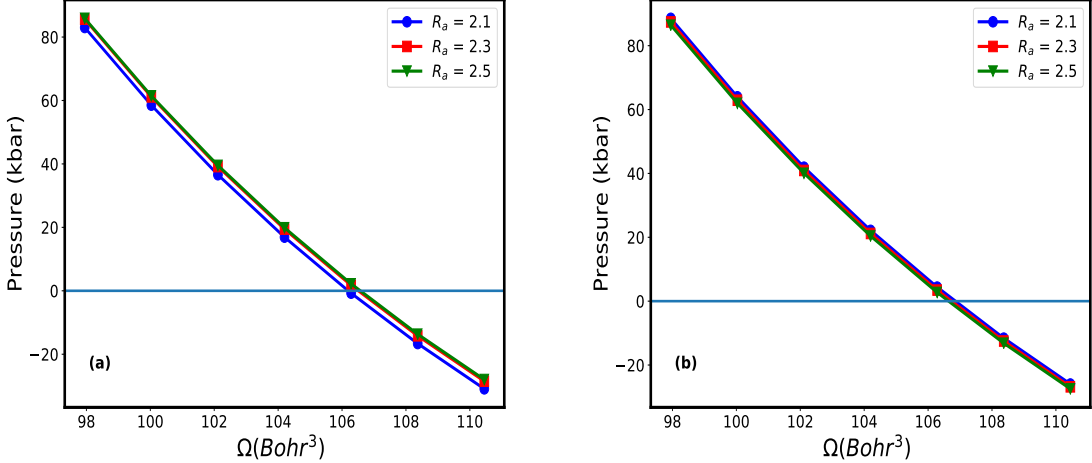


Figure 7.6: The trace of stress tensor as a function of volume for fcc Al for three different sphere sizes. The 2p states are treated as core states. The core potential outside of an atomic sphere in the panel (a) is the original potential (red curve in Fig.7.2) and in the panel (b) is the extrapolated potential (blue curve in Fig. 7.2).

In Fig. 7.6, the right panel shows that the pressure estimated via the full stress tensor agrees well with the pressure evaluated directly from the total energy (also called the numerical pressure). Both, the trace of the stress tensor and the numerical pressure exhibit a small  $R_a$  dependency. This dependency affects the estimated lattice parameter only at the third digit after the decimal point and this dependency is not problematic. However, as shown in the left panel, with the original potential the estimated pressure has a noticeable  $R_a$  dependency, and the lattice parameter has an inaccuracy at the second digit for the smaller  $R_a$ . The above analysis epitomizes that the core leakage is clearly a serious problem for both pressure and stress calculations, even though it is not the case for the total energy. The results suggested that we can mitigate the problem by either describing core states of higher energy via semi-core local orbitals or modifying the potential outside the region of the atomic-sphere. In our calculations, we adopt both techniques.

Tables 7.3 and 7.4 below show how core leakage affects the predicted lattice parameter. The calculations are the same as for Fig. 7.3.

Table 7.3: The predicted lattice parameter ( $a_0$ ) using the analytical simple pressure (SIMP) formula and directly from total energy (ENE) for three different atomic sphere sizes ( $R_a$ ). The 2p states are treated as core states and the core potential outside an atomic sphere is the original potential.

$a_0 \backslash R_a$	$R_a = 2.1$	$R_a = 2.3$	$R_a = 2.5$
$a_0$ (SIMP)	7.508	7.520	7.522
$a_0$ (ENE)	7.531	7.531	7.532

Table 7.4: Same as Table 7.3, but the 2p states are treated as semi-core states.

$a_0 \diagdown R_a$	$R_a = 2.1$	$R_a = 2.3$	$R_a = 2.5$
$a_0$ (SIMP)	7.522	7.523	7.523
$a_0$ (ENE)	7.529	7.529	7.531

# Chapter 8

## Results

In the previous chapters, we derived the stress tensor and pressure formalism within the APW based methods. In this chapter, we test the implementation in the WIEN2k code [13, 14] for various materials. With our formalism and implementation, the core calculation can be fully relativistic, but the valence calculation is limited to the non-relativistic limit. However, all results presented in this thesis are calculated using non-relativistic calculation. To validate our implementation, we compare the results of the stress tensor with the least square fit of total energy vs volume using the Birch-Murnaghan (BM) equation of state. In the following this fitted result is often referred to with the subscript or superscript BM. The BM equation is:

$$E_{BM}(\Omega) = E_0 + \frac{9\Omega_0 B_0}{16} \left( \left[ \left( \frac{\Omega}{\Omega_0} \right)^{\frac{2}{3}} - 1 \right]^3 B'_0 + \left[ \left( \frac{\Omega}{\Omega_0} \right)^{\frac{2}{3}} - 1 \right]^2 \left[ 6 - 4 \left( \frac{\Omega}{\Omega_0} \right)^{\frac{2}{3}} \right] \right), \quad (8.1)$$

where  $E_{BM}(\Omega)$  indicates the total energy that is obtained from the BM equation for the unit cell volume  $\Omega$ ,  $E_0$  is the ground state energy, and  $\Omega_0$  is the equilibrium volume.  $B_0$  and  $B'_0$  are the bulk modulus and its derivative with respect to  $\Omega$ . With  $E_{BM}(\Omega)$  we define the numerical pressure  $P^{(E)}$  as follows

$$P^{(E)}(\Omega) = -\frac{\partial E_{BM}(\Omega)}{\partial \Omega} \quad (8.2)$$

$$= \frac{3B_0}{2} \left[ \left( \frac{\Omega_0}{\Omega} \right)^{\frac{7}{3}} - \left( \frac{\Omega_0}{\Omega} \right)^{\frac{5}{3}} \right] \left\{ 1 + \frac{3}{4} (B'_0 - 4) \left[ \left( \frac{\Omega_0}{\Omega} \right)^{\frac{2}{3}} - 1 \right] \right\} \quad (8.3)$$

and it is later compared with the negative trace of the stress tensor, Eqn. (6.163) or (6.164).

$$P^{(\sigma)} = -\frac{1}{3} \sum_{\alpha} \sigma_{\alpha\alpha} = -\frac{1}{3} (\sigma_{11} + \sigma_{22} + \sigma_{33}). \quad (8.4)$$

The difference between the pressures,  $P^{(E)}$  and  $P^{(\sigma)}$ , calculated by two separate methods will be computed for different materials, and later  $P^{(\sigma)}$  is used to find the equilibrium volume and lattice parameter. Since the pressure is the slope of the energy-volume curve,  $P^{(\sigma)}$  should be zero in equilibrium. However, as will be seen later  $P^{(\sigma)}$  is not

completely zero at the minimum of the total energy, but usually very small indicating the numerical accuracy of the calculation. To obtain the equilibrium volume  $\Omega_0$ , we fit a cubic polynomial,  $P^{(\sigma)} = a\Omega^3 + b\Omega^2 + c\Omega + d$ , using  $P^{(\sigma)}$  obtained from our analytical implementation. The estimated equilibrium volume i.e  $\Omega_0^{(\sigma)}$  and corresponding lattice parameter  $a_0^{(\sigma)}$  will be presented in tables, and will be compared with result obtain using Eqn. (8.2). Moreover, the bulk modulus  $B_0^{(\sigma)}$  is calculated as  $-\frac{P^{(\sigma)}}{d\Omega}$ .

In the APW based methods, the accuracy of the results is controlled by several input parameters which are described in the following points.

- $R_a K_{max}$  where  $R_a$  is the smallest atomic sphere size among the constituent atoms, and  $K_{max}$  is the size of the largest  $\mathbf{K}$  vector of the wave functions in the reciprocal lattice.  $R_a K_{max}$  determines the size of the basis functions in the APW based methods and determines the cutoff energy of the plane waves via  $K_{max} = \sqrt{E_{max}}$ . The value of  $R_a K_{max}$  in the total energy calculation ranges from 7 to 10 depending on the atoms in the system (for elements with f-electrons even a value of 11 may be required). It is unclear, however, how the accuracy of the analytically computed stress tensor would depend on the choice of  $R_a K_{max}$ . One may anticipate that a larger value than for regular total energy calculations might be required, because the energy is variational with respect to small changes in the density according to the Hohenberg-Kohn theorems [22, 23] and thus errors in the density only enter in quadratic order, while there is no corresponding variational principle for the stress tensor so that errors may already manifest themselves in linear order. The validity of this argument is scrutinized in the following figures and tables.
- $l_{max}$ , the cutoff value of the angular momentum expansion in the atomic spheres, see Eqn. (3.1), the cutoff value  $G_{max}$  for the plane wave expansion of the charge density (Eqn. (3.28) ) and the potential (Eqn. (5.62)), and the cutoff value  $L''_{max}$  for the expansion of the non-spherical potential (Eqn. (6.104)) also have a certain impact on the accuracy of the calculation.
- In metallic systems, the size of the k-mesh in the Brillouin zone (BZ), the choice of the smearing method and, if the Fermi-Dirac (FD) method is chosen, the particular value of the corresponding temperature broadening parameter, determine the quality of results.

In the following sections we first present the convergence behavior of the stress tensor for Aluminum and Silicon, as they represent both a simple metal and a semiconductor. The results for these materials are also available in literature[17, 18, 12] for comparison. We later test our implementation on more complex crystal structures with lower symmetry in order to validate the trace of the stress tensor as well as its individual components. In the following calculations the energy difference and the charge distance difference between two self-consistent cycles are  $10^{-5}$  Ry and  $10^{-5}$   $e^-$  unless something else is specified.

## 8.1 Calculations for fcc Aluminum

The total energy and its numerical derivatives ( $P^{(E)}$ ) for different  $R_a K_{max}$  are shown in Figure 8.1(a). The pressure estimated from the negative trace of the stress tensor ( $P^{(\sigma)}$ ) is shown in Figure 8.1(b), and its deviation from the numerical pressure,  $P^{(E)}$

-  $P^{(\sigma)}$ , is shown in Figure 8.1(c). Calculations are done with  $R_a K_{max}$  of 7, 8, 9, and 10.  $R_a$  is the radius of the Al atom and corresponds to 2.5 Bohr. In the following calculations, 1s and 2s states of Al are treated as core states and all other states up to  $l_{max} = 10$  are treated as valence states. All valence states except the 2p states are described using the LAPW basis functions, and the 2p states are described using the semi-core local orbitals (LO). We choose most of the input parameters higher than necessary for a regular total energy calculation in order to exclude possible numerical errors due to these parameters. The charge density and the potential inside an atomic sphere are expanded in terms of symmetrized lattice harmonics. In the lattice harmonics only  $L = '00'$ ,  $'40'$ ,  $'44'$ ,  $'60'$ , and  $'64'$  components are presented. In the interstitial, however, both the charge density and the potential are expanded in symmetrized plane waves and its cutoff value is  $G_{max} = 20 \text{ Ry}^{\frac{1}{2}}$ . The discrete k-mesh with 24 intervals in each direction ( $24 \times 24 \times 24$ ), containing 13824 k-points in the full BZ, is reduced to 413 k-points in the irreducible BZ (IBZ) owing to symmetry. The tetrahedron method with and without Blöchl's correction [36] and a temperature broadening method with different broadening parameters are used for the integration in the IBZ. For the exchange-correlation energy ( $\epsilon_{xc}$ ) and the potential ( $\mu_{xc}$ ), the generalized gradient approximation (GGA) proposed by Perdew, Burke, and Ernzerhof (PBE) [38, 39] is used. All integrations in the interstitial region are evaluated using FFT method. In real space, the integrand is computed at grid points, and we used a FFT grid of  $90 \times 90 \times 90$ . All integrations inside the atomic spheres are evaluated using default 781 points and a logarithmic radial mesh. The marker points in the following figures represent the actual DFT calculations. The curve outside and inside is obtained via extrapolation and interpolation and consequently, the numerical pressure  $P^{(E)}$  estimated at the endpoints, at the smallest and largest volume, is not reliable.

In the following, the results shown in Figure 8.1 and Table 8.1 are calculated using the tetrahedron method with Blöchl's correction [36], and in Figure 8.2 and Table 8.2 without Blöchl's correction. The total energy curves, Figures 8.1(a) and 8.2(a), show that the equilibrium volume and  $P^{(E)}$  are insensitive to  $R_a K_{max}$  although the magnitude of the total energy changes significantly with  $R_a K_{max}$ . As a result, barely a change appears in  $P^{(E)}$ , which can also be seen from the predicted lattice parameter shown in Tables 8.1 and 8.2. However, the  $P^{(\sigma)}$  estimated from the stress tensor shown in Figures 8.1(b) and 8.2(b) clearly shows a  $R_a K_{max}$  dependency. In Tables 8.1 and 8.2 we present the lattice parameter estimated from the total energy ( $a_0^{(E)}$ ) and from the stress tensor ( $a_0^{(\sigma)}$ ) for different  $R_a K_{max}$ , and it can be seen that  $a_0^{(E)}$  is fairly constant within chosen values of  $R_a K_{max}$  but  $a_0^{(\sigma)}$  changes until  $R_a K_{max} = 9$ . Also, Figures 8.1(c) and 8.2(c) and Tables 8.1 and 8.2 show that the difference of  $P^{(\sigma)}$  and  $P^{(E)}$  becomes smaller as  $R_a K_{max}$  becomes larger and converges as  $R_a K_{max}$  reaches 9 or beyond, but a difference of about 3 kbar in pressure and 0.01 Bohr in  $a_0$  remains. The source of this discrepancy will be discussed below.

Table 8.1: Predicted equilibrium volume  $\Omega_0$  (in Bohr<sup>3</sup>) and lattice constant  $a_0$  (in Bohr) from the analytical stress tensor (superscript ( $\sigma$ )) and directly from the total energy (superscript ( $E$ )) as a function of  $R_a K_{max}$  for fcc Al. The standard tetrahedron method with Blöchl's correction is used for k-space integration and all the remaining input parameters are the same as in Figure 8.1.

$R_a K_{max}$	$\Omega_0^{(\sigma)}$	$\Omega_0^{(E)}$	$a_0^{(\sigma)}$	$a_0^{(E)}$
7	110.40	111.27	7.615	7.635
8	110.74	111.27	7.623	7.635
9	110.83	111.26	7.625	7.635
10	110.83	111.26	7.625	7.635

Table 8.2: Same as Table 8.1, but the tetrahedron method without Blöchl's correction.

$R_a K_{max}$	$\Omega_0^{(\sigma)}$	$\Omega_0^{(E)}$	$a_0^{(\sigma)}$	$a_0^{(E)}$
7	110.40	111.26	7.615	7.635
8	110.74	111.27	7.623	7.635
9	110.83	111.26	7.625	7.635
10	110.83	111.25	7.625	7.635

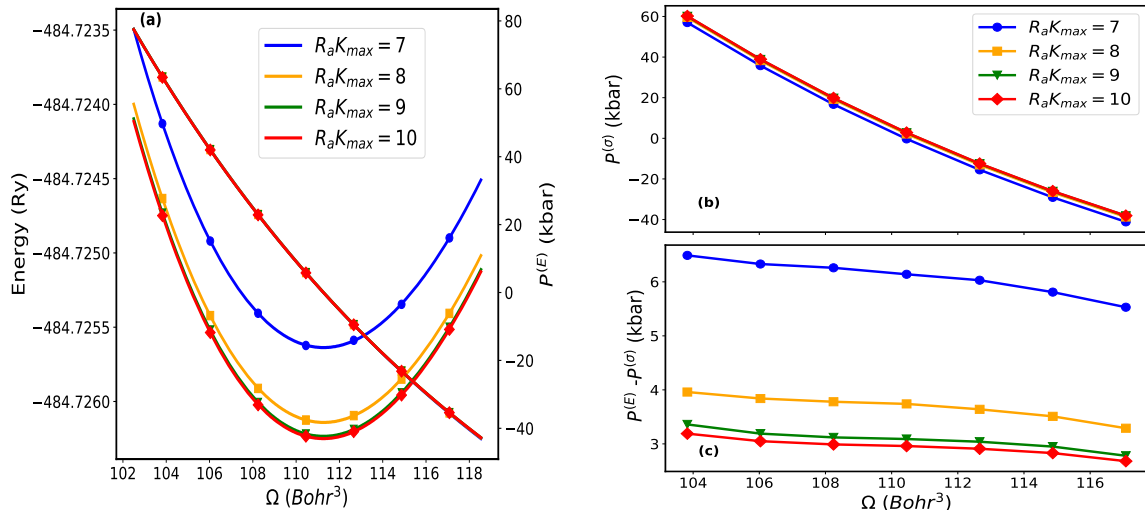


Figure 8.1: (a) Energy-volume curves as well as  $P^{(E)}$ , (b) the negative trace of the full stress tensor  $P^{(\sigma)}$  and, (c) the difference between  $P^{(\sigma)}$  and  $P^{(E)}$  as function of  $\Omega$  for various  $R_a K_{max}$  for fcc Al. The standard tetrahedron method with the Blöchl correction is used for the BZ integration.

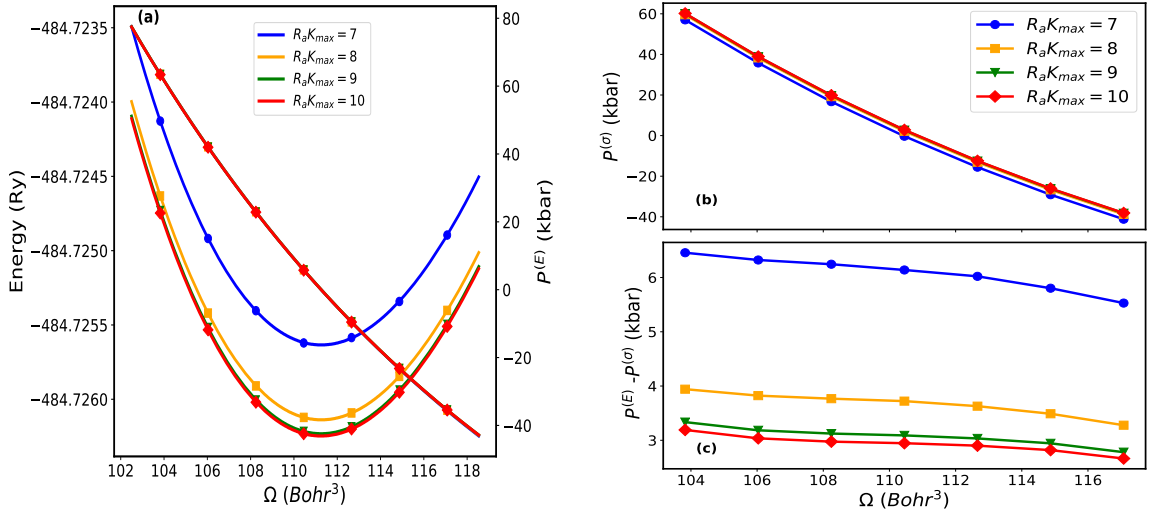
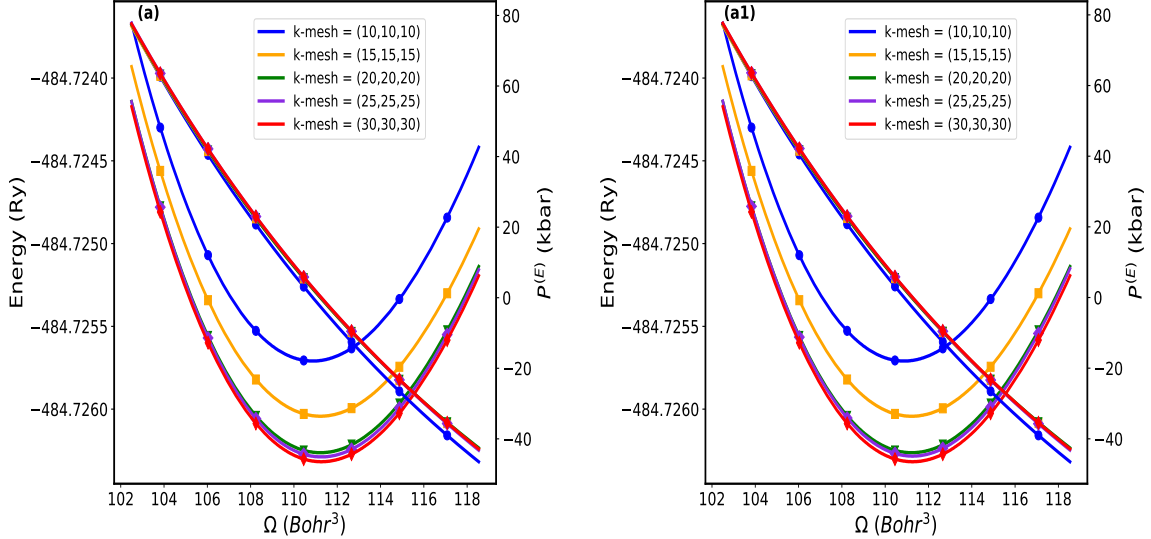


Figure 8.2: Same as Figure 8.1, but with the tetrahedron method without Blöchl's correction.



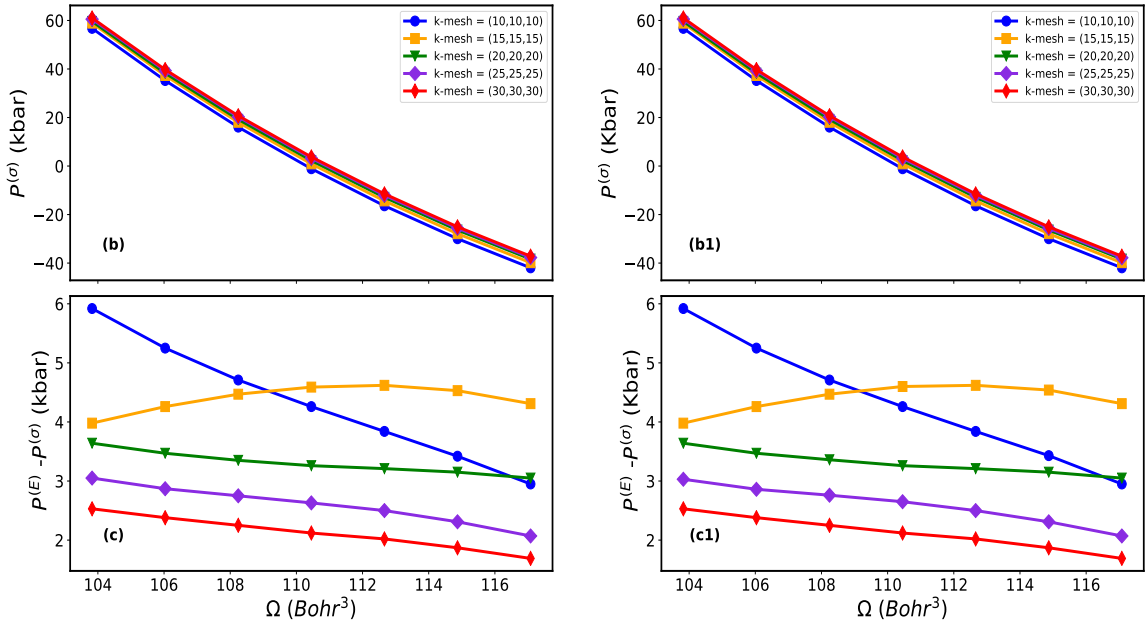


Figure 8.3: Energy-volume curves as well as  $P^{(E)}$  for different k-meshes at  $R_a K_{max} = 10$  for fcc Al. The negative trace of the full stress tensor,  $P^{(\sigma)}$ , and the difference between  $P^{(\sigma)}$  and  $P^{(E)}$  as function of  $\Omega$ . On the left panel, (a), (b), and (c) are the results using the standard tetrahedron method with Blöchl's correction. On the right panel, (a1), (b1), and (c1) are without Blöchl's correction.

Figure 8.3 shows the dependency of the trace of the stress tensor with the k-meshes. The left panel contains the results computed using the standard tetrahedron method with Blöchl's correction, and the right panel shows the results without Blöchl's correction. The figure shows that the result is independent of Blöchl's correction as was also the case for the  $R_a K_{max}$  convergence, see Figures 8.1 and 8.2. Figure 8.3 shows that the largest error ( $P^{(E)} - P^{(\sigma)}$ ) occurred for the k-mesh of  $(10 \times 10 \times 10)$ . This is due to the fact that with such a small k mesh the error is already present in the total energy and thereby in  $P^{(E)}$ . Moreover, in our stress tensor calculation we have assumed that the dependence of the occupation number in strain is of second order and its effect is neglected in stress. As a result, a relatively larger k-mesh must be used than for the total energy, which can also been seen from Figures 8.3(c) and 8.3(c1).

Aluminum is a metallic system with a complicated Fermi surface and has partial occupations close to the Fermi level. As mentioned in the above paragraph the stress tensor formulas assume that the occupancy does not depend on the strain of first-order. The results provided in Tables 8.1 and 8.2 are computed using the tetrahedron method with and without Blöchl's correction. The tables suggest that there is a non-negligible difference between  $P^{(E)}$  and  $P^{(\sigma)}$ , which is already manifested in the second digit after the decimal in the predicted lattice parameter. However, using the FD method to calculate the occupancy improves the results significantly, see Tables 8.3 and 8.4. The reasoning for this could be the argument provided in Appendix B.3. This argument is based on Ref. [48] for force calculations and we assume the same argument holds for stress calculations. As described in Appendix B.3, for a system with partial occupation the total energy provided in Eqn. (4.15) is not variational and needs to be replaced by a more general expression given in Eqn. (B.15). We expect that when calculating the strain variation of the second term of Eqn. (B.15), a similar term will

be canceled while the strain variation of the occupation number is computed. Also when we use Eqn. (B.15) to compute the total energy it is recommended to use the FD method to calculate the occupancy for better convergence and to make the total energy variational.

Table 8.3: Predicted equilibrium volume  $\Omega_0$  (in Bohr<sup>3</sup>) and lattice constant  $a_0$  (in Bohr) from the analytical stress tensor (superscript  $(\sigma)$ ) and directly from the total energy (superscript  $(E)$ ) as a function of  $R_a K_{max}$  for fcc Al. For the BZ integration, the FD method with broadening parameter 0.003 Ry is used. All other input parameters are the same as in Figure 8.4.

$R_a K_{max}$	$\Omega_0^{(\sigma)}$	$\Omega_0^{(E)}$	$a_0^{(\sigma)}$	$a_0^{(E)}$
7	110.62	111.18	7.620	7.633
8	110.97	111.19	7.628	7.633
9	111.05	111.19	7.630	7.633
10	111.06	111.18	7.630	7.633

Table 8.4: Same as Table 8.3 but temperature broadening with broadening parameter 0.005 Ry. All other input parameters are the same as in Figure 8.5.

$R_a K_{max}$	$\Omega_0^{(\sigma)}$	$\Omega_0^{(E)}$	$a_0^{(\sigma)}$	$a_0^{(E)}$
7	110.67	111.20	7.621	7.634
8	111.01	111.21	7.629	7.634
9	111.09	111.20	7.631	7.633
10	111.11	111.19	7.631	7.633

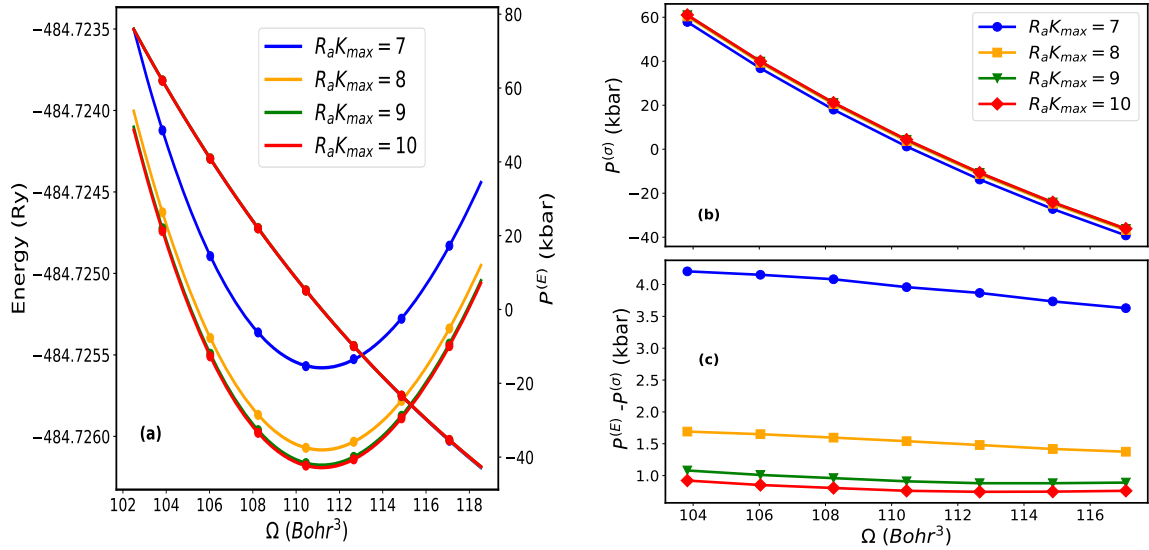


Figure 8.4: (a) Energy-volume curves as well as  $P^{(E)}$ , (b) the negative trace of the full stress tensor  $P^{(\sigma)}$  and, (c) the difference between  $P^{(\sigma)}$  and  $P^{(E)}$  as function of  $\Omega$  for various  $R_aK_{\max}$  for fcc Al. All other input parameters are the same as in Figure 8.1, but the FD method with a broadening parameter of 0.003 Ry is used for the BZ integration.

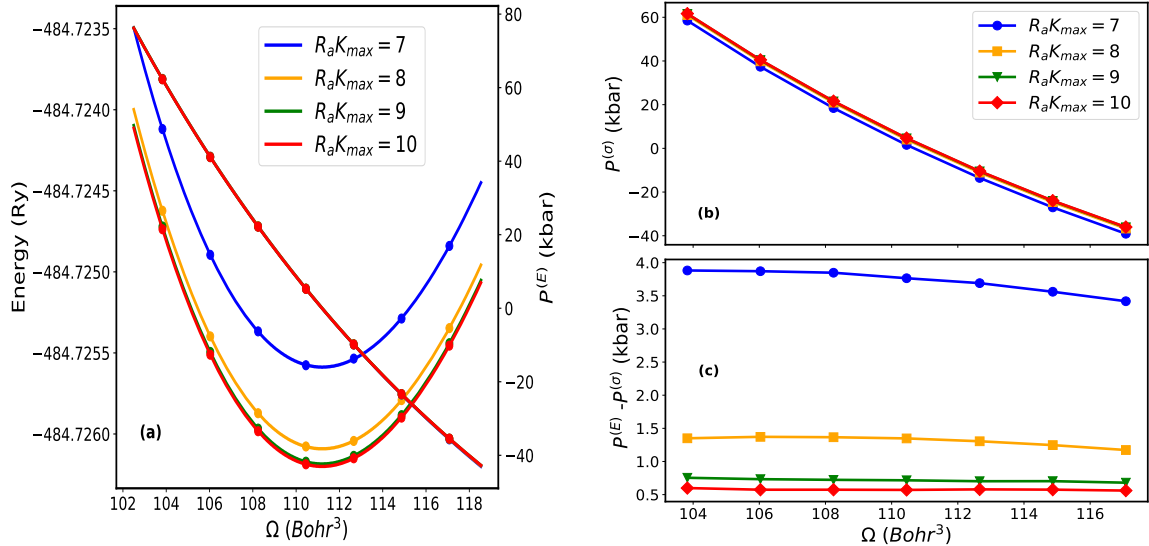


Figure 8.5: Same as Figure 8.3 but the FD method with a broadening parameter 0.005 Ry.

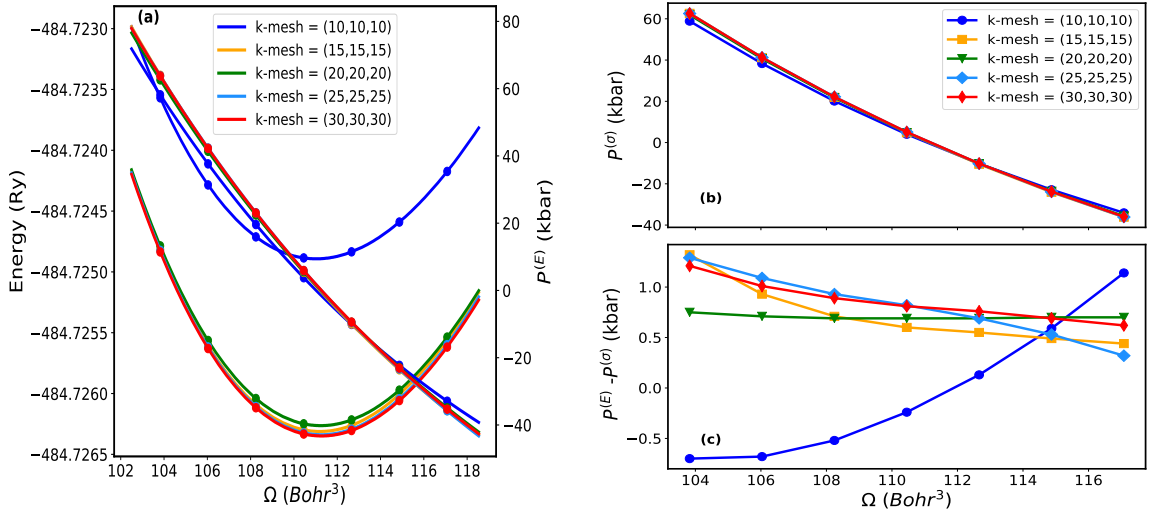


Figure 8.6: **(a)** Energy-volume curves as well as  $P^{(E)}$  for different k-meshes and  $R_a K_{max} = 10$  for fcc Al. **b)** The negative trace of the full stress tensor,  $P^{(\sigma)}$ , and **(c)** the difference between  $P^{(\sigma)}$  and  $P^{(E)}$  as function of  $\Omega$ . The integration in IBZ is carried out using the FD method with a broadening parameter of 0.005 Ry and all remaining input parameters are the same as in Figure 8.3.

In the above figures and tables we can see that the difference  $P^{(E)} - P^{(\sigma)}$  is reduced by an order of magnitude when using the temperature broadening method (the FD method) as compared to the tetrahedron method. We also see that the errors are fairly volume independent provided a sufficient k-mesh has been used. Although in the tetrahedron method errors have a bit larger volume dependency, in the temperature broadening method this dependency lies within the error bar. It also appears when the broadening parameter changes from 0.003 Ry to 0.005 Ry, the predicted lattice parameter changes in the third the decimal place. With the temperature broadening method, it seems that the size of basis set can be small ( $R_a K_{max} = 8$ ). But with the tetrahedron method, even with  $R_a K_{max} = 10$ , the difference in the lattice parameter that is predicted from the total energy and directly from stress remains at the second decimal place. In the case of the FD method, it has been shown that the choice of the k meshes is not so important and the same meshes can be used as for the calculation of the total energy. The deviation of the pressure estimated using the stress tensor from the BM equation is in the same order as in Ref. [17] when the FD method is used. In Ref. [17], 2p states are considered to be core states, sphere size is 1.89 Bohr, and  $R_a K_{max}$  equivalent to  $E_{max} = 30$  Ry is 10.35.

We can see in Eqn. (6.164) that the total stress tensor has many different contributions. Each contribution is further divided into atomic spheres and the interstitial region with the exception of the Madelung stress, the core correction stress, and the valence correction stress. To give an idea about the importance of each contribution, they are tabulated in Table 8.5 and the sum gives the total stress tensor, see the last row of the table. These numbers are getting even much bigger as the system size gets bigger or for heavier elements.

Table 8.5: The  $\sigma_{11}$  component of various stress tensor contributions of Eqn. (6.164) for fcc Al at the unit cell volume— $\Omega = 111.17 \text{ Bohr}^3$ , which is the equilibrium volume according to the total energy calculation. The stress component in the energy unit is given in the Ry column, in the pressure unit in the kbar column, and  $1\text{Ry} = \frac{147105.1641}{\Omega} \text{ kbar}$  with  $\Omega = 111.17 \text{ Bohr}^3$ .

Contributions	Methods & Units		APW+lo+LO		LAPW + LO	
	Ry	kbar	Ry	kbar	Ry	kbar
$\sigma_{11}^{es}$	-310.5584	-410944.90	-310.5580	-410944.37		
$\sigma_{11}^{core}$	239.5641	317002.04	239.5647	317002.83		
$\sigma_{11}^{val,kin}$	83.0015	109831.33	82.9903	109816.51		
$\sigma_{11}^{APW}$	-0.0076	-10.06	0.0	0.0		
$\sigma_{11}^{val,corr}$	0.0127	16.81	0.0138	18.26		
$\sigma_{11}^{xc}$	-12.0124	-15895.35	-12.0112	-15893.76		
Total	-0.0001	-0.13	-0.0004	-0.53		

In Table 8.5,  $\sigma_{11}^{es}$ ,  $\sigma_{11}^{core}$ ,  $\sigma_{11}^{val,kin}$ ,  $\sigma_{11}^{APW}$ ,  $\sigma_{11}^{val,corr}$ , and  $\sigma_{11}^{xc}$  are computed according to Eqs. (6.165a), (6.165b), (6.165c), (6.165d), (6.165e), and (6.165f). The calculation is performed with  $R_a K_{max} = 10$  and all remaining input parameters are the same as in Figure 8.5. The table shows that  $\sigma_{11}^{APW}$  disappears in LAPW+LO as expected. Note that the individual contributions are up to 7 orders of magnitude bigger than the final stress and have to cancel with high precision.

## 8.2 Silicon

In this section we present the results for silicon in the diamond structure. The 1s and 2s states of Si are described as core states, and all other states, 2p, 3s, and 3p, are treated as valence states. The valence states, with the exception of the 2p states, are described using the LAPW basis set. The 2p states, on the other hand, are regarded as the semi-core states and described using the semi-core local orbitals. In the following calculation, we used  $R_a = 2.0 \text{ Bohr}$ ,  $l_{max} = 10$ ,  $L''_{max} = 7$ ,  $G_{max} = 30 \text{ Ry}^{\frac{1}{2}}$ , a FFT grid of  $120 \times 120 \times 120$ . For the  $R_a K_{max}$  convergence test, Figure 8.7, we used 2000 k-points in the whole BZ. However, we will find later that even a reduced k-mesh of 512 k points gives the same result, see Figure 8.9. For the integration over the IBZ, the tetrahedron method is used and the PBE GGA [38, 39] is used to compute  $\epsilon_{xc}$  and  $\mu_{xc}$ .

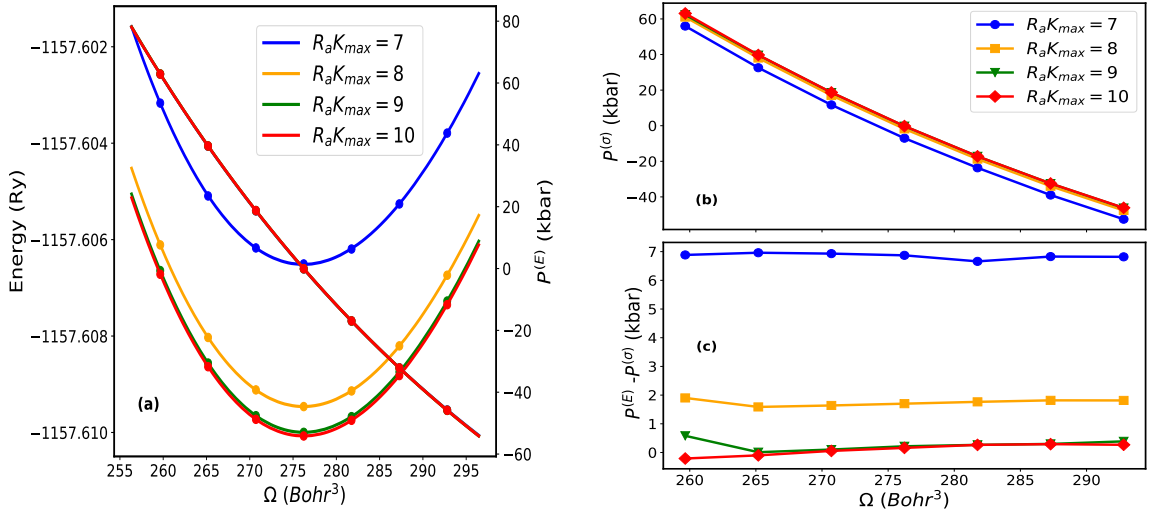


Figure 8.7: (a) Energy-volume curves as well as  $P^{(E)}$ , (b) the negative trace of the full stress tensor  $P^{(\sigma)}$  and, (c) the difference between  $P^{(\sigma)}$  and  $P^{(E)}$  as function of  $\Omega$  for various  $R_aK_{max}$  for Si in the diamond structure.

Table 8.6: Predicted equilibrium volume  $\Omega_0$  (in Bohr<sup>3</sup>) and lattice constant  $a_0$  (in Bohr) from the analytical stress tensor (superscript ( $\sigma$ )) and directly from the total energy (superscript ( $E$ )) as a function of  $R_aK_{max}$  for Si in the diamond structure.

$R_aK_{max}$	$\Omega_0^{(\sigma)}$	$\Omega_0^{(E)}$	$a_0^{(\sigma)}$	$a_0^{(E)}$
7	274.08	276.18	10.311	10.338
8	275.70	276.20	10.332	10.338
9	276.19	276.23	10.338	10.338
10	276.16	276.21	10.337	10.338

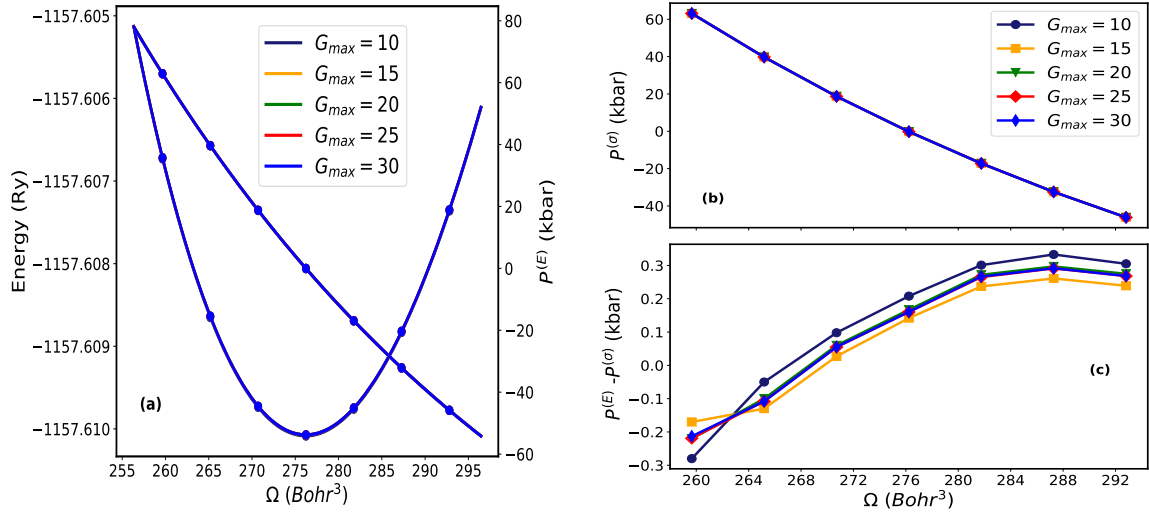


Figure 8.8: (a) Energy-volume curves as well as  $P^{(E)}$  for five different  $G_{max}$  in the expansion of the charge density and the potential for Si in the diamond structure. (b) The negative trace of the full stress tensor  $P^{(\sigma)}$  and (c) the difference between  $P^{(E)}$  and  $P^{(\sigma)}$  as function  $\Omega$ .  $R_a K_{max} = 10$  and all other input parameters are the same as in Figure 8.7.

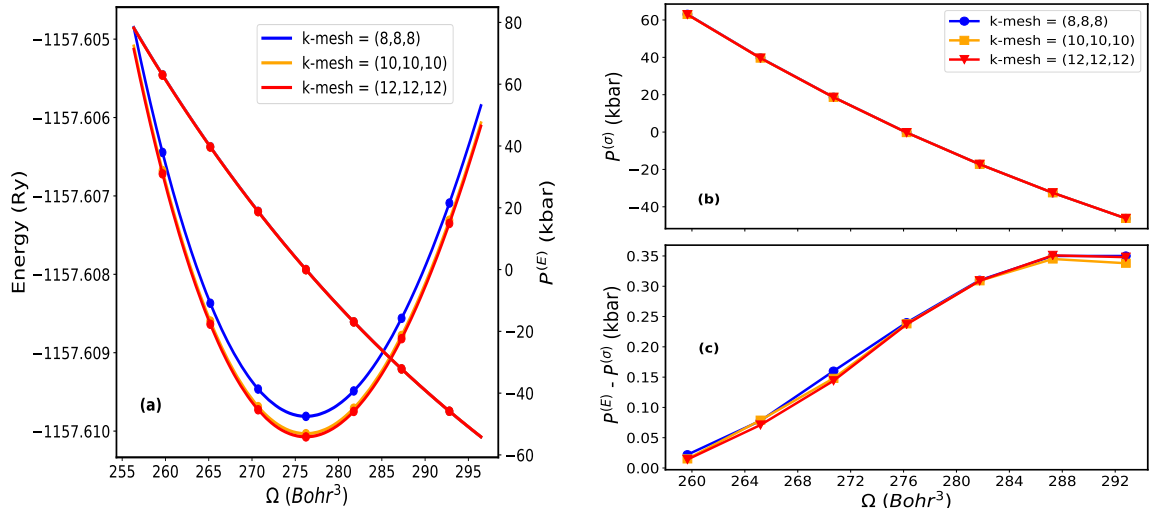


Figure 8.9: (a) Energy-volume curves as well as  $P^{(E)}$  for three different k point meshes for Si in the diamond structure. (b) The negative trace of the full stress tensor  $P^{(\sigma)}$  and (c) the difference between  $P^{(E)}$  and  $P^{(\sigma)}$  as function of  $\Omega$ .  $R_a K_{max} = 10$  and all other input parameters are the same as in Figure 8.7.

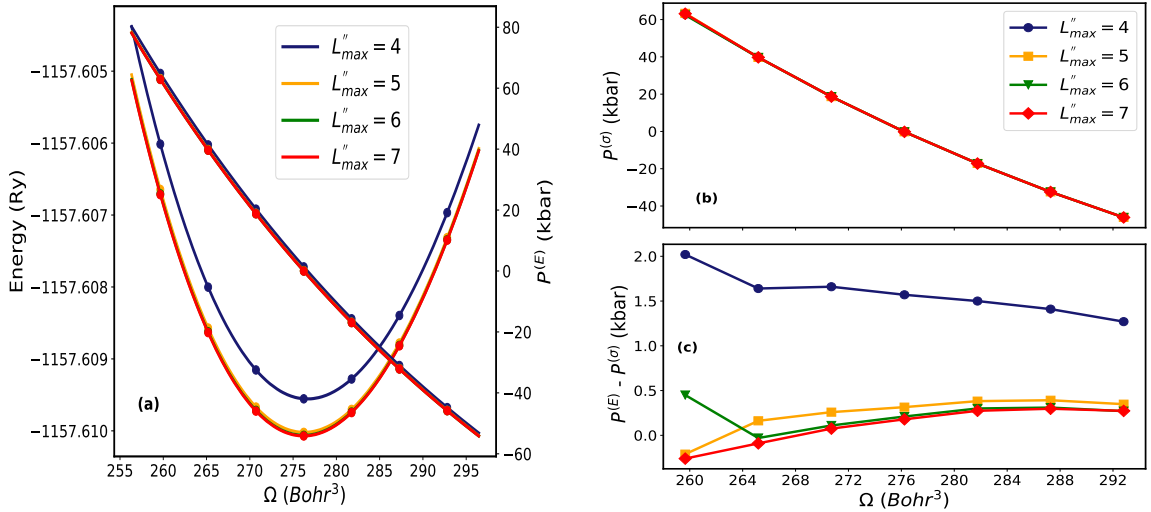


Figure 8.10: (a) Energy-volume curves as well as  $P^{(E)}$  for four different cutoff values of the angular momentum ( $L''_{max}$ ) of the non-spherical potential for Si in the diamond structure. (b) The negative trace of the full stress tensor  $P^{(\sigma)}$  and (c) the difference between  $P^{(E)}$  and  $P^{(\sigma)}$  as function of  $\Omega$ .  $R_a K_{max} = 10$  and all other input parameters are the same as in Figure 8.7.

The energy-volume curve, Figure 8.7 (a), shows that the minimum energy point as well as the slope of the curvature that represents  $P^{(E)}$  are insensitive to  $R_a K_{max}$ . As a result, barely a change appears in the numerical pressure  $P^{(E)}$ , which can also be seen in Table 8.6 via the predicted lattice parameters. However, the pressure  $P^{(\sigma)}$  estimated from the negative trace of the stress tensor for different  $R_a K_{max}$  is shown in Figure 8.7 (b) and it appears that it converges only when  $R_a K_{max} = 8$  or more. The difference between  $P^{(\sigma)}$  and  $P^{(E)}$  shown in Figure 8.7 (c) becomes smaller as  $R_a K_{max}$  becomes larger and does not change when  $R_a K_{max}$  equals 9 or more. A small discrepancy between  $P^{(E)}$  and  $P^{(\sigma)}$  at the smallest and largest volume even after  $R_a K_{max} = 9$  is because  $P^{(E)}$  at the end points are calculated with extrapolated energies. Therefore, if we discard the results for the smallest and largest volume we get a regular behavior of  $P^{(E)} - P^{(\sigma)}$  in the remaining data points. Figure 8.7 (c) together with Table 8.6 suggests that we get a desired accuracy in the predicted lattice parameter from the stress tensor calculation when  $R_a K_{max} = 7.5$  or 8, which is larger than a value normally used in the regular total energy calculation. The requirement of a larger  $R_a K_{max}$  in the stress calculation compared to the total energy calculation was also found in the calculation for Al. The difference  $P^{(\sigma)} - P^{(E)}$  given in Figure 8.7 (c) is in the same order as it is in Ref. [17]. In contrast to our results, their  $P^{(\sigma)} - P^{(E)}$  shows a rather irregular behavior. In Ref. [17], 2p states are considered to be core states. Their sphere size of Si atom is  $1.0 \text{ \AA}^3$ , which corresponds to 1.89 Bohr, which is a bit smaller than our. In our calculations, the energy cutoff ( $E_{max}$ ) of the wave functions for the largest  $R_a K_{max} = 10$  corresponds to 25 Ry, but in Ref. [17]  $E_{max} = 30$ .

The change of  $P^{(\sigma)}$  according to the different values of  $G_{max}$  in the Fourier expansion of the charge density and the potential is shown in Figure 8.8. The figure shows that both  $P^{(E)}$  and  $P^{(\sigma)}$  do not have a significant dependency and their differences ( $P^{(E)} - P^{(\sigma)}$ ) are within an acceptable limit, see Figure 8.8(c), which suggests the same  $G_{max}$  can be used for the stress calculation that is normally used for the total energy calculation. In Figure 8.9, the variations of the stress tensor according to different sizes of k-meshes are

presented, and the figure shows that both  $P^{(\sigma)}$  and  $P^{(E)}$  are independent to the choice of k-meshes. The difference between  $P^{(E)}$  and  $P^{(\sigma)}$  for the different k-meshes shown in Figure 8.9(c) shows that  $P^{(\sigma)}$  agrees with  $P^{(E)}$  very well, and that the same k mesh that is in practice for calculating the total energy can be used for calculating the stress tensor. This outcome we expected prior to calculation because, in semiconducting material like Si, there is a clear distinction between occupied and unoccupied bands. Hence, no ambiguity is presented near the Fermi level; as a result, the BZ integration is insensitive to the k-mesh grid. As we can see in the calculation for Al, however, the dependency of the stress tensor on the k-mesh grid is not negligible, especially when the tetrahedron method is used. The dependence of the stress tensor on  $L''_{max}$ , the cutoff parameter for the non-spherical potential inside the atomic spheres, is shown in Figure 8.10, and the figure shows that a value larger than 4 is sufficient for both  $P^{(\sigma)}$  and  $P^{(E)}$ . In our derivations,  $L''_{max}$  enters indirectly through Kohn-Sham eigenvalue equations and directly via the non-spherical part of the valence correction, see Eqn. (6.145).

## GaAs

In the following calculations, we take GaAs in a zinc blende crystal structure with gallium (Ga) at the corner (0,0,0) and arsenic (As) at the  $(\frac{1}{4}, \frac{1}{4}, \frac{1}{4})$  position. Both Ga and As have a sphere size of 2.21 Bohr. In the case of Ga, all states up to 3p are considered as core states. 3d, 4s, and 4p are considered as valence states and are described using the APW+lo basis set. To provide extra flexibility, we added d LOs. In the case of As, all states up to 3p are considered as core states, the valence states, 3d, 4s and 4p are described using APW+lo, and additional s and d -LOs provide more flexibility. The remaining states for both Ga and As up to  $l = 10$  are described using LAPW. Moreover, other computational parameters are:  $l_{max} = 10$ ,  $G_{max} = 30 \text{ Ry}^{\frac{1}{2}}$ ,  $L''_{max} = 8$ , 2000 k-points in the whole BZ, tetrahedron method for IBZ integration, FFT grid of  $135 \times 135 \times 135$ . The PBE GGA is used to evaluate the exchange correlation energy and potential. In Figure 8.11, the variation of the trace of the stress tensor according to different values of  $R_a K_{max}$  is shown.

Figure 8.11 shows that the estimated result for the pressure from our analytical stress formulas improves as the size of the basis set increases. The intersection of the curves with the horizontal zero pressure line corresponds to the equilibrium volume,  $\Omega_0^{(\sigma)}$  in Table 8.7. The difference in equilibrium volume estimated using the analytical stress formula from the total energy, the vertical lines in Figure 8.11, becomes small as  $R_a K_{max}$  becomes large. Similar to our previous calculations for Si the stress calculations generally require a larger basis set size and thereby a larger value of  $R_a K_{max}$ . In the case of GaAs even larger  $R_a K_{max}$  as compared to silicon is necessary, which is due to the presence of d-states in both Ga and As. From the total energy calculations it is well established that systems with d and f states require in general a larger  $R_a K_{max}$  [30].

We use the results of the stress tensor to evaluate the equilibrium volume  $\Omega_0$  and thus the lattice parameter  $a_0$ . In Table 8.7, we present  $\Omega_0$  and  $a_0$  estimated from the stress tensor (superscript( $\sigma$ )) and directly from the total energy ((superscript( $E$ ))). The deviation of the lattice parameter shown in Table 8.7 is directly related to the pressure difference in Figure 8.11. For example, in Figure 8.11 for  $R_a K_{max} = 8$ , the pressure estimated from the trace of the stress tensor (blue curve) crosses the zero pressure line (horizontal line) earlier than the value predicted from the total energy (blue vertical line). As a result, the lattice parameter already differs in the first place

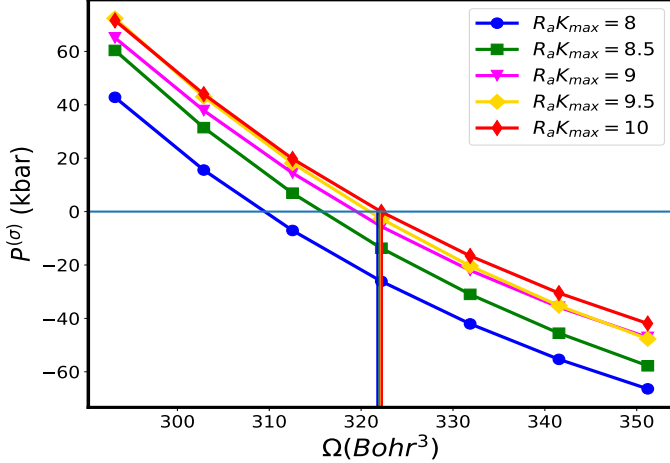


Figure 8.11: Pressure  $P^{(\sigma)}$  estimated from the trace of the full stress tensor for GaAs at different values of  $R_a K_{max}$  as function of  $\Omega$ . The vertical lines represent the equilibrium volume predicted directly from the total energy using the least square fit of BM equation.

after the decimal point, which can be clearly seen in Table 8.7. Later, when  $R_a K_{max}$  increases and reaches 10, the pressure estimated by the stress tensor passes the zero pressure line at almost the same point at which the pressure estimated by the total energy crosses. Consequently, the results shown in Table 8.7 show that the discrepancy in the predicted lattice parameter is only 0.001 Bohr.

Table 8.7: Predicted equilibrium volume  $\Omega_0$  (in Bohr<sup>3</sup>) and lattice constant  $a_0$  (in Bohr) from the analytical stress tensor (superscript  $(\sigma)$ ) and directly from the total energy (superscript  $(E)$ ) as a function of  $R_a K_{max}$  for GaAs. All input parameters are set to the same value as in Figure 8.11.

$R_a K_{max}$	$\Omega_0^{(\sigma)}$	$\Omega_0^{(E)}$	$a_0^{(\sigma)}$	$a_0^{(E)}$
8	309.32	321.77	10.736	10.878
8.5	315.61	322.01	10.808	10.880
9	319.37	322.08	10.851	10.881
9.5	320.82	322.19	10.867	10.882
10	322.18	322.25	10.882	10.883

### 8.3 Tungsten W

In this study, tungsten is considered in a body-centered cubic (bcc) crystal structure. The calculation for W is particularly important because it is a heavy transition metal that contains all of the chemically important atomic orbitals—s, p, d, and f. The calculations in Figure 8.12 were carried out with an atomic sphere of  $R_a = 2.47$  Bohr. All states up to 4d are considered as core states and they are completely confined within the atomic sphere and the remaining states as valence states. Among the valence states 5d, 5f, 6s, and 6p are described with APW+lo functions, whereas 5s, 5p, and

4f are described with the semi-core local orbitals. The remaining valence states up to  $l_{max} = 10$  are described using LAPW. The linearization energies for describing the APW+lo functions,  $E_l^a$  in Eqn.(3.13), are set in the valence region, but for describing semi-core states,  $E_{l,LO}^a$  in Eqn.(3.17) are selected to be in the semi-core region. Figure 8.12 shows the convergence with respect to the different size of the basis set controlled by  $R_a K_{max}$ . The APW+lo basis set size ranges from 73 ( $R_a K_{max} = 7$ ) to 165 ( $R_a K_{max} = 10$ ) and an additional 27 LOs are included. The other computational parameters are:  $G_{max} = 20 \text{ Ry}^{\frac{1}{2}}$ ,  $L''_{max} = 6$ , FFT grid of  $72 \times 72 \times 72$ , radial mesh contains 781 points, and k-mesh ( $21 \times 21 \times 21$ ). The FD method with a broadening parameter of 0.005 Ry is used for the integration in k-space. The exchange-correlation energy and potential are calculated using the PBE GGA approximation[38, 39]. Moreover, we repeat the calculation as in Figure 8.12 with the exception that the k space integration is performed using the standard tetrahedron method with Blöchl's correction, and the results are presented in Figure 8.13. Contrary to Al, the difference in the results between the tetrahedron and FD method is rather small, see Table 8.8. However, the FD method still provides a bit better agreement with the numerical results  $P^{(E)}$ , Figures 8.12 and 8.13.

Table 8.8: Lattice parameters  $a_0^{(E)}$  and  $a_0^{(\sigma)}$  (in units of Bohr) of bcc W as predicted from total energy and the analytical stress formalism, respectively, for four different values of  $R_a K_{max}$  and using the Fermi-Dirac (FD) and tetrahedron (Tetra) method.

$R_a K_{max}$	$a_0^{(\sigma)}(\text{FD})$	$a_0^{(E)}(\text{FD})$	$a_0^{(\sigma)}(\text{Tetra})$	$a_0^{(E)}(\text{Tetra})$
7	6.162	6.136	6.164	6.135
8	6.145	6.139	6.146	6.140
9	6.142	6.143	6.144	6.143
10	6.143	6.143	6.145	6.144

We extend our study to examine the dependence of the stress on the k-mesh with both the tetrahedron or FD smearing methods, Figure 8.14. Figure 8.14(b) shows that the calculated stress tensor with the FD method does not show any significant dependence on k points compared to the tetrahedron method. In the FD method, the difference of  $P^{(E)} - P^{(\sigma)}$  between the k-meshes ( $12 \times 12 \times 12$ ) and ( $21 \times 21 \times 21$ ) is within the error limit. In the case of the tetrahedron method this difference is a bit larger, but still has an effect only in the third decimal place (  $a_0 = 6.147$  Bohr ( $21 \times 21 \times 21$ ) and  $a_0 = 6.145$  Bohr ( $21 \times 21 \times 21$ ) ) in the predicted lattice parameter. It is also apparent that  $P^{(E)} - P^{(\sigma)}$  has a larger error and volume dependency in the tetrahedron method compared to the FD method.

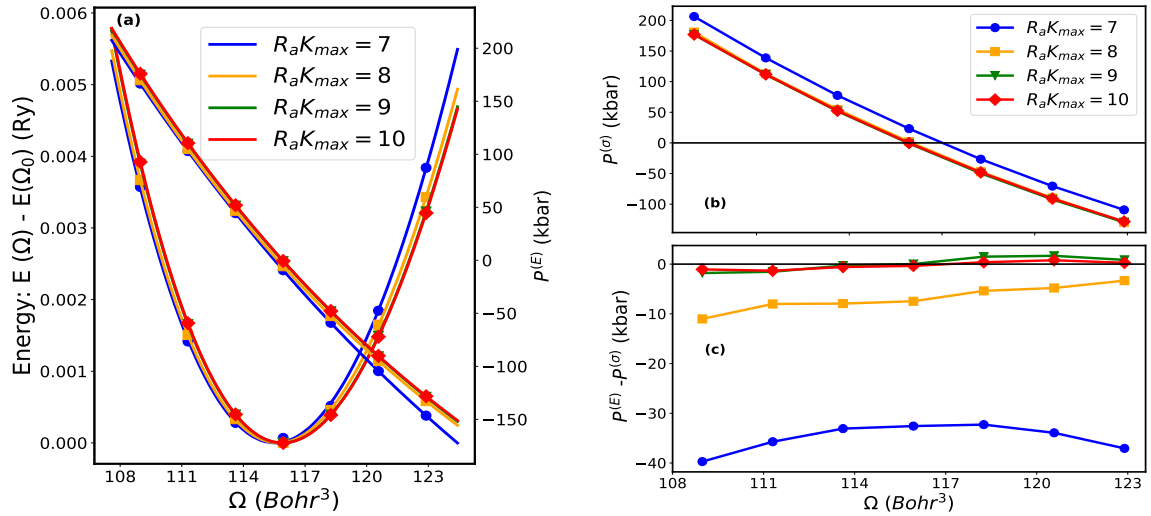


Figure 8.12: (a) Energy-volume curves as well as  $P^{(E)} = -\frac{dE(\Omega)}{d\Omega}$ , (b) the negative trace of the full stress tensor  $P^{(\sigma)}$ , and (c) the difference between  $P^{(\sigma)}$  and  $P^{(E)}$  for various  $R_aK_{max}$  as function of the unit cell volumes ( $\Omega$ ) for bcc W. Temperature broadening method with a broadening parameter of 0.005 Ry is used for the BZ integration

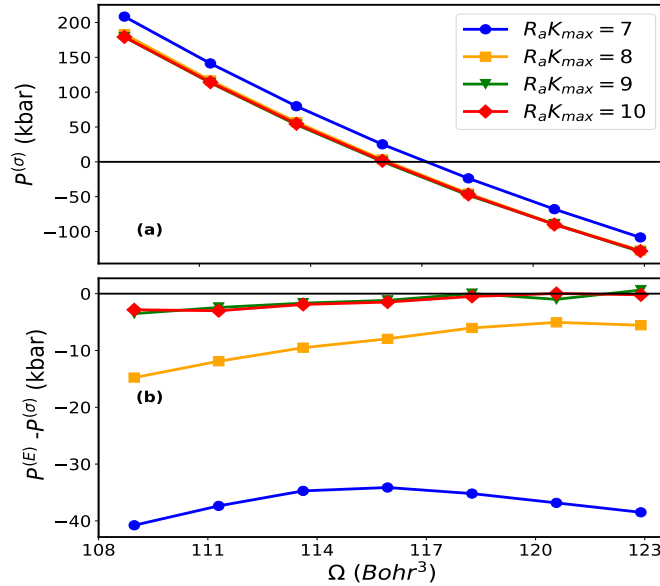


Figure 8.13: (a) The negative trace of the full stress tensor  $P^{(\sigma)}$  and (b) the difference of  $P^{(\sigma)}$  from  $P^{(E)}$  for different  $R_aK_{max}$  as function of  $\Omega$  for bcc W. The standard tetrahedron method with Blöchl's correction is used for the BZ integration and all other input parameters are the same as in Figure

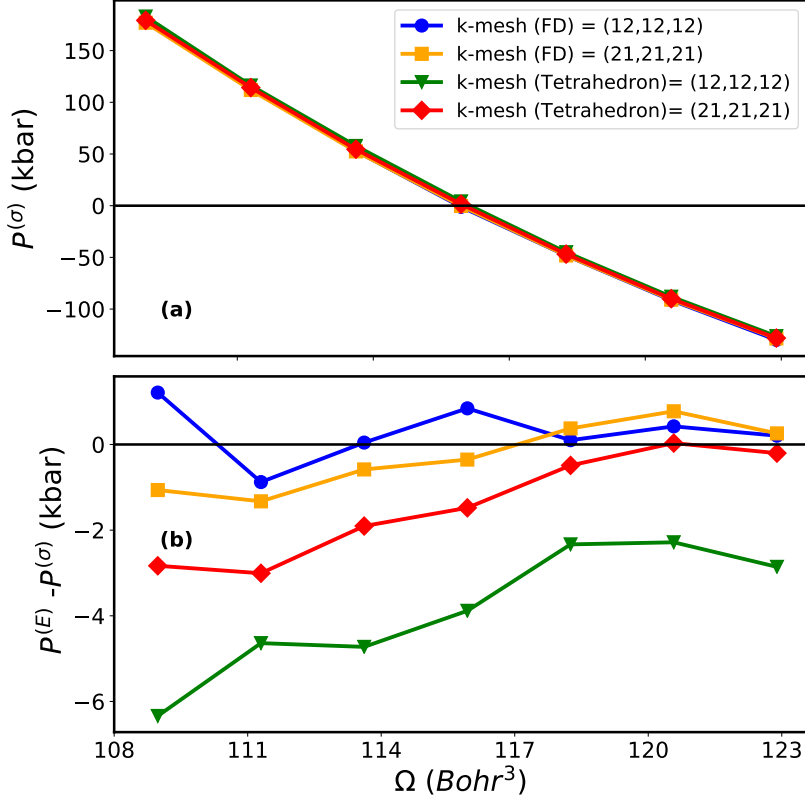


Figure 8.14: (a) The negative trace of the full stress tensor  $P^{(\sigma)}$  and (b) the deviation of  $P^{(\sigma)}$  from  $P^{(E)}$  for two different k-meshes as function of  $\Omega$  for bcc W. The standard tetrahedron method with Blöchl's correction and Fermi-Dirac (FD) smearing method are used.  $R_a K_{max} = 10$  and all other input parameters are the same as in Figure 8.12.

In section 6.3.1 we discussed the origin of the surface term  $S$  in Eqn. (6.74) when the APW method is used i.e  $\sigma_{\alpha\beta}^{APW}$  in Eqn. (6.82). In Figure 8.15 result with and without this surface term is shown. In the figure, the red and blue curves represent the negative trace of the full stress tensor with and without  $\sigma_{\alpha\beta}^{APW}$ . The horizontal green line represents the zero pressure line and the intersection of the red and blue curves with the green line corresponds to the equilibrium volume and its value directly from the total energy is represented by a vertical orange line. The equilibrium lattice parameter from the total energy is 6.143 Bohr and the predicted values by the stress tensor with and without  $\sigma_{\alpha\beta}^{APW}$  are 6.143 Bohr (red curve) and 6.174 Bohr (blue curve), respectively. This implies that without inclusion of  $\sigma_{\alpha\beta}^{APW}$  in the full stress tensor, the predicted equilibrium structure is very wrong. Moreover, in Table 8.9 the numerical value of  $\sigma_{\alpha\beta}^{APW}$  calculated at the equilibrium volume  $\Omega = 115.94 \text{ Bohr}^3$  for the APW+lo and LAPW methods is provided, and its value is practically zero in LAPW. This result is expected because in LAPW both the value and the slope of the basis functions are continuous. Consequently Eqs. (6.74) and (6.82) should vanish within numerical precision. With the APW+lo method, however, only the value of the basis functions is matched at the sphere boundary and there is no restriction with regard to the slope, which eventually requires to compute  $\sigma_{\alpha\beta}^{APW}$ .

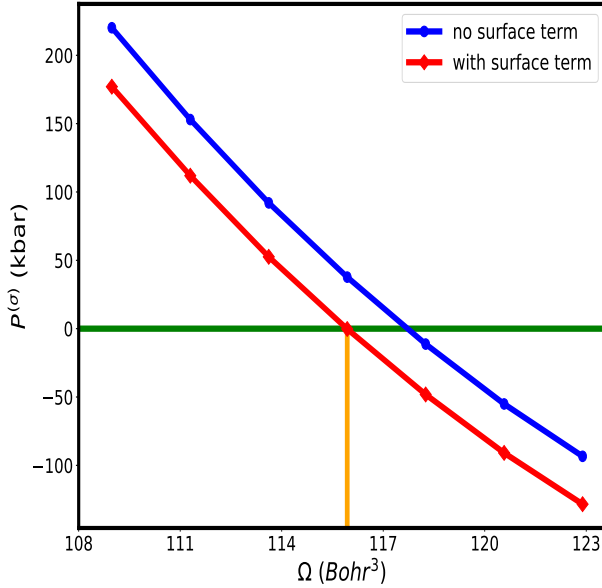


Figure 8.15: The trace of the full stress tensor with (red curve) and without (blue curve) the inclusion of APW surface term, Eqn. (6.82), as function of  $\Omega$ . The vertical orange line corresponds to the equilibrium lattice predicted directly from the total energy calculation.  $R_a K_{max} = 10$  and all the remaining input parameters are the same as in Figure 8.12.

Table 8.9:  $\sigma_{\alpha\beta}^{APW}$  (in kbar) as given in Eqn. (6.82) for  $\alpha=\beta=1$  for bcc W at the equilibrium according to the APW+lo and LAPW methods. LOs are added in the both method.  $R_a K_{max} = 10$  and all input parameters are the same as in Figure 8.12.

stress	APW+lo	LAPW
$\sigma_{11}^{APW}$	-37.96	0.0

Figure 8.16 shows the convergence of the stress tensor ( $\sigma_{11}$ ) as function of  $R_a K_{max}$  at the equilibrium volume for three different calculations: with APW+lo, LAPW with 4f electrons as valence electrons ('LAPW with 4f as valence electron' in figure legend) and LAPW with 4f electrons as core electrons ('LAPW with 4f as core electron' in figure legend). It is evident from the figure that the APW+lo stress converges much faster than in two different cases in LAPW. With APW+lo,  $R_a K_{max}=8$  already gives an acceptable result whereas  $R_a K_{max}=10$  or higher is required for the same accuracy in LAPW. The 4f wave functions in W are highly localized, and such electrons are much better described by APW+lo radial functions[27]. This can also be seen in Figure 8.16. The improvement in the LAPW calculation with 4f electrons in the core also suggests that the 4f electrons are very difficult to describe by the LAPW basis functions. The convergence of  $\sigma_{11}$  in Figure 8.16 correlates with the convergence of  $a_0$  in Figure 8.17, where  $a_0$  calculated directly from the total energy are black (APW) and orange (LAPW) dashed line and from the stress tensor are the red, green, and blue

curves. It can be seen that  $a_0$  versus  $R_a K_{max}$  in Figure 8.17 follows almost exactly the same behavior as  $\sigma_{11}$  versus  $R_a K_{max}$  in Figure 8.16.

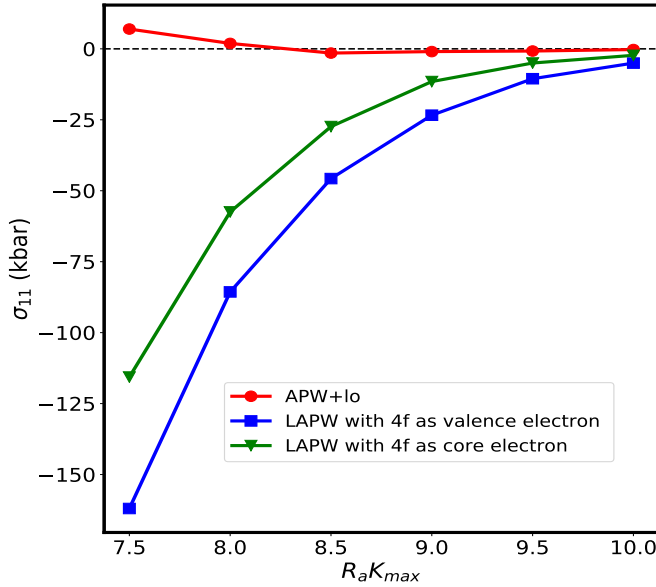


Figure 8.16: Convergence of  $\sigma_{11}$  according to different  $R_a K_{max}$  for the APW+lo and LAPW methods at the equilibrium volume for bcc W. For LAPW two different cases—4f electrons as valence or core—are considered. All other input parameters are the same as in Figure 8.12.

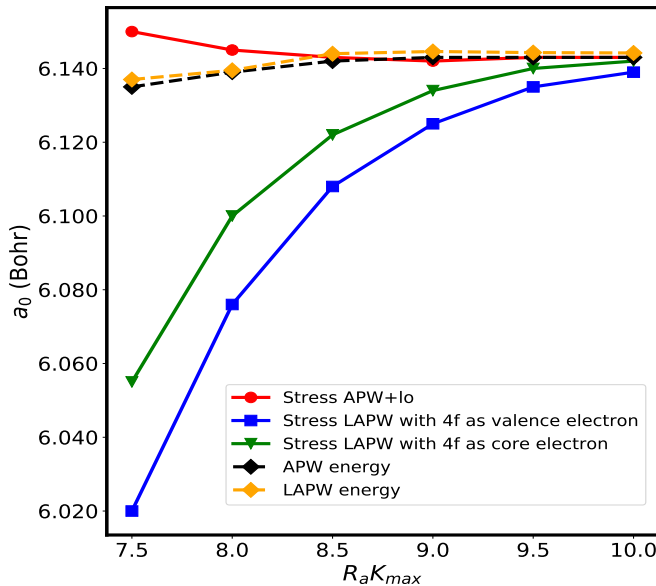


Figure 8.17: Comparison of the predicted lattice parameters from the stress tensor calculation and directly from the total energy for six different values of  $R_a K_{max}$  in the APW+lo and LAPW methods for bcc W. All other conditions are the same as Figure 8.16.

Furthermore,  $P^{(E)}$  and  $P^{(\sigma)}$  calculated with the LDA and GGA are shown in Fig. 8.18(a) and (b), respectively. The difference between  $P^{(E)}$  and  $P^{(\sigma)}$  is shown in Fig. (8.18)(c) and is just 1-2 kbar. It is smaller for GGA and slightly larger for LDA. However, the predicted lattice parameter with the LDA  $a_0^{(\sigma)}(LDA) = a_0^{(E)}(LDA)$  and GGA  $a_0^{(\sigma)}(GGA) = a_0^{(E)}(GGA)$  are the same as the results of the total energy calculations.

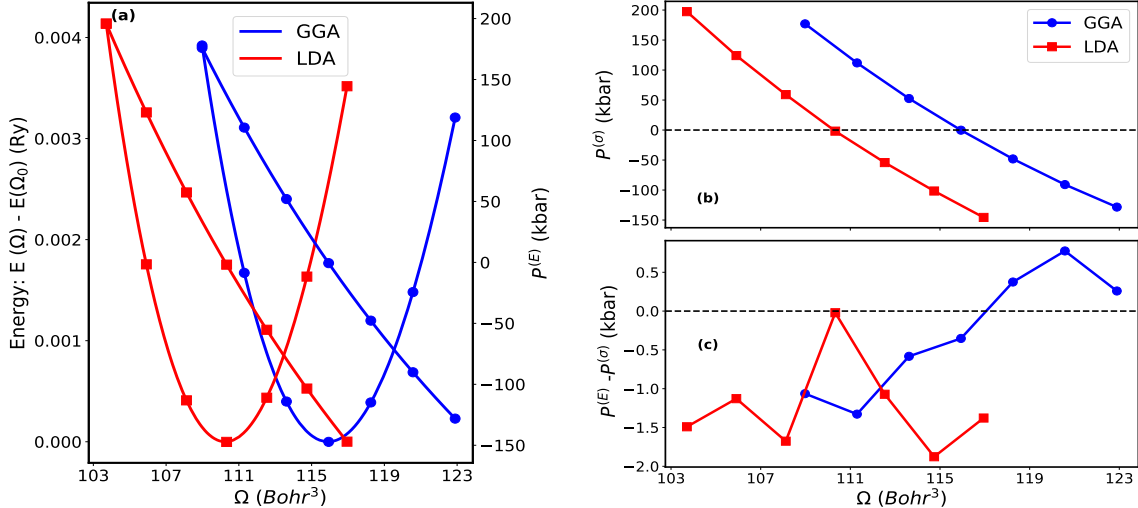


Figure 8.18: (a) Energy-volume curves as well as  $P^{(E)}$ , (b) the negative trace of the full stress tensor  $P^{(\sigma)}$ , and (c) the difference between  $P^{(\sigma)}$  and  $P^{(E)}$  for the LDA and GGA as function  $\Omega$  for bcc W.  $R_a K_{max} = 10$  and all other input parameter are the same as in Fig. 8.12 (a)-(c).

## 8.4 Low symmetry crystal structures

In this section we present results for ZnO in a hexagonal crystal structure and rutile TiO<sub>2</sub> in a tetragonal crystal structure. These calculations are important not only to check the accuracy of the trace of the stress tensor, but also of the individual elements in the diagonal. Because of two lattice parameters,  $a$  and  $c$ , the structure optimization becomes a two dimensional problem—at each volume the ratio  $\frac{c}{a}$  needs to be optimized too. If we use the traditional total energy method to calculate the numerical derivative, we need at least  $5 \times 5$  (5 different volume and 5 different  $\frac{c}{a}$ ) total energy calculation in a case when we already have a good estimate of the theoretical lattice parameters. However, in the stress calculation we perform a single DFT calculation and get the 2 components  $\sigma_{11}$  and  $\sigma_{33}$  of the stress tensor. Now the further steps would be to change the lattice parameters in such a way that we increase or decrease their values according to the positive and negative stress components. Usually a few calculations are sufficient to achieve the equilibrium configuration. The diagonal elements will be zero if both the  $\frac{c}{a}$  and the unit cell volume correspond to the minimum energy at the same time.

### 8.4.1 ZnO

In this section we present the results for ZnO in the hexagonal wurtzite structure with space group mp-2133. In this structure there are 2 Zinc and 2 Oxygen atoms per unit

cell. The positions of Zn and O in the unit cell are at (1/3,2/3,0) and (1/3,2/3,0.382), respectively. The calculations are carried out using the following input criteria:

- The sphere size of Zn and O are 1.95 Bohr and 1.68 Bohr, respectively.
- The states up to 3s in Zn and 1s in O are considered as core states. In Zn, the 3p states are regarded as semi core states and described using local orbital (LO), the valence states 3d, 4s and 4p are described using the APW+lo basis set. In the case of O, the valence 2s and 2p states are described with APW+lo and an additional LO is used to enrich the 2s basis set. All remaining valence states of both Zn and O up to  $l_{max} = 10$  are described by LAPW.
- The  $R_a K_{max}$  value is 8.5 for the oxygen atoms and the effective  $R_a K_{max}$  for Zn is 9.86. The effective  $R_a K_{max}$  for Zn is calculated as  $\frac{R_a^O K_{max}}{R_a^O} * R_a^{Zn}$ .  $R_a^O$  and  $R_a^{Zn}$  correspond to the size of the atomic sphere of oxygen and Zinc.
- The k point grid for the BZ integration is  $8 \times 8 \times 4$ .
- $G_{max} = 20 \text{ Ry}^{\frac{1}{2}}$ ,  $L''_{max} = 6$ ,  $\epsilon_{xc}$  and  $\mu_{xc}$  are calculated using the GGA, and a FFT grid of  $72 \times 72 \times 120$  is used.

We first start a calculation using the experimental lattice parameters  $a_1 = 6.142$  Bohr and  $c_1 = 9.838$  Bohr. The calculated stress tensor from our WIEN2k implementation looks like as given below.

$$\sigma_{\alpha,\beta} = \begin{pmatrix} 57.93 & 0.00 & 0.00 \\ 0.00 & 57.93 & 0.00 \\ 0.00 & 0.00 & 66.29 \end{pmatrix} \quad (8.5)$$

The stress components are shown in kbar and big positive values of the stress tensor indicate that the lattice parameters need to be increased. In the next step we change  $a_1$  and  $c_1$  in such a way that all components of the stress tensor should become smaller. But if we mistakenly increase the lattice parameters too much ( $a_2 = 6.309$  and  $c_2 = 10.182$  Bohr), the stress tensor looks like as follows.

$$\sigma_{\alpha,\beta} = \begin{pmatrix} -53.19 & 0.00 & 0.00 \\ 0.00 & -53.19 & 0.00 \\ 0.00 & 0.00 & -53.86 \end{pmatrix} \quad (8.6)$$

The calculated stress shows that the selected lattice parameters are larger than their value in the equilibrium configuration. Now, we know that our equilibrium lattice parameters can be found between the above two choices i.e the  $a$  and  $c$  of the equilibrium geometry would be larger than  $a_1$  and  $c_1$ , but smaller than  $a_2$  and  $c_2$ . Again we perform another calculation with lattice parameters  $a_0 = 6.227$  Bohr and  $c_0 = 10.026$  Bohr, and the stress tensor now looks like as follows.

$$\sigma_{\alpha,\beta} = \begin{pmatrix} -5.20 & 0.00 & 0.00 \\ 0.00 & -5.20 & 0.00 \\ 0.00 & 0.00 & -4.46 \end{pmatrix} \equiv \begin{pmatrix} -0.000035 & 0.000000 & 0.000000 \\ 0.000000 & -0.000035 & 0.000000 \\ 0.000000 & 0.000000 & -0.000030 \end{pmatrix} \quad (8.7)$$

Here the numbers in the first and second matrix are in kbar and  $\frac{\text{Ry}}{\text{Bohr}^3}$  units, respectively. With this  $a_0$  and  $c_0$ , both  $\frac{c}{a}$  and the unit cell volume correspond closely to

the minimum energy. In principle, the diagonal components should be zero at this point. However, a small non-zero value of  $P^{(E)} - P^{(\sigma)}$  in the calculations for Al, Si, and W suggests that a small non zero value in the above calculation is tolerable. It was found that a 5 kbar difference is not important in order to have the correct lattice parameters up to  $\pm 0.001$  Bohr, see Table 8.10. However, this is not always the case, for example in softer materials (Al) we have seen that a 3 kbar difference between  $P^{(E)}$  and  $P^{(\sigma)}$  affects the predicted lattice parameter from the stress tensor and the total energy already in the second place after the decimal point.

Table 8.10: Comparison of the equilibrium lattice parameters (in Bohr),  $a_0$  and  $c_0$ , of ZnO obtained from the fifth order polynomial fit to the total energy (labeled 'energy') and directly from the stress tensor formalism with and without inclusion of the non-spherical components ( $l=2$ ) in the potential when the core correction, Eqn. (6.48), is calculated.  $V_{tot}^c$  represents the sum of the both spherical potential  $V_{00}^c$  and non-spherical potential  $V_{2m}^c$ .

	$a_0$	$c_0$
energy	6.229	10.022
stress with $V_{tot}^c$	6.228	10.022
stress with $V_{00}^c$	6.195	10.129

In the total energy calculation, both the core charge density and the potential are considered to be spherically symmetric and only the  $lm=00$  term in a lattice harmonic expansion contributes when the core states are calculated. On the other hand, in our stress tensor formalism when calculating the core correction Eqn. (6.48), the potential  $V_{lm}$  can have non-spherical components, which are described by higher angular momentum quantum numbers. However, we already described in section 6.2 that due to the presence of Gaunt number  $G_{l,1,1}^{-m,t,t'}$  and Kronecker deltas  $\delta_{1,l+s}\delta_{-t',m+t}$ , only  $lm = 00$  and  $2m$  components of the potential are allowed to contribute to  $\sigma_{\alpha\beta}^{core}$ . The term with  $lm=00$  is the main contribution and the  $lm=2m$  component acts as an additional correction, which does not always exist and the trace of this term is zero because  $\sigma_{11}+\sigma_{22} = -\sigma_{33}$ . In high (cubic) symmetry crystal structures there are no  $lm=2m$  terms in a lattice harmonic expansion, but in lower symmetry crystal structures, for example, a hexagonal system, these contributions can become quite significant and neglecting this term would lead to significant errors in the predicted lattice parameters  $a_0$  and  $c_0$ , which can be verified by comparing the second and third row of Table 8.10. In the table,  $V_{tot}^c = V_{00}^c + V_{2m}^c$ . This observations is similar to what is found for the core correction of the force calculation, where a  $l=1$  contribution appears when the core contribution of the force is calculated. In contrary to our observation, the authors in Ref. [12] assumed that the charge density and the potential in the core correction are spherically symmetric i.e only  $V_{00}^c$  is considered.

### 8.4.2 Rutile TiO<sub>2</sub>

In rutile TiO<sub>2</sub> with space group  $P4_2/mnm$ , equivalent atoms are linked by complicated symmetry operations. Therefore the calculation of the stress tensor for this compound is very important to check whether the symmetry between the equivalent atoms is

being addressed correctly or not. The TiO<sub>2</sub> structure has 6 atoms (2 Ti and 4 O) with Ti at (0,0,0) and O at (0.305,0.305,0) in the unit cell. The calculations are carried out in the following setting:

- 1s, 2s and 2p states of Ti and 1s state of O are considered as core states. In Ti, the valence states 3d and 4s are described using the APW+lo basis functions, and the (3s,3p) states are described via semi core local orbitals. In oxygen, the valence states 2s and 2p are described using APW+lo. For both Ti and O, all the remaining states up to  $l = 10$  are described with LAPW.
- The atomic sphere sizes of Ti and O are 1.66 Bohr and O 1.49 Bohr, respectively.
- The calculations are performed with  $R_a K_{max} = 8.5$  and therefore the effective  $R_a K_{max}$  for Ti is 9.5.
- The k points grids for Brillouin zone integration is  $6 \times 6 \times 10$ ,  $G_{max}$  is  $20 \text{ Ry}^{\frac{1}{2}}$ ,  $L''_{max}$  is 6, a FFT grid is  $108 \times 108 \times 60$  and the exchange correlation energy and potential are calculated using the PBE GGA.

As we have described in the case of ZnO, we first take the experimental or theoretically given lattice parameter, perform the DFT calculations and get the stress tensor. With this information we change the lattice parameters until we get both individual components and the trace of the stress tensor as close as possible to zero. The lattice parameters predicted in this way are compared in Table 8.11 with those obtained directly from the total energy calculations. The table suggests that the difference in the predicted  $a_0$  and  $c_0$  from the stress tensor and total energy is within the acceptable limit. The result also verifies that the complicated symmetry operations between the equivalent atoms are implemented correctly.

Table 8.11: Comparison of the equilibrium lattice parameters (Bohr),  $a_0$  and  $c_0$ , obtained from the fifth order polynomial fit to the total energy (labeled 'energy') and directly from the stress tensor formalism.

	$a_0$	$c_0$
energy	8.805	5.611
stress	8.798	5.622

## 8.5 Lattice parameters

Here we present the lattice parameter and the bulk modulus for various elements and compounds. The calculations are done using LAPW basis functions and the LDA.

Table 8.12: Comparison of the equilibrium lattice parameter  $a_0$  (in Bohr) and the bulk modulus (in kbar) obtained from the total energy (E) and directly from the stress tensor ( $\sigma$ ) formalism for different elements.

elements	$a_0^{(\sigma)}$	$B^{(\sigma)}$	$a_0^{(E)}$	$B^{(E)}$
NaCl	10.331	324.38	10.334	323.10
MgS	10.590	620.93	10.578	616.32
LaN	9.880	1208.66	9.894	1225.79
TiN	7.900	3182.49	7.904	3192.26
NbC	8.395	3254.35	8.398	3264.59
AlAs	10.654	768.33	10.659	762.66
SrTiO <sub>3</sub>	7.295	2003.53	7.295	2006.81

## 8.6 Accuracy of individual component

So far we have validated the trace of the stress tensor as well as the individual diagonal compounds at zero strain in terms of the lattice parameters. To validate the accuracy of the individual components of the stress tensor at finite strain, our strategy is to extract them from total energy calculations of various strained systems and compare these values with those obtained from our analytical stress. In the following we take a cubic silicon in the diamond structure at the equilibrium volume (pressure = 0 and  $a_0 = 10.209$  with the LDA) and keep the lattice parameters  $a_0$  and  $b_0 = a_0 = 10.209$  fixed while varying the  $c$  lattice parameter. Using a family of such tetragonal but non-volume conserving deformations, the stress component  $\sigma_{33}$  (denoted as  $\sigma_{33}^{(E)}$  in Table 8.13) is calculated numerically by fitting total energies with a fourth order polynomial as function of strain  $\epsilon_{33} = \frac{c}{c_0} - 1$ , and  $\epsilon_{33} = 0$  and  $c_0$  corresponds to the equilibrium state at zero hydrostatic pressure. Now it is easy to see that the identity

$$\sigma_{33} = \frac{1}{\Omega_0} \frac{\partial E(\epsilon_{33})}{\partial \epsilon_{33}}, \quad (8.8)$$

holds. Therefore, differentiating the above fourth order polynomial fit, we readily obtain the stress values  $\sigma_{33}^{(E)}$  recorded in Table 8.13. On the other hand, a stress component  $\sigma_{33} \equiv \sigma_{33}^{(\sigma)}$  can be calculated directly from Eqn. (6.163).

The input settings for these calculation were:  $R_a K_{max} = 9.0$ ,  $G_{max} = 20$  Ry $^{\frac{1}{2}}$ , k-mesh =  $(12 \times 12 \times 12)$ , and  $c$  is calculated as  $c = (1 + \epsilon_{33})c_0$ . A comparison of  $\sigma_{33}^{(E)}$  and  $\sigma_{33}^{(\sigma)}$  in Table 8.13 suggests that the calculated stress is also okay for non-hydrostatic conditions. The table shows a small discrepancy between  $\sigma_{33}^{(\sigma)}$  and  $\sigma_{33}^{(E)}$ , but similar calculations for different materials show that these numerical differences are within acceptable limits.

Table 8.13: Comparison of  $\sigma_{33}$  (in kbar) calculated using Eqs. (8.8) and (6.163) for silicon in the diamond structure with seven different non-volume conserving tetragonal deformations. The superscripts  $(E)$  and  $(\sigma)$  correspond to the energy and stress.

$\epsilon_{33}$	$\sigma_{33}^{(E)}$	$\sigma_{33}^{(\sigma)}$
-0.020	33.12	34.28
-0.013	21.95	22.63
-0.007	10.90	11.17
0.000	0.00	0.00
0.007	-10.74	-10.99
0.013	-21.29	-21.70
0.020	-31.65	-32.16

A similar calculation for fcc AlAs is shown in Table 8.14 with input parameters:  $R_a K_{max} = 10.0$ ,  $G_{max} = 20 \text{ Ry}^{\frac{1}{2}}$ , k-mesh =  $(10 \times 10 \times 10)$ , PBE GGA exchange-correlation energy and potential, and the APW+lo+LO method.

Table 8.14: Comparison of  $\sigma_{33}$  (in kbar) calculated using Eqs. (8.8) and (6.163) for fcc AlAs with different non-volume conserving tetragonal deformations. The superscripts  $(E)$  and  $(\sigma)$  correspond to the energy and stress.

$\epsilon_{33}$	$\sigma_{33}^{(E)}$	$\sigma_{33}^{(\sigma)}$
-0.006	6.47	6.55
-0.004	4.29	4.35
-0.002	2.14	2.04
-0.001	1.07	0.96
0.000	0.00	0.01
0.001	-1.06	-1.13
0.002	-2.12	-2.22
0.004	-4.23	-4.37
0.006	-6.32	-6.62

## 8.7 Elastic constants

The definition of elastic constants and their relationship with the stress tensor are given briefly in Section 2.1. In Section 2.1, we have seen that the elastic constant results from the linear relationship between stress and strain within the elastic limit. Calculation of the elastic constant is important to check the accuracy of the stress tensor. In this section we present elastic constants that are calculated with two different methods— from the stress-strain relationship Eqn. (2.5) and using DFT total energies and the **ELAST** program in WIEN2k code. The details about ELAST program are described in Section 8.5 in WIEN2k usersguide [13] which calculates elastic constants  $C_{11}$  and  $C_{12}$  through the following procedure:

- First the bulk modulus

$$B = \frac{C_{11} + 2C_{12}}{3}, \quad (8.9)$$

is calculated through energy versus volume curve.

- A volume conserving tetragonal deformation

$$1 + \epsilon = \begin{pmatrix} 1 + \epsilon & 0 & 0 \\ 0 & 1 + \epsilon & 0 \\ 0 & 0 & \frac{1}{(1+\epsilon)^2} \end{pmatrix}, \quad (8.10)$$

is applied in a cubic system to calculate  $C_{11}$  -  $C_{12}$ .  $C_{11}$  -  $C_{12}$  is just the curvature of the energy versus applied strain curve i.e.

$$E(\epsilon) = E_0 + 3(C_{11} - C_{12})\Omega_0\epsilon^2 + \mathcal{O}(\epsilon^3), \quad (8.11)$$

where  $E(\epsilon)$  is the energy of a system which is under the applied strain  $\epsilon$ ,  $E_0$  is the energy of a system in its initial state with volume  $\Omega_0$ , and  $\mathcal{O}(\epsilon^3)$  represents all the higher order terms in  $\epsilon$ . Using  $C_{11} + 2C_{12}$  and  $C_{11} - C_{12}$  from Eqs. (8.9) and (8.11) we get  $C_{11}$  and  $C_{12}$ . Since these are numerical methods in which total energies are fitted into polynomials, many DFT calculations have to be performed.

In contrast, from the stress-strain relationship Eqn. (2.5), we may be able to calculate the same parameters with single DFT calculations using a single deformation with the following equations.

$$\sigma_{11} = C_{11}\epsilon_{11} \quad (8.12)$$

$$\sigma_{22} = C_{12}\epsilon_{22}, \quad (8.13)$$

Here  $\epsilon_{11}=\epsilon_{22}$  and calculated in the same way as  $\epsilon_{33}$  in Section 8.6. The calculation of elastic constants is very sensitive when choosing the input parameters. The applied strain should not be too large, otherwise it will break the linear relationship between stress and strain, and at the same time it should not be too small, otherwise numerical problems will arise in the division into stresses, Eqs. (8.12) and (8.13). In Figs. (8.19) and (8.20), we compare the elastic constants ( $C_{11}$  and  $C_{12}$ ) calculated with the stress tensor formalism using Eqs. (8.12) and (8.13) and the total energy calculations using Eqs.(8.9) to (8.11). In these figures, the marker points and the dashed lines are the results of stress and total energy calculations, respectively. The figures clearly show that a numerical instability begins to occur especially for AlAs with small strain, but with a moderate strain the elastic constants remain almost constant. However, in Figs. 8.19 and 8.20, differences of up to 2-4% between these two methods in the elastic constants (especially  $C_{11}$ ) can be seen, which seems to be the limit in accuracy of the method.

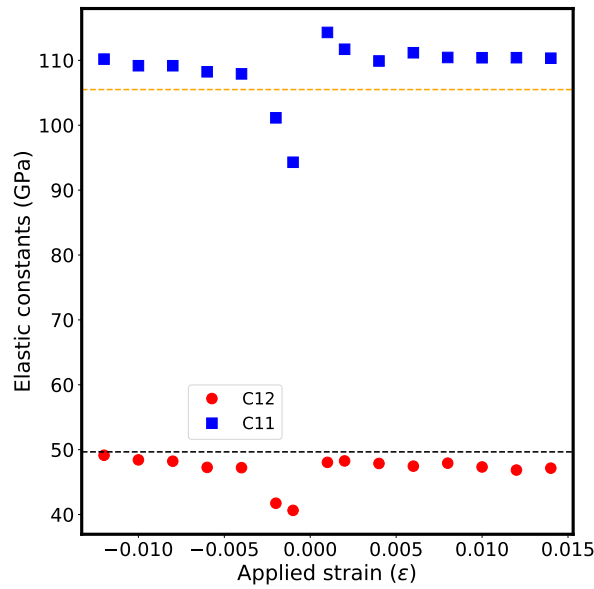


Figure 8.19: Elastic constants  $C_{12}$  and  $C_{11}$  versus the applied strain for fcc AlAs using Eqs. (8.12) and (8.13) (represented by marker points) and Eqs.(8.9) to (8.11) (represented by dashed lines). All input parameters are the same as in Table 8.14.

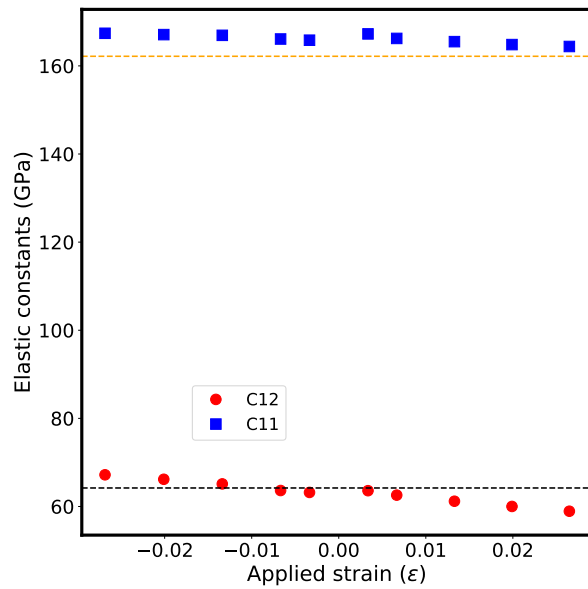


Figure 8.20: Elastic constants  $C_{12}$  and  $C_{11}$  versus the applied strain for silicon in the diamond structure using Eqs. (8.12) and (8.13) (represented by marker points) and Eqs.(8.9) to (8.11) (represented by dashed lines). All input parameters are the same as in Table 8.13.

# Chapter 9

## Discussion

In this work we present a detailed derivation of the stress tensor for the non-relativistic full potential augmented plane wave based methods. The stress tensor formalism given in equation (6.164) is implemented in the WIEN2k code[13, 14]. The formalism is adopted for LDA and GGA, the LAPW and APW+lo method with additional semi-core local orbitals (LO). In the case of GGA, the exchange-correlation energy not only depends on the charge density but also on its gradient, see equation (6.165f). Later, when the system is deformed, the gradient of the charge density is changed with respect to the applied strain, and as a result the strain derivative of this term contributes to the stress tensor, the second term of equation (6.148). In the case of APW+lo, the total stress tensor contains an additional contribution due to the presence of a surface integral as described in section 6.3.1, which later changes according to the applied strain and gives an additional contribution, equation (6.165d), which vanishes in case of LAPW. Using the LOs does not lead to an explicit change in our stress tensor formalism, but internally when expanding the basis function the index  $\lambda$  in equation (3.24) runs up to 2. Therefore, its effect can only appear in the expressions in which the wave functions are directly involved such as the valence kinetic stress and the valence correction stress. Our stress tensor formalism given in equation (6.164) is restricted for a non-relativistic treatment of the valence electrons but the core electrons can be treated fully relativistically since it contributes only via its density. With the exception of the third term, the remaining term of equation (6.164) can be used for the relativistic calculation. The third term results from the strain variation of the kinetic energy operator ( $\nabla^2$ ) and this term alone is not sufficient for the relativistic calculation. Finally, we compared the stress tensor formalism derived in this manuscript with those previously described in Refs. [12, 19, 17, 18] in the following paragraphs.

The stress formalism in Ref. [12] by Thonhauser *et. al* is limited to LDA and a pure LAPW basis. In Ref. [12] only the results of the so-called simple pressure formula, the trace of the full stress tensor, are shown for Al and Si. The authors neither provide any evidence for the usability of the proposed stress formalism for other materials nor any tests for validating the individual stress components. With Ref. [12], our formalism fundamentally differs when the scaling of the strained electronic charge density is defined, which ultimately leads to a different expression whenever the charge density is explicitly present. The scaling of the electronic charge density in Ref. [12] is similar to that in Ref. [4]. In our work, however, the strained electronic charge density of the deformed system is replaced by the charge density of the undeformed system but smeared over the deformed lattice during the calculation of the electrostatic stress tensor. The

reason for this assumption is that the number of electrons does not change, but in the deformed system the charge distribution is different due to the deformation. Moreover, the authors of Ref. [12] use a spherically symmetric core charge and potential in the core correction. The core correction in our calculation, however, contains possible non-spherical terms associated with  $lm=2m$  in the potential. The  $l = 2$  component in the potential exists only in lower symmetry structures and does not contribute to the trace of the stress tensor. In section 8.4.1, we have shown the importance of the  $l = 2$  term in the potential ( $V_{2m}^c$ ) for the prediction of the correct lattice parameters ( $a$  and  $c$ ) and showed that its influence is not negligible. Moreover, the authors in Ref[12] said that the core correction vanishes for pure pressure. We believe that the authors meant to say that the core correction in the pressure becomes the core kinetic energy as shown in Ref. [44] and its explicit form like in the stress tensor would not exist, otherwise we would not be able to validate such an argument. The existence of the discontinuity correction reported in Ref. [12] has no explicit origin other than being influenced by the LAPW force calculation [31], and later it is discarded because of the Slater form of the kinetic energy. The so-called discontinuity correction in the LAPW force calculation[31] appears due to the displacement of an atom  $\mathbf{a}$  (in our notation) into a new positions which leads to a finite change in the kinetic energy in the non-overlapping regions of the old and new atomic spheres of the atom  $\mathbf{a}$ [31]. In the stress calculation, we do not explicitly move the atoms, but change the unit cell volume by a small amount, and every change in the basis set and the adjustment of the basis set at the sphere boundary are taken into account in the so-called valence correction. A surface integral in our derivation, however, exists when the APW+lo method is used. This surface integral appears by applying Green's theorem to convert the  $\nabla^2$  form of the kinetic energy into the so-called Slater form of the kinetic energy when calculating the total energy, see sections 4.1 and 6.3.1.

Later, in a modified version of the LAPW method proposed by Soler and Williams [15, 16], a stress tensor calculation was published by Nagasako and Oguchi. They provided a rigorous mathematical formalism for both local and semilocal functionals[38, 39] in Refs. [17] and [18], respectively. They tested their implementation for many different elements with different cutoff parameters and also for some compounds. The results are in good agreement with numerical results—calculated directly from the total energies. The difference between our stress formalism and that in the paper begins with the definition of the basis function. We used the original LAPW method[25] whereas in the Soler-Williams LAPW method the basis functions are mostly defined by plane-waves and only for the chemically important  $l$  ( $l \leq l_{max} : l_{max} = 2$  or  $3$ ), the plane waves are augmented in the atomic spheres. Therefore, the definition of the charge density in Refs.[17, 18] is also different than in our work. As a result, we are not able to make a one-to-one comparison of every expressions in the atomic spheres. In the interstitial region (IR), however, both formalism use plane wave basis functions. Therefore, the different contributions in the interstitial region from our calculations are the same as in reference [17]. Furthermore, the authors in Ref. [17] stated that the stress contribution from the core kinetic energy should be zero. We found a completely contradicting result from our calculation. In our formalism the strain variation of the core kinetic energy leads to the core correction and this is an important contribution that compensates a large part of the electrostatic stress tensor, see table 8.5 for Al. We believe that the authors came to this conclusion on the basis of different definition of the basis set and thereby the charge density differently where the plane wave representation enters in

the atomic spheres. In the case of the GGA, our equation (6.148) is similar to equation (20) in Ref. [18]. Some arguments in Ref. [18], however, differ from what we observed in our calculations for the same reason as for the core kinetic energy. In Ref. [18] the authors shown even analytically that the GGA correction does not contain any contribution from the atomic spheres. But our derivations and calculations do not support such a conclusion, and this may be due to the different representation of the charge density. With our charge density representation, we found that the interstitial contribution,  $(\Omega\sigma_{\alpha\beta}^{GGA,CORR})_{Int}$  in equation (6.150), is always smaller compared to the contribution from the atomic spheres,  $(\Omega\sigma_{\alpha\beta}^{GGA,CORR})_{sph}$ . We even observed that in some cases the interstitial contribution is almost to zero, for example in the case of Al and W.

For the standard LAPW method, Klüppelberg in Ref. [19] gives a very elegant mathematical derivation of the stress tensor and also discusses an implementation into the FLEUR code [20]. Unfortunately, the calculated stress and pressure do not agree with each other as well as with the results obtained directly from the total energy. The author suggests that the possible error may be due to the equations of the electrostatic stress tensor (EST) since it is the most difficult part of total stress formulation. He also suspects that the error could be due to the valence correction or discontinuity correction term. The error in the reported results is so big that it is difficult to identify whether it is due to a numerical or a mathematical problem. Also, in Ref. [19], the result of the so called simple pressure formula is not correct, even though its expression is simple and is calculated using only the charge density and potential obtained from regular total energy calculations.

The EST is the change in the electrostatic energy according to the strain. The electrostatic energy is evaluated using the Coulomb and Madelung potentials, with the Madelung potential being a limiting case of the Coulomb potential. The Coulomb potential is calculated using Weinert's method[35]. For the EST calculation, the Coulomb potential in the deformed system is first defined and differentiated with respect to the strain. In the APW based methods, the strained Coulomb potential is computed differently in the interstitial and the atomic spheres. The strained Coulomb potential in the interstitial is computed from the Fourier components of the real interstitial charge density and the so-called pseudo-charge density in the strained system. Our calculation showed that these Fourier components do not change due to the applied strain and only the change in the reciprocal lattice vector contributes to the strain variation of the interstitial Coulomb potential. In contrast to this, in Ref. [19] the strain variation of the interstitial Coulomb potential contains the contribution due to the change in Fourier component of the pseudo charge density and the change in reciprocal lattice vector. Moreover, in the total energy calculation we often have integration of the charge density multiplied by the potential over the unit cell volume. When calculating the stress, such an integration must first be defined in the deformed system and differentiated with respect to the strain. The strained integration in Ref. [19], especially while computing the EST and the strain variation of Kohn-Sham eigen value, is first divided into the interstitial and atomic sphere, and then the derivative with respect to the strain is calculated. As a result, in Ref. [19] the strain variation of the step function has to be computed, which leads to surface integrals such as the discontinuity correction (equation (5.14b) in Ref. [19]) and the surface term in the EST (the first term in equation (5.39) in Ref. [19]). When calculating the strain variation of the double

counting term of the kinetic energy, however, the authors in Ref. [19] first transform the strain integral from the strained system to unstrained system and make a further simplification. Because of this inconsistency in solving the strain integral, they may have missed the cancellation of the similar terms. In contrast to this, we first transform all the strain integrals back from the deformed to the undeformed system, divide the integration into the interstitial and atomic sphere regions, and differentiate with respect to the strain. For this reason the surface integrals due to the strain variation of the step function are missing in our stress tensor formalism. However, as explained in the above paragraph, we get a surface term in the APW+lo method but not in the LAPW method and this surface term is completely different than the surface term in Ref. [19].

Another important finding of this work is the solution to the core leakage problem. In the original LAPW method, the valence states are orthogonal to the core states as long as the core states are confined in the region of the atomic sphere. This is only possible if the core states are deep in energy and sphere sizes are large. However, if a system has core states higher in energy such as 2p states of Al or 5s states in Pt, a portion of the core wave function will eventually spill out from the atomic spheres which is known as core leakage. In such cases, Janak's identity [44], which was used to convert the trace of the core correction into the core kinetic energy, would be invalid. The core leakage varies with the size of the atomic spheres and thus the results change with different choices of the atomic spheres. This problem was not considered in previous works Refs.[12, 19, 17, 18]. To mitigate the core leakage problem, we proposed and implemented two different ideas: 1) We treated the core states higher in energy as semi core states and described them using local orbitals (LO). 2) We approximated the core potential outside the atomic spheres, such that it more realistically resembles that of a real solid. The potential is approximated by taking three subsequent points in the vicinity of the atomic sphere boundary and extrapolated outside of the atomic sphere using a quadratic equation as long as it increases. When the potential starts to decrease, it is replaced with the value at which it starts to decrease. In a total energy calculation, a small core leakage is not as severe as compared to a stress calculation because the leak portions of core densities from many different atoms are superposed and produce a ‘crystalline’ core density, which has i) non-spherical terms due to the superposition effects, and ii) an interstitial density described by a Fourier series. The core leakage problem and the proposed solution with results of the WIEN2k implementation are presented in section 7.7. The modified potential described in section 7.7 is now also routinely used in the WIEN2k total energy calculation.

In the Chapter 8, we presented the results of our WIEN2k[13, 14] implementation for fcc Al and Si in the diamond structure, ZnO in the hexagonal wurtzite structure, and TiO<sub>2</sub> in the tetragonal structure. Since the accuracy of the results is controlled by several input parameters, we had to perform various convergence tests. The negative trace of the full stress tensor ( $P^{(\sigma)}$ ) is compared with the results directly obtained from the total energy ( $P^{(E)}$ ). The difference between  $P^{(\sigma)}$  and  $P^{(E)}$  is checked for various  $R_a K_{max}$ ,  $G_{max}$ , k-mesh grids, smearing methods, broadening parameter when the temperature broadening method is used, and the cutoff  $L''_{max}$  for the non-spherical potential in the atomic spheres. From the results we have found that the stress tensor strongly depends on  $R_a K_{max}$  and needs a larger  $R_a K_{max}$  than the total energy calculations. The dependence on the k-mesh is only sizable when the tetrahedron method is used in metallic systems. For other input parameters such as  $G_{max}$  and  $L''_{max}$ , the

dependence of the stress tensor is in the same order as in the total energy, so the same cutoff value can be used in the stress tensor calculation. For Al and W,  $P^{(E)} - P^{(\sigma)}$  has a relatively strong volume dependence in the tetrahedron method that we did not see in the temperature broadening method. With the temperature broadening method, the discrepancy between  $P^{(E)}$  and  $P^{(\sigma)}$  became smaller and even a smaller basis set than that of the tetrahedron method gave good agreement between  $P^{(E)}$  and  $P^{(\sigma)}$ . The importance of the temperature broadening in the stress calculation is discussed in Appendix B.3. In the case of Si, the analytical stress tensor only depends on the different values of  $R_a K_{max}$ . Its dependency on the other input parameters is found to be within the error limit and the same cutoff values that are used in the total energy calculation can be used in the stress calculation. Furthermore, the difference  $P^{(E)} - P^{(\sigma)}$  from our implementation is in the same order as in Refs. [17] and [18]. Later we used  $P^{(\sigma)}$  to estimate the equilibrium lattice parameter  $a_0^{(\sigma)}$  and this estimate was found to agree well with  $a_0^{(E)}$  obtained from the total energy  $P^{(E)}$ . The predicted lattice parameter  $a_0^{(\sigma)}$  from the stress tensor calculation for various materials are tabulated and given in Chapter 8.

We have also tested our implementation in complex systems such as ZnO and TiO<sub>2</sub> (rutile). Since two lattice parameters,  $a$  and  $c$ , in ZnO can be changed freely and in the optimization process, we had to optimize them simultaneously. The value of  $a$  and  $c$  at which the stress tensor is zero is closed to the values at which the total energy is minimal. As a result,  $a$  and  $c$  estimated from the stress tensor agree well with the values estimated from the total energy. The comparison of the estimated lattice parameters from the stress and total energy is presented in Table 8.10 for ZnO and 8.11 for TiO<sub>2</sub>. The calculation of rutile TiO<sub>2</sub> is particularly important to check whether the points group symmetry is correctly taken into account, since in rutile TiO<sub>2</sub> the equivalent atoms are linked via complicated symmetry operations.

In section 8.6, we tested the accuracy of the individual component of the stress tensor at finite strain. For the test, we took silicon in the diamond structure and applied non-volume conserving tetragonal deformations by increasing or decreasing the lattice parameter  $c$ , but leaving  $a$  and  $b$  the same as they were in the cubic structure. The  $\sigma_{33}$  calculated via the total energy fit ( $\sigma_{33}^{(E)}$ ) is compared with the value obtained directly from our analytical stress tensor formalism ( $\sigma_{33}^{(\sigma)}$ ). Table 8.13 shows that there is a small discrepancy between  $\sigma_{33}^{(\sigma)}$  and  $\sigma_{33}^{(E)}$ , but similar calculations for different materials—Al, Si, W, GaAs—show that these numerical differences are within acceptable limits. Finally, we tested the accuracy of the stress tensor by comparing the elastic constants calculated using the stress tensor formalism and total energy calculation in section 8.7.

In summary, we conclude that the stress tensor is accurate enough to be used for structure optimization, although deviations of a few kbar can occur. If the input parameters are selected correctly, however, this deviation only has an effect up to the third decimal place of the lattice parameters. In addition, the formalism and the implementation can be extended to the scalar relativistic kinetic energy and the spin-orbit coupling. In the future, the formalism for the automatic optimization of the lattice parameter using the stress tensor can be implemented in a similar way to the automatic optimization with force.

# Appendices

# Appendix A

## Mathematical tools

The expansion of the unit vector in terms of spherical harmonics  $Y_{1t}(\hat{\mathbf{r}})$  is

$$\hat{\mathbf{r}}_\alpha = \sum_{t=-1}^1 c_{\alpha t} Y_{1t}(\hat{\mathbf{r}}), \quad (\text{A.1})$$

where  $c_{\alpha t}$  are expansion coefficients,  $t = -1, 0, 1$  labels the spherical harmonics components  $(1, t)$  of the  $\alpha$ -coordinate of the unit vector  $\hat{\mathbf{r}}$  and  $\alpha = 1, 2, 3$  denote x, y, z of the Cartesian coordinates.

Multiply both side of the equation (A.1) by  $Y_{1t}^*(\hat{\mathbf{r}})$  and carry out a surface integral.

$$\oint_S dS \hat{\mathbf{r}}_\alpha Y_{1t}^*(\hat{\mathbf{r}}) = \sum_{t=-1}^1 c_{\alpha t} \oint_S dS Y_{1t}(\hat{\mathbf{r}}) Y_{1t}^*(\hat{\mathbf{r}}) \quad (\text{A.2})$$

Using the orthogonality property of spherical harmonic on the right hand side, we get:

$$c_{\alpha t} = \oint_S dS \hat{\mathbf{r}}_\alpha Y_{1t}^*(\hat{\mathbf{r}}) \quad (\text{A.3})$$

The values of  $c_{\alpha t}$  are given in the table A.1.

Table A.1: The value of  $c_{\alpha t}$  for different  $\alpha$  and  $t$ .  $\alpha = 1, 2, 3$  represent to x, y, z of the Cartesian coordinate system.

$\alpha \setminus t$	-1	0	1
1	$\sqrt{\frac{2\pi}{3}}$	0	$-\sqrt{\frac{2\pi}{3}}$
2	$i\sqrt{\frac{2\pi}{3}}$	0	$i\sqrt{\frac{2\pi}{3}}$
3	0	$\sqrt{\frac{4\pi}{3}}$	0

In our WIEN2k implementation, this table is programmed in the subroutine `c_alpha.m.f.`. The product of two spherical harmonics can be expanded into Gaunt number  $G_{l_3, l_1, l_2}^{m_3, m_1, m_2}$  times another spherical harmonics.

$$Y_{l_1 m_1} Y_{l_2 m_2} = \sum_{l_3 m_3} G_{l_3, l_1, l_2}^{m_3, m_1, m_2} Y_{l_3 m_3} \quad (\text{A.4})$$

$$G_{l_3, l_1, l_2}^{m_3, m_1, m_2} = \oint_S dS Y_{l_3 m_3}^* Y_{l_1 m_1} Y_{l_2 m_2} \quad (\text{A.5})$$

Here the angular quantum numbers— $l_3$ ,  $l_1$ , and  $l_2$ —of spherical harmonics has to satisfy the following conditions:

- $l_3 + l_1 + l_2$  has to be even,
- $l_3$ ,  $l_1$ , and  $l_2$  has to satisfy the triangle inequality i.e sum of any two  $l$ 's has to be greater or equal to third  $l$ ,

and  $m_3$ ,  $m_1$ , and  $m_2$  has to satisfy:  $-m_3 + m_1 + m_2 = 0$ . Therefore, indexes  $m_1$  and  $m_2$  can be interchanged but not  $m_3$  i.e  $G_{l_3, l_1, l_2}^{m_3, m_1, m_2} = G_{l_3, l_2, l_1}^{m_3, m_2, m_1}$ . Also, an integral of a product of two spherical harmonics is orthonormal.

$$\oint_S dS Y_{l_1 m_1}^* Y_{l_2 m_2} = \delta_{l_1 l_2} \delta_{m_1 m_2} \quad (\text{A.6})$$

## A.1 Variation of spherical harmonics

The component derivative of the spherical harmonics is given by

$$\partial_\alpha Y_{lm}(\hat{\mathbf{r}}) = \frac{1}{r} r \partial_\alpha Y_{lm}(\hat{\mathbf{r}}) = \frac{1}{r} \sum_{s=\pm 1} \sum_{t=-1}^1 c_\alpha^{st}(l, m) Y_{l+s, m+t}(\hat{\mathbf{r}}) \quad (\text{A.7})$$

Here the index  $s$  takes values  $\pm 1$  but not 0. If the angular quantum number  $l$  is 0,  $s$  is only  $+1$ , since  $l + s$  of a spherical harmonics can not be negative. Accordingly, the angular derivative of the spherical harmonics changes the angular quantum number by  $\pm 1$ . Also,  $c_\alpha^{st}(l, m)$  can be evaluated as following:

$$c_\alpha^{st}(l, m) = \oint_S dS r \partial_\alpha Y_{lm}(\hat{\mathbf{r}}) Y_{l+s, m+t}^*(\hat{\mathbf{r}}), \quad (\text{A.8})$$

and detailed expressions of  $c_\alpha^{st}(l, m)$  are given in section A.2. The strain derivative of the spherical harmonics is:

$$\left. \frac{\partial}{\partial \epsilon_{\alpha\beta}} \right|_{\underline{\epsilon}=0} Y_{lm}(\hat{\mathbf{r}}[\underline{\epsilon}]) = \left. \frac{\partial \mathbf{r}[\underline{\epsilon}]}{\partial \epsilon_{\alpha\beta}} \right|_{\underline{\epsilon}=0} \cdot \nabla_v Y_{lm}(\hat{\mathbf{r}}) \quad (\text{A.9a})$$

$$= \pm \frac{1}{2} (r_\beta \hat{\mathbf{e}}_\alpha + r_\alpha \hat{\mathbf{e}}_\beta) \cdot \nabla_v Y_{lm}(\hat{\mathbf{r}}) \quad (\text{A.9b})$$

$$= \pm \frac{1}{2} (r_\beta \partial_\alpha + r_\alpha \partial_\beta) Y_{lm}(\hat{\mathbf{r}}) \quad (\text{A.9c})$$

$$= \pm \frac{1}{2} (\hat{r}_\beta \cdot r \partial_\alpha + \hat{r}_\alpha \cdot r \partial_\beta) Y_{lm}(\hat{\mathbf{r}}) \quad (\text{A.9d})$$

Here the index  $v$  denotes the components of  $\nabla$ . The sign  $\pm$  in the above equations depends on the argument in the spherical harmonics:  $+(-)$  is for a direct lattice (reciprocal lattice) vector. Using equations (A.1) and (A.8) in equation (A.9d) yields

$$\frac{\partial}{\partial \epsilon_{\alpha\beta}} \left|_{\underline{\epsilon}=0} \right. Y_{lm}(\hat{\mathbf{r}}[\underline{\epsilon}]) = \pm \frac{1}{2} \sum_{s=\pm 1} \sum_{t,t'=-1}^1 [c_{\alpha t'} c_{\beta}^{st}(l,m) + c_{\beta t'} c_{\alpha}^{st}(l,m)] Y_{1t'}(\hat{\mathbf{r}}) Y_{l+s, m+t}(\hat{\mathbf{r}}). \quad (\text{A.10})$$

Also, using equation (A.4) to further simplify the product of two spherical harmonics:

$$\frac{\partial}{\partial \epsilon_{\alpha\beta}} \left|_{\underline{\epsilon}=0} \right. Y_{lm}(\hat{\mathbf{r}}[\underline{\epsilon}]) = \pm \frac{1}{2} \sum_{s=\pm 1} \sum_{t,t'=-1}^1 \sum_{l_3 m_3} [c_{\alpha t'} c_{\beta}^{st}(l,m) + c_{\beta t'} c_{\alpha}^{st}(l,m)] G_{l_3,1,l+s}^{m_3,t',m+t} Y_{l_3 m_3}(\hat{\mathbf{r}}) \quad (\text{A.11})$$

Equation (A.11) contributes to the full stress tensor, but for the hydrostatic case only the diagonal components contribute. In such a case, equation (A.11) becomes

$$\sum_{\alpha\alpha} \frac{\delta}{\delta \epsilon_{\alpha\alpha}} \left|_{\underline{\epsilon}=0} \right. Y_{lm}(\hat{\mathbf{r}}[\underline{\epsilon}]) = \pm \mathbf{r} \cdot \nabla_v Y_{lm}(\hat{\mathbf{r}}) = \pm r \frac{\partial Y_{lm}(\hat{\mathbf{r}})}{\partial r} = 0 \quad (\text{A.12})$$

Therefore, in pure pressure calculations (i.e. hydrostatic case), the strain variation of spherical harmonics does not contribute.

## A.2 c coefficients

For  $c_{\alpha}^{st}(l,m)$ , the following formulas are implemented.

$$\begin{aligned} c_{\alpha}^{-1,-1}(l,m) &= -(l+1)(\delta_{\alpha,1} + i\delta_{\alpha,2}) F_{lm}^2 \\ c_{\alpha}^{-1,0}(l,m) &= (l+1)\delta_{\alpha,3} F_{lm}^6 \\ c_{\alpha}^{-1,+1}(l,m) &= (l+1)(\delta_{\alpha,1} - i\delta_{\alpha,2}) F_{lm}^4 \\ c_{\alpha}^{+1,-1}(l,m) &= -l(\delta_{\alpha,1} + i\delta_{\alpha,2}) F_{lm}^1 \\ c_{\alpha}^{+1,0}(l,m) &= -l\delta_{\alpha,3} F_{lm}^5 \\ c_{\alpha}^{+1,+1}(l,m) &= l(\delta_{\alpha,1} - i\delta_{\alpha,2}) F_{lm}^3 \\ c_{\alpha}^{00}(l,m) &= 0 \text{(no matter what } l \text{ and } m \text{ would be)} \end{aligned}$$

where  $F_{lm}^j$  for  $j=1,6$  are given as

$$\begin{aligned} F_{lm}^1 &= \sqrt{\frac{(l-m+1)(l-m+2)}{4(2l+1)(2l+3)}} & F_{lm}^2 &= \sqrt{\frac{(l+m-1)(l+m)}{4(2l-1)(2l+1)}} \\ F_{lm}^3 &= \sqrt{\frac{(l+m+1)(l+m+2)}{4(2l+1)(2l+3)}} & F_{lm}^4 &= \sqrt{\frac{(l-m-1)(l-m)}{4(2l-1)(2l+1)}} \\ F_{lm}^5 &= \sqrt{\frac{(l+1)^2 - m^2}{4(2l+1)(2l+3)}} & F_{lm}^6 &= \sqrt{\frac{l^2 - m^2}{(2l-1)(2l+1)}} \end{aligned}$$

These formulas are coded in the subroutine c-factor. They are called for each  $l$  and  $m$  i.e `C_factor(l, m, c_alpha^st(l, m))`. This subroutine is written inside of `c_alpha.m.f`. The above expressions show that  $c_{\alpha}^{st}(0,0)$  is always zero when  $l$  and  $m$  are zero at the same time.

### A.3 Component derivative of the radial function

A vector  $\mathbf{r}$  with length  $r$  transform from a strained to un-strained system as:

$$\mathbf{r}[\underline{\epsilon}] = (1 \pm \underline{\epsilon})\mathbf{r} \quad (\text{A.13})$$

Where + (-) is for vectors of the direct (reciprocal) lattice. Also, the strain variation of the strained vector is:

$$\frac{\partial}{\partial \epsilon_{\alpha\beta}} \mathbf{r}[\underline{\epsilon}] = \pm \frac{\mathbf{r}_\alpha \mathbf{r}_\beta}{r} \quad (\text{A.14})$$

$$= \pm r \hat{\mathbf{r}}_\alpha \hat{\mathbf{r}}_\beta \quad (\text{A.15})$$

$$\stackrel{(A.1)}{=} \pm r \sum_{t,t'=-1}^1 c_{\alpha t} c_{\beta t'} Y_{1t}(\hat{\mathbf{r}}) Y_{1t'}(\hat{\mathbf{r}}) \quad (\text{A.16})$$

$$\stackrel{(A.4)}{=} \pm r \sum_{t,t'=-1}^1 c_{\alpha t} c_{\beta t'} \sum_{s=0,2} \sum_{\nu=-s}^s G_{s,1,1}^{\nu,t,t'} Y_{s\nu}(\hat{\mathbf{r}}) \quad (\text{A.17})$$

Variation of the unit cell volume:

$$\frac{\partial}{\partial \epsilon_{\alpha\beta}} \Omega[\underline{\epsilon}] = \frac{\partial}{\partial \epsilon_{\alpha\beta}} \det(1 + \underline{\epsilon}) \Omega = \delta_{\alpha\beta} \Omega \quad (\text{A.18})$$

Also,

$$r = \sqrt{\sum_{\alpha} \mathbf{r}_{\alpha}^2} \quad (\text{A.19})$$

$$\frac{\partial r}{\partial \mathbf{r}_{\alpha}} = \frac{\mathbf{r}_{\alpha}}{\sqrt{\sum_{\alpha} \mathbf{r}_{\alpha}^2}} = \frac{\mathbf{r}_{\alpha}}{r} = \hat{\mathbf{r}}_{\alpha} \quad (\text{A.20})$$

Recalling the equation (A.13) for a vector in direct space:

$$\mathbf{r}[\underline{\epsilon}] = (1 + \underline{\epsilon})\mathbf{r}$$

$$\frac{1}{|\mathbf{r}[\underline{\epsilon}]|} = \frac{1}{|(\mathbf{r} + \epsilon \mathbf{r})|} = \frac{1}{\sqrt{(\mathbf{r} + \epsilon \mathbf{r})(\mathbf{r} + \epsilon \mathbf{r})}} \quad (\text{A.21})$$

$$= \frac{1}{\sqrt{\mathbf{r}^2 + 2\mathbf{r}\epsilon\mathbf{r} + (\epsilon\mathbf{r})^2}} \quad (\text{A.22})$$

$$= \frac{1}{|\mathbf{r}|} \frac{1}{\sqrt{1 + \frac{2\mathbf{r}\epsilon\mathbf{r}}{\mathbf{r}^2} + \frac{(\epsilon\mathbf{r})^2}{\mathbf{r}^2}}} \quad (\text{A.23})$$

If the strain tensor is small i.e  $|\underline{\epsilon}| \ll 1$

$$\frac{1}{|\mathbf{r}[\epsilon]|} \approx \frac{1}{|\mathbf{r}|} \left( 1 - \frac{\mathbf{r}\epsilon\mathbf{r}}{\mathbf{r}^2} \right) \quad (\text{A.24})$$

Now the strain variation is:

$$\frac{d}{d\epsilon_{\alpha\beta}} \left|_{\underline{\epsilon}=0} \right. \frac{1}{|\mathbf{r}[\epsilon]|} = -\frac{d}{d\epsilon_{\alpha\beta}} \left|_{\underline{\epsilon}=0} \right. \frac{\mathbf{r}\epsilon\mathbf{r}}{|\mathbf{r}|^3} = -\frac{1}{|\mathbf{r}|^3} \frac{d}{d\epsilon_{\alpha\beta}} \left|_{\underline{\epsilon}=0} \right. \sum_{\gamma\delta} \mathbf{r}_\gamma \epsilon_{\gamma\delta} \mathbf{r}_\delta \quad (\text{A.25})$$

$$= -\frac{1}{|\mathbf{r}|^3} \sum_{\gamma\delta} \mathbf{r}_\gamma \frac{d\epsilon_{\gamma\delta}}{d\epsilon_{\alpha\beta}} \Big|_{\underline{\epsilon}=0} \mathbf{r}_\delta \quad (\text{A.26})$$

$$= -\frac{1}{|\mathbf{r}|^3} \sum_{\gamma\delta} \mathbf{r}_\gamma \mathbf{r}_\delta \delta_{\alpha\gamma} \delta_{\beta\delta} \quad (\text{A.27})$$

$$= -\frac{1}{|\mathbf{r}|^3} \mathbf{r}_\alpha \mathbf{r}_\beta \quad (\text{A.28})$$

$$= -\frac{\hat{\mathbf{r}}_\alpha \hat{\mathbf{r}}_\beta}{|\mathbf{r}|} \quad (\text{A.29})$$

This expression is important to simplify the electrostatic stress tensor. In the electrostatic stress tensor it is required to evaluate the strain variation of  $\frac{1}{|\mathbf{r}[\epsilon]-\mathbf{s}[\epsilon]|}$ ,  $\frac{1}{|\mathbf{r}[\epsilon]-\boldsymbol{\tau}_a[\epsilon]|}$ , and  $\frac{1}{|\boldsymbol{\tau}_a[\epsilon]-\boldsymbol{\tau}_b[\epsilon]|}$ , which is:

$$\frac{d}{d\epsilon_{\alpha\beta}} \frac{1}{|\mathbf{r}[\epsilon]-\mathbf{s}[\epsilon]|} = -\frac{(\mathbf{r}-\mathbf{s})_\alpha (\mathbf{r}-\mathbf{s})_\beta}{(|\mathbf{r}-\mathbf{s}|^3)} = -\frac{\widehat{(\mathbf{r}-\mathbf{s})}_\alpha \widehat{(\mathbf{r}-\mathbf{s})}_\beta}{(|\mathbf{r}-\mathbf{s}|)} \quad (\text{A.30})$$

$$\frac{d}{d\epsilon_{\alpha\beta}} \frac{1}{|\mathbf{r}[\epsilon]-\boldsymbol{\tau}_a[\epsilon]|} = -\frac{(\mathbf{r}-\boldsymbol{\tau}_a)_\alpha (\mathbf{r}-\boldsymbol{\tau}_a)_\beta}{(|\mathbf{r}-\boldsymbol{\tau}_a|^3)} = -\frac{\widehat{(\mathbf{r}-\boldsymbol{\tau}_a)}_\alpha \widehat{(\mathbf{r}-\boldsymbol{\tau}_a)}_\beta}{(|\mathbf{r}-\boldsymbol{\tau}_a|)} \quad (\text{A.31})$$

$$\frac{d}{d\epsilon_{\alpha\beta}} \frac{1}{|\boldsymbol{\tau}_a[\epsilon]-\boldsymbol{\tau}_b[\epsilon]|} = -\frac{(\boldsymbol{\tau}_a-\boldsymbol{\tau}_b)_\alpha (\boldsymbol{\tau}_a-\boldsymbol{\tau}_b)_\beta}{(|\boldsymbol{\tau}_a-\boldsymbol{\tau}_b|^3)} = -\frac{\widehat{(\boldsymbol{\tau}_a-\boldsymbol{\tau}_b)}_\alpha \widehat{(\boldsymbol{\tau}_a-\boldsymbol{\tau}_b)}_\beta}{(|\boldsymbol{\tau}_a-\boldsymbol{\tau}_b|)} \quad (\text{A.32})$$

Here  $\boldsymbol{\tau}_a$  represents a position of an atom ‘a’ with respect to the global coordinate system.

## A.4 Integration over the whole unit cell

To solve an integral over the whole unit cell in APW based methods, the integration domain divides into a region of atomic spheres with radius  $R_a$  located at  $\boldsymbol{\tau}_a$  and an interstitial region. Lets consider a regular function  $F(\mathbf{r})$  and, its integration over the whole unit cell volume ( $\Omega$ ) is

$$\int_{\Omega} d^3\mathbf{r} F(\mathbf{r}) = \int_{\Omega} d^3\mathbf{r} F(\mathbf{r}) \left[ \sum_a \Theta(R_a - |\mathbf{r} - \boldsymbol{\tau}_a|) + \right. \quad (\text{A.33})$$

$$\left. \left( 1 - \sum_a \Theta(R_a - |\mathbf{r} - \boldsymbol{\tau}_a|) \right) \right] \quad (\text{A.34})$$

$$= \int_{\Omega} d^3\mathbf{r} F(\mathbf{r}) \sum_a \Theta(R_a - |\mathbf{r} - \boldsymbol{\tau}_a|) + \int_{\Omega} d^3\mathbf{r} F(\mathbf{r}) \left( 1 - \sum_a \Theta(R_a - |\mathbf{r} - \boldsymbol{\tau}_a|) \right) \quad (\text{A.35})$$

Here  $\Theta(R_a - |\mathbf{r} - \boldsymbol{\tau}_a|)$  is the Heavyside step function, and it is used to distinguish atomic spheres and interstitial regions. It is zero in the interstitial, and 1 in the atomic spheres centered at  $\boldsymbol{\tau}_a$ . For the sake of brevity,  $\Theta(R_a - |\mathbf{r} - \boldsymbol{\tau}_a|)$  will be replaced by

$\Theta_a(\mathbf{r})$  and  $\left(1 - \sum_a \Theta(R_a - |\mathbf{r} - \boldsymbol{\tau}_a|)\right)$  by the  $\Theta_{IS}(\mathbf{r})$ .  $\Theta_{IS}(\mathbf{r})$  is the Heavyside step function for the interstitial region and has zero value inside the atomic spheres. Here, the  $F(\mathbf{r})$  is a general function, but in practice, it refers to the charge density, total or exchange-correlational potential, or some other real physical quantity.

$$\int_{\Omega} d^3\mathbf{r} F(\mathbf{r}) = \sum_a \int_{\Omega} d^3\mathbf{r} \Theta_a(\mathbf{r}) F(\mathbf{r}) + \int_{\Omega} d^3\mathbf{r} \Theta_{IS}(\mathbf{r}) F(\mathbf{r}) \quad (\text{A.36})$$

The second integral of equation (A.36) is solved by expressing the function  $F(\mathbf{r})$  and  $\Theta_{IS}(\mathbf{r})$  as Fourier series expansions.

$$F(\mathbf{r}) = \sum_{\mathbf{G}} F(\mathbf{G}) e^{i\mathbf{G}\cdot\mathbf{r}}, \quad \Theta_{IS}(\mathbf{r}) = \sum_{\mathbf{G}} \Theta_{IS}(\mathbf{G}) e^{i\mathbf{G}\cdot\mathbf{r}} \quad (\text{A.37})$$

Now,

$$\int_{\Omega} d^3\mathbf{r} \Theta_{IS}(\mathbf{r}) F(\mathbf{r}) = \sum_{\mathbf{GG}'} \int_{\Omega} d^3\mathbf{r} F(\mathbf{G}) e^{i\mathbf{G}\cdot\mathbf{r}} \Theta_{IS}(\mathbf{G}') e^{i\mathbf{G}'\cdot\mathbf{r}} \quad (\text{A.38})$$

$$= \sum_{\mathbf{GG}'} F(\mathbf{G})^* \Theta_{IS}(\mathbf{G}') \underbrace{\int_{\Omega} d^3\mathbf{r} e^{-i\mathbf{G}\cdot\mathbf{r}} e^{i\mathbf{G}'\cdot\mathbf{r}}}_{\Omega \delta_{\mathbf{GG}'}} \quad (\text{A.39})$$

$$= \Omega \sum_{\mathbf{G}} F(\mathbf{G})^* \Theta_{IS}(\mathbf{G}) \quad (\text{A.40})$$

Here  $F(\mathbf{G})$  and  $\Theta_{IS}(\mathbf{G})$  are the Fourier coefficients of functions  $F(\mathbf{r})$  and  $\Theta_{IS}(\mathbf{r})$ , and they are determined via Fourier transform.

$$F(\mathbf{G}) = \frac{1}{\Omega} \int_{\Omega} d^3\mathbf{r} F(\mathbf{r}) e^{-i\mathbf{Gr}} \quad (\text{A.41})$$

The  $\Theta_{IS}(\mathbf{G})$  is also evaluated in the same manner. However, in the program, the Fourier coefficients of a step function— $\Theta_{IS}(\mathbf{G})$ —are calculated as given below:

$$\Theta_{IS}(\mathbf{G}) = \begin{cases} 1 - \sum_a \frac{4\pi R_a^3}{3\Omega} & \mathbf{G} = 0 \\ -\frac{4\pi}{\Omega|\mathbf{G}|} \sum_a e^{i\mathbf{G}\cdot\mathbf{r}} R_a^2 j_l(|\mathbf{G}|R_a) & \mathbf{G} \neq 0 \end{cases} \quad (\text{A.42})$$

Here  $j_l$  is a spherical Bessel function,  $|\mathbf{G}|$  is the length of the vector  $\mathbf{G}$ ,  $\mathbf{r}$  is a spatial vector defined with respect to the global coordinates system such that  $\mathbf{r} = \mathbf{r}_a + \boldsymbol{\tau}_a$ , and  $\mathbf{r}_a$  is a position vector with respect to the local coordinate system. The index  $a$  in the sum ( $\sum$ ) runs over all equivalent and non-equivalent atoms. In most expressions where the  $\Theta(\mathbf{G})$  function appears, the unit cell volume appears as a multiplier. Therefore, in our code, instead of equation (A.42),  $\Theta(\mathbf{G})$  is defined as given below:

$$\Omega \Theta_{IS}(\mathbf{G}) = \begin{cases} \Omega - \sum_a \frac{4\pi R_a^3}{3} & \mathbf{G} = 0 \\ -\frac{4\pi}{|\mathbf{G}|} \sum_a e^{i\mathbf{G}\cdot\mathbf{r}} R_a^2 j_l(|\mathbf{G}|R_a) & \mathbf{G} \neq 0 \end{cases} \quad (\text{A.43})$$

If the system possesses an inversion symmetry the exponential function ( $e^{i\mathbf{G}\cdot\mathbf{r}}$ ) can be replaced by  $\cos(\mathbf{G}\cdot\mathbf{r})$ .

# Appendix B

## Real and complex spherical harmonics and density

All of our stress tensor formulas are computed using complex spherical harmonics, while the total energy computation is performed using real spherical harmonics. In order to use quantities such as charge density and potential from the calculation of the total energy, we must either express our formulas in real spherical harmonics or the quantities calculated with real spherical harmonics must be converted into a complex form. In the stress calculation, the second option is chosen. The transformation relations between real spherical harmonics ( $y_{l|m|}^{\pm}$ ) and the complex spherical harmonics ( $Y_{l,\pm|m|}$ ) are

$$\begin{aligned} Y_{l,+|m|}(\hat{\mathbf{r}}) &= \frac{(-1)^m}{\sqrt{2}} \left( y_{l|m|}^+(\hat{\mathbf{r}}) + iy_{l|m|}^-(\hat{\mathbf{r}}) \right) & m > 0 \\ Y_{l,-|m|}(\hat{\mathbf{r}}) &= \frac{1}{\sqrt{2}} \left( y_{l|m|}^+(\hat{\mathbf{r}}) - iy_{l|m|}^-(\hat{\mathbf{r}}) \right) & m < 0 \\ Y_{l0}(\hat{\mathbf{r}}) &= y_{l0}^+(\hat{\mathbf{r}}) & m = 0 \end{aligned} \quad (\text{B.1})$$

Inverse transformation of equation (B.1) is:

$$\begin{aligned} y_{l|m|}^+(\hat{\mathbf{r}}) &= \frac{1}{\sqrt{2}} \left( (-1)^m Y_{l,+|m|}(\hat{\mathbf{r}}) + Y_{l,-|m|}(\hat{\mathbf{r}}) \right) & m > 0 \\ y_{l|m|}^-(\hat{\mathbf{r}}) &= \frac{1}{i\sqrt{2}} \left( (-1)^m Y_{l,+|m|}(\hat{\mathbf{r}}) - Y_{l,-|m|}(\hat{\mathbf{r}}) \right) & m < 0 \\ y_{l0}^+(\hat{\mathbf{r}}) &= Y_{l0}(\hat{\mathbf{r}}) & m = 0 \end{aligned} \quad (\text{B.2})$$

The pre-factors before the complex spherical harmonics are different for different  $l$  and  $m$  and are listed in Table B.1.

Table B.1: Pre-factors for different  $l$  and  $m$ .

	$m > 0$	$m < 0$
$l^+$	$\frac{(-1)^m}{\sqrt{2}}$	$\frac{1}{\sqrt{2}}$
$l^-$	$\frac{(-1)^m}{i\sqrt{2}}$	$-\frac{1}{i\sqrt{2}}$

In the code, these factors are evaluated in a subroutine **multfc.f**. Using equation (B.2), the charge density can be expressed in terms of real spherical harmonics.

$$\rho(\mathbf{r}) = \sum_{lm} \rho_{l|m|}^+(r) y_{l|m|}^+(\hat{\mathbf{r}}) + \sum_{lm} \rho_{l|m|}^-(r) y_{l|m|}^-(\hat{\mathbf{r}}) \quad (\text{B.3})$$

The relationship between  $\rho_{l\pm|m|}(r)$  and  $\rho_{l|m|}^\pm(r)$  is

$$\rho_{l+|m|}(r) = \frac{(-1)^m}{\sqrt{2}} \left( \rho_{l|m|}^+(r) - i \rho_{l|m|}^-(r) \right) \quad m > 0 \quad (\text{B.4})$$

$$\rho_{l-|m|}(r) = \frac{1}{\sqrt{2}} \left( \rho_{l|m|}^+(r) + i \rho_{l|m|}^-(r) \right) \quad m < 0 \quad (\text{B.5})$$

$$\rho_{00}(r) = \rho_{00}(r) \quad l = 0, m = 0 \quad (\text{B.6})$$

Inverse of the above relation is

$$\rho_{l|m|}^+(r) = \frac{1}{\sqrt{2}} \left( (-1)^m \rho_{l+|m|}(r) + \rho_{l-|m|}(r) \right) \quad m > 0 \quad (\text{B.7})$$

$$\rho_{l|m|}^-(r) = \frac{1}{i\sqrt{2}} \left( -(-1)^m \rho_{l+|m|}(r) + \rho_{l-|m|}(r) \right) \quad m < 0 \quad (\text{B.8})$$

$$\rho_{00}^+(r) = \rho_{00}(r) \quad l = 0, m = 0 \quad (\text{B.9})$$

In WIEN2k calculations,  $\rho_{lm}^+(\mathbf{r})$  and  $\rho_{lm}^-(\mathbf{r})$  are saved in a file with the extension '`.clmsum`'. The pre-factor specified in the table (B.1) is computed in subroutine `multfc.f` for different  $l$  and  $m$ , and the charge density is multiplied by this pre-factor in subroutine `multsu.f`. Note, that for 'cubic harmonics' slightly different factors and linear combinations appear [49].

## B.1 Sum over atoms

In our final stress tensor formula we see the notation  $\sum_a$ , which implies a sum over non-equivalent and equivalent atoms in the unit cell. The equivalent atoms are symmetrically related atoms, and therefore the charge density and the potential in each atom are the same. Consequently, the stress tensor, which is calculated using the charge density and potential, does not need to be computed explicitly in every equivalent atom. Instead, we evaluate it for one of the equivalent atoms and rotate it correctly for the remaining equivalent atoms. The rotation is performed using a  $3 \times 3$  matrix constructed using the point group symmetry of the crystal structure.

Let us consider a system containing  $n$  equivalent atoms i.e  $a_1, a_2 \dots, a_n$ , and  $R_i$  ('rotij' in WIEN2k code) is the rotational part of the symmetry operation that transforms the atom  $a_1$  into  $a_i$ . If  $\sigma_1$  and  $\sigma_i$  are the stress tensor of atoms  $a_1$  and  $a_i$  respectively, then  $\sigma_i$  can be calculated as follows

$$\sigma_i = R_i^{-1} \sigma_1 R_i \quad (\text{B.10})$$

and the stress tensor of all equivalent atoms is

$$\sigma_{eqv} = \sum_i^n \sigma_i \quad (B.11)$$

In addition, if the local coordinate system of atoms does not coincide with the global coordinate system or crystal axes, the evaluation of charge density and potential requires more LM combinations in their lattice harmonics expansion. This ultimately increases the computational cost. In an alternative approach, we rotate the local coordinate system of atoms to match the global coordinate system. As a result, a few LM combinations are sufficient in the charge density and potential. In the WIEN2k code, this transformation is achieved using the ROTLOC matrix.

## B.2 $\mathbf{k}$ points symmetrization

In the stress tensor formalism, the wave functions appear explicitly in contributions to the valence kinetic stress, the valence correction stress, and the stress tensor due to an additional surface term in the case of APW+lo. In their calculations, we need to perform a summation over all  $\mathbf{k}$ -vectors of the first Brillouin zone. In practice, however, we only perform the summation over the irreducible part of the first Brillouin zone. In the summation, we take one  $\mathbf{k}$ -vector from the group of symmetrically related  $\mathbf{k}$ -vectors. This is very helpful for speeding up the calculations, especially in metallic systems where a lot of  $\mathbf{k}$ -vectors are required to get a decent result. For example, in the case of a simple element like fcc Aluminum, 15000  $\mathbf{k}$ -vectors in the first Brillouin zone reduce to only 413  $\mathbf{k}$ -vectors in the irreducible Brillouin zone. Once we have computed the stress tensor in the irreducible Brillouin zone, the following transformation operation must be performed to extend it to the full first Brillouin zone.

$$\sigma_{\alpha\beta}^{FBZ} = \frac{1}{N_{sy}} \sum_{\mathbf{k} \in IBZ} \sum_{i=1}^{N_{sy}} S_i^{-1} \sigma_{\alpha\beta}^{\mathbf{k}} S_i, \quad (B.12)$$

where  $\sigma_{\alpha\beta}^{FBZ}$  is the total stress tensor in the first Brillouin zone,  $N_{sy}$  is number of symmetry operations, IBZ is the irreducible Brillouin zone, and  $\mathbf{k} \in IBZ$  denotes all  $\mathbf{k}$  vectors that belong to the irreducible Brillouin zone.  $S_i$  is the  $i^{th}$  symmetry operation and  $S_i^{-1}$  is its inverse.  $\sigma_{\alpha\beta}^{\mathbf{k}}$  is the stress tensor for a given  $\mathbf{k}$  vector of the IBZ.

## B.3 Occupation number

During the derivation we assumed that the occupancy of each band does not depend on strain in a first order approximation. This assumption is motivated by the force calculations, but is not tested explicitly for the stress. Because of this assumption, the occupancy of each state must be carefully calculated. In practice, we use the tetrahedron or the Fermi-Dirac method with suitable temperature broadening parameters to evaluate the occupancy in the electronic structure calculation. In the traditional tetrahedron method, often referred to as the linear tetrahedron method, the irreducible part of the Brillouin zone is divided into many tetrahedra, eigenvalues and matrix elements for each k-point are evaluated only at the corner of the tetrahedron, and via

linear interpolation the quantities at any point within the tetrahedron are evaluated.

In the Brillouin zone, the integration of  $\epsilon_{v\mathbf{k}}$ , which depend on the band index  $v$  and on the  $\mathbf{k}$  vector, is evaluated by a sum over a discrete grid of  $\mathbf{k}$ -points i.e.

$$\sum_v \frac{1}{\Omega_{BZ}} \int_{\Omega_{BZ}} \epsilon_{v\mathbf{k}} \theta(\epsilon_{v\mathbf{k}} - E_F) d\mathbf{k} \rightarrow \sum_v \frac{1}{\Omega_{BZ}} \sum_{\mathbf{k}} w_{\mathbf{k}} \epsilon_{v\mathbf{k}} \theta(\epsilon_{v\mathbf{k}} - E_F), \quad (\text{B.13})$$

where  $w_{\mathbf{k}}$  is the weight corresponding to k-point  $\mathbf{k}$ , and  $\Omega_{BZ}$  is the volume of the Brillouin zone. The step function  $\theta$  is equals to 1 if  $\epsilon_{v\mathbf{k}} \leq E_F$  and 0 otherwise.  $E_F$  is the Fermi level that distinguish the occupied and unoccupied energy bands. In semiconductors and insulators, there is a clear distinction between occupied and unoccupied energy bands, and thus the Fermi energy lies between the valence and conduction bands. Therefore,  $\theta$  is 1 for all the occupied energy bands ( $\epsilon_{v\mathbf{k}} \leq E_F$ ) and 0 for all the unoccupied energy bands ( $\epsilon_{v\mathbf{k}} > E_F$ ). In this case, calculation of Eq. (B.13) poses no problem numerically. In the case of a metallic system, however, the story is a little different. A valence band near the Fermi level can be partially occupied and changes abruptly for a neighboring unoccupied band, which makes convergence of Eq. (B.13) or  $\theta(\epsilon_{v\mathbf{k}} - E_F)$  exceedingly slow with respect to the number of k-points. Therefore, for metals, in order to speed up the calculations, the step function is replaced by a much smooth function  $f(\epsilon_{v\mathbf{k}})$  whose smoothness can be controlled by the temperature. In practice,  $f(\epsilon_{v\mathbf{k}})$  is usually chosen to be a Fermi-Dirac function:

$$f(\epsilon_{v\mathbf{k}}) = \frac{1}{e^{\frac{\epsilon_{v\mathbf{k}} - E_F}{\sigma}} + 1}, \quad (\text{B.14})$$

where  $\sigma = k_B T$ ,  $k_B$  is the Boltzmann's constant, and  $T$  is temperature. In the calculation,  $\sigma$  should be chosen so that  $T$  does not exceed room temperature too much.

Weinert *et. al.* discussed in Ref. [48] that the total energy given by equation (4.15) is no longer variational for a system with partial occupation numbers. In this case, the total energy must be replaced by a more general expression as given in equation (B.15), and for the force calculation, energy given in equation (B.15) must be used instead of equation (4.15). Furthermore, the authors showed in Ref. [48] that in the force calculation the derivative of the occupation number with respect to atomic position is canceled with a similar expression from the entropy-like term (second term in equation (B.15)).

$$F = E - \sum_{vk} n_{vk} \sigma S, \quad (\text{B.15})$$

where  $F$  is the free energy and  $S$  is the entropy. We also expect this approach to be applicable to stress calculation as it is also a derivative, albeit with respect to the strain.

# Appendix C

## Contribution from the double counting term

The strain variation of the effective potential, which appears in the double counting term of the kinetic energy, is identical for core and valence electrons.

$$\begin{aligned} -\frac{1}{\Omega} \frac{\delta}{\delta \epsilon_{\alpha\beta}} \left[ \int_{\Omega[\underline{\epsilon}]} d^3 r \rho[\underline{\epsilon}](\mathbf{r}_\epsilon) V_{eff}[\underline{\epsilon}](\mathbf{r}_\epsilon) \right]_{\underline{\epsilon}=0} &= -\frac{\delta}{\delta \epsilon_{\alpha\beta}} \left[ \underbrace{\det(1 + \underline{\epsilon})}_{=1+\text{tr}\underline{\epsilon}+O(\underline{\epsilon}^2)} \int_{\Omega} d^3 r \rho[\underline{\epsilon}](\mathbf{r}[\underline{\epsilon}]) V_{eff}[\underline{\epsilon}](\mathbf{r}[\underline{\epsilon}]) \right]_{\underline{\epsilon}=0} \\ &= -\frac{\delta_{\alpha\beta}}{\Omega} \int_{\Omega} d^3 r \rho[\underline{\epsilon}](\mathbf{r}) V_{eff}(\mathbf{r}) \end{aligned} \quad (\text{C.1a})$$

$$-\frac{1}{\Omega} \int_{\Omega} d^3 r V_{eff}(\mathbf{r}) \frac{\delta \rho[\underline{\epsilon}](\mathbf{r}[\underline{\epsilon}])}{\delta \epsilon_{\alpha\beta}} \Big|_{\underline{\epsilon}=0} \quad (\text{C.1b})$$

$$-\frac{1}{\Omega} \int_{\Omega} d^3 r \rho(\mathbf{r}) \frac{\delta V_{eff}[\underline{\epsilon}](\mathbf{r}[\underline{\epsilon}])}{\delta \epsilon_{\alpha\beta}} \Big|_{\underline{\epsilon}=0} \quad (\text{C.1c})$$

Equation (C.1a) is a purely hydrostatic contribution due to the change of the unit cell volume. Equation (C.1c) describes the variation of the effective potential resulting

from the deformation of the unit cell. The variation  $\frac{\delta V_{eff}[\underline{\epsilon}](\mathbf{r}[\underline{\epsilon}])}{\delta \epsilon_{\alpha\beta}} \Big|_{\underline{\epsilon}=0}$  depends on  $\underline{\epsilon}$  both explicitly via linear response and implicitly via its smeared argument  $\mathbf{r}[\underline{\epsilon}]$ , which means

$$\frac{\delta V_{eff}[\underline{\epsilon}](\mathbf{r}[\underline{\epsilon}])}{\delta \epsilon_{\alpha\beta}} \Big|_{\underline{\epsilon}=0} = \frac{\delta V_{eff}[\underline{\epsilon}](\mathbf{r})}{\delta \epsilon_{\alpha\beta}} \Big|_{\underline{\epsilon}=0} + \frac{\delta \mathbf{r}[\underline{\epsilon}]}{\delta \epsilon_{\alpha\beta}} \cdot \nabla V_{eff}(\mathbf{r}) \quad (\text{C.2})$$

As we know,

$$\frac{\delta \mathbf{r}[\underline{\epsilon}]}{\delta \epsilon_{\alpha\beta}} = \frac{r}{2} (\hat{r}_\beta \hat{\mathbf{e}}_\alpha + \hat{r}_\alpha \hat{\mathbf{e}}_\beta) \quad (\text{C.3})$$

Substituting equation (C.3) in (C.2):

$$\frac{dV_{eff}[\underline{\epsilon}](\mathbf{r}[\underline{\epsilon}])}{d\epsilon_{\alpha\beta}} \Big|_{\underline{\epsilon}=0} = \frac{\delta V_{eff}[\underline{\epsilon}](\mathbf{r})}{\delta \epsilon_{\alpha\beta}} \Big|_{\underline{\epsilon}=0} + \frac{1}{2} (r_\beta \partial_\alpha + r_\alpha \partial_\beta) V_{eff}(\mathbf{r}) \quad (\text{C.4})$$

Then

$$\begin{aligned}
-\frac{1}{\Omega} \frac{\delta}{\delta \epsilon_{\alpha\beta}} \left[ \int_{\Omega[\underline{\epsilon}]} d^3 r_\epsilon \rho[\underline{\epsilon}](\mathbf{r}_\epsilon) V_{eff}[\underline{\epsilon}](\mathbf{r}_\epsilon) \right]_{\underline{\epsilon}=0} &= -\frac{\delta_{\alpha\beta}}{\Omega} \int_{\Omega} d^3 r \rho(\mathbf{r}) V_{eff}(\mathbf{r}) - \frac{1}{\Omega} \int_{\Omega} d^3 r V_{eff}(\mathbf{r}) \frac{\delta \rho[\underline{\epsilon}](\mathbf{r}[\underline{\epsilon}])}{\delta \epsilon_{\alpha\beta}} \Big|_{\underline{\epsilon}=0} \\
&\quad - \frac{1}{\Omega} \int_{\Omega} d^3 r \rho(\mathbf{r}) \left[ \frac{\delta V_{eff}[\underline{\epsilon}](\mathbf{r})}{\delta \epsilon_{\alpha\beta}} \Big|_{\underline{\epsilon}=0} + \frac{1}{2} (r_\beta \partial_\alpha + r_\alpha \partial_\beta) V_{eff}(\mathbf{r}) \right]
\end{aligned} \tag{C.5}$$

Also, with the expression  $V_{eff}(\mathbf{r}) = V_C(\mathbf{r}) + \mu_{xc}(\mathbf{r})$ , the above equation would be:

$$\begin{aligned}
-\frac{1}{\Omega} \frac{\delta}{\delta \epsilon_{\alpha\beta}} \left[ \int_{\Omega[\underline{\epsilon}]} d^3 r_\epsilon \rho[\underline{\epsilon}](\mathbf{r}_\epsilon) V_{eff}[\underline{\epsilon}](\mathbf{r}_\epsilon) \right]_{\underline{\epsilon}=0} &= -\frac{\delta_{\alpha\beta}}{\Omega} \int_{\Omega} d^3 r \rho(\mathbf{r}) V_{eff}(\mathbf{r}) - \frac{1}{\Omega} \int_{\Omega} d^3 r V_C(\mathbf{r}) \frac{\delta \rho[\underline{\epsilon}](\mathbf{r}[\underline{\epsilon}])}{\delta \epsilon_{\alpha\beta}} \Big|_{\underline{\epsilon}=0} \\
-\frac{1}{\Omega} \int_{\Omega} d^3 r \mu_{xc}(\mathbf{r}) \frac{\delta \rho[\underline{\epsilon}](\mathbf{r}[\underline{\epsilon}])}{\delta \epsilon_{\alpha\beta}} \Big|_{\underline{\epsilon}=0} &- \frac{1}{\Omega} \int_{\Omega} d^3 r \rho(\mathbf{r}) \frac{\delta V_{eff}[\underline{\epsilon}](\mathbf{r})}{\delta \epsilon_{\alpha\beta}} \Big|_{\underline{\epsilon}=0} - \frac{1}{2\Omega} \int_{\Omega} d^3 r \rho(\mathbf{r}) (r_\beta \partial_\alpha + r_\alpha \partial_\beta) V_{eff}(\mathbf{r})
\end{aligned} \tag{C.6}$$

The second term of the equation (C.6) cancels with a similar expression from the electrostatic stress, and the third term is balanced by a similar term from our exchange-correlation stress. Also, the fourth term is balanced after combining the strain derivative of the Kohn-Sham eigenvalue for both valence and core states. The valence part of the last term cancels out while the core part persists, and is named as core correction, whose detailed discussion is provided in Chapter 6.2.

# Appendix D

## Janak's Identity

Janak identity asserts that the core correction is equal to twice of the core kinetic energy.

$$-\frac{1}{2} \int_{R_a} d^3 r_a \rho_c^a(\mathbf{r}_a) (r_\alpha \partial_\beta + r_\beta \partial_\alpha) V_{eff}^a(\mathbf{r}_a) = \int_{R_a} d^3 r_a \psi_c^{a*}(\mathbf{r}_a) (\partial_\alpha \partial_\beta + \partial_\beta \partial_\alpha) \psi_c^a(\mathbf{r}_a) \quad (D.1)$$

In APW based methods, all valence states are orthogonal to core states, and this assumption is valid as long as core states are confined entirely inside an atomic sphere. In principle, the core states and their radial derivatives should vanish outside the atomic spheres, but numerically always a small portion of core charge spills out from the region of the atomic spheres. This is known as core leakage, which can be avoided to some extent by either making an atomic sphere bigger or representing semi-core states with local orbitals. Here, the point has to be noted that in case of bigger core leakage this identity would not be valid.

Proof: Let us consider the Kohn-Sham equation and its complex conjugate for the core states.

$$(-\nabla^2 + V_{eff}^a(\mathbf{r}_a)) \psi_c^a(\mathbf{r}_a) = \epsilon_c^a \psi_c^a(\mathbf{r}_a) \quad (D.2a)$$

$$(-\nabla^2 + V_{eff}^a(\mathbf{r}_a)) \psi_c^{a*}(\mathbf{r}_a) = \epsilon_c^a \psi_c^{a*}(\mathbf{r}_a) \quad (D.2b)$$

Now, first apply  $r_\alpha \partial_\beta$  and multiple by  $\psi_c^{a*}(\mathbf{r}_a)$  from the left side in (D.2a) and integrate over the sphere.

$$\begin{aligned} & \int_{R_a} d^3 r_a \psi_c^{a*}(\mathbf{r}_a) r_\alpha \partial_\beta (-\nabla^2 + V_{eff}^a(\mathbf{r}_a)) \psi_c^a(\mathbf{r}_a) \\ &= - \int_{R_a} d^3 r_a \psi_c^{a*}(\mathbf{r}_a) r_\alpha \partial_\beta \nabla^2 \psi_c^a(\mathbf{r}_a) + \int_{R_a} d^3 r_a \psi_c^{a*}(\mathbf{r}_a) r_\alpha \left[ \frac{\partial V_{eff}^a(\mathbf{r}_a)}{\partial r_\beta} \psi_c^a(\mathbf{r}_a) + V_{eff}^a(\mathbf{r}_a) \frac{\partial \psi_c^a(\mathbf{r}_a)}{\partial r_\beta} \right] \\ &= - \int_{R_a} d^3 r_a \psi_c^{a*}(\mathbf{r}_a) r_\alpha \partial_\beta \nabla^2 \psi_c^a(\mathbf{r}_a) + \int_{R_a} d^3 r_a \rho_c^a(\mathbf{r}_a) r_\alpha \partial_\beta V_{eff}^a(\mathbf{r}_a) + \int_{R_a} d^3 r_a \psi_c^{a*}(\mathbf{r}_a) r_\alpha V_{eff}^a(\mathbf{r}_a) \partial_\beta \psi_c^a(\mathbf{r}_a) \end{aligned} \quad (D.3)$$

Again, in another way equations (D.2a) und (D.2b) can be used.

$$\begin{aligned} & \int_{R_a} d^3 r_a \psi_c^{a*}(\mathbf{r}_a) r_\alpha \partial_\beta (-\nabla^2 + V_{eff}^a(\mathbf{r}_a)) \psi_c^a(\mathbf{r}_a) \stackrel{(D.2a)}{=} \epsilon_c^a \int_{R_a} d^3 r_a \psi_c^{a*}(\mathbf{r}_a) r_\alpha \partial_\beta \psi_c^a(\mathbf{r}_a) \\ & \stackrel{(D.2b)}{=} \int_{R_a} d^3 r_a [(-\nabla^2 + V_{eff}^a(\mathbf{r}_a)) \psi_c^{a*}(\mathbf{r}_a)] r_\alpha \partial_\beta \psi_c^a(\mathbf{r}_a) \\ &= - \int_{R_a} d^3 r_a [\nabla^2 \psi_c^{a*}(\mathbf{r}_a)] r_\alpha \partial_\beta \psi_c^a(\mathbf{r}_a) + \int_{R_a} d^3 r_a \psi_c^{a*}(\mathbf{r}_a) V_{eff}^a(\mathbf{r}_a) r_\alpha \partial_\beta \psi_c^a(\mathbf{r}_a) \end{aligned} \quad (D.4)$$

From equations (D.3) and (D.4)

$$\int_{R_a} d^3 r_a \rho_c^a(\mathbf{r}_a) r_\alpha \partial_\beta V_{eff}^a(\mathbf{r}_a) = \int_{R_a} d^3 r_a \psi_c^{a*}(\mathbf{r}_a) r_\alpha \partial_\beta \nabla^2 \psi_c^a(\mathbf{r}_a) - \overbrace{\int_{R_a} d^3 r_a \psi_c^{a*}(\mathbf{r}_a) r_\alpha V_{eff}^a(\mathbf{r}_a) \partial_\beta \psi_c^a(\mathbf{r}_a)}^{(D.5)}$$

$$- \overbrace{\int_{R_a} d^3 r_a [\nabla^2 \psi_c^{a*}(\mathbf{r}_a)] r_\alpha \partial_\beta \psi_c^a(\mathbf{r}_a) + \int_{R_a} d^3 r_a \psi_c^{a*}(\mathbf{r}_a) V_{eff}^a(\mathbf{r}_a) r_\alpha \partial_\beta \psi_c^a(\mathbf{r}_a)}^{(D.6)}$$

With the identity

$$\begin{aligned} \partial_i [\psi_c^{a*}(\mathbf{r}_a) r_\alpha \partial_\beta \partial_i \psi_c^a(\mathbf{r}_a)] &= [\partial_i \psi_c^{a*}(\mathbf{r}_a)] r_\alpha \partial_\beta \partial_i \psi_c^a(\mathbf{r}_a) + \psi_c^{a*}(\mathbf{r}_a) \delta_{i\alpha} \partial_\beta \partial_i \psi_c^a(\mathbf{r}_a) + \psi_c^{a*}(\mathbf{r}_a) r_\alpha \partial_\beta \partial_i \partial_i \psi_c^a(\mathbf{r}_a) \\ &= [\nabla \psi_c^{a*}(\mathbf{r}_a)] r_\alpha \partial_\beta \nabla \psi_c^a(\mathbf{r}_a) + \psi_c^{a*}(\mathbf{r}_a) \partial_\beta \partial_\alpha \psi_c^a(\mathbf{r}_a) + \psi_c^{a*}(\mathbf{r}_a) r_\alpha \partial_\beta \nabla^2 \psi_c^a(\mathbf{r}_a) \\ \partial_i \{[\partial_i \psi_c^{a*}(\mathbf{r}_a)] r_\alpha \partial_\beta \psi_c^a(\mathbf{r}_a)\} &= [\nabla^2 \psi_c^{a*}(\mathbf{r}_a)] r_\alpha \partial_\beta \psi_c^a(\mathbf{r}_a) + [\partial_\alpha \psi_c^{a*}(\mathbf{r}_a)] \partial_\beta \psi_c^a(\mathbf{r}_a) + [\nabla \psi_c^{a*}(\mathbf{r}_a)] r_\alpha \partial_\beta \nabla \psi_c^a(\mathbf{r}_a) \end{aligned} \quad (D.7)$$

Let us use this identity in equation (D.6)

$$\begin{aligned} \int_{R_a} d^3 r_a \rho_c^a(\mathbf{r}_a) r_\alpha \partial_\beta V_{eff}^a(\mathbf{r}_a) &= \int_{R_a} d^3 r_a \nabla \{ \psi_c^{a*}(\mathbf{r}_a) r_\alpha \partial_\beta \nabla \psi_c^a(\mathbf{r}_a) \} - \overbrace{\int_{R_a} d^3 r_a [\nabla \psi_c^{a*}(\mathbf{r}_a)] r_\alpha \partial_\beta \nabla \psi_c^a(\mathbf{r}_a)}^{} - \overbrace{\int_{R_a} d^3 r_a \psi_c^{a*}(\mathbf{r}_a) \partial_\beta \partial_\alpha \psi_c^a(\mathbf{r}_a)}^{} \\ &\quad - \int_{R_a} d^3 r_a \nabla \{ [\nabla \psi_c^{a*}(\mathbf{r}_a)] r_\alpha \partial_\beta \psi_c^a(\mathbf{r}_a) \} + \int_{R_a} d^3 r_a [\partial_\alpha \psi_c^{a*}(\mathbf{r}_a)] \partial_\beta \psi_c^a(\mathbf{r}_a) + \overbrace{\int_{R_a} d^3 r_a [\nabla \psi_c^{a*}(\mathbf{r}_a)] r_\alpha \partial_\beta \nabla \psi_c^a(\mathbf{r}_a)}^{} \\ &= \underbrace{\oint_{\partial B R_a(\mathbf{0})} d\mathbf{A} \{ \psi_c^{a*}(\mathbf{r}_a) r_\alpha \partial_\beta \nabla \psi_c^a(\mathbf{r}_a) \}}_{=0} - \overbrace{\int_{R_a} d^3 r_a \psi_c^{a*}(\mathbf{r}_a) \partial_\beta \partial_\alpha \psi_c^a(\mathbf{r}_a)}^{} - \underbrace{\oint_{\partial B R_a(\mathbf{0})} d\mathbf{A} \{ [\nabla \psi_c^{a*}(\mathbf{r}_a)] r_\alpha \partial_\beta \psi_c^a(\mathbf{r}_a) \}}_{=0} \\ &\quad + \int_{R_a} d^3 r_a [\partial_\alpha \psi_c^{a*}(\mathbf{r}_a)] \partial_\beta \psi_c^a(\mathbf{r}_a) \end{aligned} \quad (D.8)$$

In the above equation the surface integrals are zero due to the fact that core wave functions vanish at the boundary.

$$\int_{R_a} d^3 r_a \rho_c^a(\mathbf{r}_a) r_\alpha \partial_\beta V_{eff}^a(\mathbf{r}_a) = - \int_{R_a} d^3 r_a \psi_c^{a*}(\mathbf{r}_a) \partial_\beta \partial_\alpha \psi_c^a(\mathbf{r}_a) + \int_{R_a} d^3 r_a [\partial_\alpha \psi_c^{a*}(\mathbf{r}_a)] \partial_\beta \psi_c^a(\mathbf{r}_a) \quad (D.9)$$

The last term in the above equation can be further simplified as given below:

$$\begin{aligned} \int_{R_a} d^3 r_a [\partial_\alpha \psi_c^{a*}(\mathbf{r}_a)] \partial_\beta \psi_c^a(\mathbf{r}_a) &= \mathbf{e}_\alpha \cdot \int_{R_a} d^3 r_a [\nabla \psi_c^{a*}(\mathbf{r}_a)] \partial_\beta \psi_c^a(\mathbf{r}_a) \\ &= \mathbf{e}_\alpha \cdot \int_{R_a} d^3 r_a \nabla [\psi_c^{a*}(\mathbf{r}_a) \partial_\beta \psi_c^a(\mathbf{r}_a)] - \mathbf{e}_\alpha \cdot \int_{R_a} d^3 r_a \psi_c^{a*}(\mathbf{r}_a) \nabla \partial_\beta \psi_c^a(\mathbf{r}_a) \\ &= \mathbf{e}_\alpha \cdot \underbrace{\oint_{\partial B R_a(\mathbf{0})} d\mathbf{A} \psi_c^{a*}(\mathbf{r}_a) \partial_\beta \psi_c^a(\mathbf{r}_a)}_{=0} - \int_{R_a} d^3 r_a \psi_c^{a*}(\mathbf{r}_a) \partial_\alpha \partial_\beta \psi_c^a(\mathbf{r}_a) \end{aligned} \quad (D.10)$$

The remaining expression is:

$$\int_{R_a} d^3 r_a \rho_c^a(\mathbf{r}_a) r_\alpha \partial_\beta V_{eff}^a(\mathbf{r}_a) = -\frac{1}{2} \int_{R_a} d^3 r_a \psi_c^{a*}(\mathbf{r}_a) (\partial_\beta \partial_\alpha + \partial_\alpha \partial_\beta) \psi_c^a(\mathbf{r}_a) \quad (D.11)$$

Interchanging  $\alpha$  and  $\beta$

$$\int_{R_a} d^3 r_a \rho_c^a(\mathbf{r}_a) r_\beta \partial_\alpha V_{eff}^a(\mathbf{r}_a) = -\frac{1}{2} \int_{R_a} d^3 r_a \psi_c^{a*}(\mathbf{r}_a) (\partial_\beta \partial_\alpha + \partial_\alpha \partial_\beta) \psi_c^a(\mathbf{r}_a) \quad (D.12)$$

Adding equations (D.11) and (D.12)

$$\frac{1}{2} \int_{R_a} d^3 r_a \rho_c^a(\mathbf{r}_a) \left( r_\alpha \partial_\beta V_{eff}^a(\mathbf{r}_a) + r_\beta \partial_\alpha V_{eff}^a(\mathbf{r}_a) \right) = -\frac{1}{2} \int_{R_a} d^3 r_a \psi_c^{a*}(\mathbf{r}_a) (\partial_\beta \partial_\alpha + \partial_\alpha \partial_\beta) \psi_c^a(\mathbf{r}_a) \quad (D.13)$$

In case of a **hydrostatic** deformation

$$\sum_{\alpha=\beta} \frac{1}{2} \int_{R_a} d^3 r_a \rho_c^a(\mathbf{r}_a) (r_\alpha \partial_\beta V_{eff}^a(\mathbf{r}_a) + r_\beta \partial_\alpha V_{eff}^a(\mathbf{r}_a)) = - \sum_{\alpha=\beta} \frac{1}{2} \int_{R_a} d^3 r_a \psi_c^{a*}(\mathbf{r}_a) (\partial_\beta \partial_\alpha + \partial_\alpha \partial_\beta) \psi_c^a(\mathbf{r}_a) \quad (\text{D.14})$$

$$\int_{R_a} d^3 r_a \rho_c^a(\mathbf{r}_a) \mathbf{r}_a \nabla V_{eff}^a(\mathbf{r}_a) = - \int_{R_a} d^3 r_a \psi_c^{a*}(\mathbf{r}_a) \nabla^2 \psi_c^a(\mathbf{r}_a) = 2E_{kin}^{core} \quad (\text{D.15})$$

The last equation suggests that the core correction for pure (i.e. hydrostatic) pressure is twice the core kinetic energy. This result is contradicting the argument made by Thonhauser *et al.* in section 4.1 in Ref. [12]: ‘for pure pressure the core correction vanishes’.

# Appendix E

## Variation of the electrostatic energy

The simplifications provided in this chapter are used in section 5.2 while the strained variation of the electrostatic energy is simplified. The following steps are used to convert equation (5.23) into equation (5.24). Here, we first consider equation (5.21) and then transform the integral back from the strained system to the un-strained system.

$$\begin{aligned}
E_C[\underline{\epsilon}] &= +\frac{1}{2} \det(\underline{1} + \underline{\epsilon}) \int_{\Omega} d^3r \rho[\underline{\epsilon}](\mathbf{r}[\underline{\epsilon}]) \left[ \det(\underline{1} + \underline{\epsilon}) \int d^3r' \frac{\rho[\underline{\epsilon}](\mathbf{r}'[\underline{\epsilon}])}{|\mathbf{r}[\underline{\epsilon}] - \mathbf{r}'[\underline{\epsilon}]|} - \sum_b \frac{Z_b}{|\mathbf{r}[\underline{\epsilon}] - \boldsymbol{\tau}_b[\underline{\epsilon}]|} \right] \\
&= +\frac{1}{2} \det(\underline{1} + \underline{\epsilon})^2 \int_{\Omega} d^3r \int d^3r' \frac{\rho[\underline{\epsilon}](\mathbf{r}[\underline{\epsilon}]) \rho[\underline{\epsilon}](\mathbf{r}'[\underline{\epsilon}])}{|\mathbf{r}[\underline{\epsilon}] - \mathbf{r}'[\underline{\epsilon}]|} \\
&\quad - \frac{1}{2} \sum_b Z_b \det(\underline{1} + \underline{\epsilon}) \int_{\Omega} d^3r \frac{\rho[\underline{\epsilon}](\mathbf{r}[\underline{\epsilon}])}{|\mathbf{r}[\underline{\epsilon}] - \boldsymbol{\tau}_b[\underline{\epsilon}]|}
\end{aligned} \tag{E.1}$$

The strain variation is

$$\begin{aligned}
\left. \frac{dE_C[\underline{\epsilon}]}{d\underline{\epsilon}_{\alpha\beta}} \right|_{\underline{\epsilon}=0} &= \frac{1}{2} \int_{\Omega} d^3r \int d^3r' \frac{\frac{\partial \rho[\underline{\epsilon}](\mathbf{r}[\underline{\epsilon}])}{\partial \underline{\epsilon}_{\alpha\beta}} \Big|_{\underline{\epsilon}=0} \rho(\mathbf{r}') + \rho(\mathbf{r}) \frac{\partial \rho[\underline{\epsilon}](\mathbf{r}'[\underline{\epsilon}])}{\partial \underline{\epsilon}_{\alpha\beta}} \Big|_{\underline{\epsilon}=0}}{|\mathbf{r} - \mathbf{r}'|} \\
&\quad - \frac{1}{2} \sum_b Z_b \int_{\Omega} d^3r \frac{\frac{\delta \rho[\underline{\epsilon}](\mathbf{r}[\underline{\epsilon}])}{\delta \underline{\epsilon}_{\alpha\beta}} \Big|_{\underline{\epsilon}=0}}{|\mathbf{r} - \boldsymbol{\tau}_b|} + \frac{1}{2} \frac{\partial}{\partial \underline{\epsilon}_{\alpha\beta}} \Bigg|_{\underline{\epsilon}=0} \left\{ \det(\underline{1} + \underline{\epsilon})^2 \int_{\Omega} d^3r \int d^3r' \frac{\rho(\mathbf{r}) \rho(\mathbf{r}')}{|\mathbf{r}[\underline{\epsilon}] - \mathbf{r}'[\underline{\epsilon}]|} \right. \\
&\quad \left. - \frac{1}{2} \sum_b Z_b \det(\underline{1} + \underline{\epsilon}) \int_{\Omega} d^3r \frac{\rho(\mathbf{r})}{|\mathbf{r}[\underline{\epsilon}] - \boldsymbol{\tau}_b[\underline{\epsilon}]|} \right\}
\end{aligned} \tag{E.2}$$

Because of the periodicity of the density  $\rho(\mathbf{r})$ , the first two terms in the first line give the same contribution. In the second line, an inverse transformation (i.e.  $(\underline{1} + \underline{\epsilon})^{-1} = (\underline{1} - \underline{\epsilon}) + O(\underline{\epsilon}^2)$ ) will be used.

$$\begin{aligned}
\left. \frac{dE_C[\underline{\epsilon}]}{d\underline{\epsilon}_{\alpha\beta}} \right|_{\underline{\epsilon}=0} &= \int_{\Omega} d^3r \frac{\partial \rho[\underline{\epsilon}](\mathbf{r}[\underline{\epsilon}])}{\partial \underline{\epsilon}_{\alpha\beta}} \Big|_{\underline{\epsilon}=0} \left[ \int d^3r' \frac{\rho(\mathbf{r}')}{|\mathbf{r} - \mathbf{r}'|} - \frac{1}{2} \sum_b \int_{\Omega} d^3r \frac{Z_b}{|\mathbf{r} - \boldsymbol{\tau}_b|} \right] \\
&\quad + \frac{1}{2} \frac{\partial}{\partial \underline{\epsilon}_{\alpha\beta}} \Bigg|_{\underline{\epsilon}=0} \left\{ \int_{\Omega[\underline{\epsilon}]} d^3r_{\epsilon} \rho((\underline{1} - \underline{\epsilon})\mathbf{r}_{\epsilon}) \left[ \int d^3r'_{\epsilon} \frac{\rho((\underline{1} - \underline{\epsilon})\mathbf{r}'_{\epsilon})}{|\mathbf{r}_{\epsilon} - \mathbf{r}'_{\epsilon}|} - \sum_b \frac{Z_b}{|\mathbf{r}_{\epsilon} - \boldsymbol{\tau}_b[\underline{\epsilon}]|} \right] \right\}
\end{aligned} \tag{E.3}$$

Similarly the strain variation of the Madelung energy is

$$\begin{aligned}
\frac{dE_M[\underline{\epsilon}]}{d\epsilon_{\alpha\beta}} \Bigg|_{\underline{\epsilon}=0} &= -\frac{1}{2} \int d^3r \frac{\partial \rho[\underline{\epsilon}](\mathbf{r}[\underline{\epsilon}])}{\partial \epsilon_{\alpha\beta}} \Bigg|_{\underline{\epsilon}=0} \sum_{a \in \Omega} \frac{Z_a}{|\mathbf{r} - \boldsymbol{\tau}_a|} - \frac{1}{2} \frac{\partial}{\partial \epsilon_{\alpha\beta}} \left[ \sum_{a \in \Omega[\underline{\epsilon}]} Z_a \int d^3\mathbf{r}_\epsilon \frac{\rho((\underline{\epsilon} - \underline{\epsilon})\mathbf{r}_\epsilon)}{|\mathbf{r}_\epsilon - \boldsymbol{\tau}_a[\underline{\epsilon}]|} \right]_{\underline{\epsilon}=0} \\
&\quad + \frac{1}{2} \frac{\partial}{\partial \epsilon_{\alpha\beta}} \left[ \sum_{a \in \Omega} Z_a \sum_{b \neq a} \frac{Z_b}{|\boldsymbol{\tau}_a[\underline{\epsilon}] - \boldsymbol{\tau}_b[\underline{\epsilon}]|} \right]_{\underline{\epsilon}=0} \\
&= -\frac{1}{2} \int d^3r \frac{\partial \rho[\underline{\epsilon}](\mathbf{r}[\underline{\epsilon}])}{\partial \epsilon_{\alpha\beta}} \Bigg|_{\underline{\epsilon}=0} \sum_{a \in \Omega} \frac{Z_a}{|\mathbf{r} - \boldsymbol{\tau}_a|} \\
&\quad - \frac{1}{2} \sum_{a \in \Omega} Z_a \frac{\partial}{\partial \epsilon_{\alpha\beta}} \left[ \int d^3\mathbf{r}_\epsilon \frac{\rho((\underline{\epsilon} - \underline{\epsilon})\mathbf{r}_\epsilon)}{|\mathbf{r}_\epsilon - \boldsymbol{\tau}_a[\underline{\epsilon}]|} - \sum_{b \neq a} \frac{Z_b}{|\boldsymbol{\tau}_a[\underline{\epsilon}] - \boldsymbol{\tau}_b[\underline{\epsilon}]|} \right]_{\underline{\epsilon}=0} \tag{E.4}
\end{aligned}$$

Now, combine the strain derivative of the Coulomb and Madelung energy and separate the variation of the charge density with respect to strain:

$$\begin{aligned}
\frac{d[E_C[\underline{\epsilon}] + E_M[\underline{\epsilon}]]}{d\epsilon_{\alpha\beta}} \Bigg|_{\underline{\epsilon}=0} &= \int_{\Omega} d^3r \frac{\partial \rho[\underline{\epsilon}](\mathbf{r}[\underline{\epsilon}])}{\partial \epsilon_{\alpha\beta}} \Bigg|_{\underline{\epsilon}=0} \left[ \int d^3r' \frac{\rho(\mathbf{r}')}{|\mathbf{r} - \mathbf{r}'|} - \sum_b \int_{\Omega} d^3r \frac{Z_b}{|\mathbf{r} - \boldsymbol{\tau}_b|} \right] \\
&\quad + \frac{1}{2} \frac{\partial}{\partial \epsilon_{\alpha\beta}} \left\{ \int_{\Omega[\underline{\epsilon}]} d^3r_\epsilon \rho((\underline{\epsilon} - \underline{\epsilon})\mathbf{r}_\epsilon) \left[ \int d^3r'_\epsilon \frac{\rho((\underline{\epsilon} - \underline{\epsilon})\mathbf{r}'_\epsilon)}{|\mathbf{r}_\epsilon - \mathbf{r}'_\epsilon|} - \sum_b \frac{Z_b}{|\mathbf{r}_\epsilon - \boldsymbol{\tau}_b[\underline{\epsilon}]|} \right] \right\}_{\underline{\epsilon}=0} \\
&\quad - \frac{1}{2} \sum_{a \in \Omega} Z_a \frac{\partial}{\partial \epsilon_{\alpha\beta}} \left[ \int d^3\mathbf{r}_\epsilon \frac{\rho((\underline{\epsilon} - \underline{\epsilon})\mathbf{r}_\epsilon)}{|\mathbf{r}_\epsilon - \boldsymbol{\tau}_a[\underline{\epsilon}]|} - \sum_{b \neq a} \frac{Z_b}{|\boldsymbol{\tau}_a[\underline{\epsilon}] - \boldsymbol{\tau}_b[\underline{\epsilon}]|} \right]_{\underline{\epsilon}=0} \tag{E.5}
\end{aligned}$$

Replace the expression in the square brackets with the Coulomb potential ( $V_C(\mathbf{r})$ ), the strained Coulomb potential ( $V_C[\underline{\epsilon}](\mathbf{r}_\epsilon)$ ) and the strained Madelung potential ( $V_M[\underline{\epsilon}](\mathbf{r}_\epsilon)$ ) in the first, second, and third lines of the above equation.

$$\begin{aligned}
\frac{d[E_C[\underline{\epsilon}] + E_M[\underline{\epsilon}]]}{d\epsilon_{\alpha\beta}} \Bigg|_{\underline{\epsilon}=0} &= \int_{\Omega} d^3r \frac{\delta \rho[\underline{\epsilon}](\mathbf{r}[\underline{\epsilon}])}{\delta \epsilon_{\alpha\beta}} \Bigg|_{\underline{\epsilon}=0} V_C(\mathbf{r}) + \frac{1}{2} \frac{\delta}{\delta \epsilon_{\alpha\beta}} \left\{ \int_{\Omega[\underline{\epsilon}]} d^3r_\epsilon \rho((\underline{\epsilon} - \underline{\epsilon})\mathbf{r}_\epsilon) V_C[\underline{\epsilon}](\mathbf{r}_\epsilon) \right\}_{\underline{\epsilon}=0} \\
&\quad - \frac{1}{2} \sum_{a \in \Omega} Z_a \frac{\delta}{\delta \epsilon_{\alpha\beta}} V_M[\underline{\epsilon}](\mathbf{r}_\epsilon) \Bigg|_{\underline{\epsilon}=0} \tag{E.6}
\end{aligned}$$

Hence

$$\begin{aligned}
\frac{dE_{es}[\underline{\epsilon}]}{d\epsilon_{\alpha\beta}} \Bigg|_{\underline{\epsilon}=0} &= \int_{\Omega} d^3r \frac{\delta \rho[\underline{\epsilon}](\mathbf{r}[\underline{\epsilon}])}{\delta \epsilon_{\alpha\beta}} \Bigg|_{\underline{\epsilon}=0} V_C(\mathbf{r}) + \frac{1}{2} \frac{\delta}{\delta \epsilon_{\alpha\beta}} \left\{ \int_{\Omega[\underline{\epsilon}]} d^3r_\epsilon \rho((\underline{\epsilon} - \underline{\epsilon})\mathbf{r}_\epsilon) V_C[\underline{\epsilon}](\mathbf{r}_\epsilon) \right\}_{\underline{\epsilon}=0} \\
&\quad - \frac{1}{2} \sum_{a \in \Omega} Z_a \frac{\delta}{\delta \epsilon_{\alpha\beta}} V_M[\underline{\epsilon}](\mathbf{r}_\epsilon) \Bigg|_{\underline{\epsilon}=0} \tag{E.7}
\end{aligned}$$

# Appendix F

## Calculation of the strain variation of Kohn-Sham eigenvalue

The effective one-electron Kohn-Sham equation for valence states  $\psi_{v\mathbf{k}}(\mathbf{r})$  is

$$\left(-\frac{1}{2}\nabla^2 + V_{eff}(\mathbf{r})\right)\psi_{v\mathbf{k}}(\mathbf{r}) = \epsilon_{v\mathbf{k}}\psi_{v\mathbf{k}}(\mathbf{r}) \quad (\text{F.1})$$

Multiply from the left by  $\psi_{v\mathbf{k}}^*(\mathbf{r})$  and integrate over  $\Omega$ :

$$\int_{\Omega} d^3r \psi_{v\mathbf{k}}^*(\mathbf{r}) \left(-\frac{1}{2}\nabla^2 + V_{eff}(\mathbf{r})\right) \psi_{v\mathbf{k}}(\mathbf{r}) = \epsilon_{v\mathbf{k}} \int_{\Omega} d^3r \psi_{v\mathbf{k}}^*(\mathbf{r}) \psi_{v\mathbf{k}}(\mathbf{r}) \quad (\text{F.2})$$

In the strained environment, equation F.2 would be

$$\int_{\Omega[\underline{\epsilon}]} d^3r_{\epsilon} \psi_{v\mathbf{k}[\underline{\epsilon}][\underline{\epsilon}]}^*(\mathbf{r}_{\epsilon}) \left(-\frac{1}{2}\nabla_{\epsilon}^2 + V_{eff}[\underline{\epsilon}](\mathbf{r}_{\epsilon})\right) \psi_{v\mathbf{k}[\underline{\epsilon}][\underline{\epsilon}]}(\mathbf{r}_{\epsilon}) = \epsilon_{v\mathbf{k}[\underline{\epsilon}][\underline{\epsilon}]} \int_{\Omega[\underline{\epsilon}]} d^3r_{\epsilon} \psi_{v\mathbf{k}[\underline{\epsilon}][\underline{\epsilon}]}^*(\mathbf{r}_{\epsilon}) \psi_{v\mathbf{k}[\underline{\epsilon}][\underline{\epsilon}]}(\mathbf{r}_{\epsilon})$$

Using the integral transformation  $\int_{\Omega[\underline{\epsilon}]} d^3r_{\epsilon} = \det(\underline{1} + \underline{\epsilon}) \int_{\Omega} d^3r$

$$\begin{aligned} & \cancel{\det(\underline{1} + \underline{\epsilon})} \int_{\Omega} d^3r \psi_{v\mathbf{k}[\underline{\epsilon}][\underline{\epsilon}]}^*(\mathbf{r}[\underline{\epsilon}]) \left(-\frac{1}{2}[(\underline{1} - \underline{\epsilon})\nabla]^2 + V_{eff}[\underline{\epsilon}](\mathbf{r}[\underline{\epsilon}])\right) \psi_{v\mathbf{k}[\underline{\epsilon}][\underline{\epsilon}]}(\mathbf{r}[\underline{\epsilon}]) \\ &= \epsilon_{v\mathbf{k}[\underline{\epsilon}][\underline{\epsilon}]} \cancel{\det(\underline{1} + \underline{\epsilon})} \int_{\Omega} d^3r \psi_{v\mathbf{k}[\underline{\epsilon}][\underline{\epsilon}]}^*(\mathbf{r}[\underline{\epsilon}]) \psi_{v\mathbf{k}[\underline{\epsilon}][\underline{\epsilon}]}(\mathbf{r}[\underline{\epsilon}]) \end{aligned} \quad (\text{F.3})$$

Rearranging the terms to get strained Kohn-Sham eigen value

$$\epsilon_{v\mathbf{k}[\underline{\epsilon}][\underline{\epsilon}]} = \frac{\int_{\Omega} d^3r \psi_{v\mathbf{k}[\underline{\epsilon}][\underline{\epsilon}]}^*(\mathbf{r}[\underline{\epsilon}]) (-\frac{1}{2}[(\underline{1} - \underline{\epsilon})\nabla]^2 + V_{eff}[\underline{\epsilon}](\mathbf{r}[\underline{\epsilon}])) \psi_{v\mathbf{k}[\underline{\epsilon}][\underline{\epsilon}]}(\mathbf{r}[\underline{\epsilon}])}{\int_{\Omega} d^3r \psi_{v\mathbf{k}[\underline{\epsilon}][\underline{\epsilon}]}^*(\mathbf{r}[\underline{\epsilon}]) \psi_{v\mathbf{k}[\underline{\epsilon}][\underline{\epsilon}]}(\mathbf{r}[\underline{\epsilon}])} \quad (\text{F.4})$$

We consider an operator  $\widehat{O}$  which depends explicitly on  $\mathbf{r}$  and implicitly on  $\underline{\epsilon}$ .

$$O(\underline{\epsilon}) = \frac{\sum_{a \in \Omega} \int_{\Omega} d^3r \psi_{v\mathbf{k}[\underline{\epsilon}][\underline{\epsilon}]}^*(\mathbf{r}_{\epsilon}) \widehat{O}[\underline{\epsilon}](\mathbf{r}_{\epsilon}) \psi_{v\mathbf{k}[\underline{\epsilon}][\underline{\epsilon}]}(\mathbf{r}_{\epsilon})}{\sum_{a \in \Omega} \int_{\Omega} d^3r \psi_{v\mathbf{k}[\underline{\epsilon}][\underline{\epsilon}]}^*(\mathbf{r}_{\epsilon}) \psi_{v\mathbf{k}[\underline{\epsilon}][\underline{\epsilon}]}(\mathbf{r}_{\epsilon})} \quad (\text{F.5})$$

For the sake of brevity take only the numerator

$$\begin{aligned} \frac{d(\text{numerator}[\underline{\epsilon}])}{d\epsilon_{\alpha\beta}} \Big|_{\underline{\epsilon}=0} &= \sum_{a \in \Omega} \int_{\Omega} d^3r \frac{d\psi_{v\mathbf{k}[\underline{\epsilon}][\underline{\epsilon}]}^*(\mathbf{r}_{\epsilon})}{d\epsilon_{\alpha\beta}} \Big|_{\underline{\epsilon}=0} \widehat{O}(\mathbf{r}) \psi_{v\mathbf{k}}(\mathbf{r}) + \sum_{a \in \Omega} \int_{\Omega} d^3r \psi_{v\mathbf{k}}^*(\mathbf{r}) \widehat{O}(\mathbf{r}) \frac{d\psi_{v\mathbf{k}[\underline{\epsilon}][\underline{\epsilon}]}(\mathbf{r}_{\epsilon})}{d\epsilon_{\alpha\beta}} \Big|_{\underline{\epsilon}=0} \\ &+ \sum_{a \in \Omega} \int_{\Omega} d^3r \psi_{v\mathbf{k}}^*(\mathbf{r}) \frac{d\widehat{O}[\underline{\epsilon}](\mathbf{r}_{\epsilon})}{d\epsilon_{\alpha\beta}} \Big|_{\underline{\epsilon}=0} \psi_{v\mathbf{k}}(\mathbf{r}) \end{aligned}$$

In more compact form

$$\begin{aligned} \frac{d(\text{numerator}[\underline{\epsilon}])}{d\epsilon_{\alpha\beta}} \Big|_{\underline{\epsilon}=0} &= \left\langle \frac{d\psi_{v\mathbf{k}}[\underline{\epsilon}](\mathbf{r}[\underline{\epsilon}])}{d\epsilon_{\alpha\beta}} \Big|_{\underline{\epsilon}=0} \middle| \widehat{O}(\mathbf{r}) \middle| \psi_{v\mathbf{k}}(\mathbf{r}) \right\rangle + \left\langle \psi_{v\mathbf{k}}(\mathbf{r}) \middle| \widehat{O}(\mathbf{r}) \middle| \frac{d\psi_{v\mathbf{k}}[\underline{\epsilon}](\mathbf{r}[\underline{\epsilon}])}{d\epsilon_{\alpha\beta}} \Big|_{\underline{\epsilon}=0} \right\rangle \\ &\quad + \left\langle \psi_{v\mathbf{k}}(\mathbf{r}) \middle| \frac{d\widehat{O}[\underline{\epsilon}](\mathbf{r}[\underline{\epsilon}])}{d\epsilon_{\alpha\beta}} \Big|_{\underline{\epsilon}=0} \middle| \psi_{v\mathbf{k}}(\mathbf{r}) \right\rangle \end{aligned}$$

The denominator is derived simply by replacing  $\widehat{O}(\mathbf{r}) \rightarrow 1$ :

$$\frac{d(\text{denominator}[\underline{\epsilon}])}{d\epsilon_{\alpha\beta}} \Big|_{\underline{\epsilon}=0} = \int_{\Omega} d^3 r \frac{d\psi_{v\mathbf{k}}^*[\underline{\epsilon}](\mathbf{r}[\underline{\epsilon}])}{d\epsilon_{\alpha\beta}} \Big|_{\underline{\epsilon}=0} \psi_{v\mathbf{k}}(\mathbf{r}) + \int_{\Omega} d^3 r \psi_{v\mathbf{k}}^*(\mathbf{r}) \frac{d\psi_{v\mathbf{k}}[\underline{\epsilon}](\mathbf{r}[\underline{\epsilon}])}{d\epsilon_{\alpha\beta}} \Big|_{\underline{\epsilon}=0}$$

In more compact form

$$\frac{d(\text{denominator}[\underline{\epsilon}])}{d\epsilon_{\alpha\beta}} \Big|_{\underline{\epsilon}=0} = \left\langle \frac{d\psi_{v\mathbf{k}}[\underline{\epsilon}](\mathbf{r}[\underline{\epsilon}])}{d\epsilon_{\alpha\beta}} \Big|_{\underline{\epsilon}=0} \middle| \psi_{v\mathbf{k}}(\mathbf{r}) \right\rangle + \left\langle \psi_{v\mathbf{k}}(\mathbf{r}) \middle| \frac{d\psi_{v\mathbf{k}}[\underline{\epsilon}](\mathbf{r}[\underline{\epsilon}])}{d\epsilon_{\alpha\beta}} \Big|_{\underline{\epsilon}=0} \right\rangle \quad (\text{F.6})$$

For the total calculation the chain rule is adopted.

$$\begin{aligned} \frac{dO(\underline{\epsilon})}{d\epsilon_{\alpha\beta}} \Big|_{\underline{\epsilon}=0} &= \frac{1}{\text{denominator}[0]} \frac{d(\text{numerator}[\underline{\epsilon}])}{d\epsilon_{\alpha\beta}} \Big|_{\underline{\epsilon}=0} - \frac{\text{numerator}[0]}{(\text{denominator}[0])^2} \frac{d(\text{denominator}[\underline{\epsilon}])}{d\epsilon_{\alpha\beta}} \Big|_{\underline{\epsilon}=0} \\ &= \frac{1}{1} \frac{d(\text{numerator}[\underline{\epsilon}])}{d\epsilon_{\alpha\beta}} \Big|_{\underline{\epsilon}=0} - \frac{\text{numerator}[0]}{1} \frac{d(\text{denominator}[\underline{\epsilon}])}{d\epsilon_{\alpha\beta}} \Big|_{\underline{\epsilon}=0} \quad (\text{F.7}) \end{aligned}$$

Also

$$O_v(\mathbf{k}) = \left\langle \psi_{v\mathbf{k}} \middle| \widehat{O}(\mathbf{r}) \middle| \psi_{v\mathbf{k}} \right\rangle \quad (\text{F.8})$$

and

$$\text{numerator}[0] = O_v(\mathbf{k}) \quad (\text{F.9})$$

Now, collecting all above terms

$$\begin{aligned} \frac{dO(\underline{\epsilon})}{d\epsilon_{\alpha\beta}} \Big|_{\underline{\epsilon}=0} &= \left\langle \frac{d\psi_{v\mathbf{k}}[\underline{\epsilon}](\mathbf{r}[\underline{\epsilon}])}{d\epsilon_{\alpha\beta}} \Big|_{\underline{\epsilon}=0} \middle| \widehat{O}(\mathbf{r}) \middle| \psi_{v\mathbf{k}}(\mathbf{r}) \right\rangle + \left\langle \psi_{v\mathbf{k}}(\mathbf{r}) \middle| \widehat{O}(\mathbf{r}) \middle| \frac{d\psi_{v\mathbf{k}}[\underline{\epsilon}](\mathbf{r}[\underline{\epsilon}])}{d\epsilon_{\alpha\beta}} \Big|_{\underline{\epsilon}=0} \right\rangle \\ &\quad + \left\langle \psi_{v\mathbf{k}}(\mathbf{r}) \middle| \frac{d\widehat{O}[\underline{\epsilon}](\mathbf{r}[\underline{\epsilon}])}{d\epsilon_{\alpha\beta}} \Big|_{\underline{\epsilon}=0} \middle| \psi_{v\mathbf{k}}(\mathbf{r}) \right\rangle - O_v(\mathbf{k}) \left\{ \left\langle \frac{d\psi_{v\mathbf{k}}[\underline{\epsilon}](\mathbf{r}[\underline{\epsilon}])}{d\epsilon_{\alpha\beta}} \Big|_{\underline{\epsilon}=0} \middle| \psi_{v\mathbf{k}} \right\rangle \right. \\ &\quad \left. + \left\langle \psi_{v\mathbf{k}}(\mathbf{r}) \middle| \frac{d\psi_{v\mathbf{k}}[\underline{\epsilon}](\mathbf{r}[\underline{\epsilon}])}{d\epsilon_{\alpha\beta}} \Big|_{\underline{\epsilon}=0} \right\rangle \right\} \quad (\text{F.10}) \end{aligned}$$

i.e

$$\begin{aligned} \frac{dO(\underline{\epsilon})}{d\epsilon_{\alpha\beta}} \Big|_{\underline{\epsilon}=0} &= \left\langle \frac{d\psi_{v\mathbf{k}}[\underline{\epsilon}](\mathbf{r}[\underline{\epsilon}])}{d\epsilon_{\alpha\beta}} \Big|_{\underline{\epsilon}=0} \middle| \widehat{O}(\mathbf{r}) - O_v(\mathbf{k}) \middle| \psi_{v\mathbf{k}}(\mathbf{r}) \right\rangle + \left\langle \psi_{v\mathbf{k}}(\mathbf{r}) \middle| \widehat{O}(\mathbf{r}) - O_v(\mathbf{k}) \middle| \frac{d\psi_{v\mathbf{k}}[\underline{\epsilon}](\mathbf{r}[\underline{\epsilon}])}{d\epsilon_{\alpha\beta}} \Big|_{\underline{\epsilon}=0} \right\rangle \\ &\quad + \left\langle \psi_{v\mathbf{k}}(\mathbf{r}) \middle| \frac{d\widehat{O}[\underline{\epsilon}](\mathbf{r}[\underline{\epsilon}])}{d\epsilon_{\alpha\beta}} \Big|_{\underline{\epsilon}=0} \middle| \psi_{v\mathbf{k}}(\mathbf{r}) \right\rangle \end{aligned}$$

For further simplification, the following steps are adopted.

$$\hat{O}(\mathbf{r}) \equiv \hat{H}_{eff}(\mathbf{r}) = -\frac{1}{2}\nabla^2 + V_{eff}(\mathbf{r}), \quad O_v(\mathbf{k}) = \epsilon_v(\mathbf{k}) \quad (\text{F.11})$$

Then

$$\hat{O}[\underline{\epsilon}](\mathbf{r}[\underline{\epsilon}]) = -\frac{1}{2}[(\underline{1} - \underline{\epsilon})\nabla]^2 + V_{eff}[\underline{\epsilon}](\mathbf{r}[\underline{\epsilon}]) \quad (\text{F.12})$$

We know

$$\begin{aligned} [(\underline{1} - \underline{\epsilon})\nabla]^2 &= (\delta_{\gamma\delta} - \epsilon_{\gamma\delta})(\delta_{\gamma\sigma} - \epsilon_{\gamma\sigma})\partial_\delta\partial_\sigma &= [\delta_{\delta\sigma} - \epsilon_{\delta\sigma} - \epsilon_{\sigma\delta} + O(\underline{\epsilon}^2)]\partial_\delta\partial_\sigma \\ &= \nabla^2 - \epsilon_{\delta\sigma}\partial_\delta\partial_\sigma - \epsilon_{\sigma\delta}\partial_\delta\partial_\sigma + O(\underline{\epsilon}^2) \end{aligned} \quad (\text{F.13})$$

so

$$\hat{O}[\underline{\epsilon}](\mathbf{r}[\underline{\epsilon}]) = -\frac{1}{2}[\nabla^2 - \epsilon_{\delta\sigma}\partial_\delta\partial_\sigma - \epsilon_{\sigma\delta}\partial_\delta\partial_\sigma + O(\underline{\epsilon}^2)] + V_{eff}[\underline{\epsilon}](\mathbf{r}[\underline{\epsilon}]) \quad (\text{F.14})$$

from which

$$\frac{d\hat{O}[\underline{\epsilon}](\mathbf{r}[\underline{\epsilon}])}{d\epsilon_{\alpha\beta}} \Big|_{\underline{\epsilon}=0} = \frac{1}{2}(\partial_\alpha\partial_\beta + \partial_\beta\partial_\alpha) + \frac{dV_{eff}[\underline{\epsilon}](\mathbf{r}[\underline{\epsilon}])}{d\epsilon_{\alpha\beta}} \Big|_{\underline{\epsilon}=0} \quad (\text{F.15})$$

follows. Thus we obtain

$$\begin{aligned} \frac{d\epsilon_{v\mathbf{k}}[\underline{\epsilon}]}{d\epsilon_{\alpha\beta}} \Big|_{\underline{\epsilon}=0} &= \left\langle \frac{d\psi_{v\mathbf{k}}[\underline{\epsilon}](\mathbf{r}[\underline{\epsilon}])}{d\epsilon_{\alpha\beta}} \Big|_{\underline{\epsilon}=0} \right\rangle \left| \hat{H}_{eff}(\mathbf{r}) - \epsilon_{v\mathbf{k}} \right| \psi_{v\mathbf{k}}(\mathbf{r}) + \left\langle \psi_{v\mathbf{k}}(\mathbf{r}) \right| \hat{H}_{eff}(\mathbf{r}) - \epsilon_{v\mathbf{k}} \left| \frac{d\psi_{v\mathbf{k}}[\underline{\epsilon}](\mathbf{r}[\underline{\epsilon}])}{d\epsilon_{\alpha\beta}} \Big|_{\underline{\epsilon}=0} \right\rangle \\ &\quad + \left\langle \psi_{v\mathbf{k}}(\mathbf{r}) \right| \frac{1}{2}(\partial_\alpha\partial_\beta + \partial_\beta\partial_\alpha) + \frac{dV_{eff}[\underline{\epsilon}](\mathbf{r}[\underline{\epsilon}])}{d\epsilon_{\alpha\beta}} \Big|_{\underline{\epsilon}=0} \left| \psi_{v\mathbf{k}}(\mathbf{r}) \right\rangle \end{aligned} \quad (\text{F.16})$$

or

$$\begin{aligned} \frac{d\epsilon_{v\mathbf{k}}[\underline{\epsilon}]}{d\epsilon_{\alpha\beta}} \Big|_{\underline{\epsilon}=0} &= 2\Re \left\langle \frac{d\psi_{v\mathbf{k}}[\underline{\epsilon}](\mathbf{r}[\underline{\epsilon}])}{d\epsilon_{\alpha\beta}} \Big|_{\underline{\epsilon}=0} \right\rangle \left| \hat{H}_{eff}(\mathbf{r}) - \epsilon_{v\mathbf{k}} \right| \psi_{v\mathbf{k}}(\mathbf{r}) + \left\langle \psi_{v\mathbf{k}}(\mathbf{r}) \right| \frac{1}{2}(\partial_\alpha\partial_\beta + \partial_\beta\partial_\alpha) \left| \psi_{v\mathbf{k}}(\mathbf{r}) \right\rangle \\ &\quad + \left\langle \psi_{v\mathbf{k}}(\mathbf{r}) \right| \frac{dV_{eff}[\underline{\epsilon}](\mathbf{r}[\underline{\epsilon}])}{d\epsilon_{\alpha\beta}} \Big|_{\underline{\epsilon}=0} \left| \psi_{v\mathbf{k}}(\mathbf{r}) \right\rangle \end{aligned} \quad (\text{F.17})$$

where  $\frac{d\psi_{v\mathbf{k}}[\underline{\epsilon}](\mathbf{r}[\underline{\epsilon}])}{d\epsilon_{\alpha\beta}} \Big|_{\underline{\epsilon}=0}$  has an explicit dependency in  $\underline{\epsilon}$  and implicit dependency through

$\mathbf{r}_\epsilon$ . Using of the frozen augmentation approximation[31, 37], an explicit dependency on  $\underline{\epsilon}$  as a result of linear response is discarded in the matching condition while keeping an implicit dependency. Also, in the equation (F.17) the first and the second terms are the valence correction and the valence kinetic stress. They are denoted as follows.

$$\sigma_{\alpha\beta}^{val,corr} = \frac{2}{\Omega} \sum_{v\mathbf{k}} n_{v\mathbf{k}} \Re \left\langle \frac{d\psi_{v\mathbf{k}}[\underline{\epsilon}](\mathbf{r}[\underline{\epsilon}])}{d\epsilon_{\alpha\beta}} \Big|_{\underline{\epsilon}=0} \right\rangle \left| \hat{H}_{eff}(\mathbf{r}) - \epsilon_{v\mathbf{k}} \right| \psi_{v\mathbf{k}}(\mathbf{r}) \quad (\text{F.18a})$$

$$\sigma_{\alpha\beta}^{val,kin} = \frac{1}{2\Omega} \sum_{v\mathbf{k}} n_{v\mathbf{k}} \langle \psi_{v\mathbf{k}}(\mathbf{r}) | \partial_\alpha\partial_\beta + \partial_\beta\partial_\alpha | \psi_{v\mathbf{k}}(\mathbf{r}) \rangle \quad (\text{F.18b})$$

$\sigma_{\alpha\beta}^{val,corr}$  is the valence correction originating due to the finite size of the basis function, and sometimes referred to as an incomplete basis set correction. This correction would have vanished if we had used either a basis set that does not depend on atomic positions or a complete basis set to describe the valence states.  $\sigma_{\alpha\beta}^{val,kin}$  is the valence kinetic stress tensor. Also, if the calculations are converged,  $\psi_{v\mathbf{k}}(\mathbf{r})$  and its first derivative should be continuous at the sphere boundary (at least for sufficiently large  $l_{max}$ ).

# Bibliography

# Bibliography

- [1] R. M. Dreizler and E. K. U. Gross, *Density Functional Theory*, Springer-Verlag (1990), ISBN 3-540-51993-9.
- [2] R. G. Parr, W. Yang, *Density-functional theory of atoms and molecules*, Oxford University Press, New York (1989).
- [3] O. H. Nielsen and R. M. Martin, Phys. Rev. Lett. **50**, 697 (1983).
- [4] O. H. Nielsen and R. M. Martin, Phys. Rev. B **32**, 3792 (1985).
- [5] D. M. Ceperley and B. J. Alder, Phys. Rev. Lett. , **45**, 566 (1980).
- [6] J. P. Perdew and A. Zunger, Phys. Rev. B**23**, 5048 (1981).
- [7] A. D. Corso and R. Resta, Phys. Rev. B **50**, 4327 (1994).
- [8] M. Torrent, F. Jollet, F. Bottin, G. Zrah, and X. Gonze, Comput. Mater. Sci. **42**, 337 (2008).
- [9] T. L. Loucks, *Augmented Plane Wave method: a guide to performing electronic structure calculations*, Benjamin, New York (1967).
- [10] S. Cottenier, *Density Functional Theory and the family of (L)APW-methods: a step-by-step introduction*, 2002-2013 2<sup>nd</sup> Ed., ISBN 978-90-807215-1-7.
- [11] J.O. Dimmock, J. Phys. C: Solid State Phys, **26**, 103 (1971)
- [12] T. Thonhauser, C. Ambrosch-Draxl, and D. J. Singh, Solid State Commun. **124** 275 (2002).
- [13] P. Blaha, K. Schwarz, G. K. H. Madsen, D. Kvasnicka, J. Luitz, R. Laskowski, F. Tran, and L. D. Marks, Vienna University of Technology, Vienna, Austria.
- [14] P. Blaha, K. Schwarz, F. Tran, R. Laskowski, G. K. H. Madsen, and L. D. Marks, J. Chem. Phys. **152**, 074101 (2020).
- [15] J. M. Soler and A. R. Williams, Phys. Rev. B **40**, 1560 (1989).
- [16] J. M. Soler and A. R. Williams, Phys. Rev. B **42**, 9728 (1990).
- [17] N. Nagasako and T. Oguchi, J. Phys. Soc. Jap **80**, 024701 (2011).
- [18] N. Nagasako and T. Oguchi, J. Phys. Soc. Jap **82**, 044701 (2013).
- [19] D. A. Klüppelberg, Diploma thesis, RWTH Aachen, 2011.

- [20] <https://www.flapw.de/MaX-5.1/>
- [21] [https://en.wikipedia.org/wiki/Stress%E2%80%93strain\\_curve](https://en.wikipedia.org/wiki/Stress%E2%80%93strain_curve)
- [22] P. Hohenberg and W. Kohn, Phys. Rev. **136**, B864 (1964).
- [23] W. Kohn and L. J. Sham, Phys. Rev. **140**, A1133 (1965).
- [24] J. C. Slater, Phys. Rev. B **51**, 846 (1937).
- [25] O. K. Anderson, Phys. Rev. B**12**, 3060 (1975).
- [26] D. D. Koelling and G.O. Arbman, J. Phys. F **5**, 2041 (1975).
- [27] E. Sjöstedt, L. Nordström, and D. J. Singh, Solid State Commun. **114**, 15 (2000).
- [28] G. K. H. Madsen, P. Blaha, K. Schwarz, E. Sjöstedt, and L. Nordström, Phys. Rev. B**64**, 195134, (2001).
- [29] D. J. Singh, Phys. Rev. B **43**, 6388 (1991).
- [30] D. J. Singh and L. Nordström, *Planewaves, Pseudopotentials, and the LAPW method*, 2<sup>nd</sup> Ed. (Springer, New York, 2006).
- [31] R. Yu, D. Singh, and H. Krakauer, Phys. Rev. B **43**, 6411 (1991).
- [32] P. J. Feibelman, Phys. Rev. B **44**, 3916 (1991).
- [33] M. Kara and K. Kurki-Suonio, Acta Crystallogr. Sect. A **37**, 201 (1981)
- [34] M. Weinert, E. Wimmer, and A. J. Freeman, Phys. Rev. **26**, 4571 (1982)
- [35] M. Weinert, J. Math. Phys. **22**, 2433 (1981)
- [36] P. E. Blöchl, O. Jepsen, and O. K. Anderson, Phys. Rev. B **49**, 16223 (1994).
- [37] S. Goedecker and K. Maschke, Phys. Rev. B **45**, 1597 (1992).
- [38] J. P. Perdew, K. Burke, and M. Ernzerhof, Phys. Rev. Lett. **77**, 3865 (1996)
- [39] J. P. Perdew, K. Burke, and M. Ernzerhof, Phys. Rev. Lett. **78**, 1396 (1997)
- [40] <https://www.tddft.org/programs/libxc/manual/>
- [41] [http://www.netlib.org/lapack/explore-html/d7/d2b/dgemm\\_8f.html](http://www.netlib.org/lapack/explore-html/d7/d2b/dgemm_8f.html)
- [42] [http://www.netlib.org/lapack/explore-html/d7/d76/zgemm\\_8f.html](http://www.netlib.org/lapack/explore-html/d7/d76/zgemm_8f.html)
- [43] F. Knuth, C. Carbogno, V. Atalla, V. Blum, and M. Scheffler, Com. Phys. Comm. **190**, 33-50 (2015).
- [44] J. F. Janak, Phys. Rev. B **9**, 3985 (1974).
- [45] F. Giustino, *Materials modelling using density functional theory*, Oxford University press, p98, 2014
- [46] A. R. Edmonds, *Angular Momentum in Quantum Mechanics*, Princeton University Press (1985).

- [47] D. D. Koelling and B. N. Harmon, J. Phys. C: Solid St. Phys. **10**, 3107 (1977)
- [48] M. Weinert and J. W. Davenport, Phys. Rev. B **45**, 13709 (1992)
- [49] M. Kara and K. Kuri-Suonig, Acta Cryst., A37:201. xiii, 150 (1981)

# Chapter 10

## List of Publication

1. **K. Belbase**, A. Tröster and P. Blaha. Extension of the stress tensor for the augmented plane wave method with local orbital and the Generalized Gradient Approximation. (preparation)
2. **K. Belbase**, A. Tröster and P. Blaha. Stress tensor in the linearized augmented plane wave method, Phys. Rev. B 104, 174113 (2021).
3. A. Tröster, W. Schranz, S. Ehsan, **K. Belbase** and P. Blaha. Symmetry Adapted Finite Strain Landau Theory Applied to KMnF<sub>3</sub>, Crystals 2020, 10(2), 124.
4. A. Tröster, S. Ehsan, **K. Belbase**, P. Blaha, J. Kreisel and W. Schranz. Finite strain Landau theory applied to the high pressure phase transition of lead titanate. Phys. Rev. B 95, 064111 (2017).

# Stress tensor in augmented plane wave methods II: Extension to APW+lo and GGA

Kamal Belbase,<sup>1</sup> Andreas Tröster,<sup>2</sup> and Peter Blaha<sup>1</sup>

<sup>1</sup>*Institute of Materials Chemistry, Vienna University of Technology,  
Getreidemarkt 9/165-TC, A-1060 Vienna, Austria*

<sup>2</sup>*Faculty of Physics, University of Vienna, Boltzmannngasse 5, A-1090 Vienna, Austria*

In this paper we present a detailed extension of our previously derived stress tensor formalism for the linearized augmented plane wave (LAPW) method and the local density approximation (LDA) to the APW plus local orbital (lo) method and the generalized gradient approximation (GGA). The final formalism is implemented in the WIEN2k code and tested by comparing the result of the stress tensor formalism with the corresponding results derived from total energies. Convergence tests with respect to the basis set size are carried out and prove the superior convergence of the stress tensor in the APW+lo method as compared to LAPW. The basis set size needs to be increased slightly compared to total energy calculations. The importance of the additional surface term in the APW+lo method and the additional contribution for GGA is discussed in detail and their influence on the calculated lattice parameters is shown.

## I. INTRODUCTION

A primary goal of density functional theory (DFT) based electronic structure calculations in crystalline systems is the determination of the equilibrium crystal structure at a prescribed external stress. This generally implies that the forces on all atoms must vanish and the calculated stress should also vanish or adopt the pre-selected nonzero hydrostatic or uniaxial stress. Forces and stress, however, are not directly controllable parameters, but are determined by the individual atomic positions as well as the lattice vectors. Therefore, our task is to relax the atomic positions and – at the same time – determine the correct set of lattice vectors, or, sometimes more simple, one or more unit cell parameters, that yield the desired external stress. In order to carry out this task efficiently, it is mandatory to develop efficient algorithms that allow to compute all derivatives of the total energy with respect to atomic positions and strain based on a single DFT run, thus avoiding a tedious and expensive naive approach of fitting an excessive number of single DFT calculations of carefully selected individual configurations. For a low symmetry system, which can easily have tens to hundreds of structural parameters, such a brute force strategy would obviously become completely intractable.

The mathematics of plane wave-based pseudopotential methods is comparatively simple, and a convenient force and stress formalism has indeed been already developed a long time ago<sup>1,2</sup> and implemented into DFT codes that use plane waves as basis functions. In contrast, for all-electron augmented plane wave (APW) based codes, up to recently only a force formalism has been successfully developed<sup>3,4</sup>. In two papers<sup>5,6</sup> a stress tensor for the Soler-Williams LAPW method<sup>7,8</sup> was finally offered, but unfortunately these works are not compatible with the standard linear augmented plane wave (LAPW) method proposed by Anderson<sup>9</sup>. These two methods differ in particular in the definition of the basis functions inside the atomic spheres and the representation of the charge

density, which induces grave differences between the corresponding stress formalisms. Therefore, the work presented in Refs. 5 and 6 cannot be directly adopted to standard APW-based methods. It should also be mentioned that almost 20 years ago Thonhauser et al.<sup>10</sup> published a formalism for the stress in the LAPW method, but apparently it worked only for hydrostatic pressure in cubic systems. Hence it is fair to say that only recently the present authors developed and implemented a fully functioning stress tensor formalism for the standard LAPW method<sup>11</sup>.

The purpose of our present paper is to extend our previous formalism<sup>11</sup> for the standard LAPW method and the local density approximation (LDA)<sup>12</sup> to (i) the much more efficient augmented plane wave plus local orbital (APW+lo)<sup>13–16</sup> method and (ii) to the generalized gradient approximation (GGA)<sup>17,18</sup>, which is the standard family of DFT functionals in present solid state calculations.

This manuscript is organized as follows: Section II introduces and summarizes the APW based methods and the semi-core local orbitals (LO). Section III A deals with the modifications of the LAPW stress tensor formalism for APW+lo and the derivation of additional contributions in the GGA. Section IV presents numerical tests probing the accuracy of the stress tensor with respect to the choice of various numerical parameters and the significance of the earlier mentioned surface integral. We summarize our study in Section V.

## II. REVIEW OF THE APW BASED METHODS

In APW based methods<sup>14,19</sup> the unit cell is divided into non-overlapping atomic spheres and an interstitial region. The basis functions are adapted to the character of the atomic wave functions in the corresponding regions and in the interstitial ( $\mathbf{r} \in IS$ ) plane waves are used to represent the tails of the atomic orbitals. Inside the atomic spheres ( $\mathbf{r} \in R_a$ ) the plane waves are augmented by an angular momentum expansion into spherical harmonics

$Y_L(\hat{\mathbf{r}})$  times numerical radial basis functions  $u_l^a(r, E)$ :

$$\phi_{\mathbf{k}\mathbf{K}}^{APW}(\mathbf{r}) = \begin{cases} \frac{1}{\sqrt{\Omega}} e^{i(\mathbf{k}+\mathbf{K}) \cdot \mathbf{r}} & \mathbf{r} \in IS \\ \sum_L a_L^{a\mathbf{k}\mathbf{K}} u_l^a(r, E) Y_L(\hat{\mathbf{r}}) & \mathbf{r} \in R_a \end{cases} \quad (1)$$

Here  $L$  represents a tuple  $L \equiv \{lm\}$  of angular momentum quantum numbers,  $\Omega$  denotes the unit cell volume,  $\mathbf{r} \equiv \mathbf{r}_a + \boldsymbol{\tau}_a$ :  $\mathbf{r}_a$  is the local position vector defined with respect to the atomic position  $\boldsymbol{\tau}_a$ ,  $\mathbf{k}$  is a wave vector and  $\mathbf{K}$  denotes a reciprocal lattice vector. The coefficients  $a_L^{a\mathbf{k}\mathbf{G}}$  are chosen such that continuity of the basis functions at the sphere boundaries  $r_a = R_a$  is established. In Slater's original APW method<sup>19</sup>  $u_l^a(r, E)$  is the solution of the radial Schrödinger equation with the spherically symmetric potential ( $V_{00}$ ) at the (unkonwn) eigenenergy  $E$ , which leads to a non-linear eigenvalue problem and a computationally very expensive process. In Andersson's LAPW method<sup>9</sup> the energy dependency of  $u_l^a(r, E)$  was linearized by choosing a linear combination of  $u_l^a(r, E_l^a)$  at a fixed energy  $E_l^a$  and it's energy derivative  $\dot{u}_l^a(r, E_l^a)$ . This leads to two coefficients  $a_L^{a\mathbf{k}\mathbf{K}}$  and  $b_L^{a\mathbf{k}\mathbf{K}}$ , which are determined by continuity of the basis functions in value and slope at the sphere boundary. However, it was noted by Koelling and Arbman<sup>20</sup> that the APW method converges relatively faster than the LAPW method with the number of plane waves. Therefore another linearization scheme, the APW plus local orbital (APW+lo)<sup>13</sup> method, was introduced. The authors of Ref. 13 used an APW basis but at a fixed energy  $E_l^a$  and linearized the energy dependency by a set of local orbitals (lo). These local orbitals, Eq. (2), are defined as linear combination of  $u_{l,lo}^a(r, E_l^a)$  and  $\dot{u}_{l,lo}^a(r, E_l^a)$  (like in the traditional LAPW method), but are local in the sense that they are zero outside the corresponding atomic sphere and not connected to a plane wave.

$$\phi_{lo}^a(\mathbf{r}) = \begin{cases} 0 & \mathbf{r} \in IS \\ [a_{l,lo}^a u_{l,lo}^a(r, E_l^a) + b_{l,lo}^a \dot{u}_{l,lo}^a(r, E_l^a)] Y_L(\hat{\mathbf{r}}), & \mathbf{r} \in R_a \end{cases} \quad (2)$$

Later Madsen *et.al.*<sup>15</sup> limited the APW+lo basis set to the chemically important angular momenta ( $l = 0, 1, 2$  or  $3$ , depending on the atom) and used LAPW for higher  $l$ . They provided an extensive study of the superior efficiency of the (L)APW+lo method as compared to other linearization strategies. Another type of local orbitals Eq. (3), the so-called LOs, were first introduced by Singh<sup>21</sup> to describe semi-core states. These are states whose energy is higher (lower) compared to that of core states (valence states) and they are not fully confined within an atomic sphere. Since the linearization in the LAPW or APW+lo methods can only capture the energy variation of the radial function for energies close to  $E_l^a$  (valence states), they cannot handle such semi-core

states. As a result, LOs need to be defined with different linearization energies ( $E_{l,LO}^a$ ) close to the semi-core eigenenergies:

$$\phi_{LO}^a(\mathbf{r}) = \begin{cases} 0 & \mathbf{r} \in IS \\ [a_{l,LO}^a u_l^a(r, E_l^a) + c_{l,LO}^a u_{l,LO}^a(r, E_{l,LO}^a)] Y_L(\hat{\mathbf{r}}) & \mathbf{r} \in R_a \end{cases} \quad (3)$$

Here  $u_l^a(r, E_l^a)$  and  $u_{l,LO}^a(r, E_{l,LO}^a)$  denote the solutions of the Schrödinger equation for energies  $E_l^a$  and  $E_{l,LO}^a$ , respectively. The two coefficients  $a_{l,LO}^a$  and  $c_{l,LO}^a$  are fixed by imposing the conditions of normalization and that the value of the LO functions vanish at the sphere boundaries.

Using basis functions as defined above, Eqs. (1) to (3), the wave function  $\psi_{v\mathbf{k}}(\mathbf{r})$  for band  $v$  and wave vector  $\mathbf{k}$  is:

$$\psi_{v\mathbf{k}}(\mathbf{r}) = \sum_{\mathbf{K}} c_{v\mathbf{k}\mathbf{K}} \phi_{\mathbf{k}\mathbf{K}}^{APW}(\mathbf{r}) + \sum_{lo} c_{v\mathbf{k},lo} \phi_{lo}^a(\mathbf{r}) + \sum_{LO} c_{v\mathbf{k},LO} \phi_{LO}^a(\mathbf{r}), \quad (4)$$

with expansion coefficients  $c_{v\mathbf{k}\mathbf{K}}$ ,  $c_{v\mathbf{k},lo}$  and  $c_{v\mathbf{k},LO}$ . The summation over reciprocal lattice vectors  $\mathbf{K}$  is truncated at  $|\mathbf{K}| \leq K_{max}$ , and the summation over lo and LO runs over all atoms in the unit cell. Later, Eq. (4) will be used to define the charge density  $\rho(\mathbf{r}) = \sum_{v\mathbf{k}} n_{v\mathbf{k}} |\psi_{v\mathbf{k}}(\mathbf{r})|^2$ , where  $n_{v\mathbf{k}}$  is the corresponding occupation number. The charge density representation follows the APW spirit and is expanded into a Fourier series in the interstitial and into symmetry adapted lattice harmonics ( $Y_{LM}$ ) inside the atomic spheres<sup>14</sup>. In a Fourier expansion of  $\rho(\mathbf{r})$ , the expansion is truncated at reciprocal vectors  $G$  with magnitude  $G_{max}$ , which should therefore be chosen at least as large as  $2K_{max}$ :

$$\rho(\mathbf{r}) \equiv \begin{cases} \sum_G^{G_{max}} \rho(G) e^{iG \cdot \mathbf{r}} & \mathbf{r} \in IS \\ \sum_{LM} \rho_{LM}(r) Y_{LM}(\hat{\mathbf{r}}) & \mathbf{r} \in R_a, \end{cases} \quad (5)$$

The APW based methods are described in detail by Singh and Nordström<sup>14</sup> and the (L)APW+lo method forms the basis of the WIEN2k code<sup>16,22</sup>.

### III. STRESS TENSOR

The stress tensor in a given state is defined as the derivative

$$\sigma_{\alpha\beta} = \frac{1}{\Omega} \frac{dE_{tot}[\underline{\epsilon}]}{d\epsilon_{\alpha\beta}} \Big|_{\underline{\epsilon}=0}, \quad (6)$$

of the total energy with respect to strain, taken at zero strain with respect to this state. Here  $\sigma_{\alpha\beta}$  and  $\epsilon_{\alpha\beta}$  represent Cartesian components of the stress and the strain tensor, respectively, and  $E_{tot}[\underline{\epsilon}]$  is the DFT total energy

for the system at strain  $\underline{\epsilon}$ . To compute Eq.(6), we first need the DFT total energy expression<sup>23</sup>, which is as follows

$$\begin{aligned} E_{tot} = & \sum_{v\mathbf{k}} n_{v\mathbf{k}} \epsilon_{v\mathbf{k}} - \int_{\Omega} d^3\mathbf{r} \rho(\mathbf{r}) V_{eff}(\mathbf{r}) \\ & + \frac{1}{2} \int_{\Omega} d^3\mathbf{r} \rho(\mathbf{r}) V_C(\mathbf{r}) - \frac{1}{2} \sum_a Z_a V_M(\boldsymbol{\tau}_a) \\ & + \int_{\Omega} d^3\mathbf{r} \rho(\mathbf{r}) \epsilon_{xc}(\rho), \end{aligned} \quad (7)$$

$\epsilon_{v\mathbf{k}}$  represents the Kohn-Sham eigenvalue for the  $v$ th band at wave vector  $\mathbf{k}$  and  $V_{eff}(\mathbf{r})$  is the effective potential, which is the sum of the Coulomb  $V_C(\mathbf{r})$  and the

exchange correlation potential  $\mu_{xc}(\rho)$ .  $Z_a$  is the nuclear charge of an atom  $a$  located at  $\boldsymbol{\tau}_a$  and  $V_M(\boldsymbol{\tau}_a)$  is the Madelung potential.  $\epsilon_{xc}(\rho)$  is the exchange correlation energy per particle which is a local function of the total charge density  $\rho$  in the LDA and of  $\rho$  as well as of the gradient of the density ( $\nabla\rho$ ) in the GGA. In Eq.(7), the first two terms represent the non-interacting kinetic energy, the sum of the third and fourth terms is the electrostatic energy, and the last term corresponds to the exchange correlation energy.

In the stress tensor calculation, Eq.(7) should be defined in the strained or deformed system and differentiated with respect to strain. The calculation of the stress tensor with Eqs. (6) and (7) in the standard LAPW method and for the LDA has already been presented in our previous paper<sup>11</sup>. For the sake of clarity, we present the final expression once again in Eq.(8).

---


$$\begin{aligned} \Omega\sigma_{\alpha\beta}^{LAPW} = & \frac{1}{2} \sum_{v\mathbf{k}} n_{v\mathbf{k}} \int_{\Omega} d^3\mathbf{r} \psi_{v\mathbf{k}}^*(\mathbf{r}) (\partial_{\alpha}\partial_{\beta} + \partial_{\beta}\partial_{\alpha}) \psi_{v\mathbf{k}}(\mathbf{r}) + 2 \sum_{v\mathbf{k}} n_{v\mathbf{k}} \text{Re} \left\langle \frac{d\psi_{v\mathbf{k}}[\underline{\epsilon}](\mathbf{r}[\underline{\epsilon}])}{d\underline{\epsilon}_{\alpha\beta}} \right|_{\underline{\epsilon}=0} \left| \widehat{H}_{eff}(\mathbf{r}) - \epsilon_{v\mathbf{k}} \right| \psi_{v\mathbf{k}}(\mathbf{r}) \rangle^{R_a} \\ & - \frac{1}{2} \sum_{a \in \Omega} \int_{R_a} d^3\mathbf{r}_a \rho_c^a(\mathbf{r}_a) (r_{\beta}\partial_{\alpha} + r_{\alpha}\partial_{\beta}) V_{eff}(\mathbf{r}) - \frac{\delta_{\alpha\beta}}{2} \int_{\Omega} d^3\mathbf{r} \rho(\mathbf{r}) V_C(\mathbf{r}) + \frac{1}{2} \int_{\Omega} d^3\mathbf{r} \rho(\mathbf{r}) \frac{dV_C[\underline{\epsilon}](\mathbf{r}[\underline{\epsilon}])}{d\underline{\epsilon}_{\alpha\beta}} \Big|_{\underline{\epsilon}=0} \\ & - \frac{1}{2} \sum_{a \in \Omega} Z_a \frac{d}{d\underline{\epsilon}_{\alpha\beta}} V_M[\underline{\epsilon}](\boldsymbol{\tau}_a[\underline{\epsilon}]) \Big|_{\underline{\epsilon}=0} + \delta_{\alpha\beta} \int_{\Omega} d^3\mathbf{r} \rho(\mathbf{r}) [\epsilon_{xc}(\rho) - \mu_{xc}(\rho)] \end{aligned} \quad (8)$$


---

where the symbol Re denotes the real part of a complex number,  $\langle \cdot | \cdot | \cdot \rangle^{R_a}$  refers to the integral only within the atomic spheres which is equivalent to  $\int_{R_a} d^3\mathbf{r}_a$ ,  $H_{eff}(\mathbf{r})$  is the effective Hamiltonian,  $\int_{\Omega} d^3\mathbf{r}$  is an integration over the whole unit cell, and the total electronic charge density  $\rho(\mathbf{r})$  is the sum of the core [ $\rho_c^a(\mathbf{r}_a)$ ] and valence charge density.  $\psi_{v\mathbf{k}}^*(\mathbf{r})$  is the complex conjugate of  $\psi_{v\mathbf{k}}(\mathbf{r})$  and  $\partial_{\alpha}$  is a shorthand notation for the partial derivative along the Cartesian direction  $\alpha$ . The summation  $\sum_{a \in \Omega}$  runs over all equivalent and non-equivalent atoms of the unit cell,  $\delta_{\alpha\beta}$  denotes the Kronecker delta.

As already mentioned, the main objective of this paper is to extend the stress tensor formalism previously derived for the LAPW method and LDA to the APW+lo method and GGA. As described in Section II, in the APW+lo formalism the basis functions are not restricted to have a continuous slope at the atomic sphere boundary. This gives rise to an additional contribution to the kinetic energy, see Section III A, which subsequently yields a corresponding additional contribution to the stress tensor in the same fashion as in the force formalism<sup>3</sup>. Moreover, the additional contributions to the stress tensor formalism when using a GGA-type exchange-correlation functional will be discussed in Section III B.

### A. Additional surface term in APW+lo

In standard quantum mechanics, the kinetic energy density per unit cell volume  $\Omega$  for a Bloch function  $\psi_{v\mathbf{k}}(\mathbf{r})$  is given by the expectation value  $\mathcal{T}^{(H)} \equiv \frac{1}{2} \int_{\Omega} d^3\mathbf{r} \psi_{v\mathbf{k}}^*(\mathbf{r}) (-\nabla^2) \psi_{v\mathbf{k}}(\mathbf{r})$ . By continuity and periodicity of  $\psi_{v\mathbf{k}}$ , this is strictly equal to the so-called **Slater** form  $\mathcal{T}^{(S)} \equiv \frac{1}{2} \int_{\Omega} d^3\mathbf{r} \nabla \psi_{v\mathbf{k}}^*(\mathbf{r}) \nabla \psi_{v\mathbf{k}}(\mathbf{r})$  as shown by a simple partial integration. Nevertheless, in the context of APW basis functions, there is a subtle difference between these two expressions. Indeed, if we expand  $\psi_{v\mathbf{k}}(\mathbf{r}) = \sum_{\mathbf{K}} c_{v\mathbf{k}\mathbf{K}} \phi_{\mathbf{k}\mathbf{K}}(\mathbf{r})$  in terms of basis functions  $\phi_{\mathbf{k}\mathbf{K}}(\mathbf{r})$ , then in both cases the algebraic contribution to the kinetic energy for Bloch wave vector  $\mathbf{k}$  will be given by

$$T_{\mathbf{k}} = \sum_{\mathbf{K}'\mathbf{K}} c_{v\mathbf{k}\mathbf{K}'}^* T_{\mathbf{K}'\mathbf{K}}(\mathbf{k}) c_{v\mathbf{k}\mathbf{K}} \quad (9)$$

However, the above Hamiltonian (H) and Slater (S) form of the kinetic energy will give two different matrix elements:

$$T_{\mathbf{K}'\mathbf{K}}^{(H)}(\mathbf{k}) = \frac{1}{2} \int_{\Omega} d^3\mathbf{r} \phi_{\mathbf{k}\mathbf{K}'}^*(\mathbf{r}) (-\nabla^2) \phi_{\mathbf{k}\mathbf{K}}(\mathbf{r}) \quad (10)$$

$$T_{\mathbf{K}'\mathbf{K}}^{(S)}(\mathbf{k}) = \frac{1}{2} \int_{\Omega} d^3\mathbf{r} \nabla \phi_{\mathbf{k}\mathbf{K}'}^*(\mathbf{r}) \nabla \phi_{\mathbf{k}\mathbf{K}}(\mathbf{r}) \quad (11)$$

The important point is that the matrix  $T_{\mathbf{K}'\mathbf{K}}$  (which is

part of the Hamiltonian matrix  $\mathcal{H}_{\mathbf{K}'\mathbf{K}}$ ) needs to be *hermitian*, i.e.  $T_{\mathbf{K}'\mathbf{K}}^* = T_{\mathbf{K}\mathbf{K}'}$  needs to hold just like it needs to hold for the whole Hamiltonian, because otherwise it

would yield complex (and thus unphysical) eigenvalues. Hermiticity of the matrix with elements  $T_{\mathbf{K}'\mathbf{K}}^{(S)}(\mathbf{k})$  derived from the Slater form is obvious, but using Green's identity we can show that

$$T_{\mathbf{K}'\mathbf{K}}^{(H)}(\mathbf{k}) = T_{\mathbf{K}'\mathbf{K}}^{(S)}(\mathbf{k}) - \frac{1}{2} \sum_{a \in \Omega} \oint dS \left[ \phi_{\mathbf{k}\mathbf{K}'}^{a*}(\mathbf{r}) \frac{\partial \phi_{\mathbf{k}\mathbf{K}}^a(\mathbf{r})}{\partial r} - \phi_{\mathbf{k}\mathbf{K}'}^{*IS}(\mathbf{r}) \frac{\partial \phi_{\mathbf{k}\mathbf{K}}^{IS}(\mathbf{r})}{\partial r} \right] \quad (12)$$

In Eq.(12),  $\oint dS$  is a surface integral at the atomic sphere boundary, the superscripts  $a$  and  $IS$  in  $\phi_{\mathbf{k}\mathbf{K}}^a(\mathbf{r})$  and  $\phi_{\mathbf{k}\mathbf{K}}^{IS}(\mathbf{r})$  indicate the basis functions in the atomic spheres and the interstitial region, and  $\frac{\partial}{\partial r}$  represents the partial derivative. Thus the Hamiltonian matrix element  $T_{\mathbf{K}'\mathbf{K}}^{(H)}(\mathbf{k})$  is *not* hermitian unless the surface integral vanishes, which is guaranteed only if the basis functions are continuous in value and slope, which is fulfilled for the LAPW basis set, but not for APW. In summary, while the standard Hamiltonian form for the kinetic energy density is suitable for LAPW, Eq. (12) shows that maintaining hermiticity in an APW setting requires the mandatory use of Slater's version of the kinetic energy density, or equivalently, the consideration of an additional surface integral, which in terms of the full wave function is tantamount to calculate

$$\mathcal{S} = \frac{1}{2} \oint dS \left( \psi_{v\mathbf{k}}^{*a}(\mathbf{r}) \frac{\partial \psi_{v\mathbf{k}}^a(\mathbf{r})}{\partial r} - \psi_{v\mathbf{k}}^{*IS}(\mathbf{r}) \frac{\partial \psi_{v\mathbf{k}}^{IS}(\mathbf{r})}{\partial r} \right) \quad (13)$$

When the unit cell is strained or deformed through increasing or decreasing the unit cell volume  $\Omega$ , the interstitial part of the basis functions immediately undergoes a change due to the factor  $1/\sqrt{\Omega}$ , see Eq.(1), which makes it necessary to redefine the matching coefficients  $a_L^{ak\mathbf{K}}$  in Eq. (1) at the atomic sphere boundary. As a result, both  $\psi_{v\mathbf{k}}^a$  and  $\psi_{v\mathbf{k}}^{IS}$  in Eq. (13) will be affected. To address the resulting change of the surface integral  $\mathcal{S}$  of Eq. (13), we differentiate its counterpart  $\mathcal{S}[\underline{\epsilon}]$  defined in the deformed system with respect to the applied strain:

$$\sigma_{\alpha\beta}^S = \frac{1}{\Omega} \frac{d\mathcal{S}[\underline{\epsilon}]}{d\underline{\epsilon}_{\alpha\beta}} \Big|_{\underline{\epsilon}=0}, \quad (14)$$

Here the superscript  $S$  indicates the origin of this new strain contribution  $\sigma_{\alpha\beta}^S$  to the total stress tensor  $\sigma_{\alpha\beta}$  of Eq. (6). A detailed evaluation of Eq. (14) is presented in Appendix A, and its final expression is

$$\begin{aligned} \sigma_{\alpha\beta}^S &= \frac{1}{2\Omega} \sum_L \mathbf{D}_L^{avk}(\alpha, \beta) u_l^a(R_a) \left\{ \sum_{\lambda'} \mathbf{A}_{L\lambda'}^{avk} u_{l\lambda'}'(R_a) - F_L^{avk} \right\} \\ &+ \frac{1}{2\Omega} \sum_L \sum_{\lambda} \mathbf{A}_{L\lambda}^{avk*} u_l^a(R_a) \left\{ \mathbf{D}_L^{avk}(\alpha, \beta) u_l^{a'}(R_a) - \mathbf{F}_L^{avk}(\alpha, \beta) \right\} \end{aligned} \quad (15)$$

See Appendix A for the definitions of the shorthand notations  $\lambda$ ,  $u_{l\lambda}^a(R_a)$ ,  $u_{l\lambda'}'(R_a)$ , and  $\mathbf{A}_{L\lambda}^{avk}$ .  $\mathbf{D}_L^{avk}(\alpha, \beta)$  is the strain variation of  $A_L^{avk}$  calculated from Eq. (A15).  $F_L^{avk}$  is evaluated according to Eq. (A7) and  $\mathbf{F}_L^{avk}(\alpha, \beta)$  is the strain variation of  $F_L^{avk}$ , see Eq. (A16).

## B. Exchange-Correlation Stress for GGA

In the LDA, the exchange correlation energy per particle  $\epsilon_{xc}(\rho)$  depends exclusively on the density  $\rho$  while in the GGA<sup>17,18</sup> it features also an additional dependence on the density gradient  $\nabla\rho$ .

$$E_{xc}^{GGA} = \int_{\Omega} d^3r \rho(\mathbf{r}) \epsilon_{xc}(\rho, \nabla\rho) \quad (16)$$

When the system is deformed, the gradient of the charge density changes according to the applied deformation and in the stress tensor this changed quantity gets differentiated by the strain. In comparison to LDA, this introduces an additional contribution for the GGA

$$\begin{aligned} \sigma_{\alpha\beta}^{xc, GGA} &= \frac{1}{\Omega} \frac{dE_{xc}^{GGA}[\underline{\epsilon}]}{d\underline{\epsilon}_{\alpha\beta}} \Big|_{\underline{\epsilon}=0} \\ &= \frac{\delta_{\alpha\beta}}{\Omega} \int_{\Omega} d^3r \rho(\mathbf{r}) \epsilon_{xc} + \frac{1}{\Omega} \int_{\Omega} d^3r \frac{d\rho[\underline{\epsilon}](\mathbf{r})}{d\underline{\epsilon}_{\alpha\beta}} \mu_{xc} \\ &\quad - \frac{2}{\Omega} \int_{\Omega} d^3r \rho(\mathbf{r}) \partial_{\alpha}\rho(\mathbf{r}) \partial_{\beta}\rho(\mathbf{r}) \frac{\partial \epsilon_{xc}}{\partial \boldsymbol{\sigma}}, \end{aligned} \quad (17)$$

for GGA, where  $E_{xc}^{GGA}[\underline{\epsilon}]$  is the exchange correlation energy of Eq. (16) but is defined in the deformed system.  $\delta_{\alpha\beta}$  is the Kronecker delta function and indicates that the first term only contributes to the diagonal elements of  $\sigma_{\alpha\beta}^{xc, GGA}$ . In the last term,  $\epsilon_{xc}$  equivalent to  $\epsilon_{xc}(\rho, \nabla\rho)$ . Moreover, we shall use the notation

$$\frac{\partial \epsilon_{xc}}{\partial \boldsymbol{\sigma}} \equiv \frac{\partial \epsilon_{xc}}{\partial (\partial_{\alpha}\rho \cdot \partial_{\alpha}\rho)}, \quad \boldsymbol{\sigma} = \nabla\rho \cdot \nabla\rho \quad (18)$$

The first two terms in Eq. (17) are identical to the corresponding terms in the stress tensor for LDA<sup>11</sup> and the third term is an additional contribution that is solely due to the change of the gradient of the charge density as the system deforms. Therefore, Eq. (17) can generally be stated in a form that is valid for both, LDA and GGA exchange correlation functionals:

$$\begin{aligned} \Omega \sigma_{\alpha\beta}^{xc} &= \Omega \sigma_{\alpha\beta}^{xc, LDA} \\ &- 2\delta_{GGA} \int_{\Omega} d^3r \rho(\mathbf{r}) \partial_{\alpha}\rho(\mathbf{r}) \partial_{\beta}\rho(\mathbf{r}) \frac{\partial \epsilon_{xc}}{\partial \boldsymbol{\sigma}}, \end{aligned} \quad (19)$$

were the presence of  $\delta_{GGA}$  distinguishes whether a GGA ( $\delta_{GGA} = 1$ ) or LDA ( $\delta_{GGA} = 0$ ) type of exchange correlation energy is used. While implementing Eq.(19) in the WIEN2k code<sup>22</sup>, the Libxc library<sup>24</sup> has been used particularly to get  $\frac{\partial \epsilon_{xc}}{\partial \boldsymbol{\sigma}}$ . Our Eq.(19) is similar to Eq.(19)

in Ref. 6 for the Soler-William LAPW method. However, since the charge density representation is different in their method, the contributions from different terms is very different as will be discussed later on (see Fig.7).

### C. Total stress tensor

With the consideration of the discussion given in Sections III A and III B, the final expression for the stress tensor that covers all flavors of (L)APW+lo+LO and is applicable to both, LDA and GGA, is

$$\Omega\sigma_{\alpha\beta} = \Omega\sigma_{\alpha\beta}^{LAPW} + \delta_{APW}\Omega\sigma_{\alpha\beta}^S + \delta_{GGA}\Omega\sigma_{\alpha\beta}^{xc\text{ GGA}}, \quad (20)$$

where the expression for  $\sigma_{\alpha\beta}^{LAPW}$  is given in Eq. (8). In formula (20) the notation  $\delta_{APW}$  and  $\delta_{GGA}$  is used to single out contributions that are only relevant for APW+lo and GGA, respectively.

## IV. RESULTS

In the following we present the results of the stress tensor given by Eq. (20) as implemented in the WIEN2k code<sup>16,22</sup>. In addition the Birch-Murnaghan (BM) equation of state<sup>25</sup> fitted to total energies at different volumes is used to obtain the numerical pressure  $P^{(E)} = -\frac{dE(\Omega)}{d\Omega}$ . The pressure  $P^{(E)}$  can then be compared to the negative trace of the stress tensor  $P^{(\sigma)} = -(\sigma_{11} + \sigma_{22} + \sigma_{33})/3$  calculated directly from our analytical expression Eq. (20). The difference between  $P^{(E)}$  and  $P^{(\sigma)}$  is an indicator of the accuracy and reliability of our formalism.

### A. Tungsten

As our first example, we consider body-centered cubic (bcc) tungsten (W). The case of W is particularly important since it is a heavy transition metal that features all chemically important atomic orbitals s, p, d, and f (the semi-core 4f states are included as valence states). Results shown in Fig. 1 are calculated with an atomic sphere radius  $R_a = 2.47$  Bohr. All states up to 4d are treated as core states since they are completely confined within the atomic sphere. The 5s, 5p, and 4f states are represented with semi-core local orbitals (LO), see Eq. (3), while the valence s, p, d and f states are described with APW+lo basis functions (Eq. (1) and (2)) and higher angular momentum states (up to  $l=10$ ) with LAPW. The linearization energies for the different basis functions are set automatically to the centers of the corresponding occupied bands<sup>22</sup>. Fig. 1 shows the convergence with respect to the size of the basis set, which is controlled by the product  $R_a K_{max}$  of the smallest atomic sphere radius  $R_a$  and  $K_{max}$ , the modulus of the largest reciprocal lattice vector. The APW basis set size ranges

TABLE I. Lattice parameters  $a_0^{(E)}$  and  $a_0^{(\sigma)}$  (in Bohr) of bcc tungsten as predicted from the total energy and the analytical stress formalism, respectively, for four different values of  $R_a K_{max}$  and using the Fermi-Dirac (FD) and tetrahedron (Tetra) method.

$R_a K_{max}$	$a_0^{(\sigma)}$ (FD)	$a_0^{(E)}$ (FD)	$a_0^{(\sigma)}$ (Tetra)	$a_0^{(E)}$ (Tetra)
7	6.162	6.136	6.164	6.135
8	6.145	6.139	6.146	6.140
9	6.142	6.143	6.144	6.143
10	6.143	6.143	6.145	6.144

from 73 ( $R_a K_{max} = 7$ ) to 165 ( $R_a K_{max} = 10$ ) and additional 27 lo+LOs are always included. The  $G_{max}$  in Eq. (5) is  $20 \text{ Ry}^{\frac{1}{2}}$ . The cutoff value for the angular momentum for the non spherical potential expansion  $L_{max}^{ns}$  is 6 and the Brillouin zone (BZ) is sampled with a k-mesh of  $21 \times 21 \times 21$ . We used the Fermi-Dirac (FD) smearing method with a broadening parameter of 0.005 Ry for Fig. 1 (a)-(c), while the standard tetrahedron method is used for Fig. 1(d). The exchange-correlation energy and the potential  $\epsilon_{xc}$  and  $\mu_{xc}$  in Eq. (17), are calculated using the Perdew-Burke-Ernzerhof (PBE) GGA<sup>17,18</sup>. All integrations in the interstitial region are evaluated using the Fast Fourier Transform (FFT) method with a FFT grid of  $72 \times 72 \times 72$ . The convergence criteria for the energy and charge distance in the self consistency cycle are set to  $10^{-5}$  Ry and  $10^{-5}$  e<sup>-</sup> unless otherwise specified. Fig. 1(a)-(c) and Table I show that the equilibrium lattice parameter (or volume) from the total energy converges a bit faster than from the stress tensor with  $R_a K_{max}$ , so that for an accuracy of 0.01 Bohr at least  $R_a K_{max}=8$  is necessary for the stress tensor while only  $R_a K_{max}=7$  is needed for total energy calculations.

Moreover, the difference between  $P^{(\sigma)}$  and  $P^{(E)}$  in the tetrahedron method [Fig. 1(d)] is fairly similar to that of the FD method [Fig. 1(c)], which is in strong contrast to the fcc Al example presented in our previous LAPW-stress paper<sup>11</sup>, where the errors in  $P^{(\sigma)}$  in the tetrahedron method were much larger. For W the tetrahedron method has only a little larger volume dependency of  $P^{(\sigma)} - P^{(E)}$ , see Figs. 1(c) and 1(d).

Continuing the comparison of the tetrahedron and FD smearing method for BZ integration, the dependence of the stress tensor on different choices of k-mesh grid sizes for both methods is shown in Fig. 2. Fig. 2(b) reveals no significant dependence of the calculated stress tensor on the chosen k meshes for the FD method and the difference  $P^{(\sigma)} - P^{(E)}$  for k-meshes  $(12 \times 12 \times 12)$  and  $(21 \times 21 \times 21)$  is within the accuracy limit of the stress tensor. In the case of the tetrahedron method, however, this deviation is a bit larger even though it has only an effect in the third digit in the predicted lattice parameter  $a_0^{(\sigma)}$ (Tetra) = 6.147 Bohr ( $12 \times 12 \times 12$ ) and 6.144 Bohr ( $21 \times 21 \times 21$ ).

In Section III A we discussed the origin and importance

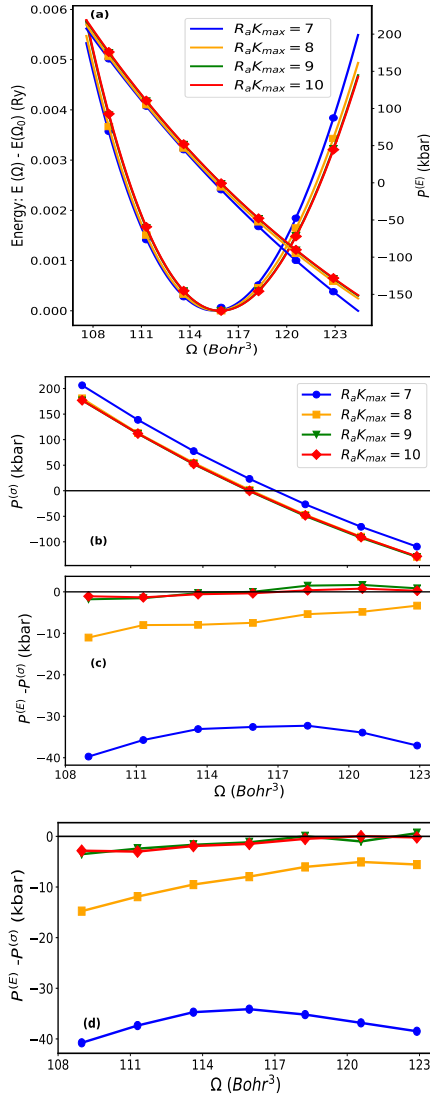


FIG. 1. (a) Energy-volume curves as well as  $P^{(E)}$ , (b) the negative trace of the full stress tensor  $P^{(\sigma)}$ , and (c) the difference between  $P^{(\sigma)}$  and  $P^{(E)}$  for four different  $R_a K_{max}$  values as function of  $\Omega$  for bcc W. The FD method with a broadening parameter of 0.005 Ry is used for (a)-(c) and the standard tetrahedron method is used for (d).

of the surface term  $\mathcal{S}$  in Eq. (13) for the kinetic energy and thereby for the stress tensor formalism  $\sigma_{\alpha\beta}$ , Eq. (20). Fig. 3 confirms its significance. In the figure, the red and blue curves represent the negative trace of Eq. (20) with and without  $\sigma_{\alpha\beta}^S$ . The horizontal green line represents the zero pressure line and the intersection of the red and blue curves with the green line corresponds to the equilibrium volume that is estimated from the stress tensor. The corresponding value estimated using the total energy calculation is also shown by the vertical orange line. This implies that without inclusion of  $\sigma_{\alpha\beta}^S$  in Eq. (20) the equilibrium lattice parameter predicted from the stress tensor

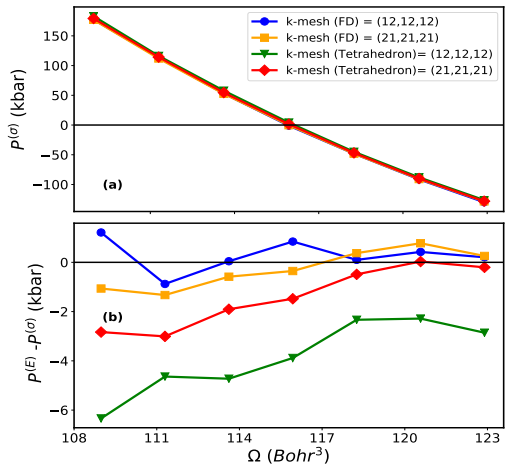


FIG. 2. (a) The negative trace of the full stress tensor  $P^{(\sigma)}$  and (b) the difference between  $P^{(\sigma)}$  and  $P^{(E)}$  for two different k-mesh grids as function of  $\Omega$  for bcc W. The standard tetrahedron and FD methods are used.  $R_a K_{max} = 10$  and all other input parameters are the same as in Fig. 1.

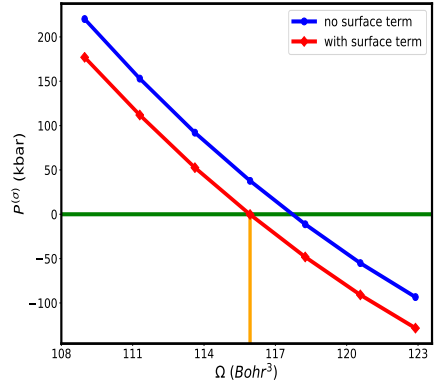


FIG. 3. The trace of the full stress tensor with (red curve) and without (blue curve)  $\sigma_{\alpha\beta}^S$  in Eq. (20) as function of  $\Omega$  for bcc W. The vertical orange line corresponds to the equilibrium lattice predicted from the total energy calculation.  $R_a K_{max} = 10$ , and all the remaining input parameters are the same as in Fig. 1(b).

would be 0.03 Bohr larger than that predicted from the total energy, which cannot be ignored. Moreover, the fifth row of Table II gives the numerical value of  $\sigma_{\alpha\beta}^S$  calculated at the equilibrium volume  $\Omega = 115.94$  Bohr<sup>3</sup> for the APW+lo and LAPW methods and, as expected, its value is zero for LAPW.

In order to demonstrate the superior convergence behavior of APW+lo versus the standard LAPW method, we show in Fig. 4 the convergence of the stress tensor element  $\sigma_{11}$  with respect to the basis set size represented by  $R_a K_{max}$  for APW+lo and LAPW. Since the calculation is performed at the equilibrium volume, the calculated

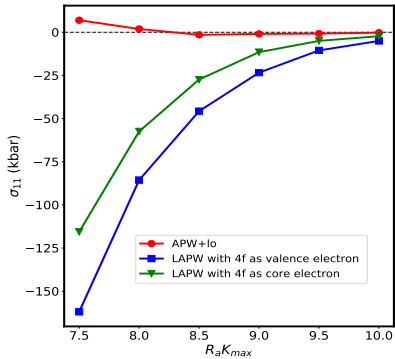


FIG. 4. Convergence of  $\sigma_{11}$  with  $R_a K_{max}$  in the APW+lo and LAPW methods for W at a volume  $\Omega = 115.94 \text{ Bohr}^3$ . For LAPW two different cases – 4f electrons treated as valence or core states – are considered. All other input parameters are the same as in Fig. 1 (b).

$\sigma_{11}$  is expected to be zero within the numerical accuracy of the calculation. The figure shows results for three different cases: with APW+lo, LAPW with 4f electrons as valence electrons and as core electrons. It is clear from the figure that the stress tensor in the APW+lo method converges much faster than for the two LAPW cases. Indeed, with APW+lo,  $R_a K_{max} = 8$  already gives an acceptable result, whereas  $R_a K_{max} = 10$  is required for LAPW with 4f electrons as core electron or even higher for LAPW with 4f electrons as valence electrons. The 4f wave functions in W are highly localized and difficult to converge, but the APW+lo basis set is much more efficient than the LAPW method. The convergence of  $\sigma_{11}$  in Fig. 4 correlates with the convergence of the equilibrium lattice parameter  $a_0$  in Fig. 5, where  $a_0$  calculated directly from the total energy is represented by the black and orange dashed line for APW+lo and LAPW, respectively. It can be seen that  $a_0$  versus  $R_a K_{max}$  follows almost exactly the same behavior as  $\sigma_{11}$  versus  $R_a K_{max}$  and APW+lo converges significantly faster than LAPW.

In Fig. 6 we compare LDA and GGA calculations for  $P^{(E)}$  and  $P^{(\sigma)}$ , respectively. The difference between  $P^{(E)}$  and  $P^{(\sigma)}$  is shown in Fig. (6)(c) and is just 1-2 kbar. It is smaller for GGA and slightly larger with LDA, but all results are within the expected accuracy limit. Also the predicted lattice parameters  $a_0^{(\sigma)} = a_0^{(E)}$  are identical up to the third decimal point for both, LDA and GGA.

$\sigma_{\alpha\beta}^{xc}$  of Eq. (19) represents the contribution of the exchange-correlation energy to the stress tensor. It consists of a LDA-like term  $\sigma_{\alpha\beta}^{xc, LDA}$  (the name reflects the fact that this term is the only contribution when the LDA exchange-correlation functional is used) and the second term of Eq. (19), which represents the effect of the change of the gradient of the density on the stress tensor and is obviously only present in GGA calculations. The integral involved in the second term of Eq. (19) is computed by following the standard procedure of APW+lo based methods, where the integration over the whole unit

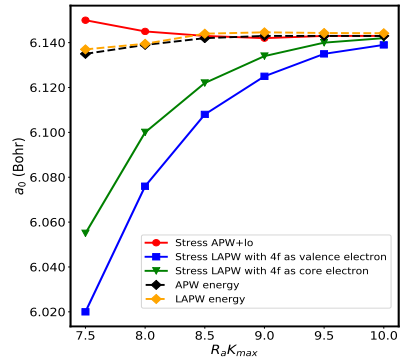


FIG. 5. Comparison of the calculated equilibrium lattice parameter for W from the stress tensor or from the total energy for different values of  $R_a K_{max}$  in the APW+lo and LAPW methods. For LAPW two different cases – 4f electrons as valence or core states – are considered. All other input parameters are the same as in Fig. 1(b).

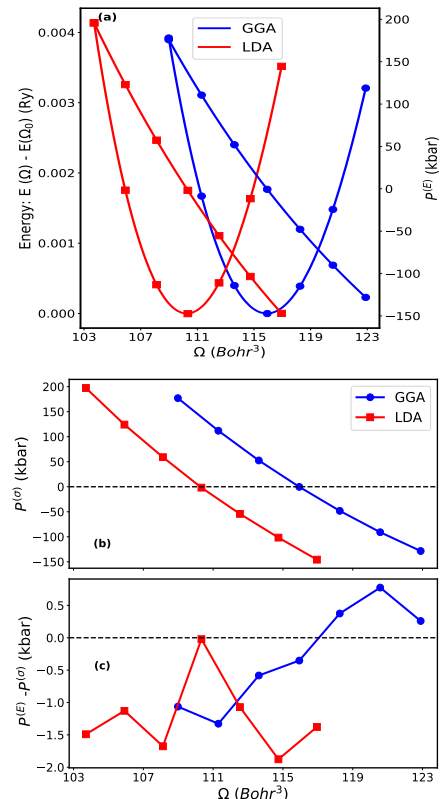


FIG. 6. (a) Energy-volume curves as well as  $P^{(E)}$ , (b) the negative trace of the full stress tensor  $P^{(\sigma)}$ , and (c) the difference between  $P^{(\sigma)}$  and  $P^{(E)}$  for LDA and GGA as function of  $\Omega$  for bcc W.  $R_a K_{max} = 10$  and all other input parameter are the same as in Fig. 1 (a)-(c).

cell is divided into the atomic spheres and the interstitial. Our Eq. (19) is similar to Eq. (20) in Ref. 6 for the Soler-Williams LAPW method. However, the authors in Ref. 6 show analytically that the GGA correction comes solely from their Fourier representation of the charge density and does not contain any contribution from inside the atomic spheres. In contrast, we found that the interstitial contribution (given by the Fourier expansion) is always small compared to the contribution from the atomic spheres. We even observed that in some cases, for example for Aluminum and W, the interstitial contribution is close to zero as can be seen in Fig. 7, where the negative trace of the second term of Eq. (19)  $P_{tot}^{(xc,GGA)}$  as well as the contributions from the atomic sphere  $P_{R_a}^{(xc,GGA)}$  and the interstitial region  $P_{IS}^{(xc,GGA)}$  are given for W. It is clear that the major contribution to  $P_{tot}^{(xc,GGA)}$  is from the atomic spheres [ $P_{R_a}^{(xc,GGA)}$ ] and the contribution from the interstitial [ $P_{IS}^{(xc,GGA)}$ ] is zero within the error limit of the calculation. However, this is not always the case. For example for silicon the interstitial contribution can not be neglected. The reason for the discrepancy between our results and the claim in Ref. 6 is probably the different representation of the charge density, where in the Soler-Williams LAPW method the Fourier expansion of the charge density contributes in the whole unit cell.

Finally we would like to present the magnitude of the different contributions to the stress tensor in order to demonstrate how the extremely large individual contributions partially cancel each other and which accuracy is necessary and can be achieved. Table II lists the different contributions to  $\sigma_{11}$  for an APW+lo and a LAPW calculation for W, where  $\sigma_{11}^{val,kin}$ ,  $\sigma_{11}^{val,corr}$ ,  $\sigma_{11}^{core,corr}$  and  $\sigma_{11}^{es}$  represent the first, second, third and the sum of the fourth, fifth and sixth term of Eq.(8), respectively. In addition  $\sigma_{11}^S$ ,  $\sigma_{11}^{xc,LDA}$  and  $\sigma_{11}^{GGA,corr}$  correspond to the second term of Eq.(20) and the first and second term of Eq.(19), respectively. The largest contributions (of opposite sign) are  $\sigma_{11}^{core,corr}$  and  $\sigma_{11}^{es}$  with magnitudes of about  $10^7$  kbar, followed by  $\sigma_{11}^{val,kin}$  with a magnitude of  $10^6$  kbar. They represent the partial cancellation of the kinetic and electrostatic energy contributions, which are so large because of the core electrons. The xc-contributions  $\sigma_{11}^{xc,LDA}$  and  $\sigma_{11}^{GGA,corr}$  are still in the order of  $10^5$  kbar, while the incomplete basis set correction  $\sigma_{11}^{val,corr}$  and the surface discontinuity correction  $\sigma_{11}^S$  in the APW+lo case account only for rather small corrections. The latter is, as expected, zero for the LAPW basis set. All those huge numbers cancel in the APW+lo case to almost zero (since the calculation is for the equilibrium volume), while for LAPW a 5 kbar residual remains, since with  $R_a K_{max} = 10$  the stress tensor is not fully converged for LAPW (see above). Nevertheless, the 5 kbar correspond only to small changes in the third decimal place of the lattice parameter.

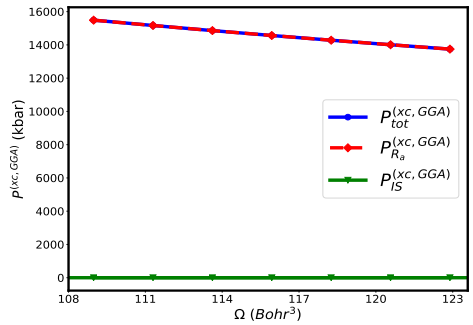


FIG. 7. The negative trace of the second term of Eq. (19),  $P_{tot}^{(xc,GGA)}$ , as well as its spatial decomposition into  $P_{R_a}^{(xc,GGA)}$  and  $P_{IS}^{(xc,GGA)}$  as function of the unit cell volume for bcc W.  $R_a K_{max} = 10$  and all other input parameters are the same as in Fig. 1(a)-(c).

TABLE II. The  $\sigma_{11}$  component of the stress tensor for W calculated with APW+lo and LAPW at the equilibrium unit cell volume  $\Omega = 115.94$  Bohr<sup>3</sup>. The total tensor element is decomposed into contributions according to Eqs.(8) and (20). All other input parameters are the same as in Fig. 1 (b).

stress	APW+lo (kbar)	LAPW (kbar)
$\sigma_{11}^{val,kin}$	1102905.56	1102971.88
$\sigma_{11}^{val,corr}$	45.09	20.50
$\sigma_{11}^{core,corr}$	24760504.93	24760437.09
$\sigma_{11}^{es}$	-25607153.70	-25607170.14
$\sigma_{11}^S$	-37.96	0.00
$\sigma_{11}^{xc,LDA}$	-241699.29	-241699.56
$\sigma_{11}^{GGA,corr}$	-14564.88	-14564.78
total	-0.25	-5.01

## B. Anatase TiO<sub>2</sub>

The calculation for anatase TiO<sub>2</sub> is especially important to verify that the symmetry between the equivalent atoms has been addressed correctly and the code works also for a non-symmorphic space group. In the anatase structure, TiO<sub>2</sub> has 6 atoms (2 Ti and 4 O) in the unit cell. All states up to 2p for Ti and the 1s state of O are considered as core states. The sphere sizes of Ti and O are 1.66 and 1.49 Bohr, respectively. Calculations are performed with  $R_a K_{max} = 8.5$ , a k-point mesh of  $6 \times 6 \times 10$ ,  $G_{max} = 20$  Ry<sup>½</sup> and  $L_{max}^{ns} = 6$ . The exchange correlation energy and potential are calculated using the PBE GGA and a FFT grid of  $108 \times 108 \times 60$  is used. The predicted lattice parameters from the stress tensor ( $a_0^{(\sigma)}$  = 7.182 Bohr,  $c_0^{(\sigma)}$  = 18.304 Bohr) and the total energy calculations are virtually identical up to 3 digits. This

result confirms that the complicated symmetry operations between equivalent atoms have been implemented correctly and the stress tensor also works for non-cubic symmetry.

## V. DISCUSSION

In this paper we have presented the stress tensor formalism for the APW+lo(+LO) method and included additional corrections for the GGA functionals. With this formalism we can do a fully relativistic core calculation, but the valence calculation is limited to being non-relativistic, since the scalar relativistic corrections are not yet implemented in the terms involving directly the valence wave functions. In Eq.(8), the first term results from the strain variation of the kinetic energy operator, but this term alone is not sufficient for a scalar-relativistic calculation. Therefore, with the exception of the first term, the remaining terms of Eq.(8) can be used for the relativistic calculation.

Moreover, convergence tests of the stress tensor with respect to  $R_a K_{max}$  and k-meshes were carried out for both, the tetrahedron and the FD method. Compared to LAPW, superior convergence properties of both the stress tensor and the derived equilibrium lattice parameters in APW+lo are observed. The importance of the additional surface contribution in the APW+lo stress formalism due to the kink in the basis set at the sphere boundary is discussed in detail. An additional contribution for the GGA is derived and included in our stress tensor formalism. In addition, the result for anatase TiO<sub>2</sub> confirm that the stress tensor has been correctly implemented also for non-cubic cases.

### Appendix A: Details of the strain variation of the surface term.

The surface term from Eq.(13) is

$$\mathcal{S} = \frac{1}{2} \oint dS \left( \psi_{v\mathbf{k}}^* \frac{\partial \psi_{v\mathbf{k}}^a(\mathbf{r})}{\partial r} - \psi_{v\mathbf{k}}^{IS} \frac{\partial \psi_{v\mathbf{k}}^{IS}(\mathbf{r})}{\partial r} \right) \quad (A1)$$

The wave functions in the atomic sphere  $\psi_{v\mathbf{k}}^a(\mathbf{r})$  and the interstitial region  $\psi_{v\mathbf{k}}^{IS}(\mathbf{r})$  are defined as

$$\begin{aligned} \psi_{v\mathbf{k}}^a(\mathbf{r}) &= \sum_L [A_L^{avk} u_l^a(r, E_l^a) + B_L^{avk} \dot{u}_l^a(r, E_l^a)] Y_L(\hat{\mathbf{r}}) \\ &\quad + C_{L,LO}^{avk} u_{l,LO}^a(r, E_{LO}^a) \end{aligned} \quad (A2)$$

$$\psi_{v\mathbf{k}}^{IS}(\mathbf{r}) = \sum_K c_{v\mathbf{k}\mathbf{K}} \frac{1}{\sqrt{\Omega}} e^{i(\mathbf{k}+\mathbf{K}) \cdot \mathbf{r}}, \quad (A3)$$

with

$$A_L^{avk} = \sum_{\mathbf{K}} c_{v\mathbf{k}\mathbf{K}} a_L^{avk} \quad (A4)$$

In Eq. (A2), the second term (energy derivative of  $u_l$ ) is coming from the small  $lo$  and the third term from capital  $LO$  (semi-core) as described in Section II. The partial derivative is

$$\frac{\partial \psi_{v\mathbf{k}}^a(\mathbf{r})}{\partial r} \Big|_{r=R_a} = \sum_L \sum_{\lambda} \mathbf{A}_{L\lambda}^{avk} u_{l\lambda}^a(R_a, E_{l\lambda}^a) Y_L(\hat{\mathbf{r}}), \quad (A5)$$

where  $|_{r=R_a}$  indicates that the radial derivative is evaluated only at the sphere boundary and for the sake of brevity the label  $\lambda$  is introduced to distinguish the radial function ( $\lambda=0$ ), its energy derivative ( $\lambda=1$ ), and semi-core local orbital ( $\lambda=2$ ).

$$\mathbf{A}_{L\lambda}^{avk} \text{ or } u_{l\lambda}^a(R_a, E_{l\lambda}^a) \equiv \begin{cases} A_L^{avk} \text{ or } u_l^a(R_a, E_l^a) & \lambda = 0 \\ B_L^{avk} \text{ or } u_l^a(R_a, E_l^a) & \lambda = 1 \\ C_{L,LO}^{avk} \text{ or } u_l^a(R_a, E_{LO}^a) & \lambda = 2 \end{cases}$$

To compute the partial derivative in the interstitial region, first the radial vector  $\mathbf{r}$  is defined in terms of local coordinates i.e.  $\mathbf{r} = \mathbf{r}_a + \boldsymbol{\tau}_a$ , then we use a Rayleigh expansion to expand  $e^{i(\mathbf{k}+\mathbf{K}) \cdot \mathbf{r}_a}$  in terms of spherical Bessel functions ( $j_l$ ) and spherical harmonics, which yields

$$\frac{\partial \psi_{v\mathbf{k}}^{IS}(\mathbf{r})}{\partial r} \Big|_{r_a=R_a} = F_L^{avk} Y_L(\hat{\mathbf{r}}), \quad (A6)$$

with

$$\begin{aligned} F_L^{avk} &= \sum_{\mathbf{K}} \frac{c_{v\mathbf{k}\mathbf{K}}}{\sqrt{\Omega}} 4\pi i^l e^{i(\mathbf{k}+\mathbf{K}) \cdot \boldsymbol{\tau}_a} Y_L^*(\widehat{\mathbf{k}+\mathbf{K}}) \\ &\quad |\mathbf{k}+\mathbf{K}| j_l(|\mathbf{k}+\mathbf{K}| R_a) \end{aligned} \quad (A7)$$

Substitution of Eqs. (A6) and (A5) into (A1) yields

$$\mathcal{S} = \frac{1}{2} \sum_L \sum_{\lambda} \mathbf{A}_{L\lambda}^{avk*} u_{l\lambda}^a(R_a) \left\{ \sum_{\lambda'} \mathbf{A}_{L\lambda'}^{avk} u_{l\lambda'}^a(R_a) - F_L^{avk} \right\}, \quad (A8)$$

where  $u_{l\lambda}^a(R_a, E_{l\lambda}^a)$  is replaced by  $u_{l\lambda}^a(R_a)$  for the sake of brevity, and this convention will be used from now on. To calculate the contribution of the above surface term to the stress tensor, first Eq. (A8) is defined in the deformed system and differentiated with respect to strain.

$$\begin{aligned} \mathcal{S}_{[\underline{\epsilon}]} &= \frac{1}{2} \sum_L \sum_{\lambda} \mathbf{A}_{L\lambda}^{avk*} [\underline{\epsilon}] u_{l\lambda}^a[\underline{\epsilon}](R_a) \\ &\quad \left\{ \sum_{\lambda'} \mathbf{A}_{L\lambda'}^{avk} [\underline{\epsilon}] u_{l\lambda'}^a[\underline{\epsilon}](R_a) - F_L^{avk} [\underline{\epsilon}] \right\} \end{aligned} \quad (A9)$$

In what follows,  $[\underline{\epsilon}]$  labels quantities defined in the deformed system. Using the frozen augmentation

approximation<sup>3,26</sup> we can discard the implicit dependency due to the linear response i.e.  $u_{l\lambda}^a(\underline{\epsilon})(R_a) \rightarrow u_{l\lambda}^a(R_a)$ . When calculating the strain variation of Eq.(A9), the following relationships will be used:

$$\frac{d(\mathbf{k}[\underline{\epsilon}] + \mathbf{K}[\underline{\epsilon}])}{d\epsilon_{\alpha\beta}} = -\frac{(\mathbf{k} + \mathbf{K})_\alpha(\mathbf{k} + \mathbf{K})_\beta}{|\mathbf{k} + \mathbf{K}|} \quad (\text{A10})$$

$$\begin{aligned} \frac{dY_L(\widehat{\mathbf{k}[\underline{\epsilon}]} + \widehat{\mathbf{K}[\underline{\epsilon}]})}{d\epsilon_{\alpha\beta}} &= -\frac{1}{2} \sum_{s=\pm 1} \sum_{t,t'=-1}^1 \left[ (\widehat{\mathbf{k} + \mathbf{K}})_\alpha c_\beta^{st}(l, m) \right. \\ &\quad \left. + (\widehat{\mathbf{k} + \mathbf{K}})_\beta c_\alpha^{st}(l, m) \right] Y_{l+s, m+t}(\widehat{\mathbf{k} + \mathbf{K}}) \end{aligned} \quad (\text{A11})$$

$$\frac{d}{d\epsilon_{\alpha\beta}} \frac{1}{\sqrt{\Omega[\underline{\epsilon}]}} = -\frac{\delta_{\alpha\beta}}{2\sqrt{\Omega}} \quad (\text{A12})$$

The coefficient  $c_\alpha^{st}(l, m)$  is computed as

$$c_\alpha^{st}(l, m) = \oint dS r \partial_\alpha Y_{lm}(\hat{r}) Y_{l+s, m+t}^*(\hat{r}) \quad (\text{A13})$$

Since both *lo* and *LO* vanish at the sphere boundary and beyond, in the calculation of  $\frac{d\mathbf{A}_{L\lambda}^{avk}[\underline{\epsilon}]}{d\epsilon_{\alpha\beta}}$  we only need to explicitly deal with the APW matching coefficients  $A_L^{avk}$ , which are obtained by equating the dual representation of the basis function at the sphere boundary:

$$A_L^{avk} = \sum_{\mathbf{K}} \frac{c_{v\mathbf{k}\mathbf{K}}}{\sqrt{\Omega}} 4\pi i^l e^{i(\mathbf{k} + \mathbf{K}) \cdot \tau_a} Y_L^*(\widehat{\mathbf{k} + \mathbf{K}}) \frac{j_l'(|\mathbf{k} + \mathbf{K}| R_a)}{u_l(R_a)} \quad (\text{A14})$$

and the derivative of the  $A_L^{avk}[\underline{\epsilon}]$  with respect to strain  $\epsilon_{\alpha\beta}$  is:

$$\begin{aligned} \mathbf{D}_L^{avk}(\alpha, \beta) &= \frac{dA_L^{avk}[\underline{\epsilon}]}{d\epsilon_{\alpha\beta}} \\ &= -\frac{\delta_{\alpha\beta}}{2} A_L^{avk} + \sum_{\mathbf{K}} \frac{c_{v\mathbf{k}\mathbf{K}}}{\sqrt{\Omega}} 4\pi i^l e^{i(\mathbf{k} + \mathbf{K}) \cdot \tau_a} \\ &\quad \left( \frac{Y_{lm}^*(\widehat{\mathbf{k} + \mathbf{K}})}{u_l(R_a)} \frac{d j_l(|\mathbf{k}[\underline{\epsilon}] + \mathbf{K}[\underline{\epsilon}]| R_a)}{d\epsilon_{\alpha\beta}} + \right. \\ &\quad \left. \frac{dY_{lm}^*(\widehat{\mathbf{k} + \mathbf{K}})}{d\epsilon_{\alpha\beta}} \frac{j_l(|\mathbf{k} + \mathbf{K}| R_a)}{u_l(R_a)} \right) \end{aligned} \quad (\text{A15})$$

Further simplification of Eq.(A15) can be achieved by using Eqs.(A10) and (A11). Moreover, the strain variation of  $F_L^{avk}[\underline{\epsilon}]$  is

$$\mathbf{F}_L^{avk}(\alpha, \beta) = \frac{dF_L^{avk}[\underline{\epsilon}]}{d\epsilon_{\alpha\beta}}, \quad (\text{A16})$$

which is simplified by defining Eq.(A7) in the deformed system and differentiating as in Eq.(A15). By collecting Eqs.(A15) and (A16), we get the strain variation of the surface integral

$$\begin{aligned} \frac{dS[\underline{\epsilon}]}{d\epsilon_{\alpha\beta}} &= \frac{1}{2} \sum_L \mathbf{D}_L^{avk*}(\alpha, \beta) u_{l\lambda}^a(R_a) \left\{ \sum_{\lambda'} \mathbf{A}_{L\lambda'}^{avk} u_{l\lambda'}^a(R_a) - F_L^{avk} \right\} \\ &\quad + \frac{1}{2} \sum_L \sum_{\lambda} \mathbf{A}_{L\lambda}^{avk*} u_{l\lambda}^a(R_a) \left\{ \mathbf{D}_L^{avk}(\alpha, \beta) u_{l\lambda}^a(R_a) - \mathbf{F}_L^{avk}(\alpha, \beta) \right\} \end{aligned} \quad (\text{A17})$$

This expression is used in Eq. (14) to calculate  $\sigma_{\alpha\beta}^S$ .

- 
- <sup>1</sup> O. H. Nielsen and R. M. Martin. *Phys. Rev. Lett.*, 50:697, 1983.  
<sup>2</sup> O. H. Nielsen and R. M. Martin. *Phys. Rev. B*, 32:3780, 1985.  
<sup>3</sup> R. Yu, D. Singh, and H. Krakauer. *Phys. Rev. B*, 43:6411, 1991.  
<sup>4</sup> B. Kohler, S. Wilke, M. Scheffler, R. Kouba, and C. Ambrosch-Draxl. *Comput. Phys. Commun.*, 94:31, 1996.  
<sup>5</sup> N. Nagasako and T. Oguchi. *J. Phys. Soc. Jap.*, 80:024701, 2011.  
<sup>6</sup> N. Nagasako and T. Oguchi. *J. Phys. Soc. Jap.*, 82:044701, 2011.  
<sup>7</sup> J. M. Soler and A. R. Williams. *Phys. Rev. B*, 40:1560, 1989.  
<sup>8</sup> J. M. Soler and A. R. Williams. *Phys. Rev. B*, 42:9728, 1990.  
<sup>9</sup> O. K. Anderson. *Phys. Rev. B*, 12:3060, 1975.  
<sup>10</sup> T. Thonhauser, C. Ambrosch-Draxl, and D.J. Singh. *Solid State Commun.*, 124:275, 2002.  
<sup>11</sup> K. Belbase, A. Tröster, and P. Blaha. *Phys. Rev. B*, (ac-

- cepted), 2021.  
<sup>12</sup> J. P. Perdew and A. Zunger. *Phys. Rev. B*, 23:5048, 1981.  
<sup>13</sup> E. Sjöstedt, L. Nordström, and D. J. Singh. *Solid State Commun.*, 114:15, 2000.  
<sup>14</sup> D. J. Singh and L. Nordström, editors. *Planewaves, Pseudopotentials, and the LAPW method 2<sup>nd</sup> Ed.* Springer, New York, 2006.  
<sup>15</sup> G. K. H. Madsen, P. Blaha, K. Schwarz, E. Sjöstedt, and L. Nordström. *Phys. Rev. B*, 64:195134, 2001.  
<sup>16</sup> P. Blaha, K. Schwarz, F. Tran, R. Laskowski, G. K. H. Madsen, and L. D. Marks. *J. Chem. Phys.*, 152:074101, 2020.  
<sup>17</sup> J. P. Perdew, K. Burke, and M. Ernzerhof. *Phys. Rev. Lett.*, 77:3865, 1996.  
<sup>18</sup> J. P. Perdew, K. Burke, and M. Ernzerhof. *Phys. Rev. Lett.*, 78:1396, 1997.  
<sup>19</sup> J. C. Slater. *Phys. Rev. B*, 51:846, 1937.  
<sup>20</sup> D. Koelling and G. O. Arbman. *J. Phys. F: Met. Phys.*, 5:2041, 1975.  
<sup>21</sup> D. Singh. *Phys. Rev. B*, 43:6388, 1991.  
<sup>22</sup> P. Blaha, K. Schwarz, G. K. H. Madsen, D. Kvasnicka,

- J. Luitz, R. Laskowski, F. Tran, and L. D. Marks, editors. *Wien2k:An Augmented Plane Wave Plus Local Orbitals Program for Calculating Crystal Properties*. Vienna University of Technology, Vienna, 2021.
- <sup>23</sup> M. Weinert, E. Wimmer, and A. J. Freeman. *Phys. Rev.*, 26:4571, 1982.
- <sup>24</sup> S. Lehtola, C. Steigemann, M. J. T. Oliveira, and M. A. L. Marques. *SoftwareX*, 7:1, 2018.
- <sup>25</sup> F. D. Murnaghan. *Proc. Natl. Acad. Sci. U.S.A.*, 30:244, 1944.
- <sup>26</sup> S. Goedecker and K. Maschke. *Phys. Rev. B*, 45:1597, 1992.

## Stress tensor in the linearized augmented plane wave method

Kamal Belbase<sup>1</sup>, Andreas Tröster<sup>2</sup>, and Peter Blaha<sup>1</sup>

<sup>1</sup>*Institute of Materials Chemistry, Vienna University of Technology, Getreidemarkt 9/165-TC, A-1060 Vienna, Austria*

<sup>2</sup>*Faculty of Physics, University of Vienna, Boltzmanngasse 5, A-1090 Vienna, Austria*



(Received 7 October 2021; accepted 10 November 2021; published 29 November 2021)

In this paper we present a detailed derivation of the stress tensor for the nonrelativistic full potential linearized augmented plane wave (LAPW) method. The formalism has been implemented into the WIEN2K code and has been thoroughly tested for the equilibrium lattice parameters in various solids. Hydrostatic and nonhydrostatic conditions have been applied and the accuracy of individual stress components has been tested at finite strain. We also tested the convergence of the stress tensor with respect to the basis set and found it necessary to increase the basis set a bit as compared to total energy calculations. The effect of the tetrahedron and Fermi-Dirac (FD) methods on the calculated stress is studied for aluminum and found that the FD method improves the results. Finally, a brief comparison with previous attempts in the literature on this topic is given.

DOI: [10.1103/PhysRevB.104.174113](https://doi.org/10.1103/PhysRevB.104.174113)

### I. INTRODUCTION

The minimization of the total energy ( $E_{\text{tot}}$ ) with respect to the structural parameters of a material under a specific set of constraints is one of the fundamental tasks of modern solid state theory. Since in compounds with lower symmetry there could be tens to hundreds of structural parameters, determining the total energy alone is not sufficient for this goal and additional observables must be considered. One is the derivative of  $E_{\text{tot}}$  with respect to the atomic positions, i.e., the forces acting on the atoms [1–3]. Basically all major codes for solid state simulations have implemented efficient algorithms to determine these forces, and various force relaxation methods for optimizations of the atomic positions exist [4]. Another ingredient is knowledge of the stress tensor [5,6], i.e., the derivative of  $E_{\text{tot}}$  with respect to strain, which is necessary to optimize the lattice parameters and angles in low symmetry cases.

The stress tensor formalism was first adapted to density functional theory (DFT) [7,8] by Nielsen and Martin in Refs. [5,6], and verified using a plane wave based pseudopotential implementation. Their work was limited to the local density approximation (LDA), but later the derivation was extended to a semilocal exchange-correlation functional by Dal Corso and Resta [9]. A further extension to the projector augmented wave (PAW) method was published by Torrent *et al.* [10]. An alternative but less common way to calculate the stress tensor is via density functional perturbation theory (DFPT) [11], since strain may be regarded as a parametric perturbation. However, the application of strain also changes the periodic boundary conditions of the eigenfunctions of a Hamiltonian, which creates difficulties in the perturbative expansions used in DFPT [11]. These problems were finally overcome by an elegant reduced coordinate formulation in terms of strain-dependent metric tensors [12–14].

In plane wave pseudopotential calculations, a full structural optimization of both the atomic positions and the shape and size of the unit cell has thus been made possible and has been

implemented in many such DFT codes. On the other hand, in all-electron linearized augmented plane wave (LAPW) methods [15,16], depending on the symmetry of the system at hand, a unit cell optimization could only be achieved by tedious if not prohibitively expensive procedures based on fitting lattice parameters to a possibly large number of total energy calculations, putting the all-electron LAPW approach at a significant disadvantage as compared to the pseudopotential plane wave based methods. Therefore, it is only too understandable that a number of efforts [17–21] have been made within the last two decades to remove this shortcoming of the LAPW approach. However, only the work of Nagasako and Oguchi [19,20] led to a fully functional stress tensor implementation, but their approach was based on the Soler-Williams LAPW method [22,23], which is somewhat different from standard LAPW. Thus it is fair to say that the task of implementing a fully functional stress tensor into a standard LAPW DFT code persisted to represent a long-standing and pressing problem. This task has finally been accomplished in our present paper.

Below, we shall present a thorough description of the formalism of the stress tensor within the LAPW method. The implementation into our WIEN2k code [24,25] is tested in terms of convergence and accuracy on a couple of examples. Then a brief comparison with previous respective work is given in the discussion. We limit ourselves to a nonrelativistic description of the valence states, while the core states can be handled fully relativistically.

### II. STRESS TENSOR IN LAPW BASED METHODS

#### A. Basis function

The introduction of a set of basis functions is necessary to numerically solve Kohn-Sham single-particle equations in density functional theory (DFT) and to represent the electron density. In the LAPW method [16], the basis functions are defined according to the behavior of the potential and its effect on wave functions. Near the nuclei, the potential is very strong

but still approximately spherical, and the wave functions are similar to those of a free atom, and thus may contain several nodes and a cusp at the nucleus. In the so-called interstitial (IS) region farther away from the nuclei, the potential is weaker, and the wave functions are much smoother. Based on these observations, the unit cell of a crystal with volume  $\Omega$  is divided into nonoverlapping atom-centered spheres with radii  $R_a$  and the remaining IS region. The LAPW basis functions are defined by smoothly augment plane waves  $\frac{1}{\sqrt{\Omega}}e^{i(\mathbf{k}+\mathbf{K})\cdot\mathbf{r}}$  in

$$\phi_{kK}(\mathbf{r}) = \begin{cases} \frac{1}{\sqrt{\Omega}}e^{i(\mathbf{k}+\mathbf{K})\cdot\mathbf{r}}, & \mathbf{r} \in \text{IS}, \\ \sum_{l=0}^{l_{\max}} \sum_{m=-l}^l [a_{lm}^{akK} u_l(r_a, E_l^a) + b_{lm}^{akK} \dot{u}_l(r_a, E_l^a)] Y_{lm}(\hat{\mathbf{r}}_a), & \mathbf{r} \in R_a. \end{cases} \quad (1)$$

Here,  $\mathbf{r}_a = \mathbf{r} - \boldsymbol{\tau}_a$  denotes the local position vector of a nucleus of an atom  $a$  with length  $r_a = |\mathbf{r}_a|$  and directional unit vector  $\hat{\mathbf{r}}_a = \mathbf{r}/r_a$ , whereas the position vector  $\mathbf{r}$  is defined with respect to the global coordinate system, which is often the crystal coordinate system.  $Y_{lm}$  is a spherical harmonic for angular momentum quantum numbers  $lm$  and  $\mathbf{k}$  denotes a wave vector in the first Brillouin zone while  $\mathbf{K}$  denotes a reciprocal lattice vector. In Eq. (1) each interstitial plane wave is augmented within the atomic spheres by a linear combination of radial functions plus their energy derivative times spherical harmonics. Imposing continuity in value and slope of the basis functions at the sphere boundary  $r_a = R_a$  fixes the unknown coefficients  $a_{lm}^{akK}$  and  $b_{lm}^{akK}$  in Eq. (1).

In the presence of energetically high lying core states, which are often referred to as semicore states, the so-called local orbitals  $\phi_{\text{LO}}$  (LOs) as described in Ref. [16] can be added. These additional functions contain an additional radial basis function at an energy  $E_l^{a,\text{sc}}$  close to the semicore (sc) eigenvalues and are nonzero only within the region of the atomic spheres.

The basis functions Eq. (1) and the LOs are used to represent the wave function  $\psi_{vk}(\mathbf{r})$  for the band  $v$  and wave vector  $\mathbf{k}$ ,

$$\psi_{vk}^v(\mathbf{r}) = \sum_K c_{vkK} \phi_{kK}(\mathbf{r}) + \sum_{\text{LO}} c_{vk,\text{LO}} \phi_{\text{LO}}(\mathbf{r}), \quad (2)$$

with expansion coefficients  $c_{vkK}$  and  $c_{vk,\text{LO}}$ , where the summation runs over all reciprocal lattice vectors with  $|\mathbf{K}| \leq K_{\max}$  and all LOs of all atoms in the cell.

In the calculation of the total energy, the valence wave functions enter implicitly only through the valence charge density  $\rho_v(\mathbf{r}) = \sum_{vk} n_{vk} |\psi_{vk}^v(\mathbf{r})|^2$ , where  $n_{vk}$  is the corresponding occupation number. When calculating the stress tensor, however, the individual wave functions are explicitly involved in the valence kinetic energy stress and the valence correction stress, as will be shown below.

The valence electron density is expanded into a Fourier series in the interstitial and into symmetry adapted lattice harmonics inside the spheres [16],

$$\rho_v(\mathbf{r}) \equiv \begin{cases} \sum_K \rho(\mathbf{K}) e^{i(\mathbf{K}) \cdot \mathbf{r}}, & \mathbf{r} \in \text{IS}, \\ \sum_{LM} \rho_{LM}(r) Y_{LM}(\hat{\mathbf{r}}), & \mathbf{r} \in R_a, \end{cases} \quad (3)$$

the IS with an atomiclike angular momentum expansion in the atomic spheres, where  $\mathbf{K}$  is a reciprocal lattice vector with modulus  $|\mathbf{K}| \leq K_{\max}$  smaller than a chosen cutoff. Specifically, inside the atomic spheres around nucleus of an atom  $a$  at position  $\boldsymbol{\tau}_a$ , for each  $l \leq l_{\max}$  we solve the radial Schrödinger equation using the spherically symmetric potential at certain prescribed energies  $E_l^a$  and obtain the resulting numerical solutions  $u_l(r_a, E_l^a)$  and their energy derivatives  $\dot{u}_l(r_a, E_l^a)$  as our radial basis functions:

where  $G_{\max}$  should be chosen at least as large as  $2K_{\max}$ . The total charge density and the potential are also expanded analogously to Eq. (3).

## B. Stress tensor

The stress tensor is defined as the first-order variation in the total energy with respect to strain. The DFT Kohn-Sham total energy [26],

$$E_{\text{tot}} = E_{\text{kin}} + E_{\text{es}} + E_{\text{xc}}, \quad (4)$$

is therefore an appropriate starting point of its calculation. Here,

$$E_{\text{kin}} = \sum_{vk} n_{vk} \epsilon_{vk} - \int_{\Omega} d^3 \mathbf{r} \rho(\mathbf{r}) V_{\text{eff}}(\mathbf{r}), \quad (5a)$$

$$E_{\text{es}} = \frac{1}{2} \int_{\Omega} d^3 \mathbf{r} \rho(\mathbf{r}) V_C(\mathbf{r}) - \frac{1}{2} \sum_a Z_a V_M(\boldsymbol{\tau}_a), \quad (5b)$$

$$E_{\text{xc}} = \int_{\Omega} d^3 \mathbf{r} \rho(\mathbf{r}) \epsilon_{\text{xc}}(\mathbf{r}), \quad (5c)$$

are the noninteracting kinetic, electrostatic, and exchange-correlation energy, respectively.  $\epsilon_{vk}$  represents the Kohn-Sham eigenvalue for the  $v$ th band at wave vector  $\mathbf{k}$  and  $V_{\text{eff}}(\mathbf{r})$  is the effective potential, which is the sum of the Coulomb and the exchange-correlation potential  $\mu_{\text{xc}}(\rho)$ . In (5b),

$$V_C(\mathbf{r}) = \int d^3 \mathbf{r}' \frac{\rho(\mathbf{r}')}{|\mathbf{r} - \mathbf{r}'|} - \sum_a \frac{Z_a}{|\mathbf{r} - \boldsymbol{\tau}_a|}, \quad (6a)$$

$$V_M(\boldsymbol{\tau}_a) = \int d^3 \mathbf{r}' \frac{\rho(\mathbf{r}')}{|\mathbf{r}' - \boldsymbol{\tau}_a|} - \sum_{a \neq b} \frac{Z_a}{|\boldsymbol{\tau}_a - \boldsymbol{\tau}_b|}, \quad (6b)$$

are the Coulomb and Madelung potential, respectively.  $Z_a$  is the nuclear charge of an atom  $a$  located at  $\boldsymbol{\tau}_a$ . In the local density approximation (LDA) the exchange-correlation energy per particle  $\epsilon_{\text{xc}}(\mathbf{r})$  is a local function of the total charge density  $\rho$ .

In order to compute the stress tensor, the total energy  $E_{\text{tot}}[\underline{\epsilon}]$  of a strained system needs to be differentiated with

respect to the strain tensor components  $\epsilon_{\alpha\beta}$ :

$$\sigma_{\alpha\beta} = \frac{1}{\Omega} \frac{dE_{\text{tot}}[\underline{\underline{\epsilon}}]}{d\epsilon_{\alpha\beta}} \Big|_{\underline{\underline{\epsilon}}=0}. \quad (7)$$

The symbol  $[\underline{\underline{\epsilon}}]$  will be generally used to denote quantities after deformation. Greek letters  $\alpha$  and  $\beta$  are used to denote the Cartesian coordinate components. The substitution of Eq. (4) in Eq. (7) suggests that in order to calculate the stress tensor,

the strain variation of  $E_{\text{kin}}$ ,  $E_{\text{es}}$ , and  $E_{\text{xc}}$  must first be assessed, which is done in the following sections.

### 1. The strain variation of the kinetic energy

This contribution results from the change in kinetic energy upon deforming the system. Formally,  $E_{\text{kin}}[\underline{\underline{\epsilon}}]$  is given by Eq. (5a) evaluated in the strained system. Taking the strain derivative of  $E_{\text{kin}}[\underline{\underline{\epsilon}}]$  results in

$$\frac{dE_{\text{kin}}[\underline{\underline{\epsilon}}]}{d\epsilon_{\alpha\beta}} \Big|_{\underline{\underline{\epsilon}}=0} = \frac{d}{d\epsilon_{\alpha\beta}} \Bigg|_{\underline{\underline{\epsilon}}=0} \sum_{v\mathbf{k}[\underline{\underline{\epsilon}}]} n_{v\mathbf{k}[\underline{\underline{\epsilon}}]}[\underline{\underline{\epsilon}}] \epsilon_{v\mathbf{k}[\underline{\underline{\epsilon}}]}[\underline{\underline{\epsilon}}] - \frac{d}{d\epsilon_{\alpha\beta}} \Bigg|_{\underline{\underline{\epsilon}}=0} \int_{\Omega[\underline{\underline{\epsilon}}]} d^3\mathbf{r}_\epsilon \rho[\underline{\underline{\epsilon}}](\mathbf{r}_\epsilon) V_{\text{eff}}[\underline{\underline{\epsilon}}](\mathbf{r}_\epsilon). \quad (8)$$

To calculate the first term, the strain derivative of the occupation number is required. In parallel with the calculation of LAPW forces [3], we assume that the strain dependence of the occupation numbers  $n_{v\mathbf{k}[\underline{\underline{\epsilon}}]}[\underline{\underline{\epsilon}}]$  vanishes to linear order, i.e.,  $\frac{dn_{v\mathbf{k}[\underline{\underline{\epsilon}}]}[\underline{\underline{\epsilon}}]}{d\epsilon_{\alpha\beta}} \Big|_{\underline{\underline{\epsilon}}=0} \rightarrow 0$ . The strain variation of the total Kohn-Sham eigenvalues  $\frac{d\epsilon_{v\mathbf{k}[\underline{\underline{\epsilon}}]}[\underline{\underline{\epsilon}}]}{d\epsilon_{\alpha\beta}} \Big|_{\underline{\underline{\epsilon}}=0}$  is split into the change of core eigenvalues  $\frac{d\epsilon_c[\underline{\underline{\epsilon}}]}{d\epsilon_{\alpha\beta}} \Big|_{\underline{\underline{\epsilon}}=0}$  and valence eigenvalues  $\frac{d\epsilon_{v\mathbf{k}[\underline{\underline{\epsilon}}]}[\underline{\underline{\epsilon}}]}{d\epsilon_{\alpha\beta}} \Big|_{\underline{\underline{\epsilon}}=0}$ . We first calculate the strain variation of the core eigenvalues using the Hellmann-Feynman theorem similar to the strategy used in the LAPW force calculations:

$$\begin{aligned} \sum_c n_c \frac{d\epsilon_c[\underline{\underline{\epsilon}}]}{d\epsilon_{\alpha\beta}} \Big|_{\underline{\underline{\epsilon}}=0} &= \sum_c n_c \frac{d}{d\epsilon_{\alpha\beta}} \left\langle \psi_c^a[\underline{\underline{\epsilon}}](\mathbf{r}_\epsilon) | -\frac{1}{2} \nabla[\underline{\underline{\epsilon}}]^2 + V_{\text{eff}}[\underline{\underline{\epsilon}}](\mathbf{r}_\epsilon) | \psi_c^a[\underline{\underline{\epsilon}}](\mathbf{r}_\epsilon) \right\rangle \Big|_{\underline{\underline{\epsilon}}=0} \\ &= \sum_{a \in \Omega} \int_{R_a} d^3 r_a \rho_c^a(\mathbf{r}_a) \frac{dV_{\text{eff}}[\underline{\underline{\epsilon}}](\mathbf{r}_a)}{d\epsilon_{\alpha\beta}} \Big|_{\underline{\underline{\epsilon}}=0}. \end{aligned} \quad (9)$$

Here,  $\psi_c^a(\mathbf{r})$  denotes a core state  $c$  of an atom  $a$ ,  $\langle \cdot | \cdot | \cdot \rangle$  refers to the volume integration within the unit cell, the sum  $\sum_{a \in \Omega}$  runs over all atoms and core states of the unit cell,  $\rho_c^a$  refers to the core electron density of an atom  $a$ , and  $\int_{R_a} d^3 r_a$  indicates that the integration is limited to atomic spheres because the core wave functions vanish outside the spheres.

In the following we evaluate the strain variation of the valence eigenvalues,

$$\frac{d\epsilon_{v\mathbf{k}[\underline{\underline{\epsilon}}]}^v}{d\epsilon_{\alpha\beta}} = \frac{d}{d\epsilon_{\alpha\beta}} \frac{\int_{\Omega[\underline{\underline{\epsilon}}]} d^3 r_\epsilon \psi_{v\mathbf{k}[\underline{\underline{\epsilon}}]}^{v*}[\underline{\underline{\epsilon}}](\mathbf{r}_\epsilon) \hat{H}_{\text{eff}}[\underline{\underline{\epsilon}}](\mathbf{r}_\epsilon) \psi_{v\mathbf{k}[\underline{\underline{\epsilon}}]}^v(\mathbf{r}_\epsilon)}{\int_{\Omega[\underline{\underline{\epsilon}}]} d^3 r_\epsilon \psi_{v\mathbf{k}[\underline{\underline{\epsilon}}]}^{v*}[\underline{\underline{\epsilon}}](\mathbf{r}_\epsilon) \psi_{v\mathbf{k}[\underline{\underline{\epsilon}}]}^v(\mathbf{r}_\epsilon)}. \quad (10)$$

- (1) The volume integration is transformed back to the unstrained unit cell as  $\int_{\Omega[\underline{\underline{\epsilon}}]} d^3 \mathbf{r}_\epsilon \rightarrow \det(1 + \underline{\underline{\epsilon}}) \int_{\Omega} d^3 \mathbf{r}$ .
- (2) Differentiation with respect to the strain is simplified as described in Appendix B.
- (3) The strain variation of the effective Hamiltonian is computed as

$$\frac{dH_{\text{eff}}[\underline{\underline{\epsilon}}](\mathbf{r}[\underline{\underline{\epsilon}}])}{d\epsilon_{\alpha\beta}} \Big|_{\underline{\underline{\epsilon}}=0} = \frac{1}{2} (\partial_\alpha \partial_\beta + \partial_\beta \partial_\alpha) + \frac{dV_{\text{eff}}[\underline{\underline{\epsilon}}](\mathbf{r}[\underline{\underline{\epsilon}}])}{d\epsilon_{\alpha\beta}} \Big|_{\underline{\underline{\epsilon}}=0}. \quad (11)$$

The first term results from the strain variation of the nonrelativistic kinetic energy  $\frac{d\nabla^2[\underline{\underline{\epsilon}}]}{d\epsilon_{\alpha\beta}}$  of the Hamiltonian operator and the second term results from a change in the total potential according to the strain. The symbol  $\partial_\alpha = \hat{\mathbf{r}}_\alpha \frac{\partial}{\partial r}$  is shorthand for the partial derivative along the Cartesian direction  $\alpha$ .

Using Eq. (11) and Appendix B, Eq. (10) can be brought into the form

$$\begin{aligned} \frac{d\epsilon_{v\mathbf{k}[\underline{\underline{\epsilon}}]}^v}{d\epsilon_{\alpha\beta}} &= 2 \operatorname{Re} \left\langle \frac{d\psi_{v\mathbf{k}[\underline{\underline{\epsilon}}]}^v[\underline{\underline{\epsilon}}](\mathbf{r}[\underline{\underline{\epsilon}}])}{d\epsilon_{\alpha\beta}} \Big|_{\underline{\underline{\epsilon}}=0} \mid \hat{H}_{\text{eff}}(\mathbf{r}) - \epsilon_{v\mathbf{k}}^v \mid \psi_{v\mathbf{k}}^v(\mathbf{r}) \right\rangle + \frac{1}{2} \int_{\Omega} d^3 r \psi_{v\mathbf{k}}^v(\mathbf{r}) (\partial_\alpha \partial_\beta + \partial_\beta \partial_\alpha) \psi_{v\mathbf{k}}^v(\mathbf{r}) \\ &\quad + \int_{\Omega} d^3 r \rho_v(\mathbf{r}) \frac{dV_{\text{eff}}[\underline{\underline{\epsilon}}](\mathbf{r}[\underline{\underline{\epsilon}}])}{d\epsilon_{\alpha\beta}} \Big|_{\underline{\underline{\epsilon}}=0}. \end{aligned} \quad (12)$$

Here,  $\operatorname{Re}$  denotes the real part of a complex number. The first term of Eq. (12), which is similar to the Pulay term in the force calculation, is the so-called valence correction or incomplete basis-set (IBS) correction. To compute this IBS correction, the valence states described in Eq. (2) need to be defined in the strained environment followed by differentiation with respect to the

strain:

$$\left. \frac{d\psi_{vk[\underline{\epsilon}]}^v(\mathbf{r}[\underline{\epsilon}])}{d\epsilon_{\alpha\beta}} \right|_{\underline{\epsilon}=0} = \sum_K \left( \frac{d}{d\epsilon_{\alpha\beta}} \left[ \frac{c_{vk[\underline{\epsilon}]K[\underline{\epsilon}][\underline{\epsilon}]}[\underline{\epsilon}]}{\sqrt{\Omega[\underline{\epsilon}]}} \right]_{\underline{\epsilon}=0} \sqrt{\Omega} \phi_{kK}(\mathbf{r}) + \frac{c_{vkK}}{\sqrt{\Omega}} \frac{d}{d\epsilon_{\alpha\beta}} \left[ \sqrt{\Omega[\underline{\epsilon}]} \phi_{k[\underline{\epsilon}]K[\underline{\epsilon}][\underline{\epsilon}]}(\mathbf{r}[\underline{\epsilon}]) \right]_{\underline{\epsilon}=0} \right). \quad (13)$$

(1) The first term on the right-hand side of (13) is proportional to the basis functions, so it does not contribute to the valence correction at all.

(2) The second term does not contribute in the interstitial region since the  $\Omega$  times the basis function do not change with strain in first order [see Eq. (D1) of Appendix D]. Therefore, it suffices to calculate the total integral  $\langle \cdot | \cdot | \cdot \rangle$  only within the atomic spheres  $\langle \cdot | \cdot | \cdot \rangle^{R_a}$ . Inside the atomic spheres, using the so-called *frozen augmentation approximation* [3], we discard an explicit strain dependency in  $\phi_{k[\underline{\epsilon}]K[\underline{\epsilon}][\underline{\epsilon}]}(\mathbf{r}[\underline{\epsilon}])$  while keeping an implicit dependency via its smeared argument, i.e.,  $\phi_{k[\underline{\epsilon}]K[\underline{\epsilon}][\underline{\epsilon}]}(\mathbf{r}[\underline{\epsilon}]) \rightarrow \phi_{k[\underline{\epsilon}]K[\underline{\epsilon}]}(\mathbf{r}[\underline{\epsilon}])$  [see Eq. (D6)].

Substitution of Eqs. (9) and (12) into (8), and the evaluation of the second integral of Eq. (8) along the lines of Appendix B, results in

$$\begin{aligned} \left. \frac{dE_{\text{kin}}[\underline{\epsilon}]}{d\epsilon_{\alpha\beta}} \right|_{\underline{\epsilon}=0} &= 2 \sum_{vk} n_{vk} \operatorname{Re} \left\langle \frac{d\psi_{vk[\underline{\epsilon}]}^v(\mathbf{r}[\underline{\epsilon}])}{d\epsilon_{\alpha\beta}} \right\rangle_{\underline{\epsilon}=0} |\widehat{H}_{\text{eff}}(\mathbf{r}) - \epsilon_{vk}| \psi_{vk}^v \Bigg|_{\underline{\epsilon}=0}^{R_a} + \frac{1}{2} \sum_{vk} n_{vk} \int_{\Omega} d^3 r \psi_{vk}^{v*}(\mathbf{r}) (\partial_{\alpha} \partial_{\beta} + \partial_{\beta} \partial_{\alpha}) \psi_{vk}^v(\mathbf{r}) \\ &\quad - \delta_{\alpha\beta} \int_{\Omega} d^3 r \rho(\mathbf{r}) V_{\text{eff}}(\mathbf{r}) - \int_{\Omega} d^3 r \frac{d\rho[\underline{\epsilon}](\mathbf{r}[\underline{\epsilon}])}{d\epsilon_{\alpha\beta}} V_{\text{eff}}(\mathbf{r}) - \frac{1}{2} \sum_{a \in \Omega} \int_{R_a} d^3 r_a \rho_c^a(\mathbf{r}_a) (r_{\beta} \partial_{\alpha} + r_{\alpha} \partial_{\beta}) V_{\text{eff}}(\mathbf{r}). \end{aligned} \quad (14)$$

The evaluation of the above integrals is straightforward:

(1) Integrals over the unit cell are divided into integrals over atomic spheres and over the interstitial region.

(2) The first and second terms can be simplified using Eq. (D3) and Eqs. (C1) and (C9), respectively.

(3) The third term is easy to evaluate using the corresponding expressions for  $\rho(\mathbf{r})$  and  $V_{\text{eff}}(\mathbf{r})$  in terms of the spherical harmonics expansion inside atomic spheres and the Fourier expansion in the interstitial region.

(4) The fourth term will get canceled in combination with similar terms appearing in the electrostatic and exchange-correlation stress, and hence does not contribute to the final stress tensor.

(5) The last term is referred to as the core correction stress. When the unit cell is deformed, the core states change in two different ways. On the one hand, the core states will move along with the nuclei to a new position in the strained unit cell. On the other hand, the total potential in the unit cell is changed, and core states will interact with this modified potential. The explicit expression of the core correction in Eq. (14) illustrates that the core correction resembles the latter change. For a detailed evaluation, see Appendix E.

## 2. Strain variation of electrostatic energy

This contribution results from the change in electrostatic energy according to strain. In the following the electrostatic energy given in Eq. (5b) is first formulated in the strained system, i.e.,  $E_{\text{es}}[\underline{\epsilon}]$ , and then differentiated with respect to strain:

$$\begin{aligned} \left. \frac{dE_{\text{es}}[\underline{\epsilon}]}{d\epsilon_{\alpha\beta}} \right|_{\underline{\epsilon}=0} &= \frac{1}{2} \frac{d}{d\epsilon_{\alpha\beta}} \Bigg|_{\underline{\epsilon}=0} \int_{\Omega[\underline{\epsilon}]} d^3 r_{\epsilon} \rho[\underline{\epsilon}](\mathbf{r}_{\epsilon}) V_C[\underline{\epsilon}](\mathbf{r}_{\epsilon}) \\ &\quad - \frac{1}{2} \sum_{a \in \Omega[\underline{\epsilon}]} Z_a \frac{dV_M[\underline{\epsilon}](\boldsymbol{\tau}_a[\underline{\epsilon}])}{d\epsilon_{\alpha\beta}} \Bigg|_{\underline{\epsilon}=0}. \end{aligned} \quad (15)$$

Using Eq. (B1) to evaluate the strained variation of the integral, we obtain  $\sigma_{\alpha\beta}^{\text{es}}$  as

$$\begin{aligned} \left. \frac{dE_{\text{es}}[\underline{\epsilon}]}{d\epsilon_{\alpha\beta}} \right|_{\underline{\epsilon}=0} &= \frac{\delta_{\alpha\beta}}{2} \int_{\Omega} d^3 r \rho(\mathbf{r}) V_C(\mathbf{r}) \\ &\quad + \int_{\Omega} d^3 r \frac{d\rho[\underline{\epsilon}](\mathbf{r}[\underline{\epsilon}])}{d\epsilon_{\alpha\beta}} \Bigg|_{\underline{\epsilon}=0} V_C(\mathbf{r}) \\ &\quad + \frac{1}{2} \int_{\Omega} d^3 r \rho(\mathbf{r}) \frac{dV_C[\underline{\epsilon}](\mathbf{r}[\underline{\epsilon}])}{\epsilon_{\alpha\beta}} \Bigg|_{\underline{\epsilon}=0} \\ &\quad - \frac{1}{2} \sum_{a \in \Omega} Z_a \frac{dV_M[\underline{\epsilon}](\boldsymbol{\tau}_a[\underline{\epsilon}])}{d\epsilon_{\alpha\beta}} \Bigg|_{\underline{\epsilon}=0}, \end{aligned} \quad (16)$$

where  $\delta_{\alpha\beta}$  denotes the Kronecker delta.

(1) The first term contributes only to the diagonal elements of  $\sigma_{\alpha\beta}^{\text{es}}$ . The corresponding integral is straightforward to obtain.

(2) The second term cancels with a corresponding term in Eq. (14).

(3) When calculating the strain variation of  $V_C(\mathbf{r})$  and  $V_M(\mathbf{r})$ , the strained charge density  $\rho[\underline{\epsilon}](\mathbf{r}[\underline{\epsilon}])$  is replaced by the charge density of the unstrained system but smeared over the strained system, i.e.,  $\rho((1 - \underline{\epsilon})\mathbf{r}_{\epsilon})$ .

It is clear from the above equation that to evaluate the electrostatic stress tensor we need to calculate the strain variation of the Coulomb and Madelung potentials. Two different approaches are available in Refs. [17,21] to calculate the change in the potential under infinitesimal strain, but due to the lack of sufficient results it is unclear which approach works best for the original LAPW method. In Ref. [17], the authors suggest that the strain potential can be determined directly from the strained charge density using Poisson's equation. In contrast, in Ref. [21] an explicit derivation of the strain variation of the Coulomb potential using Weinert's method

[27] was presented. We tried to work with the expression provided in Ref. [21] first, but unfortunately this resulted in huge errors in the calculated stress tensor and we could not figure out where the problem was actually originating from. Similar problems are reported by Klüppelberg in Ref. [21]. Therefore, after some painstaking numerical testing we finally decided to resort to a different approach to simplify the electrostatic stress tensor. In our derivation we first transform all the integrals from the strained to the unstrained system. Following the standard procedure of the LAPW method, the total integral is divided into the interstitial and the atomic sphere parts. When solving the strain variation of the Coulomb potential in the interstitial, we assume that the Fourier component of both the real interstitial charge density and the pseudocharge density are invariant under strain [see Eqs. (F3) and (F4)], and that the change in the potential is only due to the change in the reciprocal lattice vector. This leads to our expression of the electrostatic stress tensor in the interstitial region similar to that in Refs. [5,19]. In the atomic sphere region, we only consider the change in  $V_C(\mathbf{r})$  due to the change in the unit cell volume and the change in the radial vector.

### 3. The strain variation of the exchange-correlation energy

The LDA exchange-correlation energy per particle  $\epsilon_{xc}(\rho)$  depends exclusively on the density  $\rho$ . When the system is

$$\sigma_{\alpha\beta} = \sigma_{\alpha\beta}^{\text{val,kin}} + \sigma_{\alpha\beta}^{\text{val,corr}} + \sigma_{\alpha\beta}^{\text{core,corr}} + \sigma_{\alpha\beta}^{\text{es}} + \sigma_{\alpha\beta}^{\text{xc,LDA}}, \quad (18)$$

with

$$\sigma_{\alpha\beta}^{\text{val,kin}} = \frac{1}{2\Omega} \sum_{vk} n_{vk} \int_{\Omega} d^3 r \psi_{vk}^*(\mathbf{r}) (\partial_{\alpha} \partial_{\beta} + \partial_{\beta} \partial_{\alpha}) \psi_{vk}^{\text{v}}(\mathbf{r}), \quad (19)$$

$$\sigma_{\alpha\beta}^{\text{val,corr}} = \frac{2}{\Omega} \sum_{vk} n_{vk} \text{Re} \left\langle \frac{d\psi_{vk}^{\text{v}}(\mathbf{r}[\underline{\epsilon}])}{d\epsilon_{\alpha\beta}} \right|_{\underline{\epsilon}=0} \left| \widehat{H}_{\text{eff}}(\mathbf{r}) - \epsilon_{vk} \right| \psi_{vk}^{\text{v}} \left. \right\rangle^{R_a}, \quad (20)$$

$$\sigma_{\alpha\beta}^{\text{core,corr}} = -\frac{1}{2\Omega} \sum_{a \in \Omega} \int_{R_a} d^3 r \rho_c^a(\mathbf{r}) (r_{\beta} \partial_{\alpha} + r_{\alpha} \partial_{\beta}) V_{\text{eff}}(\mathbf{r}), \quad (21)$$

$$\sigma_{\alpha\beta}^{\text{es}} = -\frac{\delta_{\alpha\beta}}{2} \int_{\Omega} d^3 r \rho(\mathbf{r}) V_C(\mathbf{r}) + \frac{1}{2} \int_{\Omega} d^3 r \rho(\mathbf{r}) \frac{dV_C(\underline{\epsilon})(\mathbf{r}[\underline{\epsilon}])}{\epsilon_{\alpha\beta}} \Big|_{\underline{\epsilon}=0} - \frac{1}{2} \sum_{a \in \Omega} Z_a \frac{d}{d\epsilon_{\alpha\beta}} V_M(\underline{\epsilon})(\boldsymbol{\tau}_a[\underline{\epsilon}]) \Big|_{\underline{\epsilon}=0}, \quad (22)$$

$$\sigma_{\alpha\beta}^{\text{xc,LDA}} = \delta_{\alpha\beta} \int_{\Omega} d^3 r \rho(\mathbf{r}) [\epsilon_{xc}(\rho) - \mu_{xc}(\rho)]. \quad (23)$$

The final expressions of Eqs. (19)–(23), which are implemented in the WIEN2K code, may be found in Appendix G, and the results for validating our implementation are presented in Sec. III. Note that most of the quantities such as  $\psi_{vk}(\mathbf{r})$ ,  $\rho(\mathbf{r})$ ,  $\rho_c(\mathbf{r}_a)$ ,  $V_C(\mathbf{r})$ ,  $\epsilon_{xc}$ ,  $\mu_{xc}$ , and  $\partial\epsilon_{xc}/\partial\sigma$  that appear in this formula are readily available from a regular total energy calculation. Most of the terms involved in Eqs. (19)–(23) are easy to evaluate, but the evaluation of  $\sigma_{\alpha\beta}^{\text{val,corr}}$  and  $\sigma_{\alpha\beta}^{\text{val,kin}}$ , which explicitly contains the wave functions, is both mathematically and computationally demanding.

## III. RESULTS

In the LAPW method, the accuracy of results is controlled by the selection of various input parameters. One of them is

deformed,  $E_{xc}$  changes compared to the undeformed system, which makes it necessary to evaluate the strain variation of  $E_{xc}$ . In the following,  $E_{xc}$  given in Eq. (5c) is first defined in the strained system  $E_{xc}[\underline{\epsilon}]$ , differentiated with respect to strain and using the same techniques discussed in the calculation of the kinetic energy and the electrostatic stress tensor results in

$$\frac{dE_{xc}[\underline{\epsilon}]}{d\epsilon_{\alpha\beta}} \Big|_{\underline{\epsilon}=0} = \delta_{\alpha\beta} \int_{\Omega} d^3 r \rho(\mathbf{r}) \epsilon_{xc} + \int_{\Omega} d^3 r \frac{d\rho[\underline{\epsilon}](\mathbf{r}[\underline{\epsilon}])}{d\epsilon_{\alpha\beta}} \mu_{xc}. \quad (17)$$

Due to the presence of the Kronecker delta, the first term only contributes to the diagonal elements of  $\sigma_{\alpha\beta}^{xc}$ . The second term cancels with a corresponding contribution in the double counting part of the kinetic energy—the second term of Eq. (5a). In the spin-polarized case, contributions of spin-up and spin-down charge densities must be explicitly included, yielding separate contributions to the total exchange-correlation stress tensor.

### 4. Total stress tensor

We collect the strain variation of the kinetic energy, the electrostatic energy, and the exchange-correlation energy from Eqs. (14), (16), and (17) to define the strain variation of the total energy and thereby the stress tensor, Eq. (7). Finally the stress tensor in the LAPW method is

$R_a K_{\max}$ , where  $R_a$  is the smallest atomic sphere size among the constituent atoms, and  $K_{\max}$  is the modulus of the largest reciprocal vector contributing to the Fourier expansion of wave functions.  $R_a K_{\max}$  limits the total number of basis functions in the LAPW method and determines the cutoff energy of the plane waves via  $E_{\max} = K_{\max}^2$ . The value of  $R_a K_{\max}$  in a total energy calculation typically ranges from 7 to 10 depending on the atoms in the system (for elements with  $f$  electrons even a value of 11 may be required). However, it is unclear how the accuracy of the analytically computed stress tensor would depend on the choice of  $R_a K_{\max}$ . One may anticipate that a larger value than for regular total energy calculations might be required, because the energy is variational with respect to small changes in the density according to the

Hohenberg-Kohn theorems [7,8] and thus errors in the density only enter in quadratic order, while there is no corresponding variational principle for the stress tensor so that errors may already manifest themselves in linear order.

In addition to  $R_a K_{\max}$ ,  $l_{\max}$ , the cutoff value for the expansion of basis functions in the region of the atomic spheres, the cutoff value  $G_{\max}$  for the plane wave expansion of the charge densities and the potential, the cutoff value  $L_{\max}^{\text{ns}}$  for the expansion of the nonspherical potential, and the chosen size of the  $k$  mesh in the Brillouin zone (BZ) also have a certain impact on the accuracy of the calculation. Moreover, in metallic systems, the choice of the smearing method and, if the Fermi-Dirac (FD) method is chosen, the particular value of the corresponding temperature broadening parameter, determine the quality of results.

In the sections below we provide various convergence tests of the above mentioned parameters on several systems. The results were produced using our WIEN2K [24,25] implementation using LDA for the exchange-correlation energy and potential. To validate our implementation, we compare the results of the stress tensor with the least squares fit of total energy versus volume using the Birch-Murnaghan [28] (BM) equation of state. From the BM fit we obtain the pressure  $P^{(E)} := -\frac{dE(\Omega)}{d\Omega}$  [see Fig. 1(a)]. The resulting pressures  $P^{(E)}$  are then compared with the hydrostatic pressure  $P^{(\sigma)} := -(\sigma_{11} + \sigma_{22} + \sigma_{33})/3$  as calculated directly from our analytical expression Eq. (18) of the stress tensor. The difference between  $P^{(E)}$  and  $P^{(\sigma)}$  represents an excellent measure of the accuracy and reliability of our formalism. In particular, a small remainder of  $P^{(E)} - P^{(\sigma)}$  within some acceptable limit suggests that the zero pressure equilibrium configuration predicted from the stress tensor calculation is quite close to that obtained from the minimum of the total energy.

### A. Aluminum

For fcc aluminum, the total energy and  $P^{(E)}$  as a function of  $\Omega$  for different  $R_a K_{\max}$  is plotted in Fig. 1(a).  $P^{(\sigma)}$  is shown in Fig. 1(b), and the deviation  $P^{(E)} - P^{(\sigma)}$  between  $P^{(E)}$  and  $P^{(\sigma)}$  in Fig. 1(c). Calculations are done with  $R_a K_{\max}$  of 7, 8, 9, and 10. In this case  $R_a = 2.5$  bohrs is chosen as the atomic sphere radius of the Al atom. In the following calculations, 1s and 2s states of Al are treated as core states and all other states up to  $l_{\max} = 10$  are treated as valence states. All valence states except the 2p states are described using pure LAPW basis functions Eq. (1), while 2p states are represented using semicore local orbitals (LOs)—the second term in Eq. (2). We choose most of the input parameters higher than necessary for a regular total energy calculations in order to exclude possible numerical errors due to these parameters. The  $G_{\max}$  in the expansion of the charge density [see Eq. (3)] and the potential in the interstitial is 20 Ry $^{\frac{1}{2}}$ , and a  $k$  mesh is  $(24 \times 24 \times 24)$ . The standard tetrahedron method with Blöchl's correction [29] [Figs. 1(a)–1(c)], as well as the FD method with a broadening parameter of 0.005 Ry [Fig. 1(d)], for the integration in the irreducible Brillouin zone (IBZ) are used. All integrations in the interstitial region are evaluated using the fast Fourier transform (FFT) method with a FFT grid of  $90 \times 90 \times 90$ .

The total energy curves [Fig. 1(a)] show that the equilibrium volume and  $P^{(E)}$  are insensitive to  $R_a K_{\max}$  although

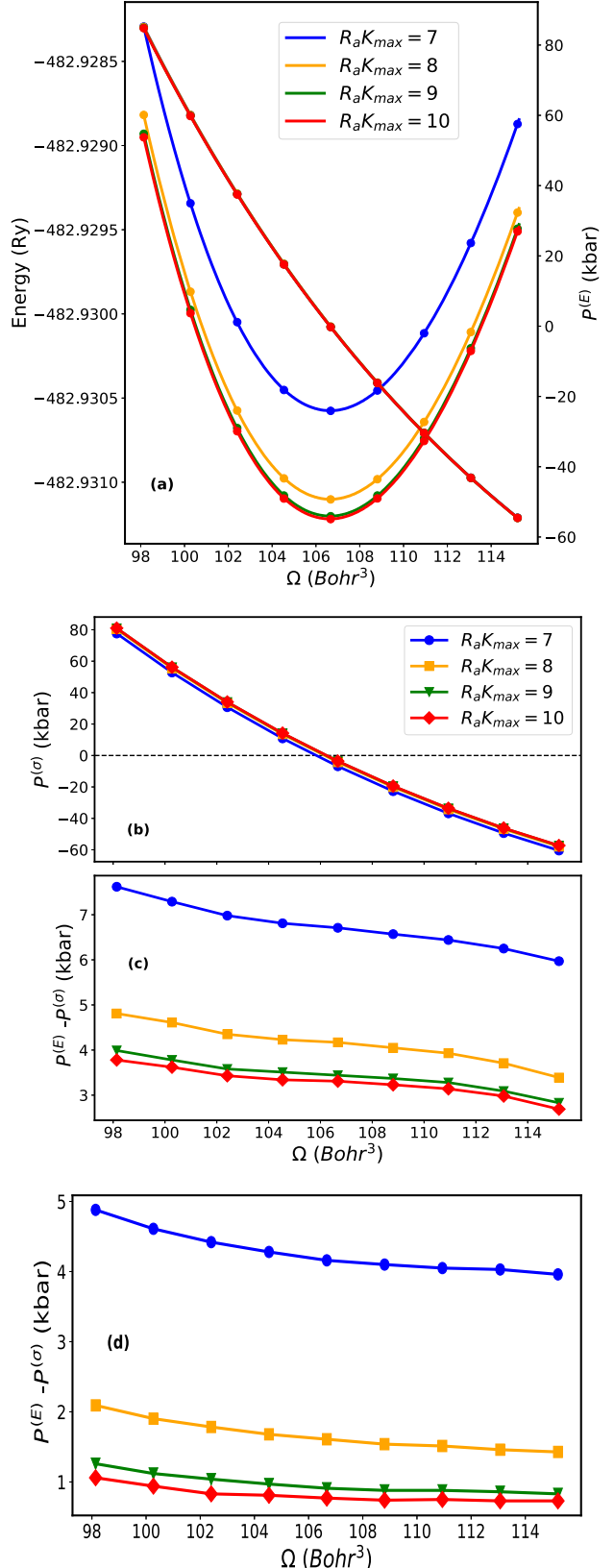


FIG. 1. (a) Energy-volume curves as well as  $P^{(E)}$ , (b) the negative trace of the full stress tensor  $P^{(\sigma)}$ , and (c) the difference between  $P^{(\sigma)}$  and  $P^{(E)}$  as a function of  $\Omega$  for various  $R_a K_{\max}$  for fcc Al. The standard tetrahedron method with the Blöchl correction is used in (a)–(c), while the FD method with a 0.005 Ry broadening parameter is used for (d).

TABLE I. Predicted lattice constant  $a_0$  (in bohrs) and bulk modulus  $B$  (in kbars) from the analytical stress tensor [superscript  $(\sigma)$ ] and directly from the total energy [superscript  $(E)$ ] as a function of  $R_a K_{\max}$  for fcc Al. The standard tetrahedron method with Blöchl's correction is used for  $k$ -space integration.

$R_a K_{\max}$	$a_0^{(\sigma)}$	$a_0^{(E)}$	$B^{(\sigma)}$	$B^{(E)}$
7	7.508	7.528	871	844
8	7.516	7.528	859	844
9	7.518	7.528	857	843
10	7.518	7.528	856	843

the magnitude of the total energy does change with  $R_a K_{\max}$ . As a result,  $P^{(E)}$  barely changes, which can also be seen in the resulting prediction for the equilibrium lattice parameter shown in Table I. The pressure  $P^{(\sigma)}$  estimated from the stress tensor shown in Fig. 1(b) clearly shows a  $R_a K_{\max}$  dependency. However, this dependency, which can also be seen in Fig. 1(c), only manifests itself at the third decimal place in the predicted lattice parameter provided  $R_a K_{\max}$  is chosen greater than 7 (see Table I). All calculations in Figs. 1(a)–1(c) were done with the Blöchl correction [29] in the tetrahedron method. We also repeated the same calculation without Blöchl's correction and found that this correction neither improved nor worsened the results. Aluminum is a metallic system with a complicated Fermi surface and has partial occupations close to the Fermi level. When deriving stress tensor formulas, we assumed that the occupancy does not depend on the strain in a first-order approximation. The underlying reasoning for this assumption, which is also supported for the closely related force calculations [3], is that the number of electrons in the system is conserved and thus the change in the occupation numbers is a second-order effect. For the system with partial occupations, however, Ref. [30] reports that when calculating forces, the total energy given in Eq. (4) is not variational and needs to be replaced by the more general expression

$$F = E_{\text{tot}} - \sum_{vk} n_{vk} \sigma S, \quad (24)$$

in which  $F$  denotes the Helmholtz free energy,  $S$  is the entropy, and  $\sigma = k_B T$ , where  $T$  and  $k_B$  denote the temperature and Boltzmann's constant, respectively. Similar to what is observed in the force formalism, we expect that when calculating the strain variation of the second term of Eq. (24), a corresponding term will be canceled when the strain variation of the occupation number is computed. In Ref. [30] an explicit equation for  $S$  is given for the Fermi-Dirac distribution function. We repeated the above calculations [Figs. 1(a)–1(c)] using the FD method which is shown in Fig. 1(d). The comparison of Figs. 1(c) and 1(d), and Tables I and II shows that the analytical stress tensor and thereby the predicted lattice constant  $a_0^{(\sigma)}$  from the stress tensor improves significantly. These tables also show that there is a small change in the total energy, affecting  $a_0^{(E)}$  only in the third digit, but more noticeable in the bulk modulus. The effect on the analytical stress calculation, on the other hand, is much stronger, as can be seen from comparing the  $a_0^{(\sigma)}$  columns of Tables I and II. Moreover, unless we choose  $R_a K_{\max}$  as small as 7, the discre-

TABLE II. Predicted lattice constant  $a_0$  (in bohrs) and bulk modulus  $B$  (in kbars) from the analytical stress tensor formalism [superscript  $(\sigma)$ ] and directly from the total energy [superscript  $(E)$ ] as a function of  $R_a K_{\max}$  for fcc Al. The FD method with a broadening parameter of 0.005 Ry is used.

$R_a K_{\max}$	$a_0^{(\sigma)}$	$a_0^{(E)}$	$B^{(\sigma)}$	$B^{(E)}$
7	7.513	7.526	854	838
8	7.521	7.526	843	839
9	7.523	7.526	841	838
10	7.523	7.526	840	837

ancy between  $P^{(E)}$  and  $P^{(\sigma)}$  manifests itself only in the third digit place of the predicted lattice constants  $a_0^{(\sigma)}$  when the FD method is used, which certainly appears to be acceptable in standard electronic structure calculations. Tables I and II show that  $R_a K_{\max} = 8$  is sufficient for the FD method, while at  $R_a K_{\max} = 10$  a difference of 0.01 bohrs between  $a_0^{(E)}$  and  $a_0^{(\sigma)}$  persist using the tetrahedron method. Figures 1(c) and 1(d) also reveal a stronger volume dependency of  $P^{(E)} - P^{(\sigma)}$  calculated using the tetrahedron method as compared to the FD method.

The convergence of the stress tensor with respect to  $k$  mesh with the two different BZ sampling methods, the tetrahedron and FD method, is shown in Fig. 2. Two different  $k$ -mesh grids of  $15 \times 15 \times 15$  and  $24 \times 24 \times 24$  are used. The results show that  $P^{(E)} - P^{(\sigma)}$  in the FD method is fairly insensitive to the choice of the  $k$  mesh while with the tetrahedron method there

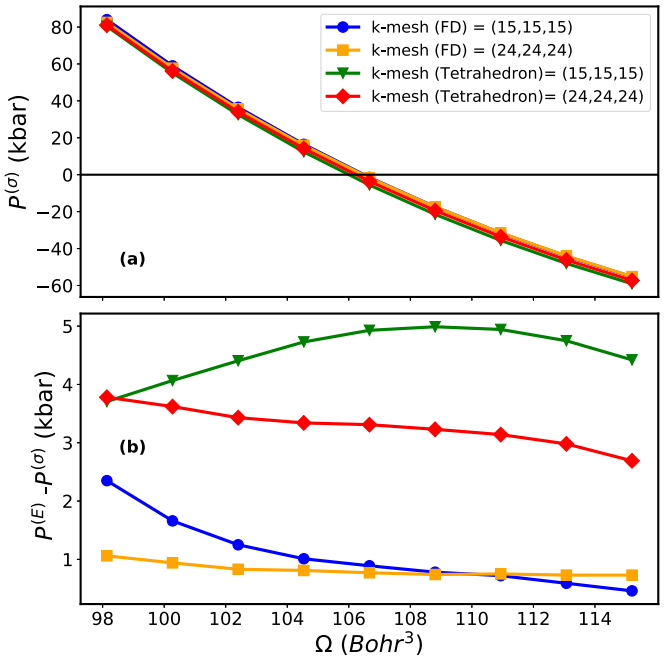


FIG. 2. (a) Analytical pressure  $P^{(\sigma)}$  and (b) the difference between  $P^{(\sigma)}$  and  $P^{(E)}$  for two different  $k$ -mesh grids as function of  $\Omega$  for fcc Al. The BZ is sampled using the FD method with smearing 0.005 Ry and the tetrahedron method with Blöchl's correction.  $R_a K_{\max} = 10$  and all the remaining input parameters are the same as in Fig. 1.

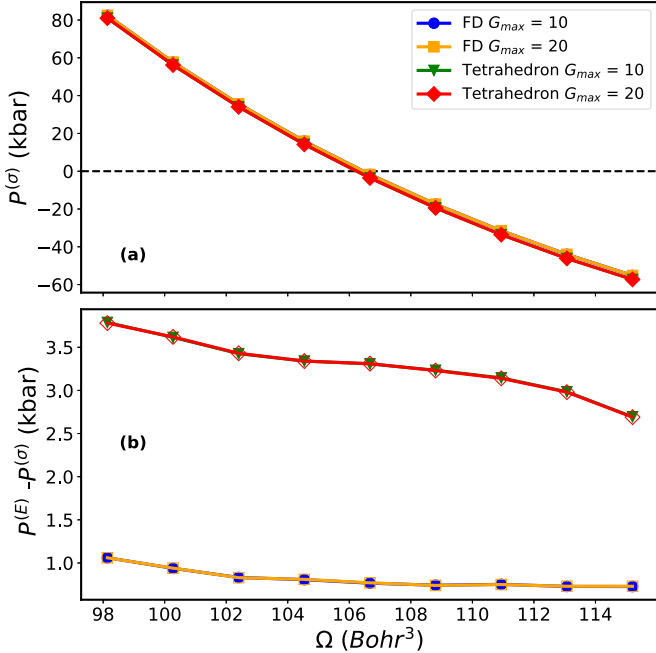


FIG. 3. (a) Analytical pressure  $P^{(\sigma)}$  and (b) the difference between  $P^{(\sigma)}$  and  $P^{(E)}$  for the different  $G_{\max}$  for the charge density and the potential as function of  $\Omega$  for fcc Al. The FD method and tetrahedron method with Blöchl's correction are used for BZ sampling.  $R_a K_{\max} = 10$  and all the remaining input parameters are the same as in Fig. 1.

is a change in the predicted lattice constant  $a_0^\sigma = 7.512$  bohrs ( $15 \times 15 \times 15$ ) to 7.518 bohrs ( $24 \times 24 \times 24$ ).

The convergence of the stress tensor with respect to the value of the cutoff  $G_{\max}$  of the expansion of the charge density and the potential in the interstitial is shown in Fig. 3. The figure shows that  $P^{(\sigma)}$  is insensitive to the choice of  $G_{\max}$ . Thus, the same value of  $G_{\max}$  can be used for the total energy and stress calculations.

## B. SrTiO<sub>3</sub>

Next, we considered SrTiO<sub>3</sub> in the cubic perovskite structure with space group  $Pm\bar{3}m$ . All states up to  $3d$ ,  $2p$ , and  $1s$  are considered as the core states for Sr, Ti, and O, respectively. All other states are treated as valence states and described with LAPW+LO basis functions. Calculations are carried out with  $G_{\max} = 20$  Ry<sup>½</sup>,  $L_{\max}^{\text{ns}}$  equals 6, and the BZ is sampled on a tetrahedron mesh with ten intervals in each direction. The convergence of the stress tensor according to the different values of  $R_a K_{\max}$  is presented in Fig. 4. Calculated pressure  $P^{(\sigma)}$  from the negative trace of the stress tensor is shown in Fig. 4(a) and its difference with the pressure  $P^{(E)}$  is shown in Fig. 4(b). The lattice parameters resulting from the stress tensor are 7.273, 7.286, 7.292, and 7.295 bohrs for  $R_a K_{\max} = 7.5$ , 8, 8.5, and 9, respectively. This value is fairly close to the 7.295 bohrs predicted from total energy, with the exception of  $R_a K_{\max} = 7.5$ . This indicates that  $R_a K_{\max} = 8$  is sufficient to obtain the lattice parameter with a precision 0.01 bohrs.

Figure 5 shows the convergence of the stress tensor with respect to three different  $k$  meshes  $8 \times 8 \times 8$ ,  $10 \times 10 \times 10$ ,

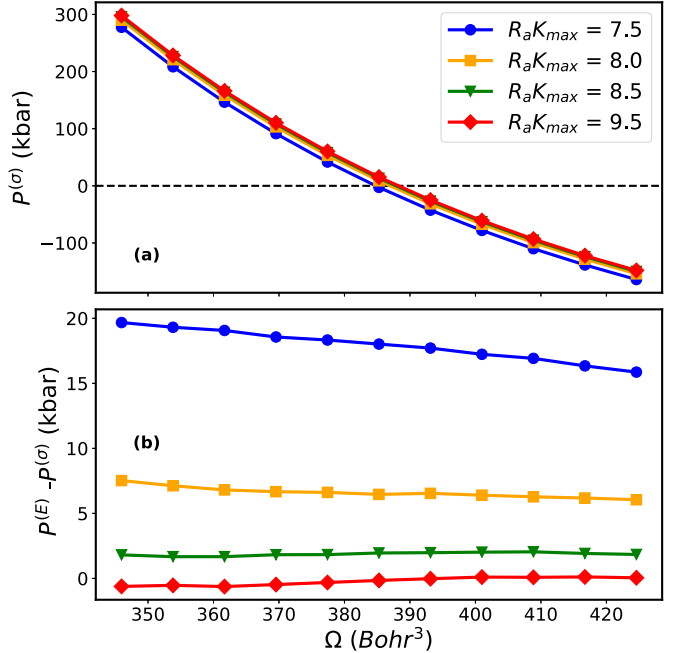


FIG. 4. (a) Analytical pressure  $P^{(\sigma)}$  and (b) the difference between  $P^{(\sigma)}$  and  $P^{(E)}$  for the four different values of  $R_a K_{\max}$  as a function of  $\Omega$  for SrTiO<sub>3</sub>.

and  $15 \times 15 \times 15$  with  $R_a K_{\max} = 8.5$ . Since SrTiO<sub>3</sub> is an insulator, a smaller  $k$  mesh should be sufficient in calculation, which can also be seen in Fig. 5. Figure 5(b) indicates that the difference  $P^{(E)} - P^{(\sigma)}$  between the trace of the stress tensor and the energy-based pressure estimate  $P^{(E)}$  remains the same

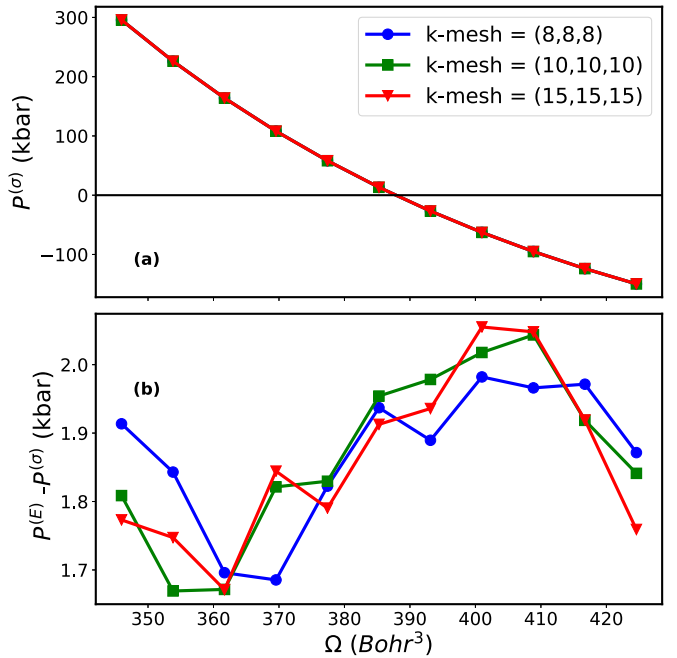


FIG. 5. (a) Analytical pressure  $P^{(\sigma)}$  and (b) the difference between  $P^{(\sigma)}$  and  $P^{(E)}$  for the three different  $k$  meshes as a function of  $\Omega$  for SrTiO<sub>3</sub>.  $R_a K_{\max} = 8.5$  and all the remaining input parameters are the same as in Fig. 4.

TABLE III. Comparison of the equilibrium lattice parameter  $a_0$  (in bohrs) and the bulk modulus (in kbars) obtained from the total energy and directly from the stress tensor for different compounds.

Elements	$a_0^{(\sigma)}$	$a_0^{(E)}$	$B^{(\sigma)}$	$B^{(E)}$
NaCl	10.331	10.334	324	323
LaN	9.880	9.894	1209	1226
TiN	7.900	7.904	3182	3192
NbC	8.395	8.398	3254	3265
MgS	10.590	10.578	621	616
AlAs	10.654	10.659	768	763
SrTiO <sub>3</sub>	7.295	7.295	2004	2007

for all selected  $k$  meshes. Table III compares the structural parameters of several cubic compounds obtained from  $P^{(E)} = 0$  and  $P^{(\sigma)} = 0$ , and very good overall agreement has been found.

### C. ZnO

Calculations for ZnO in the hexagonal wurtzite structure are carried out with sphere sizes of 1.95 and 1.68 bohrs for Zn and O, respectively. For Zn all states up to  $3s$  and for O the  $1s$  states are considered as core states. We choose a cutoff of  $G_{\max} = 20$  Ry $^{\frac{1}{2}}$  in the expansion of the charge density and the potential. The  $R_a K_{\max}$  value is 9.5, the  $k$ -point grid is  $12 \times 12 \times 6$ ,  $L_{\max}^{\text{ns}} = 6$ , and the exchange-correlation energy and potential are calculated using the LDA. Our investigation starts with a total energy calculation for a unit cell based on the experimental lattice parameters. We performed a two-dimensional (2D) optimization of  $a$  and  $c$ , using either the calculated total energies or the stress tensor elements  $\sigma_{11}$  and  $\sigma_{33}$ . The first and second rows of Table IV offer a comparison of these values with their corresponding counterparts predicted from the stress tensor formalism.

In the total energy calculation, both the core charge density and the potential are considered to be spherically symmetric and only the  $lm = 00$  term in a lattice harmonic expansion contributes. On the other hand, in our stress tensor formalism when calculating the core correction Eq. (21), the potential  $V_{\text{eff}}$  can have nonspherical components, which are described by higher angular momentum quantum numbers. However, in the final expression Eq. (E3), due to the presence of Gaunt number  $G_{l,l,1}^{-m,t,t'}$  and Kronecker deltas  $\delta_{1,l+s}\delta_{-t',m+t}$ , only  $lm = 00$  and  $2m$  components of the potential are allowed to be nonzero, such that we are left with  $V_{\text{tot}}^c = V_{00}^c + V_{2m}^c$ , in which the term

TABLE IV. Comparison of the equilibrium lattice parameters  $a_0$  and  $c_0$  of ZnO obtained from a fifth-order polynomial fit to the total energy and directly from the stress tensor with ( $V_{\text{tot}}^c$ ) and without ( $V_{00}^c$ ) inclusion of the nonspherical components ( $l = 2$ ) in the potential when the core correction is calculated using Eq. (G6).

	$a_0$ (bohrs)	$c_0$ (bohrs)
Energy	6.056	9.763
Stress with $V_{\text{tot}}^c$	6.057	9.762
Stress with $V_{00}^c$	6.030	9.849

TABLE V. Comparison of  $\sigma_{33}$  (in kbars) calculated using Eqs. (25) and (18) for silicon in the diamond structure with seven different nonvolume conserving tetragonal deformations. The superscripts  $(E)$  and  $(\sigma)$  correspond to the energy and stress.

$\epsilon_{33}$	$\sigma_{33}^{(E)}$	$\sigma_{33}^{(\sigma)}$
-0.020	33.12	34.28
-0.013	21.95	22.63
-0.007	10.90	11.17
0.000	0.00	0.00
0.007	-10.74	-10.99
0.013	-21.29	-21.70
0.020	-31.65	-32.16

with  $lm = 00$  is the main contribution and the  $lm = 2m$  component acts as an additional correction, which may or may not be zero. For instance, in highly (cubic) symmetric crystal structure there are no  $lm = 2m$  terms in a lattice harmonic expansion, but in even in slightly lower symmetric crystal structures such as a hexagonal system, it was found that these contributions can become quite significant and neglecting this term would lead to substantial errors in the predicted lattice parameters  $a$  and  $c$ , as can be verified by comparing the second and third rows of Table IV.

In passing we note that similar observations can be made for the core correction of the force calculation, where the  $l = 1$  contribution appears in the potential upon displacing the atoms. In contrary to our present approach, the authors in Ref. [17] assumed that the potential in the core correction is only spherically symmetric.

### D. Accuracy of individual stress tensor components

So far we have validated the trace of the stress tensor as well as the individual diagonal compounds at zero strain in terms of the lattice parameters. To validate the accuracy of the individual components of the stress tensor at finite strain, our strategy is to extract them from total energy calculations of various strained systems and compare these values with those obtained from our analytical stress. In the following we take a cubic silicon structure at the equilibrium volume (pressure = 0 and  $a_0 = 10.209$ ) and keep the lattice parameters  $a_0$  and  $b_0 = a_0 = 10.209$  fixed while varying the  $c$  lattice parameter. Using a family of such tetragonal but volume nonconserving deformations, the stress component  $\sigma_{33}$  [denoted as  $\sigma_{33}^{(E)}$  in Table V] is calculated numerically by fitting total energies with a fourth-order polynomial as a function of strain  $\epsilon_{33} = \frac{c}{c_0} - 1$ , and  $\epsilon_{33} = 0$  and  $c_0$  correspond to the equilibrium state at hydrostatic pressure zero. Now it is easy to see that the identity

$$\sigma_{33} = \frac{1}{\Omega_0} \frac{\partial E(\epsilon_{33})}{\partial \epsilon_{33}} \quad (25)$$

holds. Therefore, differentiating the above fourth-order polynomial fit, we readily obtain the stress values  $\sigma_{33}^{(E)}$  recorded in Table V. On the other hand, a stress component  $\sigma_{33} \equiv \sigma_{33}^{(\sigma)}$  can be calculated directly from Eq. (18). The input settings for these calculation were  $R_a K_{\max} = 9.0$ ,  $G_{\max} = 20$  for the charge density and the potential,  $k$  mesh =  $(12 \times 12 \times 12)$ ,

and  $c$  is calculated as  $c = (1 + \epsilon_{33})c_0$ . A comparison of  $\sigma_{33}^{(E)}$  and  $\sigma_{33}^{(\sigma)}$  in Table V suggests that the calculated stress is also satisfactory for nonhydrostatic conditions. The table shows a small discrepancy between  $\sigma_{33}^{(\sigma)}$  and  $\sigma_{33}^{(E)}$ , but similar calculations for different materials show that these numerical differences are within acceptable limits.

#### IV. SURVEY OF PREVIOUS ATTEMPTS IN LITERATURE

In chronological order, previous works on the stress tensor in the LAPW method are (A) Thonhauser *et al.* [17] which summarizes his 2001 Ph.D. thesis [18], (B) the two papers by Nagasako and Oguchi [19,20], and most recently (C) the diploma thesis of Klüppelberg [21].

##### A. The implementation by Thonhauser *et al.*

A first attempt to implement the stress tensor in the LAPW method dates back to the work of Thonhauser *et al.* [18] and was implemented in the WIEN97 code [24]. However, in Ref. [17] only results for Al and Si subject to hydrostatic pressure were shown, whereas the functionality and usefulness of this formalism for low symmetric noncubic materials remained unclear. Unfortunately, in Ref. [17] the final equations that have been implemented are not explicitly stated. Therefore we can only conjecture that our present formalism probably differs from Thonhauser's by the treatment of the electrostatic part of the stress tensor. Moreover, Ref. [17] uses a spherically symmetric potential for the core correction, whereas in our derivation [Eq. (21)] the potential can have nonspherical components. In addition, in contrast to Ref. [18], our formalism does not include the so-called discontinuity correction. Furthermore, an integration in the valence correction [the first term of Eq. (12) in this paper], is calculated in Ref. [18] over the whole unit cell, but using Eq. (13) we only need to calculate this inside the atomic spheres.

##### B. The implementation by Nagasako and Oguchi

In their two papers published in 2011 and 2013, Nagasako and Oguchi present a stress tensor calculation based on a modified version of the LAPW method proposed by Soler and Williams [22,23]. In Refs. [19,20] they provide a rigorous mathematical formalism for both local and semilocal functionals [31,32], respectively, and test their implementation for many different elements with different cutoff parameters and also for some compounds. The results are in good agreement with numerical results calculated directly from total energies. Regrettably, their implementation cannot easily be transferred to the standard LAPW method, since Soler-Williams basis functions are constructed in a related but nevertheless distinctly different way. In the Soler and Williams LAPW method, the plane waves are augmented only for the chemically important  $l$  ( $l \leq l_{\max}$ :  $l_{\max} = 2$  or 3) inside the spherical region and the charge density and potential are formulated differently, which leads to a number of differences in the final expressions.

#### C. The diploma thesis of Klüppelberg

In his 2012 diploma thesis [21], Klüppelberg gave a very elegant mathematical derivation of the stress tensor and also discussed an implementation into the FLEUR code [33], which is based on the standard LAPW method. In particular, we would like to mention that this work contains a number of quite ingenious mathematical tricks, and fully tries to lay out the electrostatic part of the stress tensor. Tragically, as is honestly and in great detail documented in Klüppelberg's thesis, even for the hydrostatic component of the stress tensor the numerical tests showed a large disagreement of the resulting implementation with results of the so-called simple pressure formula and both differ from the results obtained directly from total energy fits. Our first attempt was to work with the formalism of Ref. [21], but this resulted in a huge error whose origin still remains unclear as of today. Our formalism differs from that presented in Ref. [21] by the treatment of the electrostatic part of the stress tensor and the absence of a so-called discontinuity correction.

#### V. DISCUSSION

In this paper we presented the stress tensor formalism in the all-electron full potential LAPW plus local orbital (LO) method. With this formalism, the core calculation can be fully relativistic, but the valence calculation is limited to the nonrelativistic limit. Substantial convergence tests were carried out and the calculations for metals, semiconductors, low symmetric crystal structure, and many compounds were presented. The accuracy of the stress tensor was validated by comparing the lattice parameters predicted from the stress tensor formalism and from total energy calculations. In addition, the accuracy of the individual components of the stress tensor was also tested in the nonhydrostatic case.

#### ACKNOWLEDGMENTS

K.B. and A.T. acknowledge support by the Austrian Science Fund (FWF) Project No. P27738-N28. K.B. would like to thank F. Tran for valuable discussions.

#### APPENDIX A: STRAIN DERIVATIVE OF VECTORS AND VOLUME

When strain is applied to a solid, a vector  $\mathbf{V}$  changes as  $\mathbf{V} \rightarrow \mathbf{V}[\underline{\epsilon}] = (1 \pm \underline{\epsilon})\mathbf{V}$ , the sign  $\pm$  being positive for a real space vector and negative for a reciprocal one. The unit cell volume changes as  $\Omega \rightarrow \Omega[\underline{\epsilon}] = \det(1 + \underline{\epsilon})\Omega$ . When calculating the stress, the strain derivative of these quantities at vanishing strain is calculated as

$$\frac{d\mathbf{V}[\underline{\epsilon}]}{d\underline{\epsilon}_{\alpha\beta}} \Big|_{\underline{\epsilon}=0} = \pm \frac{V}{2} (\hat{\mathbf{V}}_\alpha \hat{\mathbf{e}}_\beta + \hat{\mathbf{V}}_\beta \hat{\mathbf{e}}_\alpha) = \pm \frac{\mathbf{V}_\alpha \mathbf{V}_\beta}{V}, \quad (A1)$$

$$\frac{d\Omega[\underline{\epsilon}]}{d\underline{\epsilon}_{\alpha\beta}} \Big|_{\underline{\epsilon}=0} = \delta_{\alpha\beta} \Omega, \quad (A2)$$

where  $\frac{d}{d\underline{\epsilon}_{\alpha\beta}} \det(1 + \underline{\epsilon})|_{\underline{\epsilon}=0} = \delta_{\alpha\beta}$ ,  $V = |\mathbf{V}|$ , and  $\mathbf{V}_\alpha$  is the Cartesian component of vector  $\mathbf{V}$  in the direction  $\alpha = 1, 2, 3$ .

## APPENDIX B: STRAIN DERIVATIVE OF INTEGRALS OVER THE UNIT CELL VOLUME

The total energy given in Eq. (4) contains the integration of the charge density times the potential over the unit cell volume. To perform the stress tensor calculation, this definition must be carried over to the strained system, differentiated with respect to the strain, and subsequently evaluated at zero strain. From such a derivative we obtain two contributions: (i) one that results from the variation of the unit cell volume and (ii) another one that results from the actual strain variation of the integrand. To clarify the discussion, consider a generic integral  $\int_{\Omega} d^3 \mathbf{r} F(\mathbf{r})$  of an arbitrary function  $F(\mathbf{r})$  over the unit cell. The generic function  $F(\mathbf{r})$ , in practice, may refer to the charge density times a potential or some other physical quantity. Under application of strain it changes to  $\int_{\Omega[\underline{\epsilon}]} d^3 \mathbf{r}_\epsilon F[\underline{\epsilon}](\mathbf{r}_\epsilon)$ . Differentiation of this integral with respect to a strain component  $\epsilon_{\alpha\beta}$  gives

$$\frac{d}{d\epsilon_{\alpha\beta}} \left|_{\underline{\epsilon}=0} \int_{\Omega[\underline{\epsilon}]} d^3 \mathbf{r}_\epsilon F[\underline{\epsilon}](\mathbf{r}_\epsilon) \right| = \frac{d}{d\epsilon_{\alpha\beta}} \left|_{\underline{\epsilon}=0} \det(1 + \underline{\epsilon}) \int_{\Omega} d^3 \mathbf{r} F[\underline{\epsilon}](\mathbf{r}[\underline{\epsilon}]) \right| = \delta_{\alpha\beta} \int_{\Omega} d^3 \mathbf{r} F(\mathbf{r}) + \int_{\Omega} d^3 \mathbf{r} \frac{dF[\underline{\epsilon}](\mathbf{r}[\underline{\epsilon}])}{d\epsilon_{\alpha\beta}} \Big|_{\underline{\epsilon}=0}. \quad (\text{B1})$$

In general,  $\frac{dF[\underline{\epsilon}](\mathbf{r}[\underline{\epsilon}])}{d\epsilon_{\alpha\beta}}|_{\underline{\epsilon}=0}$  may depend on  $\underline{\epsilon}$  both explicitly via linear response and implicitly via its smeared argument  $\mathbf{r}[\underline{\epsilon}]$ , which implies that

$$\frac{dF[\underline{\epsilon}](\mathbf{r}[\underline{\epsilon}])}{d\epsilon_{\alpha\beta}} \Big|_{\underline{\epsilon}=0} = \frac{dF[\underline{\epsilon}](\mathbf{r})}{d\epsilon_{\alpha\beta}} \Big|_{\underline{\epsilon}=0} + \frac{d\mathbf{r}[\underline{\epsilon}]}{d\epsilon_{\alpha\beta}} \Big|_{\underline{\epsilon}=0} \cdot \nabla F(\mathbf{r}), \quad (\text{B2})$$

where  $\frac{d\mathbf{r}[\underline{\epsilon}]}{d\epsilon_{\alpha\beta}} = \frac{r}{2} (\hat{\mathbf{r}}_\alpha \hat{\mathbf{e}}_\beta + \hat{\mathbf{r}}_\beta \hat{\mathbf{e}}_\alpha) = r \hat{\mathbf{r}}_\alpha \hat{\mathbf{r}}_\beta$ . If we substitute Eq. (B2) into (B1), we arrive at

$$\frac{d}{d\epsilon_{\alpha\beta}} \left|_{\underline{\epsilon}=0} \int_{\Omega[\underline{\epsilon}]} d^3 \mathbf{r}_\epsilon F[\underline{\epsilon}](\mathbf{r}_\epsilon) \right| = \delta_{\alpha\beta} \int_{\Omega} d^3 \mathbf{r} F(\mathbf{r}) + \int_{\Omega} d^3 \mathbf{r} \frac{dF[\underline{\epsilon}](\mathbf{r})}{d\epsilon_{\alpha\beta}} \Big|_{\underline{\epsilon}=0} + \frac{1}{2} \int_{\Omega} d^3 \mathbf{r} (r_\beta \partial_\alpha + r_\alpha \partial_\beta) F(\mathbf{r}). \quad (\text{B3})$$

## APPENDIX C: PARTIAL DERIVATIVE OF THE WAVE FUNCTION

Spatial partial derivatives of the wave function  $\psi_{vk}^v(\mathbf{r})$  in the LAPW basis representation [Eq. (2)] are required to compute the second line of Eq. (14).

(1) In the interstitial region, the LAPW basis functions Eq. (1) are plane waves, and thus

$$\begin{aligned} \partial_\alpha \psi_{vk}^{\text{vIS}}(\mathbf{r}) &= \sum_{\mathbf{K}} c_{vk\mathbf{K}} \partial_\alpha \frac{1}{\sqrt{\Omega}} e^{i(\mathbf{k}+\mathbf{K}) \cdot \mathbf{r}} \\ &= \sum_{\mathbf{K}} c_{vk\mathbf{K}} i(\mathbf{k}+\mathbf{K})_\alpha \frac{1}{\sqrt{\Omega}} e^{i(\mathbf{k}+\mathbf{K}) \cdot \mathbf{r}}. \end{aligned} \quad (\text{C1})$$

(2) To compute the gradient components  $\partial_\alpha \psi_{vk}^{\text{vR}_a}(\mathbf{r})$  in the atomic spheres, where the valence wave function is represented by the spherical harmonics expansion [Eq. (1)], we need the derivatives

$$\partial_\alpha Y_{lm}(\hat{\mathbf{r}}_a) = \frac{1}{r} \sum_{s=\pm 1} \sum_{t=-1}^1 c_\alpha^{st}(l, m) Y_{l+s, m+t}(\hat{\mathbf{r}}_a), \quad (\text{C2})$$

$$\partial_\alpha u_{l\lambda}(r_a) = \hat{r}_{a\alpha} u'_{l\lambda}(r_a), \quad (\text{C3})$$

where  $c_\alpha^{st}(l, m)$  is calculated as follows,

$$c_\alpha^{st}(l, m) = \oint_S ds r \partial_\alpha Y_{lm}(\hat{\mathbf{r}}) Y_{l+s, m+t}^*(\hat{\mathbf{r}}), \quad (\text{C4})$$

Abbreviating  $u_{l\lambda}(r_a, E_{l\lambda}^a)$  and  $Y_{lm}(\hat{\mathbf{r}}_a)$  by the shorthand notations  $u_{l\lambda}(r_a)$  and  $Y_{lm}$ , respectively, we have

$$\begin{aligned} \partial_\alpha (u_{l\lambda}(r_a) Y_{lm}) &= \hat{r}_{a\alpha} u'_{l\lambda}(r_a) Y_{lm} \\ &+ \frac{u_{l\lambda}(r_a)}{r} \sum_{s=\pm 1} \sum_{t=-1}^1 c_\alpha^{st}(l, m) Y_{l+s, m+t}. \end{aligned} \quad (\text{C5})$$

The unit vector component  $\hat{\mathbf{r}}_{a\alpha}$  along the Cartesian direction  $\alpha$  can be expanded as

$$\hat{\mathbf{r}}_{a\alpha} = \sum_{t=-1}^1 c_{\alpha t} Y_{1t}(\hat{\mathbf{r}}), \quad (\text{C6})$$

where  $c_{\alpha t}$  can be obtained using the orthogonality property of spherical harmonics as follows,

$$c_{\alpha t} = \oint_S ds \hat{\mathbf{r}}_\alpha Y_{1t}^*(\hat{\mathbf{r}}), \quad (\text{C7})$$

and the product of two spherical harmonics is expanded into Gaunt numbers times another spherical harmonics, i.e.,

$$Y_{1t} Y_{lm} = \sum_{s, v} G_{s, 1, l}^{v, t, m} Y_{s, v}. \quad (\text{C8})$$

In summary, the partial derivative of the wave function inside the atomic sphere is

$$\begin{aligned} \partial_\alpha \psi_{vk}^{\text{vR}_a}(\mathbf{r}) &= \sum_{\mathbf{K}} c_{vk\mathbf{K}} \left[ \sum_{t=-1}^1 c_{\alpha t} u'_{l\lambda}(r) \sum_{s, v} G_{s, 1, l}^{v, t, m} Y_{sv}(\hat{\mathbf{r}}_a) \right. \\ &\quad \left. + \frac{u_{l\lambda}(r)}{r} \sum_{s=\pm 1} \sum_{t=-1}^1 c_\alpha^{st}(l, m) Y_{l+s, m+t}(\hat{\mathbf{r}}_a) \right]. \end{aligned} \quad (\text{C9})$$

The mathematical steps provided in this Appendix are used to simplify the valence kinetic stress tensor  $\sigma_{\alpha\alpha}^{\text{val,kin}}$  of Eq. (18).

## APPENDIX D: STRAIN VARIATION OF THE BASIS FUNCTION

The strain variation of the basis function is required to calculate the valence correction stress  $\sigma_{\alpha\beta}^{\text{val,corr}}$  of Eq. (18). In

the discussion following Eq. (13), we have argued that calculating the valence correction requires only to calculate the strain variation of  $\phi_{k[\underline{\epsilon}]} \phi_{k[\underline{\epsilon}]}^{\text{IS}}(\underline{\epsilon})(\mathbf{r}[\underline{\epsilon}]) \sqrt{\Omega[\underline{\epsilon}]}$  inside the atomic spheres. Indeed, expanding the strained version of the LAPW basis functions restricted to the interstitial region, we see that

$$\begin{aligned} \sqrt{\Omega[\underline{\epsilon}]} \phi_{k[\underline{\epsilon}]}^{\text{IS}}(\underline{\epsilon})(\mathbf{r}[\underline{\epsilon}]) &= e^{i(k+K)[\underline{\epsilon}] \cdot \mathbf{r}[\underline{\epsilon}]} \\ &= \sqrt{\Omega} \phi_{kK}^{\text{IS}}(\mathbf{r}) + O(\underline{\epsilon}^2), \end{aligned} \quad (\text{D1})$$

as claimed. Thus, in the interstitial region  $\frac{d}{d\epsilon_{\alpha\beta}} \phi_{k[\underline{\epsilon}]}^{\text{IS}}(\underline{\epsilon})(\mathbf{r}[\underline{\epsilon}]) \sqrt{\Omega[\underline{\epsilon}]} = O(\underline{\epsilon})$  and does not contribute to the valence correction stress. It remains to calculate the

---


$$\begin{aligned} \frac{d}{d\epsilon_{\alpha\beta}} \left[ \sqrt{\Omega[\underline{\epsilon}]} \phi_{k[\underline{\epsilon}]} \phi_{k[\underline{\epsilon}]}^{\text{IS}}(\underline{\epsilon})(\mathbf{r}[\underline{\epsilon}]) \right]_{\underline{\epsilon}=0} &= \sum_{lm\lambda} \left[ \frac{d}{d\epsilon_{\alpha\beta}} \sqrt{\Omega[\underline{\epsilon}]} a_{lm\lambda}^{ak[\underline{\epsilon}]K[\underline{\epsilon}]} \right]_{\underline{\epsilon}=0} u_{l\lambda}^a(r_a) Y_{lm}(\hat{\mathbf{r}}_a) \\ &+ \sqrt{\Omega} \sum_{lm\lambda} a_{lm\lambda}^{akK} \left[ \frac{d}{d\epsilon_{\alpha\beta}} u_{l\lambda}^a(r_a) \right]_{\underline{\epsilon}=0} Y_{lm}(\hat{\mathbf{r}}_a) + \sqrt{\Omega} \sum_{lm\lambda} a_{lm\lambda}^{akK} u_{l\lambda}^a(r_a) \left[ \frac{d}{d\epsilon_{\alpha\beta}} Y_{lm}(\hat{\mathbf{r}}_a) \right]_{\underline{\epsilon}=0}. \end{aligned} \quad (\text{D3})$$


---

In order to simplify this expression further, we repeatedly make use of the following relations:

(1) For the strain variation of spherical harmonics we use the general formula

$$\begin{aligned} \frac{dY_{lm}(\hat{\mathbf{V}}[\underline{\epsilon}])}{d\epsilon_{\alpha\beta}} &= \pm \frac{1}{2} \sum_{s=\pm} \sum_{t=-1}^1 [c_{\beta}^{st}(l, m) \hat{\mathbf{V}}_{\alpha} \\ &+ c_{\alpha}^{st}(l, m) \hat{\mathbf{V}}_{\beta}] Y_{l+s, m+t}(\hat{\mathbf{V}}), \end{aligned} \quad (\text{D4})$$

where the positive and negative sign applies to a real space vector and reciprocal space vector, respectively.

(2) Similarly, the strain variation of the spherical Bessel function, which is necessary to calculate the strain variation of the matching coefficient  $a_{lm\lambda}^{ak[\underline{\epsilon}]K[\underline{\epsilon}]}$ , is

$$\frac{d j_l(|\mathbf{V}[\underline{\epsilon}]| R_a)}{d\epsilon_{\alpha\beta}} = \pm j'_l(|\mathbf{V}| R_a) V \hat{\mathbf{V}}_{\alpha} \hat{\mathbf{V}}_{\beta}. \quad (\text{D5})$$

In addition, we resort to the frozen augmentation approximation, according to which the explicit strain dependency in  $u_{l\lambda}^a(r_a)$  via the linear response is discarded while keeping only an implicit dependency via  $r_a$ . Effectively,  $u_{l\lambda}^a(r_a)$  is therefore replaced by  $u_{l\lambda}(r_a)$ :

$$\frac{du_{l\lambda}(r_a)}{d\epsilon_{\alpha\beta}} = u'_{l\lambda}(r_a) r_a \hat{\mathbf{r}}_{\alpha\beta} \hat{\mathbf{r}}_{\alpha\beta}. \quad (\text{D6})$$

Armed with these relations, we may tackle the numerical evaluation of the different terms that contribute in Eq. (D3). The necessary quantities to evaluate the strain variation of the basis function such as the variation of the reciprocal lattice

first-order strain variation of  $\sqrt{\Omega[\underline{\epsilon}]} \phi_{k[\underline{\epsilon}]} \phi_{k[\underline{\epsilon}]}^{\text{IS}}(\underline{\epsilon})(\mathbf{r}[\underline{\epsilon}])$  in the atomic spheres. In the deformed system, a basis function inside the atomic sphere region as defined in Eq. (1) becomes

$$\phi_{k[\underline{\epsilon}]} \phi_{k[\underline{\epsilon}]}^{\text{IS}}(\underline{\epsilon})(\mathbf{r}[\underline{\epsilon}]) = \sum_{lm\lambda} a_{lm\lambda}^{ak[\underline{\epsilon}]K[\underline{\epsilon}]} u_{l\lambda}^a(r_a) Y_{lm}(\hat{\mathbf{r}}_a). \quad (\text{D2})$$

Here, the index  $\lambda$  ( $= 0, 1$ ) is introduced to provide a compact notation including both the radial part and the energy derivative part of the basis function Eq. (1). All terms with  $[\underline{\epsilon}]$  are meant to be defined in the strained system. Furthermore,

vector, the unit cell volume, the spherical harmonics, and the spherical Bessel function are already given explicitly.

## APPENDIX E: CORE CORRECTION STRESS TENSOR

The contribution of the core correction to the stress tensor as given in Eq. (21) is

$$\sigma_{\alpha\beta}^{\text{core,corr}} = -\frac{1}{2\Omega} \sum_{a \in \Omega} \int_{R_a} d^3 r \rho_c^a(\mathbf{r}) (r_{\beta} \partial_{\alpha} + r_{\alpha} \partial_{\beta}) V_{\text{eff}}(\mathbf{r}). \quad (\text{E1})$$

To simplify the notation we replace  $V_{\text{eff}}(\mathbf{r})$  by  $V(\mathbf{r})$ , the potential expand in terms of spherical harmonics,  $\partial_{\alpha}$  replace by  $\hat{\mathbf{r}}_{\alpha} \frac{\partial}{\partial r}$ , expand the unit vector  $\hat{\mathbf{r}}_{\alpha}$  as given in Eq. (C6), and the angular derivative of the spherical harmonics is computed as in Eq. (C5). Thus

$$\begin{aligned} r_{\beta} \partial_{\alpha} V(\mathbf{r}) &= \sum_{l,m} \left( r V'_{l,m}(r) \sum_{t,t'=-1}^1 c_{\alpha t} c_{\beta t'} Y_{lt}(\hat{\mathbf{r}}) Y_{l,t'}(\hat{\mathbf{r}}) Y_{l,m}(\hat{\mathbf{r}}) \right. \\ &\quad \left. + V_{l,m}(r) \sum_{s=\pm 1} \sum_{t,t'=-1}^1 c_{\alpha}^{st}(l, m) c_{\beta t'} Y_{lt'}(\hat{\mathbf{r}}) Y_{l+s, m+t}(\hat{\mathbf{r}}) \right). \end{aligned} \quad (\text{E2})$$

The prime in  $V'_{l,m}(r)$  denotes the radial derivative and the loop over  $l$  and  $s$  has to be such that  $l+s$  is always positive. To get the final expression of the core correction  $\sigma_{\alpha\beta}^{\text{core,corr}}$ , we replace the product of two spherical harmonics in Eq. (E2) by a Gaunt number times spherical harmonic according to Eq. (C8), interchange  $\alpha$  and  $\beta$  in the expression of  $r_{\beta} \partial_{\alpha} V(\mathbf{r})$ , substituting

Eq. (E2) in Eq. (E1), and use  $\rho_c^a(\mathbf{r}) = \rho_{00}^a(r_a)Y_{00}(\hat{r})$ ,

$$\begin{aligned} & \Omega\sigma_{\alpha\beta}^{\text{core,corr}} \\ &= \sum_{l,m} \sum_{t,t'=-1}^1 \left( I_1 c_{\alpha t} c_{\beta t'} \frac{(-1)^m}{4\pi} G_{l,1,1}^{-m,t,t'} \right. \\ &+ I_2 \sum_{s=\pm 1} \frac{c_\beta^{st}(l, m)c_{\alpha t'} + c_\alpha^{st}(l, m)c_{\beta t'}}{2} \frac{(-1)^{t'}}{4\pi} \delta_{1,l+s}\delta_{-t',m+t} \Bigg), \end{aligned} \quad (\text{E3})$$

with

$$I_1 = - \int_0^{R_a} r_a^3 dr_a \sqrt{4\pi} \rho_{00}^*(r_a) \frac{dV_{lm}(r_a)}{dr_a}, \quad (\text{E4})$$

$$I_2 = - \int_0^{R_a} dr_a \sqrt{4\pi} r_a^2 \rho_{00}^*(r_a) V_{lm}(r_a). \quad (\text{E5})$$

Recall that for a Gaunt number  $G_{l,1,1}^{-m,t,t'}$  to be nonzero, the indices  $[l, 1, 1]$  are required to satisfy the triangle rule, their sum needs to be even, and  $m + t + t'$  must be zero [34].

## APPENDIX F: VARIATION OF THE COULOMB POTENTIAL

The Coulomb potential is evaluated using Weinert's method [27]. According to this method the interstitial potential is obtained using the real interstitial charge density and a pseudocharge density, which reproduces the current multipole moments inside the spheres and is zero in the interstitial. The interstitial potential as given in Ref. [27] is

$$V_C^I(\mathbf{r}) = \sum_{\mathbf{K} \neq 0} \frac{4\pi}{\mathbf{K}^2} [\tilde{\rho}_a(\mathbf{K}) + \rho_I(\mathbf{K})] e^{i\mathbf{K} \cdot \mathbf{r}}, \quad (\text{F1})$$

where  $\rho_I(\mathbf{K})$  and  $\tilde{\rho}_a(\mathbf{K})$  are the Fourier components of the interstitial charge density and the smooth pseudocharge density, respectively. In the strained environment,

$$\rho_I[\underline{\epsilon}](\mathbf{K}[\underline{\epsilon}]) = \frac{1}{\Omega[\underline{\epsilon}]} \int_{\Omega[\underline{\epsilon}]} d^3\mathbf{r}_\epsilon \rho_I[\underline{\epsilon}](\mathbf{r}_\epsilon) e^{-i\mathbf{K}[\underline{\epsilon}] \cdot \mathbf{r}_\epsilon}. \quad (\text{F2})$$

$$\begin{aligned} \sigma_{\alpha\beta}^{\text{val,kin}} &= \frac{1}{\Omega} \left\{ - \sum_{vk} n_{vk} \sum_{KK'} c_{vk}^* c_{vkK'}(\mathbf{k} + \mathbf{K}')_\alpha (\mathbf{k} + \mathbf{K}')_\beta \Theta(\mathbf{K} - \mathbf{K}') + \frac{1}{2} \sum_{vk} n_{vk} \sum_{LL'} \sum_{\lambda\lambda'} A_{L'\lambda'}^{avk*} A_{L\lambda}^{avk} \right. \\ &\times \left\{ \sum_{t,t'=-1} (c_{\alpha t} c_{\beta t'} + c_{\beta t} c_{\alpha t'}) \sum_{s,v} G_{s,1,l}^{v,t,m} G_{l',1,s}^{m',t',v} \int_0^{R_a} r_a^2 dr_a u_{l'\lambda'}(r) u_{l\lambda}''(r) \right. \\ &+ \sum_{t,t'=-1} \sum_{s,v} \sum_{s'=\pm 1} G_{s,1,l}^{v,t,m} [c_{\alpha t} c_{\beta s'}^{s't'}(s, v) + c_{\beta t} c_{\alpha s'}^{s't'}(s, v)] \delta_{l',s+s'} \delta_{m',v+t'} \int_0^{R_a} r_a dr_a u_{l'\lambda'}(r) u_{l\lambda}'(r) \\ &+ \sum_{s=\pm 1} \sum_{t,t'=-1}^1 [c_\alpha^{st}(l, m)c_{\beta t'} + c_\beta^{st}(l, m)c_{\alpha t'}] G_{l',1,l+s}^{m',t',m+t} \int_0^{R_a} r_a^2 dr_a u_{l'\lambda'}(r) \left[ \frac{u_{l\lambda}'(r)}{r} - \frac{u_{l\lambda}(r)}{r^2} \right] \\ &+ \left. \sum_{s,s'=\pm 1} \sum_{t,t'=-1}^1 [c_\alpha^{st}(l, m)c_{\beta s'}^{s't'}(l+s, m+t) + c_\beta^{st}(l, m)c_{\alpha s'}^{s't'}(l+s, m+t)] \delta_{l',l+s+s'} \delta_{m',m+t+t'} \int_0^{R_a} dr_a u_{l'\lambda'}(r) u_{l\lambda}(r) \right\}, \end{aligned} \quad (\text{G1})$$

The physically strained electronic charge density  $\rho_I[\underline{\epsilon}](\mathbf{r}_\epsilon)$  is replaced by the “smeared” charge density  $\rho_I((\underline{1} - \underline{\epsilon})\mathbf{r}[\underline{\epsilon}])$ ,

$$\begin{aligned} \rho_I[\underline{\epsilon}](\mathbf{K}[\underline{\epsilon}]) &= \frac{1}{\Omega[\underline{\epsilon}]} \int_{\Omega[\underline{\epsilon}]} d^3\mathbf{r}_\epsilon \rho_I((\underline{1} - \underline{\epsilon})\mathbf{r}[\underline{\epsilon}]) e^{-i\mathbf{K}[\underline{\epsilon}] \cdot \mathbf{r}_\epsilon} \\ &= \frac{1}{\Omega} \int_{\Omega} d^3\mathbf{r} \rho_I((\underline{1} - \underline{\epsilon})(\underline{1} + \underline{\epsilon})\mathbf{r}) e^{-i\mathbf{K} \cdot \mathbf{r}} \\ &= \rho_I(\mathbf{K}), \end{aligned} \quad (\text{F3})$$

where  $\mathbf{r}[\underline{\epsilon}] = (\underline{1} + \underline{\epsilon})\mathbf{r}$ ,  $\mathbf{K}[\underline{\epsilon}] = (\underline{1} - \underline{\epsilon})\mathbf{K}$ , and  $\mathbf{K}[\underline{\epsilon}] \cdot \mathbf{r}[\underline{\epsilon}] = \mathbf{K} \cdot \mathbf{r}$ . A concept similar to the one used for the plane wave charge density is used for the pseudocharge density  $\tilde{\rho}_a$ :

$$\tilde{\rho}_a[\underline{\epsilon}](\mathbf{K}[\underline{\epsilon}]) = \tilde{\rho}_a(\mathbf{K}). \quad (\text{F4})$$

With the help of Eqs. (F3) and (F4), the interstitial Coulomb potential in the deformed system is written as

$$\begin{aligned} V_C[\underline{\epsilon}](\mathbf{K}[\underline{\epsilon}]) &= \frac{4\pi}{\mathbf{K}[\underline{\epsilon}]^2} [\tilde{\rho}_a[\underline{\epsilon}](\mathbf{K}[\underline{\epsilon}]) + \rho_I[\underline{\epsilon}](\mathbf{K}[\underline{\epsilon}])] \\ &= \frac{4\pi}{\mathbf{K}[\underline{\epsilon}]^2} [\tilde{\rho}_a(\mathbf{K}) + \rho_I(\mathbf{K})] \end{aligned} \quad (\text{F5})$$

For our calculations, the strain derivative of Eq. (F5) is also required. Since the Fourier components of the plane wave charge density and the pseudocharge density are independent of strain, their derivatives do not contribute to the stress. Therefore,

$$\left. \frac{d}{d\varepsilon_{\alpha\beta}} V_C[\underline{\epsilon}](\mathbf{K}[\underline{\epsilon}]) \right|_{\underline{\epsilon}=0} = \frac{4\pi}{\mathbf{K}^2} 2\hat{\mathbf{K}}_\alpha \hat{\mathbf{K}}_\beta [\tilde{\rho}_a(\mathbf{K}) + \rho_I(\mathbf{K})] = 2\hat{\mathbf{K}}_\alpha \hat{\mathbf{K}}_\beta V_C(\mathbf{K}), \quad (\text{F6})$$

where we made use of  $\frac{dK_{\underline{\epsilon}}}{d\varepsilon_{\alpha\beta}} = -\frac{\hat{\mathbf{K}}_\alpha \hat{\mathbf{K}}_\beta}{\mathbf{K}}$  and  $\hat{\mathbf{K}}_\alpha = \frac{\mathbf{K}_\alpha}{\mathbf{K}}$ , and  $V_C(\mathbf{K})$  is given in Eq. (F1). This formula is used to evaluate the Coulomb part of the electrostatic stress tensor in the interstitial region—the interstitial part of the second line of Eq. (16).

## APPENDIX G: FINAL FORMULAS

In this Appendix we present the explicit expressions of Eqs. (19)–(23) that we implemented in the WIEN2K package:

$$\begin{aligned} \sigma_{\alpha\beta}^{\text{val,kin}} &= \frac{1}{\Omega} \left\{ - \sum_{vk} n_{vk} \sum_{KK'} c_{vk}^* c_{vkK'}(\mathbf{k} + \mathbf{K}')_\alpha (\mathbf{k} + \mathbf{K}')_\beta \Theta(\mathbf{K} - \mathbf{K}') + \frac{1}{2} \sum_{vk} n_{vk} \sum_{LL'} \sum_{\lambda\lambda'} A_{L'\lambda'}^{avk*} A_{L\lambda}^{avk} \right. \\ &\times \left\{ \sum_{t,t'=-1} (c_{\alpha t} c_{\beta t'} + c_{\beta t} c_{\alpha t'}) \sum_{s,v} G_{s,1,l}^{v,t,m} G_{l',1,s}^{m',t',v} \int_0^{R_a} r_a^2 dr_a u_{l'\lambda'}(r) u_{l\lambda}''(r) \right. \\ &+ \sum_{t,t'=-1} \sum_{s,v} \sum_{s'=\pm 1} G_{s,1,l}^{v,t,m} [c_{\alpha t} c_{\beta s'}^{s't'}(s, v) + c_{\beta t} c_{\alpha s'}^{s't'}(s, v)] \delta_{l',s+s'} \delta_{m',v+t'} \int_0^{R_a} r_a dr_a u_{l'\lambda'}(r) u_{l\lambda}'(r) \\ &+ \sum_{s=\pm 1} \sum_{t,t'=-1}^1 [c_\alpha^{st}(l, m)c_{\beta t'} + c_\beta^{st}(l, m)c_{\alpha t'}] G_{l',1,l+s}^{m',t',m+t} \int_0^{R_a} r_a^2 dr_a u_{l'\lambda'}(r) \left[ \frac{u_{l\lambda}'(r)}{r} - \frac{u_{l\lambda}(r)}{r^2} \right] \\ &+ \left. \sum_{s,s'=\pm 1} \sum_{t,t'=-1}^1 [c_\alpha^{st}(l, m)c_{\beta s'}^{s't'}(l+s, m+t) + c_\beta^{st}(l, m)c_{\alpha s'}^{s't'}(l+s, m+t)] \delta_{l',l+s+s'} \delta_{m',m+t+t'} \int_0^{R_a} dr_a u_{l'\lambda'}(r) u_{l\lambda}(r) \right\}, \end{aligned} \quad (\text{G1})$$

where  $A_{L\lambda}^{av\mathbf{k}} = \sum_{\mathbf{K}} c_{v\mathbf{k}\mathbf{K}} a_{lm\lambda}^{ak\mathbf{K}}$  and  $L$  is a shorthand for the double index  $(l, m)$ ;

$$\begin{aligned} \sigma_{\alpha\beta}^{\text{val,corr}} = & \frac{2}{\Omega} \sum_a \sum_{v\mathbf{k}} n_{v\mathbf{k}} \operatorname{Re} \left\{ \sum_{L\lambda\lambda'} D_{L\lambda}^{av\mathbf{k}*}(\alpha, \beta) A_{L\lambda'}^{av\mathbf{k}} \left[ (E_l^a - \epsilon_{v\mathbf{k}}) \delta_{\lambda\lambda'} \|u_{l\lambda'}^a\|^2 + \delta_{\lambda'1} \delta_{\lambda,0} \right] \right. \\ & + \sum_{L\lambda} \sum_{L'\lambda'} A_{L\lambda}^{av\mathbf{k}*} A_{L'\lambda'}^{av\mathbf{k}} \sum_{t,t'=-1} c_{\alpha t} c_{\beta t'} \sum_{s,v} G_{s,1,1}^{v,t,t'} G_{l,l',s}^{m,m',v} \left[ (E_{l'}^a - \epsilon_{v\mathbf{k}}^v) J_{ll'}^{a\lambda\lambda'} + \delta_{\lambda'1} J_{ll'}^{a\lambda 0} \right] \\ & + \frac{1}{2} \sum_{s=\pm 1} \sum_{t,t'=-1}^1 [c_{\alpha t} c_{\beta t'}^{st}(l, m) + c_{\beta t'} c_{\alpha t}^{st}(l, m)] \sum_{L'\lambda'} A_{L\lambda}^{av\mathbf{k}*} A_{L'\lambda'}^{av\mathbf{k}} G_{l,1,1+s}^{m,t',m+t} \left\{ (E_{l'}^a - \epsilon_{v\mathbf{k}}^v) \delta_{\lambda,\lambda'} \|u_{l\lambda'}^a\|^2 + \delta_{\lambda'1} \delta_{\lambda,0} \right\} \\ & + \sum_{L''>0} \sum_{L\lambda} \sum_{L'\lambda'} D_{L\lambda}^{av\mathbf{k}*}(\alpha, \beta) A_{L'\lambda'}^{av\mathbf{k}} G_{l,l'',l'}^{m,m'',m'} V_{l,L'',l'}^{a\lambda\lambda'} \\ & + \sum_{L''>0} \sum_{L\lambda} \sum_{L'\lambda'} A_{L\lambda}^{av\mathbf{k}*} A_{L'\lambda'}^{av\mathbf{k}} \sum_{t,t'=-1} \sum_{sv} \sum_{s'v'} c_{\alpha t} c_{\beta t'} G_{s,1,1}^{v,t,t'} G_{s',l',l'}^{v',m'',m'} G_{l,s,s'}^{m,v,v'} W_{l,L'',l'}^{a\lambda\lambda'} \\ & \left. + \frac{1}{2} \sum_{s=\pm 1} \sum_{t,t'=-1}^1 [c_{\alpha t} c_{\beta t'}^{st}(l, m) + c_{\beta t'} c_{\alpha t}^{st}(l, m)] \sum_{L\lambda} \sum_{L'\lambda'} A_{L\lambda}^{av\mathbf{k}*} A_{L'\lambda'}^{av\mathbf{k}} \sum_{L''>0} \sum_{s,v} G_{s,l'',l'}^{v,m'',m'} G_{s,1,1+s}^{v,t',m+t} V_{l,L'',l'}^{a\lambda\lambda'} \right\}, \end{aligned} \quad (\text{G2})$$

where  $D_{L\lambda}^{av\mathbf{k}}(\alpha, \beta)$  contains the stress variation of the matching coefficients and is expressed as

$$D_{lm\lambda}^{av\mathbf{k}}(\alpha, \beta) = \sum_{\mathbf{K}} c_{v\mathbf{k}\mathbf{K}} d_{lm\lambda}^{ak\mathbf{K}}(\alpha, \beta), \quad (\text{G3})$$

with

$$\begin{pmatrix} d_{lm0}^{ak\mathbf{K}}(\alpha, \beta) \\ d_{lm1}^{ak\mathbf{K}}(\alpha, \beta) \end{pmatrix} \equiv \frac{1}{\sqrt{\Omega}} \frac{d}{d\epsilon_{\alpha\beta}} \left[ \sqrt{\Omega[\underline{\epsilon}]} \begin{pmatrix} a_{lm}^{ak[\underline{\epsilon}]K[\underline{\epsilon}]} \\ b_{lm}^{ak[\underline{\epsilon}]K[\underline{\epsilon}]} \end{pmatrix} \right]_{\underline{\epsilon}=0}, \quad (\text{G4})$$

and integrals  $J_{ll'}^{a\lambda\lambda'}$ ,  $V_{l,L'',l'}^{a\lambda\lambda'}$ , and  $W_{l,L'',l'}^{a\lambda\lambda'}$  are

$$\begin{aligned} J_{ll'}^{a\lambda\lambda'} &= \int_0^{R_a} r_a^3 dr_a u_{l\lambda}^{a\prime}(r_a) u_{l'\lambda'}^a(r_a), \\ V_{l,L'',l'}^{a\lambda\lambda'} &= \int_0^{R_a} r_a^2 dr_a u_{l\lambda}^a(r_a) V_{L''}^{\text{eff}}(r_a) u_{l'\lambda'}^a(r_a), \\ W_{l,L'',l'}^{a\lambda\lambda'} &= \int_0^{R_a} r_a^3 dr_a u_{l\lambda}^{a\prime}(r_a) V_{L''}^{\text{eff}}(r_a) u_{l'\lambda'}^a(r_a), \\ \sigma_{\alpha\beta}^{\text{es}} &= \frac{1}{2} \sum_{\mathbf{K}} \sum_{\mathbf{K}' \neq 0} \rho^*(\mathbf{K}) [-\delta_{\alpha\beta} V_C(\mathbf{K}') + 2\hat{\mathbf{K}}_\alpha' \hat{\mathbf{K}}_\beta' V_C(\mathbf{K}')] \Theta(\mathbf{K} - \mathbf{K}') \\ &- \frac{1}{2\Omega} \sum_a \sum_{t,t'=-1}^1 c_{\alpha t} c_{\beta t'} \int_0^{R_a} d^3\mathbf{r} \rho(\mathbf{r}) V_C(\mathbf{r}) Y_{1t}(\hat{\mathbf{r}}) Y_{1t'}(\hat{\mathbf{r}}) + \frac{1}{2\Omega} \sum_a Z_a \sum_{t,t'=-1}^1 c_{\alpha t} c_{\beta t'} V_M(\tau_a) Y_{1t}(\hat{\tau}_a) Y_{1t'}(\hat{\tau}_a), \end{aligned} \quad (\text{G5})$$

where  $\Theta(\mathbf{K})$  is the Fourier transform of the step function in the interstitial region;

$$\begin{aligned} \sigma_{\alpha\beta}^{\text{core}} = & -\frac{1}{\Omega} \sum_a \sum_{l,m} \sum_{t,t'=-1}^1 \left( c_{\alpha t} c_{\beta t'} \frac{(-1)^m}{4\pi} G_{l,1,1}^{-m,t,t'} \int_0^{R_a} r_a^3 dr_a \sqrt{4\pi} \rho_{00}^*(r_a) \frac{dV_{lm}(r_a)}{dr_a} \right. \\ & \left. + \sum_{s=\pm 1} \frac{c_{\beta}^{st}(l, m) c_{\alpha t'} + c_{\alpha}^{st}(l, m) c_{\beta t'}}{2} \frac{(-1)^{t'}}{4\pi} \delta_{1,l+s} \delta_{-t',m+t} \int_0^{R_a} dr_a \sqrt{4\pi} r_a^2 \rho_{00}^*(r_a) V_{lm}(r_a) \right), \end{aligned} \quad (\text{G6})$$

$$\sigma_{\alpha\beta}^{\text{xc}} = \frac{\delta_{\alpha\beta}}{\Omega} \int_{\Omega} d^3\mathbf{r} \rho(\mathbf{r}) [\epsilon_{\text{xc}}(\rho(\mathbf{r})) - \mu_{\text{xc}}(\rho(\mathbf{r}))]. \quad (\text{G7})$$

- [1] H. G. A. Hellmann, *Z. Phys.* **85**, 180 (1933).
- [2] R. P. Feynman, *Phys. Rev.* **56**, 340 (1939).
- [3] R. Yu, D. Singh, and H. Krakauer, *Phys. Rev. B* **43**, 6411 (1991).
- [4] L. D. Marks, *J. Chem. Theory Comput.* **17**, 5715 (2021).
- [5] O. H. Nielsen and R. M. Martin, *Phys. Rev. Lett.* **50**, 697 (1983).
- [6] O. H. Nielsen and R. M. Martin, *Phys. Rev. B* **32**, 3780 (1985).
- [7] P. Hohenberg and W. Kohn, *Phys. Rev.* **136**, B864 (1964).
- [8] W. Kohn and L. J. Sham, *Phys. Rev.* **140**, A1133 (1965).
- [9] A. Dal Corso and R. Resta, *Phys. Rev. B* **50**, 4327 (1994).
- [10] M. Torrent, F. Jollet, F. Bottin, G. Zrah, and X. Gonze, *Comput. Mater. Sci.* **42**, 337 (2008).
- [11] S. Baroni, P. Giannozzi, and A. Testa, *Phys. Rev. Lett.* **58**, 1861 (1987).
- [12] D. R. Hamann, X. Wu, K. M. Rabe, and D. Vanderbilt, *Phys. Rev. B* **71**, 035117 (2005).
- [13] D. R. Hamann, K. M. Rabe, and D. Vanderbilt, *Phys. Rev. B* **72**, 033102 (2005).
- [14] X. Wu and D. Vanderbilt, and D. R. Hamann, *Phys. Rev. B* **72**, 035105 (2005).
- [15] O. K. Anderson, *Phys. Rev. B* **12**, 3060 (1975).
- [16] D. J. Singh and L. Nordström, *Planewaves, Pseudopotentials, and the LAPW method*, 2nd ed. (Springer, New York, 2006).
- [17] T. Thonhauser, C. Ambrosch-Draxl, and D. J. Singh, *Solid State Commun.* **124**, 275 (2002).
- [18] T. Thonhauser, Stress and strain in solids: A formalism for the LAPW method, Ph.D. thesis, Karl-Franzens University Graz, 2001.
- [19] N. Nagasako and T. Oguchi, *J. Phys. Soc. Jpn.* **80**, 024701 (2011).
- [20] N. Nagasako and T. Oguchi, *J. Phys. Soc. Jpn.* **82**, 044701 (2013).
- [21] D. A. Klüppelberg, Calculation of stress tensor within the *ab initio* full-potential linearized augmented plane wave method, Diploma thesis, RWTH Aachen, 2011.
- [22] J. M. Soler and A. R. Williams, *Phys. Rev. B* **40**, 1560 (1989).
- [23] J. M. Soler and A. R. Williams, *Phys. Rev. B* **42**, 9728 (1990).
- [24] P. Blaha, K. Schwarz, and J. Luitz, WIEN97: A full potential linearized augmented plane wave package for calculating crystal properties, Vienna University of Technology, 1997.
- [25] P. Blaha, K. Schwarz, F. Tran, R. Laskowski, G. K. H. Madsen, and L. D. Marks, *J. Chem. Phys.* **152**, 074101 (2020).
- [26] M. Weinert, E. Wimmer, and A. J. Freeman, *Phys. Rev. B* **26**, 4571 (1982).
- [27] M. Weinert, *J. Math. Phys.* **22**, 2433 (1981).
- [28] F. Birch, *Phys. Rev.* **71**, 809 (1947).
- [29] P. E. Blöchl, O. Jepsen, and O. K. Andersen, *Phys. Rev. B* **49**, 16223 (1994).
- [30] M. Weinert and J. W. Davenport, *Phys. Rev. B* **45**, 13709 (1992).
- [31] J. P. Perdew, K. Burke, and M. Ernzerhof, *Phys. Rev. Lett.* **77**, 3865 (1996).
- [32] J. P. Perdew, K. Burke, and M. Ernzerhof, *Phys. Rev. Lett.* **78**, 1396(E) (1997).
- [33] <https://www.flapw.de/MaX-5.1/>
- [34] A. R. Edmonds, *Angular Momentum in Quantum Mechanics* (Princeton University Press, Princeton, NJ, 1985).

Article

# Symmetry-Adapted Finite Strain Landau Theory Applied to KMnF<sub>3</sub>

Andreas Tröster <sup>1,\*</sup>, Wilfried Schranz <sup>1</sup>, Sohaib Ehsan <sup>2</sup>, Kamal Belbase <sup>2</sup> and Peter Blaha <sup>2</sup>

<sup>1</sup> Faculty of Physics, University of Vienna, Boltzmanngasse 5, A-1090 Vienna, Austria; wilfried.schranz@univie.ac.at

<sup>2</sup> Institute of Materials Chemistry, Vienna University of Technology, Getreidemarkt 9, A-1060 Wien, Austria; sohaib.ehsan@tuwien.ac.at (S.E.); kamal.belbase@tuwien.ac.at (K.B.); peter.blaha@tuwien.ac.at (P.B.)

\* Correspondence: andreas.troester@univie.ac.at

Received: 27 January 2020; Accepted: 11 February 2020; Published: 17 February 2020



**Abstract:** In recent years, finite strain Landau theory has been gradually developed as both a conceptual as well as a quantitative framework to study high pressure phase transitions of the group-subgroup type. In the current paper, we introduce a new version of this approach which is based on symmetry-adapted finite strains. This results in a substantial simplification of the original formulation. Moreover, it allows for replacing the clumsy use of truncated Taylor expansions by a convenient functional parametrization. Both the weaknesses of the traditional Landau approach based on infinitesimal strains as well as the major improvements made possible by our new parametrization are illustrated in great detail in an application to the ambient temperature high pressure transition of the perovskite KMnF<sub>3</sub>.

**Keywords:** high pressure; phase transitions; Landau theory; nonlinear elasticity theory; perovskites

---

## 1. Introduction

Through many decades, the Landau theory (LT) of phase transitions [1,2] (PTs) has proven to be one of the most valuable conceptual tools for understanding PTs of the group-subgroup type. In particular, the field of structural PTs abounds even with successful quantitative applications, and, for many classes of materials, complete collections of the corresponding coupling coefficients have been gathered in the literature (for ferroelectrics see, e.g., Appendix A of Ref. [3]). Effects of spontaneous strain that generally accompany temperature-driven structural PTs are sufficiently parameterized in terms of infinitesimal strain tensor components defined with respect to a baseline, which is obtained by extrapolating the generally small thermal expansion changes of the high symmetry reference phase. The corresponding Landau potential then involves only terms up to harmonic order, and any temperature dependence of the relevant parameters (high symmetry phase elastic constants and other coupling constants) can usually be completely neglected [4].

The situation changes drastically for high pressure phase transitions (HPPTs). Spontaneous strain components may still be numerically small, but they now must be defined with respect to a  $P$ -dependent base line. The total strain measured with respect to the ambient pressure reference state must then be calculated from a nonlinear superposition of finite background and spontaneous strain (see Equation (11) below). Furthermore, the Landau potential may be truncated beyond harmonic order only if calculated with respect to this  $P$ -dependent elastic background reference system. Therefore, neither the elastic constants nor the other elastic couplings can be assumed to be  $P$ -independent. In a high pressure

context, clinging to the familiar infinitesimal strain Landau toolbox may result not only in a quantitatively, but also qualitatively completely erroneous description.

It is not easy to construct a mathematically consistent and yet practically useful version of Landau theory taking into account the inherent nonlinearities and anharmonic effects that accompany HPPTs. In recent years, however, such a theory, for which we have coined the name finite strain Landau theory (FSLT), has been successfully developed. FSLT constitutes a careful extension of Landau theory beyond coupling to infinitesimal strain, fully taking into account the nonlinear elastic effects at finite strain. Its capabilities have been demonstrated in a number of applications to HPPTs [5–10]. However, as it stands, the numerical scheme underlying FSLT is still quite involved, and many practical workers in the field of HPPTs may be hesitant to go through the mathematical hardships it seems to pose. It is the purpose of this paper to show that FSLT is drastically simplified by switching from a formulation in terms of Cartesian Lagrangian strains to one in terms of symmetry-adapted finite strains. The enormous reduction of overall complexity of the approach as well as the vastly reduced numerical requirements of our new version of FSLT are demonstrated on the example of the HPPT in the perovskite  $\text{KMnF}_3$  (KMF).

## 2. Review of Experimental Results on the Cubic-to-Tetragonal Transition of KMF

In what follows, we focus on the antiferrodistortive high pressure phase transition of KMF from the cubic perovskite aristophase  $Pm\bar{3}m$  to a tetragonal  $I4/mcm$  phase at room temperature which was experimentally investigated in Ref. [11] by X-ray diffraction up to 30 GPa. Since the ambient pressure Landau theory also provides a limiting reference frame for the description of the high pressure transition, we start our discussion with a detailed survey of the corresponding Landau theory.

According to Ref. [12], a similar transition observed at ambient pressure and temperature  $T_c = 186.5$  K is weakly first order but close to critical, and the mechanism underlying these transitions is the same as in the well-studied  $T = 105$  K cubic-to-tetragonal transition in strontium titanate, i.e., octahedral tilting with a critical wavevector at the  $R$ -point of the cubic Brillouin zone. Furthermore, in Ref. [12], it is argued that, even though a further structural transition to an orthorhombic phase related to further octahedral tilting at the  $M$ -point of the Brillouin zone at  $T_N = 87$  K is accompanied by antiferromagnetism, this coincidence between structural and magnetic transition temperatures may just be accidental, and actually there seems to be essentially no coupling between structural and magnetic order parameters (OPs) for these transitions. In passing we note that at  $T = 82$  K there is a further transition to an orthorhombic canted ferromagnet [12].

As discussed in Ref. [12], the  $Pm\bar{3}m \rightarrow I4/mcm$  symmetry reduction corresponds to the isotropy subgroup of the three-dimensional irreducible representation  $R_4^+$  of  $Pm\bar{3}m$  with respect to the order parameter direction  $(Q, 0, 0)$ , the corresponding Landau expansion to sixth order being

$$\begin{aligned} F = & \frac{A}{2} (Q_1^2 + Q_2^2 + Q_3^2) + \frac{B}{4} (Q_1^4 + Q_2^4 + Q_3^4) + \frac{B_2}{4} (Q_1^2 Q_2^2 + Q_2^2 Q_3^2 + Q_1^2 Q_3^2) \\ & + \frac{C}{6} (Q_1^6 + Q_2^6 + Q_3^6) + \frac{C_2}{6} (Q_1^2 Q_2^4 + Q_2^2 Q_3^4 + Q_1^2 Q_3^4 + Q_2^2 Q_1^4 + Q_3^2 Q_2^4 + Q_3^2 Q_1^4) + \frac{C_3}{6} Q_1^2 Q_2^2 Q_3^2 \\ & + \lambda_a^{(0)} (Q_1^2 + Q_2^2 + Q_3^2) \epsilon_a + \lambda_t^{(0)} (2Q_1^2 - Q_2^2 - Q_3^2) \epsilon_t + \frac{K^{(0)}}{2} \epsilon_a^2 + \frac{\mu^{(0)}}{2} \epsilon_t^2 \end{aligned} \quad (1)$$

with volume and tetragonal symmetry-adapted strains  $\epsilon_a = \epsilon_{11} + \epsilon_{22} + \epsilon_{33}$ ,  $\epsilon_t = \frac{2\epsilon_{33} - \epsilon_{11} - \epsilon_{22}}{\sqrt{3}}$  and bulk and longitudinal shear modulus related to the bare cubic elastic constants by  $K^{(0)} = (C_{11}^{(0)} + C_{12}^{(0)})/3$ ,  $\mu^{(0)} = (C_{11}^{(0)} - C_{12}^{(0)})/2$ . Targeting a transition into a single tetragonal domain where  $(Q_1, Q_2, Q_3) \equiv (Q, 0, 0)$  and  $\epsilon_{22} = \epsilon_{33}$ , we have

$$\begin{aligned} F = & \frac{A}{2}Q^2 + \frac{B}{4}Q^4 + \frac{C}{6}Q^6 + \lambda_a^{(0)}Q^2\epsilon_a + 2\lambda_t^{(0)}Q^2\epsilon_t \\ & + \frac{K^{(0)}}{2}\epsilon_a^2 + \frac{\mu^{(0)}}{2}\epsilon_t^2 \end{aligned} \quad (2)$$

In a standard Landau approach, the coefficients  $B, C, \lambda_a^{(0)}, \lambda_t^{(0)}$  are assumed to be independent of temperature (and pressure), while for  $A$  the ansatz

$$A = A_0(T - T_0) \quad (3)$$

with  $T$ -independent coefficients  $A_0, T_0$  is made and quantum saturation has been neglected [13]. The elastic equilibrium conditions  $-P = \frac{1}{V_0} \frac{\partial F}{\partial \epsilon_a} \Big|_{\bar{\epsilon}_a, \bar{\epsilon}_t}$  and  $0 = \frac{1}{V_0} \frac{\partial F}{\partial \epsilon_t} \Big|_{\bar{\epsilon}_a, \bar{\epsilon}_t}$  amount to

$$\bar{\epsilon}_a = e_a(P) - \frac{\lambda_a^{(0)}}{K^{(0)}}Q^2, \quad \bar{\epsilon}_t = -\frac{2\lambda_t^{(0)}}{\mu^{(0)}}Q^2 \quad (4)$$

with a background volume strain

$$e_a(P) = 3e(P), \quad e(P) = -\frac{P}{3K^{(0)}} \quad (5)$$

Performing a Legendre transform yields the Gibbs potential

$$G = \frac{A_R}{2}Q^2 + \frac{\tilde{B}}{4}Q^4 + \frac{C}{6}Q^6 - \frac{P^2}{2K^{(0)}} \quad (6)$$

where

$$A_R = A - 6\lambda_a^{(0)}e(P) = A - \frac{2\lambda_a^{(0)}P}{K^{(0)}} \quad (7a)$$

$$\tilde{B} = B - \frac{2(\lambda_a^{(0)})^2}{K^{(0)}} - \frac{8(\lambda_t^{(0)})^2}{\mu^{(0)}} \quad (7b)$$

The values of coefficients  $A_0 = 63.118 \text{ kPa/K}$ ,  $\tilde{B} = -1.308 \text{ MPa}$  and  $C = 13.032 \text{ MPa}$  at  $P = 0$ , which imply a first order phase transition at  $T_c = 186.15 \text{ K}$ , have been determined from calorimetric measurements by Salje and coworkers [13]. In principle, numerical values for the OP-strain coupling coefficients  $\lambda_a^{(0)}, \lambda_t^{(0)}$  may be extracted from experimental data on the temperature evolution of spontaneous strains  $\bar{\epsilon}_a, \bar{\epsilon}_t$ . Unfortunately, however, for KMF, this is easier said than done. At room temperature, the thermal expansion data  $a_{\text{cubic}}(T)$  of Ref. [14] are observed to perfectly reproduce the value of the cubic lattice constant  $a_{\text{cubic}}(T_R)$  at ambient pressure as determined in Ref. [11]. However, the measurement data of thermal lattice parameter irregularities  $a(T), c(T)$  around  $T_c \approx 186 \text{ K}$  (Refs. [15–18]) available in the literature appear to be in rather poor mutual agreement. As Figure 1 illustrates, while a discontinuous behavior of the lattice parameters is clearly visible in all three data sets, the absolute values of the measured unit cell parameters differ considerably, yet none of the data sets seem to be compatible with extrapolating the thermal expansion data of Ref. [14].

Not unexpectedly, the agreement in relative splitting between the a-and c-axis in the tetragonal phase appears to be better, albeit far from perfect. Nevertheless, the cubic parts of the data of Refs. [15,18] exhibit slopes similar to the low temperature extrapolation of the thermal expansion data of Ref. [14]. In order to be able to collapse the data onto a common “master set”, we thus shifted the data of Refs. [15,18] by

constant absolute offsets to match the extrapolated baseline of Ref. [14] in an optimal way, treating the seemingly more precise measurements of Sakashita et al. (Refs. [16,17]) as an outlier. Figure 2 illustrates our results for a corresponding effort.

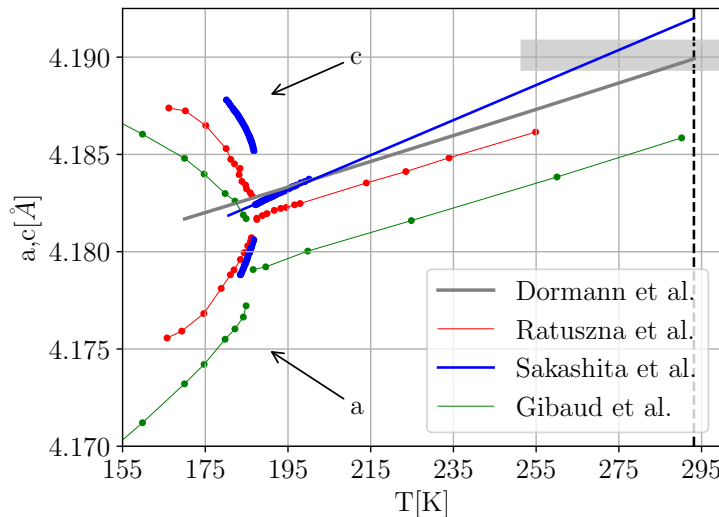


**Figure 1.** Compilation of experimental unit cell data from Refs. [15] (red) and [18] (green) (data range restricted to  $T > 155$  K) [16,17] (blue) and [14] (gray). For comparison, the value (including error bars) of the room temperature (indicated by the vertical dashed line) lattice constant at ambient pressure as measured in Ref. [11] is illustrated by the gray horizontal area.

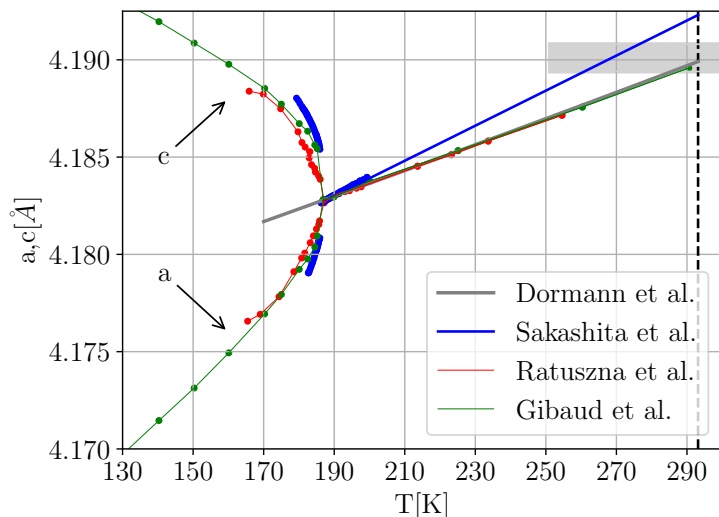


**Figure 2.** Collapse of data from Refs. [15] (red) and [18] (green), onto the low temperature expansion of the thermal expansion data of Ref. [14] (gray) by constant vertical shifts. The positive and negative branches of the data correspond to values  $\epsilon_t$  and  $\epsilon_a$  from the various references, respectively. As in Figure 1, the room temperature ambient pressure lattice constant of Ref. [11] is indicated by a horizontal gray bar for comparison. The shifted data from Ref. [16,17] (blue) clearly appear to be at odds with the other measurements.

With a meaningful baseline  $a_{\text{cubic}}(T)$  for unit cell parameters  $a(T), c(T)$  in place, we calculate the spontaneous strain components  $\epsilon_1 = a/a_{\text{cubic}} - 1$  and  $\epsilon_3 = c/a_{\text{cubic}} - 1$  and thus the (infinitesimal) spontaneous volume and tetragonal strains

$$\epsilon_a = 2\epsilon_1 + \epsilon_3 = \frac{2a + c}{a_{\text{cubic}}} - 3, \quad (8)$$

$$\epsilon_t = \frac{2(\epsilon_3 - \epsilon_1)}{\sqrt{3}} = \frac{2}{\sqrt{3}} \frac{c - a}{a_{\text{cubic}}}, \quad (9)$$

respectively. According to Equation (4), when plotted against  $\bar{Q}^2(t)$  at  $P = 0$ ,  $\epsilon_a$  and  $\epsilon_t$  should resemble straight lines with slopes  $-\lambda_a^{(0)}/K^{(0)}$  and  $-2\lambda_t^{(0)}/\mu^{(0)}$ , respectively. Figure 3 illustrates corresponding fits with results

$$\lambda_a^{(0)}/K^{(0)} = 0.002, \quad \lambda_t^{(0)}/\mu^{(0)} = -0.005 \quad (10)$$

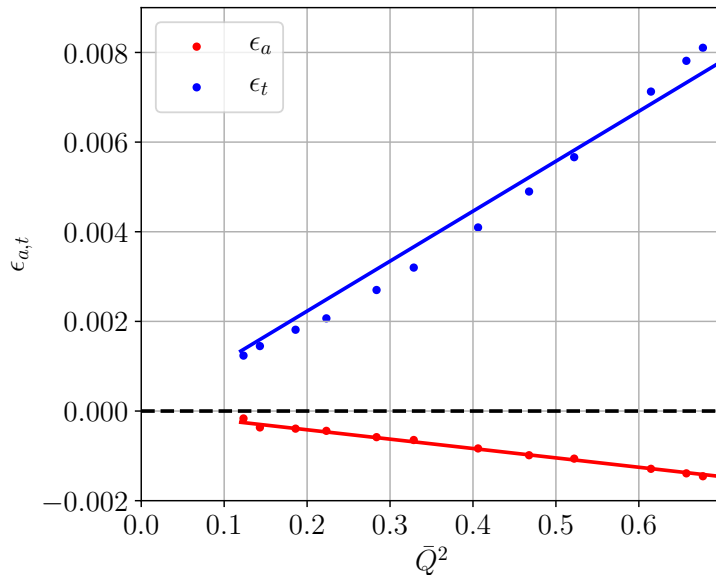


**Figure 3.** Fits of  $\epsilon_a(T)$  and  $\epsilon_t(T)$  against  $\bar{Q}^2(T)$  according to Equations (4).

With the Landau theory of the temperature-driven transition at ambient pressure available, we are tempted to analyze the ambient temperature HPPT based on the same framework. In Ref. [11], the variation of the pseudo-/cubic lattice constants of KMF under pressure at room temperature was measured with X-ray scattering (Figure 4) and the cubic part of the data was fitted to a simple Murnaghan equation of state (EOS) with  $K_0 = 64$  GPa and  $V_0 = 73.608^3$ . This provides a baseline to determine (Lagrangian) spontaneous strains  $\hat{\epsilon}_a \approx \epsilon_a, \hat{\epsilon}_t \approx \epsilon_t$  (Figure 5).

Comparing the thermal and pressure-induced spontaneous strains shown in Figures 2 and 5, respectively, we note that there is some spontaneous thermal volume strain  $\epsilon_a$  while practically  $\hat{\epsilon}_a \approx 0$  for the pressure-induced case. Furthermore, even though it may be difficult to directly relate temperature and pressure scales, the pressure-induced tetragonal spontaneous strain  $\hat{\epsilon}_t$  is observed to be roughly one order of magnitude larger than its thermal counterpart  $\epsilon_t$ . From the perspective of traditional Landau theory based on infinitesimal strain coupling, these findings are difficult to explain. Based on Equation (4), there are in principle two ways to alter the magnitude of spontaneous strains. One may either change

the value of the couplings  $\lambda_a^{(0)}/K^{(0)}$  and  $\lambda_t^{(0)}/\mu^{(0)}$  or find a mechanism to increase the magnitude of  $\bar{Q}^2$  which, of course, implicitly depends on all Landau coefficients. Since these are actually only known for  $T = 186.5$  K, one could assume a thermal drift in  $\lambda^{(0)}$  towards zero to be responsible for the vanishing of  $\hat{\epsilon}_a$  at room temperature (more than counteracting against the thermal drift of  $K_0$  which is generally expected to decrease with increasing  $T$ ). For the tetragonal strain, a similar mechanism seems to be difficult to conceive, however. On the one hand, we would need to increase  $\lambda_t^{(0)}$  dramatically to explain the large values of  $\hat{\epsilon}_t$ . On the other hand, Equation (7b) indicates that such an increase would send parameter  $\tilde{B}$  to negative values much larger than those found for the thermal transition, resulting in a pronounced first order character of the HPTP. This, however, is not observed. The only remedy therefore seems to find a way to increase  $\bar{Q}^2$ . Calculated from a standard 2–4 Landau potential,  $\bar{Q}^2$  would be inversely proportional to  $1/\tilde{B}$ . This may explain why advocates of an orthodox Landau description frequently resort to assuming HPPT's to be near a tricritical point, explicitly postulating some ad-hoc pressure dependence  $\tilde{B} = \tilde{B}(P)$  induced somehow by unspecified higher order coupling effects.

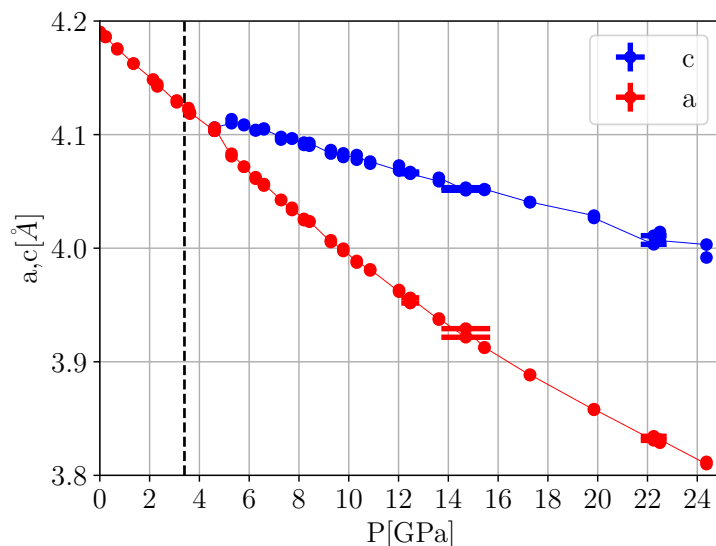


**Figure 4.** Pseudo-/cubic lattice constants of KMF under pressure at room temperature as measured in Ref. [11] with X-ray scattering. The transition pressure estimate  $P_s \approx 3.4$  GPa put forward in Ref. [11], which is indicated by the dashed vertical line, is clearly too low.

Further difficulties arise if we try to reconcile the observed value of  $P_c$  with the prediction of standard Landau theory. In Ref. [11], a brute force fit based on the above assumptions of a second order transition close to a tricritical point produced an estimate of  $P_c \approx 3.4$  GPa. In principle, for a second order or slightly first order phase transition, this pressure should coincide or be somewhat lower than the pressure value  $P_0(T_R)$  at which  $A_R(T_R, P_0(T_R))$  vanishes at room temperature  $T_R$ . Unfortunately, however, this is incompatible with extrapolating the Landau parametrization of Hayward et al. [19] to room temperature. In fact, inserting the parameter value (10) into Equation (7a) yields  $P_0(T_R) \approx 1.7$  GPa, which is completely at odds with  $P_c \approx 3.4$  GPa as reported in Ref. [11]. To reach this transition pressure at room temperature would require reducing our previous result  $\lambda_a^{(0)}/K^{(0)} = 0.002$  obtained at  $T = 186$  K by a full factor of 2 (cf. Figure 6). However, even then, any unbiased reader should have a hard time believing that the bare data of Figure 5 should indicate a continuous transition at  $P_c = 3.4$  GPa. In summary, we hope to have demonstrated that standard Landau theory is completely inadequate to describe the HPPT of KMF

unless one is willing to sacrifice any numerical meaning to Landau theory, leaving us with all coupling parameters as essentially unknown and with ad hoc pressure dependencies at room temperature.

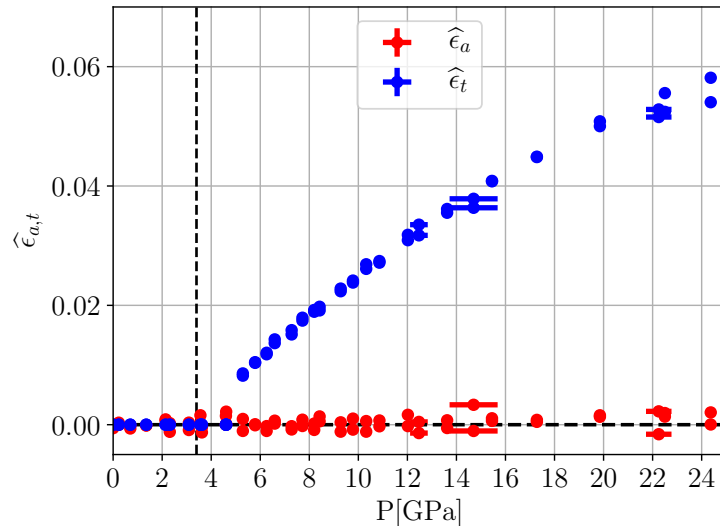


**Figure 5.** Lagrangian strains  $\hat{\epsilon}_a, \hat{\epsilon}_t$  calculated from unit cell data and Murnaghan fit of cubic part according to Ref. [11].

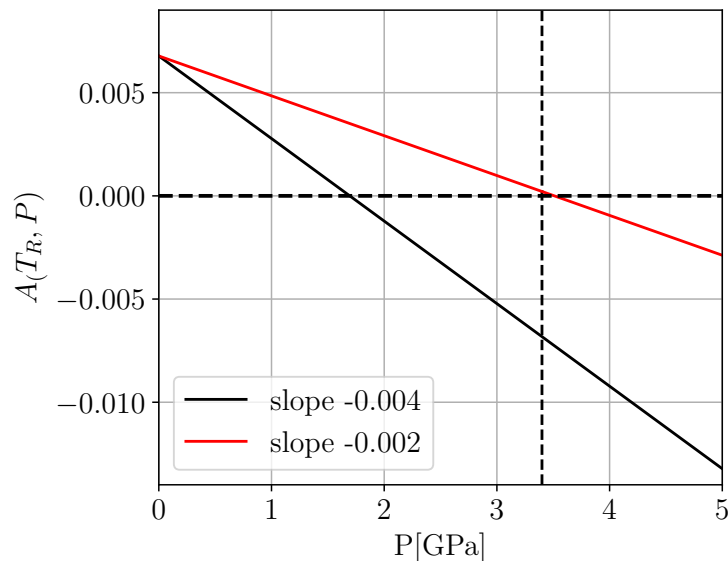


**Figure 6.**  $A_R(T = T_R, P)$  as defined in Equation (10) for correct slope  $-2\lambda_a^{(0)}/K^{(0)} = -0.004$  in comparison to a slope of  $-2\lambda_a^{(0)}/K^{(0)} \approx -0.002$  assumed in Ref. [11].

### 3. A Quick Review of FS LT

In a nutshell, in a generic high pressure experiment, a given crystal is observed to change under application of high hydrostatic pressure  $P$  from an ambient pressure “laboratory” state  $X$  to a deformed state to be denoted as  $\hat{\hat{X}} = \hat{\hat{X}}(P)$  with an accompanying total (Lagrangian) strain  $\eta_{ij}$ . Frequently, a high pressure phase transition manifests itself in such an experiment through the observation of relatively small strain anomalies on top of a much larger “background strain” that in itself is unrelated to the actual transition. Recognizing that the concept of strain is always defined with respect to a chosen elastic

reference state, in Ref. [5], a corresponding background system  $\widehat{\mathbf{X}} = \widehat{\mathbf{X}}(P)$ , defined as the (hypothetical) equilibrium state of the system with the primary OP clamped to remain zero, was introduced. Let  $\alpha_{ik}$  and  $e_{ik} = \frac{1}{2}(\sum_n \alpha_{ni}\alpha_{nk} - \delta_{ik})$  denote the deformation and Lagrangian strain tensors from  $\mathbf{X}$  to  $\widehat{\mathbf{X}}$ , respectively. The total strain  $\eta_{ij}$  may then be disentangled as a nonlinear superposition

$$\eta_{ij} = e_{ij} + \alpha_{ki}\widehat{\epsilon}_{kl}\alpha_{lj} \quad (11)$$

of the—generally large—Lagrangian background strain and a relatively small spontaneous strain  $\widehat{\epsilon}_{ij}$  measured relative to the floating “background” reference state  $\widehat{\mathbf{X}}$ . Determining the proper background strain  $e_{ij}$  in the resulting reference scheme

$$\mathbf{X} \xrightarrow[\underline{\alpha}, \underline{\eta}]{} \widehat{\mathbf{X}} \xrightarrow[\underline{\alpha}, \underline{\widehat{\epsilon}}]{} \widehat{\widehat{\mathbf{X}}} \quad (12)$$

is thus a crucial step in correctly identifying the actual spontaneous strain, which in turn is mandatory in a successful application of the concepts of Landau theory. Effectively “subtracting” the elastic baseline, the strategy of FSLT therefore consists of setting up Landau theory *within the background reference system*  $\widehat{\mathbf{X}}$ . Based on the reasonable assumption that a harmonic expansion with pressure-dependent elastic constants  $C_{ijkl}[\widehat{\mathbf{X}}]$  suffices to capture the elastic energy originating exclusively from the relatively small spontaneous strain  $\widehat{\epsilon}_{kl}$ , one arrives at the Landau free energy

$$\frac{F(Q, \widehat{\epsilon}; \widehat{\mathbf{X}})}{V[\widehat{\mathbf{X}}]} = \Phi(Q; \widehat{\mathbf{X}}) + \sum_{\mu \geq 1} Q^{2n} d_{ij}^{(2\mu)}[\widehat{\mathbf{X}}] \widehat{\epsilon}_{ij} + \frac{F_0(\widehat{\epsilon}; \widehat{\mathbf{X}})}{V[\widehat{\mathbf{X}}]} \quad (13)$$

where we have assumed a scalar OP  $Q$  for simplicity, and

$$\frac{F_0(\widehat{\epsilon}; \widehat{\mathbf{X}})}{V[\widehat{\mathbf{X}}]} \approx \sum_{ij} \tau_{ij}[\widehat{\mathbf{X}}] \widehat{\epsilon}_{ij} + \frac{1}{2} \sum_{ijkl} C_{ijkl}[\widehat{\mathbf{X}}] \widehat{\epsilon}_{ij} \widehat{\epsilon}_{kl} \quad (14)$$

denotes the pure spontaneous strain-dependent elastic free energy at hydrostatic external stress  $\tau_{ij}[\widehat{\mathbf{X}}] = -\delta_{ij}P$ . For the pure OP potential part, we assume the traditional Landau expansion

$$\Phi(Q; \widehat{\mathbf{X}}) = \frac{A[\widehat{\mathbf{X}}]}{2} Q^2 + \frac{B[\widehat{\mathbf{X}}]}{4} Q^4 + \frac{C[\widehat{\mathbf{X}}]}{6} Q^6 + \dots \quad (15)$$

with  $P$ -dependent coefficients yet to be determined. In Ref. [9], it was explicitly shown that the harmonic structure of  $\frac{F_0(\widehat{\epsilon}; \widehat{\mathbf{X}})}{V[\widehat{\mathbf{X}}]}$  yields the equilibrium spontaneous strain

$$\bar{\epsilon}_{mn} = - \sum_{\nu=1}^{\infty} \bar{Q}^{2\nu} \sum_{ij} d_{ij}^{(2\nu)}[\widehat{\mathbf{X}}] S_{mnij}[\widehat{\mathbf{X}}] \quad (16)$$

where the compliance tensor  $S_{mnij}[\widehat{\mathbf{X}}]$  is defined as the tensorial inverse of the so-called *Birch coefficients* [20,21]

$$B_{ijkl}[\widehat{\mathbf{X}}] = C_{ijkl}[\widehat{\mathbf{X}}] + \frac{1}{2} \left( \tau_{jk}[\widehat{\mathbf{X}}]\delta_{il} + \tau_{ik}[\widehat{\mathbf{X}}]\delta_{jl} + \tau_{jl}[\widehat{\mathbf{X}}]\delta_{ik} + \tau_{il}[\widehat{\mathbf{X}}]\delta_{jk} - 2\tau_{ij}[\widehat{\mathbf{X}}]\delta_{kl} \right) \quad (17)$$

of the background system  $\hat{X}$  which effectively take over the role of the elastic constants at finite strain. Furthermore, if we eliminate  $\bar{\epsilon}_{mn}$  from  $\frac{F(Q, \hat{\epsilon}; \hat{X})}{V[\hat{X}]}$  by this formula, we obtain the renormalized pure OP potential

$$\begin{aligned}\Phi_R(Q; \hat{X}) &:= \Phi(Q; \hat{X}) - \sum_{\mu, \nu=1}^{\infty} \frac{2\mu}{2\mu + 2\nu} \left( \sum_{ijkl} d_{ij}^{(2\mu)} [\hat{X}] S_{ijkl} [\hat{X}] d_{kl}^{(2\nu)} [\hat{X}] \right) Q^{2(\mu+\nu)} \\ &\equiv \frac{A_R[\hat{X}]}{2} Q^2 + \frac{B_R[\hat{X}]}{4} Q^4 + \frac{C_R[\hat{X}]}{6} Q^6 + \dots\end{aligned}\quad (18)$$

from which the equilibrium OP  $\bar{Q}$  can be determined by minimization.

Information on the  $P$ -dependence of elastic constants  $C_{ijkl}[\hat{X}]$  is usually available from density functional theory (DFT) or may be extracted from experimental measurements. At this stage, it therefore remains to relate the potential coefficients  $A[\hat{X}]$ ,  $B[\hat{X}]$ , ... and  $d_{ij}^{(2\mu)}[\hat{X}]$ , which are still defined with respect to the reference system  $\hat{X}$  i.e.,  $P$ -dependent. In a generic application of FSLT, however, one starts from knowledge of an ambient pressure Landau potential, i.e., the lowest order coefficients of the free energy

$$\begin{aligned}\frac{F(Q, \eta; X)}{V(X)} &= \Phi(Q; X) + \sum_{\mu=1}^{\infty} Q^{2\mu} \left( \sum_{ij} d_{ij}^{(2\mu,1)} \eta_{ij} + \frac{1}{2!} \sum_{ijkl} d_{ijkl}^{(2\mu,2)} \eta_{ij} \eta_{kl} + \frac{1}{3!} \sum_{ijklmn} d_{ijklmn}^{(2\mu,3)} \eta_{ij} \eta_{kl} \eta_{mn} + \dots \right) \\ &\quad + \frac{1}{2!} \sum_{ijkl} C_{ijkl}^{(2)} \eta_{ij} \eta_{kl} + \frac{1}{3!} \sum_{ijklmn} C_{ijklmn}^{(3)} \eta_{ij} \eta_{kl} \eta_{mn} + \dots\end{aligned}\quad (19)$$

(defined at  $\tau_{ij}[X] \equiv 0$ ) with  $P$ -independent coefficients are assumed to be known, which obviously places constraints on the possible  $P$ -dependence of the above coefficients  $A[\hat{X}]$ ,  $B[\hat{X}]$ , ... and  $d_{ij}^{(2\mu)}[\hat{X}]$ . To explore the relations between the two set of coefficients defined in the  $P$ -dependent background system  $\hat{X}$  and the laboratory system  $X$ , we insert the nonlinear superposition relation (11) into (19) and compare coefficients. Following Ref. [9], we content ourselves to just include OP-strain couplings of type  $Q^2 \hat{\epsilon}_{ij}$  and obtain

$$A[\hat{X}] = \frac{1}{J(\alpha)} \left[ A[X] + 2 \left( \sum_{ij} d_{ij}^{(2,0)} e_{ij} + \frac{1}{2!} \sum_{ijkl} d_{ijkl}^{(2,1)} e_{ij} e_{kl} + \frac{1}{3!} \sum_{ijklmn} d_{ijklmn}^{(2,2)} e_{ij} e_{kl} e_{mn} + \dots \right) \right] \quad (20a)$$

$$d_{st}^{(2)}[\hat{X}] = \frac{1}{J(\alpha)} \left( \sum_{ij} \alpha_{si} d_{ij}^{(2,0)} \alpha_{tj} + \sum_{ijkl} \alpha_{si} d_{ijkl}^{(2,1)} \alpha_{tj} e_{kl} + \sum_{ijklmn} \alpha_{si} d_{ijklmn}^{(2,2)} \alpha_{tj} e_{kl} e_{mn} + \dots \right) \quad (20b)$$

in addition to the trivial relations  $B[\hat{X}] = B[X]/J(\alpha)$ ,  $C[\hat{X}] = C[X]/J(\alpha)$ , where  $J(\alpha) = \det(\alpha_{il})$ .

The above parametrization scheme, although mathematically correct, is certainly not very convenient for applications in which the background reference state  $\hat{X}$  is of high symmetry. For the most important example of a cubic high-symmetry phase, the above equations simplify considerable, since the deformation tensor  $\alpha_{ij} \equiv \alpha \delta_{ij}$  is diagonal, and so is the Lagrangian background strain  $e_{ij} \equiv e \delta_{ij}$  with  $e = \frac{1}{2}(\alpha^2 - 1)$ , which yields

$$A[\hat{X}] = \frac{1}{\alpha^3} \left[ A[X] + 2 \left( e \sum_i d_{ii}^{(2,0)} + \frac{e^2}{2!} \sum_{ik} d_{iikk}^{(2,1)} + \frac{e^3}{3!} \sum_{ikm} d_{iikkmm}^{(2,2)} + \dots \right) \right] \quad (21a)$$

$$d_{st}^{(2)}[\hat{X}] = \frac{1}{\alpha} \left( d_{st}^{(2,0)} + e \sum_k d_{stkk}^{(2,1)} + e^2 \sum_{km} d_{stkkmm}^{(2,2)} + \dots \right) \quad (21b)$$

These formulas are as far as we can get without committing to a specific set of irreducible representations that determine the symmetry-allowed couplings in the Landau potential. Since the background strains  $e(P) \sim P + O(P^2)$ , they effectively represent a set of highly interrelated power series in powers of  $P$ . Unfortunately, this also comes with all the inherent drawbacks. On the one hand, going beyond the lowest order terms, which may be taken from an previously determined ambient pressure Landau potential, we are forced to truncate the above series at rather low order to limit the number of additional unknown parameters. Of course, such truncated series inevitable diverge for increasing values of  $P$ . In addition, if we want to employ the theory for the purpose of fitting experimental data, we would like to fix certain experimental observables, in particular the pressure  $P_0$  at which  $A_R[\hat{X}]$  vanishes. Given the above parametrization, this is obviously difficult to do.

In Section 2, we have demonstrated the considerable structural simplification of a standard ambient pressure Landau approach upon replacing Cartesian strain tensors by symmetry-adapted strains. Remarkably, it turns out that, despite the additional complicated nonlinearities contained in formulas (21a) and (21b), similar manipulations may also be carried out in FSLT and are found to yield equally substantial structural simplifications. In the rest of the paper, the resulting scheme will be derived and illustrated by describing the HPPT of KMF.

#### 4. Symmetry-Adapted FSLT: The Cubic-to-Tetragonal HP Phase Transition of KMF

For  $\nu = 0, 1, 2, \dots$ , we set

$$\lambda_a^{(\nu)} \equiv \frac{1}{3} \sum_{k_1 \dots k_\nu} \sum_i d_{iik_1 k_1 \dots k_\nu k_\nu}^{(2,\nu)} \quad (22a)$$

$$\lambda_t^{(\nu)} \equiv \sum_{k_1 \dots k_\nu} \frac{d_{33k_1 k_1 \dots k_\nu k_\nu}^{(2,\nu+1)} - d_{11k_1 k_1 \dots k_\nu k_\nu}^{(2,\nu)}}{2\sqrt{3}} \quad (22b)$$

in accordance with

$$\lambda_a[\hat{X}] \equiv \lambda_a(e) \equiv \frac{1}{3} \sum_s d_{ss}^{(2)}[\hat{X}] \quad (23a)$$

$$\lambda_t[\hat{X}] \equiv \lambda_t(e) \equiv \frac{d_{33}^{(2)}[\hat{X}] - d_{11}^{(2)}[\hat{X}]}{2\sqrt{3}} \quad (23b)$$

Equations (21a) and (21b) are then replaced by

$$\alpha^3 A[\hat{X}] = A[X] + 6 \sum_{\nu=0}^{\infty} \frac{\lambda_a^{(\nu)}}{(\nu+1)!} e^{\nu+1} \quad (24a)$$

$$\alpha \lambda_{a,t}[\hat{X}] = \sum_{\nu=0}^{\infty} \lambda_{a,t}^{(\nu)} e^\nu \quad (24b)$$

Furthermore, we recall from nonlinear elasticity theory [20] that for a cubic system the compliance tensor  $S_{ijkl}[\hat{X}]$  and the bulk modulus  $K[\hat{X}] = (B_{1111}[\hat{X}] + 2B_{1122}[\hat{X}])/3$  at finite pressure are related by  $\sum_i S_{iiji}[\hat{X}] = S_{1111}[\hat{X}] + 2S_{1122}[\hat{X}] = 1/3K[\hat{X}]$ , while, for the longitudinal shear modulus,  $\mu[\hat{X}] = (B_{1111}[\hat{X}] - B_{1122}[\hat{X}])/2$  the relation  $S_{1111}[\hat{X}] - S_{1122}[\hat{X}] = 1/2\mu[\hat{X}]$  holds. If we replace the Cartesian

equilibrium spontaneous strain components (16) by their symmetry-adapted volume and tetragonal counterparts using these relations, they acquire the representations

$$\bar{\epsilon}_a = -\frac{\lambda_a[\hat{X}]}{K[\hat{X}]} \bar{Q}^2, \quad \bar{\epsilon}_t = -\frac{2\lambda_t[\hat{X}]}{\mu[\hat{X}]} \bar{Q}^2 \quad (25)$$

Furthermore, it is easy to check the identity

$$\sum_{ijkl} d_{ij}^{(2)}[\hat{X}] S_{ijkl}[\hat{X}] d_{kl}^{(2)}[\hat{X}] = \frac{\lambda_a^2[\hat{X}]}{K[\hat{X}]} \quad (26)$$

which allows for similarly rewriting the renormalized potential  $\Phi_R(Q; \hat{X})$  as

$$\Phi_R(Q; \hat{X}) = \Phi(Q; \hat{X}) - \frac{Q^4}{4} \left( \frac{2\lambda_a^2[\hat{X}]}{K[\hat{X}]} + \frac{8\lambda_t^2[\hat{X}]}{\mu[\hat{X}]} \right) \quad (27)$$

Combining these equations with Equations (24a) and (24b), we can summarize the symmetry-adapted parametrization of the coefficients of the renormalized Landau potential (18), whose minimization determines the equilibrium OP  $\bar{Q}$  with

$$A_R[\hat{X}] = \frac{A[X]}{\alpha^3} + \frac{6\Delta_a[\hat{X}]}{\alpha^3} \quad (28a)$$

$$B_R[\hat{X}] = \frac{B[X]}{\alpha^3} - \frac{2(\lambda_a^{(2)}[\hat{X}])^2}{K[\hat{X}]} - \frac{8\lambda_t^2[\hat{X}]}{\mu[\hat{X}]} \quad (28b)$$

in addition to  $C_R[\hat{X}] = \tilde{C}[\hat{X}]$ , where we introduced the function

$$\Delta_a[\hat{X}] \equiv \Delta_a(e) \equiv \sum_{\nu=0}^{\infty} \frac{\lambda_a^{(\nu)}}{(\nu+1)!} e^{\nu+1} \quad (29)$$

Note the close formal similarity of Equations (28a), (28b) and (29) with their infinitesimal counterparts (7a) and (7b). In a generic application of this theory with cubic high symmetry, the lowest order Landau coefficients  $A[X], B[X], C[X]$  and the lowest order strain-OP coupling coefficients  $\lambda_{a,t}^{(0)}$  can be taken from an existing ambient pressure Landau theory. Furthermore, the (diagonal) background deformation components  $\alpha = \alpha(P)$  and the resulting Lagrangian strain  $e = e(P)$  may be determined by fitting a suitable EOS to the cubic unit cell volume data. Such a fit also immediately yields the pressure-dependent bulk modulus  $K[\hat{X}] \equiv K(P)$ . It is only for the pressure-dependence of the longitudinal shear modules  $\mu[\hat{X}] = \mu(P)$  that we are truly forced to resort to additional input from DFT. To determine the EOS and the elastic constants of KMnF<sub>3</sub>, we have performed a series of fairly standard DFT calculations. We refer to Appendix A for further details of these simulations.

Since we do not need to maintain the highest possible precision in determining  $\mu(P)$  at room temperature but can content ourselves with a reasonable approximation, we use the following heuristic strategy to promote the DFT result  $\mu_{\text{DFT}}(P)$  from  $T = 0$  to ambient temperature. Figure 7 shows a comparison of the bulk moduli  $K_{\text{DFT}}(P)$  calculated from DFT to the result for  $K(P)$  obtained from the Murnaghan fit of the data published in Ref. [11]. Numerically, one finds the fraction of these moduli stays

entirely within the narrow bounds  $0.918 \leq K(P)/K_{\text{DFT}}(P) \leq 0.92$  over the whole interval  $0 \leq P \leq 20$  GPa. We therefore postulate a similar behavior for  $\mu(P)$ , setting

$$\mu(P) \equiv \frac{K(P)}{K_{\text{DFT}}(P)} \cdot \mu_{\text{DFT}}(P) \quad (30)$$

Figure 8 illustrates the resulting behavior of  $\mu(P)$ .

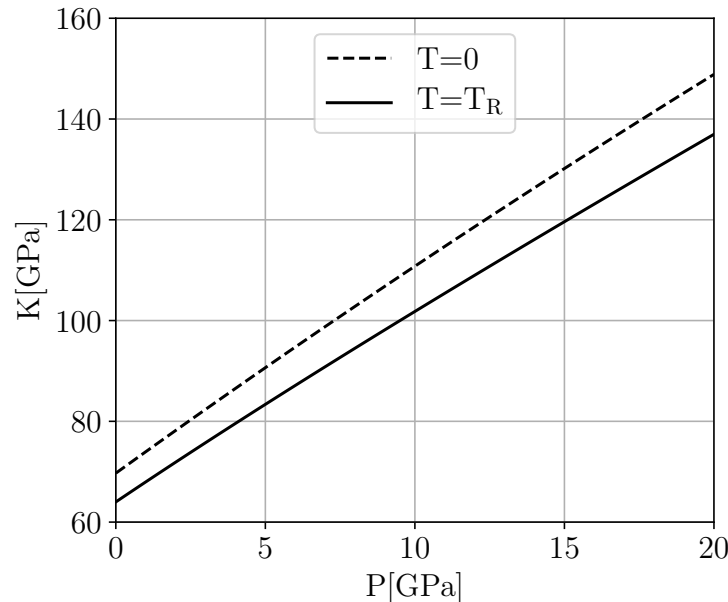


**Figure 7.** Comparison of pressure-dependent bulk modulus  $K(P)$  at room temperature  $T = T_R$  extracted from the Murnaghan fit of the cubic part of the unit cell data of Ref. [11] to the  $T = 0$  result obtained from DFT.

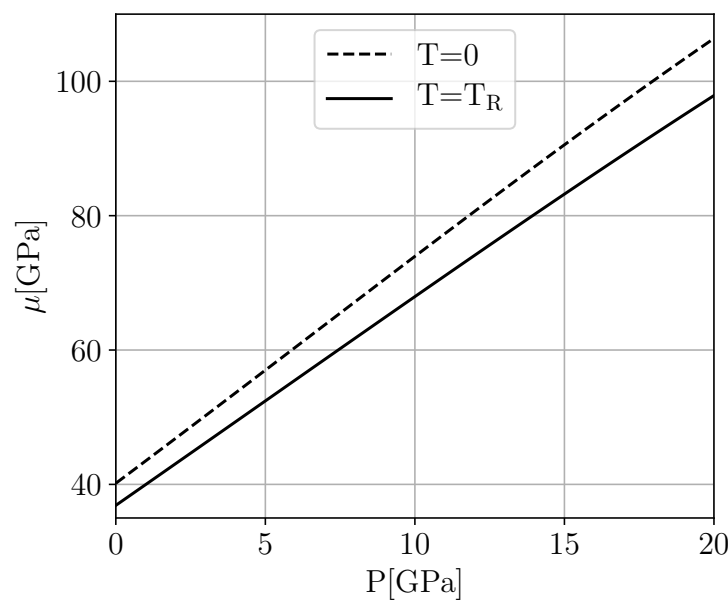


**Figure 8.** Pressure-dependent longitudinal shear modulus  $\mu(P)$  at room temperature  $T = T_R$  as determined by extrapolating the corresponding DFT result from  $T = 0$  to  $T = T_R$  based on Formula (30).

With all other ingredients in place, this leaves only the higher order coefficients  $\lambda_{a,t}^{(\nu)}, \nu > 0$  as the remaining undetermined parameters of FS LT. It therefore seems that these parameters must be treated as unknown fit parameters in a practical application. In the next section, however, we will introduce a much more convenient and powerful approach.

## 5. Efficient Parametrization

Comparing the above symmetry-adapted system of equations to what we had before, a considerable structural simplification is obvious. However, the following drawbacks seem to persist:

- Truncating the functions  $\lambda_{a,t}[\hat{X}]$  defined by Equation (24b) at finite order  $e^\nu = e^\nu(P)$  still results in divergent behavior with increasing  $P$ .
- In addition to a given set of strain measurements which we would want to feed to least squares fits based on Landau theory, rather accurate experimental information on the critical temperature  $T_c$  or the critical pressure  $P_c$  is frequently available from complementary experimental measurements. Unfortunately, least squares fitting procedures of strain measurements with an unconstrained value of  $T_c$  or  $P_c$  frequently tend to displace  $T_c$  or  $P_c$  and thus degrade the accuracy of the fit in the transition region. At least for a second order transition, the critical point is, of course, determined by the zero of the quadratic coefficient  $A_R$  of the Landau expansion. Therefore, we would like to be able to explicitly constrain the behavior of  $A_R$ , possibly fixing both its zero and/or slope at zero as a function of  $T$  or  $P$ . Unfortunately, based on a set of interrelated truncated power series, this is still hard to do.

In what follows, we propose a new scheme which finally allows for practically overcoming all of these problems in a single push. Let us start by taking a second look at Figure 6. Of course, the correct functional form of  $A_R[\hat{X}] \equiv A_R(T_R, P)$  that we are looking for should be that of a well-behaved function passing through zero around  $P_c \approx 4$  GPa. At  $P = 0$ , however, it should start out with roughly twice the initial slope of the purely linear yellow curve if we are to retain the ambient pressure Landau parameters. The pressure dependence of the correct function  $A_R(T_R, P)$  must therefore be far from linear. Experimentally, there is no indication of a re-entrant behavior below 25 GPa, so we do not expect any second crossing point in this pressure range. Unfortunately, our numerical tests quickly revealed that, using a truncated version of  $\Delta_a(e(P))$  as defined in (29), it seems virtually impossible to meet these requirements unless one is willing to go to prohibitively high truncation order, thus introducing a plethora of unknown fit parameters and the accompanying horrific numerical problems.

A way out is to propose a reasonable function  $\Delta_a(e(P))$  in closed form that meets all of the above requirements while still containing some adjustable parameters that offer a certain amount of variational flexibility to allow improvement by least squares fitting. Of course, there are many ways to do this, and the choices are only limited by the reader's ingenuity. In fact, since the summand  $\nu = 0$  of  $\Delta_a(x)$  contributes the lowest order coefficient  $x\lambda_a^{(0)}$ , which is usually fixed from knowledge of an existing ambient pressure Landau theory, all candidate functions  $\Delta_a(x)$  that start out like

$$\Delta_a(x) = \lambda_a^{(0)}x + O(x^2) \quad (31)$$

qualify as candidates for a meaningful function  $\Delta_a(x)$ . In our current application to KMF, we parametrize

$$A_R \equiv A_R(T_R, e(P)) = \frac{A_R(T_R) + 6\Delta(e(P); b, c, d)}{\alpha^3(P)} \quad (32)$$

by introducing the function

$$\Delta(e; b, c, d) := ce + 2bf_d(e) \quad (33)$$

with parameters  $b, c, d$  combining a linear part with slope  $c$  and a nonlinear contribution  $f_d(e)$ , which remains yet to be specified. Our general parametrization strategy is then as follows:

- As a function of  $e$ ,  $A_R(T_R, e)$  should start out with slope  $s = -6\lambda_a^{(0)} \equiv c + 2bf'_d(0)$ , so parameter  $b$  can be traded for the slope  $s$  of  $\Delta(e; b, c, d)$  at  $e = 0$ .
- Suppose further that  $A_R(T_R, e)$  should vanish at a critical value  $e_0 = e(P_0)$  of the background strain  $e$ . For  $\Delta(e; b, c, d)$ , this implies the constraint equation  $\alpha + \Delta(e_0; b, c, d) \equiv 0$  where  $\alpha \equiv A_R(T_R, 0)/6$ , which may be solved for parameter  $c$ .

These steps eliminate parameters  $b, c$  in favor of the constants  $\alpha$  and  $e_0$ , leaving  $d$  as the single remaining free variational parameter. We still need to reconcile this parametrization of  $A_R$  with that of the function  $\lambda_a[\hat{X}]$  as defined in Equation (24b). We focus on the power series part

$$\Lambda(x) \equiv \sum_{\nu=0}^{\infty} \lambda_a^{(\nu)} x^\nu \quad (34)$$

which is based on the same set of coefficients  $\lambda_a^{(\nu)}$  as  $\Delta_a(x)$  but lacks the accompanying factorials  $1/\nu!$ . These factorials can, however, easily be taken care of. Observe that

$$\int_0^\infty dt e^{-t} \frac{(tx)^{\nu+1}}{(\nu+1)!} = x^{\nu+1} \quad (35)$$

Therefore, using the *Borel transform*

$$(\mathcal{B}\Delta)(x) \equiv \int_0^\infty dt e^{-tx} \Delta(tx) \quad (36)$$

we may relate

$$\Lambda(x) = \frac{(\mathcal{B}\Delta)(x)}{x} \quad (37)$$

It remains to specify a suitable function  $f_d(x)$ . Beyond producing a reasonable function  $A_R(T_R, e)$ , the job profile for recruiting such a function includes at least two basic requirements:

- It would be highly desirable to be able to compute the corresponding Borel transform  $(\mathcal{B}f_d)(x)$  in closed form.
- $f_d(x)$  should also allow for solving the equation  $\alpha + \Delta(e_0; b, c, d) \equiv 0$  explicitly.

For the present goal of understanding the HPPT in KMF, we came up with the choice

$$f_d(e) := -1 + \sqrt{1 - d^2e} \quad (38)$$

(note that  $e(P) < 0$  for  $P > 0$ ) which meets both of these minimal requirements, since, in this case,  $b = (c - s)/d^2$  and

$$c = \frac{s \left( \sqrt{1 - d^2e_0} - 1 \right) - \alpha d^2/2}{d^2e_0/2 + \sqrt{1 - d^2e_0} - 1} \quad (39)$$

In this way, we have completely bypassed Taylor series expansions and their various accompanying drawbacks. Figure 9 illustrates the remaining variational freedom in our chosen parametrization.

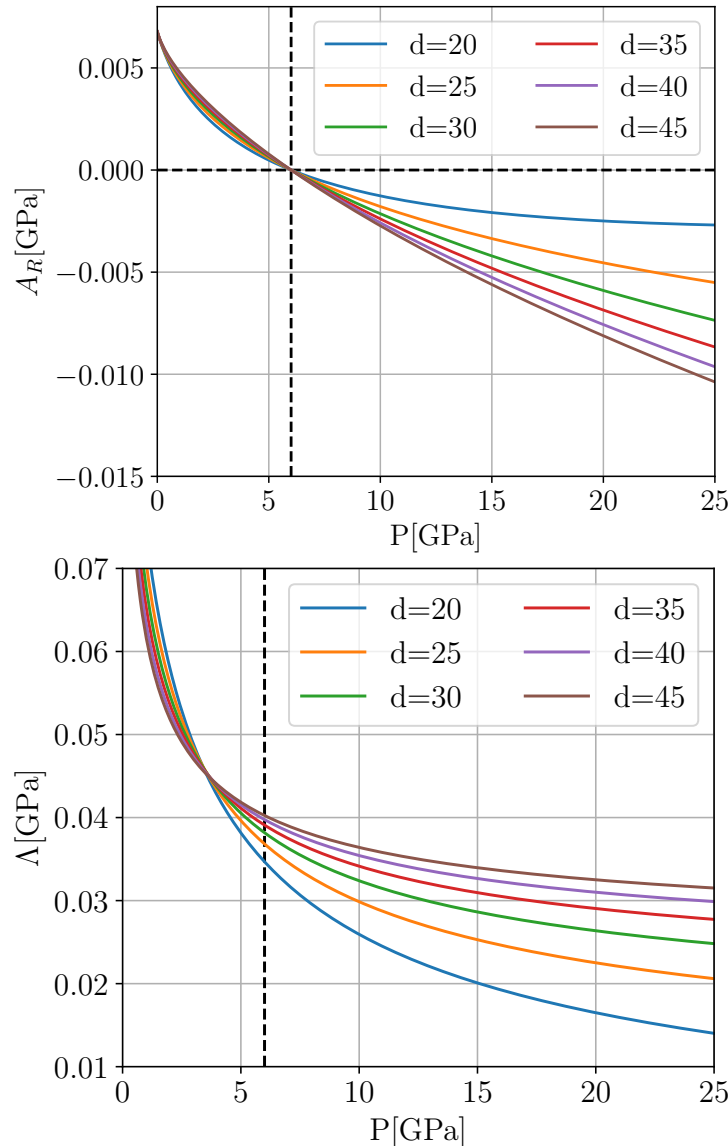


**Figure 9.** Illustration of the remaining  $d$ -dependence of the parametrization of  $A_R(T_R, e(P))$  by Equation (32) (upper panel) and the resulting function  $\Lambda(e(P))$  as given by the Borel transform Equation (37) (lower panel). Parameters  $b$  and  $c$  were eliminated in favor of parameter  $\lambda_a^{(0)} = 0.128$  GPa as prescribed from ambient pressure LT and a chosen pressure parameter  $P_0 = 6.0$  GPa.

In summary, at this stage, the function  $\Delta_a[\hat{X}]$  which governs the behavior of  $A_R[\hat{X}]$  and—through a Borel transform—also provides the coupling function  $\lambda_a[\hat{X}]$  between the spontaneous volume strain  $\hat{\epsilon}_a$  and  $\hat{Q}^2$  according to Equation (25) has been specified up to a single free parameter  $d$ . The remaining coupling function  $\lambda_a[\hat{X}] \equiv \lambda_a(P)$  explicitly determines the proportionality between the spontaneous tetragonal strain  $\hat{\epsilon}_a$  and  $\hat{Q}^2$ . However, both  $\lambda_a[\hat{X}]$  and  $\lambda_t[\hat{X}]$  also enter implicitly into the spontaneous strain via its implicit dependence on the quartic coefficient  $B_R[\hat{X}]$  of the renormalized Landau potential as given by Equation (28b), and, apart from the reasonable requirement  $\lim_{P \rightarrow 0} \lambda_t[\hat{X}] = \lambda_t^{(0)}$ , nothing is known in advance about its pressure dependence, such that introducing a truncated Taylor series and least squares

fitting seems unavoidable. However, we can actually do a lot better than this. Let us consider experimental high pressure spontaneous strain data in the form of  $n$  data points  $(P_i, \hat{\epsilon}_{a,\text{exp}}(P_i), \hat{\epsilon}_{t,\text{exp}}(P_i))_{i=1}^n$ . In fact, at a given prescribed pressure value  $P_i$  and with all other parameters in place, we can regard the room temperature values  $\hat{\epsilon}_a = \hat{\epsilon}_a(\lambda_t(P_i))$  and  $\hat{\epsilon}_t = \hat{\epsilon}_t(\lambda_t(P_i))$  as functions of the unknown function values  $\lambda_t(P_i)$ . The “best” value  $\lambda_t(P_i)$  matching the data point  $(P_i, \hat{\epsilon}_{a,\text{exp}}(P_i), \hat{\epsilon}_{t,\text{exp}}(P_i))$  may then be determined by numerically minimizing the function

$$\begin{aligned} s_i(\lambda_t(P_i)) := & w_a [\hat{\epsilon}_{a,\text{exp}}(P_i) - \hat{\epsilon}_a(\lambda_t(P_i))]^2 \\ & + w_t [\hat{\epsilon}_{t,\text{exp}}(P_i) - \hat{\epsilon}_t(\lambda_t(P_i))]^2 \end{aligned} \quad (40)$$

with weights  $w_a, w_t$  suitable adjusted to counterbalance size differences between  $\hat{\epsilon}_a$  and  $\hat{\epsilon}_t$ . Carried out for all  $i = 1, \dots, n$ , this prescription results in a collection of  $n$  “optimal” values  $\lambda_t(P_i)$  from which one may hope to recover the full function  $\lambda_t(P)$  by interpolation. Figure 10 shows the result of our corresponding effort for KMF. Amazingly, we observe that all values  $\lambda_t(P_i)$  seem to accumulate on a straight line whose extrapolation  $P \rightarrow 0$  perfectly passes through the point  $(0, \lambda_t^{(0)})$ , which is just the limiting value imposed by ambient pressure Landau theory. We believe that this behavior is not coincidental but a strong indication that the present parametrization is internally consistent and correct.

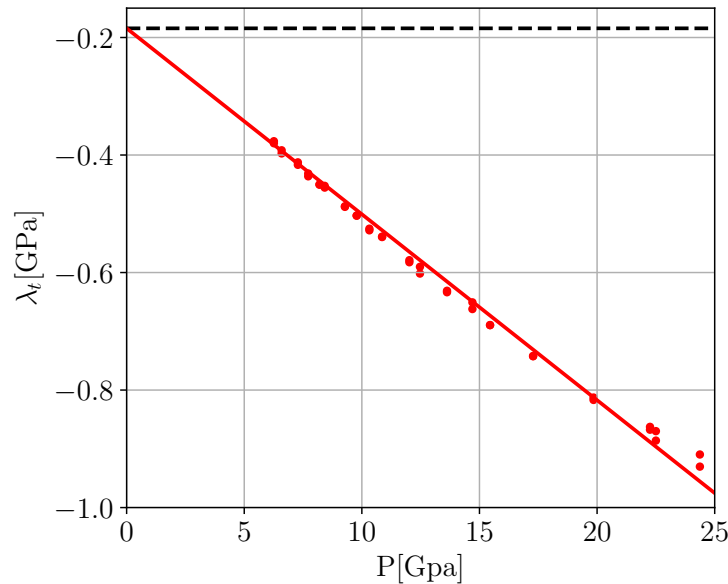


**Figure 10.** Results of minimizing the sum (40) using the relative weights  $(w_a, w_t) = (10, 1)$  and pressure parameters  $P_0 = 6\text{GPa}$ ,  $d = 40$ . The dashed horizontal line indicates the limiting value  $\lambda_t(P = 0) \equiv \lambda_t^{(0)}$ .

A simple linear fit of  $\lambda_t(P)$  therefore completes our Landau parametrization. Our results for the pressure dependence of the couplings  $A_R(P), \tilde{B}(P), \lambda_{a,t}(P)$  and the resulting pressure dependence of the equilibrium OP  $\bar{Q}(P)$  are illustrated in Figure 11. Note that in the present description the transition appears to be of first rather than second order, with  $P_0 = 6\text{GPa}$  yielding a transition pressure  $P_c \approx 4.5\text{GPa}$ . Finally, the resulting parametrization of the spontaneous strain is compared to experiment in Figure 12.

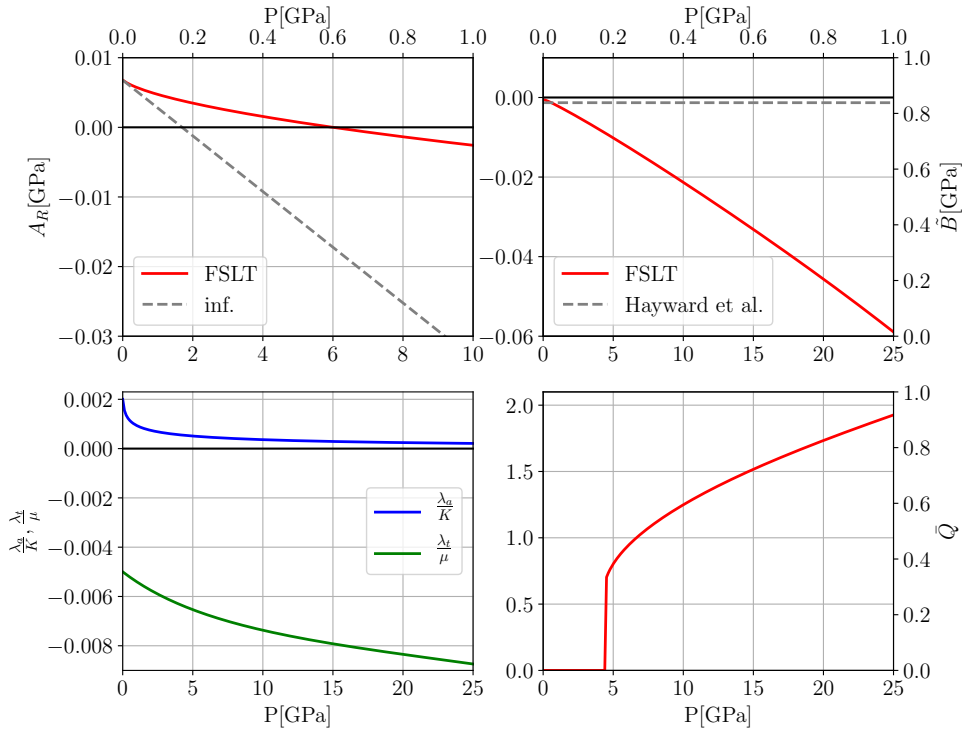


**Figure 11.** Upper left panel: pressure dependence of Landau parameters  $A_R(P)$  as compared to the simple linear behavior of infinitesimal strain LT assumed in Equation (7a). Upper right panel: pressure dependence of  $\tilde{B}(P)$ . The dashed horizontal line indicates the corresponding value from the parametrization of Hayward et al. [19] taken at  $T = 186.5$  K, which is slightly displaced from our limiting value at  $P = 0$  since we are taking into account thermal softening of  $K(P)$  and  $\mu(P)$  for room temperature. Lower left panel: pressure dependence of coupling parameters  $\lambda_a(P)/K(P)$  and  $\lambda_t(P)/\mu(P)$ . Lower right panel: resulting behavior of the equilibrium order parameter  $\bar{Q}(P)$  (right).

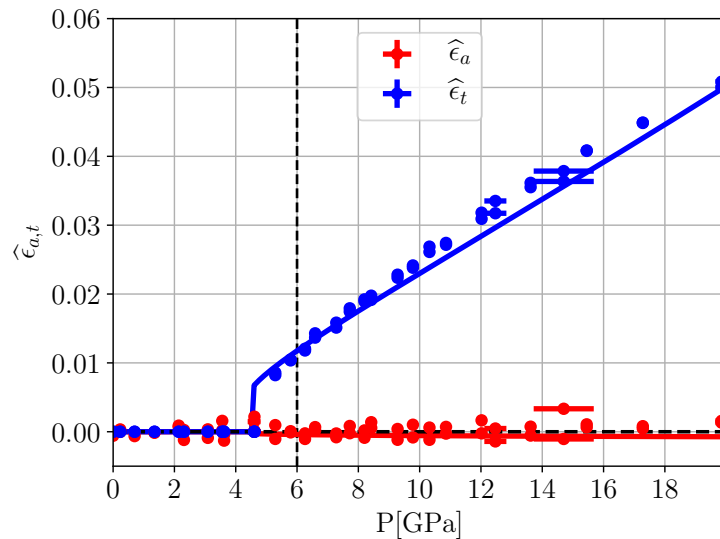


**Figure 12.** Parametrization of spontaneous strains  $\hat{\epsilon}_a, \hat{\epsilon}_t$  in comparison to experimental data from Ref. [11]. The thin vertical line indicates the pressure parameter  $P_0 = 6$  GPa.

## 6. Discussion

For the high pressure community, our present paper contains some good news and some bad news—first, the bad news. We hope to have demonstrated convincingly that classical Landau theory is usually completely inadequate for “explaining” experimental findings in the field of high pressure phase transitions, and the conclusions drawn from it will often be misleading at best. Taking the example of KMF, both the first order character of the transition and the correct value of the transition pressure are completely obscured by sticking to Landau theory with infinitesimal strain coupling, even if one is willing to distort a pre-existing ambient pressure Landau parametrization beyond recognition. The good news, however, is that with the development of FSLT a mathematically consistent alternative incorporating nonlinear elasticity has recently become available. Up to now, however, FSLT has been rather complicated in structure, which quite likely scared off many potential users and thus did not lead to the widespread use that its developers were initially hoping for. The present paper, which exploits the enormous simplifications that arise by passing (i) from Cartesian to symmetry-adapted finite strains and (ii) by virtue of (i), from truncated Taylor expansions to a functional parametrization. These improvements should pave the way for routine use of our theory in successfully describing HPPTs. In particular, the present paper illustrates that, while the former version of FSLT involved delicate least-squares fitting procedures with a large number of unknown fit parameters and dealing with all the inadequacies implicit in the use of truncated Taylor expansions, in the present scheme, the unknown pressure dependencies can be systematically determined one-by-one in a step-wise, almost “deterministic” manner.

Admittedly, even the present parametrization of the HPPT in KMF is still less than perfect. For instance, the coupling function  $\lambda_a(P)/K(P)$  shown in the lower left panel of Figure 11 exhibits a steep initial decrease with increasing pressure. Since no spontaneous strain data are available for this pressure region, this does not change the physical values produced by the theory. However, it hints at a sub-optimal choice Equation (38) for the auxiliary function  $f_d(x)$ . The reader is invited to come up with an improved candidate function.

More importantly, in a full-blown application of FSLT, we should be able to predict e.g., the  $(P, T)$  cubic-to-tetragonal phase boundary of KMF and compute pressure—and temperature-dependent elastic constants. In principle, the ability to do so depends mainly on the successful construction of a pressure—and temperature-dependent baseline, i.e., the cubic EOS  $V_{\text{cubic}} = V_{\text{cubic}}(P, T)$ . In a previous paper [10], this task has been successfully carried out for the perovskite  $\text{PbTiO}_3$  by combining zero temperature DFT calculations (see Appendix A for details) with the Debye approximation as implemented in the GIBBS2 package [22,23] to incorporate effects of thermal expansion (recently, we learned [24] that a similar approach also seems to work for  $\text{MgSiO}_3$ ). Unfortunately, our corresponding efforts to derive  $V_{\text{cubic}}(P, T)$  for KMF along the same lines have failed so far, however. This failure manifests itself e.g., in the inability to simultaneously reproduce the thermal baseline at  $P = 0$  measured experimentally and the ambient temperature EOS, even if we allowed for the introduction of a constant compensating background pressure which is frequently introduced in DFT calculations to compensate inadequacies of an employed exchange-correlation functional. Ref. [25] states that perovskites with octahedral tilting generally do not show an appreciable coupling between structural and magnetic order parameters. Nevertheless, this statement obviously does not exclude effects due to a coupling between magnetic degrees of freedom and the background volume strain. Since the Debye approximation is based exclusively on phonons, we may speculate that in KMF residual magnetic effects may be responsible for additional thermal energy consumption. An investigation of this problem is currently underway.

Finally, it may be argued that our current theory also does not “explain” the origins of the involved nonlinear  $P$ -dependencies on a fundamental level. In approaches based on infinitesimal strain couplings, similarly looking  $P$ -dependent couplings are also introduced, but in a more or less completely ad hoc

manner, blaming their existence on rather unspecific “higher order strain couplings”. As a rule, such an approach results in a mathematically inconsistent theory. In contrast, the nonlinearities that arise in FSLT result for different but well-defined reasons. On the one hand, there are couplings between powers of the background strain  $e(P)$  and the Landau potential  $\Phi_R(Q; \hat{X})$  “floating” on this background strain, and there is a pressure-dependence of the elastic moduli  $K(P)$  and  $\mu(P)$ , which is in principle accessible e.g., to DFT calculations. This leaves the task of “explaining” the residual nonlinearities in the functions  $\lambda_{a,t}(P)$  describing the couplings between order parameter and spontaneous strains. In contrast to blaming their existence on the effects of some unspecified higher order couplings, our present theory provides a practical way to numerically determine these functions. In addition, we see no reason in principle as to why such  $P$ -dependent coupling constants could not eventually be extracted from DFT calculations along the general philosophy laid out in Refs. [26,27] and the subsequent follow-up literature.

**Author Contributions:** A.T.: concept, main theory, and writing; W.S.: additional theory, comparison to previous experimental data; S.E., K.B., and P.B.: DFT calculations. All authors have read and agreed to the published version of the manuscript.

**Funding:** A.T., S.E., and K.B. acknowledge support by the Austrian Science Fund (FWF) Project P27738-N28. W.S. acknowledges support by the Austrian Science Fund (FWF) Project P28672-N36. S.E. acknowledges support from H.E.C., Pakistan.

**Acknowledgments:** A.T. would like to thank Ronald Miletich-Pawliczek for useful discussions.

**Conflicts of Interest:** The authors declare no conflict of interest.

## Abbreviations

The following abbreviations are used in this manuscript:

AFN	antiferromagnetic
DFT	density functional theory
EOS	equation of state
FSLT	finite strain Landau theory
HPPT	high pressure phase transition
KMF	$KMnF_3$
LDA	local density approximation
LT	Landau theory
OP	order parameter
PT	phase transition
NM	nonmagnetic

## Appendix A. DFT Calculation Details

The EOS and the elastic constants in the cubic phase of KMF were calculated using the WIEN2K DFT package, which is an all-electron code based on the (linearized) augmented plane-wave and local orbitals [(L)APW+lo] basis representation of the Kohn–Sham equations [28] of DFT. Here, we only content ourselves with a quick outline of the basic ideas and refer to Refs. [29,30] and the monograph Ref. [31] for more details.

In the (L)APW+lo method, the crystal’s unit cell is partitioned into a set of atomic spheres surrounding the nuclei and a remaining interstitial region. Inside these atomic spheres, the wave functions are expanded into atomic-like basis functions, i.e., numerical radial functions times spherical harmonics while they are represented by plane waves throughout the interstitial region. These two regions are glued together by requiring continuity of the basis functions in value (and, depending on the flavor of the (L)APW+lo method, in radial slope) across the sphere boundaries. These LAPW calculations require making a couple

of choices regarding cell size, standard parameter values, etc. In detail, the calculations of the present work were done with  $R_{\text{MT}}^{\min} K_{\max} = 9$  and atomic sphere radii of 2.1, 2.0, and 1.6 bohr for K, Mn and F, respectively. The energy separation between core and valance states used was  $-6.0 \text{ Ry}$ . Inside the sphere, the maximum angular momentum used in the spherical expansions was  $L_{\max} = 10$ , while the charge density in the interstitial was Fourier expanded up to a cutoff of  $G_{\max} = 14(\text{a.u.})^{-1}$ .

As to the use of exchange-correlation functionals, we have performed calculations using the standard local density approximation (LDA) [32] and three functionals of the generalized gradient approximation, namely, PBE from Perdew et al. [33,34], its solid-state optimized version PBEsol [35], and WC from Wu and Cohen [36]. For LDA and PBE, we observed the well-known tendency to underestimate and overestimate the lattice constants of solids, respectively, while PBEsol and WC produced more accurate results in between LDA and PBE [37,38].

To study the effect of magnetism on our results, we undertook calculations for a standard non-magnetic (NM) and ferromagnetic (FM) cubic perovskite unit cell with five atoms as well as an for a cubic supercell with 10 atoms in antiferromagnetic (AFM) structures of A-type, C-type and G-type [39]. After sufficient testing, we settled for a k-mesh sampling of  $10 \times 10 \times 10$  k-points for all types of structures. In FM and AFM structure, we observed a linearization error which is inherent to the basis functions inside the spheres. To overcome this problem, we use the second energy derivative of the radial part (HDLO) for d electrons for Mn atom (for more detail see Ref. [40]). Using this setup, we identified that G-type AFM structure to have lowest energy.

Cubic elastic elastic constants were calculated with the help of the WIEN2K add-on package by Charpin [41]. Results at  $T = 0$  are compiled in Table A1. In particular, we conclude that FM and AFM structures give similar value of lattice parameters and bulk modulus, which suggests that the specific magnetic ordering is not overly important for these quantities. In passing, we note that non-magnetic KMf is found to be a metal (with all functionals), but all magnetic structures lead to insulators (with all functionals). Simulations with PBEsol+U with  $U = 4 \text{ eV}$  in the AFM G-type phase would even lead to slightly better agreement with experiment for lattice constants and bulk modulus, but overall the effect is small and we therefore used the PBEsol results in Figures 7 and 8.

**Table A1.** Lattice constant ( $\text{\AA}$ ) and bulk modulus (GPa) of cubic  $\text{KMnF}_3$  for different methods used in this work.

	Present Work			Other Works	
	NM	FM	AFM (G-Type)	PBE	Expt.
Lattice constant				4.185 [42]	
LDA	3.89	4.11	4.09		
PBEsol	3.96	4.19	4.17		
PBE	4.04	4.26	4.24	4.19 [43]	
PBEsol + U ( $U = 4 \text{ ev}$ )		4.20	4.19		
Bulk modulus					
LDA	117.2	83.7	88.4		
PBEsol	97.6	70.4	69.6		
PBE	83.3	62.3	63.1		
PBEsol + U ( $U=4 \text{ ev}$ )		68.2	67.7		

Estimating an additional softening due to finite temperature with various flavors of the Debye approximation which are implemented in the GIBBS2 software [22,23], the best agreement with the cubic part of the experimental data of Ref. [11] was reached for the combination of G-type antiferromagnetic structure and PBEsol functional.

## References

1. Landau, L.; Lifshitz, E.; Pitaevskii, L. *Statistical Physics Part I*; Butterworth and Heinemann: Oxford, UK, 2001.
2. Tolédano, J.; Tolédano, P. *The Landau Theory of Phase Transitions*; World Scientific: Singapore, 1987.
3. Rabe, K.; Ahn, C.; Triscone, J.M. (Eds.) Physics of Ferroelectrics. In *Topics in Applied Physics*; Springer: Berlin/Heidelberg, Germany, 2007; Volume 105.
4. Salje, E. *Phase Transitions in Ferroelastic and Coelastic Crystals*; Cambridge University Press: Cambridge, UK, 1990.
5. Tröster, A.; Schranz, W.; Miletich, R. How to Couple Landau Theory to an Equation of State. *Phys. Rev. Lett.* **2002**, *88*, 055503. [[CrossRef](#)]
6. Koppensteiner, J.; Tröster, A.; Schranz, W. Efficient parametrization of high-pressure elasticity. *Phys. Rev. B* **2006**, *74*, 014111. [[CrossRef](#)]
7. Schranz, W.; Tröster, A.; Koppensteiner, J.; Miletich, R. Finite strain Landau theory of high pressure phase transformations. *J. Phys. Condens. Matter* **2007**, *19*, 275202. [[CrossRef](#)]
8. Tröster, A.; Schranz, W. Landau theory at extreme pressures (invited paper for contribution to the special edition of “FERROELECTRICS”) (birthday edition in honour of V. Ginzburg’s 90th birthday). *Ferroelectrics* **2007**, *354*, 208. [[CrossRef](#)]
9. Tröster, A.; Schranz, W.; Karsai, F.; Blaha, P. Fully Consistent Finite-Strain Landau Theory for High-Pressure Phase Transitions. *Phys. Rev. X* **2014**, *4*, 031010. [[CrossRef](#)]
10. Tröster, A.; Ehsan, S.; Belbase, K.; Blaha, P.; Kreisel, J.; Schranz, W. Finite-strain Landau theory applied to the high-pressure phase transition of lead titanate. *Phys. Rev. B* **2017**, *95*, 064111. [[CrossRef](#)]
11. Guennou, M.; Bouvier, P.; Garbarino, G.; Kreisel, J.; Salje, E. Pressure-induced phase transition(s) in KMnF<sub>3</sub> and the importance of the excess volume for phase transitions in perovskite structures. *J. Phys. Condens. Matter* **2011**, *23*, 485901. [[CrossRef](#)]
12. Carpenter, M.A.; Becerro, A.I.; Seifert, F. Strain analysis of phase transitions in (Ca, Sr) TiO<sub>3</sub> perovskites. *Am. Mineral.* **2001**, *86*, 348–363. [[CrossRef](#)]
13. Salje, E.K.H.; Zhang, M.; Zhang, H. Cubic–tetragonal transition in KMnF<sub>3</sub>: IR hard-mode spectroscopy and the temperature evolution of the (precursor) order parameter. *J. Physics: Condens. Matter* **2009**, *21*, 335402.
14. Dormann, E.; Copley, J.R.D.; Jaccarino, V. Temperature dependence of the MnF<sub>2</sub> and KMnF<sub>3</sub> lattice parameters from room temperature to the melting point. *J. Phys. C Solid State Phys.* **1977**, *10*, 2767–2771. [[CrossRef](#)]
15. Ratuszna, A.; Pietraszko, A.; Chelkowski, A.; Lukaszewicz, K. The Temperature Dependence of Lattice Parameters of KMeF<sub>3</sub> and KMn<sub>0.9</sub>Me<sub>0.1</sub>F<sub>3</sub> Compounds (Me = Mn<sup>2+</sup>, Co<sup>2+</sup>, and Ni<sup>2+</sup>). *Phys. Status Solidi (a)* **1979**, *54*, 739–743. [[CrossRef](#)]
16. Sakashita, H.; Ohama, N. A precursor effect in the lattice constant at the 186 K-structural phase transition in KMnF<sub>3</sub>. *Phase Transit.* **1982**, *2*, 263–276. [[CrossRef](#)]
17. Sakashita, H.; Ohama, N.; Okazaki, A. Thermal expansion and spontaneous strain of KMnF<sub>3</sub> near the 186 K-structural phase transition. *Phase Transit.* **1990**, *28*, 99–106. [[CrossRef](#)]
18. Gibaud, A.; Shapiro, S.M.; Nouet, J.; You, H. Phase diagram of KMn<sub>1-x</sub>Ca<sub>x</sub>F<sub>3</sub> ( $x < 0.05$ ) determined by high-resolution X-ray scattering. *Phys. Rev. B* **1991**, *44*, 2437–2443. [[CrossRef](#)]
19. Hayward, S.A.; Romero, F.J.; Gallardo, M.C.; del Cerro, J.; Gibaud, A.; Salje, E.K.H. Cubic-tetragonal phase transition in KMnF<sub>3</sub>: Excess entropy and spontaneous strain. *J. Phys. Condens. Matter* **2000**, *12*, 1133–1142. [[CrossRef](#)]
20. Wallace, D. *Thermodynamics of Crystals*; Dover: New York, NY, USA, 1998.
21. Morris, J.W.; Krenn, C.R. The internal stability of an elastic solid. *Philos. Mag. A* **2000**, *80*, 2827–2840. [[CrossRef](#)]
22. Otero-de-la-Roza, A.; Lúaña, V. Gibbs2: A new version of the quasi-harmonic model code. I. Robust treatment of the static data. *Comput. Phys. Commun.* **2011**, *182*, 1708–1720. [[CrossRef](#)]
23. Otero-de-la-Roza, A.; Abbasi-Pérez, D.; Lúaña, V. Gibbs2: A new version of the quasiharmonic model code. II. Models for solid-state thermodynamics, features and implementation. *Comput. Phys. Commun.* **2011**, *182*, 2232–2248. [[CrossRef](#)]

24. Liu, Z.; Sun, X.; Zhang, C.; Hu, J.; Song, T.; Qi, J. Elastic Tensor and Thermodynamic Property of Magnesium Silicate Perovskite from First-principles Calculations. *Chin. J. Chem. Phys.* **2011**, *24*, 703–710. [[CrossRef](#)]
25. Carpenter, M.A.; Salje, E.K.H.; Howard, C.J. Magnetoelastic coupling and multiferroic ferroelastic/magnetic phase transitions in the perovskite KMnF<sub>3</sub>. *Phys. Rev. B* **2012**, *85*, 224430. [[CrossRef](#)]
26. Zhong, W.; Vanderbilt, D.; Rabe, K.M. Phase Transitions in BaTiO<sub>3</sub> from First, Principles. *Phys. Rev. Lett.* **1994**, *73*, 1861–1864. [[CrossRef](#)]
27. King-Smith, R.D.; Vanderbilt, D. First-principles investigation of ferroelectricity in perovskite compounds. *Phys. Rev. B* **1994**, *49*, 5828–5844. [[CrossRef](#)]
28. Kohn, W.; Sham, L.J. Self-Consistent Equations Including Exchange and Correlation Effects. *Phys. Rev.* **1965**, *140*, A1133–A1138. [[CrossRef](#)]
29. Blaha, P.; Schwarz, K.; Madsen, G.K.H.; Kvasnicka, D.; Luitz, J. *WIEN2k: An Augmented Plane Wave and Local Orbitals Program for Calculating Crystal Properties*; Vienna University of Technology: Vienna, Austria, 2001.
30. Schwarz, K.; Blaha, P.; Trickey, S. Electronic structure of solids with WIEN2k. *Mol. Phys.* **2010**, *108*, 3147–3166. [[CrossRef](#)]
31. Singh, D.; Nordström, L. *Planewaves, Pseudopotentials and the LAPW Method*, 2nd ed.; Springer: New York, NY, USA, 2006.
32. Perdew, J.P.; Wang, Y. Accurate and simple analytic representation of the electron-gas correlation energy. *Phys. Rev. B* **1992**, *45*, 13244–13249. [[CrossRef](#)]
33. Perdew, J.P.; Burke, K.; Ernzerhof, M. Generalized Gradient Approximation Made Simple. *Phys. Rev. Lett.* **1996**, *77*, 3865. [[CrossRef](#)]
34. Perdew, J.P.; Burke, K.; Ernzerhof, M. Generalized Gradient Approximation Made Simple [Phys. Rev. Lett. 77, 3865 (1996)]. *Phys. Rev. Lett.* **1997**, *78*, 1396. [[CrossRef](#)]
35. Perdew, J.P.; Ruzsinszky, A.; Csonka, G.I.; Vydrov, O.A.; Scuseria, G.E.; Constantin, L.A.; Zhou, X.; Burke, K. Restoring the Density-Gradient Expansion for Exchange in Solids and Surfaces. *Phys. Rev. Lett.* **2008**, *100*, 136406. [[CrossRef](#)]
36. Wu, Z.; Cohen, R.E. More Accurate Generalized Gradient Approximation for Solids. *Phys. Rev. B* **2006**, *73*, 235116. [[CrossRef](#)]
37. Tran, F.; Laskowski, R.; Blaha, P.; Schwarz, K. Performance on molecules, surfaces, and solids of the Wu-Cohen GGA exchange-correlation energy functional. *Phys. Rev. B* **2007**, *75*, 115131. [[CrossRef](#)]
38. Tran, F.; Stelzl, J.; Blaha, P. Rungs 1 to 4 of DFT Jacob's ladder: Extensive test on the lattice constant, bulk modulus, and cohesive energy of solids. *J. Chem. Phys.* **2016**, *144*, 204120. [[CrossRef](#)] [[PubMed](#)]
39. Hidaka, M.; Ohama, N.; Okazaki, A.; Sakashita, H.; Yamakawa, S. A comment on the phase transitions in KMnF<sub>3</sub>. *Solid State Commun.* **1975**, *16*, 1121–1124. [[CrossRef](#)]
40. Karsai, F.; Tran, F.; Blaha, P. On the importance of local orbitals using second energy derivatives for d and f electrons. *Comput. Phys. Commun.* **2017**, *220*, 230–238. [[CrossRef](#)]
41. Charpin, T. *A Package for Calculating Elastic Tensors of Cubic Phase Using WIEN*; Laboratory of Geometrix: Paris, France, 2001.
42. Ivanov, Y.; Nimura, T.; Tanaka, K. Electron density and electrostatic potential of KMnF<sub>3</sub>: A phase-transition study. *Acta Crystallogr. Sect. B* **2004**, *60*, 359–368. [[CrossRef](#)]
43. Hayatullah; Murtaza, G.; Khenata, R.; Muhammad, S.; Reshak, A.; Wong, K.M.; Omran, S.B.; Alahmed, Z. Structural, chemical bonding, electronic and magnetic properties of KMF<sub>3</sub> (M = Mn, Fe, Co, Ni) compounds. *Comput. Mater. Sci.* **2014**, *85*, 402–408. [[CrossRef](#)]



# Finite-strain Landau theory applied to the high-pressure phase transition of lead titanate

A. Tröster,<sup>1,\*</sup> S. Ehsan,<sup>1</sup> K. Belbase,<sup>1</sup> P. Blaha,<sup>1</sup> J. Kreisel,<sup>2,3</sup> and W. Schranz<sup>4</sup>

<sup>1</sup>Vienna University of Technology, Institute of Material Chemistry, Getreidemarkt 9, A-1060 Wien, Austria

<sup>2</sup>Department of Materials Research and Technology, Luxembourg Institute of Science and Technology, 41 Rue du Brill, L-4422 Belvaux, Luxembourg

<sup>3</sup>Physics and Materials Science Research Unit, University of Luxembourg, 41 Rue du Brill, L-4422 Belvaux, Luxembourg

<sup>4</sup>University of Vienna, Boltzmanngasse 5, A-1090 Vienna, Austria

(Received 29 November 2016; revised manuscript received 6 February 2017; published 27 February 2017)

Standard Landau theory coupled to infinitesimal strain allows a concise description of the temperature-driven ferroelectric tetragonal-to-cubic phase transition in  $\text{PbTiO}_3$  at ambient pressure. Unfortunately, it fails to cover its high-pressure counterpart at ambient temperature. For example, the experimental transition pressure is vastly underestimated, and neither the change from first to second order with increasing pressure nor the unusual pressure dependence of the tetragonal unit cell parameters observed in experiment are reproduced. Here we demonstrate that a combination of density functional theory and a recently constructed finite-strain extension of Landau theory provides a natural mechanism for resolving these discrepancies between theory and experiment. Our approach also allows us to determine the full tetragonal-cubic phase boundary in the  $(P, T)$  plane including an estimate of the tricritical point. We show that a careful analysis of the thermal elastic baseline is an essential ingredient to the success of this theory.

DOI: [10.1103/PhysRevB.95.064111](https://doi.org/10.1103/PhysRevB.95.064111)

## I. INTRODUCTION

Understanding the combined effects of temperature and pressure in inducing structural phase transitions is of vital interest to a large range of scientific disciplines. In particular, the study of crystals of perovskite type with structural formula  $\text{ABX}_3$  ( $\text{A}=\text{Ba}, \text{Ca}, \text{Mg}, \text{Pb}, \text{Sr}, \text{Ln}, \text{Y}, \dots, \text{B}=\text{Ti}, \text{Zr}, \text{Si}, \text{La}, \text{Mn}$ , etc.,  $\text{X}=\text{O}, \text{F}$ ) attracts a major interest, in both materials research and earth science. As to the latter, a prominent example is the perovskite-postperovskite transition in  $(\text{Mg},\text{Fe})\text{SiO}_3$ . It was the discovery of this transition [1], which occurs only at extreme pressures up to 125 GPa and temperatures of some 2500 K, that finally elucidated the unusual seismic properties of the earth's core-mantle  $\text{D''}$  boundary layer. In addition to external hydrostatic pressure [2], electronic, magnetic, and optical properties of materials may also be strongly affected by chemical pressure [3] or uniaxial stress [4]. High pressure also plays an important role in the synthesis of bulk multiferroic materials and provides insight into the complex interplay between magnetic and electronic properties and structural instabilities [5].

The paradigm formed by traditional Landau theory (LT) [6,7] and the closely related lattice-dynamical theory of “soft modes” [8] is a cornerstone of our understanding of structural phase transitions. In transitions driven by changing the temperature at ambient pressure, strain effects are usually small enough to warrant a harmonic treatment of the elastic contributions to the Landau potential (LP), and this approach also works for transitions driven by moderate external stress. However, the last two decades have seen a rapid improvement of the experimental capabilities for studying materials at extreme pressures [9]. It has become routine to control stresses that frequently represent sizable fractions of the elastic constants of the materials investigated. Under such conditions,

a description of pressure-induced transitions based on linear elasticity is bound to fail. A pressing need arises for an adequate extension of traditional LT to include nonlinear elastic effects at high stress and strain.

In Ref. [10] such a high-pressure extension of an existing ambient-pressure LP has been constructed. The most important input required by this finite-strain Landau theory (FSLT) is a set of pressure-dependent elastic constants of the high-symmetry phase which are calculated from density functional theory (DFT). Introducing additional parameters to capture the remaining nonlinear pressure evolution of the order parameter-strain coupling coefficients then allows to give a concise numerical description of the room-temperature high-pressure phase transition  $Pm\bar{3}m \leftrightarrow I4/mcm$  of the archetype perovskite strontium titanate  $\text{SrTiO}_3$  (STO) whereas a traditional Landau approach based on truncating the elastic energy at harmonic order fails quantitatively.

The purpose of the present paper is threefold. First, it illustrates the capabilities of our theory for the example of lead titanate  $\text{PbTiO}_3$  (PTO). As we shall demonstrate below, traditional LT fails in this case not only on the quantitative but even on the qualitative level.

Of course, it would be desirable to work out a true *ab initio* description [11,12] rather than relying on a theory that involves both input from DFT and a certain number of free parameters that need to be determined from fits to experimental data. However, electronic structure methods like DFT reside at zero temperature. Imposing an arbitrary external pressure poses no particular problem in DFT, but including effects of high temperatures is difficult. On the other hand, experimentalists have accumulated a wealth of data on the temperature dependence of structural phase transitions and encoded them in terms of published sets of numerical parameters for the corresponding LPs over the years (for ferroelectric perovskites see, e.g., Appendix A of Ref. [13]). Our second goal is to present FSLT as a general framework for extending this thermal information from ambient to high pressure.

\*andreas.troester@tuwien.ac.at

Third, we shall see that separating spontaneous and background strain must be done carefully when extracting Landau parameters from experimental data.

The paper is organized as follows. Section II presents a critical survey of the main predictions obtained from conventional LT for PTO. Section III reviews basic FSLT. Finite-temperature effects are treated in Sec. IV. Section V is devoted to the application to PTO. Section VI closes the paper with a discussion of results. Some technical arguments with the potential of distracting the reader's attention from the paper's main objective are gathered in Appendices A–D.

## II. SURVEY OF EXISTING RESULTS FOR THE FERROELECTRIC TRANSITION OF LEAD TITANATE

PTO is one of the most extensively studied ferroelectrics and is generally considered as a model material for understanding structural phase transitions. Moreover, PTO is an end member of high piezoelectric materials [14] like  $\text{PbZr}_{1-x}(\text{TiO}_3)_x$  (PZT) or  $(\text{PbMg}_{1/3}\text{Nb}_{2/3}\text{O}_3)_{1-x}(\text{TiO}_3)_x$  (PMN-PT), both of which exhibit a giant electromechanical (piezoelectric) response [15] near the so-called morphotropic phase boundary. They are thus of great technological importance. In view of the vast amount of literature on PTO, here, we only provide a short summary of results that are relevant for the present work.

Our focus is on the ferroelectric displacive transition from the tetragonal space group  $P4mm$  to the prototypical cubic perovskite structure  $Pm\bar{3}m$ . At ambient pressure, this transition is of first order at a reported Curie temperature of  $T_c \approx 492^\circ\text{C}$ . Following its discovery in 1950 [16,17], the underlying soft-mode dynamics was studied by neutron scattering [18] and Raman spectroscopy [19,20]. Guided by previous work [21,22], Haun *et al.* [23] constructed a Landau-Devonshire theory [24] that accounts for all possible [25] transitions from the cubic parent phase to tetragonal, orthorhombic, or rhombohedral phases under application of external stress. In what follows, we shall use small Latin letters for 3d vector indices  $i, j, \dots = 1, 2, 3$  and Greek ones  $\mu, \nu, \dots = 1, \dots, 6$  for Voigt indices. Using this convention, the phenomenological Gibbs potential density of Haun *et al.* includes all symmetry-allowed polynomial invariants up to sixth order built from the three components  $P_i$  of the spontaneous polarization  $\mathbf{P}$  that serves as the primary order parameter (OP), linear-quadratic couplings between the components  $\sigma_\mu$  of the external stress and the primary OP components, as well as a “bare” harmonic elastic energy. We shall focus on a single domain description by setting  $P_1 = P_2 = 0$ , with  $P_3$  playing the role of the primary OP. Then it suffices to work with the Gibbs potential density

$$G(P_3, \sigma_1, \sigma_2, \sigma_3) = G(P_3) + G_c(P_3, \sigma_1, \sigma_2, \sigma_3) + G_0(\sigma_1, \sigma_2, \sigma_3), \quad (1)$$

where

$$G(P_3) = \alpha_1 P_3^2 + \alpha_{11} P_3^4 + \alpha_{111} P_3^6, \quad (2a)$$

$$G_c(P_3, \sigma_1, \sigma_2, \sigma_3) = -P_3^2 \sum_\mu q_\mu \sigma_\mu, \quad (2b)$$

$$G_0(\sigma_1, \sigma_2, \sigma_3) = -\frac{1}{2} \sum_{\mu, \nu=1}^3 S_{\mu\nu}^0 \sigma_\mu \sigma_\nu. \quad (2c)$$

TABLE I. Landau parameter values used in our present calculations for dimensionless order parameter  $Q$ . The compliance components  $S_{11}^0$  and  $S_{12}^0$  are taken from Ref. [26] and agree with those listed in Table I of Gao *et al.* [27] or Table 5 on p. 368 of Ref. [13].

Parameter	Value
$\hat{\alpha}_1$	$7.644 \times 10^{-4} \text{ GPa K}^{-1} \times (T_0 - T)$
$T_0$	751.95 K
$\hat{\alpha}_{11}$	$-7.252 \times 10^{-2} \text{ GPa}$
$\hat{\alpha}_{111}$	$2.602 \times 10^{-1} \text{ GPa}$
$\hat{q}_{11}$	$8.92 \times 10^{-2}$
$\hat{q}_{12}$	$-2.6 \times 10^{-2}$
$S_{11}^0$	$8.0 \times 10^{-12} \text{ Pa}$
$S_{12}^0$	$-2.5 \times 10^{-12} \text{ Pa}$

Here  $S_{\mu\nu}^0$  are the bare elastic compliances of the cubic high-symmetry phase and  $q_1 = q_2 = q_{12}$ ,  $q_3 = q_{11}$  in the parametrization of Haun *et al.* In Ref. [23] numerical values for the parameters  $\alpha_1, \alpha_{11}, \alpha_{111}, q_{11}, q_{12}$  are given. Their behavior follows the traditional Landau prescription; i.e.,  $\alpha_1$  depends linearly on temperature while all other coefficients are independent of  $T$ . The polarization  $P_3$  has dimension  $\text{C/m}^2$ . In the present context, however, we prefer to work with a dimensionless OP instead, since the coupling coefficients then acquire the same units as the pressure. Rescaling  $P_3 \equiv 1\text{C/m}^2 \cdot Q$ , the coefficients  $\alpha_1, \alpha_{11}, \alpha_{111}$  and  $q_\mu$  get replaced by rescaled versions  $\hat{\alpha}_1, \hat{\alpha}_{11}, \hat{\alpha}_{111}$  and  $\hat{q}_\mu$ . Table I lists those rescaled parameters that are needed in our present context.

Instead of stresses, FSLT requires a parametrization in terms of strains. Mathematically, this amounts to replacing the Gibbs by the Helmholtz potential by performing a partial Legendre transform

$$F(Q, \epsilon_1, \epsilon_2, \epsilon_3) = G(Q, \underline{\sigma}(\underline{\epsilon})) + \sum_\mu \bar{\sigma}_\mu(\underline{\epsilon}) \epsilon_\mu \quad (3)$$

of the LP of Haun *et al.* At fixed  $P$ , the required equilibrium strains are

$$\bar{\epsilon}_\mu = -\frac{\partial G}{\partial \sigma_\mu} = Q^2 \hat{q}_\mu + \sum_{\nu=1}^3 S_{\mu\nu}^0 \sigma_\nu. \quad (4)$$

Solving (4) for  $\bar{\sigma}_\mu = \sum_\alpha C_{\mu\alpha}^0 (\epsilon_\alpha - \hat{q}_\alpha Q^2)$  where  $C_{\mu\alpha}^0$  denote the cubic elastic constants, we find

$$F(Q, \epsilon_1, \epsilon_2, \epsilon_3) = G(Q) - Q^2 \sum_{\alpha\beta} C_{\alpha\beta}^0 \hat{q}_\alpha \epsilon_\beta + \frac{Q^4}{2} \sum_{\mu, \alpha} q_\mu C_{\mu\alpha}^0 \hat{q}_\alpha + \frac{1}{2} \sum_{\alpha\beta} C_{\alpha\beta}^0 \epsilon_\alpha \epsilon_\beta. \quad (5)$$

Using a more traditional parametrization, we obtain

$$F(Q, \epsilon_1, \epsilon_2, \epsilon_3) = \frac{A}{2} Q^2 + \frac{B}{4} Q^4 + \frac{C}{6} Q^6 + Q^2 \sum_\mu D_\mu \epsilon_\mu + \frac{1}{2} \sum_{\mu, \alpha} \epsilon_\mu C_{\mu\alpha}^0 \epsilon_\alpha, \quad (6)$$

where

$$A = 2\hat{\alpha}_1, \quad (7)$$

$$B = 4\hat{\alpha}_{11} + 2 \sum_{\mu,\nu} \hat{q}_\mu C_{\mu\nu}^0 \hat{q}_\nu, \quad (8)$$

$$C = 6\hat{\alpha}_{111}, \quad (9)$$

$$D_\mu = - \sum_\nu C_{\mu\nu}^0 \hat{q}_\nu. \quad (10)$$

Figures 4 and 5 of Ref. [23] suggest that for vanishing stress, the potential  $G$  (or equally  $F$ ) is capable of offering a remarkable concise numerical description of both equilibrium OP as well as spontaneous strain components over a wide temperature range of nearly 500 K. In this parametrization the spontaneous strain components

$$\bar{\epsilon}_\mu(T) = \hat{q}_\mu \bar{Q}^2(T) \quad (11)$$

appear to be exactly proportional over this temperature range with a  $T$ -independent proportionality factor  $\hat{q}_\mu$ . In Refs. [13,26–28] the parameters published by Haun *et al.* in Ref. [23] have been taken over without any changes and can thus be regarded as well established in the literature. We shall reconsider the validity of this parametrization later on.

Unfortunately, the good agreement between data and theory for the temperature-driven transition at ambient pressure is spoiled for the pressure-driven case at ambient temperature. For hydrostatic stress  $\sigma_{ij} = -P\delta_{ij}$  the above Landau Gibbs potential density becomes

$$G(Q, P) = -\frac{P^2}{2K_0} + [\alpha_1 + (2q_{12} + q_{11})P]Q^2 + \alpha_{11}Q^4 + \alpha_{111}Q^6, \quad (12)$$

where  $K_0$  denotes the bulk modulus of the cubic parent phase. Note the linear  $P$  dependence of the harmonic contribution in contrast to the  $P$  independence of  $\alpha_{11}$ . For  $\alpha_{11} < 0$  this yields a first-order phase transition

$$P_c^{\text{Haun}} = \frac{\hat{\alpha}_1 + \frac{\hat{\alpha}_{11}^2}{4\hat{\alpha}_{111}}}{\hat{q}_{11} + 2\hat{q}_{12}} \quad (13)$$

with a corresponding OP discontinuity

$$\Delta Q_c = \sqrt{\frac{-\hat{\alpha}_{11}}{2\hat{\alpha}_{111}}} \quad (14)$$

at  $T_c$  and accompanying jumps

$$\Delta\epsilon_\mu = \Delta Q^2 \hat{q}_\mu, \quad \mu = 1, 2, 3 \quad (15)$$

of the spontaneous strain components. Note that with the given parametrization these jumps are mere constants independent of both  $P$  and  $T$ . At room temperature  $T_R$ , the parameter values listed in Table I produce

$$P_c^{\text{Haun}}(T_R) = 2.92 \text{ GPa}, \quad (16a)$$

$$\Delta\epsilon_\mu^{\text{Haun}} = \begin{cases} -0.0036, & \mu = 1, 2, \\ +0.0124, & \mu = 3. \end{cases} \quad (16b)$$

Our present work is motivated by the fact that these predictions are both qualitatively and quantitatively strikingly far from experiment. Instead, at room temperature in both the classic Raman study Ref. [29] and the high-pressure x-ray and Raman experiments conducted by Janolin *et al.* in Ref. [30] a second-order phase transition at a much larger critical pressure was detected.

In the single-crystal Raman experiments of Ref. [29], the merging of the tetragonal Raman-active  $E(jTO)$  and  $A_1(jTO)$  modes is observed at  $P_c \approx 12$  GPa, beyond which they are reported to vanish abruptly. In addition, close to  $P_c$  the squared frequencies of the lowest modes  $E(1TO)$  and  $A_1(1TO)$  are found to vanish like  $|P - P_c|$ . Early x-ray diamond anvil cell experiments [31] on U-doped PTO confirmed the absence of any transition up to 6 GPa at room temperature and yielded a similar estimate for  $P_c$ . On pure PTO, both x-ray and Raman scattering measurements were finally carried out at room temperature in Ref. [30], covering a much larger pressure range from ambient pressure up to 63 GPa. Up to 12 GPa, the x-ray results are consistent with the  $P4mm$  space group, while from 12 GPa to 20 GPa the unit cell parameters appear to be metrically cubic. The accompanying Raman data, which were obtained from powder, point more towards  $P_c \approx 13$  GPa but also show some features that are not well understood. Nevertheless, the fact that some Raman modes continue to be observed above this pressure and are found to harden again is not necessarily incompatible with the assignment of the prototypical cubic perovskite structure  $Pm\bar{3}m$  to this cubic phase. Similar observations are also made in the Raman spectra of  $\text{BaTiO}_3$  and  $\text{KNbO}_3$  (KNO) and are attributed to the existence of so-called nanopolar regions (cf. Ref. [32] and references therein). Summarizing, there is little doubt [33] that at room temperature lead titanate is of  $Pm\bar{3}m$  symmetry within the pressure range of 12–20 GPa. In passing we note that above 20 GPa, further tetragonal phases are reported in Ref. [30], which hints at the rather complicated topology of the full phase diagram of PTO in the  $(P, T)$  plane [34]. Concise DFT calculations [35] reveal that at zero temperature a tetragonal ground state is followed by monoclinic and rhombohedral phases, but below some 200 K the existence of a cubic phase seems to be ruled out [34].

In quantitative terms, a discrepancy of some 300% between the experimentally observed critical pressure  $P_c$  and the prediction  $P_c^{\text{Haun}}$  deduced from the theory of Haun *et al.* should be sufficient to make advocates of the traditional Landau approach scratch their heads. To illustrate the even more severe qualitative failures, Fig. 1 shows a compilation of powder and single-crystal x-ray results from Ref. [30] up to 20 GPa. Two aspects of these data appear to be particularly remarkable. (i) On the one hand, the transition appears to be continuous within experimental resolution. Tentatively calculating the jumps that the lattice parameters would undergo according to the prediction (16b), we would obtain discontinuities  $\Delta a = \Delta b \approx -0.014 \text{ \AA}$  and  $\Delta c = 0.048 \text{ \AA}$ . Jumps of this magnitude are, however, clearly ruled out by experiment (cf. Fig. 1). Indeed, the second-order character of the transition at elevated pressure and the possibility of a tricritical point has already been noted some time ago in the classic Raman study Ref. [29]. Interestingly, such a change from first to second

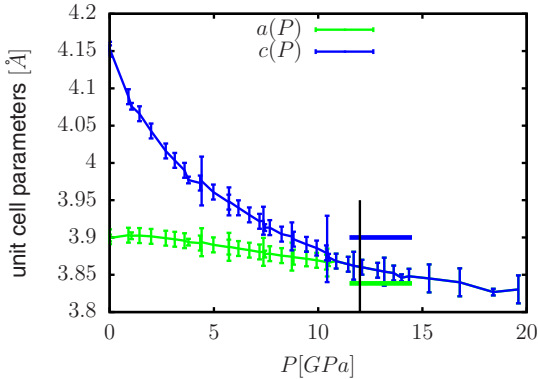


FIG. 1. Raw axis data for PTO obtained in Ref. [30] in the pressure range  $0 \leq P \leq 20$  GPa. The value  $P_c = 12$  GPa is indicated by the vertical line. The unobserved first-order jumps predicted from (16b) are marked by the two horizontal lines.

order character with increasing pressure is not only observed in the tetragonal-to-cubic transition of PTO but, for instance, also in that of KNO [32]. (ii) Equally puzzling is the observed curvature of the data that seems to increase as one lowers the pressure from  $P_c$  to ambient pressure. Given a second-order transition, the traditional Landau approach would predict a linear pressure dependence of the squared order parameter, inducing a similar  $P$  dependence of the spontaneous strain on top of the elastic background. In contrast, the observed behavior is neither expected nor explainable using standard Landau theory.

In summary, we observe serious inconsistencies between the traditional Landau approach and the experimental facts. Thus, it comes as no surprise that up to date we are not aware

of any attempt to analyze these data further within the Landau framework. In what follows we shall demonstrate that our recently developed extension of Landau theory [10] allows us to carry out such an analysis successfully. However, the case of PTO turns out to pose some special challenges that may not be encountered in simpler applications of this theory. We therefore add a short discussion of the cornerstones of our flavor of Landau theory before we present its application to PTO in detail.

### III. FINITE-STRAIN LANDAU THEORY

In a Landau-type approach, it is essential to recognize that a possible dependence on an external stress can be fully encoded in a double expansion of the Landau free energy  $F(Q, \eta; X)$  in powers of the OP components  $Q_i$  and the components of the total strain tensor  $\eta_{ij}$  defined with respect to the zero-pressure (“lab”) system  $X$ . In previous literature, to capture strain effects beyond linear elasticity, some authors have tried to modify LPs of the above type by introducing  $P$ -dependent potential parameters in a more or less *ad hoc* manner. Frequently, this leads to “Landau potentials” in which both strains and stresses appear simultaneously. Such a strategy is neither mathematically consistent nor physically satisfying. Our present method strictly employs expansions in the strain components, even though our final results are parametrized by the underlying external pressure  $P$ , which nevertheless has always the status of a derived quantity, i.e., is a function of the applied strain. This is also very natural from the perspective of DFT.

Considering for simplicity the case of a scalar order parameter  $Q$ , in the laboratory system  $X_0$  such an expansion generally reads

$$\begin{aligned} \frac{F(Q, \eta; X_0)}{V(X_0)} &\equiv \Phi(Q; X_0) + \sum_{ijkl} \frac{C_{ijkl}^{(2)}[X_0]}{2!} \eta_{ij} \eta_{kl} + \sum_{ijklmn} \frac{C_{ijklmn}^{(3)}[X_0]}{3!} \eta_{ij} \eta_{kl} \eta_{mn} + \dots \\ &+ \sum_{N=1}^{\infty} Q^{2N} \sum_{ij} \eta_{ij} \left( D_{ij}^{(2N,1)}[X_0] + \sum_{kl} \frac{D_{ijkl}^{(2N,2)}[X_0]}{2!} \eta_{kl} + \sum_{klmn} \frac{D_{ijklmn}^{(2N,3)}[X_0]}{3!} \eta_{kl} \eta_{mn} + \dots \right), \end{aligned} \quad (17)$$

where

$$\Phi(Q; X_0) = \frac{A[X_0]}{2} Q^2 + \frac{B[X_0]}{4} Q^4 + \frac{C[X_0]}{6} Q^6 + \dots \quad (18)$$

denotes the “pure” OP contribution. Unfortunately, as it stands such an expansion is of very little use in practical applications. The presence of any strain powers beyond harmonic order results in a set of nonlinear coupled equilibrium equations which are extremely hard to handle. Furthermore, evaluating these powers would require knowledge of the numerical values of a rapidly increasing number of third, fourth, and higher order elastic constants  $C_{ijklmn\dots}^{(p)}[X_0]$  as well as of the higher order coupling parameters  $D_{ijkl\dots}^{(2N,p)}[X_0]$ , neither of which are easily available in general. Consequently, the “traditional” attempts to apply Landau theory (LT) in a high-pressure context thus

continue to regard  $\eta_{ij}$  as “infinitesimal” and truncate the above expansion at harmonic order in the strain. The terms ignored by such a crude approximation are precisely the ones that encode the nonlinear elastic effects inevitably accompanying high pressure. In cases where nonlinear effects are too obvious to be swept under the rug, the infinitesimal strain approach is therefore frequently augmented by *ad hoc* assumptions about an additional pressure dependence of elastic constants and strain-OP couplings that are difficult to justify.

On the other hand, one should realize that an expansion of type (17) actually contains much more information than needed. In fact, if we knew (17) to high orders, this would in principle allow us to compute the response of the system to an arbitrary external stress  $\sigma_{ij}$ . When only *hydrostatic* external stress is applied, however, all effects of elastic anisotropy necessarily originate solely from the emergence of a nonzero OP coupled to strain that effectively exerts a *nonhydrostatic*

*internal* stress. A much more economic approach should therefore exist for determining the response to hydrostatic external stress. Indeed, such a theory has recently been presented in Ref. [10] and was shown to yield a concise description of the ambient-temperature high-pressure phase transition in STO. We refer to Ref. [10] for a more detailed exposition of the machinery underlying FSLT. Here we content ourselves with summarizing its core ideas.

We start by emphasizing that “strain” is a relative concept. An expansion of a structure similar to (17) must therefore be possible also for another choice  $\mathbf{X}_P$  of elastic reference system. To identify a particularly convenient “background” system, we argue that even though the total observed strain may be large, at least near  $P_c$  of a second-order or weakly first-order transition the spontaneous strain caused solely by emergence of nonzero equilibrium OP must necessarily be small enough to warrant a harmonic treatment. Thus we decompose the total strain  $\eta_{ij} = \eta_{ij}(P)$  into

$$\eta_{ij} = e_{ij} + \alpha_{ki}\widehat{\epsilon}_{kl}\alpha_{lj}, \quad (19)$$

where  $\alpha_{ik}$  denotes the deformation tensor [10] relating the zero-pressure ambient (“lab”) system  $\mathbf{X}_0$  to the chosen background system  $\mathbf{X}_P$ , which is therefore defined as the (hypothetical) equilibrium state of the system with the OP constrained to zero, and  $e_{ik} = \frac{1}{2}(\sum_n \alpha_{ni}\alpha_{nk} - \delta_{ik})$  is the—possibly large—Lagrangian background strain. We emphasize that it is only with respect to the decomposition (19) that we are allowed to write

$$\begin{aligned} \frac{F(Q, \widehat{\epsilon}; \mathbf{X}_P)}{V[\mathbf{X}_P]} &\approx \Phi(Q; \mathbf{X}_P) + Q^2 D_{ij}[\mathbf{X}_P] \widehat{\epsilon}_{ij} + \sum_{ij} \tau_{ij}[\mathbf{X}_P] \widehat{\epsilon}_{ij} \\ &\quad + \frac{1}{2} \sum_{ijkl} C_{ijkl}[\mathbf{X}_P] \widehat{\epsilon}_{ij} \widehat{\epsilon}_{kl}. \end{aligned} \quad (20)$$

For the pure OP potential part we assume

$$\Phi(Q; \mathbf{X}_P) = \frac{A[\mathbf{X}_P]}{2} Q^2 + \frac{B[\mathbf{X}_P]}{4} Q^4 + \frac{C[\mathbf{X}_P]}{6} Q^6 \quad (21)$$

with coefficients yet to be determined. As shown in Ref. [10], the OP equilibrium value  $\bar{Q}$  minimizes a *renormalized background pure OP potential density*

$$\Phi_R(Q; \mathbf{X}_P) = \frac{A_R[\mathbf{X}_P]}{2} Q^2 + \frac{B_R[\mathbf{X}_P]}{4} Q^4 + \frac{C_R[\mathbf{X}_P]}{6} Q^6, \quad (22)$$

which is simply related to  $\Phi(Q; \mathbf{X}_P)$  by

$$\begin{aligned} \Phi_R(Q; \mathbf{X}_P) &= \Phi(Q; \mathbf{X}_P) - \frac{Q^2}{2} \sum_{ijkl} D_{ij}[\mathbf{X}_P] S_{ijkl} \\ &\quad \times [\mathbf{X}_P] D_{kl}[\mathbf{X}_P], \end{aligned} \quad (23)$$

where the compliance tensor  $S_{mnij}[\mathbf{X}_P]$  is the tensorial inverse of the *Birch coefficients*

$$\begin{aligned} B_{ijkl}[\mathbf{X}_P] &= C_{ijkl}[\mathbf{X}_P] + \frac{1}{2}(\tau_{jk}[\mathbf{X}_P]\delta_{il} + \tau_{ik}[\mathbf{X}_P]\delta_{jl} \\ &\quad + \tau_{jl}[\mathbf{X}_P]\delta_{ik} + \tau_{il}[\mathbf{X}_P]\delta_{jk} - 2\tau_{ij}[\mathbf{X}_P]\delta_{kl}) \end{aligned} \quad (24)$$

of the background system  $\mathbf{X}_P$  which replace the elastic constants [36,37] at finite strain. A comparison of common

powers in  $\widehat{\epsilon}_{ij}$  yields the following expansions of the coefficients  $A_R[\mathbf{X}_P], B_R[\mathbf{X}_P], C_R[\mathbf{X}_P]$ , and  $D_{ij}[\mathbf{X}_P]$  in powers of the background strain  $e_{ij} = e_{ij}(P)$ , with the laboratory couplings constituting (17) appearing as coefficients. One obtains

$$\begin{aligned} JD_{st}[\mathbf{X}_P] &= \sum_{ij} \alpha_{si} D_{ij}^{(2,1)}[\mathbf{X}_0] \alpha_{tj} + \sum_{ijkl} \alpha_{si} D_{ijkl}^{(2,2)}[\mathbf{X}_0] \alpha_{tj} e_{kl} \\ &\quad + \sum_{ijklmn} \alpha_{si} D_{ijklmn}^{(2,3)}[\mathbf{X}_0] \alpha_{tj} e_{kl} e_{mn} + \dots, \end{aligned} \quad (25)$$

$$\begin{aligned} JA_R[\mathbf{X}_P] &= A[\mathbf{X}_0] + 2 \left( \sum_{ij} D_{ij}^{(2,1)}[\mathbf{X}_0] e_{ij} \right. \\ &\quad \left. + \frac{1}{2!} \sum_{ijkl} D_{ijkl}^{(2,2)}[\mathbf{X}_0] e_{ij} e_{kl} + \frac{1}{3!} \sum_{ijklmn} D_{ijklmn}^{(2,3)} \right. \\ &\quad \left. \times [\mathbf{X}_0] e_{ij} e_{kl} e_{mn} + \dots \right), \end{aligned} \quad (26)$$

$$JB_R[\mathbf{X}_P] = B[\mathbf{X}_0] - 2J \sum_{ijkl} D_{ij}[\mathbf{X}_P] S_{ijkl}[\mathbf{X}_P] D_{kl}[\mathbf{X}_P], \quad (27)$$

$$JC_R[\mathbf{X}_P] = C[\mathbf{X}_0], \quad (28)$$

where  $J := \det(\alpha_{ij})$ . Relation (25) indicates a pressure dependence of the strain-OP coupling constants resulting from nonlinear elastic effects, while (26) generalizes the linear pressure dependence of the harmonic Landau parameter familiar from the traditional infinitesimal strain approach. Relation (27), which is written in a compact way thanks to the previous relation (25) for  $D_{kl}[\mathbf{X}_P]$ , gives a pressure-dependent generalization of the constant negative renormalization of the fourth-order Landau parameter accompanying a linear-quadratic strain-OP coupling. Such a shift of the fourth-order coefficient is familiar from infinitesimal-strain Landau theory, where it is discussed as a possible mechanism for explaining the appearance of tricritical or first-order behavior. However, it is crucial to note that within the simple linearized theory no fully consistent explanation of an observed *pressure-dependent* change of the order of transition (second order, tricritical, first order) based on this device can be given. Finally, according to (28) the sixth-order Landau parameter acquires only a trivial renormalization with the current assumptions made.

Superficially, the equilibrium value  $\widehat{\epsilon}_{mn}$  of the spontaneous strain

$$\widehat{\epsilon}_{mn} = -\bar{Q}^2 \sum_{ij} D_{ij}[\mathbf{X}_P] S_{mnij}[\mathbf{X}_P] \quad (29)$$

still seems to follow the traditional Landau rule of thumb that for linear-quadratic coupling the spontaneous strain is proportional to the square of the OP. However, while the accompanying proportionality factor represents a mere constant in the infinitesimal approach, relation (29) indicates that this factor must be expected to become pressure-dependent in a nontrivial way as a result of the interplay between the pressure-dependent elastic constants and coupling constants in the nonlinear regime.

For an application to PTO we specialize equations (26) and (25) to a cubic background reference system  $X_P$ . Then  $J = V(P)/V(0)$ , which yields a diagonal deformation tensor  $\alpha_{ij} \equiv \alpha\delta_{ij}$  with  $\alpha = \sqrt[3]{J}$  and a diagonal Lagrangian background strain  $e_{ij} \equiv e\delta_{ij}$  with  $e = \frac{1}{2}(\alpha^2 - 1)$ . While this specialization leaves (27) and (28) unchanged, Eqs. (25) and (26) simplify to

$$\begin{aligned}\alpha(P)D_\mu[X_P] &= D_\mu[X_0] + e(P)E_\mu[X_0] + e^2(P)F_\mu[X_0] \\ &\quad + e^3(P)G_\mu[X_0] + \dots, \quad \mu = 1, 2, 3,\end{aligned}\quad (30)$$

$$\begin{aligned}\alpha^3(P)A_R[X_P] &= A[X_0] + 2\left(e(P)D[X_0] + \frac{e^2(P)}{2!}E[X_0]\right. \\ &\quad \left.+ \frac{e^3(P)}{3!}F[X_0] + \frac{e^4(P)}{4!}G[X_0] + \dots\right) + \dots,\end{aligned}\quad (31)$$

where we introduced the abbreviations

$$\begin{aligned}D_\mu[X] &:= D_\mu^{(2,1)}[X], \quad E_\mu[X] := \sum_v D_{\mu v}^{(2,2)}[X], \\ F_\mu[X] &:= \sum_{v\sigma} D_{\mu v\sigma}^{(2,3)}[X], \quad G_\mu[X] := \sum_{v\sigma\tau} D_{\mu v\sigma\tau}^{(2,4)}[X], \quad \dots\end{aligned}\quad (32)$$

and

$$\begin{aligned}D[X] &:= \sum_\mu D_\mu[X], \quad E[X] := \sum_\mu E_\mu[X], \\ F[X] &:= \sum_\mu F_\mu[X], \quad G[X] := \sum_\mu G_\mu[X], \quad \dots\end{aligned}\quad (33)$$

FSLT is constructed to serve as a high-pressure extension of an existing ambient-pressure LT. The minimal required input of FSLT for a successful application in this respect consists of the following ingredients:

(1) A preexisting ambient-pressure LT, supplying the laboratory coefficients  $A[X_0], B[X_0], C[X_0], D_\mu^{(2,1)}[X_0] \equiv D_\mu[X_0]$  and possibly ambient-pressure elastic constants  $C_{\mu\nu}[X_0]$ . Obviously, such a LT constitutes a “boundary condition” that any high-pressure extension must meet. Our theory fulfills this requirement by construction, since  $X_P = X_0$  implies  $\alpha_{ij} = \delta_{ij}$  and thus  $e_{ij} = 0$ .

(2) The pressure dependence  $e_{ij} = e_{ij}(P)$ , i.e.,  $\alpha_{ij} = \alpha_{ij}(P)$ , defining the “floating” reference system  $X_P$  must be known. If the high-symmetry phase is cubic, as it is in the present case, this amounts to knowledge of the equation of state (EOS)  $V = V(P)$  from experiment or *ab initio* simulations.

(3) Similarly, we rely on knowledge of the pressure-dependent elastic constants  $C_{ijkl}[X_P] \equiv C_{ijkl}(P)$ , constituting a relatively small set of  $P$ -dependent functions that encode the effects of higher order elastic constants at purely hydrostatic stress in a way that is much easier to handle. Unfortunately, experimental high-pressure measurements of pressure-dependent elastic constants are only available in rare cases. While in a precursor to our present theory [38] this  $P$  dependence had to be encoded in an expansion in powers of  $P$  constrained only by consistency with the pressure-dependent bulk modulus  $K(P)$ , which gave rise to additional fit parameters, in the present version pressure-dependent elastic constants are calculated from DFT.

Given these additional data, the only remaining free parameters are the higher order coupling coefficients  $D_{ijkl}^{(2,2)}[X_0], D_{ijklmn}^{(2,3)}[X_0], \dots$  appearing in the ambient pressure LP (17). Theoretically it could be possible to actually determine these coefficients (as well as higher order elastic constant components) from some sophisticated simulation or experiment. In practice, however, it is probably fair to say that in a genuine application of FSLT these couplings must be taken as unknown parameters to be determined from fitting the predictions of the theory to a set of experimental measurements. This may sound disturbing, since in a low-symmetry situation the number of independent components constituting these tensors can be quite substantial. However, in cases where the “high symmetry” paraphrase—defined by the requirement that the OP vanishes identically—is, e.g., of cubic symmetry, Eqs. (30) and (31) indicate that only certain sums of these coefficients actually enter into our expansions. Thus, if the background system is highly symmetric, the actual number of independent free parameters is drastically reduced. For instance, Eqs. (30) and (31) reveal that to describe a cubic-to-tetragonal transition one needs to determine only two free parameters at each order in the background strain  $e$ . In situations of lower symmetry we may find ourselves in a less favorable situation. Unfortunately, however, there seems to be no consistent way of simplifying the problem any further without sacrificing key elements of nonlinear elasticity.

The theory we have summarized so far was developed in Ref. [10] to describe the high-pressure extension of the 105 K transition  $Pm\bar{3}m \leftrightarrow I4/mcm$  in STO. In particular, it assumes that the low-pressure phase coincides with the high-symmetry parent phase. For the ferroelectric transition in PTO, however, this aspect seems to be reversed. The ambient temperature and pressure phase  $P4mm$  of PTO is ferroelectric, and the transition to the cubic  $Pm\bar{3}m$  reference phase mediated by a soft mode at the  $\Gamma$  point [29] heuristically conforms to the rule of thumb that pressure tends to suppress ferroelectricity [39] at least up to some critical pressure [40,41]. From the point of view of traditional LT, this difference, which also manifests itself in the different sign of the Clapeyron slopes  $dP_c/dT$  computed for both transitions, seems to be merely related to the signs of the OP-strain coupling constants. However, in setting up a FSLT extension, some extra care is needed. This becomes obvious if one takes into account that at ambient pressure and temperature the background strain  $e$  vanishes by definition if measured with respect to the laboratory state  $X_0$ , which in turn implies that the total strain  $\eta = \epsilon$  is all spontaneous. This state of affairs seems to thwart our plans developed above, which explicitly rest on the assumption that  $\epsilon$  would be small and  $e$  large. A remedy is, of course, to trade the  $X_0$  for a different reference system  $X_{P_r} \equiv X_r$  defined for some pressure  $P_r > P_c$ , which is always possible, since strain, as we once more emphasize, is a relative concept. The resulting slight technical complications in applying FSLT are described in Appendix A.

#### IV. FINITE TEMPERATURE

For notational reasons we have suppressed an additional temperature dependence of the constituents entering the theory sketched above. Assuming that the  $T$  dependence of the

ambient-pressure LP is known, this still leaves us with determining that of all remaining coupling parameters defined with respect to the background reference system  $X_R$ . In particular, we should find a way to “heat up” the EOS and pressure-dependent elastic constants that we have obtained from DFT to the desired temperature. If one studies a transition at rather low temperatures one may try to get away with ignoring effects related to finite temperature such as thermal expansion or temperature changes in the elastic constants in a first approximation. This applies, e.g., to the cubic-to-tetragonal transition of STO used as a test bed for FSLT in Ref. [10], which takes place at a modest  $T_c = 105$  K. In the case of PTO, neglecting finite-temperature effects would be much harder to justify, since the ambient-pressure ferroelectric transition takes place at the rather elevated temperature of  $T_c \approx 765$  K.

Some time ago, a very interesting and ambitious strategy to obtain finite-temperature results from DFT has been worked out [42–47] with the declared objective to obtain a parameter-free description. It consists of (i) isolating those unstable deformation modes that initiate the symmetry breaking accompanying the transition, (ii) calculating an effective lattice Hamiltonian for these modes, including couplings to further important deformations such as lattice strain, and (iii) feeding this into Monte Carlo [46] or molecular dynamics [48]. This approach has indeed offered remarkable qualitative and semiquantitative insight into the mechanisms underlying, e.g., structural phase transitions. In addition, it also shares a lot of common ground with Landau theory due to its strong emphasis of group theory. However, the effective Hamiltonian approach typically fails to reproduce the experimentally observed critical temperatures in perovskites, sometimes by several tens of kelvins or more. In Ref. [49] these problems were traced back to an insufficient incorporation of noncritical anharmonic effects.

Our present approach does not aim at calculating coupling parameters of energy contributions involving the OP. It only requires determining the dependence of the background system  $X_P$  on  $P$  and  $T$  for zero OP. However,  $X_P$  is—by definition—thermodynamically unstable within the broken-symmetry phase, and therefore it is not straightforward how to determine the  $T$  dependence of the EOS and elastic constants of the high-symmetry reference phase. Of course, this problem is not at all specific to high-pressure situations (in the context of effective Hamiltonians cf. Ref. [42]). Indeed, it should arise any time that a secondary OP (i.e., a tensorial quantity that does not break as many symmetry elements as the primary OP when assuming a nonzero value [50]) is included in LT. To disentangle the transition anomalies related to such a secondary OP from possible noncritical contributions, some potentially  $T$ -dependent “baseline” always needs to be subtracted. Drawing such a thermal “base line” to disentangle transition-related anomalies of a secondary order parameter from some background not related to broken symmetry may be considered a trivial matter. However, it is not. In the ferroelectric literature, elastic baselines have been defined at ambient pressure in various ways. For instance, Ref. [22] explicitly defines a pseudocubic unit cell parameter as the third root of the noncubic unit cell volume, whereas conveniently imposing the condition of  $T$  independence for the coupling

parameters between strain and polarization [23] constitutes an implicit one. Of course, the fitted Landau parameters emerging from such an *ad hoc* prescription inherit a similar degree of arbitrariness. Moreover, the resulting elastic baseline is likely to be incompatible with one obtained from a thermal extension of an EOS calculated from DFT. While these issues may remain unnoticed at modest pressures, they are bound to surface in an attempt to construct FSLT as the high-pressure extension of this LP.

For solid state systems, a standard way of passing from energies to free energies is the quasiharmonic approximation (QHA) [36,51–53]. In principle the QHA requires computing the zero-temperature phonon frequencies at any given volume of the high-symmetry phase which is well mastered by DFT. By definition, however, the high-symmetry reference structure of a structurally unstable system will exhibit at least one unstable phonon mode characterized by an imaginary frequency. In the lattice-dynamical description of structural phase transitions this imaginary frequency corresponds to the “soft mode” that becomes unstable at the transition. Indeed, the phonon dispersions calculated for typical perovskites generally feature several rather “flat” branches of imaginary modes stretching into extended regions of the Brillouin zone (see, e.g., the phonon dispersion graphs on p. 135 of Ref. [13]). The corresponding large spikes in the phonon density of states (DOS)  $g(\omega)$  make it impossible to simply neglect these phonon branches. It is due to the presence of these imaginary phonons that standard techniques for incorporating thermal effects such as the quasiharmonic approximation (QHA) and Grüneisen theory [54,55] cannot be applied. Ways to overcome the fundamental difficulties posed by the presence of imaginary phonon modes and strong anharmonicity continue to constitute an active area of current research (see, e.g., Refs. [56,57]).

The nonapplicability of the QHA is a recurrent theme in high-pressure and mineral physics even in the absence of imaginary phonons simply because precise information on the phonon DOS is frequently unavailable due to the complexity of the corresponding systems. In these fields different types of Debye approximations (DAs) are therefore still essential [58–61]. As we recall in Appendix C, where we recollect the most relevant facts of the DA in the present context for the reader’s convenience, the simplest forms of the DA require only knowledge of the underlying EOS and a rough guess of the Poisson ratio  $\sigma$ . It is these modest requirements that make the Slater-Debye approximation equally appealing in our present situation, in which the phonon DOS of the high-symmetry structure is available but nevertheless unusable due to the imaginary frequency contributions.

A general solution of the issues raised by the presence of an imaginary contribution to the phonon spectrum must be postponed to future work. For now, our proposed strategy for determining the finite-temperature dependence of a (e.g., cubic) high-symmetry reference structure consists of performing constrained DFT calculations of the corresponding cubic EOS and elastic constants followed by a subsequent application of the DA. In view of the rather drastic simplifications implied by such strategy, we shall take a pragmatic point of view with respect to the choice of DA flavor described above. In a typical problem at hand, we may have experimental volume data at several temperatures available, and we shall choose

the combination of DFT and DA type that exhibits the most satisfactory overall agreement with the available data.

We close this section with some practical advice. A generic application of this theory will typically involve fitting a set of  $P$ -dependent strain data, for which rather precise additional information on the actual value of the critical pressure  $P_c$  may frequently be available. By its very nature, a least-squares fitting procedure may however numerically trade a better fit to data points far away from the transition for a shift of  $P_c$  to some other value. To avoid such a numerical smearing of the transition pressure region, we recommend numerically eliminating one of the free fit parameters, say  $E_1[X_0]$ , in favor of  $P_c$ . Provided we are dealing with a second-order transition, this can be accomplished, for example, by solving the equation  $A_R[X_{P_c}] \equiv 0$  for  $E_1[X_0]$ .

## V. APPLICATION TO LEAD TITANATE

The above discussion has underlined that a prerequisite for a successful description of the ambient-temperature high-pressure phase transition in lead titanate reported in Ref. [30] is the determination of a meaningful background system  $X_P$  at a given temperature  $T$ . This amounts to calculating the EOS  $V = V(P, T)$  and the elastic constants  $C_{11}(P, T), C_{12}(P, T)$  for the cubically constrained system. At  $T = 0$  we accomplish this task by performing a series of standard DFT calculations. Details are deferred to Appendix B.

The behavior of the resulting elastic baselines at finite temperature and pressure is analyzed using the GIBBS2 package [52,53]. Further details can be found in Appendix C. As stated above, we take a pragmatic point of view and try to single out the type of DA that yields the best overall agreement of the thermally extrapolated cubic EOS  $V = V(P, T)$  with the available data. On the one hand, at ambient pressure, this function should reproduce the one of Haun *et al.* [23] for  $T > T_c$ . On the other hand, at room temperature it should match the volume data of Janolin *et al.* [30] for  $12 \text{ GPa} \leq P \leq 20 \text{ GPa}$ . In addition, between 0 and 7.8 GPa high-temperature cubic EOSs have been measured rather recently using synchrotron x-ray diffraction by Zhu *et al.* [33] at temperatures  $T = 674 \text{ K}, 874 \text{ K}, \text{ and } 1074 \text{ K}$ . Unfortunately, no matter which type of the DAs implemented in GIBBS2 was invoked, it proved to be impossible to perfectly match these requirements simultaneously.

In detail, the Dugdale-McDonald and Vaschenko-Zubarev flavors of Debye-Grueneisen approximations (see Appendix C) admittedly produced the best-fitting baseline to the volume data of Janolin *et al.* Also, they yielded good agreement with those of Zhu *et al.* However, these approximations produced a certain small but non-negligible offset to the  $T > T_c$  part of the baseline of Haun *et al.* Concise agreement with the high-temperature part of this baseline must, however, be regarded as an important constraint in our search, since our set of Landau coefficients is directly based on these data.

Interestingly, the simple DA is not only found to perform excellent in this respect (Fig. 2), but also to produce an ambient-temperature baseline for the high-temperature volume data that is in reasonable agreement with the volume data of Janolin *et al.* between 12 and 20 GPa (cf. Fig. 2), which is an indispensable prerequisite for application of our FSLT.

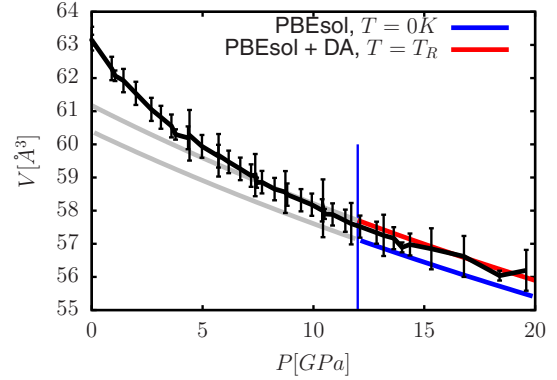


FIG. 2. Comparison of raw volume data of Janolin *et al.* [30] (black line) to the thermal EOS derived from the PBEsol functional and the DA (red line). To illustrate the effect of thermal expansion, the EOS resulting from zero-temperature DFT is also shown (blue line).

The values obtained from the simple DA are, however, in excess of the synchrotron data of Zhu *et al.* by some 3.5%. The reason for the discrepancy is currently not understood. It may very well result from the intrinsic imperfections of the DA (as well as those of the QHA) at high temperatures. On the other hand, Zhu *et al.* also report certain disagreements of the accompanying values they obtained for the bulk modulus with those previously obtained by other authors.

In summary, for our present purposes a combination of PBEsol and a simple DA emerged as a reasonable choice for producing a suitable  $T$ - and  $P$ -dependent EOS. Based on the strategy outlined in Appendix C, this also allows us to extend the pressure-dependent elastic constants obtained from DFT from zero to finite temperature.

Looking at Fig. 3, one notices that upon lowering the temperature from  $T_c$  down to  $T_R$  our new baseline steadily deviates from the one of Haun *et al.*, and the spontaneous strain components emerging from these data have to be redefined with respect to this new baseline. This, in turn, requires revising the

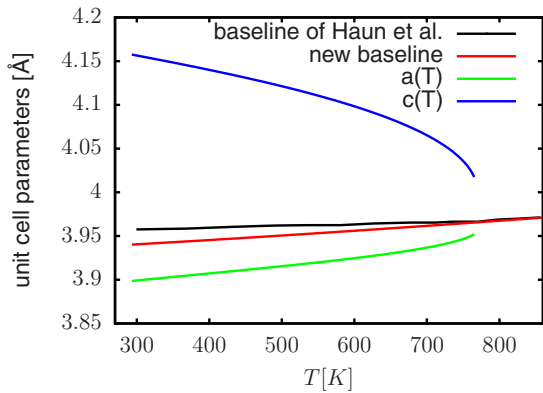


FIG. 3. Comparison of elastic baseline used in Haun *et al.* [23] (black) to our new baseline (red) as obtained from the Debye approximation. The temperature-dependent ambient pressure unit cell parameters  $a(T)$  (green) and  $c(T)$  (blue) are also shown for convenience.

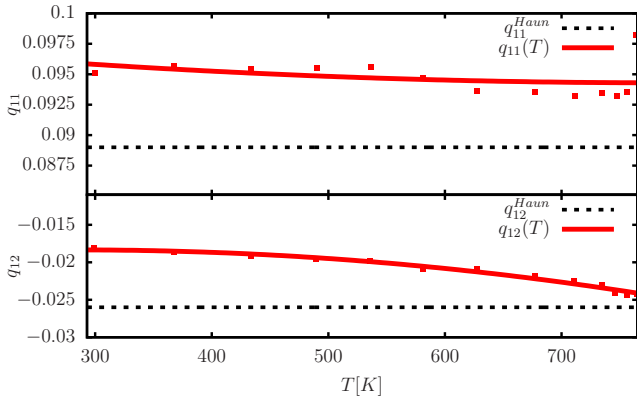


FIG. 4. Comparison of the  $T$ -independent coupling coefficients values  $\hat{q}_{ij}$  obtained by Haun *et al.* (black horizontal dashed lines; cf. Table I) to those obtained from redefining the elastic baseline using PBEsol and the DA [red data points, fitted by Eqs. (D1) (red line)].

values of the  $T$ -independent coupling coefficients  $\hat{q}_\mu$  of Haun *et al.* As demonstrated in Appendix D, one obtains a new set of somewhat shifted and slightly  $T$ -dependent coupling coefficients  $\hat{q}_\mu = \hat{q}_\mu(T)$ . In principle, the thereby acquired  $T$  dependence may still appear rather weak (cf. Fig. 4) and could very well be neglected. More importantly, however, Fig. 4 reveals that the overall levels of the couplings have also undergone certain small but definitely non-negligible shifts. These readjustments of the OP-strain coupling parameters may appear small. Nevertheless, in retrospect they proved to be crucial for obtaining a good fit of FSLT to the high-pressure transition data.

Once the thermal baseline and a redefined set of strain-OP couplings have been established, we can extract (Lagrangian [36]) spontaneous strain components from the raw data of Janolin *et al.* The results, which are shown in Fig. 5, reveal that any discontinuous behavior of these components with respect to variations in the pressure cannot virtually exceed the size of the error bars, and certainly must be at least much smaller than the first-order discontinuities observed in the corresponding spontaneous strain components at the critical temperature of

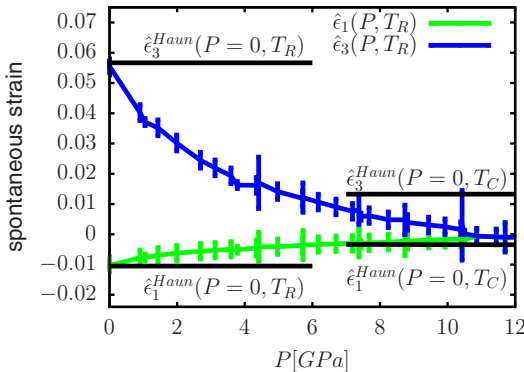


FIG. 5. Spontaneous Lagrangian strain components computed from the raw data of Janolin *et al.* [30] (shown in Fig. 1) after implementation of our new baseline at  $T = T_R$ . The corresponding spontaneous strains  $\hat{\epsilon}_\mu(P = 0, T_R)$  and the critical jumps  $\hat{\epsilon}_\mu(T_C)$  of the ambient-pressure ferroelectric transition are also indicated.

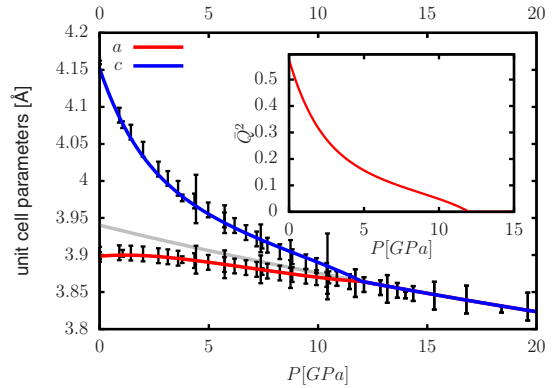


FIG. 6. Main plot: Fit of FSLT to experimental lattice parameters. The vertical line indicates the critical pressure  $P_c = 12$  GPa. The gray line indicates the elastic thermal background reference system resulting from the use of PBEsol and the simple DA. Inset: Resulting  $P$  dependence of squared equilibrium OP.

the ambient-pressure ferroelectric transition. This supports our initial hypothesis that the high-pressure transition at room temperature exhibits a second-order character. In contrast, Eq. (16b) derived from traditional LT predicts discontinuous jumps of the spontaneous strains with sizes independent of both  $T$  and  $P$ , that are clearly not observed.

With the above preparations completed, setting up the least-squares fit is rather straightforward. In detail, we placed our background reference system  $X_r$  at  $P_r = 20$  GPa. As explained above, fixing  $P_c = 12$  GPa allows us to eliminate  $E_3[X_r]$  from the list of free parameters, which thus reads  $E_3[X_r], F_1[X_r], F_3[X_r], G_1[X_r], G_3[X_r]$ . In a simultaneous fit of the two data sets for the total strains  $\eta_1(P)$  and  $\eta_3(P)$  all of these parameters are initially put to zero.

The resulting fits to the experimental unit cell parameters  $a, c$  and the accompanying pressure dependence of the squared equilibrium OP  $\bar{Q}^2(P)$  are shown in Fig. 6. In the inset to this figure, one immediately notices the strong deviation of  $\bar{Q}^2(P)$  from the generally assumed linear  $P$  dependence predicted by infinitesimal-strain LT. Via Eq. (29), this pronounced nonlinearity is passed on to the unit cell parameters  $a$  and  $c$ , precisely producing the unusual curvatures of  $a(P)$  and  $c(P)$  away from their common baseline, as the main plot of Fig. 6 shows. It is the combined effects of the  $P$  dependence of elastic constants and the nonlinear strain-OP coupling terms that have made it possible to understand the unusual effects of nonlinear elasticity reflected in these experimental data.

The resulting  $P$  dependence of  $A_R$  is roughly linear as expected from standard LT (left upper corner of Fig. 7). However, while it necessarily reduces to the corresponding ambient-temperature value of the potential of Haun *et al.* for  $P = 0$ , its slope as a function of pressure is markedly reduced due to the fact that our FSLT is able to take the  $P$  dependence of elastic constants properly into account. This immediately resolves the discrepancy between the experimentally observed critical pressure  $P_c = 12$  GPa and the value  $P_c = 2.9$  GPa predicted by the infinitesimal-strain approach, in which any pressure dependence of elastic constants had been implicitly neglected.

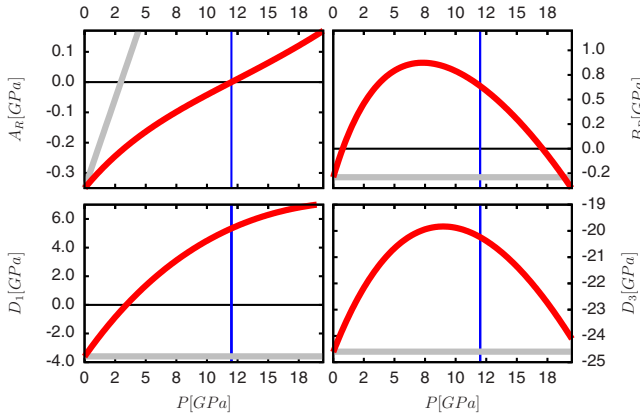


FIG. 7.  $P$  dependence of Landau coefficient  $A_R, B_R, D_1, D_3$  at room temperature  $T_R$  (red lines). Vertical blue lines mark the critical pressure  $P_c = 12$  GPa. For comparison, gray lines indicate the  $P$  dependence of the coefficients (7), (8), and (10) as computed from the Landau potential (2) of Haun *et al.*

Parameters  $D_\mu$  show some  $P$  dependence, with  $D_1$  remaining small in modulus and  $D_3$  evolving in the range between  $-22$  GPa and  $-19$  GPa.

The  $P$  dependence of  $B_R$  is most interesting. In fact, it is the key to understanding the change of the character of the transition from first to second order with increasing pressure. For a scalar OP subject to a given LP, a second-order transition is expected for a positive sign of the quartic coupling constant  $B > 0$ . In contrast, for  $B < 0$  a sixth-order term with a positive coupling constant  $C > 0$  must be present in the LP for reasons of stability, and (since fluctuations are neglected [62]) standard LT always predicts a first-order transition [6]. In particular, the presence of a linear-quadratic coupling between OP and infinitesimal strain yields a negative renormalization [63] of the “bare” quartic OP coefficient  $B$  to a smaller value  $B_R < B$  after the strain terms have been eliminated from the LP by using the elastic equilibrium conditions. In infinitesimal LT, this mechanism constitutes the standard theoretical quantitative device to explain the rule of thumb that strong elastic coupling is often accompanied by a first-order transition character. However, infinitesimal-strain LT only allows for a  $P$ -independent renormalization from  $B$  to  $B_R$ , while the observed change in transition character for PTO from first to second order with increasing  $P$  can only be due to a  $P$ -dependent change of sign of  $B_R$ , a behavior that is impossible to implement consistently in such an approach. In contrast, the coupling coefficient  $B_R$  resulting from FSLT naturally acquires a nontrivial  $P$  dependence, as immediately anticipated from a glance at Eq. (27). As displayed in the right upper corner of Fig. 7,  $B_R$  indeed starts out negative at ambient pressure, but quickly changes its sign with increasing  $P$ . Thus, the observed  $P$  dependence of  $B_R$  provides the sought-after explanation of the change in order of the transition from first to second order. In principle, this should not come as a surprise, since our theory was just designed as an interpolation capable of describing both the first-order ambient-pressure transition as well as second-order transition at 12 GPa. However, we emphasize once more that

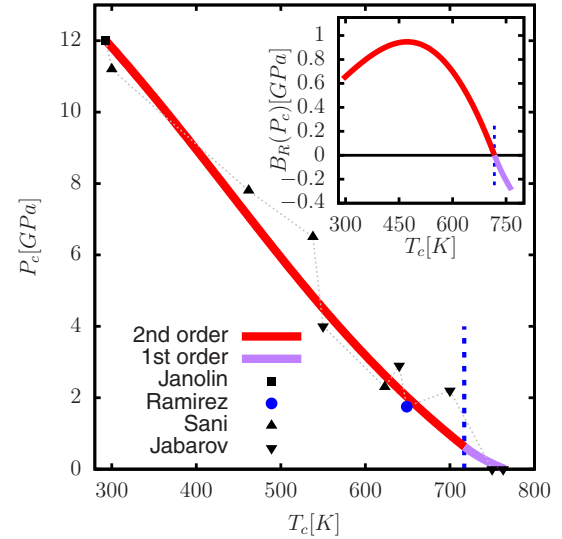


FIG. 8. Main plot: Comparison of tentative second-order (red line) and first-order (purple line) phase boundary  $P_c = P_c(T_c)$  for  $T_R \leq T \leq T_c$  as computed from our theory to literature values including the well-known ferroelectric transition at  $T = T_c$  for which  $P_c = 0$ , the  $P_c = 12$  GPa transition at  $T = T_R$  measured by Janolin *et al.* [30]. The blue data point indicates the estimate of the tricritical point derived by Ramirez *et al.* in Ref. [64]. The remaining data points represent experimental results compiled from Refs. [65] and [66]. Inset: Values of  $B_R$  along the phase boundary. The tricritical temperature  $T_{\text{tric}} \approx 717$  K derived from FSLT is indicated in both plots by the vertical dashed blue line.

a similar mechanism cannot consistently be introduced in a LT based on infinitesimal strain.

Varying both pressure and temperature, the combined dependence of  $A_R$  and  $B_R$  on  $(P, T)$  allows us to estimate the location of the tricritical point in the phase diagram, which is defined as the state on the cubic-tetragonal phase boundary that separates the line of first-order transitions from that of second-order ones. Indeed, for variable temperature  $T$  the location of  $A_R(P, T) \equiv 0$  as a function of pressure defines the cubic-tetragonal phase boundary  $P_c = P_c(T_c)$ , provided that the corresponding value  $B_R$  is positive. Otherwise, as follows from standard Landau reasoning, the transition pressure must be located by numerically solving the equation  $A_R(P, T) \equiv \frac{3B_R^2(T, P)}{16C_R(P, T)}$ . The resulting tentative phase diagram for PTO in the pressure range  $0 \leq P \leq 20$  GPa is shown in Fig. 8. As shown in the inset of Fig. 8,  $B_R$  indeed changes sign along the phase boundary, and we estimate the corresponding tricritical point to be

$$(T_{\text{tric}}, P_{\text{tric}}) \approx (717 \text{ K}, 0.64 \text{ GPa}). \quad (34)$$

In closing this section we note that upon further increasing the pressure  $B_R$  drops towards large negative values for  $P > 18$  GPa after passing through a maximum at approximately 7.5 GPa. It is tempting to interpret this behavior as an indication of the instability of the cubic phase for high pressure experimentally observed in Ref. [30].

## VI. DISCUSSION AND CONCLUSION

We have presented an in-depth discussion of the application of FSLT to the room-temperature high-pressure ferroelectric phase transition of PTO, for which the conventional Landau approach based on truncating the free energy expansion in the strain tensor components beyond harmonic contributions fails. In contrast, FSLT allows us to understand the peculiar behavior of the tetragonal unit cell parameters as functions of pressure, the change of the character of the transition from first to second order with increasing pressure, to predict the phase boundary separating the cubic and tetragonal phase in the  $(P, T)$  plane, and to localize the corresponding tricritical point. In this final section we would like to comment on several points.

(i) While Fig. 8 indicates that the cubic-tetragonal phase boundary derived from our theory is in reasonable agreement with experimental data from the literature, we note that the predicted location (34) of the tricritical point differs somewhat from previous estimates in the literature. In particular, Samara [67] estimates the tricritical pressure of PTO to be  $P_{\text{tric}} \approx 4.5$  GPa by analyzing dielectric measurements, while Ramirez *et al.* [64] gather evidence for  $(T_{\text{tric}}, P_{\text{tric}}) = (649 \text{ K}, 1.75 \text{ GPa})$ . To understand these discrepancies, one has to take into account that dielectric measurements on pure PTO crystals are usually hampered by their large room conductivity resulting from lead deficiency. This problem is greatly reduced for slightly  $U^{5+}$ -doped single crystals [21], which had therefore been used for the measurements of Ref. [67], on which also the estimate of Ref. [64] was based. Unfortunately, as Ref. [8] reports, it later turned out that reproducibility of dielectric measurement results for different U-doped crystal specimens was not very reliable, with peak values of the dielectric constant at  $T_c$  varying by factors up to 3 and specific heat and slope  $dP_c/dT$  by factors up to 2.

(ii) From a pure *ab initio* perspective, our present approach cannot compete with the elaborate and parameter-free effective Hamiltonian method sketched in Sec. IV. Still, since it is not plagued by its lack of precision in determining  $T_c$ , it is able to offer much greater numerical accuracy in describing a given set of experimental data. This is only possible because the knowledge of a  $T$ -dependent LP at ambient pressure is already presupposed, and we merely construct a DFT-aided extension of this existing thermal theory from ambient to high pressure.

In passing, we note that even if we were in possession of a perfect microscopic effective Hamiltonian, it would still be far from trivial to determine the resulting temperature-dependent Landau parameters from Monte Carlo simulations (as shown in Refs. [68,69], one pitfall is the unavoidable occurrence of phase separation below  $T_c$ ).

(iii) As we have shown, the construction of the finite-temperature extensions of the EOS and elastic constants of the cubic reference phase turned out to be an essential prerequisite for the successful description of the high-pressure transition of PTO and also enforced a redefinition of Landau parameters previously established in the literature. The main obstacle in determining this thermal extension is the presence of imaginary phonon modes indicating the low-temperature instability of this reference phase. It is important to realize that such problems are unavoidable in any attempt to combine LT

with *ab initio* calculations. Electronic structure methods like DFT generally work at  $T = 0$ , whereas a high-symmetry (and thus, in general, high-temperature) reference state is pivotal to LT. In the present work, this difficulty was circumvented by employing a DA based on the EOS and elastic constants obtained from DFT, but a more fundamental and controlled solution of this problem, which might be based on, e.g., ideas of Refs. [56,70] or [71] is definitely welcome. Work in this direction is currently in progress.

(iv) We certainly do not want to leave the impression that our work is the only one that accounts for the effects of nonlinear elasticity and large strains at structural phase transformations. For instance, the last decade has witnessed considerable progress in the description of strong first-order martensitic phase transformations in shape memory alloys and steels (see, e.g., Refs. [72–77] and references therein). For the construction of the corresponding phase field models a finite-strain treatment turns out to be mandatory. However, strong martensitic transformations are not of the standard group-subgroup type, but rather fall under the class of reconstructive transitions [78], for which it is impossible to define an OP in the strict sense of orthodox LT (i.e., based on a single irreducible representation of a high-symmetry reference group). Accordingly, the mechanism of these martensitic transitions is not related to a particular phonon instability; i.e., the soft-mode picture does not apply.

## ACKNOWLEDGMENTS

A.T. is grateful to A. Otero-de-la-Roza for advice using the GIBBS2 program package. A.T. and K.B. acknowledge support by the Austrian Science Fund (FWF) Project No. P27738-N28. S.E. acknowledges support from HEC, Pakistan, and would like to thank F. Tran for help with the DFT calculations. S.E. and P.B. acknowledge support from FWF SFB F41 (ViCom). J.K. acknowledges support from the Fonds National de la Recherche, Luxembourg, through a Pearl grant (FNR/P12/4853155/Kreisel). W.S. acknowledges support by the Austrian Science Fund (FWF) Project No. P28672-N36.

## APPENDIX A: BROKEN SYMMETRY AT HIGH VS LOW PRESSURE

The success of the strategy of FSLT as outlined in Sec. III hinges on (i) knowledge of the LP as defined with respect to the ambient pressure reference system  $X_0$ , (ii) the possibility to split the total strain into a spontaneous contribution  $\hat{\epsilon}_{ij}$  assumed small enough to warrant harmonic treatment for a second-order transition close to  $P_c$ , and a “large” background strain  $e$  taking care of all pressure effects that are unrelated to the primary OP. Equating coefficients of a power series in  $\hat{\epsilon}_{ij}$  allowed us then to calculate the pressure dependence of Landau parameters. For STO, this strategy worked great. For the “upside-down” case of PTO the decomposition of total strain into background and spontaneous part may still be useful around  $P_c$ , but it fails exactly where we need it the most: at ambient pressure. Relative to the zero-pressure reference

system  $X_0$ , the background strain must vanish, and the total strain is all spontaneous. With every coefficient vanishing, it makes also no sense to equate common powers of  $\hat{\epsilon}_{ij}$ .

An obvious solution to the described “upside-down” situation would be to choose another reference system  $X_r$ . If one tries to mirror the case of STO, the state at a reference pressure  $P_r \equiv 20$  GPa appears to be a logical choice. The drawback is, of course, that the parameters of the initial LT are still given

with respect to the laboratory system  $X_0$ . We therefore have to transfer these values first to the new reference system  $X_r$ , before we can employ them in a thereby slightly generalized version of FSLT. To construct this theory, one notices that the basic strategy of imposing invariance of the description under a change of elastic reference frame and the strategy of comparing common powers of the spontaneous strain components remain intact under such a generalization. In terms of

$$j_r(P) = \frac{V(P)}{V(P_r)}, \quad \alpha_r(P) = j_r^{1/3}(P), \quad e_r(P) = \frac{1}{2}[\alpha_r^2(P) - 1], \quad (A1)$$

we now find

$$\alpha_r(P)D_\mu[X_P] = D_\mu[X_r] + e_r(P)E_\mu[X_r] + e_r^2(P)F_\mu[X_r] + e_r^3(P)G_\mu[X_r] + \dots, \quad \mu = 1, 2, 3, \quad (A2)$$

$$\alpha_r^3(P)A_R[X_P] = A[X_r] + 2\left(e_r(P)D[X_r] + \frac{e_r^2(P)}{2!}E[X_r] + \frac{e_r^3(P)}{3!}F[X_r] + \frac{e_r^4(P)}{4!}G[X_r] + \dots\right) + \dots. \quad (A3)$$

It remains to transfer our knowledge of the ambient-pressure LP parameters to the new reference system  $X_r$ . Specializing to  $P = 0$ , one gets

$$D_\mu[X_r] = \alpha_r(0)D_\mu[X_0] - e_r(0)E_\mu[X_r] + e_r^2(0)F_\mu[X_r] + e_r^3(0)G_\mu[X_r] + \dots, \quad \mu = 1, 2, 3. \quad (A4)$$

This also carries over to the other couplings. For instance, in terms of the sums (33) we similarly obtain

$$A[X_r] = \alpha_r^3(0)A_R[X_0] - 2\left(e_r(0)D[X_r] + \frac{e_r^2(0)}{2!}E[X_r] + \frac{e_r^3(0)}{3!}F[X_r] + \frac{e_r^4(0)}{4!}G[X_r] + \dots\right) + \dots. \quad (A5)$$

In this way, we are retaining the information about the  $X_0$  couplings constituting the ambient-pressure LT, while trading the—usually unknown—quantities  $E_\mu[X_0]$ ,  $F_\mu[X_0]$ ,  $G_\mu[X_0]$ , … for the equally unknowns  $E_\mu[X_r]$ ,  $F_\mu[X_r]$ ,  $G_\mu[X_r]$ , …, which thus serve as yet another set of fit parameters in a practical application.

## APPENDIX B: DFT CALCULATION OF EOS AND ELASTIC CONSTANTS

The EOS and elastic constants of the cubic phase were performed using the WIEN2K DFT package [81], an all-electron code including relativistic effects. WIEN2K is based on the full-potential (linearized) augmented plane-wave ((L)APW) + local orbitals (lo) method [82], one among the most accurate schemes for band structure calculations. For the present calculation, an APW + lo type basis set was employed. Its size, which is the main parameter governing the quality of convergence of a given simulation, depends on the product  $R_{MT}^{\min} \times K_{\max}$ , where  $R_{MT}^{\min}$  is the smallest muffin tin radius in the unit cell and  $K_{\max}$  is the largest reciprocal lattice vector considered. Using muffin-tin radii of  $R_{MT} = 2.1$  bohrs, 1.77 bohrs, and 1.6 bohrs for lead, titanium, and oxygen, respectively, the safe choice [82]  $R_{MT}^{\min} \times K_{\max} \equiv 8$  produces  $K_{\max} = 5$  bohr $^{-1}$ . For total energy calculations a  $10 \times 10 \times 10$   $k$  mesh in the Brillouin zone turned out to be sufficient to establish convergence.

As to the choice of XC functional, it is worth mentioning that the well-documented inadequacy [83] of both LDA and PBE functionals in application to ferroelectric perovskites is particularly severe for the tetragonal phase of PTO. In fact, this

very issue has played an important role in the improvement of GGA functionals for applications to solids [84–86]. While we have also explored standard LDA as well as PBE [87,88] functionals, we can confirm previous observations [10,89] according to which for perovskites the Wu-Cohen [84] and PBEsol functionals [85] give overall satisfying agreement with experiment. In passing we mention that we have also included spin-orbit coupling to account for the relativistic effects due to the presence of lead. However, not unexpectedly the corresponding effects turned out to be rather small.

Our procedure to determine the behavior of the background system  $X_P$  starts by computing the total energy per unit cell for a number of different volumes roughly covering the expected pressure range between 0 and 20 GPa. A standard third-order Birch-Murnaghan EOS [90] is found to allow for an excellent fit to these data. For the choice of PBEsol, on which we shall focus from now on, it produces the zero-temperature EOS parameters  $V_0 = 60.388$  bohr $^3$ ,  $K_0 = 190.7$  GPa, and  $K'_0 = 4.5$ . Armed with this zero-temperature EOS  $V = V(P)$ , we determined the cubic zero temperature elastic constants  $C_{ij}(P)$  by performing a systematic series of hydrostatic, uniaxial, and rhombohedral deformations, fitting the resulting energy curves to polynomials, and extracting the corresponding curvatures at the minimum. Within the WIEN2K environment, this task is in principle conveniently performed using the corresponding package by Charpin [81]. Results are shown in Fig. 9.

Table II provides a comparison of our all-electron results for the ambient pressure cubic phase of PTO to previous ones from the literature. In particular, it should serve to warn nonspecialists of DFT not to expect different DFT codes to yield identical results even if the corresponding calculations are based on

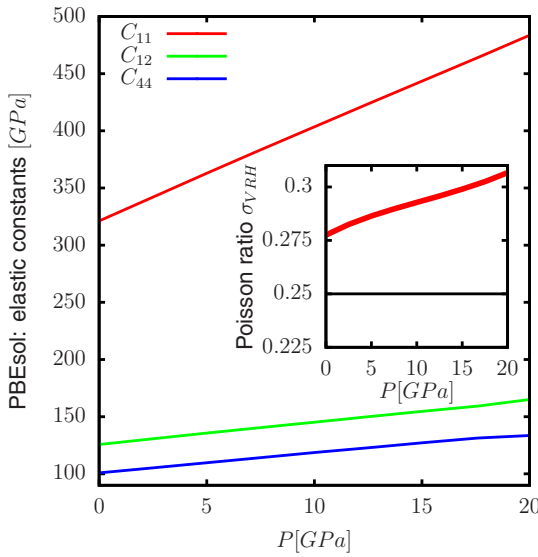


FIG. 9. Main plot: Pressure dependence of zero-temperature elastic constants of PTO as obtained from DFT using the PBEsol functional. Inset:  $P$  dependence of Poisson ratio as computed from Eq. (C4). The default value  $\sigma = 1/4$  used in the GIBBS2 package, which corresponds to a Cauchy solid, is also indicated as a guide to the eye.

the same choice of XC functional. In practice the quality of the obtained results may depend significantly on various other ingredients such as the type of pseudopotential used, the basis set employed, the number of  $k$ -mesh points, and so on. For instance, the tendency of LDA to produce overbinding is well known [91]. Therefore, the fact that the lattice constant  $a_0 = 4.09 \text{ \AA}$  obtained in Ref. [80] from an LDA calculation appears to be larger than all other corresponding values in Table II should raise severe doubts on the validity of the elastic constants reported in this reference as well. But Table II also reveals that even if two calculations show nice agreement of the equilibrium lattice parameters and bulk moduli, that does not necessarily guarantee that the corresponding elastic constants derived from these calculations do so. In summary, keeping in mind that elastic constants already represent a second-order quantity with respect to the total energy, Table II illustrates the importance of aiming for the highest possible

numerical precision when conducting calculations of elastic constants. When it comes to reliability and precision, however, a recent meta-study [92] confirms that all-electron codes like WIEN2K represent the past as well as current state-of-the-art.

As a further caveat, we note that unfortunately the procedure implemented to calculate elastic constants in the Charpin package is not based on the use of the Lagrangian strain tensor required in the proper definition of elastic constants [36], but only on the linearized strain tensor. While this subtle difference is irrelevant at zero pressure, at nonzero external pressure such an approach actually yields the so-called Voigt elastic constants  $V_{ijkl}[X_P]$  which differ from the sought-after elastic constants  $C_{ijkl}[X_P]$  by [93]

$$C_{ijkl}[X_P] = V_{ijkl}[X_P] + \frac{P}{2}(\delta_{ik}\delta_{jl} + \delta_{il}\delta_{jk}). \quad (\text{B1})$$

Without this important correction (i.e. accidentally identifying the tensors  $C_{ijkl}[X_P]$  and  $V_{ijkl}[X_P]$ ), the “elastic constants” obtained differ from the correct values by systematic errors of order no less than  $P$ . We have found this to be a pitfall to which even some prominent DFT-based codes seem to be vulnerable. Whenever in doubt, a calculated set of elastic constants can be numerically checked for consistency with an underlying EOS by (i) computing the corresponding set of Birch coefficients  $B_{\mu\nu}[X_P]$  from Eqs. (C5) and (C6), (ii) inverting the resulting tensor to obtain the compliances  $S_{\mu\nu}[X_P]$ , and (iii) making use of the general relation  $K(P) = 1/\sum_{\mu,\nu=1}^3 S_{\mu\nu}[X_P]$  to obtain the bulk modulus  $K(P)$ , which can be compared to the corresponding value directly obtained from the EOS [94].

Having determined the set of Birch coefficients  $B_{\mu\nu}[X_P]$ , it is also straightforward to determine the pressure-dependent Poisson ratio  $\sigma(P)$  as described in Appendix C. For PTO, using the PBEsol functional, we find that the ambient-pressure value of  $\sigma \approx 0.28$  (cf. inset of Fig. 9) is only slightly in excess of the GIBBS2 default value  $\sigma = 1/4$  corresponding to a Cauchy solid [53]. Within the calculated pressure range  $0 \leq P \leq 20 \text{ GPa}$  we also note a weak, roughly linear rise of  $\sigma$  to  $\sigma \approx 0.31$  at  $P = 20 \text{ GPa}$ . The observed overall dependence of the DA on  $\sigma$  is, however, observed to be quite weak. Therefore we settled for a value of  $\sigma = 0.28$ , which was used subsequently in the DA.

TABLE II. Comparison of  $T = 0$  *ab initio* results for ambient-pressure elastic constants of cubic PTO (NCP=norm-conserving pseudopotential, USPP = ultrasoft pseudopotential, LCAO = linear combination of atomic orbitals, HF = Hartree-Fock, included here for comparison).

Ref.	Method	XC functional	Remarks	$a_0 (\text{\AA})$	$C_{11}^0 (\text{GPa})$	$C_{12}^0 (\text{GPa})$	$C_{44}^0 (\text{GPa})$	$K_0 (\text{GPa})$
[79]	HF		LCAO (CRYSTAL)	3.94	398.3	169.0	172.0	245.4
[42]	DFT	LDA	USPP	3.889	341.4	148.8	102.7	208.9
[46]	DFT	LDA	NCP (CASTEP 2.1)	3.883	320.2	141.2	187.4	203.0
[79]	DFT	LDA	LCAO (CRYSTAL)	3.93	450.3	261.4	112.8	324.3
[80]	DFT	LDA	NCP (ABINIT)	4.090	321.7	113.3	83.9	179.7
this work	DFT	LDA	APW+lo (WIEN2K)	3.888	352.8	133.7	104.4	206.7
[79]	DFT	PBE	LCAO (CRYSTAL)	3.96	342.3	155.2	109.6	217.5
this work	DFT	PBE	APW+lo (WIEN2K)	3.970	282.0	117.3	97.1	172.2
this work	DFT	PBEsol	APW+lo (WIEN2K)	3.923	321.1	125.5	100.9	190.7

### APPENDIX C: NOTES ON OUR USE OF THE DEBYE APPROXIMATION

Recall [61,95] that the DA replaces the original system by an effective isotropic model containing only acoustic phonons. From their longitudinal and transverse sound velocities  $v_P, v_S$ , respectively, one defines a directionally averaged sound velocity  $\bar{v}$  with

$$\frac{3}{\bar{v}^3} = \frac{1}{v_P^3} + \frac{2}{v_S^3}. \quad (\text{C1})$$

Given the mass density  $\rho$ , the bulk modulus  $K$ , and the Poisson ratio [96]  $\sigma$ , Slater [97] has shown that

$$\bar{v} = f(\sigma) \sqrt{K/\rho}, \quad (\text{C2})$$

where

$$f(\sigma) \equiv \sqrt[3]{3} \left[ \left( \frac{1+\sigma}{3(1-\sigma)} \right)^{\frac{3}{2}} + 2 \left( \frac{2(1+\sigma)}{3(1-2\sigma)} \right)^{\frac{3}{2}} \right]^{-\frac{1}{3}}; \quad (\text{C3})$$

$\rho$  and  $K$  may be directly extracted from a given EOS while  $\sigma$  usually [53] takes values around 0.25 and exhibits only a very weak volume dependence.

Bearing in mind that the Debye approximation rests on approximating the underlying system as isotropic, it may not be obvious which value to plug into (C2) for the Poisson ratio  $\sigma$ , since in a crystal this represents, of course, a direction-dependent combination of elastic constants. Indeed it has been shown [98] that the Debye temperature may be calculated with excellent accuracy using the Voigt-Reuss-Hill (VRH) averaging scheme [99] of elastic constants which had been primarily invented to assess the elastic properties of granular material consisting of randomly oriented microcrystallites. In detail, given a crystal with elastic constants  $C_{\mu\nu}$  and corresponding compliances  $S_{\mu\nu}$ , one defines Voigt (V), Reuss (R), and VRH averages of the bulk modulus  $K$ , the shear modulus  $G$ , and Poisson's ratio  $\sigma$ . Our present purposes only require the cubic formulas, for which the Voigt and Reuss averages both agree with the unaveraged result  $K_V = K_R = K$ , whereas one obtains  $5G_V = (C_{11} - C_{12}) + 3C_{44}$  and  $5/G_R = 4(S_{11} - S_{12}) + 3S_{44}$ . From their arithmetic average  $G_{VRH} = (G_V + G_R)/2$  one finally obtains a VRH-averaged Poisson ratio

$$\sigma \equiv \sigma_{VRH} = \frac{1}{2} \left( 1 - \frac{3G_{VRH}}{3K + G_{VRH}} \right) \quad (\text{C4})$$

in accordance with the formulas of standard elasticity theory (cf. Ref. [100]). In our present context, the elastic constants  $C_{\mu\nu}$  entering the Voigt-Reuss-Hill formulas should, however, be replaced by the corresponding Birch coefficients  $B_{\mu\nu}[X_P]$ . This follows from the observation that at nonzero pressure the  $B_{ij}$  are the tensor components that actually enter into the Christoffel equations determining the acoustic sound velocities (see Ref. [36]). In passing we note that for hydrostatic pressure  $\sigma_{ij} = -P\delta_{ij}$  (and only then) the Birch coefficients (24) can indeed be written in Voigt notation as [36]

$$B_{\alpha\beta}[X_P] = C_{\alpha\beta}[X_P] + \Delta_{\alpha\beta}(P), \quad (\text{C5})$$

TABLE III. Comparison of various results for cubic bulk modulus of PTO at  $T = T_c$ .

Ref.	Method	$K_0$ (GPa)
[65]	synchrotron x-ray diffraction	237(4)
[106]	synchrotron x-ray diffraction	195(3)
[33]	synchrotron x-ray diffraction	141(5)
[107]	Brillouin scattering	143.6
this work	DFT PBEsol+DA, $\sigma = 0.28$	161.3

where

$$\Delta(P) = \begin{pmatrix} -P & P & P \\ P & -P & P \\ P & P & -P \\ & & -P \\ & & -P \\ & & -P \end{pmatrix}. \quad (\text{C6})$$

A complication worth mentioning is that the assumption that  $\sigma$  is completely independent of volume should, as already noted by Slater [97], result in an improper QHA. Attempts to fix this yield the class of so-called Debye-Grueneisen approximations [52,53], notably the Dugdale-McDonald [101], Vaschenko-Zubarev [102], and mean-free-volume [103,104] approximations (see Ref. [105] for details). All of these have been implemented in the computer code GIBBS2 [52,53], which—depending on the details of the available phonon information—also supports various other levels of the QHA as well as high-quality fitting routines for a large number of popular types of EOSs. As mentioned in Sec. V, the combination of PBEsol with a simple DA based on a Poisson ratio of  $\sigma = 0.28$  yields the overall best agreement to the available volume data. For comparison, Table III also lists some experimental results on the bulk modulus of the cubic phase.

Even after having successfully promoted the EOS of the background system  $X_P$  from zero to finite temperature, we are still left with determining the much more difficult problem of also determining the  $T$  dependence of the corresponding background elastic constants  $C_{ijkl}[X_P] = C_{ijkl}[X_P(T)]$ . Our strategy to overcome this final obstacle is reminiscent of the one put together in Ref. [38] for the purpose of parametrizing an unknown  $P$  dependence of elastic constants. We start by observing that since the  $T$  dependence of the bulk modulus  $K(P,T)$  is fully determined from the EOS based on our choice PBEsol+DA, the identity  $1/K[X_P](T) = \sum_{\mu,\nu=1}^3 S_{\mu\nu}[X_P](T)$  can be regarded as a constraint for any possible  $T$  variations of the elastic constants  $C_{\mu\nu}[X_P]$  for  $\mu, \nu = 1, 2, 3$ . Given a set of compliances  $S_{ij}[X_P](T=0)$  calculated from DFT, the compliances from the left upper quadrant  $\mu, \nu \leq 3$  satisfy

$$S_{\mu\nu}[X_P](T) = \frac{K[X_P](0)}{K[X_P](T)} S_{\mu\nu}[X_P](T) + \dots \quad (\text{C7})$$

Of course, the  $T$  dependence of transverse elastic constants like  $C_{\mu\mu}$ ,  $\mu = 4, 5, 6$  cannot be expected to be assessed in the

above way. Fortunately, in the transition under investigation shear strains play no role, so this is of no concern for our present problem.

Taking the example of a cubic system, this leaves a single function  $\delta S(P, T)$  that accounts for any possible remaining trade-off between the compliance tensor components  $S_{11}[X_P](T)$  and  $S_{12}[X_P](T)$  not covered by the overall factor  $K[X_P](0)/K[X_P](T)$ . Since this function must vanish for  $T = 0$ , it follows that it might be possible to expand  $\delta S(P, T)$  into a power series in  $T$  with  $P$ -dependent coefficients. However, for our present purposes we refrain from introducing such further complications and content ourselves with the lowest order approximation as indicated in Eq. (C7). Results are included in Table III.

Owing to the fact that the cubic phase is only thermodynamically stable above  $T_c$ , published experimental data on the cubic elastic constants of PTO are rather scarce. In the DFT-related literature (cf., e.g., Refs. [79, 108, 109]), Brillouin scattering results  $C_{11} \approx 229$  GPa,  $C_{12} \approx 101$  GPa, and  $C_{44} \approx 100$  GPa for the cubic phase are frequently attributed to Ref. [107]. Actually, however, the value of  $C_{12}$  reported in Ref. [107] refers only to the room-temperature tetragonal phase, while we are unable to spot any explicit value for the cubic elastic constant  $C_{12}$  in Ref. [107]. We therefore suspect that the above frequently cited value for  $C_{12}$  represents only a conjecture vaguely related to the observation that the value of the tetragonal elastic constant  $C_{13} \approx 98.8$  GPa reported in Ref. [107] almost agrees with said value of  $C_{12}$ . Adopting this hypothesis for the moment, one would derive a cubic bulk modulus of  $K_0 \approx 143.6$  GPa. On the other hand, using the simple strategy outlined in Eq. (C7) to extrapolate our DFT results to  $T_c$ , we obtain the numbers  $C_{11}^0 \approx 271$  GPa and  $C_{12}^0 \approx 106$  GPa yielding a bulk modulus  $K_0 \approx 161.3$  GPa in reasonable agreement with and certainly in the same ballpark as the experimental results gathered in Table III.

It is interesting to compare these results to the compliance values  $S_{11}^0 = 8.0 \times 10^{-12} \text{ m}^2/\text{N}$  and  $S_{12}^0 = -2.5 \times 10^{-12} \text{ m}^2/\text{N}$  listed in the very influential paper Ref. [26] and reproduced in a number of subsequent publications by other authors (see, e.g., Refs. [13, 27]). Inverting the compliance tensor, we obtain values  $C_{11}^0 = 174.6$  GPa,  $C_{12}^0 = 79.3$  GPa, and  $K = 111.11$  GPa that are much lower than those listed above. Puzzled by this discrepancy, we traced the origin of these values, which the authors of Ref. [26] had themselves taken from other sources, back to Ref. [28], which also lists the same value for  $S_{12}^0$  as Ref. [26] but for  $S_{11}^0$  gives a value of  $S_{11}^0 = 6.785 \times 10^{-12} \text{ m}^2/\text{N}$  instead. This set of compliances

now results in  $C_{11}^0 = 258.5$  GPa and  $C_{12}^0 = 150.8$  GPa with an accompanying bulk modulus of  $K = 186.7$  GPa, in much better agreement with the values listed before. Some readers may find this discussion lengthy. However, while we are only speculating about the actual source of the detected discrepancy; in any case such sizable errors in the values of elastic constants may have the potential to seriously affect the results of, e.g., calculations dealing with uniaxial stresses appearing in epitaxial layers of PTO on substrates. For the Landau theory of the ferroelectric transition at ambient pressure, these problems are fortunately of no concern, since for  $P = 0$  the values of the elastic constants drop out of the corresponding calculations. In summary, there is clear evidence that not only the values of the couplings  $q_\mu$  but also the compliances  $S_{11}, S_{12}$ , and  $S_{44}$  need to be revised in the published tables of Landau parameters for PTO.

#### APPENDIX D: REDEFINING THE ELASTIC BASELINE

Any time a LT contains secondary order parameters, a definition of their spontaneous equilibrium values should always require defining a corresponding baseline in advance. A correct definition of the spontaneous strain components from a given set of  $P$ -dependent unit cell parameters thus relies on the determination of a meaningful elastic reference system  $X_P(T)$  together with a compatible set of elastic constants  $C_{\mu\nu}[X_P(T)]$ , and Appendix C summarizes our corresponding efforts. In principle, only then fits of (4) to the resulting spontaneous strain data allow us to obtain the strain-OP coupling coefficients  $\hat{q}_\mu$ . This raises the question of how Haun *et al.* had overcome this difficulty in the first place without having to go through all the arguments we have given above. A careful reading of their paper reveals that the answer to this question is disarmingly simple. In fact, their baseline has been defined *a posteriori* based on the convenient requirement that the proportionality factors between the squared OP and the spontaneous strain components, which are just the Landau coefficients  $\hat{q}_\mu$  according to Eq. (11), should be constants independent of  $T$ . Our present baseline preserves this proportionality, albeit with a new set of coupling coefficients  $\hat{q}_\mu = \hat{q}_\mu(T)$  that are now inevitably  $T$ -dependent. For a DA with  $\sigma = 0.28$ , a rough polynomial fit up to second order produces (Fig. 4)

$$\begin{aligned}\hat{q}_{11}(T) &\approx +0.09816 - 9.764 \times 10^{-6} T + 6.11 \times 10^{-9} T^2, \\ \hat{q}_{12}(T) &\approx -0.02055 + 1.486 \times 10^{-5} T - 2.561 \times 10^{-8} T^2.\end{aligned}\quad (\text{D1})$$

- 
- [1] M. Murakami, K. Hirose, K. Kawamura, N. Sata, and Y. Ohishi, *Science* **304**, 855 (2004).
  - [2] A. Jaffe, Y. Lin, C. M. Beavers, J. Voss, W. L. Mao, and H. I. Karunadasa, *ACS Central Science* **2**, 201 (2016).
  - [3] H. J. Zhao, X. Q. Liu, X. M. Chen, and L. Bellaiche, *Phys. Rev. B* **90**, 195147 (2014).
  - [4] H. Sharma, J. Kreisel, and P. Ghosez, *Phys. Rev. B* **90**, 214102 (2014).
  - [5] E. Gilioli and L. Ehm, *IUCrJ* **1**, 590 (2014).
  - [6] J. Tolédano and P. Tolédano, *The Landau Theory of Phase Transitions* (World Scientific, Singapore, 1987).
  - [7] L. Landau, E. Lifshitz, and L. Pitaevskii, *Statistical Physics, Part I* (Butterworth and Heinemann, Oxford, 2001).
  - [8] M. Lines and A. Glass, *Principles and Applications of Ferroelectrics and Related Materials* (Clarendon Press, Oxford, 1977).

- [9] T. Duffy, *Nature (London)* **506**, 427 (2014).
- [10] A. Tröster, W. Schranz, F. Karsai, and P. Blaha, *Phys. Rev. X* **4**, 031010 (2014).
- [11] B. Karki, L. Stixrude, and R. Wentzcovitch, *Rev. Geophys.* **39**, 507 (2001).
- [12] A. Togo, F. Oba, and I. Tanaka, *Phys. Rev. B* **78**, 134106 (2008).
- [13] *Physics of Ferroelectrics*, Vol. 105 of Topics in Applied Physics, edited by K. Rabe, C. Ahn, and J.-M. Triscone (Springer, Berlin, 2007).
- [14] B. Noheda, *Curr. Opin. Solid State Mater. Sci.* **6**, 27 (2002).
- [15] Z. Kutnjak, J. Petzelt, and R. Blinc, *Nature (London)* **441**, 956 (2006).
- [16] G. Shirane, S. Hoshino, and K. Suzuki, *Phys. Rev.* **80**, 1105 (1950).
- [17] G. Shirane and S. Hoshino, *J. Phys. Soc. Jpn.* **6**, 265 (1951).
- [18] G. Shirane, J. D. Axe, J. Harada, and J. P. Remeika, *Phys. Rev. B* **2**, 155 (1970).
- [19] G. Burns and B. A. Scott, *Phys. Rev. Lett.* **25**, 167 (1970).
- [20] G. Burns and B. A. Scott, *Phys. Rev. B* **7**, 3088 (1973).
- [21] J. Remeika and A. Glass, *Mater. Res. Bull.* **5**, 37 (1970).
- [22] A. Amin, M. J. Haun, B. Badger, H. McKinstry, and L. E. Cross, *Ferroelectrics* **65**, 107 (1985).
- [23] M. J. Haun, E. Furman, S. J. Jang, H. A. McKinstry, and L. E. Cross, *J. Appl. Phys.* **62**, 3331 (1987).
- [24] A. F. Devonshire, *The London, Edinburgh, and Dublin Philosophical Magazine and Journal of Science* **40**, 1040 (1949).
- [25] D. Vanderbilt and M. H. Cohen, *Phys. Rev. B* **63**, 094108 (2001).
- [26] N. A. Pertsev, A. G. Zembilgotov, and A. K. Tagantsev, *Phys. Rev. Lett.* **80**, 1988 (1998).
- [27] J. Gao, F. Li, Z. Xu, C. Zhang, Y. Liu, G. Liu, T. Zhang, and H. He, *J. Phys. D* **46**, 215304 (2013).
- [28] G. A. Rossett, K. R. Udayakumar, M. J. Haun, and L. E. Cross, *J. Am. Ceram. Soc.* **73**, 3334 (1990).
- [29] J. A. Sanjurjo, E. López-Cruz, and G. Burns, *Phys. Rev. B* **28**, 7260 (1983).
- [30] P.-E. Janolin, P. Bouvier, J. Kreisel, P. A. Thomas, I. A. Kornev, L. Bellaiche, W. Crichton, M. Hanfland, and B. Dkhil, *Phys. Rev. Lett.* **101**, 237601 (2008).
- [31] R. J. Nelmes and A. Katrusiak, *J. Phys. C* **19**, L725 (1986).
- [32] P. Pruzan, D. Gourdaine, and J. C. Chervin, *Phase Transitions* **80**, 1103 (2007).
- [33] J. Zhu, H. Xu, J. Zhang, C. Jin, L. Wang, and Y. Zhao, *J. Appl. Phys.* **110**, 084103 (2011).
- [34] M. Ahart, M. Somayazulu, R. E. Cohen, P. Ganesh, P. Dera, H.-k. Mao, R. J. Hemley, Y. Ren, P. Liermann, and Z. Wu, *Nature (London)* **451**, 545 (2008).
- [35] P. Ganesh and R. E. Cohen, *J. Phys.: Condens. Matter* **21**, 064225 (2009).
- [36] D. Wallace, *Thermodynamics of Crystals* (Dover, New York, 1998).
- [37] J. W. Morris and C. R. Krenn, *Philos. Mag. A* **80**, 2827 (2000).
- [38] A. Tröster, W. Schranz, and R. Miletich, *Phys. Rev. Lett.* **88**, 055503 (2002).
- [39] Z. Wu and R. E. Cohen, *Phys. Rev. Lett.* **95**, 037601 (2005).
- [40] I. A. Kornev, L. Bellaiche, P. Bouvier, P.-E. Janolin, B. Dkhil, and J. Kreisel, *Phys. Rev. Lett.* **95**, 196804 (2005).
- [41] I. A. Kornev and L. Bellaiche, *Phase Transitions* **80**, 385 (2007).
- [42] R. D. King-Smith and D. Vanderbilt, *Phys. Rev. B* **49**, 5828 (1994).
- [43] K. M. Rabe and J. D. Joannopoulos, *Phys. Rev. Lett.* **59**, 570 (1987).
- [44] W. Zhong, D. Vanderbilt, and K. M. Rabe, *Phys. Rev. Lett.* **73**, 1861 (1994).
- [45] W. Zhong, D. Vanderbilt, and K. M. Rabe, *Phys. Rev. B* **52**, 6301 (1995).
- [46] U. V. Waghmare and K. M. Rabe, *Phys. Rev. B* **55**, 6161 (1997).
- [47] A. Kumar, K. M. Rabe, and U. V. Waghmare, *Phys. Rev. B* **87**, 024107 (2013).
- [48] H. Krakauer, R. Yu, C.-Z. Wang, K. M. Rabe, and U. V. Waghmare, *J. Phys.: Condens. Matter* **11**, 3779 (1999).
- [49] S. Tinte, J. Íñiguez, K. M. Rabe, and D. Vanderbilt, *Phys. Rev. B* **67**, 064106 (2003).
- [50] A. D. Bruce and R. A. Cowley, *Structural Phase Transitions* (Taylor and Francis Ltd., London, 1981).
- [51] O. Anderson, *Equations of State of Solids for Geophysics and Ceramic Science* (Oxford University Press, Oxford, 1995).
- [52] A. Otero-de-la-Roza and V. Luña, *Comput. Phys. Commun.* **182**, 1708 (2011).
- [53] A. Otero-de-la-Roza, D. Abbasi-Pérez, and V. Luña, *Comput. Phys. Commun.* **182**, 2232 (2011).
- [54] M. Dove, *Introduction to Lattice Dynamics* (Cambridge University Press, Cambridge, 2004).
- [55] B. Fultz, *Phase Transitions in Materials* (Cambridge University Press, Cambridge, 2014).
- [56] O. Hellman, I. A. Abrikosov, and S. I. Simak, *Phys. Rev. B* **84**, 180301 (2011).
- [57] P. Souvatzis, S. Arapan, O. Eriksson, and M. I. Katsnelson, *Europhys. Lett.* **96**, 66006 (2011).
- [58] S. W. Kieffer, *Rev. Geophys.* **17**, 1 (1979); **17**, 20 (1979); **17**, 35 (1979); **18**, 862 (1980); **20**, 827 (1982).
- [59] A. Oganov, in *Treatise on Geophysics*, edited by G. Schubert (Elsevier, Amsterdam, 2007), pp. 121–152.
- [60] L. Stixrude and R. Jeanloz, in *Treatise on Geophysics*, edited by G. Schubert (Elsevier, Amsterdam, 2007), pp. 775–803.
- [61] *An Introduction to High-Pressure Science and Technology*, edited by J. M. Recio, J. M. Menendez, and A. Otero-de-la-Roza (CRC Press, Boca Raton, FL, 2016).
- [62] A. Tröster, *Phys. Rev. Lett.* **100**, 140602 (2008).
- [63] E. Salje, *Phase Transitions in Ferroelastic and Coelastic Crystals* (Cambridge University Press, Cambridge, 1990).
- [64] R. Ramirez, M. F. Lapena, and J. A. Gonzalo, *Phys. Rev. B* **42**, 2604 (1990).
- [65] A. Sani, M. Hanfland, and D. Levy, *J. Solid State Chem.* **167**, 446 (2002).
- [66] S. G. Jabarov, D. P. Kozlenko, S. E. Kichanov, A. I. Mamedov, R. Z. Mehdieva, E. V. Lukin, B. N. Savenko, and C. Lathe, *Surface Engineering and Applied Electrochemistry* **48**, 69 (2012).
- [67] G. A. Samara, *Ferroelectrics* **2**, 277 (1971).
- [68] A. Tröster, C. Dellago, and W. Schranz, *Phys. Rev. B* **72**, 094103 (2005).
- [69] A. Tröster and C. Dellago, *Ferroelectrics* **354**, 225 (2007).
- [70] P. Souvatzis, O. Eriksson, M. I. Katsnelson, and S. P. Rudin, *Phys. Rev. Lett.* **100**, 095901 (2008).
- [71] J. C. Thomas and A. Van der Ven, *Phys. Rev. B* **88**, 214111 (2013).

- [72] V. I. Levitas, D. L. Preston, and D.-W. Lee, *Phys. Rev. B* **68**, 134201 (2003).
- [73] V. I. Levitas, *Int. J. Plast.* **49**, 85 (2013).
- [74] V. A. Levin, V. I. Levitas, K. M. Zingerman, and E. I. Freiman, *Int. J. Solids Struct.* **50**, 2914 (2013).
- [75] V. I. Levitas, *J. Mech. Phys. Solids* **70**, 154 (2014).
- [76] A. Vattré and C. Denoual, *J. Mech. Phys. Solids* **92**, 1 (2016).
- [77] C. Denoual and A. Vattré, *J. Mech. Phys. Solids* **90**, 91 (2016).
- [78] P. Toledano and V. Dmitriev, *Reconstructive Phase Transitions in Crystals and Quasicrystals* (World Scientific, Singapore, 1996).
- [79] S. Piskunov, E. Heifets, R. Egglitis, and G. Borstel, *Comput. Mater. Sci.* **29**, 165 (2004).
- [80] W. Huang, H. Yang, G. Lu, and Y. Gao, *Physica B* **411**, 56 (2013).
- [81] P. Blaha, K. Schwarz, G. K. H. Madsen, D. Kvasnicka, and J. Luitz, *WIEN2k: An Augmented Plane Wave and Local Orbitals Program for Calculating Crystal Properties* (Vienna University of Technology, Austria, 2001).
- [82] D. Singh and L. Nordström, *Planewaves, Pseudopotentials and the LAPW Method*, 2nd ed. (Springer, New York, 2006).
- [83] Z. Wu, R. E. Cohen, and D. J. Singh, *Phys. Rev. B* **70**, 104112 (2004).
- [84] Z. Wu and R. E. Cohen, *Phys. Rev. B* **73**, 235116 (2006).
- [85] J. P. Perdew, A. Ruzsinszky, G. I. Csonka, O. A. Vydrov, G. E. Scuseria, L. A. Constantin, X. Zhou, and K. Burke, *Phys. Rev. Lett.* **100**, 136406 (2008).
- [86] F. Tran, R. Laskowski, P. Blaha, and K. Schwarz, *Phys. Rev. B* **75**, 115131 (2007).
- [87] J. P. Perdew, K. Burke, and M. Ernzerhof, *Phys. Rev. Lett.* **77**, 3865 (1996).
- [88] J. P. Perdew, K. Burke, and M. Ernzerhof, *Phys. Rev. Lett.* **78**, 1396 (1997).
- [89] R. Wahl, D. Vogtenhuber, and G. Kresse, *Phys. Rev. B* **78**, 104116 (2008).
- [90] F. Birch, *Phys. Rev.* **71**, 809 (1947).
- [91] A. van de Walle and G. Ceder, *Phys. Rev. B* **59**, 14992 (1999).
- [92] K. Lejaeghere *et al.*, *Science* **351**, aad3000 (2016).
- [93] D. C. Wallace, *Phys. Rev.* **162**, 776 (1967).
- [94] J. Koppensteiner, A. Tröster, and W. Schranz, *Phys. Rev. B* **74**, 014111 (2006).
- [95] J.-P. Poirier, *Introduction to the Physics of the Earth's Interior*, 2nd ed. (Cambridge University Press, Cambridge, 2000).
- [96] G. N. Greaves, A. L. Greer, R. S. Lakes, and T. Rouxel, *Nat. Mater.* **10**, 823 (2011).
- [97] J. Slater, *Introduction to Chemical Physics* (McGraw-Hill, New York, 1939).
- [98] O. L. Anderson, *J. Phys. Chem. Solids* **24**, 909 (1963).
- [99] R. Hill, *Proc. Phys. Soc., London, Sect. A* **65**, 349 (1952).
- [100] G. Grimvall, *Thermophysical Properties of Materials* (Elsevier, Amsterdam, 1999).
- [101] J. S. Dugdale and D. K. C. MacDonald, *Phys. Rev.* **89**, 832 (1953).
- [102] V. Vashenko and V. Zubarev, *Sov. Phys. Solid State* **5**, 653 (1963).
- [103] M. A. Barton and F. D. Stacey, *Phys. Earth Planet. Inter.* **39**, 167 (1985).
- [104] F. D. Stacey, *Phys. Earth Planet. Inter.* **89**, 219 (1995).
- [105] L. Vočadlo, J. Poirier, and G. Price, *Am. Mineral.* **85**, 390 (1985).
- [106] A. Sani, M. Hanfland, and D. Levy, *J. Phys.: Condens. Matter* **14**, 10601 (2002).
- [107] Z. Li, M. Grimsditch, C. Foster, and S.-K. Chan, *J. Phys. Chem. Solids* **57**, 1433 (1996).
- [108] J. Long, L. Yang, and X. Wei, *J. Alloys Compd.* **549**, 336 (2013).
- [109] Y. Liu, G. Xu, C. Song, Z. Ren, G. Han, and Y. Zheng, *Mater. Sci. Eng., A* **472**, 269 (2008).

# Curriculum Vitae

# Kamal Belbase

PhD Student  
TU Wien

Techical University of Vienna  
Institute of Material chemistry  
(+43) 6608429341  
kamal.belbase@tuwien.ac.at

## Education

- 2021 **PhD, Computational Material Science, TU Wien**, Vienna, Austria.
- 2015 **Postgraduate Diploma, The Abdus Salam Interantional Centre for Theoretical Physics (ICTP)**, Trieste, Italy.
- 2013 **M.Sc. Physics, Tri-Bhuvan University**, Kathmandu, Nepal.
- 2010 **B.Sc. Physics, Tri-Bhuvan University**, Kathmandu, Nepal.

## Experiences

- 2015-2021 **Research Assistant, TU Wien, Institute of Material Chemistry**, Vienna, Austria.
- 2013 **Research Assistant, Central Department of Physics, Tri-Bhuvan University**, Kathmandu, Nepal.

## Skills

- Codes WIEN2k, Quantum ESPRESSO
- Languages FORTRAN, Python
- Miscellaneous Linux, Shell script, Latex, gnuplot,google colab, jupyter-notebook

## Languages

- English Fluent
- German A2 Level
- Hindi Fluent
- Nepal Native

## Publications

- **K. Belbase**, A. Tröster and P. Blaha. Extension of the stress tensor for the augmented plane wave method with local orbital and the Generalized Gradient Approximation. (submitted to PRB)
- **K. Belbase**, A. Tröster and P. Blaha. Stress tensor in the linearized augmented plane wave method, Phys. Rev. B 104, 174113 (2021).
- A. Tröster, W. Schranz, S. Ehsan, **K. Belbase** and P. Blaha. Symmetry Adapted Finite Strain Landau Theory Applied to KMnF<sub>3</sub>, Crystals 2020, 10(2), 124.
- A. Tröster, S. Ehsan, **K. Belbase**, P. Blaha, J. Kreisel and W. Schranz. Finite strain Landau theory applied to the high pressure phase transition of lead titanate. Phys. Rev. B 95, 064111 (2017).
- N. Pantha, **K. Belbase**, and N. P. Adhikari. First-principles study of the interaction of hydrogen molecular on Na-adsorbed graphene. Applied Nanoscience 5, 393-402 (2015).

## Talks and Posters

- “Implementation of Stress Tensor in the LAPW method with Emphasis on WIEN2k”, DPG Spring Meetings 2019, Regensburg, Germany, 3/4/2019 (Talk).
- “Implementation of Stress Tensor in the LAPW method with Emphasis on WIEN2k package”, The Summer School of Solid4Fun, Schlosshotel Waidhofen an der Ybbs, Austria, 5/7/2019 (Talk).
- “Implementation of Stress Tensor in the LAPW method”, Mainz Materials Simulation Days 2017, CECAM-DE-SMSM, Mainz, Germany, 31/06/2017 (Poster Presentation).
- “Implementation of Stress Tensor in the LAPW method”, 32 Workshop on Novel Materials and Superconductors, Obertraun, Austria, 12-18, February (Poster Presentation).

## Conference Participation

- \* VDSP-ESI Winter School 2020, “Machine learning in Physics” at the University of Vienna, Austria 10-20, February, 2020.
- \* The International Summer School, “Ab initio Modeling in Solid State Chemistry – MSSC2019” at the Imperial College London, UK, 16-20, September, 2019.
- \* “Paris International School on Advanced Computational Materials Science 2019 – PISACMS2019”, Sorbonne University, Paris, France, 26-30, August, 2019.
- \* “26th WIEN2k – WORKSHOP, DFT based simulations of solids with the WIEN2k code”, Vienna, Austria, 13-17, August, 2019.
- \* “Hands-on course on ab-initio calculations”, Clausthal University of Technology, Göttingen, Germany, 3-7, September, 2018.
- \* “Psi-K/CECAM/CCP9 graduate school in electronic-structure methods”, Daresbury Laboratory, UK, 5-9, September, 2016.

## References

- 1 Prof. Dr. Peter Blaha  
Technical University of Vienna  
Vienna, Austria  
[pbla@theochem.tuwien.ac.at](mailto:pbla@theochem.tuwien.ac.at)  
[peter.blaha@theochem.tuwien.ac.at](mailto:peter.blaha@theochem.tuwien.ac.at)
- 2 Dr. Andreas Troester  
University of Vienna  
Vienna, Austria  
[andreas.troester@univie.ac.at](mailto:andreas.troester@univie.ac.at)